

Leveraging Remote Sensing, Field Surveys, and Numerical Modelling to Understand the Prek System of the Cambodian Mekong Delta - From Hydrological Processes to Ecosystem Services

Christina Orieschnig

▶ **To cite this version:**

Christina Orieschnig. Leveraging Remote Sensing, Field Surveys, and Numerical Modelling to Understand the Prek System of the Cambodian Mekong Delta - From Hydrological Processes to Ecosystem Services. Earth Sciences. AgroParisTech, 2022. English. ⟨NNT : 2022AGPT0009⟩. ⟨tel-03943648⟩

HAL Id: tel-03943648

https://pastel.hal.science/tel-03943648v1

Submitted on 17 Jan 2023

HAL is a multi-disciplinary open access archive for the deposit and dissemination of scientific research documents, whether they are published or not. The documents may come from teaching and research institutions in France or abroad, or from public or private research centers.

L'archive ouverte pluridisciplinaire **HAL**, est destinée au dépôt et à la diffusion de documents scientifiques de niveau recherche, publiés ou non, émanant des établissements d'enseignement et de recherche français ou étrangers, des laboratoires publics ou privés.



HAL Authorization

THÈSE POUR OBTENIR LE GRADE DE DOCTEUR DE L'INSTITUT DES SCIENCES ET INDUSTRIES DU VIVANT ET DE L'ENVIRONNEMENT - AGROPARISTECH

N° : 2022 AGPT 0009

En STE - SCIENCES DE L'EAU

École doctorale GAIA – Biodiversité, Agriculture, Alimentation, Environnement, Terre, Eau – n°584

Portée par l'Université de Montpellier

Unité Mixte de Recherche G-EAU

Leveraging Remote Sensing, Field Surveys, and Numerical Modelling to Understand the Prek System of the Cambodian Mekong Delta - From Hydrological Processes to Ecosystem Services

(Exploiter la télédétection, les enquêtes de terrain et la modélisation numérique pour comprendre le système Prek du delta du Mékong cambodgien - des processus hydrologiques aux services écosystémiques)

Présentée par Christina ORIESCHNIG

Le 07 Juillet 2022

Sous la direction de Gilles BELAUD

et le co-encadrement de Sylvain MASSUEL et Jean-Philippe VENOT

Devant le jury composé de

Gilles BELAUD, Professeur, Institut Agro Montpellier	Directeur de thèse
Jean-Philippe VENOT, Chargé de recherche, IRD	Co-encadrant
Charlotte DE FRAITURE, Professeure, IHE Delft (Pays-Bas)	Rapporteure
Hélène ROUX, Professeure, Institut National Polytechnique de Toulouse	Rapporteure
Karsten SCHULZ, Professeur, BOKU Wien (Autriche)	Membre du jury
Carole DELENNE, Maîtresse de conférences, Université de Montpellier	Membre du jury
Dominique COURAULT, Directrice de recherche, INRAE Avignon	Presidente
Sylvain MASSUEL, Chargé de recherche, IRD	Invité

AgroParisTech

UNIVERSITÉ DE MONTPELLIER

Abstract

This thesis provides insights into the hydrological processes in the Cambodian Mekong delta, as well as their relationship to ecosystem services from which the local population benefits. In particular, the role of the Prek channels is examined. First constructed during the period of the French protectorate in the early 20th century, these channels diverge perpendicularly from the Mekong and its deltaic distributary, the Bassac, and provide a connection between the river mainstream and its low-lying floodplains by breaching the elevated river banks. The aim of this thesis is to assess how large-scale changes in the Mekong basin, such as climate and land use change, as well as hydropower development, are reflected at a local scale in its delta. It also aims to elucidate how local infrastructure such as Preks catalyzes these processes and could help mitigate negative effects of future scenarios.

To address all of these research questions, a multi-method approach was chosen. First, a thorough literature review of the complex challenges facing the Mekong basin and its delta was carried out. Subsequently, an analysis of long-term trends in water levels, precipitation patterns, and inundation extents and dynamics at the scale of the Cambodian Mekong delta is provided. Water level time series at four hydrological stations maintained by the Mekong River Commission (MRC) are subjected to a trend and break point analysis. Furthermore, precipitation data from three in-situ stations, as well as remotely sensed CHIRPS data are compared. Inundation extents are assessed on the basis of a new model developed in the course of this thesis: WAFL - Water Level Flood Link. WAFL uses in-situ water level time series and inundation maps derived from Sentinel-1 and -2 images taken between 2017 and 2020, and establishes a correlative link between them, accounting for flood propagation delays and attenuation. It can then be used to reconstruct past inundation extents based on water levels, overcoming spatial data sparsity. It is able to reconstruct earlier events (floods in the 1990's and 2000s) with good accuracy, in comparison to historical Landsat-derived maps. This indicates that long-term changes of flood patterns are mostly due to shifts in boundary inflow, rather than in the local configuration of the link between the river

and its floodplains. Overall, average inundation durations have declined by 19 days and the incidence of inundations in the early wet season (July and August) has decreased by an average of to 21%.

Furthermore, fieldwork was carried out in a case study area on the banks of the Bassac river, which encompasses ten Preks. Local stakeholders, such as farmers and village chiefs, were interviewed to gain a better understanding of the ecosystem services linked to local hydrological processes, and the capacity in which the Preks catalyze these processes. The interviews also served as a basis to characterize typical cropping patterns and practices, from irrigation to average and maximum yield. To further enhance the understanding of the role of the Preks for local communities and agricultural practices archival research was undertaken. In addition, local land use and its variations depending on the spatial configuration of hydrological processes and Preks was analyzed using a land use - land cover (LULC) classification based on Sentinel imagery and a supervised Gradient Tree Boosting machine learning approach.

Finally, to formalize the understanding of the role of Preks for local hydrological processes and ecosystem services in the Cambodian Mekong delta, and to simulate future scenarios, a numerical model was constructed in Python. It uses the data generated through interviews, literature research, and remote sensing analyses as input and simulates four future scenarios with respect to local climate variables, the configuration of Prek channels and river water levels, the latter depending on basin-wide climate change and hydropower development. Flood-related and non-flood related ecosystem services were simulated separately, to central role of annual monsoon inundations. The results show that under likely future precipitation, temperature, and water level patterns, agricultural production is set to decrease, but that this decrease could be compensated by Prek rehabilitation.

Keywords: Mekong, remote sensing, hydrological modeling, inundations, ecosystem services

Résumé

Cette thèse fournit des informations sur les processus hydrologiques dans le delta du Mékong cambodgien, ainsi que sur leur relation avec les services écosystémiques dont bénéficie la population locale. En particulier, le rôle des canaux de Prek est examiné. Construits à l'époque du protectorat français, au début du 20e siècle, ces canaux divergent perpendiculairement du Mékong et de son distributaire deltaïque, le Bassac, et assurent une connexion entre le cours principal du fleuve et ses plaines inondables de faible altitude en ouvrant des brèches dans les berges élevées du fleuve. L'objectif de cette thèse est d'évaluer comment les changements à grande échelle dans le bassin du Mékong, tels que le changement climatique et l'utilisation des terres, ainsi que le développement de l'hydroélectricité, se reflètent à une échelle locale dans son delta. Elle vise également à élucider comment les infrastructures locales telles que Preks catalysent ces processus et pourraient contribuer à atténuer les effets négatifs des scénarios futurs.

Pour répondre à toutes ces questions de recherche, une approche multi-méthodes a été choisie. Tout d'abord, une analyse documentaire approfondie des défis complexes auxquels sont confrontés le bassin du Mékong et son delta a été réalisée. Ensuite, une analyse des tendances à long terme des niveaux d'eau, des modèles de précipitations, de l'étendue et de la dynamique des inondations à l'échelle du delta du Mékong cambodgien est fournie. Les séries chronologiques des niveaux d'eau de quatre stations hydrologiques maintenues par la Commission du Mékong (MRC) sont soumises à une analyse des tendances et des points de rupture. De plus, les données de précipitation de trois stations in situ, ainsi que les données de télédétection CHIRPS sont comparées. L'étendue des inondations est évaluée sur la base d'un nouveau modèle développé au cours de cette thèse : WAFL - Water Level Flood Link. WAFL utilise des séries temporelles de niveaux d'eau in-situ et des cartes d'inondation dérivées d'images Sentinel-1 et -2 prises entre 2017 et 2020, et établit un lien corrélatif entre elles, en tenant compte des délais de propagation et de l'atténuation des inondations. Elle peut ensuite être utilisée pour reconstruire les étendues d'inondation passées sur la base des niveaux d'eau, en surmontant la rareté des données spatiales. Elle est capable de

reconstruire des événements plus anciens (inondations des années 1990 et 2000) avec une bonne précision, en comparaison avec les cartes historiques dérivées de Landsat. Cela indique que les changements à long terme des modèles d'inondation sont principalement dus à des changements dans le flux d'entrée frontalier, plutôt que dans la configuration locale du lien entre la rivière et ses plaines d'inondation. Globalement, la durée moyenne des inondations a diminué de 19 jours et l'incidence des inondations au début de la saison des pluies (juillet et août) a diminué en moyenne de 21%.

En outre, le travail de terrain a été réalisé dans une zone d'étude de cas sur les rives du fleuve Bassac, qui englobe dix Preks. Les parties prenantes locales, telles que les agriculteurs et les chefs de village, ont été interrogées afin de mieux comprendre les services écosystémiques liés aux processus hydrologiques locaux et la capacité des Preks à catalyser ces processus. Les entretiens ont également servi de base pour caractériser les modèles et pratiques culturales typiques, de l'irrigation au rendement moyen et maximal. Afin d'améliorer la compréhension du rôle des Preks pour les communautés locales et les pratiques agricoles, des recherches archivistiques ont été entreprises. En outre, l'utilisation locale des terres et ses variations en fonction de la configuration spatiale des processus hydrologiques et des Preks ont été analysées à l'aide d'une classification de l'utilisation des terres et de la couverture des terres (LULC) basée sur l'imagerie Sentinel et une approche d'apprentissage automatique supervisée de type Gradient Tree Boosting.

Enfin, pour formaliser la compréhension du rôle des Preks pour les processus hydrologiques locaux et les services écosystémiques dans le delta du Mékong cambodgien, et pour simuler des scénarios futurs, un modèle numérique a été construit en Python. Il utilise les données générées par les entretiens, la recherche documentaire et les analyses de télédétection comme données d'entrée et simule quatre scénarios futurs en ce qui concerne les variables climatiques locales, la configuration des canaux Prek et les niveaux d'eau du fleuve, ces derniers dépendant du changement climatique à l'échelle du bassin et du développement de l'hydroélectricité. Les services écosystémiques liés et non liés aux inondations ont été simulés séparément, en tenant compte du rôle central des inondations annuelles dues à la mousson. Les résultats montrent que dans le cadre des modèles probables de précipitations, de températures et de niveaux d'eau futurs, la production agricole devrait diminuer, mais que cette diminution pourrait être compensée par la réhabilitation des Preks.

Mots-clés: Mékong,télédétection, modélisation hydrologique, inondations, services écosystémiques

Abstrakt

Diese Arbeit bietet Einblicke in die hydrologischen Prozesse im kambodschanischen Mekong-Delta sowie deren Beziehung zu den Ökosystemleistungen, von denen die lokale Bevölkerung profitiert. Dabei wird insbesondere die Rolle der Prek-Kanäle untersucht. Diese Kanäle, die erstmals während des französischen Protektorats im frühen 20. Jahrhundert angelegt wurden, zweigen senkrecht vom Mekong und seinem Nebenfluss, dem Bassac, ab und stellen eine Verbindung zwischen dem Hauptstrom des Flusses und seinen Überschwemmungsflächen her, indem sie die durch Sedimentablagerungen erhöhten Flussufer durchbrechen. In dieser Arbeit soll untersucht werden, wie sich großräumige Veränderungen im Mekong-Becken, vor allem Änderungen in Klima und Landnutzung, sowie der Ausbau der Wasserkraft, auf lokaler Ebene im Delta widerspiegeln. Außerdem soll geklärt werden, wie lokale Infrastrukturelemente wie Preks diese Prozesse katalysieren und dazu beitragen, negative Auswirkungen künftiger Szenarien zu mildern.

Zur Beantwortung all dieser Forschungsfragen wurde ein multimethodischer Ansatz gewählt. Zunächst wurde eine gründliche Literaturrecherche zu den komplexen Herausforderungen des Mekong-Beckens und seines Deltas durchgeführt. Anschließend wurde eine Analyse der langfristigen Trends bei Wasserständen, Niederschlagsmustern, Überschwemmungsausmaß und -dynamik auf der Ebene des kambodschanischen Mekong-Deltas durchgeführt. Die Zeitreihen der Wasserstände an vier von der Mekong River Commission (MRC) betriebenen hydrologischen Stationen wurden einer Trend- und Bruchpunktanalyse unterzogen. Darüber hinaus wurden Niederschlagsdaten von drei In-situ-Stationen sowie CHIRPS-Fernerkundungsdaten verglichen. Das Ausmaß der Überschwemmung wurde auf der Grundlage eines neuen, im Rahmen dieser Arbeit entwickelten Modells abgeschätzt: WAFL - Water Level Flood Link. WAFL verwendet in-situ Wasserstandszeitreihen und Überschwemmungskarten, die aus Bildern der Sentinel-Konstellation aus den Jahren 2017 bis 2020 abgeleitet wurden und stellt eine korrelative Verbindung zwischen ihnen her, wobei Verzögerungen bei der Ausbreitung von Überschwemmungen berücksichtigt werden. Anschließend kann WAFL zur Rekonstruktion früherer Überschwemmungsaus-

dehnungen auf der Grundlage der Wasserstände verwendet werden. Es ist in der Lage, frühere Ereignisse (Überschwemmungen in den 1990er und 2000er Jahren) mit großer Genauigkeit zu rekonstruieren, im Vergleich mit historischen Landsat-Bildern. Dies deutet darauf hin, dass langfristige Veränderungen der Überschwemmungsmuster auf Verschiebungen der Zuflüsse aus dem Einzugsgebiets des Mekongs zurückzuführen sind, nicht auf die Verbindung zwischen dem Fluss und seinen Überschwemmungsflächen. Insgesamt ist die durchschnittliche Überschwemmungsdauer um 19 Tage zurückgegangen, und die Häufigkeit von Überschwemmungen in der frühen Regenzeit (Juli und August) hat sich um durchschnittlich 21% verringert. Darüber hinaus haben umfangreiche lokale Landnutzungsänderungen, insbesondere die Entwaldung, erhebliche Auswirkungen auf die hydrologische Dynamik und die Erfassungsgenauigkeit.

Darüber hinaus wurde Feldarbeit in einem Fallstudiengebiet am Ufer des Bassac-Flusses durchgeführt, das zehn Preks umfasst. Lokale Stakeholder wie Bauern und Dorfvorsteher wurden befragt, um ein besseres Verständnis der mit den hydrologischen Prozessen verbundenen Ökosystemleistungen und der Fähigkeit der Preks, diese Prozesse zu katalysieren, zu gewinnen. Die Interviews dienten auch als Grundlage für die Charakterisierung typischer Anbaumuster und -praktiken, von der Bewässerung bis zum durchschnittlichen und maximalen Ertrag. Um das Verständnis für die Rolle der Preks für die lokalen Gemeinschaften und die landwirtschaftlichen Praktiken weiter zu vertiefen, wurden Archivrecherchen durchgeführt. Darüber hinaus wurden die lokale Landnutzung und ihre Variationen in Abhängigkeit von der räumlichen Konfiguration der hydrologischen Prozesse und der Preks mit Hilfe einer Klassifizierung von Landnutzung und Bodenbedeckung (LULC) auf der Grundlage von Sentinel-Bildern und einem supervised Gradient Tree Boosting-Ansatz analysiert.

Um das Verständnis der Rolle von Preks für hydrologische Prozesse und Ökosystemleistungen im kambodschanischen Mekong-Delta zu formalisieren und Szenarien zu simulieren, wurde ein numerisches Modell in Python erstellt. Es nutzt die durch Interviews, Literaturrecherche und Fernerkundungsanalysen gewonnenen Daten als Input und simuliert vier mögliche Szenarien in Bezug auf Klimavariablen, die Konfiguration der Preks und die Wasserstände der Flüsse, letztere in Abhängigkeit vom einzugsgebietsweiten Klimawandel und der Entwicklung der Wasserkraft. Überschwemmungsbedingte und nicht überschwemmungsbedingte Ökosystemleistungen wurden getrennt simuliert. Die Ergebnisse zeigen, dass bei den wahrscheinlichen zukünftigen Niederschlags-, Temperatur- und Wasserstandsmustern die landwirtschaftliche Produktion zurückgehen wird, dass dieser Rückgang jedoch durch den Ausbau der Preks kompensiert werden könnte.

Stichwörter: Mekong, Fernerkundung, hydrologische Modellierung, Überschwemmungen, Ökosystemleistungen

We at the height are ready to decline.
There is a tide in the affairs of men
Which, taken at the flood, leads on to fortune;
Omitted, all the voyage of their life
Is bound in shallows and in miseries.
On such a full sea are we now afloat,
And we must take the current when it serves,
Or lose our ventures.

Julius Cesar (IV.iii)

William Shakespeare

Résumé en Français

Exploiter la télédétection, les enquêtes de terrain et la modélisation numérique pour comprendre le système Prek du delta du Mékong cambodgien - des processus hydrologiques aux services écosystémiques

Introduction

Dans le monde entier, les deltas font partie des zones les plus riches en biodiversité et les plus productives en termes d'agriculture et de pêche. Ils ne couvrent que 0,57% de la surface de la planète, mais abritent plus de 4,5% de sa population. Depuis l'aube des hautes civilisations antiques, les deltas tels que ceux du Yangtze et du Nil ont été des plaques tournantes pour le développement de la société humaine. Cependant, les deltas sont également confrontés à un éventail étonnant de pressions en raison de leur intersection à la frontière des systèmes terrestres et aquatiques, marins et d'eau douce.

Le delta du Mékong, le plus grand fleuve d'Asie du Sud-Est, est représentatif de cette situation. Il s'étend sur le sud du Cambodge et du Vietnam, à partir de la capitale cambodgienne Phnom Penh. Connu comme le grenier à riz de la région pour son immense productivité agricole, il fait également partie du système de pêche intérieure le plus productif au monde. Les processus hydrologiques sont au cœur de cette productivité. Chaque année, pendant la mousson, de vastes étendues de la plaine inondable du delta sont inondées. Pendant cette période, qui dure traditionnellement de juillet à novembre, les eaux souterraines sont rechargées, les populations de poissons se régénèrent dans les eaux peu profondes des plaines d'inondation, et des sédiments riches en nutriments sont déposés.

Cependant, une multitude de changements ont un impact négatif sur cette dynamique traditionnelle. Le développement de l'hydroélectricité en amont et les changements dans l'occupation des sols, la

température et les précipitations modifient le débit des rivières. Le changement climatique dans le delta lui-même a un impact sur les modes d'utilisation des terres et les processus hydrologiques. Les activités humaines telles que l'exploitation du lit du fleuve et la construction d'infrastructures de contrôle hydraulique compliquent encore la situation. Sans parler du problème de l'affaissement des sols dû au compactage des sédiments et à l'extraction des eaux souterraines, et l'élévation du niveau de la mer.

Cette thèse vise à examiner comment tous ces changements à grande échelle ont un impact sur les processus hydrologiques dans la partie cambodgienne du delta du Mékong, et comment ces processus, à leur tour, sont liés aux services écosystémiques dont bénéficie la population locale. Le Mékong cambodgien a été choisi parce que, contrairement à son homologue vietnamien, il ne dispose toujours pas d'infrastructures de contrôle hydraulique étendues telles que des digues et des vannes. Au lieu de cela, les plaines d'inondation sont intimement liées au cours principal du fleuve par des *Preks*. Il s'agit de canaux trapézoïdaux qui divergent perpendiculairement du Mékong et de son distributaire deltaïque, le Bassac. Ils ouvrent une brèche dans les berges élevées du fleuve et servent de vecteur d'inondation et de drainage, de transport de sédiments et de migration des poissons. Ils sont intégralement liés à la fourniture d'une variété de services écosystémiques. Cependant, de nombreux Preks se sont détériorés au fil des ans en raison de la sédimentation, de l'érosion et d'un manque d'entretien. Par conséquent, des projets de développement internationaux et des initiatives locales ont cherché à restaurer leurs fonctionnalités.

Les objectifs de cette thèse sont d'analyser les changements hydrologiques à long terme dans le delta du Mékong cambodgien, et de les relier à ceux documentés à l'échelle du bassin. En outre, elle vise à examiner comment ces changements se traduisent au niveau local, et, par conséquent, sur les services écosystémiques dont bénéficient les communautés du delta. En particulier, elle a cherché à élucider le rôle des Preks dans la catalyse de ces processus. Enfin, un objectif de cette thèse était également de comprendre à quoi pourraient ressembler les développements futurs dans la région, et comment les infrastructures locales telles que les Preks pourraient aider à atténuer les impacts négatifs.

Pour répondre à toutes ces questions, une approche multi-méthodes a été choisie. Tout d'abord, un examen approfondi de la littérature disponible a été réalisé afin d'acquérir une compréhension globale des facteurs de changement dans le bassin du Mékong dans son ensemble et dans son delta en particulier, et de définir le contexte conceptuel de ce travail. Ensuite, une analyse des processus hydrologiques à l'échelle du delta du Mékong cambodgien a été réalisée. Elle comprenait un examen des séries chronologiques de données sur les niveaux d'eau, des données sur les précipitations, ainsi que des modèles et des étendues d'inondation. Ensuite, l'accent a été mis sur une zone d'étude dans la partie sud du delta cambodgien. Là, un travail de terrain approfondi a été mené pour mieux comprendre le rôle des Preks pour les communautés

locales, les pratiques agricoles et les services écosystémiques. Ces travaux ont été complétés par des recherches aux Archives Nationales de Phnom Penh sur l'histoire des Preks, ainsi que par une classification de la couverture terrestre basée sur la télédétection. Enfin, un modèle numérique a été construit en Python pour formaliser ce qui avait été appris sur la relation des Preks avec les processus hydrologiques et les services écosystémiques, et pour simuler les impacts de scénarios futurs. Ci-dessous, chaque section est résumée et discutée brièvement et une conclusion générale et des perspectives sont présentées.

Revue de la littérature : Contexte conceptuel et défis pour le bassin du Mékong et son delta

Cette thèse s'appuie sur un ensemble interdisciplinaire d'approches et de concepts bien établis. Elle utilise le cadre des services écosystémiques pour aborder l'analyse des différentes façons dont la population locale du delta du Mékong cambodgien bénéficie des systèmes naturels et des agro-écosystèmes. Elle exploite également des concepts et des méthodes issus des domaines de l'écohydrologie et de la socio-hydrologie. L'écohydrologie s'efforce de comprendre comment les processus hydrologiques interagissent et s'intègrent aux processus écologiques. La socio-hydrologie, en revanche, vise à comprendre les interactions entre la société et l'eau - la dynamique et les boucles de rétroaction des systèmes couplés homme-eau. Les Preks sont une caractéristique anthropogénique définissant le paysage qui a une influence fondamentale sur les processus hydrologiques de la région, mais qui dépend également des activités humaines telles que la réhabilitation et l'entretien. Le système Prek peut donc être conceptualisé comme l'un de ces systèmes couplés homme-eau.

En ce qui concerne les défis auxquels sont confrontés le Mékong et son delta, l'examen de la littérature a permis d'identifier une multitude de pressions. Tout d'abord, le développement de l'hydroélectricité modifie fondamentalement le régime d'écoulement du fleuve. Globalement, le bassin du Mékong a un potentiel cumulé de production d'hydroélectricité de 268 000 GWh/an. Actuellement, environ la moitié est exploitée. La construction de barrages a commencé dans les années 1960, mais ce n'est que dans les années 2000 que le nombre de barrages et leur capacité ont augmenté de manière exponentielle. En 2008, la capacité de stockage active totale de tous les réservoirs ne représentait que 2% de son débit annuel. En 2025, cette capacité aura été multipliée par dix. Globalement, l'exploitation des barrages entraîne une diminution du débit en saison humide et une augmentation du débit en saison sèche. Un autre facteur de changement est le changement d'occupaation des sols dans le bassin, en particulier la déforestation. Cela a un impact sur le ruissellement et augumente l'apport de sédiments dans le fleuve par l'érosion. Par contre, les charges sédimentaires dans le fleuve sont réduites par le piégeage des sédiments dans les réservoirs. En outre, le changement climatique modifie les régimes de précipitations et de températures

dans le bassin, les températures devant augmenter en moyenne de 0.4 à 3.3 degrés.

Le delta du Mékong est confronté à une série de défis complexes. L'affaissement des sols dû au tassement naturel des sédiments et à la surextraction des eaux souterraines a atteint une ampleur moyenne de 18 cm au cours des 25 dernières années. Dans le même temps, le niveau de la mer s'élève. L'altitude moyenne du delta n'étant que de 0.8 m, une élévation du niveau de la mer de 1 m pourrait entraîner le déplacement de 70 % de sa population. L'apport de sédiments en provenance de l'amont étant limité, ce processus ne peut pas non plus servir de contre-mesure. Actuellement, le delta est déjà confronté à l'intrusion d'eau salée plus loin dans les terres qu'au cours des décennies précédentes.

Analyse hydrologique

Pour l'analyse des tendances des niveaux d'eau, on a utilisé les séries chronologiques enregistrées par la Commission du Mékong (MRC) dans quatre stations. Ces stations étaient Koh Khel et Chau Doc sur le Bassac et Neak Luong et Tan Chau sur le Mékong. Koh Khel et Neak Luong sont situés en amont au Cambodge, et Tan Chau et Chau Doc juste de l'autre côté de la frontière au Vietnam. À Neak Luong, les mesures quotidiennes du niveau d'eau remontent à 1926. À Tan Chau et Chau Doc, les données sont disponibles depuis 1981, et à Koh Khel depuis 1991. Toutes ces séries ont été soumises à une analyse des tendances et des points de rupture. En outre, des données en temps quasi réel - enregistrées à des intervalles de 15 minutes - à Phnom Penh, Koh Khel, à un enregistreur situé à env. 30 km au sud de Koh Khel, et à Chau Doc ont été utilisées pour examiner la dynamique infra-quotidienne des niveaux d'eau par le biais d'une analyse statistique et d'un modèle numérique dans HEC-RAS.

L'analyse des tendances à long terme des niveaux d'eau a indiqué que l'année 2008 peut être considérée comme un point de rupture hydrologique local, conformément aux études menées à l'échelle du bassin. En outre, elles ont montré que la montée des crues se produisait nettement plus tard et la décrue nettement plus tôt après cette date qu'avant, réduisant ainsi la durée globale des crues. La comparaison de la dynamique des stations en amont et en aval a indiqué un modèle caractéristique à trois pics pendant l'arrivée de la crue, avec deux pics mineurs avant le pic principal de la saison des crues. Cela indique la présence de seuils pour les connexions de plaine d'inondation, ou de processus en amont tels que l'écoulement inverse dans le lac de Tonle Sap. La présence de tels seuils est également indiquée par la dynamique des niveaux d'eau à Phnom Penh et à Koh Khel pendant la montée des crues. Les deux stations augmentent de façon presque synchrone, jusqu'à un niveau d'environ 6 m, lorsque Koh Khel atteint un pic secondaire et décline avant de remonter. De plus, une influence claire de la marée peut être observée à toutes les stations, mais surtout à Chau Doc et à Koh Khel.

Pour l'analyse des données de précipitations, des séries temporelles provenant de trois stations in-situ ont été utilisées. Il s'agit d'une station MRC à Koh Khel, d'une station maintenue par le Programme des Nations Unies pour le Développement (UNDP) à Koh Thom, et d'une station installée au cours du projet dont cette thèse fait partie à environ 5 km au sud de Koh Thom. De plus, les données de précipitations télédétectées par CHIRPS ont été analysées à titre de comparaison.

Les résultats ont montré une distribution bimodale des précipitations, avec des pics en avril et en octobre. Ils ont montré que les données CHIRPS ont tendance à surestimer le nombre d'événements de précipitations de faible intensité et à sous-estimer le nombre d'événements de forte intensité. Cependant, la comparaison a également révélé une hétérogénéité considérable entre les stations locales, avec des valeurs d'erreur quadratique moyenne (RMSE) comprises entre 51.42 et 83.16. L'analyse à long terme des données du CHIRPS n'a montré aucun point de rupture significatif et une augmentation significative des sommes de précipitations mensuelles en décembre.

L'analyse des distributions d'inondation s'est avérée peu aisée en raison de la rareté des données historiques, notamment des images satellites historiques qui pourraient être utilisées pour établir des cartes d'inondation à intervalles réguliers. Pour résoudre ce problème, une nouvelle méthode a été développée pour reconstruire les cartes d'inondation. Elle prend la forme d'une liaison niveau d'eau - inondation (WAFL), qui utilise le modèle de corrélation de Lamagat pour relier les niveaux d'eau mesurés localement aux étendues d'inondation dérivées des images de télédétection Sentinel-1 et -2, prises entre 2017 et 2020, et fournies par l'Agence Spatiale Européenne (ESA). La robustesse du WAFL a été testée à l'aide du modèle d'élévation haute résolution de 12 m de TanDEM-X, ainsi que des cartes d'inondation dérivées des quelques scènes de saison humide disponibles à partir d'images historiques (Landsat-5 et -8). Il a ensuite été utilisé pour reconstruire les cartes d'inondation quotidiennes en remontant jusqu'au début de la série chronologique des niveaux d'eau en 1991, et pour calculer les changements dans l'incidence, l'étendue et le moment des inondations depuis lors.

Les résultats ont montré que les étendues d'inondation simulées par le WAFL peuvent atteindre une bonne concordance avec les cartes d'inondation directement dérivées de Landsat-5 et -8, ainsi que de Sentinel. En tenant compte de l'effet d'obscurcissement de la couverture végétale, les valeurs de concordance atteignent une moyenne de 87%, avec des valeurs maximales allant jusqu'à 93% La comparaison des modèles et de la dynamique des inondations pour les périodes précédant et suivant le point de rupture hydrologique local en 2008 révèle que la durée des inondations a diminué de 19 jours en moyenne. En outre, les résultats indiquent que l'incidence des inondations basée sur les pixels a considérablement diminué au début de la saison traditionnelle des inondations, en juillet et dans la

première moitié du mois d'août.

Comprendre la zone d'étude - Travail de terrain, recherche archivistique et classification des LULC

Après avoir acquis une compréhension de base de la dynamique à l'échelle du delta du Mékong cambodgien, il était nécessaire de se concentrer davantage sur le niveau local. À cette fin, une zone d'étude de 43 km^2, englobant 10 Preks, et située à environ 70 km au sud de Phnom Penh a été choisie. Des entretiens approfondis y ont été menés avec les habitants de la zone, notamment les agriculteurs et les chefs de village, afin de mieux comprendre les pratiques agricoles et le rôle des Preks dans la fourniture de services écosystémiques aux communautés locales. Au total, quatre voyages sur le terrain ont été effectués - en décembre 2018, juin 2019, novembre 2019 et février-mai 2020, dont le dernier a été écourté en raison de la pandémie de COVID-19. Pour compenser, d'autres enquêtes de terrain ont été menées par un collègue de l'Université royale d'agriculture (RUA) de Phnom Penh en novembre 2020 et au printemps 2021. Un vaste questionnaire de terrain de 12 pages relatif aux pratiques agricoles et aux services écosystémiques a été élaboré et affiné.

Au total, 96 personnes ont été interviewéees, dont 67 en utilisant la forme finale du questionnaire destiné aux agriculteurs. Les résultats ont permis de quantifier les pratiques agricoles moyennes en termes d'irrigation, de culture et de rendement pour différents types de cultures dans la zone d'étude: le riz (récession, saison sèche, début de saison humide, saison humide), le maïs, les arbres fruitiers comme la mangue et le lemut, les haricots (blancs, verts, longs), les légumes comme les aubergines, les concombres et les tomates, ainsi que les cultures typiquement locales comme le melon amer et la cire. Ils ont également révélé que le principal avantage que les personnes interrogées tirent des Preks est la fourniture d'eau pendant la saison sèche, en particulier à des fins d'irrigation mais aussi pour abreuver le bétail et satisfaire les besoins domestiques non alimentaires des ménages. En outre, les habitants utilisent la végétation naturelle qui pousse le long des Preks pour se nourrir, se chauffer et se soigner. Certaines personnes pêchent également dans les Preks, bien qu'elles aient toutes noté que les rendements en poissons ont considérablement diminué au cours des dernières années, beaucoup d'entre elles accusant les changements hydrologiques et les pratiques de pêche illégales. La réhabilitation des Preks est généralement perçue de manière positive car elle augmente la disponibilité de l'eau en saison sèche. Comme les Preks servent de canaux d'inondation et de drainage, les services écosystémiques que la population locale tire de l'inondation ont également été inclus dans les questionnaires. Les agriculteurs ont cité le dépôt de sédiments riches en nutriments, la régulation des populations de rats et la recharge en

eau du sol pour la culture du riz de décrue comme les principaux effets positifs des inondations annuelles dues à la mousson.

Afin de mieux comprendre l'histoire des Preks et leur développement au fil du temps, des recherches supplémentaires ont été entreprises aux Archives Nationales de Phnom Penh. Des rapports d'ingénierie datant de la période coloniale française y ont été examinés afin de comprendre l'histoire des Preks et leur évolution. Le document le plus ancien qui a pu être trouvé date de 1908 - un rapport rédigé par un ingénieur colonial, le lieutenant Barthélemy, détaillant la possibilité de construire des Preks afin d'élever des terres pour la culture de plantes à haute valeur ajoutée. Il a ensuite été réédité en 1910 et 1913. À l'époque, la construction des Preks consistait simplement à créer une brèche dans les berges surélevées du fleuve pour permettre l'entrée d'eau dans les plaines inondables, puis à laisser le système à la dynamique naturelle de sédimentation. Sa première priorité n'était pas l'approvisionnement en eau d'irrigation, mais la création de terres arables non affectées par les inondations. Barthélemy rapporte une histoire orale qui raconte comment les Preks ont été construits au début du 19ème siècle après qu'un pêcheur ait découvert l'efficacité des processus de sédimentation en ouvrant des brèches dans les berges du fleuve pour transporter son nouveau bateau. Pendant la période coloniale française, au début du 20ème siècle, les Preks ont été construits systématiquement sur les rives du Mékong et du Bassac. Après la Seconde Guerre Mondiale, les archives deviennent rares. Pendant la période des Khmers Rouges, un réseau de canaux et de digues a été construit dans les plaines inondables de la zone d'étude dans le cadre de programmes de travaux forcés. En raison de la réinstallation à grande échelle de la population cambodgienne durant cette période, les liens locaux avec la terre ont été rompus et, après la chute des Khmers Rouges, de nombreux agriculteurs ne connaissaient pas les terres qu'ils cultivaient désormais, ni leurs caractéristiques hydrologiques. Dans les années 1990, les projets de réhabilitation des Preks ont commencé. De nombreux Preks s'étaient dégradés en raison d'un manque d'entretien et de processus tels que le dépôt de sédiments dans les canaux et l'érosion des berges. Ces projets visaient à restaurer la fonctionnalité des Preks en approfondissant leur lit et en augmentant leur surface de profil. Ces projets ont été mis en œuvre par l'Agence française de développement (AFD), le ministère australien des Affaires étrangères et du Commerce (AusAID/DFAT), ainsi que l'Agence japonaise de coopération internationale (JICA). Plus récemment, les projets WASP (Water and Agriculture Sector Programme) et WAT4CAM (Water-Resource Management and Agro-Ecological Transition in Cambodia) de l'AFD ont inclus des composantes de réhabilitation des Preks.

Pour compléter l'image de l'impact de Preks sur l'utilisation des terres et les pratiques agricoles locales, une analyse par télédétection de l'occupation des sols dans la zone de l'étude a été réalisée. À l'aide de la plateforme de cloud computing Google Earth Engine (GEE), une classification supervisée a été réalisée à

partir des images Sentinel-1 et -2. Comme données d'entrée, deux ensembles de données différents ont été comparés : des données in situ collectées pendant le travail sur le terrain et des points définis manuellement sur la base de l'imagerie SPOT à haute résolution. En outre, différents ensembles de bandes, de textures et d'images spectrales calculés sur la base des données Sentinel ont été comparés en tant qu'entrées pour la classification. Enfin, toutes les méthodes de classification supervisée disponibles sur GEE ont été comparées : Naive Bayes, arbres de classification et de régression, machines à vecteurs de support, Random Forest et Gradient Tree Boosting. Les résultats ont montré que les données d'entraînement basées sur SPOT, associées à un ensemble de bandes contenant un sous-ensemble sélectionné de bandes et d'indices disponibles, et utilisant l'algorithme Gradient Tree Boosting, présentaient les meilleures performances de classification, jusqu'à 94%. Cette combinaison a ensuite été utilisée pour classifier l'occupation du sol dans la zone d'étude de cas pour chaque mois entre avril 2020 et mars 2021.

Modélisation numérique en Python : Représentation des précipitations, des processus hydrologiques et des services écosystémiques

Enfin, pour formaliser la compréhension du rôle des Preks, et la relation entre les processus hydrologiques et les services écosystémiques dans la zone d'étude de cas, et pour simuler des scénarios futurs, un modèle numérique a été construit en Python. Il représente la zone d'étude comme un réseau de 30 segments de biefs (Preks et canaux plus petits dans les plaines d'inondation) et 129 unités de surface (zones de dynamique de couverture terrestre, d'élévation et de dynamique d'inondation similaires).

Les services écosystémiques sont calculés en deux catégories distinctes : les services écosystémiques liés aux inondations et les services écosystémiques non liés aux inondations. La première catégorie englobe des processus tels que la recharge des eaux souterraines, la régulation des populations des rats, le dépôt de sédiments et la fourniture d'habitats pour la reproduction des poissons. Ils sont calculés sur la base de la WAFL à un pas de temps quotidien. En revanche, les services écosystémiques non liés aux inondations consistent principalement en la fourniture d'eau d'irrigation pendant la saison sèche, permettant ainsi la production agricole. Pour calculer ce type de service écosystémique, la couverture du sol et donc les besoins en irrigation pour chaque unité de surface sont calculés sur la base de la classification de la couverture du sol par télédétection et des données des entretiens. Ensuite, un calcul du bilan hydrique quotidien est effectué pour chaque unité afin de déterminer si les besoins en eau des cultures peuvent être satisfaits ou si le rendement est réduit en raison du stress hydrique. Le débit à travers les segments du bief est calculé sur la base d'une équation de déversoir, résolue avec un schéma Runge-Kutta de quatrième ordre.

Le modèle a été calibré et validé en utilisant les données des enregistreurs de niveau d'eau installés dans la zone de l'étude de cas. Des tests de sensibilité ont été effectués pour le choix des produits de précipitation, les paramètres du sol et la configuration des canaux de Prek. Enfin, quatre scénarios ont été simulés pour le développement futur, avec des températures, des précipitations et des niveaux d'eau des rivières modifiés pour tenir compte de deux scénarios de changement climatique - RCP 4.5 et 8.5 - et du développement complet de l'hydroélectricité en amont. Le calcul des futurs niveaux d'eau des rivières repose sur une étude de Hoan et al. 2019, qui fournit des projections des changements de débit à la station hydrologique MRC d'ici 2050, en utilisant une base de référence de valeurs moyennes de 1971 à 2000. Le débit futur projeté a été converti en niveaux d'eau à l'aide d'une courbe d'évaluation rétrocalculée à la station à Kratie, puis transféré aux stations en aval à Koh Khel et dans la zone d'étude à l'aide d'une approche de corrélation. Chaque scénario de changement climatique a été simulé deux fois - une fois avec la configuration actuelle des Prek et une fois en supposant que tous les Prek ont été réhabilités.

Les résultats montrent que le simulateur de débit utilisant l'équation du déversoir peut réaliser une prédiction assez précise des niveaux d'eau de Prek avec un RMSE de 0.11. Les tests de sensibilité ont montré que la connaissance limitée des paramètres du sol dans la zone de l'étude de cas était une source considérable d'incertitude, avec des variations de plusieurs magnitudes dans la recharge des eaux souterraines - de 530 l/m^2 par saison à 33285 l/m^2 par saison - selon les valeurs de la littérature sélectionnées. En outre, elle a également montré que l'utilisation de différents produits de précipitation peut entraîner des augmentations des rendements calculés allant jusqu'à 28.47%, en particulier dans les zones situées le long des Preks qui connaissent une pénurie d'eau pendant la saison sèche. De même, la diminution du niveau présumé du lit de Preks a entraîné une augmentation des rendements allant jusqu'à 8.32%. En revanche, son élévation de 0.5 à 1 m a eu des effets relativement mineurs, entraînant des pertes de rendement allant jusqu'à 0.4%.

La simulation de scénarios montre qu'avec la configuration actuelle de Preks, on peut s'attendre à une diminution des services écosystémiques de saison sèche allant jusqu'à 16.27%. En revanche, si la réhabilitation de la couverture était mise en œuvre, on pourrait s'attendre à une augmentation considérable de ces services - jusqu'à 42.53% - en raison de la disponibilité accrue de l'eau d'irrigation. Les services écosystémiques liés aux inondations devraient augmenter pour les niveaux d'eau futurs calculés sur la base des changements de débit prévus à Kratie. Le niveau d'eau maximum passerait de 5.89 à 6.35 m, et il se produirait plus tard - début novembre. (Cela s'explique en partie par le scénario de base choisi, qui s'appuie sur des données plus anciennes pour les projections.) En outre, l'étendue moyenne et maximale des inondations augmenterait jusqu'à 17,98%. De même, le volume maximal retenu augmenterait considérablement, jusqu'à 40,80%. En revanche, la quantité de recharge des eaux

souterraines n'augmenterait que légèrement (jusqu'à 8,01%) et les niveaux d'eau ne seraient toujours pas assez élevés pour entraîner une régulation des populations des rats.

Cependant, plusieurs limitations s'appliquent au modèle dans sa forme actuelle. Tout d'abord, les processus de subsurface n'ont pas été pris en compte car très peu d'informations sont disponibles sur les propriétés du sol ou sur les dimensions des aquifères et des aquitards. De plus, le ruissellement de surface dans les champs a également été négligé jusqu'à présent. La raison en est que la faible déclivité du terrain et les structures à petite échelle telles que les digues basses entourant les champs individuels rendent ce processus très complexe, et que très peu d'informations précises sont connues sur la configuration spatiale exacte de ces éléments. En outre, on a supposé que le stockage de l'eau en surface dans l'ensemble d'une unité de surface est négligeable pendant la saison sèche, lorsque la pénurie d'eau règne généralement. Une autre simplification et donc source d'incertitude est l'utilisation du WAFL pour estimer l'étendue des inondations à chaque pas de temps. Le WAFL a été construit à l'aide d'images satellites des années 2017-2020. Il repose sur l'hypothèse que la nature des connexions hydrauliques entre les plaines d'inondation et le cours principal du fleuve reste plus ou moins statique. Plus le nombre de Preks à réhabiliter est important, plus il est probable que la connexion hydraulique rivière-plaine d'inondation change à un point tel que le WAFL n'est plus applicable. Une dernière limite tient au fait que seules deux études ont été utilisées pour estimer les débits, les précipitations et les températures futurs des cours d'eau, et que l'applicabilité de ces études est encore plus limitée. Par exemple, les projections des futurs débits d'eau à Kratie sont basées sur une courbe de crue moyenne des années de référence 1971-2000.

Afin d'améliorer le modèle, davantage d'informations devraient être collectées sur les propriétés du sol et du sous-sol dans les zones d'étude, ainsi que sur la configuration moyenne des digues à petite échelle pour permettre des généralisations, et sur les niveaux du lit de Prek. En outre, l'utilisation de modèles plus sophistiqués peut être envisagée pour le calcul des services inondés. En outre, il serait souhaitable d'affiner les projections des niveaux d'eau futurs. Actuellement, la base de référence s'appuie sur les données d'une station en amont sur laquelle s'appuient les scénarios futurs. Cependant, les données observées au cours des dernières années dépassent déjà ces projections. En plus, les rétroactions, comme des choix de cultures différents et des variations dans la plantation, pourraient être pris en considération - notamment dans une perspective de socio-hydrologie. Enfin, il serait bénéfique d'investir plus de temps dans la définition de scénarios plus nuancés, notamment en vue des projections futures des niveaux d'eau.

Conclusion générale et perspectives

Cette thèse illustre que les tendances hydrologiques à l'échelle du bassin, bien connues des études

à grande échelle, se reflètent étroitement dans le delta du Mékong cambodgien. Les inondations ont maintenant tendance à arriver plus tard et à se retirer plus tôt qu'avant le point de rupture hydrologique de 2008, avec des pics de crue plus courts et plus marqués. En moyenne, l'incidence des inondations au début de la saison traditionnelle des inondations a diminué en juillet et aout, et la durée totale des inondations a diminué de 19 jours. Cette situation a des répercussions négatives sur de multiples services écosystémiques, de la fourniture d'habitats pour la reproduction des poissons à la recharge des eaux souterraines et des sols. Les entretiens avec les habitants ont montré que les effets de ces développements sont déjà fortement ressentis par les communautés locales.

Les entretiens ont également illustré l'importance accordée aux infrastructures locales sous la forme de Preks - et à leur réhabilitation. Aux yeux des agriculteurs interrogés, leur principal avantage est la fourniture d'eau d'irrigation pendant la saison sèche. L'abaissement du niveau de leur lit par excavation permet de fournir cette eau pendant de plus longues périodes et avec une plus grande fiabilité. D'une manière générale, cette étude a mis en évidence que les Preks jouent un double rôle en termes de fourniture de services écosystémiques. Ils servent de vecteur aux inondations et au drainage et contribuent ainsi aux services écosystémiques liés aux inondations tels que le dépôt de sédiments. Et ils ont un rôle majeur d'approvisionnement en eau pendant la saison sèche, ainsi qu'en végétation naturelle tout au long de l'année. Depuis leurs origines au début du 19ème siècle, en passant par leur prolifération sous le régime colonial au début du 20ème siècle, et les décennies turbulentes qui ont suivi, les Preks n'ont cessé de définir le paysage du delta du Mékong cambodgien et les communautés qui y vivent.

Leur capacité future à le faire dépend de leur entretien et de leur réhabilitation. Bien que le modèle utilisé pour simuler les scénarios futurs n'en soit qu'à ses débuts, et qu'il reste encore beaucoup à améliorer sur plusieurs points, il montre qu'avec la configuration actuelle des Preks, il faut s'attendre à une diminution significative des services écosystémiques non liés aux inondations. En revanche, si une réhabilitation de la couverture était mise en œuvre, ces services augmenteraient. La simulation des services écosystémiques liés aux inondations montre que la majorité d'entre eux sont appelés à augmenter dans le scénario projeté. Cependant, cette observation même souligne l'importance de projections précises des niveaux d'eau futurs, car celles qui sont actuellement utilisées reposent sur une période de référence entre 1971 et 2000 et ne reflètent pas les modèles de ruissellement typiques observés dans les séries chronologiques récentes dans la zone d'étude.

Declaration

This dissertation is the result of my own work and includes nothing which is the outcome of work done in collaboration except as declared in the Preface and specified in the text. I further declare that this thesis has not been submitted, in whole or in part, in any previous application for a degree.

Parts of this work (incorporated in Chapters 3 and 5) have been published in:

Orieschnig, C., Venot, J.P., Massuel, S., Eang, K.E., Chhuon, K., Lun, S., Siev, S. and Belaud, G., 2022. A Multi-Method Approach to Flood Mapping: Reconstructing Inundation Changes in the Cambodian Upper Mekong Delta. Journal of Hydrology, p.127902.

Orieschnig, C.A., Venot, J.P, Massuel, S., Eang, K.E., Kong, C., Lun, S., and Belaud, G., Datasets for the assessment of changes in the incidence, extents, and spatial patterns of inundations in in the Cambodian Mekong Delta, based on a water level - flood link calculated from in-situ water levels, and Sentinel-derived inundation maps, *Data In Brief*. In Press.

Orieschnig, C. A., Belaud, G., Venot, J. P., Massuel, S., and Ogilvie, A. (2021). Input imagery, classifiers, and cloud computing: Insights from multi-temporal LULC mapping in the Cambodian Mekong Delta. *European Journal of Remote Sensing*, 54(1), 398-416.

Part of the work outlined here was also presented at conferences:

Orieschnig, C., Belaud, G., Venot, J.P. and Massuel, S., 2022, June. Retro- and forecasting inundation extents for trend analysis in the Cambodian Mekong Delta - a new method combining

Sentinel-1 and 2 and local water level measurements. IAHS Scientific Assembly, Montpellier.

Orieschnig, C., Belaud, G., Venot, J.P. and Massuel, S., 2022. Assessing long-term changes in annual monsoon inundations in the Mekong Delta (Cambodia): Testing an innovative approach linking remote sensing and in-situ measurements to overcome data scarcity (No. EGU22-9619). Copernicus Meetings.

Orieschnig, C.A., Belaud, G., Venot, J.P. and Massuel, S., 2021, April. Cultivated floodplains of the Cambodian Mekong delta: understanding the changing balance between the flow regime and the agricultural practices. In EGU General Assembly Conference Abstracts (pp. EGU21-1248).

Orieschnig, C.A., Belaud, G., Massuel, S. and Venot, J.P., 2020, May. Irrigation canal systems of the Cambodian Mekong delta: Assessing changes in ecosystem services for rural communities after wide-ranging rehabilitation plans. In EGU General Assembly Conference Abstracts (p. 2732).

Orieschnig, C.A., Belaud, G., Ogilvie, A., and Venot, J.P., 2019, July. Combining Optical and SAR Remote Sensing Approaches for Optimal Flood Mapping in the Mekong Delta (Cambodia) using Google Earth Engine. IUGG General Assembly, Montreal.

Christina Anna Orieschnig

September 6, 2022

Acknowledgements

This thesis would not have become possible without the passion, proficiency, and endurance of my supervisors, colleagues, and friends.

First and foremost, I want to thank my supervisors. Professor Gilles Belaud was always there to help me surmount both academic challenges and the intricacies of the bureaucratic system. His advice, patience, and wisdom has been invaluable in the course of my PhD. I could not have been luckier in finding a Doktorvater. Jean-Philippe Venot has kept me on my toes and helped me sharpen my academic thinking and eye for detail, and opened my mind to multiple dimensions of water-related research that I had never considered before. And Sylvain Massuel's advice and guidance has been invaluable both during the modelling process, and in the field. Without his dedication and management of the installation of measurement stations, there would have been no data on the basis of which to build the model.

I also want to thank everyone who made the fieldwork in Cambodia possible. It was one of the most enriching experiences of my (academic) life. In particular, I want to thank our esteemed colleagues at the Royal University of Cambodia, and the Institute of Technology of Cambodia. Special thanks go out to Raksmey Phoeuk, Somaly Oum, and Sreypich Sinh, whose local expertise and translation skills made it possible to rattle along Preks on motorbikes, have engaging conversations with farmers, and get insights from village chiefs. A huge thank you also goes to Paul Vandôme, my two-term stagiaire and dear friend and colleague, who navigated our Cambodian adventure with far greater proficiency than me.

Finally, I want to thank my family - especially my mother and my husband Florian. Without their unwavering moral support, words of encouragement, and willingness to listen to my latest tirade, I would have thrown in the towel long ago. Thank you also to my fantastic friends and office mates, especially Chloe, who have made both our little hub at SupAgro and our weekend adventures unforgettable.

Contents

1 Introduction **57**

1.1 Research Questions 60

1.2 Overall Research Methodology 61

1.3 Conceptual Context: Integrative Approaches, Ecohydrology, and Ecosystem Services 63

1.3.1 Ecohydrology 64

1.3.2 Sociohydrology 65

1.3.3 Quantifying Nature's Benefits - The Transformational Concept of Ecosystem Services 67

1.3.4 The Necessity for Interdisciplinary Work and Transdisciplinary Approaches in a Development Context 71

2 The Research Site: Introducing the Mekong, its (Cambodian) Delta, and the Preks 73

2.1 Southeast Asia's Centering Line - The Mekong 74

2.1.1 The Mekong's Traditional Hydrological Dynamics 77

2.1.2 Ecological Importance 78

2.1.3 Socio-Economic and Political Significance 80

2.1.4 Pressures on the River: Between Climate Change and Economic Development 83

2.1.4.1 Hydropower Development 83

2.1.4.2 Land Use Change 87

2.1.4.3 Climate Change 88

2.1.5 The Mekong River Commission - Between Governance and Mediating Conflicting National Interests 90

2.2 The Mekong Delta: A Hub of Human Activity, Hydrological Dynamics, and Biodiversity 92

2.2.1 Geographical Location 92

2.2.2 Geology and Pedological Characteristics 93

2.2.3 Overall Hydro(geo)logical Dynamics 95

2.2.3.1 Annual Monsoon Inundations 95

2.2.3.2 Sediment Dynamics 96

2.2.3.3 Groundwater Dynamics 97

2.2.4 Socio-Economic Factors 99

2.2.5 Biodiversity and Conservation 100

2.2.6 Hydraulic Infrastructure: The Canals of the Vietnamese and Preks of the Cambodian Mekong Delta 102

2.2.7 Challenges in the Delta: From Subsidence to Salinity Intrusion 104

2.2.8 From the Regional to the Local: Understanding Delta-Wide Changes in the Prek System in Cambodia 105

3 Understanding Large-Scale Hydrological Processes in the Region: Past Changes and Current Reality 107

3.1 Delineating the Areas of Interest 109

3.2 Local Hydrological Dynamics and Changes in River Flow 110

3.2.1 Data Availability: Mekong River Commission Time Series and In-Situ Loggers 111

3.2.2 Methods 115

3.2.2.1 Assessing the Dynamics of Tidal Influence and Relationships Between Upstream and Downstream Stations 115

3.2.2.2 Change Point and Trend Analysis 116

3.2.3 Results and Discussion 116

3.3 Comparing Precipitation Datasets and Identifying Trends 127

3.3.1 Data Availability: Local Rainfall Measurements vs. Remotely Sensed Series 128

3.3.2 Methods 131

3.3.3 Results and Discussion 132

3.4 Identifying Inundation Dynamics and Trends Through Satellite Imagery 137

3.4.1 Materials and Methods 138

3.4.1.1 Sentinel-1 and 2 139

3.4.1.2 Landsat 141

3.4.1.3 Google Earth Engine 142

3.4.1.4 Detecting Flood Extents Using Sentinel-1 and 2 143

3.4.1.5 Establishing a Water Level - Flood Link (WAFL) 144

3.4.1.6 Comparing the Flood Link With Inundation Extents Derived from Landsat and TanDEM-X 146

3.4.1.7 Land Use Classification: Detecting Natural Vegetation 149

3.4.1.8 Flood Dynamics Analysis: Calculating Inundation Durations and Incidences 149

3.4.2 Results 150

3.4.2.1 Detection of Inundation Extents 150

3.4.2.2 The Water level flood link (WAFL) 152

3.4.2.3 Comparison of Calculated Inundation Extents with Flood Maps Derived from Sentinel and Landsat and Influence of Natural Vegetation 152

3.4.2.4 Comparison of Calculated Inundation Extents with Flood Maps Derived from TanDEM-X 158

3.4.2.5 Changes in Inundation Incidence, Durations, and Patterns Pre- and Post-2008 161

3.4.3 Discussion 164

3.4.3.1 Local Hydrological Trends and their Reflection of Basin-Wide Changes 164

3.4.3.2 Inundation Mapping Using Sentinel: Between Biases and the Value of Observing Local Dynamics 164

3.4.3.3 Validity of the WAFL: Balancing Natural Vegetation, Sedimentation, and Terrain Correspondence 164

3.4.3.4 Decreasing Flood Incidence and Durations in the Cambodian Mekong Delta: Patterns and Impacts 167

3.5 Conclusion : Characterising the Hydrological Dynamics of the Cambodian Mekong Delta 169

4 Understanding Preks - their Origins, Management, and Significance for Local Agroecosystems 171

4.1 Case Study Area: Location and Characteristics 172

4.2 Exploring the History of Preks: From Historical to Modern Engineering Reports 175

4.2.1 From Indigenous Discoveries to Colonial Priority 176

4.2.2 Post-Colonial Period and the Khmer Rouge 183

4.2.3 Development after the Khmer Rouge and Rehabilitation Projects since the 1990s 186

4.3 Understanding the Significance of Preks for Agriculture and Communities . . . 192

4.3.1 Overview of Field Work and Interview Methodology 193

4.3.2 Geographic and Demographic Information on Respondents 196

4.3.3 Outlining Ecosystem Services and their Relation to Prek Channels . . . 198

4.3.3.1 Provisioning Ecosystem Services 198

4.3.3.2 Regulating Ecosystem Services 205

4.3.3.3 Cultural Ecosystem Services 208

4.3.4 Characterising Agricultural Practices 208

4.3.4.1 Characteristics of Survey Respondents' Holdings 209

4.3.4.2 Average Cropping Practices 211

4.3.4.3 Livestock 217

4.3.4.4 Crop Losses Due to Droughts, Floods, and Pests 218

4.3.5 Assessing Alternative Roles: Perspective of a Landless Scavenger . . . 220

4.3.6 The Role of Local Governance: Outlining the Roles of Village Chiefs and Prek User Committees 222

4.3.6.1 Information from Village Chiefs 222

4.3.7 Summarizing the Results of Fieldwork 229

4.4 Conclusion:Appreciating the Influence of Communities and Individual Actors on Hydrological Processes 230

5 Assessing Landcover Dynamics through Supervised Classification Remote Sensing Approaches 233

5.1 Data Used 236

5.2 Image Pre-Processing 237

5.3 Creation of Image Datasets 239

5.4 Classifiers and Parameter Tuning 240

5.4.1 Naïve Bayes (NB) 240

5.4.2 Classification and Regression Trees (CART) 241

5.4.3 Random Forest (RF) 241

5.4.4 Gradient Tree Boosting (GTB) 242

5.4.5 Support Vector Machines (SVM) 242

5.5 Validation and Statistical Analysis 243

5.6 Results 244

5.6.1 Optimal Tuning Parameters 244

5.6.2 Overall Accuracy 245

5.6.3 SAR- and Optical-Only vs. Combined Imagery 246

5.6.4 Choice of Training Data and Band Sets 248

5.6.5 Accuracy by Class 248

5.7 Discussion 250

5.7.1 Benefits of Combining Imagery 250

5.7.2 Configuring Input Parameters and Data for Optimal Results 251

5.7.3 Overall Classifier Performance 252

5.7.4 Final Classification Configuration and LULC Development Throughout the Year 253

5.8 Conclusion - Understanding Ecosystem Services and Landcover Dynamics on a Local Scale through Earth Observation 255

6 Linking Hydrology and Ecosystem Services to Understand Current Challenges and Assess Future Perspectives 257

6.1 Objectives: Representing the Links Between Hydrological Processes and Flood-Related and Not-Flood-Related Ecosystem Services 258

6.2 Conceptualisation of the Model Configuration and Description of Calculation of Processes Relevant to ES 262

6.2.1 Flooded Areas 264
6.2.2 Non-Flood Areas 266
6.2.2.1 Surface Units 266
6.2.2.2 Reach Segments 267
6.2.2.3 Connections Between Reach Segments 270
6.2.3 External Drivers 270
6.3 Modelling Methodology 271
6.3.1 Choice of Modelling Platform 271
6.3.2 Data Used 274
6.3.2.1 Land Cover Data 274
6.3.2.2 Soil Data 275
6.3.2.3 Water Levels: Hydraulic Boundary Conditions 276
6.3.2.4 Climate Data: Temperature and Precipitation 276
6.3.3 Delineating the Prek System into Modelling Units 277
6.3.4 Choice of Modelling Period, Time Step, and Baseline Scenario 279
6.3.5 Preliminary Calculations 280
6.3.5.1 Validating the WAFL in the case Study Area 280
6.3.5.2 Estimating the Maximum Infiltration From Recession Dynamics 282
6.3.6 Calculation Workflow 285
6.3.6.1 Overview of Calculation Workflow 285
6.3.6.2 Calculation of Inundation Extents using WAFL 288

6.3.6.3 Calculating Flood-Related Ecosystem Services 288

6.3.6.4 Calculating Not-Flood-Related Ecosystem Services 293

6.3.6.5 Summary of Model Outputs 300

6.3.7 Parametrization and Sensitivity 301

6.3.7.1 Parametrization and Validating Channel Flow Through In-Situ Water Levels 301

6.3.7.2 Sensitivity Testing 303

6.4 Formalizing Future Perspectives: Defining and Simulating Possible Scenarios . 308

6.5 Results and Discussion: Different Scenario Impacts on the Prek System and the Ecosystem Services it Provides 313

6.6 Limitations and Possibilities for Further Model Development 317

6.7 Conclusion: Deriving a Systematic Understanding and Possible Future Outlooks from Numerical Modelling 322

7 Conclusion, Discussion, Perspectives **325**

Bibliography **339**

A Overview of Mekong River Commission Observation Network **389**

B Description and Documentation of Each Prek in the Case Study Area **393**

B.1 Prek Cham Kroum 393

B.2 Prek Me Srok 397

B.3 Prek Lok 399

B.4 Prek Pok 400
B.5 Prek Hom 403
B.6 Prek Nou 405
B.7 Prek Put 406
B.8 Prek Chann 407
B.9 Prek Touch 410
B.10 Prek Thom 412

C Translations of Quotations from Archival Research in Cambodia 415

D Tables of Values Used in Eco-Hydrological Model 417

E Questionnaires used in the field surveys 419

E.1 Farmers - Initial Survey on Ecosystem Services June 2019 419
E.2 Farmers - Field Work February-March 2020 422
E.3 Village Chiefs - Field Work February-March 2020 437
E.4 Heads of Prek Water User Committees - Field Work February and March 2020 446
E.5 Shortened Farmer Questionnaire - Field Work November 2020 and Spring 2021 456

F Runge Kutta Solution 467

G Revision of Paper Published in the European Journal of Remote Sensing 469

H Revision of Paper Published in the Journal of Hydrology 513

List of Figures

1.1 Overall methodology of the research approach used in this thesis. 61

1.2 Conceptualization of the role of ecosystem services according to the MEA. Image reproduced under Creative Commons Licensing. 70

2.1 An overview of the course of the Mekong and the Lancang throughout Southeast Asia, the elevation of its basin, as well as the extent of water courses draining into the river. 76

2.2 Distribution of dams in the Mekong basin, by status (right) and capacity (left). Data courtesy of the Stimson Center Mekong Dam Monitoring Project 85

2.3 Cumulative capacity of dams on the Mekong and its tributaries since the 1940s. Data courtesy of CGIAR. 85

2.4 Online view of the MRC data portal, providing access to a wide variety of data. 91

2.5 Overview o the Mekong Delta and the Provinces of Cambodia and Vietnam that form part of it. 93

2.6 Overview of the official conservation areas in the Mekong Delta. 101

2.7 Excavation of the Cho Cao canal, ca. 1878, attributed to Émile Gsell, courtesy of the Université Côte d'Azur (ark:/17103/5hfh). In 1875 the French colonial authorities decided to construct a canal connecting Cua Tiêu to the Vaïco river as a transport route for rice by steamship. 103

3.1 Location of the areas of interest in the Cambodian Mekong delta. 110

3.2 All water level measurement stations from which data was used in this thesis, except Phnom Penh Chaktomuk. 113

3.3 The MRC's online portal visualizing the daily water level measurements at Chau Doc. 114

3.4 The HEC-RAS modelling interface. 115

3.5 Comparison of NRT data at Phnom Penh (PP), Koh Khel (KK), at the logger in the study area (SA), Angkor Borey (AB), and Chau Doc (CD) at the end of November 2020. 118

3.6 Comparison of NRT data at Koh Khel (KK), at the logger in the study area (SA), and Chau Doc (CD) with the results of the HEC-RAS simulation for water level dynamics at the logger location. 119

3.7 Comparison of daily water levels at Phnom Penh, Koh Khel, Angkorborey, and Chau Doc 2017-2021. 119

3.8 Comparison of daily water levels at Phnom Penh, Koh Khel, and Chau Doc 1992-2021. 120

3.9 Comparison of daily water levels at Phnom Penh, Koh Khel, Angkorborey, and Chau Doc during January-June 2020. 120

3.10 Results of hydrological analysis at Koh Khel. 123

3.11 Results of hydrological analysis at Neak Luong, short time series. 124

3.12 Results of hydrological analysis at Neak Luong, long time series. 125

3.13 Results of hydrological analysis at Tan Chau. 126

3.14 Results of hydrological analysis at Chau Doc. 127

3.15 Location of rainfall stations in and near the area of interest. 129

3.16 The pluviometer at Koh Khel meteorological station, photographed in 2020 by Sylvain Massuel. 131

3.17 Comparison of daily rainfall sums registered by CHIRPS, and by the stations in Koh Thom, Prek Chann, and Koh Khel in October 2021. 134

3.18 Comparison of monthly rainfall sums registered by CHIRPS, and by the stations in Koh Thom, Prek Chann, and Koh Khel in October 2021. 135

3.19 Comparison of frequency of rainfall events by intensity registered by CHIRPS, and measured at the meteorological field station at Prek Chann, the MRC station in Koh Khel, and by the UNDP Station at Kho Thom in 2021. 135

3.20 Comparison of monthly rainfall sums since 1981 as registered by CHIRPS . . . 136

3.21 Comparison of average rainfall sums per month in every decade since the 1980s as registered by CHIRPS. 136

3.22 Overall analysis workflow for the assessment of inundation trends in the study area. 139

3.23 The online Javascript interface of Google Earth Engine. 143

3.24 Logic workflow for creating the water level - flood link (WAFL). Example of an area with 4 pixels, and 4 images corresponding to 4 different water levels at Koh Khel. Blue areas represent flooded pixels. 146

3.25 Elevation-area curves according to TanDEM 148

3.26 Example of classification using k-means and optical Sentinel data on 2018-10-01 151

3.27 Dynamics of inundation extents and water levels measured at Koh Khel in the areas of interest 2017-2020. 151

3.28 Side-by-side comparison of the water level at which each pixel becomes flooded, according to the WAFL, and the TanDEM-X terrain elevation model. 152

3.29 Comparison of WAFL-derived inundation extents, and extents directly derived from Sentinel-2 images in 2018, 2019, and 2020. 154

3.30 Comparison of inundated areas - time series derived from the WAFL, and individual Landsat-5 and -8 images 155

3.31 Comparison of inundation extents derived from the WAFL and Landsat-5 and -8 images 156

3.32 Distribution of natural vegetation in the early 1990s, 2000s, 2010s, and present. 157

3.33 Local comparison of TanDEM-X-derived flood extent and WAFL-derived flood extent observed through Sentinel images. 159

3.34 Comparison of DEM with local water level data. 160

3.35 Comparison of inundation extents derived from TanDEM-X, and calculated from the WAFL, and as observed from Sentinel-1 for four dates during the 2020 flood season. 161

3.36 Change in inundation durations pre- and post-2008 162

3.37 Visual comparison of inundation incidences pre- and post-2008 163

4.1 Landscape configuration in the Prek Area during the wet and dry season, by Sylvain Massuel. 173

4.2 Location of the case study area in the Cambodian Mekong delta. 174

4.3 Figures from Lt. Barthélemy's report, illustrating the difference between flood patterns with and without Preks. 180

4.4 Figures from Lt. Barthélemy's report, illustrating the difference between flood patterns with and without Preks. 180

4.5 Figure from Lt. Barthelemy's report, illustrating sediment deposition in the Boeung following a Prek's construction. 181

4.6 A "Pol Pot" gate in the dyke that forms the southern border of the case study area. 186

4.7 Aerial view of rehabilitated and not rehabilitated Preks. 190

4.8 Pumping at the end of the Prek. 190

4.9 Aerial view of the rehabilitated Prek Chann, the gate at its head, and the Bassac in the background. 190

4.10 Common issues with rehabilitated Preks. 192

4.11 Local excavation initiative at Prek Thom. 192

4.12 HTML-based data entry portal to consolidate fieldwork results. 193

4.13 Interviews in the case study area. 195

4.14 Ages of the farmers who were interviewed. 197

4.15 Preks at which farmers were interviewed. 197

4.16 Pond dug in the inter-Prek area. the extracted soil was used to raise land elsewhere. 199

4.17 Uses of natural vegetation in the study area. 201

4.18 Boats used for transport in the study area. 202

4.19 Cattle in the case study area. 203

4.20 Three simple graphs 205

4.21 Crop distribution in the case study area. 210

4.22 Cropping practices for different crops in the study area, as characterized by Vandôme (2020). 212

4.23 Irrigation practices in the area. 216

4.24 Livestock in the study area. 218

4.25 Construction projects at the Preks. 228

5.1 Landcover dynamics in the study area during the dry season, RGB Image. . . . 234

5.2 Temporal distribution of training images and image time series used in this analysis, throughout the wet and dry season in the study area. 237

5.3 Classification workflow 237

5.4 Box plot of overall accuracies by imagery used and classifier, and significance of variation of accuracies depending on imagery type used. 247

5.5 Comparison of classification results using the best-performing configuration of NB, CART, RF, and SVM (linear). SVM (RBF) is not included due to low accuracies. 249

5.6 Time series of areas classified as bare / fallow using the training point set based on SPOT-images and RF, CART and SVM (linear) between October 2019 and September 2020. NB and SVM (RBF) are not included due to low accuracies. 250

6.1 The case study area during different seasons. 259

6.2 Simplified conceptual model. 263

6.3 Overall conceptualisation and relevant elements of the model. 264

6.5 RGB Sentinel-2 image taken in the case study area on 2018/09/13 (left) and flood extent detected using the unsupervised classifier (right). 265

6.4 Flood extents in the case study area. 265

6.6 Comparison of water levels registered by all loggers in Prek Chann and the Bassac, 2020-2021. 268

6.7 Comparison of water levels registered by all loggers in Prek Chann and the Bassac, 20-22 June 2020 268

6.8 Comparison of water levels registered by all loggers in Prek Chann and the Bassac, 24-6 September 2020 269

6.9 Logger set-up at the bridge at Prek Touch. Figure by Sylvain Massuel. 269

6.10 Comparison of water levels registered by the logger at Prek Touch bridge and the one in the Bassac, July-September 2021. 270

6.11 OpenFLUID interface. 273

6.12 Code and visualisations of the module for non-flood-related ES in Jupyter Notebook. 274

6.13 Delineation of RS and SUs, carried out manually in QGIS. 278

6.14 Delineation of modelling units. Background image: Google Earth. 278

6.15 Comparison of inundation extents estimated from WAFL and observed in Sentinel-1 imagery for the 2021 flood. 282

6.16 Comparison of observed inundation extents and inundation extents calculated on the basis of WAFL for the 2021 wet season. 282

6.17 Pseudowaterlevel in the case study area 2017-2022 and detail of the quasi-linear phase of recession of each year, as well as the average recession rates during this time. 284

6.18 Model architecture and calculation workflow. 287

6.19 TSS concentrations measured at Koh Khel 1993-2017 291

6.20 Example of simulation run with α=0.016 and z_{weir} = 0.5 at Prek Chann 302

6.21 Example of simulation run with α=0.018 and z_{weir} = 0.3 at Prek Touch 303

6.22 Variation of calculated yield as fraction of optimal yield, depending on the precipitation product used. 305

6.23 Percentage change of yield depending on the use of precipitation product. . . . 305

6.24 Variation of calculated yield as fraction of optimal yield, depending on the bed level of Preks. 306

6.25 Percentage change in comparison to the baseline using in-situ precipitation products, depending on the bed level of Preks. 307

6.26 Variation of water level in Preks [in m above Prek bed level] depending on bed elevation. 308

6.27 Comparison of water levels in m asl at Kratie, Koh Khel, and in the case study area in 2020-21. 310

6.28 Rating curve at Kratie, showing water levels in relation to discharge. 311

6.29 Comparison of water levels provided by the MRC and water levels back-calculated from provided discharge values on the basis of the reconstructed rating curve. . 311

6.30 Future water level projections according to climate change scenarios RCP 4.5 and RCP 8.5. 312

6.31 Calculated yield as fraction of optimal yield: Scenarios, 1, 2, 3, and 4. 314

6.32 Percentage change of yield in comparison to the baseline scenario. 315

6.33 Maximum inundation extents for each climate change scenario. 317

A.1 All MRC measurement stations in the vicinity of the areas of interest in the Cambodian Mekong Delta. 390

B.1 Visual documentation of Prek Cham Kroum. 396

B.2 Visual documentation of Prek Me Srok. 398

B.3 Visual documentation of Prek Lok. 400

B.4 Visual documentation of Prek Pok 402

B.5 Visual documentation of Prek Hom 404

B.6 Visual documentation of Prek Nou 405

B.7 Visual documentation of Prek Put 407

B.8 Visual documentation of Prek Chann 409

B.9 Visual documentation of Prek Touch 412

B.10 Visual documentation of Prek Thom 414

List of Tables

3.1 Meta data for all MRC water level measurement stations in the vicinity of the areas of interest. 114

3.2 Overview of average dates of flood rise and recession, flood duration, maximum water level, and date of maximum water level pre- and post-2008 at Koh Khel, Neak Luong, Chau Doc, and Tan Chau. 123

3.3 Overview of all rainfall measurement stations from which data was used in the course of this thesis 130

3.4 RMSE of monthly precipitation sums [mm] compared between stations. 135

3.5 Sentinel-1 bands, their resolutions, and wavelengths. 140

3.6 Sentinel-2 bands, their resolutions, and wavelengths. 141

3.7 Landsat 8 bands. 142

3.8 Landsat 5 bands. 142

3.9 A comparison of the agreement and discrepancies between the WAFL-derived inundation extents (WAFL) and the Landsat-derived flood maps (LS). 158

3.10 Average changes in inundation incidence and durations in Zone A and B pre- and post-2008 for individual pixels. Given are the largest increase in flood incidence and duration for any individual pixel in the study area (Max +), the largest decrease for the same (Max -), as well as the average change in incidence and duration across all pixels in the study area. 163

4.1 Overview of information on the ten Preks in the case study area. 175

4.2 Average practices for different crops grown in the case study area. 211

4.3 Overview of Preks in the case study area with regard to whether they are supplied with water via pumps during the dry season. State 2020. 216

4.4 Average irrigation hours (per day and hectare), and yield for all crops in the study area. 217

5.1 Overview of image datasets used. 236

5.2 Spectral indices calculated for optical Sentinel-2 imagery 239

5.3 Band sets of spectral indices and texture features. For the combined imagery set, these bands are stacked. 240

5.4 Optimal tuning parameters. 245

5.5 Overall accuracies 246

5.6 Producer and Consumer accuracies for NB, CART, RF and SVM using a linear kernel. SVM (RBF) is not included due to low accuracies. 249

6.1 The ecosystem services calculated in the model, and the hydrological factors on which they depend. 261

6.2 Average monthly TSS And SSC concentrations at Phnom Penh since 2011. . . 291

6.3 Weir height and α values for flow calibration at Prek Touch and Prek Chann, with resulting RMSE 302

6.4 Variation in seasonal groundwater recharge in the baseline scenario, depending on K_s (in m/d) and average inundation extents. 304

6.5 Percentage change of yield in comparison to the baseline scenario using local precipitation measurements of the three main types of crop in the case study area. 307

6.6 Percentage change of yield in the main crops in the case study area in comparison to the baseline scenario. 315

6.7 Results of simulation of flood-related ecosystem services for Scenario 1 and 2. . 316

A.1 Overview of MRC measurement stations in the vicinity of the areas of interest in the Cambodian Mekong Delta. 391

A.2 Overview of MRC measurement stations in Vietnam. 392

D.1 K_C and K_Y values for all land cover classes. 417

D.2 K_C and K_Y values for all vegetable crops. 418

D.3 Agricultural characteristics of the crops recorded in the interviews. For vegetable crops, average values depending on their relative areas were calculated. 418

D.4 Hydraulic soil properties according to Carsel and Parrish (1988), with θ_r = residual water content, $\theta_s at$ = saturated water content, α and n = fitting parameters related to particle-size distribution, and K_s = saturated hydraulic conductivity. . 418

D.5 Different curve number values according to land use, hydrological soil group, and antecedent soil moisture. 418

Glossary

3S River Basin Transboundary river basin of the Se Kong, Se San, and Sre Pok rivers.

ADCP Acoustic Doppler Current Profiler.

AET Actual Evapotranspiration.

AFD Agence Française de Développement, French Development Agency.

AHS Automatic Hydrological Stations.

AMC Antecedent Moisture Conditions.

ANN Artificial Neural Networks.

API Application Programming Interface.

ARIES ARtificial Intelligence for Ecosystem Services.

ASEAN Association of Southeast Asian Nations.

ASM Angular Second Moment.

AWS Automatic Weather Stations.

BOA Bottom of the Atmosphere Reflectance.

CART Classification and Regression Trees.

CAVAC Cambodia Agricultural Value Chain Program.

CCD Cold Cloud Duration.

CHANS Coupled human and natural system.

CHIRPS Climate Hazards group Infrared Precipitation with Stations.

CMPI6 Coupled Model Intercomparison Project Phase 6.

CORR Correlation.

CPK Communist Party of Kampuchea.

DEM Digital Elevation Model.

DFAT Australian Department of Foreign Affairs and Trade.

DISS Dissimilarity.

DNN Deep Neural Networks.

ENSO El Niño Southern Oscillation.

ENT Entropy.

ES Ecosystem services.

ESA European Space Agency.

ESs Water ecosystem services.

ET Evapotranspiration.

EVI Enhanced Vegetation Index.

EWS Early Wet Season.

FAO Food and Agriculture Organization of the United Nations.

FCNN Fully Convolutional Neural Networks.

FEWS NET Famine Early Warning Systems Network of the United States Agency for International Development.

GBM Stochastic Gradient Boosting Methods.

GDP Gross Domestic Product.

GEE Google Earth Engine.

GLCM Grey Level Co-occurence Matrix.

HES Hydrological ecosystem services.

IDM Inverse Difference Moment.

InVEST Integrated Valuation of Ecosystem Services and Tradeoffs.

IOD Indian Ocean Dipole.

IRD Institut de Recherche pour le Développement, French National Research Institute for Sustainable Development.

ITC Institute of Technology of Cambodia.

IW Interferometric wide swath.

JICA Japan International Cooperation Agency.

KNN K Nearest Neighbour.

LMB Lower Mekong Basin.

LULC Land Use and Land Cover Change.

LVQ Learning Vector Quantization.

MEA Millennium Ecosystem Assessment.

MODIS Moderate Resolution Imaging Spectroradiometer.

MoWRAM Ministry of Water Resources and Meteorology .

MRC Mekong River Commission.

MSS Multi-spectral scanner.

NASA North American Space Agency.

NB Naive Bayes.

NDMI Normalized Difference Moisture Index.

NDVI Normalized Difference Vegetation Index.

NDWI Normalized Difference Water Index.

NOAA US National Oceanographic and Atmospheric Administration.

NRT Near-realtime.

NWISP Northwest Irrigation Sector Project.

PET Potential Evapotranspiration.

PUC Prek User Committees.

RF Random Forest.

RFE2 Rainfall Estimate dataset by NOAA.

RMSE Root mean square error.

RPART Recursive Partitioning Regression Trees.

RS Reach Segments.

SAR Synthetic aperture radar.

SCS The USDA's Soil Conservation Service.

SPOT-6 Sattelite pour l'observation de la terre.

SSC Suspended Sediment Concentration.

SSP-RCP Shared Socioeconomic Pathway-representative Concentration Pathway.

STS Science and technology studies.

STV Standard Total View.

SU Surface Unit.

SVM Support Vector Machines.

SWAT Soil Water Assessment Tool.

TAMSAT Tropical Applications of Meteorology using SATellite.

TARCAT TAMSAT African Rainfall Climatology And Time series by the University of Reading.

TEEB The Economics of Ecosystems and Biodiversity.

TMPA 3B42 v7 Tropical Rainfall Measuring Mission Multi-satellite Precipitation Analysis version 7.

TOA Top of the Atmosphere Reflectance.

TRMM Tropical Rainfall Measuring Mission.

TSS Total Suspended Solids.

UMB Upper Mekong Basin.

UNDP United Nations Development Programme.

WAFL Water level - flood link.

1

Introduction

Globally, deltas hold a disproportionate importance. They take up only 0.57% of the earth's surface, yet are home to over 4.5% of the world population (Edmonds et al., 2020). They have been hubs of both biodiversity and, since the dawn of ancient high cultures in the deltas such as those of the Yangtze and the Nile, the development of human society (Stanley and Warne, 1997; Renaud et al., 2013).

However, due to being located at the intersection between terrestrial and aquatic, as well as freshwater and marine ecosystems, these areas also have to cope with pressure from multiple angles (Kuenzer and Renaud, 2012; Kuenzer et al., 2011; Edmonds et al., 2020; Szabo et al., 2016). This is perfectly illustrated in the delta of the Mekong, Southeast Asia's largest river, which stretches across southern Cambodia and Vietnam. Home to over 19 million people, the delta is also known as the "rice bowl" of the region (Duc Tran et al., 2018; Kuenzer et al., 2013). It is the source of 50% of Vietnam's food production, with similarly high percentages in Cambodia,

and, through rice exports, provides sustenance for over 200 million people (Minderhoud et al., 2017). Yet the Mekong faces an wide array of pressure factors. Along the coastline of its delta in Vietnam, rising sea levels are causing more frequent storm surges, and are pushing saline water further inland, threatening agricultural systems in these areas (Meselhe et al., 2017; Szabo et al., 2016; Wassmann et al., 2019). Climatic shifts over the delta itself, and the entire catchment of the Mekong, are changing hydrological cycles, altering precipitation patterns, and modifying runoff dynamics (Binh et al., 2020; Pokhrel et al., 2018). In addition, human activities like overfishing (Vu et al., 2021), groundwater extraction (Minderhoud et al., 2017), land use change (Liu et al., 2020), riverbed mining (Xing et al., 2017; Park et al., 2020), infrastructure construction, and water power development (Hecht et al., 2018; Yang et al., 2019) are further drivers of change that are straining existing ecosystems and systems of production.

Yet the scale at which the impacts of these processes can most clearly be seen is a different, local one. While local areas within the Mekong Delta all exhibit their idiosyncratic characteristics, with unique configurations of socioeconomic and physical factors, delta- and basin-wide processes are keenly felt at these scales, and their impacts on individual communities and people are plainly discernible, both directly and indirectly (Hanington et al., 2017; Stewart and Coclanis, 2011; Shrestha et al., 2018). More importantly, measures can be taken at this level to mitigate the negative impact of changes and increase the resilience of local communities and their economic foundations.

In this context, with funding from the French Development Agency (AFD), the French National Research Institute for Sustainable Development (IRD) and its Cambodian partners launched an interdisciplinary research project in the framework of which this thesis was carried out - *COSTEA Cambodia - Understanding and Managing the Cambodian Floodplains, the Preks of Kandal Province*. It is centred on Kandal Province, in the Cambodian part of the Mekong Delta, south of the capital, Phnom Penh. This region has been the object of relatively few studies in comparison to its more accessible Vietnamese counterpart. However, its comparative lack of hydraulic infrastructure means that the agricultural and fishing communities in the area are still far more dependent on the natural timing and magnitude of the annual Monsoon flood in terms of cultivation practices. Another distinguishing characteristic of the area are the so-called Prek channels (Venot and Jensen, 2021). These are large-scale channels with a trapezoidal cross-section which diverge perpendicularly from the Mekong and its larger distributaries. They

breach the elevated river banks and establish connections between the river main stream and the low-lying floodplains in its vicinity. Originally, they were constructed in the early 20th century, during the period of the French protectorate, to facilitate the deposition of sediments in the floodplains during the annual inundations and thus raise land (Barthélemy, 1913). Nowadays, they still fulfill this vector-like function for both flooding and drainage, but they have also become important avenues of transport by boat, as well as sources of water for dry-season irrigation, watering cattle, and household purposes. Nevertheless, many Preks have fallen into disrepair over the past decades, with banks collapsing due to erosion, and sediment deposits clogging up the channels. Since the 1990s, several international development agencies, in cooperation with local government agencies, have implemented projects to rehabilitate Preks and re-establish their full functionality (SOFRECO, 2017). These projects involve geotechnical works to lower Preks' bed levels and facilitate water flows, restore their profiles, install regulation infrastructure such as gates, and construct accompanying infrastructure such as roads along the banks of the Preks.

However, there is still much that is unknown about the hydrological processes in the area, their impact on ecology and agronomy, the role of Preks, and how exactly basin-wide changes translate to this local level. Without this information, it is difficult to assess the efficacy of past projects and to develop sustainable plans to increase the resilience and prosperity of local agricultural communities in the face of global change.

The aim of this thesis is to shed light on the link between hydrological processes and agro-ecosystems in the Cambodian Mekong Delta, and the role that Preks play in catalyzing them. It further strives to gain an understanding of how drivers of change at the scale of the entire Mekong basin and delta influence these local processes and what impacts likely future developments could have.

To do so, it takes a broad approach. Since the objectives of this thesis are diverse, so are the methods it employs to reach them. Like theses in similar contexts, (cf. Leauthaud et al. (2013)), it draws from a variety of disciplines. Ultimately, it combines remote sensing using a cloud-computing platform, a numerical ecohydrological model, archival research, field studies, and sociological interviews to pursue answers to the research questions.

Finally, it must be noted that a partial aim of this thesis was also to develop a larger-scale understanding of the challenges similar deltas face worldwide, and to develop methods that can

be transferred to similar contexts. For instance, other major deltas worldwide, such as the Yellow River, Ganges–Brahmaputra, and Amazon deltas (Szabo et al., 2016; Singha et al., 2020) are also facing drivers of change such as climate change and land cover change, which significantly shift their hydrological patterns and impact local ecosystems and agricultural communities.

1.1 Research Questions

In general, this thesis aims to better understand the long-term hydrological dynamics in the Cambodian Mekong delta, specifically in the Prek area. Due to a comparative absence of hydraulic infrastructure such as dykes, gates, and dams, these dynamics differ considerably from those in the neighbouring Vietnamese part of the delta, which has been the object of a multitude of studies on subjects ranging from sediment deposition (Nhan and Cao, 2019; Zoccarato et al., 2018) to the sustainability of the development of hydraulic infrastructure on the deltaic plains(Tri, 2012; Quoc Thanh et al., 2019). More specifically, the objective of this thesis is to understand how hydrological processes impact ecosystem services in the Prek area - that is, the benefits that humans derive from nature. This anthropocentric approach was chosen as it reflects the priorities of the development projects in the area, to sustain and improve ecosystem functionality in order to increase the resilience of local communities. A central point is also to gain an understanding of how Preks shape these hydrological processes and ecosystem services, and what measures could be taken with regard to them to minimize future negative impacts on the communities in the area.

Formally, the research questions of this thesis are as follows.

- What are the current patterns of regional hydrological dynamics at the scale of the Cambodian upper Mekong delta, and which trends have manifested themselves over the past three decades?
- How are regional and local hydrological processes being affected by reported basin- and delta-wide changes?
- What are the roles that Preks play in catalyzing these processes at the local level?

- What are the ecosystem services from which people in the Prek area benefit? How are these linked to hydrological processes?
- How will future developments and trends impact hydrology in the Prek area, and in consequence, the ecosystem services to which it is linked? What measures can be taken to mitigate or prevent negative impacts?

1.2 Overall Research Methodology

As can be seen above, the research questions tackled in this thesis apply at different scales. Therefore, the methodology employed progressively zooms in onto smaller scales, beginning at the scale of the entire Mekong basin.

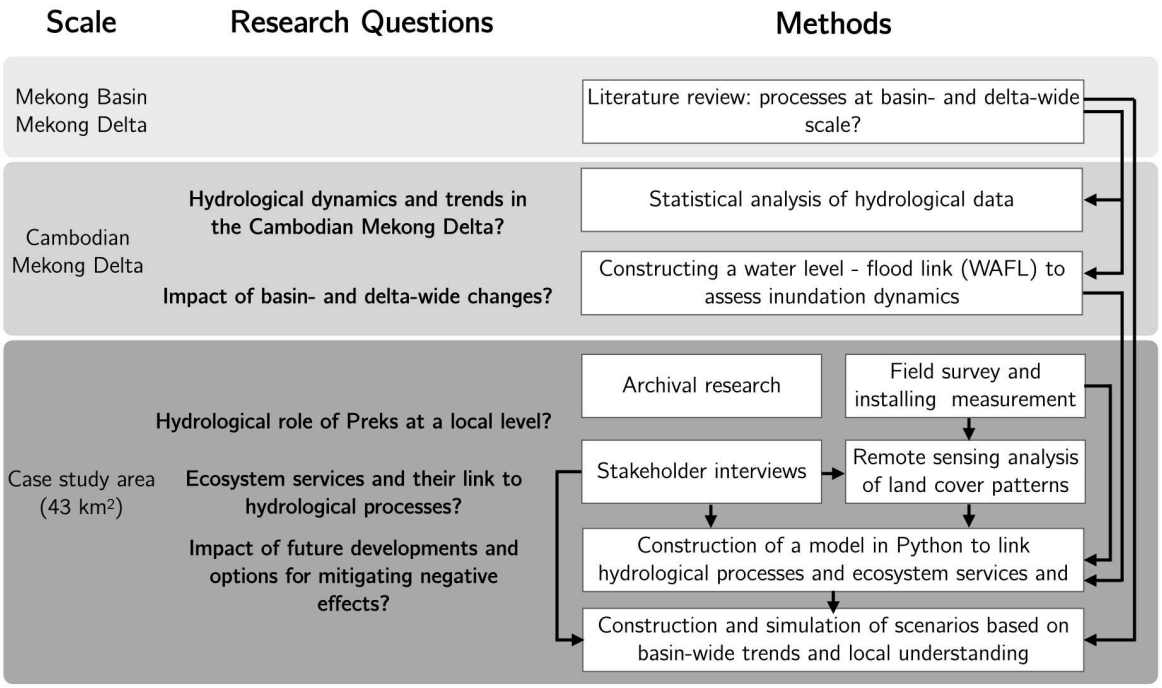

Figure 1.1: Overall methodology of the research approach used in this thesis.

First, it was necessary to gain a thorough understanding of the drivers of change at work in the basin of the Mekong. Only once these large-scale processes have been understood can it be investigated how they are reflected at smaller scales. To this end, a thorough literature review was conducted. The results are presented in chapter 2.1, which provides a broad introduction

to the Mekong River, its role in Southeast Asia in general and Cambodia in particular, and the challenges it faces. It further provides an overview of the Mekong's delta, exploring aspects such as climatic patterns, geology, hydrogeology, socio-economic characteristics, and drivers of change at work in the region.

Subsequently, the focus of this thesis shifts to the scale of the Cambodian Mekong Delta and its overall hydrological dynamics. The area of interest are two zones in the Cambodian part of the Delta, which collectively cover 400 km^2. At this scale, the aim was to identify recent hydrological trends and how they reflect or differ from basin- and delta-wide dynamics documented in the literature. To this end, current hydrological dynamics were explored using in-situ water level measurements in combination with remote sensing images. A statistical analysis of shifts in river water levels and in precipitation patterns was carried out. Furthermore, a method for linking water levels to inundated areas was developed, which allows the re-construction of flood maps over the past three decades. Based on this, changes in inundation patterns during this timespan could be explored and related to basin-wide trends. To complement this, a general analysis of land use change during the same period was conducted, specifically with a view towards the reduction in natural forest and shrubland. The results of these analyses are presented in Chapter 3.

Next, the thesis zooms in onto a local level, a study area of 43 km^2, which encompasses 10 Prek channels along the Bassac river, one of the Mekong's deltaic distributaries, and is representative of the diversity of agricultural practices and ecosystems in the Cambodian part of the delta. At this level, the aim is to understand the current role of the Preks for both ecosystems and agricultural practices, to gain insights into their historical development, and the relationship and attitudes that local communities have towards them. With this knowledge, the final research question can be addressed - how future developments are likely to impact the Prek system, and how possible negative impacts can be mitigated. The methods employed and results obtained at this scale are presented in Chapters 4, 5, and 6.

Chapter 4 provides an in-depth history of the Preks based on archival research and engineering reports from the beginning of the 20th century to now. Furthermore, the Preks' current functions and significance for economic, especially agricultural, activities in the area are explored on the basis of field studies and interviews conducted with local stakeholders, such as farmers and

village chiefs. In addition, a characterization of agricultural systems based on the interviews is presented.

Chapter 5 then complements the information acquired during field work through an analysis of seasonal land use and land cover based on remote sensing imagery. A monthly land cover classification for the entire case study area is produced using radar Sentinel-1 and optical Sentinel-2 imagery and a supervised classification approach. To ensure maximum accuracy for the classification, several classifiers available on the cloud computing platform Google Earth Engine, several combinations of input imagery, and two training datasets were compared.

Chapter 6 aims to explore future scenarios. To this end, a numerical ecohydrological model was constructed, building on the information available at multiple scales, presented in previous chapters. First, the Prek system as a whole is conceptually formalized, along with the future scenarios to be modelled. Then, the construction of the model itself is outlined, from its conceptual basis and simplifications to the process of its calibration and validation. Subsequently, the results of the simulations are presented and discussed.

Finally, Chapter 7 provides a synthesis and discussion of the results of this thesis and the insights they provide. Local processes and future outlooks are related to basin-wide projections, and their significance for local communities and engineering projects such as Prek rehabilitations are explored. To close this thesis, a reflection on its larger significance and limitations are provided, together with questions for future research and a larger outlook. However, before the concrete work done in the framework of this thesis can be delved into, it is necessary to gain a better sense of the conceptual context in which this work was conducted. Without a thorough grounding in theory and a meta-understanding of the mechanisms which are at work both in the study area and the process of research, many insights would remain occluded.

1.3 Conceptual Context: Integrative Approaches, Ecohydrology, and Ecosystem Services

This section outlines the general conceptual context of this thesis. It begins by introducing the domain of ecohydrology, which links ecology and hydrology, taking into account biophysical

dynamics. Then, it segues into socio-hydrology and related disciplines, which highlights the interdependency between society and water and requires the human dimension to be taken into account in the understanding and modeling of water resource dynamics. Subsequently, it introduces the general framework of ecosystem services which strives to quantify the benefits that humans derive from ecosystems. An anthropocentric concept, the use of ecosystem services to categorize and qualify the processes described in this thesis, more firmly establishes the link to socio-hydrological approaches. Finally, a brief discussion is given of the necessity and value of interdisciplinary approaches in studies such as the one presented in this thesis.

1.3.1 Ecohydrology

Ecohydrology is one of the concepts most central to this thesis. At its core, the model introduced in Chapter 6 is an ecohydrological one, and many aspects of the fieldwork were informed by ecohydrological considerations, as will be outlined in detail Chapter 4.

Ecohydrology as a term and, subsequently, discipline was introduced in the late 1990s. As defined by Zalewski et al. (2008), it strives to find an understanding of how hydrological processes interact and integrate with ecological ones. Ultimately, it aims to "describe a new way of managing the water cycle in order to achieve the sustainable use of water by societies" (p. 1). In order to do so, ecohydrological research employs innovative and multidisciplinary approaches, drawing not just on hydrology and ecology, but also on disciplines such as chemistry, genetics, the legal sciences, molecular biology, and socio-economic research.

There are three distinct dimensions to ecohydrology. The first, which is most relevant in this thesis, focuses on interactions between plants and water in terrestrial environments. The second relates to the water cycle itself and how changes in the available water quantity impact river ecology. The third dimension, finally, approaches the subject from a more integrated point of view, aiming to explore the role of both physical and biotic processes in the dynamic evolution of river basins (Harper et al., 2008).

Another term that needs to be mentioned in the context of ecohydrology, even if only to delineate it, is hydroecology. During the early years of research in the domain of intersection between hydrology and ecology, these two terms were often used interchangeably, without

agreement on a clear canonical definition (Kundzewicz, 2009). To a certain degree, they still are used synonymously, though hydroecology now seems to appear more rarely and many institutions in this domain of research favour the alternative, for instance the journal *Ecohydrology*, which began its publication in 2009. Wood et al. (2007) suggested a delineation of the terms, proposing to apply ecohydrology to more focused plant-water interactions, while hydroecology should encompass a much broader scope.

In this thesis, the term ecohydrology is used in its broadest contemporary sense - "a transdisciplinary sustainability science based on an understanding of hydrosphere/ecosphere interactions from the molecular to the catchment scale" (Zalewski et al. (2021) p. 1). In the context of this thesis, it encompasses many of the the questions outlined in Section 1.1, specifically those questions pertaining to the interactions between vegetation patterns and the hydrological processes in the Mekong Delta on a regional scale (see Section 3.2) and the local-scale processes catalyzed by the Prek System. Strictly speaking, since the area of interest in the Cambodian Mekong Delta is an agro-ecosystem, with the landscape being fundamentally shaped by agricultural practices and anthropogenic modifications, the processes studied in this thesis could be referred to as agro-eco-hydrological (cf. Chen et al. (2020)), though such terminological distinctions have little bearing on the actual practical work conducted or on the results presented in subsequent chapters.

1.3.2 Sociohydrology

Socio-hydrology, the second key discipline from which this thesis draws, shares several features with ecohydrology, though there are several crucial distinguishing characteristics. The science of socio-hydrology takes its origin in the early 2010s. Sivapalan et al. (2012) conceptualised the discipline as the "science of people and water, [...] a science that is aimed at understanding the dynamics and co-evolution of coupled human-water systems". It aims to treat humans as an endogenous element of the water cycle. The authors of this foundational paper envision socio-hydrology as a "discovery-based fundamental science", which must strive to be quantitative to appropriately test hypotheses, model systems, and predict possible future scenarios.

Furthermore, they especially emphasize the aspect of co-evolution. Socio-hydrology, Siva-

palan et al. (2012) underline, accounts for "the future co-evolution of coupled human-water systems". This especially involves taking the generation of previously unobserved variations into account, as well as 'emergent behaviour'. Similarly, socio-hydrological approaches are meant to take into account the possibility of the exceedance of 'tipping points', which can lead to the evolution of systems to these previously unobserved states.

Furthermore, even this early on in the genesis of socio-hydrology, the papers' authors outline significant parallels to ecohydrology that, they argue, can serve as a basis to advance knowledge and methods, for instance by the adoption of the principles of optimality and co-evolution, and bring about a similar broadening of hydrology as a discipline. However, they add the caveat that socio-hydrology is dealing with greater complexity overall, because "humans possess more powerful ways and means of controlling water cycle dynamics beyond the optimality, adaptation, and acclimation strategies that natural vegetation possesses". More recently, other studies have explored the close-knit heuristic relationship and epistemological parallels between socio- and ecohydrology. Bertassello et al. (2021), for instance, examines the application of both disciplines in the space-time dynamics of human-altered catchments and observes that "in the emerging Anthropocene, humans are no longer mere external drivers or boundary conditions in ecohydrologic systems. Rather, humans are dynamically related to both water and ecosystems" (p. 1395). This reasoning also stands behind the use of the ecosystem services concept in the course of this thesis.

Since its inception, socio-hydrology has seen a proliferation of publications related to the discipline and the parallel development of fields similarly dealing with coupled human-water systems, such as hydrosociology and hydroeconomics.The perceived overlap with other disciplines considering human agency in studying hydrological systems, inherent in socio-hydrology's interdisciplinary approach, has also left it open to criticism. Madani and Shafiee-Jood (2020), for example, suggest that the focus on socio-hydrology has led to the dismissal of work in fields such as water resources systems and coupled human and natural systems (CHANS). Furthermore, there is some controversy about the originality of socio-hydrology in comparison to previously existing fields such as hydrosociology. Sivakumar (2012), for instance, argues that socio-hydrology is merely a reformulation of hydrosociology as the science of people and water, defined previously by Falkenmark (1977).

In any case, the Prek System that forms the core focus of this thesis can easily be construed as a coupled human-water system and thus as falling within the domain of socio-hydrology. As will be outlined in the qualitative description of the study area and the results of the fieldwork in Chapter 4.3, Preks have shaped the landscape of the Cambodian Mekong Delta for decades, and have equally impacted social organisation and structures. Bi-directional feedbacks furthermore exist in the very nature of water management and Prek maintenance and rehabilitation. The cultivation pattern along Preks, for instance, depends largely on water availability. Water ability, in turn, is governed to a large extent by the rehabilitation status of Preks. Whether Preks are rehabilitated, though, is also decided based on cultivation practices in the area. These feedbacks and relationships will be discussed to a greater extent in Section 4.3.4. However, they are not explicitly considered in the model presented in Chapter 6. While the inclusion of socio-hydrological components offers an interesting perspective for future research, the added complexity would have taken it beyond the scope of this thesis, as it would have required much more in-depth interactions with local stakeholders than the utilitarian ones described in Chapter 4, which were focused on quantifying current practices.Nonetheless, a basic understanding of of ecohydrological processes in the Prek area requires the inclusion of the interface between humans and society. To a certain degree, this is achieved here through the use of the ecosystem services concept.

1.3.3 Quantifying Nature's Benefits - The Transformational Concept of Ecosystem Services

Ecosystem services are the multitude of benefits humans derive from their natural environment in general, and from healthy ecosystems in particular. The range of ecosystems subsumable to this approach is broad, including terrestrial and aquatic systems, as well as anthropologically shaped forms such as agroecosystems. Implicitly, these benefits had been a consideration in scientific studies for decades before the term ecosystem services (ES) was coined. However, with the formalization of the concept in the early 2000s as part of efforts such as the Millennium Ecosystem Assessment (MEA) and The Economics of Ecosystems and Biodiversity studies (TEEB studies), ES took centre stage in the international environmental and ecological discourse. At its core, the ES concept is essentially anthropocentric - it focuses entirely on how ecosystems

can enhance the quality of life of humans. In doing so, any intrinsic value of ecosystems is neglected. To a certain degree, this is by design, as the concept of ES was originally aimed to demonstrate the value of the natural environment and, by extension, conservation efforts, to stakeholders in the realm of business and government (Grunewald and Bastian, 2015).

In an analysis of the history of the ES concept, Gómez-Baggethun et al. (2010) traces its origins far back into classical economics, though limited, in essence, by the fact that ecology did not exist as a discipline for much of the period under scrutiny. However, Gómez-Baggethun et al. (2010) points to a baseline awareness of the benefits and value of natural systems in the work of several prominent economists in the 18th and 19th century. Such an awareness, the authors point out, is evidenced in the work of Karl Marx, who wrote: "Labor is not the source of all wealth. Nature is just as much the source of use values (and it is surely of such that material wealth consists!) as labor, which itself is only the manifestation of a force of nature." (Marx (1891) p. 7, cited in Gómez-Baggethun et al. (2010)). Yet, Gómez-Baggethun et al. (2010) also adds the caveat that Marx's focus remains on the singular role of labour in producing exchange value, and the irrelevance of the "dull and tedious quarrel over the part played by Nature in the formation of exchange-value. Since exchange-value is a definite social manner of expressing the amount of labor bestowed upon an object, Nature has no more to do with it, than it has in fixing the course of exchange." (Marx (1887), p. 40, cited in Gómez-Baggethun et al. (2010)).

It was only starting in the 1960s that the economic school of environmental and resource economics began to frame nature's benefits as monetizable in themselves, and ecological economics framed the discourse over controversies on monetizing and commodifying these benefits (Hubacek and van den Bergh, 2006; Gómez-Baggethun et al., 2010). The origins of the concept of ES in its modern form lie in the late 1970s, when scientists explicitly began to frame the beneficial functions of ecosystems in a utilitarian light (Westman, 1977; de Groot, 1987). The focus of these efforts was as yet pedagogical in nature. They aimed to inspire general public interest in conservation efforts and biodiversity. The term "ecosystem services" was first used by Ehrlich and Mooney (1983) in their seminal analysis of the role of ES in the mechanisms of species extinction and substitution. In the 1990s, the ES concept began to enter the scientific mainstream, with a focus on developing methodologies of estimating the economic value of individual services (Constanze and Daly, 1992; Perrings et al., 1992). Costanza et al. (1997), for instance, estimates that the "services of ecological systems and the natural capital stocks

that produce", which are "critical to the functioning of the Earth's life-support system" carry an economic value of "USD 16-54 trillion per year, with an average of USD 33 trillion per year", compared to an annual global GDP of USD 18 trillion.

A landmark in the history of the ES concept is the MEA. The result of a four-year international scientific effort launched by the United Nations in 2001, the MEA presented a systematic, global overview of 24 key ecosystem services. It concluded that 15 out of these 24 were in a state of advanced degradation, posing a threat to human well-being and quality of life. The MEA places considerable emphasis on the anthropocentric approach to ES, highlighting the role of functioning ecosystems and the processes they catalyze for society. Following the publication of the MEA report in 2005, the number of publications harnessing the ES concept multiplied. McDonough et al. (2017) report that in 2005, publications around the subject of ecosystem services numbered in the realm of 200, a figure based on an analysis using data from SCOPUS and Web of Science. Eleven years later, in 2016, this number lay at approximately 3000. Significant large-scale studies, analyses, and programs also followed, such as TEEB, which aimed to quantify the costs of a decline in ES stemming from a failure to halt the global loss of biodiversity (Kumar, 2012).

The majority of analyses on ES conducted over the past two decades adheres to the structure outlined in the MEA report (see Figure 1.2), which subdivides ecosystem services into four general types: provisioning, regulating, cultural, and supporting. To begin with, provisioning ES are the most readily visible benefits humans derive from ecosystems in the form of goods - food, raw materials for production and energy generation, but also medicinal resources and, on a more general level, genetic resources that may be of future use. Regulating services contribute to the provision of an environment in which both humans and ecosystems can prosper. They include, for instance, climate regulation through carbon sequestration, air and water purification, flood protection, biological disease control, and waste decomposition. More abstract but no less important are cultural ES. These encompass the cultural, spiritual, historical, and recreational value of ecosystems and the natural environment. Benefits which fall into this category can range from ecotourism and ecotherapy to the heritage and religious value of important natural sites. Finally, supporting services such as nutrient cycling, soil formation, and primary production form be basis of ecosystem functioning and thus the provision of all other types of ES. In some categorizations, including the one used in this thesis, they are subsumed under regulating services (Jacobs, 2002; Grunewald and Bastian, 2015).

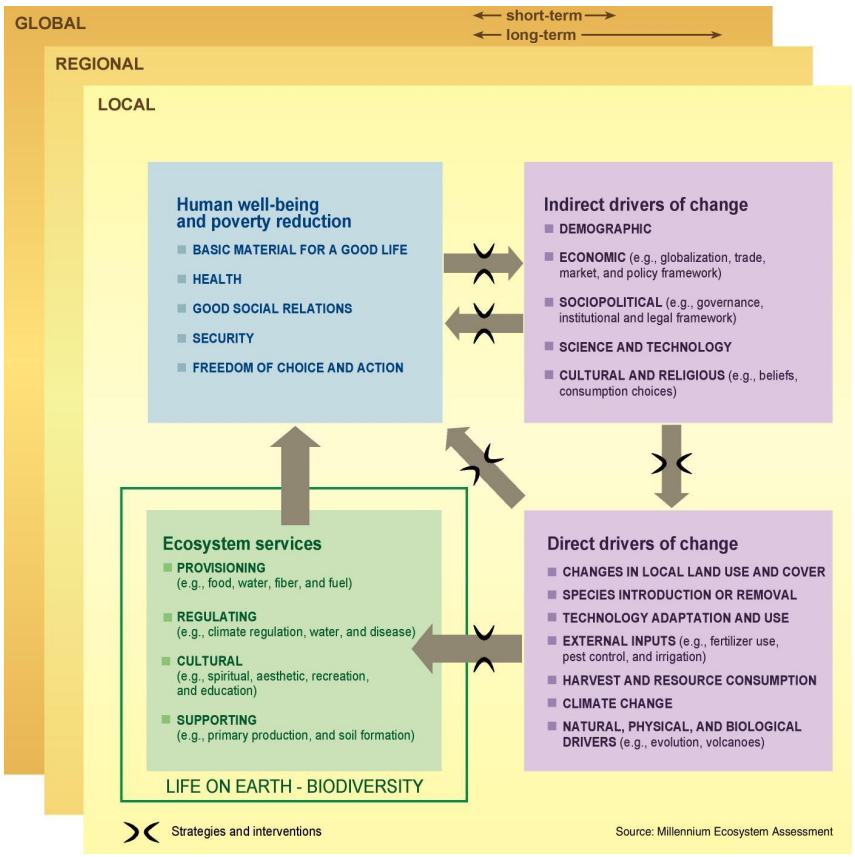

Figure 1.2: Conceptualization of the role of ecosystem services according to the MEA. Image reproduced under Creative Commons Licensing.

Building on this classification and further developing the ES concept, many studies have contributed in-depth sub-classifications in various disciplines to the scientific discourse on ES over the years. One such sub-focus which is particularly relevant for the purposes of this thesis are hydrological ES (HES), alternatively termed water ES (ESS). Brauman et al. (2007), for instance, specifically discusses the biophysical generation of hydrological services such as in-situ water supply for hydropower generation, recreation, transportation, and the supply of fish, the mitigation of water-related damage such as floods, as well as the benefits derived from diverted water supply for agricultural, commercial, and municipal use. HES have been highlighted in several studies, due to the prominent interface between ES science and policymaking in freshwater ecosystems (Harrison-Atlas et al., 2016).

However, despite the broad establishment of the ES concept in the scientific community, its application is frequently still a matter of dispute (Grizzetti et al., 2016). In particular, the development of ES indicators in order to quantify, monetize, and assess ES still arouses con-

tentious discourse. While specially designed ES models such as INVEST (Integrated Valuation of Ecosystem Services and Tradeoffs) and ARIES (ARtificial Intelligence for Ecosystem Services) exist, many studies challenge whether they are sufficient to quantify ES that rely on a complex nexus of factors, such as is commonly the case for HES, and question whether integrating ES into discipline-specific models instead would not entail more methodological benefits (Hallouin et al., 2018). The very type of valuation and the various analytical elements involved are often under discussion. Hackbart et al. (2017), for instance, concludes that the current state of knowledge about HES gives "the false impression that the ecosystem services valuation is sufficiently consolidated to support decisions about payments for ESw".

This thesis follows the general methodology outlined in Grunewald and Bastian (2015) for the analysis and evaluation of ES. The general procedure of the application of the ES concept has been outlined briefly in the introduction above and will be further expanded in Section 4.3.3. A thorough characterisation of the area of interest is provided in Chapter 4.3 together with a definition of terminology and a selection of ES to be evaluated. The evaluation procedures and indicators chosen are outlined in Chapters 4.3 and 6, alongside the basis for biophysical assessment and an approximation of monetary evaluation. Furthermore, spatial and temporal aspects are considered through distributed modelling as outlined in Chapter 6, as well as scenario building, a common approach to identify losses and gains in ESw (Ávila-García et al., 2020). However, further steps suggested in Grunewald and Bastian (2015), such as a differentiated cost/benefit analysis, a consideration of trade-offs, knowledge communication, and recommendations for ES management and monitoring are not within the scope of this thesis.

1.3.4 The Necessity for Interdisciplinary Work and Transdisciplinary Approaches in a Development Context

In the previous sections of this chapter, the terms "interdisciplinary" and "multidisciplinary" have been used largely synonymously. However, there are differences between these terms. "Interdisciplinary" is sometimes defined as describing the intersection between two disciplines, while "multidisciplinary" emphasizes that participation and cooperation of multiple disciplines. By and large, though, these terms are used to refer to approaches that combine methods and

theoretical frameworks from multiple disciplines. In contrast, "transdisciplinary" denotes the involvement of non-academic stakeholders in the process of knowledge production (Rigolot, 2020).

This PhD took place in the frame of a broader transdisciplinary research project financed by the French Development Agency (AFD), which aimed to rehabilitate Preks and increase one particular type of ES - the provisioning of water for agricultural purposes. The thesis took the AFD project as an entry point to further explore both the hydrological functioning of the Prek system and the other ES it provides. Furthermore, the research presented here has benefited from the insights gained by researchers from other disciplines, from sociologists to geohydrologists, working in the framework of the same project, through methods such participatory games (Venot et al., 2022) and chemical water quality analysis (Tweed et al., 2020). The results of their research have served as a foundation for both the fieldwork approach presented below (cf. Chapter 4), and as an aid in the construction of the model presented in Chapter 6.

On a meta-scale, an interdisciplinary approach also allows for advanced reflection on the limitations of individual methodologies and the foundational assumptions that underlie methodological choices. This is invaluable in terms of gaining insights into the cultural constructs and power relations on which the knowledge ultimately generated is often contingent, and into the "unequal material and socio-economic effects of discursive and methodological framings" (Venot et al., 2021).

As with the domain of socio-hydrology, this thesis strives to demonstrate an awareness rather than a full incorporation of these views. As outlined in the introduction and detailed further below, a multi-method approach encompassing classical statistical hydrological analysis, interviews, remote sensing, and computational modelling was utilized to answer the research questions outlined in Section 1.1. However, no in-depth meta-analysis of the interactions between these methods was undertaken, nor was an approach from the perspective of science and technology studies (STS) employed. These analyses were within the purview of studies conducted in the framework of the same project, some even within the same case study area, such as Venot and Jensen (2021), which draws on STS and critical water research to explore the multiplicity of Preks and construe them in the context of a "socionatural mosaic landscape", and Venot et al. (2022), which examines the use of serious games as a participative way of generating knowledge.

2

The Research Site: Introducing the Mekong, its (Cambodian) Delta, and the Preks

While the methods presented below are transferable, and can thus be applied to river basins and deltaic areas facing similar challenges, a thorough understanding of the Mekong basin's unique configuration is necessary to comprehend the approaches chosen to address research questions of this thesis. This chapter aims to set the stage, as it were. It introduces the Mekong, Southeast Asia's largest river, tracing its course from its spring on the Tibetan plateau to its delta in the South China Sea, introducing its traditional hydrological dynamics, and giving a brief outline of its economic and ecological importance, as well as of the multiple pressures it faces and the varying projections of its future development. The subsequent section then focuses on the Mekong Delta in Cambodia and Vietnam, giving in-depth insights into its hydrology, geology, biodiversity, and socio-economic characteristics. Most immediately relevant to this thesis, it also

provides an initial overview of the Prek system of the Cambodian Mekong delta, which is the centerpiece of this dissertation.

2.1 Southeast Asia's Centering Line - The Mekong

The Mekong river's headwaters originate on the Tibetan Plateau in China, in the Sanjiangyuan National Nature Reserve (SNNR) of Qinghai province. The reserve is also known as Three Rivers Nature Reserve, as two other major Asian rivers also take their spring here - the Yangtze and the Huang He (Yellow) River. The SSNR was China's first national park (Li et al., 2012). From here, the Mekong runs over a length of over 4,800 kilometers through China, Myanmar, Laos, Thailand, Cambodia, and Vietnam, making it the 12th longest river in the world (Nhan and Cao, 2019). In China, the river carries the name Lancang or Lancang Jiang River. From its spring in Qinghai province at an altitude of over 5,200 m (Campbell, 2009), the river flows through the Tibetan Autonomous Region and on into China's Yunnan Province, where its channel descends steeply through deep canyons. In this section of its course, also known as the Three Rivers Region, the Mekong is once more in close proximity to two other major rivers. At one point, the distance between the Mekong, the Yangtze, and the Salween Rivers is less than 120 kilometers (Eyler, 2019; Wang et al., 2017), though the rivers are separated by high mountain ranges. No tributaries enter the Mekong in this section of its course. Further South, the Mekong also passes in close proximity to the Red River, which forms one of the most vital waterways in northern Vietnam.

In southern Yunnan province, the Mekong leaves the narrow confines of gorges. Its valley opens out, its floodplain widens, and its flow velocity decreases. In this section, the river continuously drops in elevation, between 3000 and 2000 meters above sea level, and transitions to mid- and lowland reaches. At the southern tip of Yunnan, the Mekong briefly flows along the border with Myanmar, then leaves China. Subsequently, it forms the border between Laos and Myanmar for approximately 100 kilometers before reaching the Golden Triangle. This name is used to refer to the tripoint where the borders of Myanmar, Laos, and Thailand meet. Furthermore, this is the location of the confluence between the Mekong and the Ruak River, which forms the border between Thailand and Myanmar further upstream. This area in the

Northeast of Myanmar and the North of Thailand and Laos is also known as the Northern Highlands. Here, several large tributaries flow into the Mekong, such as the the Nam Ta, Nam Ou, Nam Soung and Nam Khan on its left bank, and the the Nam Mae Kok and Nam Mae Ing on its right bank (Piman and Shrestha, 2017).

After the Golden Triangle, the Mekong passes through a series of rapids, also known as Khon Pi Luang Lin and Grundy-Warr (2020), and flows through Laos for about 400 kilometres, before defining the border between this country and Thailand for another 850 kilometers. Here, the Mekong passes through the low-lying Khorat Plateau, with an average elevation of only 200 m. In this region, the confluences between the Mekong and several important tributaries can be found, such as the Songkhram and Mun rivers on its right bank, and the Nam Ca Dinh, Se Bang Fai, and Se Bang Hiang on the left bank. South of the Laotian capital of Vientiane, if once more passes into the country's interior. After passing the city of Pakse, it turns south and crosses into Cambodia (Kondolf et al., 2018; Molle et al., 2009). Here, at the border between Laos and Vietnam, a natural fault line intersects the river in the Four Thousand Island (Siphandone) area, resulting in a series of waterfalls that makes the river impassable to boats.

This border area is characterised by three tributaries of the Mekong - the Se Kong, Se San, and Sre Pok. Together, they form a transboundary river basin (also known as the 3S RIVER BASIN), which spans across Laos, Vietnam, and Cambodia, and drains into the Mekong. The 3S Basin provides an important contribution to the Mekong in terms of discharge and sediment load, accounting for 17-20% of the river's flow, and 20% of its sediment input (Piman et al., 2013a; Shrestha et al., 2016). As will be explained in more detail below, it also plays a crucial role in terms of aquatic biodiversity, providing habitats and migration routes for fish.

Further south in Cambodia, one of the most outstanding features of the Mekong River Basin can be found - the Tonle Sap system. The centerpiece of this system is the Tonle Sap Lake, a seasonal freshwater lake connected to the Mekong through the Tonle Sap River. It is located in an extensive lacustrine and alluvial floodplain system, in a depression formed by the tectonic dynamics of the Indian an Eurasian Plate. The lake's core characteristic is the seasonal variation of its extent and water volume. During the dry season, it drains into the Mekong via the Tonle Sap River. As the water level in the Mekong rises during the annual Monsoon season, the river's flow reverses and replenishes the lake. Studies estimate that the average extent of the lake's

surface tallies in at about 2,500 km^2 at the close of the dry season, but increases to as much as 16,000 km^2 at the peak of the wet season (Mekong River Commission MRC, 2005; Kummu et al., 2014, 2004; Qu et al., 2018).

The Tonle Sap river flows into the Mekong in Phnom Penh, Cambodia's capital. However, not even a kilometer further downstream, the Bassac River, one of the Mekong's major distributaries, diverges from the main stream. This marks the beginning of the Mekong Delta, which branches out into a network of natural and man-made channels across southern Cambodia and Vietnam. In Vietnam, the Bassac is called the Hau River (alternatively Hau Giang and Song Hau), while the Mekong's main branch carries the name Tien Giang. Further notable distributaries include the My Tho, Ba Li, Ham Luong, and Co Chien Rivers. The delta is also known as the Nine Dragon River Delta (Dong Bang Song Cuu Long), because nine major river channels draw their way through the low-lying expanse of the area (Renaud and Kuenzer, 2012; Quoc Thanh et al., 2019; Liu et al., 2017).

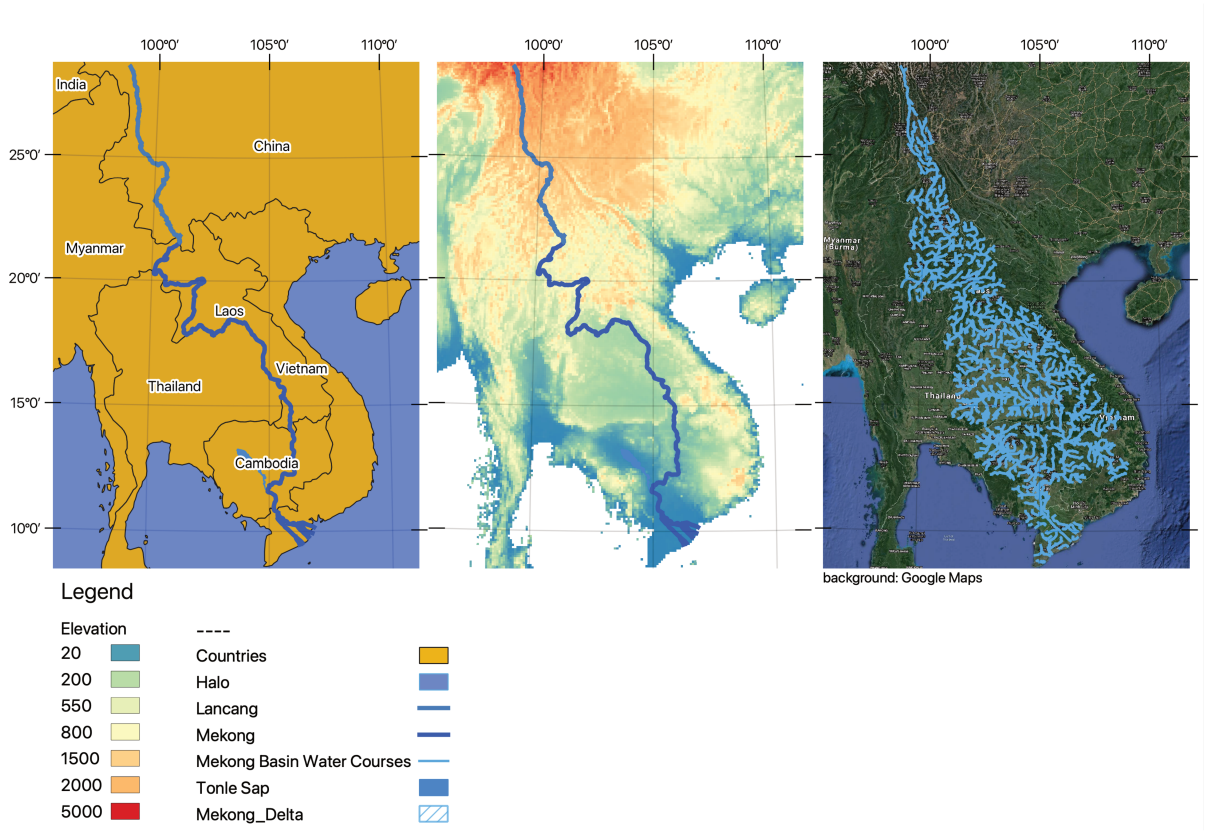

Figure 2.1: An overview of the course of the Mekong and the Lancang throughout Southeast Asia, the elevation of its basin, as well as the extent of water courses draining into the river.

Overall, the Mekong river basin drains a total area of 795,000 km^2. It is divided into the Upper Mekong Basin (UMB), which includes the Tibetan Plateau, the Three Rivers Area, as well as its basin area in Yunnan province and Myanmar. The UMB only contributes an average of 18% of the Mekong's annual discharge, even though it accounts for 23.2% of the river basin's surface area (186,356 km^2) and the first 1,800 km of the river's length (Mekong River Commission, 2019). The reason for this is that tributary systems in the UMB are typically small. During the dry season, however, this contribution is higher, accounting for 45% of river flow. In addition, the UMB also carries major ecological importance for downstream areas, since the the majority of sediment input into the river system originates in this region. However, the UMB's steep riverbed gradients and narrow gorges provide an advantageous framework for the development of hydroelectric infrastructure (Stone, 2011; Hecht et al., 2018). To date, seven dams have been completed on the Upper Mekong, with over 20 more in their planning or construction phase (Stimson Center, 2022). The resulting economic, ecological, and hydrological impacts are explored in further detail below.

The Lower Mekong Basin (LMB) encompasses the Northern Highlands, the Khorat Plateau, the Tonle Sap Basin, and the Mekong Delta. Similar to the UMB, the Northern Highlands provide attractive opportunities for hydropower development. For instance the Xayaburi Dam, which began its operation in 2019, is located in Laos in this area. In contrast, the Khorat Plateau, Tonle Sap Basin, and especially the Mekong Delta are characterised by lower terrain gradients. However, these areas, in particular the Mekong's floodplains in Cambodia and Vietnam, constitute an essential element in the Mekong system in terms of biodiversity and food security. Agricultural productivity in the LMB provides food security for over 90 million people, and the region is home to the world's largest inland fishery (Piman et al., 2013b; Nhan and Cao, 2019). However, both fisheries and agricultural productivity in the LMB depend on established hydrological cycles, which have seen significant changes in recent years.

2.1.1 The Mekong's Traditional Hydrological Dynamics

The Mekong presents a complex systems in terms of hydrology, with high inter- and intra-annual variations in its discharge. The most marked characteristic in terms of hydrology is the annual mono-modal flood pulse in its discharge during the monsoon period, which is typical for tropical

rivers (Junk et al., 1989). The Mekong Basin's climate is fundamentally influenced by the south-west monsoon, with a dry season lasting from December to May, and a wet season lasting from June to November (Mekong River Commission MRC, 2005; Delgado et al., 2012a). Rainfall in the basin is distributed along an east-to-west gradient, with highlands in Laos and Cambodia receiving as much as 3,000 mm of precipitation per year. In contrast, the Khorat Plateau in Thailand can be classified as semi-arid, with annual rainfall amounts of merely 1,000-1,600 mm, and annual rainfall on the Tibetan Plateau can amount to as little as 600 mm. In total, over 75% of the river's discharge is generated by precipitation during the wet season between July and October (Hoang et al., 2019). Dry season flows, in turn, depend on glacial meltwater from the Lancang river basin to a considerable degree, which is why the UMB's contribution to discharge is proportionally higher during the months between December and May.

During the wet season, wide swaths of the LMB, including the Tonle Sap Floodplain and the Mekong Delta in Cambodia and Vietnam, are inundated. This annual inundation, with a flood pulse typically beginning in late June or July, peaking in September, and receding in October and November, forms a major contribution to the high aquatic biodiversity, agricultural productivity, and rich fisheries of downstream systems (Hoang et al., 2018, 2019). The average annual benefits resulting from these regular inundations have been estimated to lie at USD 8-10 billion (Piman and Shrestha, 2017). However, extreme floods also pose a serious risk to the safety of downstream communities. While people in these areas have adapted to regular inundations in their agricultural practices, architecture, and everyday way of life, disproportionately extensive floods can still cause extensive damage to crops as well as infrastructure, and the loss of lives and livelihoods (Heng et al., 2021; Boretti, 2020; Kondolf et al., 2018; Kummu and Sarkula, 2008). The latest of these severe floods occurred in 2011, with one of the highest discharge values ever recorded in the LMB. Typically, these floods can be traced back to the impact of severe tropical storms and cyclones (Heng et al., 2021).

2.1.2 Ecological Importance

Globally speaking, the Mekong's is one of the most biodiverse river basins in the world, beside the Amazon and the Congo (Winemiller et al., 2016). It stretches across a wide spectrum of habitat types and climate frameworks, from arid alpine to tropical lowland and deltaic ecosystems.

Southeast Asia in general is considered a biodiversity hot-spot, characterised by considerable species diversity and high levels of endemism. In fact, this bio-region is home to the highest proportion of endemic and mammal species worldwide, as well as the second-highest proportion of endemic vascular plants (at country level) (Morand and Lajaunie, 2017). Partially, the reason for this is the region's geological and paleoecological history, with tectonic plate dynamics as well as shifting paleo-climatic conditions and sea levels promoting diversification (Claude, 2017)

The ecology and biodiversity of the Mekong Basin is also closely linked to its hydrology, specifically its annual flood pulse. Many ecological processes within the basin's fluvial system follow an annual cycle synchronised with the river's flow dynamics. Consequently, the hydro-biological cycle between terrestrial and aquatic ecosystems equally displays a distinct seasonality (Piman et al., 2013a; Junk et al., 1989).

The way that hydrological dynamics in the Mekong basin influence its biodiversity is best illustrated by looking at its diversity of fish species and their collective behavioural characteristics. While it is generally agreed that the diversity of fish in the Mekong is extraordinary, estimates of species numbers vary wildly. Coates et al. (2003) gives an estimated species number of 1200, while van Zalinge et al. (2004) states that there are over 2000 species to be found in the Mekong. According to Winemiller et al. (2016), the river is home to 599 species, 213 of them endemic. Hortle (2009a) gives a species number of 1100, 850 of which are freshwater fish. He further notes that some of the variations in estimates may well be due to taxonomic shifts, with species being split or lumped on the basis of new analyses, as well as the discovery of new species in the system. Baran et al. (2012), for instance, notes that in the decade between 2000 and 2001, 279 new species were found in the Mekong. However, Hortle (2009a) also notes what he calls "escalation bias", "where a figure is quoted that supports a commonly-held belief (the Mekong has 'high' biodiversity) while ignoring the actual counts of species from the system", which in turn "creates a credibility issue for those seeking to promote conservation of the system's biodiversity, as well as highlighting the practical problems of classification and nomenclature facing those engaged in field studies or management of habitat for fisheries" (p.6).

While the exact estimates of species numbers may vary, some of them buoyed by escalation bias, the overall diversity of the system is not in doubt. As Eyler (2019) aptly summarizes: "Only the Amazon outranks the Mekong in terms of fish diversity, but the Amazon is near twice the

length and its watershed nearly ten times the Mekong's. No river on earth has more migratory fish than the Mekong" (p.11).

The role of the hydrological cycle in sustaining this diversity among fish species is pronounced. For instance, the annual flood pulse creates a wide range of shallow-water habitats on the floodplains of Cambodia and Vietnam, across the Tonle Sap Lake area and in the Mekong Delta. These habitats, with structural elements in the form of submerged vegetation, provide ideal habitats for population regeneration. Many fish species spawn either directly in the floodplains or migrate there in their juvenile phases. As the floods recede, mature fish return to the river mainstream, its distributaries, lakes such as the Tonle Sap, as well as swamps (Halls and Hortle, 2021; Burbano et al., 2020). In addition, the annual flood provides an almost unlimited nutrient base for fish species, which has the capacity to sustain immense population sizes. The floods transfer nutrients from the river main stream to the adjacent floodplains. Simultaneously, mineralized nutrients are released from the inundated soils. In turn, these nutrients form the basis of the growth of periphyton, phytoplankton, and subsequently zooplankton, valuable food resources for fish (Hortle, 2009b). Furthermore, certain fish species continue their growth as long as sufficient nutrient levels are available. Consequently, the Mekong supports some of the world's largest fish species, such as the Mekong Giant Catfish *Pangasianodon gigas* and the giant freshwater stingray *Urogymnus polylepis* (Eyler, 2019).

2.1.3 Socio-Economic and Political Significance

Overall, approximately 66 million people live in the Lower Mekong Basin alone, including almost the entire population of Laos and Cambodia, a third of the population of Thailand, and a fifth of the population of Vietnam. However, population distribution is uneven. For instance, the Upper Mekong Basin is comparatively sparsely populated, excepting Jinghong, the capital of the prefecture of Xishuangbanna, with a population of half a million. Along the majority of the river, small villages and towns form the centers of population, alongside a few large urban capitals like Vientiane and Phnom Penh. In the Mekong Delta, a contrasting situation can be found. Here, the river is bustling with traders and floating markets, and its banks, as well as those of the man-made canals, are lined with continuous rows of houses. Population density in the delta tallies in at 425 people per square kilometer, five times higher than in the UMB

(Eyler, 2019). In recent years, urban centers along the Mekong have seen considerable rates of expansion. Between 2008 and 2017, for example, the population of the Cambodian capital Phnom Penh grew from 1.3 to 2 million people. During the same time span, the population of Vientiane increased by 400%, from 208,000 to almost 800,000 Eyler (2019).

Impressive as these numbers may be, however, the Mekong Basin provides food security for an even larger number of people. Especially the fertile floodplains in Cambodia and Vietnam are hubs of agricultural production. The Vietnamese Mekong Delta, for instance, is the source of 75% of the country's rice production, even though it occupies less than 12% of its land surface (Eyler, 2019). Through exports the Delta provides nutrition for an estimated 200 million people (Minderhoud et al., 2017).

Along the Mekong itself, the majority of the population - especially the rural population - depends on the river for their livelihoods or part of their diet. 40% of the basin's population lives within 15 km of the river's mainstream (Soukhaphon et al., 2021). In the LMB, 80% of the population are small-scale farmers, with an average of 1.8 ha on which to cultivate their crops. They substitute their diet with fish caught for household consumption as well as products from local forests (Carew-Reid and Taylor, 2017). In Cambodia, for instance, 60% of the protein in people's diet comes from fish caught in the Mekong system, including the Tonle Sap Lake and the delta Ahmed et al. (1998). Overall, the Mekong is the most productive system of inland fisheries in the world, with an annual catch of 2.3 million tonnes, at a value of USD 11 billion (Mekong River Commission, 2019). Campbell and Barlow (2020) further note that the economic importance of fisheries in the Mekong basin is likely undervalued due to the fact that a large proportion of the catch is taken in by artisanal and subsistence fishers.

In addition, the Mekong also carries a large political and social importance in the region. Historically, the river has acted as a border in several sections. For instance, it has traditionally delineated the zones of influence of the Vietnamese and Thai kingdoms in Southeast Asia. This delineation has deeply permeated popular conscience. In northeast Thailand, for example, a Thai province bordering the Mekong carries the name of "Loei", which translates as "the beyond" (Eyler, 2019).

In general, political relations in the Mekong Basin are traditionally marked by a large degree of isolation. Historically, overland travel in the area was difficult. In the mid-19th century, for

example, French explorer Henri Mahout noted that a journey by land from Saigon to Luang Prabang in the north of Laos took longer than a voyage by sea from Saigon to Paris (Eyler, 2019). This inhibited trade relations between Southeast Asian countries and limited the sphere of influence of central governments. It also contributed towards the large diversity in ethnicities, languages, and political systems in the region, especially in the mountainous uplands. These latter areas have been described as refuges for ethnic minorities retreating from the expanding influence from the Chinese, Vietnamese, and Thai in the lowlands. Some scholars have even coined a particular term to describe these high-elevation areas of the Mekong Basin - Zomia, used to denote Southeast Asia's mainland massif (Scott, 2009). The social and political diversity of this region is illustrated by official statistics. Yunnan Province in the UMB is the home to 26 of the 56 officially recognized ethnic groups in China. The Laotian part of the Mekong Basin is home to 149 official ethnic groups, whose languages stretch across 8 linguistic families (Eyler, 2019). As Scott (2009) emphasizes, the influence of central governments in this area is traditionally limited, as difficult terrain conditions impede the enforcement of centralist policies as well as the deployment of both civil servants and the military (Giersch, 2010) In the 21st century, technology as well as modern infrastructure projects have done much to bridge the remoteness of the region. However, a considerable degree of isolation from central governance and control remains. For instance, the Golden Triangle is one of the world's hot-spots for the production of illicit drugs - with farmers producing opium and carrying it down narrow mountain paths that provide protection from policing (Luong, 2020).

In addition, tensions exist between upstream- and downstream countries on the Mekong in terms of water management, which are partly due to political and geographical fragmentation having entered into popular consciousness. One of the major points of conflict is the development of hydropower and irrigation infrastructure upstream, which modifies flow and sediment load to the detriment of downstream countries. China, Thailand and Laos have already completed construction on numerous hydropower plants on both the Mekong's mainstream and its tributaries, the consequences of which are already being felt. In addition, Thailand is diverting considerable volumes of water from the Mekong mainstream for large-scale irrigation projects. Furthermore, upstream land management practices, especially deforestation have negative downstream impacts (cf. Section 3.4.1.7).

To a certain degree, this conflict stems from a lack of awareness. For example, in China

the Mekong also carries the name Lancang or Lancang Jiang River, as noted above. This terminological discrepancy has led to some confusion, as many people in China were not aware until relatively recently that the Mekong and the Lancang were, in fact, the same river. This cognitive disconnect is exemplified in a 2006 documentary, *Where Have All the Fish Gone*, which examines the effects of hydropower construction on the Lancang. Here, a Chinese diplomat goes on record to say that he fails to understand the preoccupation of downstream countries with developments on the Lancang river - since they cannot affect the Mekong, as they are two different rivers (Eyler, 2019).

However, over the past decades, the conflicts over water management have thrown into sharp relief the need for intergovernmental coordination in the region, and have increased the awareness of the Mekong as one complex, interconnected system. Attempts at coordination and mediation between Southeast Asian countries exist, most notably in the form of the Mekong River Commission (cf. Section 2.1.5). Nonetheless, tensions persist, as each country prioritizes its own interests in the face of the fast economic growth in the region.

2.1.4 Pressures on the River: Between Climate Change and Economic Development

In recent years, the pressures that the Mekong River has faced have been manifold. They range from the development of hydropower infrastructure and destructive practices such as riverbed mining, over the cascading effects of changing land practices, to more large-scale shifts in precipitation and temperature patterns over the basin due to global change. The effects of these pressures, acting in tandem on the river system, partially balance and partially magnify each other (Hecht et al., 2018).

2.1.4.1 Hydropower Development

One of the most widely-studied drivers of change on the Mekong is the development of hydropower dams, especially upstream in the Chinese part of the basin, and in Laos, where the Mekong's mainstream passes through narrow gorges, which offer ideal conditions for dam

construction from the point of view of geotechnics and civil engineering. Overall, the Mekong Basin has a cumulative potential for hydropower generation of 268,000 GWh/year. Currently, approximately half is being exploited, and the basin has sometimes been referred to the "battery of Southeast Asia" (Schmitt et al., 2019). At the moment, eleven dams are operating on the Mekong's mainstream, and 130 on its tributaries. A further 36 are currently being constructed, and a further 291 are in their planning stages, though both planning and construction on some has been delayed by the COVID-19 pandemic and its various economic consequences (Stimson Center, 2022). In addition to hydropower generation, many dams also fulfill a water provisioning role for agricultural systems. Water from their reservoirs is diverted for irrigation purposes during the dry season (Hecht et al., 2018).

Dam construction in the Mekong basin began in the 1960s. In November 1965, the first hydropower dam in the region was opened - Nam Pung Dam, in the Sakon Nakhorn Province in northeastern Thailand. This was followed by a series of other dams throughout Thailand and Laos. However, hydropower dam development was slowed by the Cold War throughout the 1960s, 70s, and 80s. It was only in the early 1990s, that hydropower infrastructure development sped up, with construction commencing on the Pak Mun Dam on the Mun River in Thailand in 1990. The first dam on the Mekong's mainstream was completed in 1993 in China - the Manwan Dam. Towards the end of the 1990s, dam construction was once more slowed due the the 1998-99 Asian financial crisis, which led to a decrease in demand for hydropower (Jacobs, 2002; Soukhaphon et al., 2021). After the turn of the millennium, construction began once more in earnest, with more ambitious, large-scale projects, and at a greater speed. In 2008, the Mekong basin was still one of the least regulated in the world, with the total active storage capacity of hydropower stations along its main course and tributaries amounting to a mere 2% of its annual discharge, at 8.6 km^3. In the late 2010s, however, several large reservoirs, many financed by Chinese investors, began to impound and commence hydropower generation. By 2025, active reservoir storage is expected to increase tenfold in comparison to its 2008 value, to over 86.8 km^3 (Hecht et al., 2018). In the UMB, the economic value of hydropower is estimated at an annual USD 4 billion, while an MRC Council Study (Mekong River Commission, 2018b) estimates gains from hydropower development to tally in at a cumulative USD 160 billion by 2040 in the LMB.

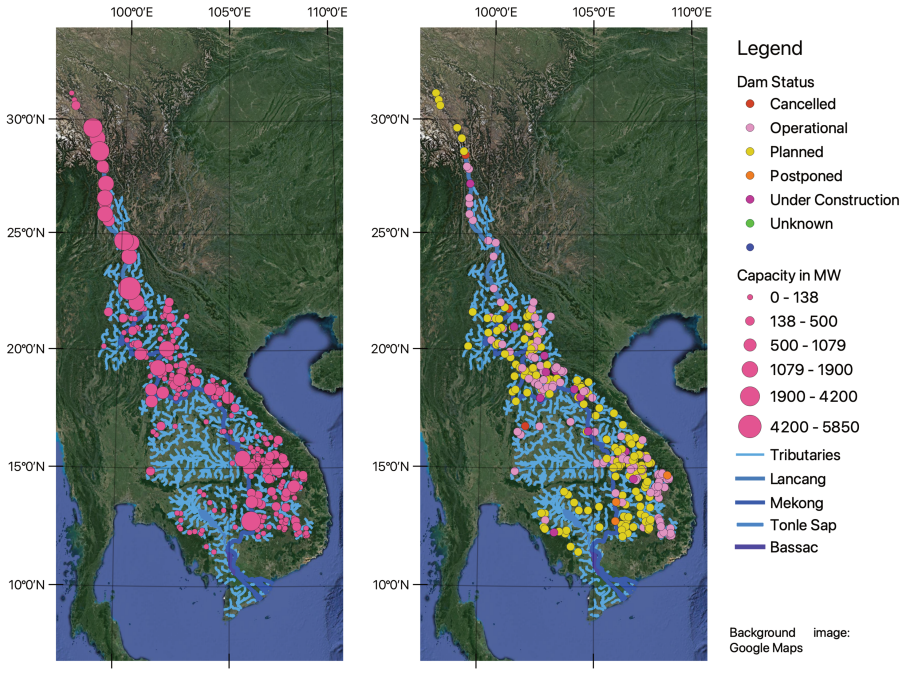

Figure 2.2: Distribution of dams in the Mekong basin, by status (right) and capacity (left). Data courtesy of the Stimson Center Mekong Dam Monitoring Project

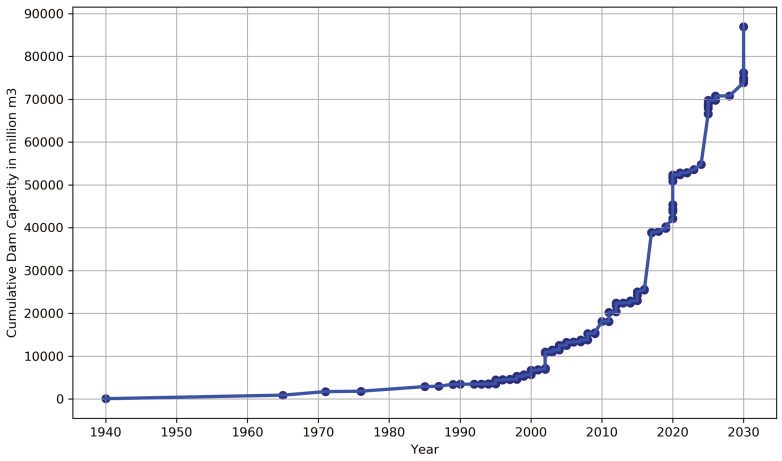

Figure 2.3: Cumulative capacity of dams on the Mekong and its tributaries since the 1940s. Data courtesy of CGIAR.

The negative impacts of hydropower construction on the riverine ecosystem have been detailed extensively. Flow modifications are of primary concern, with a general consensus that hydropower development decreases average wet season flows and increases dry season flows. Hoang et al. (2019) predict dry season flows to double as a result of hydropower development,

and flows during the wet season to decrease by 16% by 2050 on the Mekong mainstream. In Räsänen et al. (2017) already reported an increase in discharge of 121–187% during the peak dry season in northern Thailand, while wet season discharge decreased by 32–46%. Many studies have also examined the effects in tributary systems, such as the 3S river basin. Here, Piman et al. (2016) project a 98% increase in dry season flows if seven large proposed dams are built. In the lowland areas, Dang and Tran (2016) projects an increase in dry season water levels by up to 70% and a decrease in wet season water levels by up to -6%.

In addition, the numerous dams on the Mekong's main stream and its tributaries reduce the sediment load in the river, with negative impacts for downstream areas, especially the river's deltaic floodplains. Bussi et al. (2021) predict that dams will reduce the sediment flux to the Mekong Delta by 50% under the most realistic development scenario in the next twenty years. Kondolf et al. (2014) even found that if all currently planned dams are constructed to their full capacity, 96% of sediments that would usually reach the delta to be deposited on its floodplains would remain trapped in reservoirs. This is expected to have pronounced adverse effects on ecosystems and agriculture in the delta, which depend on the nutrient input from sediment deposition during the annual Monsoon inundations. For instance, phosphorus concentrations are projected to decrease by 47 to 53% and nitrogen concentrations between 57 and 62% (Piman and Shrestha, 2017).In addition, a lack of sedimentation can pose an existential threat to the delta, which is facing both land subsidence and sea level rise (Minderhoud et al., 2019).

Furthermore, hydropower dams have more immediate negative effects on ecosystems and individual species. As mentioned above, the majority of Mekong fish species are migratory. Hydropower infrastructure disrupts the river continuum and cuts numerous species off from their spawning grounds. For instance, Laos' Xayaburi dam, with a capacity of 1285 MW, has been criticised for imperiling the migratory route of the Mekong Giant Catfish and the Giant Pangasius Catfish. Moreover, hydropower dams reduce the nutrient levels in the water, as outlined above, thus restricting the nutritional basis available for aquatic species (Yoshida et al., 2020; Campbell and Barlow, 2020). While some projects have taken measures to mitigate these negative impacts on aquatic species, many of them have fallen short. For example, at the Pak Mun Dam on the Mun River in Thailand, a fish ladder was added after the construction of the actual dam had been completed. It was reportedly poorly designed and unsuccessful in allowing larger numbers of fish to migrate upstream (Baird et al., 2020). According to the Mekong River Commission, the

negative effects from hydropower infrastructure could lead to a decline of fisheries by 2040 that could cost a cumulative USD 23 billion (Soukhaphon et al., 2021).

Finally, hydropower infrastructure has also had negative impacts on the communities living in their immediate vicinity, as well as cascading upstream and downstream effects. Entire communities have been resettled to create space for dam construction, some of them to unsuitable areas. Fish yields have fallen considerably in many places due to the disruption of aquatic ecosystems, threatening food security. Water quality, too, has reportedly declined in many areas adjacent to dams. For example, in the area of the Yali Falls Dam, villagers have reported negative health impacts linked to poor water quality, including stomach infections, rashes, and eye irritations. In 2009, toxic blue-green algae were found in the dam's reservoir (Yoshida et al., 2020).

2.1.4.2 Land Use Change

Another factor that is causing major shifts in the hydrology of the Mekong basin and, by extension, its delta, is land use and land cover (LULC) change. As the economy of the Mekong sub-region grew in the course of recent decades, traditional land use patterns have been succeeded by new uses, many of them causing a cascade of consequences that manifests large-scale impacts on hydrological processes.

The most evident and widely-studied instance of land use change in the Mekong Basin is deforestation. The entirety of the Mekong region has seen high rates of deforestation for the past six decades. Hirsch (2010) noted that between the early 1960s and the late 1990s, Thailand lost half of its forest cover, while Laos' decreased from covering two thirds of the country's surface to one half. Furthermore, Vietnam lost two million hectares of forests during the Second Indochina War alone, due to concerted chemical deforestation operations and bombings by the US Air Force. Lacombe and Pierret (2013) note that even thirty years later, in 2002, degraded forest still covers those areas that were bombed heavily during the war. In Cambodia, one of the highest rates of deforestation has been observed, especially with the beginning of unregulated logging operations after the collapse of the Khmer Rouge Regime. Lohani et al. (2020) note an overall forest loss of 19% in the country since 1993. The same study furthermore found that the

rate of loss is increasing, doubling its pace after 2011. In the entirety of the LMB, Leinenkugel et al. (2015) 2015 find an annual forest loss rate of 0.4% between 2001 and 2011. Potapov et al. (2019) find that between 2000 and 2017, 9.4% of the region's overall forest cover disappeared, but that 16.6% of forests extant at the end of this period were stand replacement following reforestation. This study too highlights the particularly high rate of forest loss in Cambodia, at 22.5%. According to a report by the FAO (Costenbader et al., 2015), the major driving factors of forest loss in the region are agricultural expansion, especially high-value cash crops such as oil palms and cocoa, the construction of infrastructure such as dams and roads, the extraction of resources like minerals and gas, unsustainable and unregulated logging practices, and forest fires. However, the predominance of these factors in the loss of forests, as well as the rates of that loss exhibit a large spatial heterogeneity.

Overall, the effects of this change in land cover are far-reaching, especially in hydrological terms. Forests regulate processes such as water flow and infiltration, they impact the dynamics of seasonal flooding, as well as nutrient cycling. Generally, forest loss decreases evapotranspiration and thus increases the annual basin water yield, alongside erosion. However, when forests are converted to intensive cropland, the reverse can be the case, with increased evapotranspiration fuelled by irrigation decreasing the overall water yield (Netzer et al., 2019). Ultimately, LULC developments are one of the largest uncertainty factors in the future hydrological developments in the Mekong Basin. For instance, Shrestha et al. (2017) compares three different LULC scenarios and their impact on the future hydrological development of the 3S Basin. The results indicate major variations between scenarios, with a decrease in annual streamflow ranging between 3 and 22% and a change in annual sediment load varying between -8% and +249%.

2.1.4.3 Climate Change

Climate change is another significant driver of change in the Mekong Basin, with the impacts of shifts in temperature and precipitation already evident in various manifestations across the region, and more severe effects forecast for the medium- to long-term future. In fact, the LMB has been identified as one of the regions most vulnerable to climate change on a global basis (Mercado and Asia Times, 2021; Eyler, 2019)

The most immediate impact of climate change across the Mekong basin lies in the increase in average temperatures throughout the year. Projections see an overall increase in temperatures between 0.4 °C and 3.3 °C across the basin by the year 2060 (Mekong River Commission, 2021; IPCC, 2013).

In addition, precipitation patterns are changing as well, with high-intensity rainfall events becoming more frequent and the temporal and spatial distribution of rainfall shifting. Whether the overall development of rainfall patterns is towards increased or decreased annual rainfall sums varies according to which climate scenario is being analysed, with some projections predicting an average decrease of 16% while others prognosticate an increase of 17% (Mekong River Commission, 2021, 2018b)

These changes are likely to cause a riptide of effects for ecosystems, agriculture, and human settlements (Johnston et al., 2020; Trisurat et al., 2018; Try et al., 2020). To compensate the adverse impacts, adaptations in agricultural practices such as technological improvements in irrigation systems will be necessary. Furthermore, economic effects on sectors such as hydropower production and navigation are to be expected (Mekong River Commission, 2018a). More fundamental impacts are also expected on processes such as soil erosion, with increases of up to 17% predicted by 2060, and flooding in the deltaic areas (cf. Chapter 2.2.3.1) (Mekong River Commission, 2021).

Part of the reason for the severe effects of climate change on the Mekong region is that it is not only regional processes that are fundamentally altered. Large-scale ocean-atmospheric processes such as the El Niño Southern Oscillation (ENSO), the Indian Ocean Dipole (IOD), and monsoon cycles impact hydroclimatic conditions in the Mekong Basin (Mekong River Commission, 2021; Kiem, 2017).

A final aspect of the impact of climate change on the hydroclimatic development of the Mekong basin that needs to be mentioned at this point is that the effects of several of the processes described thus far counteract each other. For instance, Yun et al. (2020) found that climate change in the basin would increase flood magnitude by 14% and flood incidence by 45%, while hydropower development would decrease them by 16% and 36% respectively.

2.1.5 The Mekong River Commission - Between Governance and Mediating Conflicting National Interests

As outlined above, many conflicting interests are related to the development of the Mekong region, with upstream valorisation often infringing on the potential benefits of downstream riparian states.

To mediate conflicts arising from this field and provide support for sustainable development and management, the Mekong River Commission (MRC) was founded in 1995 by LMB countries - Cambodia, Laos, Thailand and Vietnam (Piman et al., 2013a). Its stated aim is to "promote, support, cooperate, and coordinate in the development of the full potential of sustainable benefits to all riparian states and the prevention of wasteful use of the Mekong River Waters." Its mandate includes various sectors, encompassing agriculture (especially irrigation), climate change adaptation, drought monitoring, fisheries, flood control, hydropower, and navigation (Mekong River Commission MRC, 1995).

Over the past twenty-seven years, the MRC has evolved into a well-established independent intergovernmental body coordinating the exchange of knowledge and resources across the LMB. It regularly releases *State of the Basin* reports to outline the main development advances and challenges facing the Mekong, it maintains large-scale hydrological models predicting the future of the river, and it provides a central point of access to extensive data on the Mekong system for parameters ranging from water levels and river discharge to evapotranspiration, sediment load, and zoo-plankton abundance [1].

However, the MRC has also faced harsh criticism in the past, with some even seeing it as a wholly "failed institution" due to its lack of success in preventing unsustainable dam projects from posing a threat to communities and ecosystem services (Eyler, 2019). Principally, this is due to the MRC's limited institutional reach. It lacks the power to overrule member states, as well as mechanisms to resolve disputes between stakeholders. Furthermore, the fact that key riparian countries like Myanmar and China are not members of the MRC impedes its reach (Cronin et al., 2016; Hirsch et al., 2006; Suhardiman et al., 2012).

[1] Information is available via the MRC's Data Portal and has been used extensively in the analyses for this thesis, see Figure 2.4

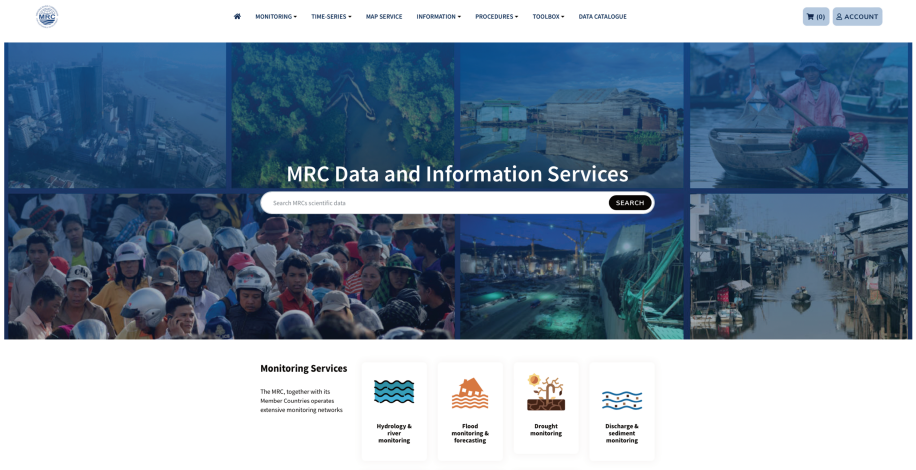

Figure 2.4: Online view of the MRC data portal, providing access to a wide variety of data.

International disenchantment with the MRC's work found financial expression in 2016. To a large degree, the MRC depends on financial support from international donors such as the World Bank, the Asian Development Bank, the Swedish International Development Agency, and the Australian Agency for International Development. According to its 2012 Annual Report, over 90% of the MRC's annual budget stems from these sources (Mekong River Commission, 2014). However, after the organisation failed to sway Laos on the question of constructing the Xayaburi and Don Sahong Dams on the Mekong mainstream, donors scaled back their contributions significantly. Where international donors provided $115 million for the 2011-2015 funding period, this budget fell to a mere $53 million for the period 2016-2020, forcing the MRC to restrict its operations and its staff (Kossov et al., 2016; Kossov and The Phnom Penh Post, 2016; Hunt, 2016).

For the 2021-2025 funding period, the MRC has seen significant contributions by the US (Sochan and The Phnom Penh Post, 2021), Australia, Germany, and Switzerland (Sivutha and The Phnom Penh Post, 2021b), as well as Japan (Khmer Times, 2021). Nevertheless, criticism persists. Specifically, the MRC's failure to urge the postponement of planned hydropower dams even in the face of the climate crisis and documented detrimental effects on food security, agricultural productivity, and fisheries has been noted (Mercado and Asia Times, 2021).

2.2 The Mekong Delta: A Hub of Human Activity, Hydrological Dynamics, and Biodiversity

The delta of the Mekong, which fans out across southern Cambodia and Vietnam, is one of the most productive areas in the world in terms of agriculture and fisheries. This region of fertile alluvial soils has been a hub of human activity for millennia. Currently, it is home to over 19 million people, and 10,000 km^2 of rice paddies. However, the Delta is also facing a wide array of challenges, ranging from population pressure and soil acidification to changes in the Mekong's runoff regime and thus the annual monsoon inundations (Stewart and Coclanis, 2011). In that, it is epitomatic of the threats looming over (tropical) deltas worldwide, especially those seeing intensive agriculture (Szabo et al., 2016; Renaud et al., 2013; Loucks, 2019).

This section outlines the characteristics of the Mekong Delta, with a particular focus on its Cambodian part. It gives an overview of the Delta's geographical location, its geology and pedological characteristics, and its value in terms of biodiversity. Then, it proceeds to review the recent literature available on the Delta's hydro-geological dynamics and its socio-economic development. Finally, the various challenges affecting the Mekong Delta as a whole are outlined.

2.2.1 Geographical Location

The exact delineations of the Mekong Delta vary, but it takes its origin at the Cambodian capital, Phnom Penh. Here, the Tonle Sap river flows into the Mekong. Only a few kilometers downstream, the Mekong's first distributary, the Bassac river, diverges from the mainstream, marking the start of the delta (Renaud et al., 2013). It then stretches across the southern Cambodian provinces of Takeo, Kandal, and Prey Veng, as well as the Southern Vietnamese provinces of An Giang, Bac Lieu, Ben Tre, Ca mau, Dong Thap, Hau Giang, Kien Giang, Long An, Soc Trang, Tien Giang, Tra Vinh, Vin Longh and Can Tho City.

Overall, the Mekong's catchment area spans 760 000 km^2. Its delta stretches over circa 55 000 km^2 (Mekong River Commission MRC, 2005), 40 000 km^2 of which are in Vietnam (Stewart and Coclanis, 2011). In terms of area, the Mekong Delta is the third largest deltaic plain in the world, after the Amazon and Ganges- Brahmaputra Deltas (Coleman and Roberts, 1989).

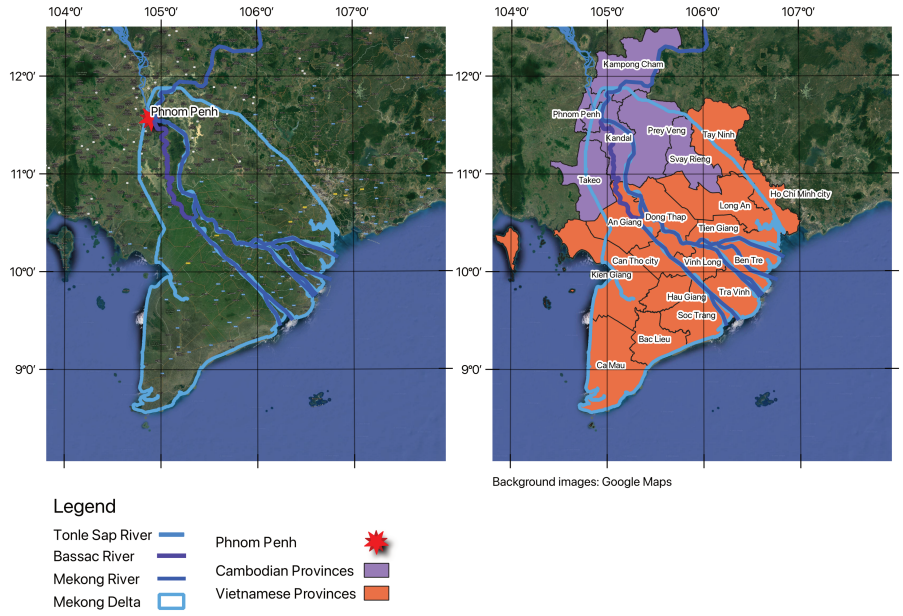

Figure 2.5: Overview o the Mekong Delta and the Provinces of Cambodia and Vietnam that form part of it.

2.2.2 Geology and Pedological Characteristics

The Mekong Delta's rich alluvial soils, nourished by annual sediment deposits during the monsoon floods, are the basis for its considerable productivity and biodiversity. However, the delta's geology and pedology also contribute to the challenges the region is facing today, for instance in terms of subsidence and arsenic contamination. It is therefore useful to gain insights into how the delta developed and what its most dominant hydro-geological and pedological features are.

The formation of the Mekong Delta began about 7,500 years ago during the Holocene period as a result of decelerating post-glacial rates of sea level rise (Stanley and Warne, 1994; Bird et al., 2010; Hanebuth et al., 2012). Stratigraphic studies of over 20 deep boreholes in the deltaic plain (Hanebuth et al., 2012; Tamura et al., 2012a,b) indicate that ca. 4,800 years ago, sea level regression commenced along the delta front, signalling the beginning of the development of a subaerial delta.[2] From this point onwards, the center of sediment deposition shifted seaward,

[2]Subaerial deltaic areas are above water. They typically consist of the upper deltaic plain, including migratory channels and lacustrine deposits, and the lower delta plain with bay-filled deposits (Coleman and Roberts, 1989).

initiating delta progradation[3]. Since the beginning of its formation, the Mekong Delta has prograded over 220 km into the South China Sea, at an average long-term rate of 30 m per year (Hanebuth et al., 2012). In deeper sediment layers, however, evidence of earlier subaqueous[4] phases of delta development are still evident. The current coastal zone of the Mekong Delta as well as its subaqueous section have been formed over the course of the last 1,000 years. In comparison to other deltas in the wider region, such as that of the Yangtze, the Pearl River, and the Red River, these are relatively young deltaic forms (Liu et al., 2017).

In terms of sediment typology, the Holocene sediment deposition left behind largely unconsolidated, fine-grained, clayey sediments (Zoccarato et al., 2018). These sediments contain arsenic (As), bound in Fe(III) (oxyhydro)oxides. Problematically, geohydrological conditions in the Mekong Delta promote dissimilatory reductive dissolution of these Fe(III) complexes, coupled with the anaerobic oxidation of organic matter, and thus the release of geogenic As into the groundwater contained in the Mekong Delta's alluvial aquifers (Stopelli et al., 2020). This is problematic since these aquifers are the main source of water supply in the Mekong Delta, for household consumption as well as agricultural activity and industry (Duy et al., 2021) (see Chapter 2.2.3.3).

As for the soils of the Mekong Delta, there are three main types: alluvial, acid sulfate, and saline. The first of these, alluvial soils, tend to be located along main rivers and cover approximately 31% of the delta. These are the most agriculturally productive soils. In contrast, acid sulfate soils are acidic and only possess limited fertility. They make up ca. 41% of the delta. The third type, saline soils, covering ca. 19% of the delta, are located in areas where the water table is low, and saline intrusion during the dry season is frequent (Torell and Salamanca, 2003). In terms of international soil classifications, the soils in the Mekong Delta correspond to Fluvisols, Gleysols, Luvisols, Acrisols, Arenosols and Plinthosols according to the World Reference Base system, and to Entisols, Inceptisols, and Ultisols of USDA Soil Taxonomy system. As for mineralogy, the dominating clay mineral is muscovite in more recent alluvial soils and kaolinate in old alluvial soils (Nguyen et al., 2015).

[3]Progradation is the process in which a river supplies sediment to coastal and shelf areas in faster than marine processes can disperse it. Consequently, regressive sedimentary deposits begin to form(Coleman and Roberts, 1989).

[4]The subaqueous parts of a delta lie below low-tide elevation and extend towards deeper marine areas. River sediments are deposited until depths of 300 m and over a width of up to several tens of kilometers. (Coleman and Prior, 1982)

2.2.3 Overall Hydro(geo)logical Dynamics

As mentioned above, part of the reason for the Mekong Delta's fertility and productivity comes from the periodic deposition of sediments during the annual monsoon inundations. This illustrates the large significance of hydrological dynamics for the economic and ecological lifeblood of the area. In addition to sediment deposition, groundwater recharge is an important process linked to this defining feature of the Mekong Delta's hydrology.

2.2.3.1 Annual Monsoon Inundations

Every year during the flood season, which typically lasts from July until November, considerable swaths of the delta are inundated. This is the result of the Mekong and its distributaries overtopping their banks and inundating the floodplains. The exact extents of inundations vary inter-annually.

According to Toan (2014) 35-50% of the Vietnamese Delta is flooded every year, with inundations reaching depths of up to 4.0 m, and lasting for three to six months. Dinh et al. (2019) found that in the hydrological year 2016/2017, flood extents rose consistently starting at the beginning of August, with 25-30% of the Delta inundated by September, and 46% at the flood peak in mid-October. This study further underlined that Vietnamese Provinces most affected by inundations were An Giang, Dong Thap, Long An, Kien Giang and Can Tho. The reason for this, Dinh et al. (2019) postulate, is that inundations emanate principally from the main branches of the Mekong centered in these provinces. Other studies record far smaller overall flood extents in the delta. Kuenzer et al. (2013), for instance, found a maximum flood extent of 13.4% of the delta area for the 2007 wet season.

It must be noted, that these annual monsoon inundations are not the only type of flood in the Mekong Delta. In fact, previous research has identified three more flood types in the region (Delgado et al., 2012b; Tri, 2012; Apel et al., 2012). The first of these results from the artificial distribution of flood waters via an extensive network of canals regulated through control structures such as sluice gates and dykes. The second additional flood type is the result of extreme local precipitation events. Floods of the third type in the coastal provinces and result

from high tides during storms. Kuenzer et al. (2013) notes that most floods in the delta are a result of a combination of these flood types. However, it must be noted that this is only true for the Vietnamese part of the Mekong Delta. In the Cambodian part, no coastal areas are present, and the dense system of hydraulic infrastructure that characterizes the landscape of the Vietnamese Mekong Delta is absent here. Nonetheless, short-term inundations can also result from heavy precipitation on the Cambodian side of the border.

In itself, the impact of the Vietnamese system of dykes and gates on flood and sediment dynamics has been the subject of scientific interest. Triet et al. (2017) found the dyke system to impact flood dynamics downstream, increasing flood hazards due to the risk of dyke breaks. This study found an average increase of 9–13 cm in water levels at flood peak in the central Delta, and an increase in duration of 15 days. Duc Tran et al. (2018) noted that upstream dyke systems increase peak water levels in areas located in the downstream reaches of the delta. Furthermore, Quoc Thanh et al. (2019) found that the network of dykes also led to a decrease in minimum water levels and impacted tidal fluctuation on the Mekong's main branches.

Another aspect of the flood dynamics in the Mekong Delta that needs to be highlighted is that inundations do not only carry positive implications. In general, the local population, especially those working in the agricultural sector, are adapted to and even dependent on the annual inundations. However, when these inundations deviate from their usual patterns, they can cause serious damage and loss of life and livelihoods. For example, if inundations arrive sooner than anticipated, they can damage crops that have not yet been harvested (cf. Section 4.3.4). If floods have a higher magnitude than usual, they can damage infrastructure, from hydraulic control structures to farmsteads (Hoang et al., 2018). For instance, the historic 50-year flood in 2000 resulted in estimated economic losses in excess of US$ 200 million (Cosslett and Cosslett, 2014).

2.2.3.2 Sediment Dynamics

As outlined above, one of the main benefits of annual inundations in the Mekong Delta is the deposition of nutrient-rich sediments, which enhance the fertility and productivity in the region. Historically, in its unregulated state, the Mekong transported 160 Mt of suspended sediments

annually (Bussi et al., 2021). A considerable percentage of this sediment load would eventually be deposited on the floodplains, as flow velocities decreased or ceased entirely during inundations. In the early 2000s and 2010s, Hung et al. (2014) described an average annual deposition of 6.86 kg/m^2 in Tam Nong district in Dong Thap province of the Vietnamese Mekong delta, which corresponds to approximately 6 mm in depositional height.

However, the amounts of deposited sediments in the Delta have been continuously declining for several decades. Upstream hydropower development on the mainstream is one of the reasons for this development, as sediments become trapped in reservoirs. Another factor is the further development of hydraulic infrastructure in the Vietnamese part of the delta. For instance, Manh et al. (2014) note that the rates of sediment deposition on floodplains of the Cambodian delta is up to six times higher - from 19 to 23% of the annual sediment load recorded at the Kratie measurement station maintained by the MRC - rather than the 1 to 6% deposited in the heavily enclosed floodplains in Vietnam.

According to Manh et al. (2015), the combination of various drivers will significantly decrease the Mekong's sediment load until the middle of the century. A comparison of scenarios revealed that even median changes would result in an overall decrease in floodplain sedimentation by 40%. Maximum-change scenarios in all drivers would lead to a 95% reduction in the rates of sediment deposition in the delta. Similarly, Bussi et al. (2021) note that the decline in suspended sediment flux would reach 50% at the apex of the delta if all currently planned hydropower projects on the Mekong were built.

2.2.3.3 Groundwater Dynamics

In the Mekong Delta, groundwater is an important resource, especially during the dry season, serving as a basis for household water supply as well as for irrigation in agriculture. Typically, people use private tube-wells to access ground water, with more than 1 million of these shallow wells reported across the delta (Danh and Khai, 2015). Their depths reach 80-120 m. In addition, there are groundwater abstraction wells penetrating into depths of 200-450 m, which belong to official water supply plants. In total, daily groundwater abstraction was estimated at 2.5 million m^3 in 2015 (Minderhoud et al., 2017; Duy et al., 2021).

The source for these groundwater abstractions is a multi-layered aquifer system in the Delta's alluvial basin. Due to the various stages of sediment deposition during the formation of the delta, the stratigraphy of the aquifers is complex. Furthermore, there are older stratigraphic units under the deltaic forms of the Holocene, with aquifers dating back to the Pleistocene, Pliocene, and Miocene (Wagner et al., 2012). According to Duy et al. (2021), these aquifers, composed of sand and gravel, form four layers, separated by aquitards consisting of silt and clay, at depths of 0-49 m, 31-193 m, 153-381 m, and 275-550 m. Broadly, the hydraulic conductivity of the aquitards lies at 3-40*10^2 m/s, while the aquifers exhibit a hydraulic conductivity of 1-20*10^2 m/s (Wagner et al., 2012; Minderhoud et al., 2017; Hung Van Pham et al., 2019).

Past studies have found shallow groundwater dynamics to be closely linked to the river system and to inundation dynamics in the floodplains. Kazama et al. (2007) found that reductions in inundation extents lead to severe reductions in groundwater storage in the Cambodian part of the Mekong Delta. Modelling three flood seasons, the authors found that a 19% decrease in inundation areas in 1993 led to a 31% reduction in groundwater storage. For 1998, these numbers were 44% and 42% respectively. In contrast, deeper groundwater layers in the Mekong Delta are relatively uninfluenced by surface water dynamics. Hung Van Pham et al. (2019), for instance, found that most fresh groundwater in the Mekong Delta was recharged 60,000 - 120,000 years ago. During this time, sea levels were relatively low and top layers exhibited high hydraulic conductivity. However, during the Holocene a clayey sedimentary layer was deposited that now inhibits groundwater recharge of the deeper aquifers.

Groundwater management efforts in the Mekong Delta, especially in Vietnam, have been disparate over the past few decades, leading to overexploitation, which, in turn, causes a cascade of negative impacts (Renaud and Kuenzer, 2012; Danh and Khai, 2015; Wagner et al., 2012). One of the consequences has been a decline in groundwater levels, with average rates of decline ranging between 0.01 and 0.55 m/year over the past twenty years (Duy et al., 2021; Erban et al., 2014). Another effect is land subsidence. To a certain extent, subsidence in deltaic areas such as the Mekong Delta is natural. Due to the overburden of the gravitational load, underlying sediments are compacted through pore collapse. However, this process is accelerated significantly by aquifer depletion as a result of groundwater exploitation. Pores that were formerly filled by groundwater are exposed to compaction, leading to increases in subsidence rates. In their landmark 2017 study, Minderhoud et al. (2017) found that the Mekong Delta sank by an average

18 cm over the past quarter century. Furthermore, the authors highlight that subsidence rates have been increasing, with average rates currently at 1.1 cm per year, and peak rates at 2.5 cm per year.

2.2.4 Socio-Economic Factors

The Mekong Delta carries an economic importance in both Cambodia and Vietnam that is disproportionate to the relative surface area it occupies in either country. The Delta's high agricultural productivity has even earned it the moniker of being the "rice bowl" of the region. In fact, the Mekong Delta is a globally important source of rice, shrimp, and Catfish exports (Olson and Morton, 2018).

The Mekong Delta contributes 75% of Vietnam's total production in the sectors of agriculture, fisheries, and forestry. Furthermore, 50% of the country's agricultural exports come from the Delta, in particular 90% of its rice exports (Liao et al., 2016). In fact, the Vietnamese Mekong delta contributes a total of 15% to global rice exports, accounting for 5.7 million tons of milled rice in 2018, and exceeding a value of 2.5 $ billion (Quyen et al., 2018). In Cambodia, agriculture makes up 23.5% of the country's total GDP, with over 33% of the working population employed in the sector (National Institute of Statistics, 2020). Cambodia's total rice production in the 2019–20 season reached 10.9 million metric tons, slightly lower than the previous season's harvest due to unfavourable weather conditions. Average yield per hectare lay at 3.09 metric tons (World Bank, 2021). In Vietnam, agriculture accounted for 15% of the GDP. Fisheries comprise 10-15% of Vietnam's GDP in the Agricultural, Fishery and Forestry Sector. In Cambodia, fisheries account for approximately 10% of GDP (Yoshida et al., 2020).

Furthermore, it must be noted that for the population of the Mekong Delta, agriculture and fisheries play a key role in ensuring livelihoods. Even if their primary economic activities lie elsewhere, such as in garment manufacturing or tourism, many people fish and maintain agricultural activities to meet household needs. Furthermore, economic activities have become diversified, with many people moving away from full-time farming and towards seeking employment in industries such as tourism and construction. However, part-time agricultural activities are often maintained (Vandôme, 2020). In Cambodia, for instance, 67% of families living on the Mekong

floodplains who have agricultural holdings report that agriculture makes up a higher or similarly high percentage of their household income as other economic activities (World Bank, 2021).

2.2.5 Biodiversity and Conservation

Despite being, as outlined above, heavily modified by human activity in terms of land cover and hydrology, the Mekong Delta can still boast substantial levels of biodiversity. Significant mammals from the point of view of conservation include the Hairy-nosed Otter (*Lutra sumatrana*), the Small Clawed Otter (*Aonyx cinerea*), and the Dugong (*Dugong dugong*) (Campbell, 2012).

Furthermore, the wetlands of the delta serve as an important habitat for numerous species of birds. Buckton and Safford (2004) reviewed the avifauna of the delta between 1988 and 2004 and found a total of 247 bird species, half of which can be considered wetland-dependant, and twenty of which were listed globally as threatened or near-threatened. Species of interest include the South-East Asian Sarus Crane (*Grus antigone sharpii*), the Indian Cormorant (*Phalacrocorax fuscicollis*), and the Little Cormorant (*Phalacrocorax niger*).

In terms of fish biodiversity, approximately 460 species can be found in the Mekong Delta. As noted above, the Mekong River is the second most biodiverse riverine habitat in the world, after the Amazon. The Delta contributes a large share of this biodiversity, as both freshwater and marine species are present here. The predominant species groups are carps, barbs, minnows (cyprinids), and gobies (gobiids). Furthermore, four endemic species can be found in the Mekong Delta: the Dwarf Catfish (*Akysis filifer*, the Mekong Sea Catfish (*Hemipimelodus daugueti*), the Mekong Goby (*Stenogobius mekongensis*), and the Mekong Blind Sole (*Typhlachirus elongates*) (Tran, 2016; Vidthayanon, 2008).

In terms of vegetation it must be noted that many natural habitation types such as natural grasslands, sedge-lands, and regularly flooded forests have been replaced by agricultural areas or destroyed during the Vietnam War. For instance, data from the 1950s documents approximately 200,000 hectares of Mangrove forests in the Mekong Delta, most of which were destroyed by exfoliants during the 1960s and 70s (Tran, 2016). Since the end of the war, conversion into rice paddies and shrimp aquaculture has led to a further reduction of these habitats, which is particularly detrimental since they have a high floristic diversity (Truong and Do, 2018; Duke,

2013).

Nevertheless, some notable vegetation communities remain in the Mekong Delta, such as the peat swamps of the U minh wetlands, the remnant Mangrove forests, and the Kien Karst outcrops in the Ca Mau Peninsula. The latter form the habitat of several endemic plants, including recently-described species such as *Begonia bataiensis* and *Calanthe kienluongensis* (Campbell, 2012; Campbell et al., 2020).

According to Triet et al. (2017), 14 areas of the Mekong delta are under official conservation protection, 12 of them in Vietnam and 2 in Cambodia. They are either national or international protected areas, such as National Parks or Ramsar sites. In total, however, they cover a mere 84,000 ha - 1.5% of the Delta. The government of Vietnam announced in 2014 that an additional 9 protected areas would be established in the Mekong Delta, encompassing an area of 51,264 ha. In addition, two sites are listed as Important Areas of Cambodia. However, these areas enjoy no formal protection.



Figure 2.6: Overview of the official conservation areas in the Mekong Delta.

2.2.6 Hydraulic Infrastructure: The Canals of the Vietnamese and Preks of the Cambodian Mekong Delta

As outlined in previous sections, the Mekong Delta has undergone extensive human modifications in terms of hydraulic infrastructure. How exactly this modification has taken shape, however, varies considerably between the Cambodian and the Vietnamese part of the delta.

In Vietnam, an extensive network of dykes, canals, and hydraulic control infrastructure such as gates exists today. In total, the dyke network in this part of the Delta has a length of over 13,000 km, 8,000 km of which are low dykes (crest levels 1.5 - 4.0 m a.s.l). High dykes, (crest levels 4.0 - 6.0 m) are concentrated in Gi-ang and Dong Thap provinces (Triet et al., 2017).

This network of canals and dykes in the Mekong Delta has a long history. While pre-colonial textual evidence is sparse, oral histories and archaeological evidence point towards canals being built at large scale as early as prior to 700 CE. For instance, ancient canals were discovered by a French archaeologist in 1931 while looking at aerial photographs of the region around Chau Doc. These canals reach a length of over 100 km, stretching from the coast of the Delta to Angkor Borei, across the border in Cambodia (Paris, 1931; Biggs, 2004).

However, it was only in the early 19th century that a systematic series of major public works initiated by the court of the Nguyen Empire more permanently shaped the delta landscape. These included the Bao Dinh canal, which widened a waterway first created in 1705, the Vinh Te canal, and the Thoai Ha canal. The latter two projects aimed to increase the Nguyen's control over Vietnam's border with Cambodia (Biggs, 2004). During the French colonial rule, canals were regarded as a tool to tie the Mekong Delta more intimately into the colonial state. The years between 1866 and 1930 saw an extensive expansion of waterways (Biggs, 2004, 2010). Overall, 174 million m^3 of earth were dredged - a scale comparable to the construction of the canals in Suez and Panama during the same period, at 260 and 210 million m^3 respectively. The situation during World War II the Vietnam War led to a fragmentation of the majority of hydraulic projects and a surge in small-scale local adaptation projects initiated by farmers. After 1975, projects initiated by the central government in the sectors of irrigation, land reclamation, and rice production revived and recentralized the construction of hydraulic infrastructure, with over 10,000 km of canals being built (Huu Nguyen et al., 2016; Biggs, 2004, 2011; Benedikter,

2014).



Figure 2.7: Excavation of the Cho Cao canal, ca. 1878, attributed to Émile Gsell, courtesy of the Université Côte d'Azur (ark:/17103/5hfh). In 1875 the French colonial authorities decided to construct a canal connecting Cua Tiêu to the Vaïco river as a transport route for rice by steamship.

On the Cambodian side of the border, the system of hydraulic infrastructure is less extensive, largely lacking a systematic network of dykes and control infrastructure such as gates. Instead, the defining characteristics are Preks. Located along the banks of the Bassac and the Mekong, these large-scale, trapezoidal canals form a connection between the river and the low-lying floodplains. They do so by breaching the elevated river banks, which were formed through centuries of sediment deposition (Kazama et al., 2007). The majority of these canals was constructed during the early 20th century. Unlike for the hydraulic infrastructure on the Vietnamese side of the border, an in-depth review of the Preks is as of yet lacking. Some aspects of their history, through the lens of engineering reports across the centuries, will be explored in Section 4.2. In addition to the Preks, a network of smaller-scale canals exists on the floodplains of the Cambodian Mekong Delta. Some of them are connected to the Preks and thus, by extension, to the river mainstream. The origin of these canals largely lies in the period of the Khmer Rouge regime in the 1970s. During this time, extensive resettlement and public work projects aimed to extend Cambodia's network of canals by forced manual labour. According to a UN survey from the 1990s, approximately 75% of Cambodia's canal networks originate from these work programmes (Fuller, 2008).

2.2.7 Challenges in the Delta: From Subsidence to Salinity Intrusion

From the previous sections in this chapter it emerges that the Mekong Delta is currently facing a multitude of challenges that pose existential threats to its ecological balance and economy and, consequently, the livelihoods of its population. Most serious are changes in the hydrological regime of the Mekong, climate change, and land subsidence. To make matters worse, various facets of these threats amplify each other's effects.

For instance, the Mekong Delta is in serious danger of becoming entirely inundated year-round due to a combination of land subsidence, sediment starvation, and sea level rise. As noted above, Minderhoud et al. (2017)'s results indicate that the entire Delta has already sunk approximately 18 cm over the past 25 years as a result of land subsidence. Part of that subsidence is due to natural sediment compaction due to overburden. Part of it, however, is also due to groundwater extraction at unsustainable rates. Simultaneously, sedimentation on the floodplains, which would normally counteract subsidence by raising land, is declining due to sediments becoming trapped in upstream hydropower reservoirs. Moreover, economic activities such as riverbed mining further reduce sediment load and increase erosive processes. In addition, sea level rise driven by climate change is further decreasing the relative elevation of the delta. Minderhoud et al. (2019) found that the average elevation of the Delta is a mere 0.8 m above sea level, rather than the previously assumed 2.6 m. Consequently, large swaths of the Delta will fall below sea level if current rates of sea level rise continue, or if they accelerate. For example, Minderhoud et al. (2019) states that over 70% of the population in the Delta would be displaced following a sea level rise of 1 meter.

Another problem that is aggravated by the processes described above is salinity intrusion into the delta. Several studies and reports have highlighted that saline sea water now intrudes further inland, especially during the dry season, than previously reported (Trung et al., 2020; Toan, 2014). This causes considerable difficulties for farmers who use the freshwater from the rivers and canals for irrigation. Part of the reason for this more extensive salinity intrusion is climate change, in particular shifts in precipitation patterns and sea level rise. Eslami et al. (2019) also report that channel incision resulting from sediment starvation and riverbed mining significantly increases tidal amplification and salinity intrusion. As a consequence, farmers in the Mekong Delta have been forced to adapt agricultural practices and livelihood models, for instance by

adopting the prawn rice rotational crop (Paik et al., 2020; Loc et al., 2021).

Apart from trapping sediments that could counteract land subsidence and prevent channel incision, upstream hydropower construction also has more direct negative effects on the Mekong Delta. Agriculture and fisheries are affected by its altered hydrological regime, decreasing wet season flows and thus inundation extents. Yoshida et al. (2020) found that if all 11 proposed mainstream dams in the LMB were to be constructed, the fish yields would decrease by 366,570 t and 267,429 t annually in Vietnam and Cambodia respectively. This would have severe economic impacts, the authors point out, with losses ranging from 6% to 9% of GDP in the Agriculture, Fishery and Forestry sector in Vietnam, and exceeding 3% of total GDP in Cambodia. Furthermore, this study also highlights that while total loss under this scenario would be smaller in Cambodia than in Vietnam, the vulnerable volume would be greater in the former country.

2.2.8 From the Regional to the Local: Understanding Delta-Wide Changes in the Prek System in Cambodia

As this chapter has outlined, the Mekong region as a whole and its delta in particular is facing a range of far-reaching changes, many of which have negative implications for its ecosystems and the livelihoods of its inhabitants. More broadly, many of these processes - from conflicts over hydropower development to subsidence are representative of similar issues that (tropical) deltas worldwide are facing.

From the literature cited in the preceding sections, it is clear that many of these processes of change and their impacts have been studied extensively at supra-regional and regional scales. However, few studies so far have assessed their impacts at more local scales, especially in the Cambodian Mekong Delta. In the following chapters, this thesis zooms in first on the Cambodian part of the Mekong Delta, then on an even smaller case study area. First, the hydrological groundwork will be laid to understand large-scale processes and land use patterns in this part of the delta. Then, the focus will fall entirely on the landscape-defining features of the case study area - the Preks, and the ecohydrological system of which they form the basis.

3

Understanding Large-Scale Hydrological Processes in the Region: Past Changes and Current Reality

To assess the regional and local impacts of the basin- and delta-wide changes outlined above, it is necessary to take a step-wise approach - to "zoom in", as it were, progressively. This chapter discusses the hydrological characteristics of the Cambodian Mekong Delta. It also strives to assess the hydrological changes that the region has experienced over the past decades. Thus, it lays the groundwork for the understanding of local-scale analyses of ecohydrological and sociohydrological processes, as well as their formal modelisation in subsequent chapters.[1]

[1]Part of this chapter is based on a paper published in: Orieschnig, C., Venot, J.P., Massuel, S., Eang, K.E., Chhuon, K., Lun, S., Siev, S. and Belaud, G., 2022. A Multi-Method Approach to Flood Mapping: Reconstructing Inundation Changes in the Cambodian Upper Mekong Delta. Journal of Hydrology, p.127902.

The processes that are examined in this chapter are changes in river flow, precipitation, inundations, and, to a certain extent, land use. Changes in river flow are assessed through a statistical analysis of the water levels of the Mekong and its distributary, the Bassac river. In the Cambodian Mekong Delta, time series of water level measurements stretch back as far as 1926, in the form of daily manual measurements. More modern, near-realtime records at a time step of 15 minutes exist since 2008 at some stations. A trend analysis and break point detection was carried out at four hydrological stations maintained my the MRC in order to pinpoint patterns of change in the hydrological series. Furthermore, the data at several local stations was compared to better understand upstream and downstream dynamics. Similar analyses were implemented for the time series of precipitation measurements. In addition, several sources of precipitation measurements were compared - manual and automatic in-situ measurements at various stations in the area, as well as remotely sensed precipitation measurements.

Detecting changes in regional inundation patterns proved to be a more difficult challenge due to the paucity of data that allows analyses on this subject. Satellite images provide a valuable avenue to assess how the temporal dynamics and extents of annual inundations have changed in the Cambodian Mekong Delta. However, images with sufficient temporal and spatial resolution to satisfactorily track highly dynamic processes such as inundations have only been consistently recorded since 2014. In order to track floods that lie farther back in time, a new method was developed to link locally measured water levels with flood maps derived from satellite images. Once this water level - flood link (WAFL) was established, it was used to re-construct a time series of daily inundation extents going back to 1991. The accuracy of the link itself was checked using a high-resolution digital elevation model, as well as historical remote sensing imagery.

A final element of the regional context that needs to be understood in the framework of this thesis is the general shift in land use, reflecting economic trends and influencing ecohydrological processes. To this end, a classification of natural vegetation was carried out using historical Landsat images and spectral indices. This classification was also used to draw conclusions on the impact of vegetation on the performance of WAFL.

3.1 Delineating the Areas of Interest

The study area for which the aspects discussed above is explored in more detail in this chapter is located ca. 50 km south of the Cambodian capital Phnom Penh, in the floodplains adjacent to the Mekong and the Bassac river, one of the Mekong's deltaic distributaries. It can further be subdivided into two zones, denominated A and B.

Zone A is located on the right bank of the Bassac. In the North and West is delineated by the Stung, a small stream that debranches from the Bassac. Its southern limit is formed by the Vinh Te canal, which in itself forms the border to Vietnam. This zone's landscape is fundamentally characterised by Prek channels, which establish a connection between the main rivers and their floodplains by breaching the river banks, elevated by sediment deposition. The terrain characteristically slopes away from the river banks towards the floodplains to the West, and from the banks of the Preks to the inter-Prek areas in the North and South. The elevated terrain areas along the banks of the Bassac and the Preks are called *Chamkar* in the local language and are rarely flooded. Here, flood-sensitive crops such as fruit trees and vegetables are grown. The lower-lying areas in the floodplains are called *Boeung*. These are flooded on a regular basis during the rainy season and are cultivated with crops such as rice and maize during the dry season. While flooded, they serve as nurseries for a large variety of fish species (Hortle, 2009b). In addition, these floodplain areas are criss-crossed by a rectangular network of canals that were excavated during the Khmer Rouge period in the 1970s. This landscape configuration and its socio- and eco-hydrological characteristics will be explored further in subsequent chapters.

Zone B differs from Zone A in that its landscape is less defined by Preks and more by large interior floodplains at its center. This zone is bracketed between the Mekong in the East and the Bassac in the West. In the North, its border is formed by a dyke and a canal, and in the South, as in Zone A, by the Vinh Te canal and the border to Vietnam. While Preks do exist in Zone B, along both the Mekong and the Bassac, their lengths are shorter and the distances between them bigger. Instead, the defining landscape elements are the extensive floodplains at the center of Zone B. Here too, a network of Khmer Rouge canals is embedded in the floodplain. In addition, there are shallow, artificial reservoirs, also excavated at the same time. In these areas, rice cultivation dominates. In addition, fishing used to be a predominant activity here at sufficient water levels, with fish benefiting from the broad expanses of submerged natural vegetation.

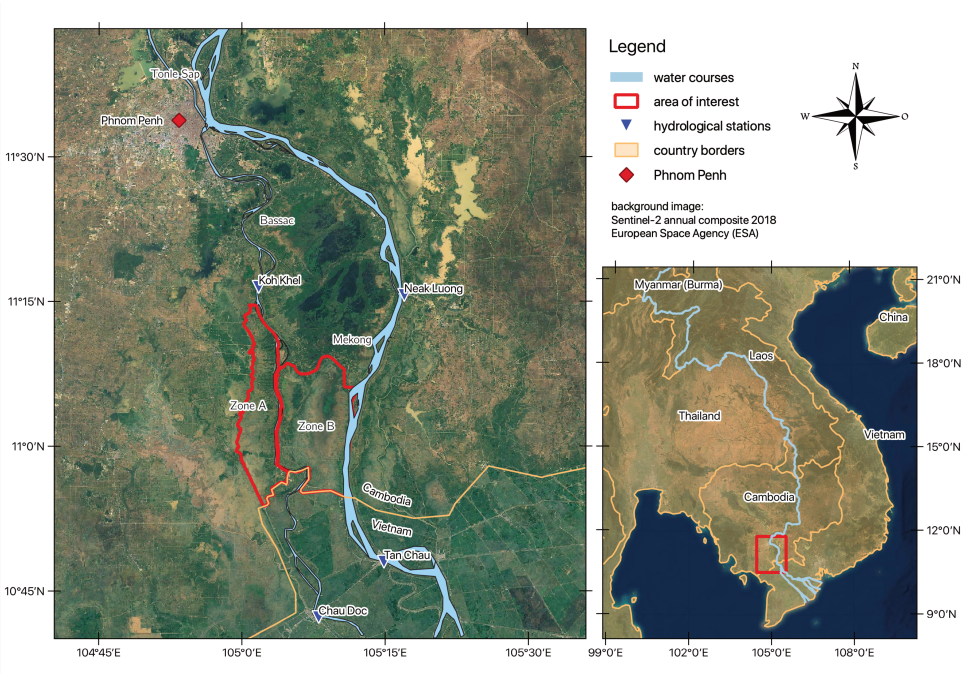

Figure 3.1: Location of the areas of interest in the Cambodian Mekong delta.

3.2 Local Hydrological Dynamics and Changes in River Flow

To begin with, it is necessary to gain more in-depth insights into the dynamics of the Mekong and its tributary the Bassac in the Cambodian Mekong Delta. The water level in these river sections is a crucial determining factor of the inundations in the delta. Their rise and fall in the course of the wet season plays a significant part in determining the dates of the onset of inundations, their peak, and recession. This, in turn, provides the framework for the agricultural practices that farmers can engage in. If river water levels rise too early in the year, and inundations thus start to soon, crops that have not yet been harvested may be lost, for instance.

For this reason, this section focuses on characterising river water level dynamics. To this end, data from several hydrological stations maintained by the MRC in Cambodia and Vietnam is used and a statistical analysis as well as a simplistic modelling approach using HEC-RAS are carried out. The interest lies in identifying long-term dynamics, as well as trends, change points, and parallelisms to shifts observed at delta- and basin-wide scales.

3.2.1 Data Availability: Mekong River Commission Time Series and In-Situ Loggers

The hydrological data used in this analysis, and in the wider context of the thesis, comes from several stations maintained by the MRC, as well as water level measurements taken with a series of differential pressure loggers (Onset Hobo MX2001) in a sub-section of Zone A, which corresponds to the smaller-scale study area on which Chapters 4.3 and 6 focus. These loggers were installed in 2020 by a team from IRD and ITC in the course of the project of which this thesis forms a part. The locations of all measurement stations are given in Figure 3.2, except for two stations in Phnom Penh, which are located approximately 50 river kilometers upstream of Koh Kehl (cf. Figure 3.1). Furthermore, a pressure logger that was installed near the hydrological station at Koh Khel is equally not visible in the map since its location coincides with that of the MRC station.

The loggers have been collecting information at a temporal resolution of 15 minutes since late spring 2020, though with varying consistency as will be explained in subsequent chapters. The MRC stations, too, have different periods of coverage. Table 3.1 gives the specifics for each water level measurement station in the vicinity of the areas of interest and shown in Figure 3.2, including the measurement interval and the temporal range of measurements. Here, it can be seen that several water level measurement stations ceased their activity in 2005-2006, such as Kompong Trabek, Stung Slot, and Tuk Chhoo, as well as the measurement of daily minimum and maximum water levels in Chau Doc and Tan Chau. These measurements will thus not be considered any further. Furthermore, some measurement stations, such as Angkorborey, Phnom Penh Port, Koh Khel, Chau Doc, and Tan Chau provide both manual and telemetry measurements. Manual measurements are nominally taken at an interval of 1-6 days, though for the stations in the study area twice-daily measurements have been provided since 2006, and once-daily measurements were recorded before then. Telemetry measurements, in contrast, provide near-realtime data at an interval of 15 minutes. While this data resolution is useful for gaining insights into daily dynamics such as the propagation of tidal influence, they span shorter durations than the daily time series. For instance, telemetry data goes as far back as 2008 at Phnom Penh Chaktomuk and 2010 at Chau Doc, but only to June 2021 at Koh Kehl. In contrast, manual measurements at Neak Luong provide a fairly consistent time series since 1926.

For the purpose of the analysis in this section, water level time series at six MRC stations were used: Phnom Penh Chaktomuk, Koh Kehl, Angkorborey, and Neak Luong in Cambodia and Tan Chau and Chau Doc in Vietnam. The Koh Kehl and Chau Doc stations measure data on the Bassac, Tan Chau and Neak Luong on the Mekong. The Phnom Penh Chaktomuk station is located near the diffluence of the Mekong and the Bassac and can thus be seen to represent water levels in both rivers. The Angkorborey measurement station is located further inland in the Cambodian floodplain and measures the water level in the Prek Ambel, a distributary of the Bassac. Long-term daily data from the Neak Luong, Koh Khel, Tan Chau, and Chau Doc stations on the Mekong and the Bassac were used for an analysis of hydrological trends in these rivers just upstream and downstream of the area of interest.

Furthermore, near-realtime water levels at Phnom Penh Chaktomuk, Koh Khel, and Chau Doc were harnessed for a simplified HEC-RAS model to examine the amplitude and dynamics of tidal influence in this river section.[2] To complement these insights, near-realtime (NRT) data from Phnom Penh, Angkorborey, Koh Khel, Chau Doc, and the logger in the study area located on the Bassac were used to compare sub-daily dynamics and tidal influences upstream and downstream of the areas of interest.

At Koh Khel, a continuous time series of daily water level measurements since autumn 1991 is available. At Neak Luong, a series is available since 1926, which is, apparently, remarkably complete save for two larger gaps in 1946 and 1952-3. For this series, the tests were carried out twice: once on the entirety of the series, and once on a shortened series corresponding to the same duration as that available at Koh Khel. At both Chau Doc and Tan Chau, series are available since 1980 and the analysis was conducted on the entirety of the series.

Furthermore, river cross sections provided by the MRC at Koh Khel and Chau Doc[3] were used to estimate the geometry of the river between these two sections in order to construct a hydraulic model in HEC-RAS to simulate the water level slope on the Bassac. In addition to these profiles, two profiles near Koh Khel and Koh Thom, measured with an Acoustic Doppler Current Profiler (ADCP) in 2018 were used. These measurements were performed in the framework of the project of which this thesis forms a part.

[2] At the time that this analysis was first carried out in early 2019, near-realtime data was not yet available at Koh Khel or from loggers in the study area. It was re-run in early 2022 when that data became available.

[3] Available at http://ffw.mrcmekong.org/overview.php

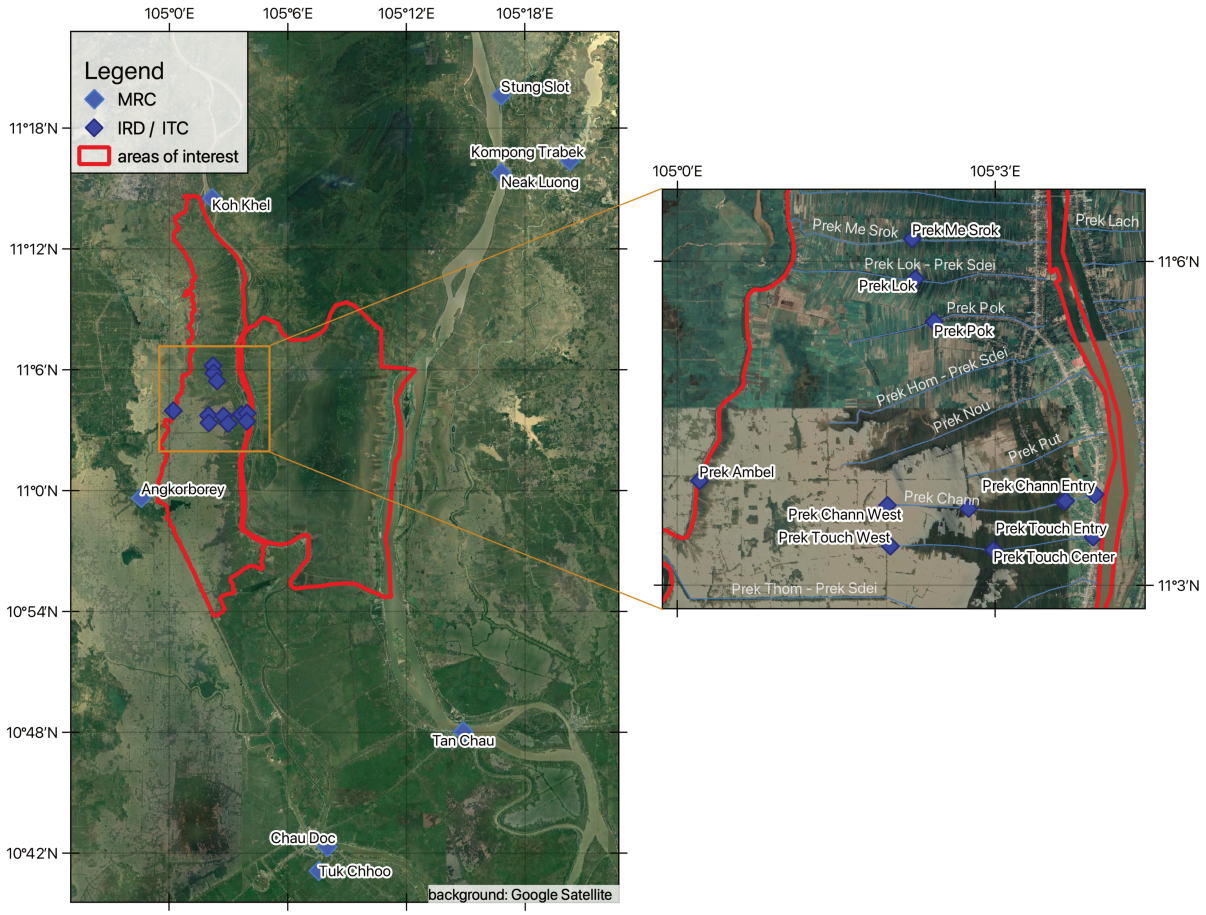

Figure 3.2: All water level measurement stations from which data was used in this thesis, except Phnom Penh Chaktomuk.

One issue that must be noted at this point are certain doubts appertaining to the quality and transparency of data downloaded from the MRC. While it provides an invaluable basis for analyses and deeper insights into hydrological conditions in the area, it is unfortunate that little metadata is available relating to how the data was collected and post-processed. For instance, it is unclear when, how, or where exactly the river cross sections were measured. Similarly, many of the measurements in the water level time series stem from before the foundation of the MRC, meaning they represent an amalgamation of data series originating from national observation networks. In the case of Neak Luong, the data reaches back almost a century, to the colonial period of the French Protectorate. Yet it is unclear how these series were consolidated, how the gauge placement may have changed over time, and whether and how interpolation was used to fill gaps in the series. These caveats were considered as the data was employed throughout this thesis.

Country	Station	Measurement Type	Interval	Start	End	River
Cambodia	Angkorborey	Telemetry	15 minutes	2018-06-02	2021-02-20	Stung Angkor Borey
	Koh Khel	Manual	1-6 times p/day	1990-09-05		Bassac
		Telemetry	15 minutes	2021-06-16		Bassac
	Kompong Trabek	Manual	1-6 times p/day	2001-01-01	2006-12-26	
	Neak Luong	Manual	1-6 times p/day	1926-01-01		Mekong
	Phnom Penh Port	Manual	1-6 times p/day	1960-01-01		Mekong
	Phnom Penh Chaktomuk	Manual	1-6 times p/day	1960-01-01		Bassac / Mekong
		Telemetry	15 minutes	2008-08-01		Bassac / Mekong
	Stung Slot	Manual	1-6 times p/day	1987-05-10	2006-12-31	
	Tuk Chhoo	Manual	1-6 times p/day	2001-01-01	2005-12-31	Kamchay
Viet Nam	Chau Doc	Daily Minimum	Daily	1962-01-01	2006-12-31	Bassac
		Daily Maximum	Daily	1962-01-01	2006-12-31	Bassac
		Manual	1-6 times p/day	1960-06-29		Bassac
		Telemetry	15 minutes	2010-08-15		Bassac
	Tan Chau	Manual	1-6 times p/day	1979-04-01		Mekong
		Telemetry	15 minutes	2010-08-16		Mekong
		Daily Minimum	Daily	1969-04-06	2006-12-31	Mekong
		Daily Maximum	Daily	1969-04-07	2006-12-31	Mekong

Table 3.1: Meta data for all MRC water level measurement stations in the vicinity of the areas of interest.

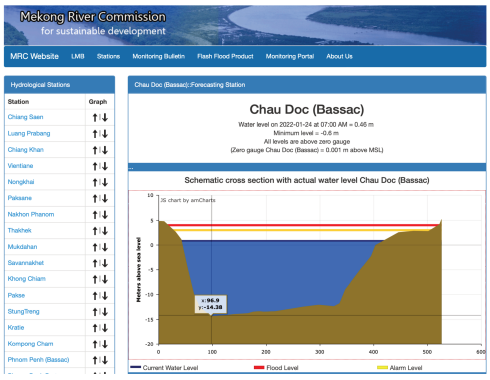

Figure 3.3: The MRC's online portal visualizing the daily water level measurements at Chau Doc.

3.2.2 Methods

3.2.2.1 Assessing the Dynamics of Tidal Influence and Relationships Between Upstream and Downstream Stations

In order to assess the evolution of water levels along the section of the Bassac that passes through the area of interest, near-realtime water levels at Phnom Penh, Koh Khel, Angkorborey, Prek Chann, and Chau Doc were compared, as well as daily water level measurements at Phnom Penh, Koh Khel, Angkorborey, and Chau Doc. Of particular interest was the propagation of diurnal tidal variations in water levels upstream. To further investigate this aspect, a basic hydraulic model was constructed in HEC-RAS.

HEC-RAS, which stands for *Hydrologic Engineering Center River Analysis System*, is a software platform developed by the US Army Corps of Engineers. It makes it possible to simulate one-dimensional steady flow as well as two-dimensional unsteady flow conditions and perform calculations related to sediment transport and water temperature and quality. Two cross-sections from the MRC ADCP measurements were used to construct a river channel representing the Bassac between Phnom Penh and Chau Doc. In addition to the input profiles, 489 cross-sections were interpolated to create a continuous river channel. Four Manning's roughness coefficients were compared (0.03, 0.035, 0.04, 0.045) for the entire profile (cf. Chow (1959)). Subsequently, a 1-D unsteady flow simulation was performed in which the NRT water level measurements at Phnom Penh, Koh Khel, and Chau Doc from the period 27/11/2020-30/11/2020, the flood peak of the year, were used as boundary conditions in order to simulate the water level evolution at the location of the logger in the study area.

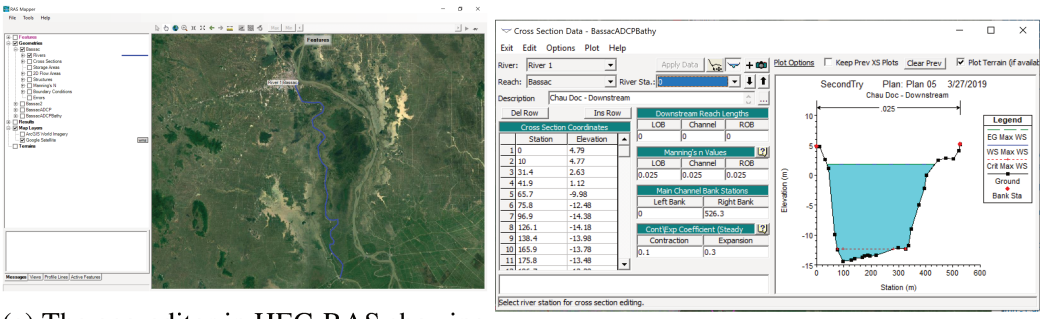

(a) The geo-editor in HEC-RAS showing the course of the Bassac.

(b) The cross-section tab in HEC-RAS.

Figure 3.4: The HEC-RAS modelling interface.

3.2.2.2 Change Point and Trend Analysis

To analyze the long-term hydrological trends in river water levels, a trend analysis was implemented using the non-parametric Mann-Kendall test (Hamed and Ramachandra Rao, 1998). Then, a change point detection was carried out using the Pettitt test (Pettitt, 1979), Buishand's range test (Buishand, 1982), and the standard normal homogeneity test (Alexandersson (1986)). This approach follows the analyses by Mallakpour and Villarini (2016), Yun et al. (2020), and Zhou et al. (2019). The parameters tested were the dates of the flood rise and recession, the overall flood duration, the duration of water levels above local threshold[4], the average water level during the flood, and the maximum water level, along with the date at which it was reached each year.

These parameters reflect the immediate considerations of farmers with regard to their cultivation practices. The date of the flood arrival, for example, determines whether early wet season crops can be harvested in time, or whether they will suffer damage from the oncoming inundations. Similarly, the date of the flood recession dictates when crops can be planted on the formerly inundated fields and the extent to which they will depend on irrigation at the end of their growing cycle. The dates of the flood rise and recession - and thus the overall flood duration - were defined on the basis of the rate at which water levels rise and fall (Δwl). The date of the largest positive Δwl was taken as the start of the flood, the date of the largest negative Δwl as the date of recession. The number of days between these two dates was taken as the flood duration. All elevations are given in the local Ha Tien 1960 elevation datum.

3.2.3 Results and Discussion

The comparisons of near-realtime and daily water levels are given in Figures 3.5 and 3.7. From the comparison of NRT data, at the end of November 2020, it emerges that tidal influence can be registered at all stations, though at different amplitudes. In Chau Doc, daily water level variations

[4]Local thresholds of 5 m at Koh Khel, 4 m at Neak Luong, and 2 m at both Tan Chau and Chau Doc were chosen. At Koh Khel, the threshold was selected based on information gathered from local stakeholders about necessary water levels for fish reproduction - see Section 4.3. A local threshold of 4 m rather than 5 m was set at Neak Luong because there were several years in the time series when water levels did not exceed 5 m at all. The downstream thresholds of 2 m similarly take account of the lowest water level exceeded every year as well as the water surface slope.

according to the tides reach amplitudes of up to 1 m. At Phnom Penh, in contrast, the variation is only several centimeters. It is notable that the tidal influence is clearly discernible at the station in the case study area on the Bassac mainstream, but hardly noticeable in Angkorborey, even though the latter station is further downstream in absolute terms. Furthermore, it is important to note that the average registered water levels decline much more sharply between stations further downstream than between Phnom Penh and Koh Khel. For instance, the average water level during the period shown in Figure 3.5 (27/11/2020 - 30/11/2020) is 3.20 m in Phnom Penh and 2.98 m at Koh Khel. This results in a difference of 22 cm over ca. 50 river kilometers, meaning an average slope of the water surface of 0.4 cm per kilometer. In contrast, the average water level registered by the logger in the study area is 2.37 m, even though it is only ca. 21 river kilometers downstream of Koh Khel. This means that there is a total decline of 61 cm, which translates to 2.9 cm per river kilometer. Similarly striking is the difference between the logger in the case study area and the station at Chau Doc, which tallies in at 92 cm, or 1.8 cm per river kilometer.[5] It can furthermore be observed that at Chau Doc, both the diurnal and the semi-diurnal tidal regimes that influence the Mekong Delta can be observed. According to Dung et al. (2011) and Phan et al. (2019), the Mekong Delta sees two tidal influences: the semidiurnal tide originating in the South China Sea and the diurnal tide, stemming from the Gulf of Thailand[6]

Similarly, propagation times vary. For example, on 28/11/2020, the maximum water level at Chau Doc at high tide is registered at 21:30. At the logger in the case study area, this maximum level is registered at 06:30 on 29/11/2020, eight hours later. In contrast, the maximum water level at Koh Khel is registered only three hours later. Between Koh Khel and Phnom Penh, the delay is a mere five and a half hours, with the maximum water level being reached at 15:00. This means the average propagation speed of the tidal wave between Chau Doc and the logger is 6.4 km/h, between the logger and Koh Khel 7 km/h, and between Koh Khel and Phnom Penh ca. 9.1 km/h.

These results indicate that the lateral connection between the Bassac River and the floodplains

[5]It must, however, be noted that due to the high tidal amplitudes at Chau Doc, the average water level here is less meaningful than further upstream.

[6]Dung et al. (2011) further notes that high tides can lead to salinity intrusion into the delta, especially during the dry season. However, the southernmost bounds of the area of interest of this thesis are located approximately 215 km upstream of the sea. Since maximum recorded upstream salinity intrusion distances in the Mekong Delta have been 130 km (Nga, 2021), and maximum projected distances are 150 km under future scenarios, this does not impact the study area of this thesis.

is more pronounced downstream of Koh Khel, likely due to the increased presence of Preks here. This conjecture is also supported by the results of the HEC-RAS model. Here, the tidal wave shows a quasi-uniform speed. As illustrated in Figure 3.6, the simulation of water levels at the logger in the study area shows lower water levels, but mirroring the dynamics at Chau Doc almost exactly, with a temporal delay. The propagation of tidal influence is simulated as being far faster and as having a higher amplitude at the logger in the case study area than was actually measured. Partly this is due to the lateral floodplain connections that were not taken into consideration. Other sources of uncertainty exist as well, though, such as the fact that other deltaic distributaries join and diverge from the Bassac in the area between the two measurement points. There is even a lateral connection to the Mekong via a canal. In addition, some uncertainties exist related to the geometry used. The profiles by the MRC appear to have been measured in the early 2010s - approximately 10 years ago. However, due to riverbed mining activities and sediment starvation, there have been significant incision rates reported in the channels of the Mekong Delta, ranging from -0.26 m/year to 0.5 m/year (Hackney et al., 2020, 2021). Consequently, the entire river section is likely to be lower than represented in the model. In addition, pools and ridges are likely to exist between the two measurement stations, which were not represented in the interpolated sections.

The additional NRT data at Angkor Borey also reveals that a slight variation of water levels due to tides can still be registered further inland, though it remains minor.

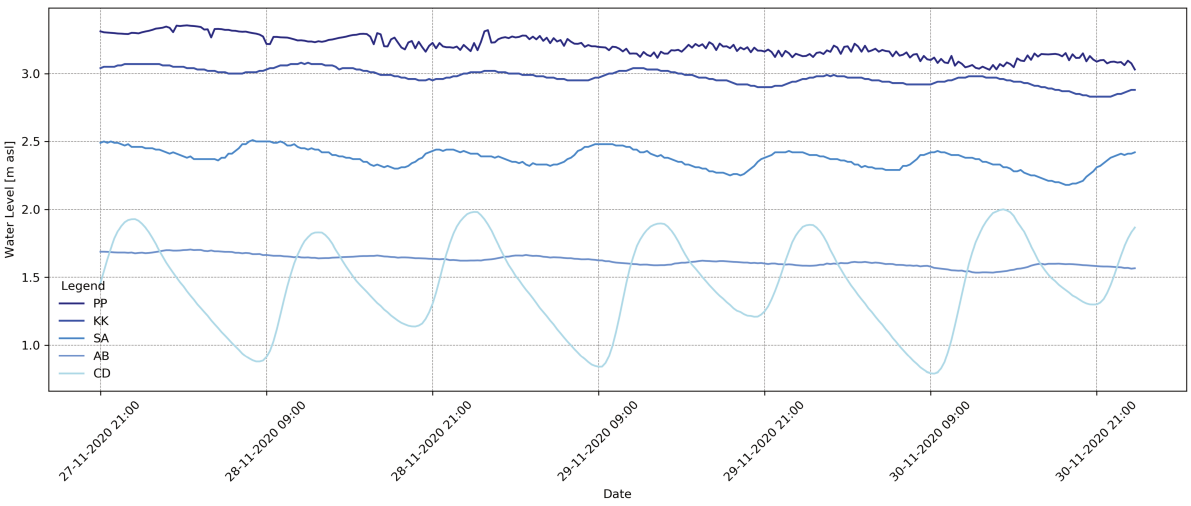

Figure 3.5: Comparison of NRT data at Phnom Penh (PP), Koh Khel (KK), at the logger in the study area (SA), Angkor Borey (AB), and Chau Doc (CD) at the end of November 2020.

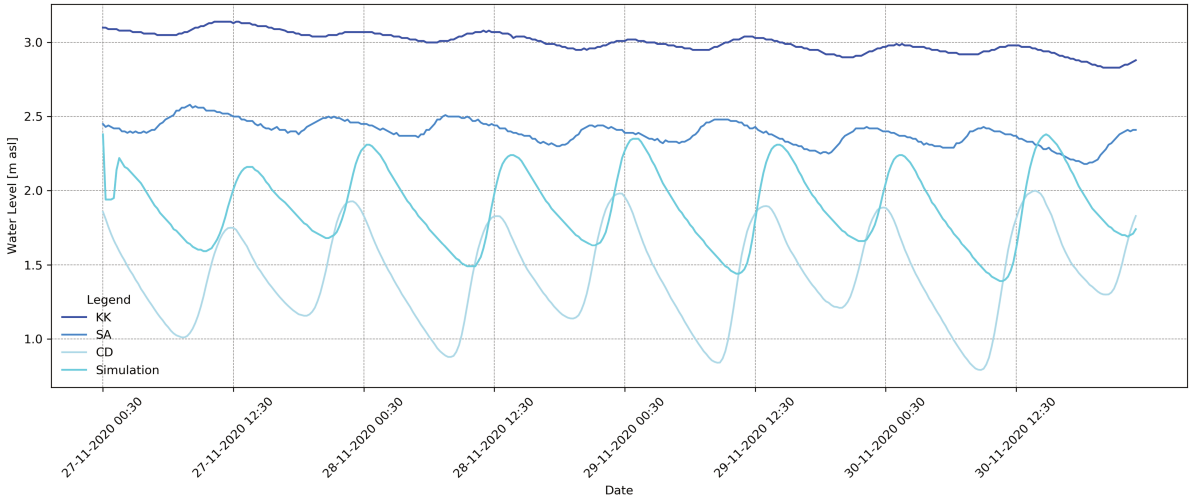

Figure 3.6: Comparison of NRT data at Koh Khel (KK), at the logger in the study area (SA), and Chau Doc (CD) with the results of the HEC-RAS simulation for water level dynamics at the logger location.

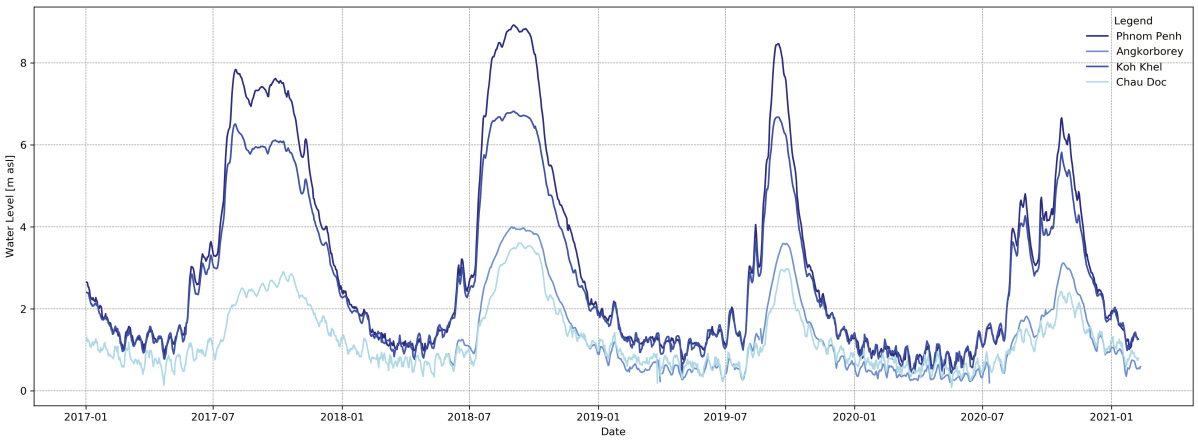

Figure 3.7: Comparison of daily water levels at Phnom Penh, Koh Khel, Angkorborey, and Chau Doc 2017-2021.

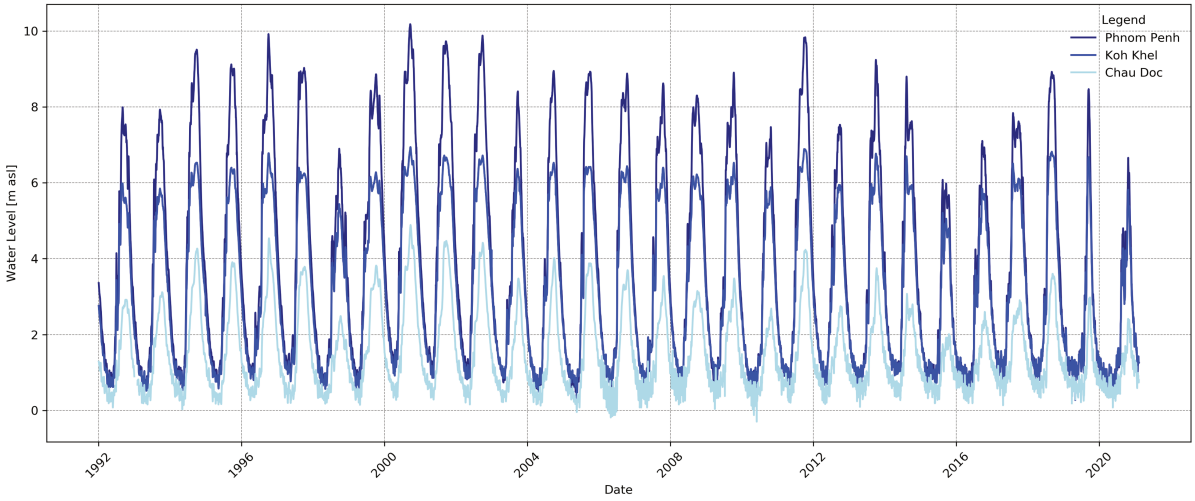

Figure 3.8: Comparison of daily water levels at Phnom Penh, Koh Khel, and Chau Doc 1992-2021.

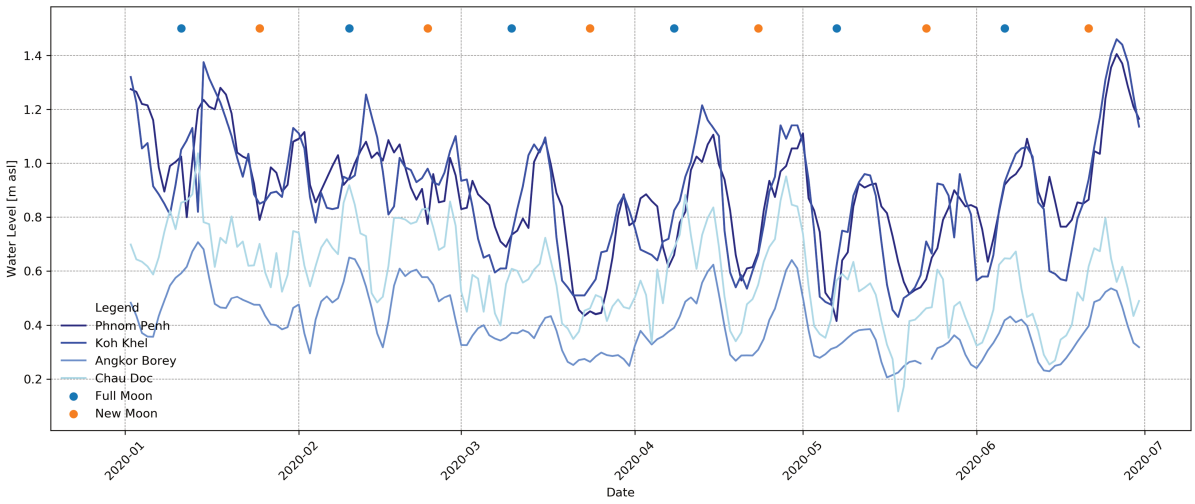

Figure 3.9: Comparison of daily water levels at Phnom Penh, Koh Khel, Angkorborey, and Chau Doc during January-June 2020.

In observing daily water levels across the course of an entire year, several trends emerge. First, there is the fact that the distinct seasonality of water levels can be observed at every station, though at different magnitudes. Seasonal water level variations upstream at Phnom Penh amount to almost 10 m, with the minimum water level recorded since 1992 being 0.33 m at the height of the dry season in 2005 (19/05/2005) and the highest water level recorded during the wet season being 10.18 m, on 19/09/2000 - 20/09/2000. At Koh Khel, variations range in the realm of 6.5 m (max: 6.94 m on 21/09/2000 and min 0.28 m on 04/30/2019). Further downstream at Chau Doc, the maximum difference between the flood and the dry season is still pronounced

at approximately 5 m (min:-0.3 m on 01/06/2010, max: 4.89 m on 23/09/2000). This lines up well with the values reported by (Lanh, 2005), as well as Dung et al. (2011), which give the seasonal amplitude at Tan Chau and Chau Doc at 3-5 m. Furthermore, as Figure 3.7 illustrates, the seasonal water level dynamics at Angkor Borey more closely mirror those at Chau Doc than at Koh Khel, even though it is located an approximately equal distance (40 river km) between the two.

Furthermore, the daily data also illustrates that the water slope along the Bassac is far steeper during the flood season, as could be expected due to the backwater effect. This becomes especially evident when looking at the long-term time series available at Phnom Penh, Koh Khel, and Chau Doc, shown in Figure 3.8. At the peak of the flood season, up to 6 m separate the water level elevations between Phnom Penh and Chau Doc, while during the dry season this difference decreases to approximately 0.5 m. Equally notable is the evolution of the water level slope between Phnom Penh and Koh Khel, which is practically non-existent during the height of the dry season, with only a few cm of difference in water elevation between the two stations, even though they are separated by over 50 km. During the wet season, in contrast, this difference reaches over 4.5 m. It is notable that the water levels at Phnom Penh and Koh Khel evolve in almost perfect sync, with small water level differences between the two stations, during the majority of the flood rise. Then, however, the levels at Koh Khel peak at 6 - 6.5 m while those at Phnom Penh continue to rise. This points towards a threshold for floodplain connectivity in the section between these two stations, which leads to significant attenuation effects at Koh Kehl.

One more phenomenon that can be observed is a bi-weekly oscillation in water levels at all stations, which becomes particularly evident during the height of the dry season. An example is given for the months of January to June 2020 in Figure 3.9. It is likely that these oscillations are due to the lunar cycle. Previous studies have reported that the lunar phases have an impact on the observed migratory behaviour of several fish in the Mekong system (Poulsen et al., 2004; Baird et al., 2020), especially the delta, though it appears that no detailed studies on the effect exist yet.

Finally, the comparison of daily water levels between stations also evidences a triple-peaking pattern, especially at Phnom Penh and Koh Khel. This pattern is particularly visible when looking at the long-term time series in Figure 3.8. A first, sharp peak typically occurs relatively early in the wet season, followed by an equally sharp, short descent before the flood rise continues. Then,

as the flood nears its peak, the water levels at Koh Khel, which have thus far risen almost in sync with those at Phnom Penh, decrease slightly before peaking a few days later. At Phnom Penh, the water levels continue to rise sharply for another few days, then decrease slightly, and finally peak. It can be conjectured that these peaks are related to thresholds for floodplain connectivity, or perhaps even the reverse flow of the Mekong into the Tonle Sap Lake.

The results of the analysis of long-term hydrological trends related to flood characteristics are given in Figures 3.10 to 3.14. The water level time series at Koh Khel shows trends towards a later flood rise and an earlier flood recession (the latter is significant at $p < 0.1$). Most significant is the decrease of the duration of water levels at over 5 m ($p=0.022$). A break point is detected by all three homogeneity tests for the hydrological year 2007/08.

The water level series at Neak Luong since 1926 exhibits significant trends towards a later flood arrival ($p=0.03$), decreasing maximum water levels ($p<0.001$), and decreasing flood durations at over 5 m ($p<0.001$). The short time series (1990-2020) shows a trend towards an earlier flood recession ($p=0.06$), a shorter flood duration ($p=0.09$), and especially a decreasing average water level during the flood ($p=0.03$), as well as a decrease in the incidence of water levels above 4 m ($p=0.03$). Significant break points were detected 17 years into the time series, which corresponds to the break 2009/10.

At both Tan Chau and Chau Doc, break points were detected for the hydrological year 2007/08. In addition, there is a significant decreasing trend in terms of maximum water levels and flood durations of over 2 m at Tan Chau ($p<0.001$).

Overall, it emerged from the analyses that the hydrological year 2007/2008 significantly separates two statistically homogeneous periods characterised by different flood durations, dates of flood rise and recession, and flood peaks. This closely mirrors trends observed in basin-wide studies, with shorter flood durations and lower wet season water levels, and a break point in 2008 (Yun et al., 2020; Heng et al., 2021). Consequently, the years pre- and post-2008 were used as comparison periods for the analysis of long-term trends in land cover and inundation dynamics (see Chapter 3.4). When comparing some flood characteristics of the pre- and post-2008 periods, several common trends emerge (see Table 3.2). Flood durations decrease by approximately 16-32 days and average peak water levels decrease by between 10 and over 50 cm. While it must be noted that many of these differences are not statistically significant, certainly in part due to

Station	Period	Flood Rise [DOY]	Flood Recession [DOY]	Flood Duration [D]	Max WL [M]	Max WL DOY
Koh Khel	**Pre 2008**	198	291	92,17	6,38	267
	Post 2008	208	269	60,75	6,28	262
Chau Doc	**Pre 2008**	186	304	116,29	2,73	280
	Post 2008	198	275	86,27	2,17	282
Neak Luong	**Pre 2008**	200	298	97,44	6,82	267
	Post 2008	206	274	68,08	6,28	263
Tan Chau	**Pre 2008**	199	329	137,32	3,86	276
	Post 2008	203	324	121,00	3,43	273

Table 3.2: Overview of average dates of flood rise and recession, flood duration, maximum water level, and date of maximum water level pre- and post-2008 at Koh Khel, Neak Luong, Chau Doc, and Tan Chau.

the short length of the data series post-2008, a picture of shorter, less intense floods emerges nonetheless.

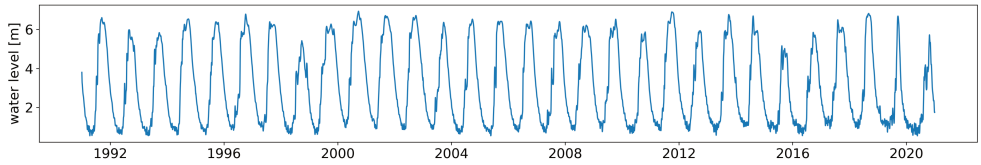

(a) Water levels at Koh Kehl 1990-present.

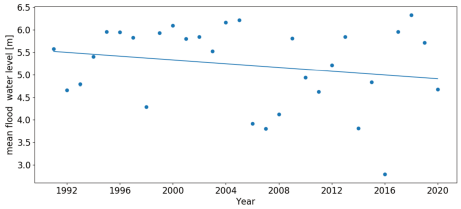

(b) Mean flood water levels at Koh Khel.

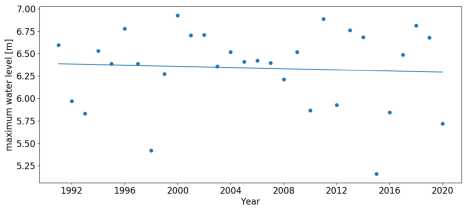

(c) Maximum water level at Koh Kehl.

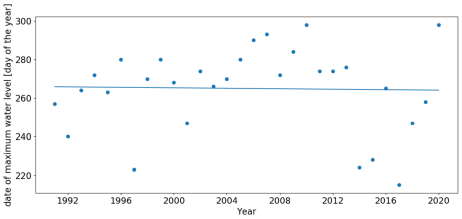

(d) Date of maximum water level at Koh Khel.

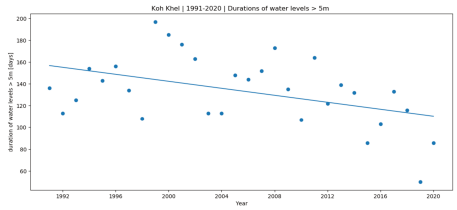

(e) Flood duration over 4 m at Koh Khel.

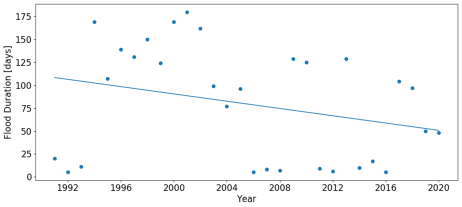

(f) Overall flood duration at Koh Kehl.

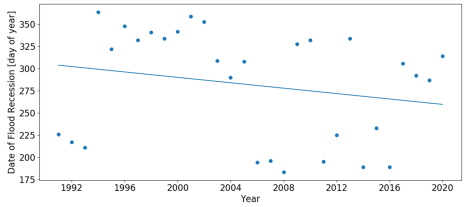

(g) Date of flood recession at Koh Khel.

Figure 3.10: Results of hydrological analysis at Koh Khel.

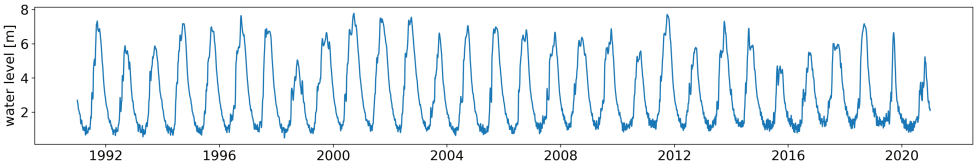

(a) Water levels at Neak Luong 1990-present.

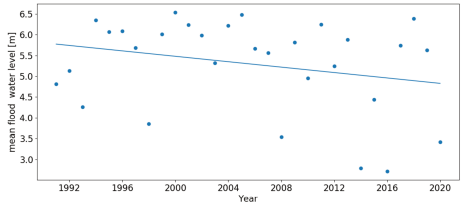

(b) Mean flood water levels at Neak Luong.

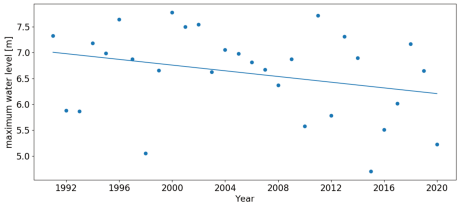

(c) Maximum water level at Neak Luong.

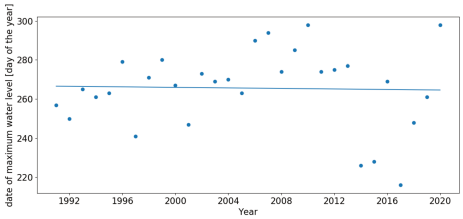

(d) Date of maximum water level at Neak Luong.

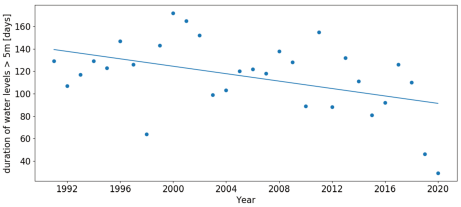

(e) Flood duration over 4 m at Neak Luong.

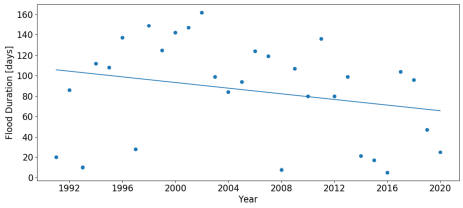

(f) Overall flood duration at Neak Luong.

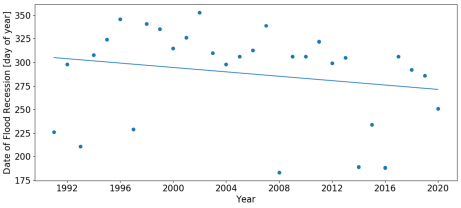

(g) Date of flood recession at Neak Luong.

Figure 3.11: Results of hydrological analysis at Neak Luong, short time series.

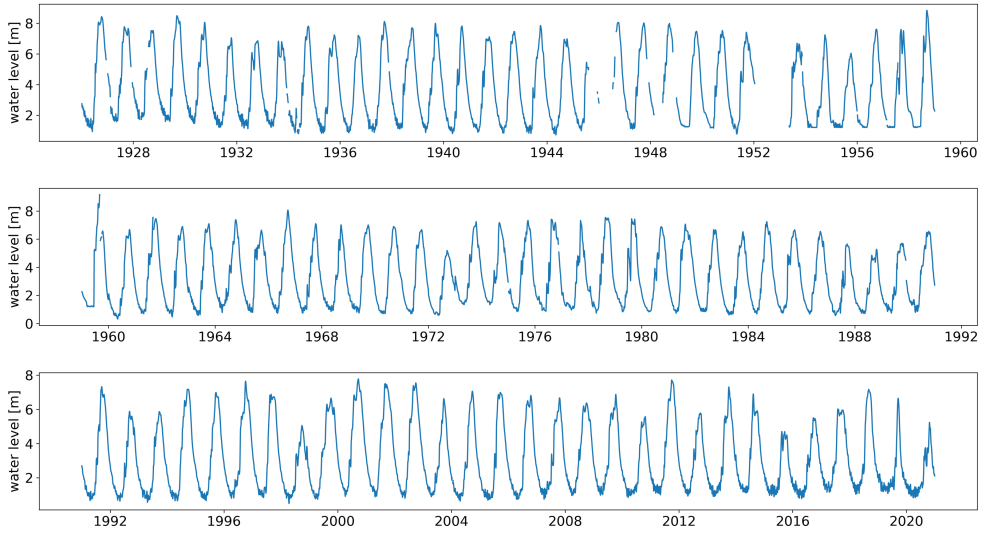

(a) Water levels at Neak Luong 1926-present.

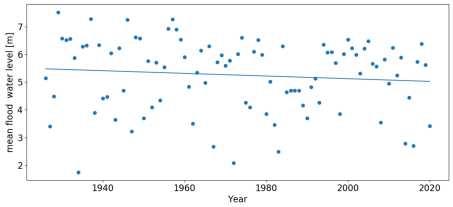

(b) Mean flood water levels at Neak Luong.

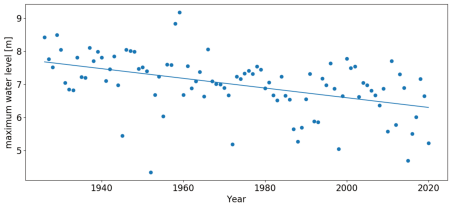

(c) Maximum water level at Neak Luong.

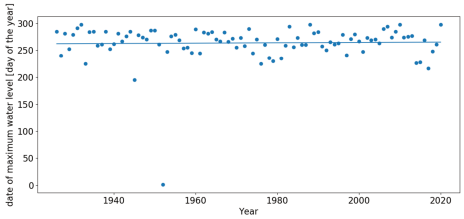

(d) Date of maximum water level at Neak Luong.

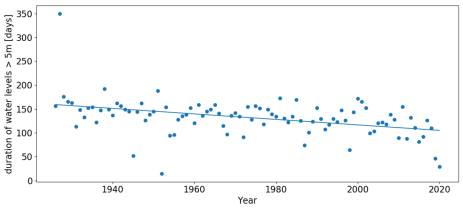

(e) Flood duration over 4 m at Neak Luong.

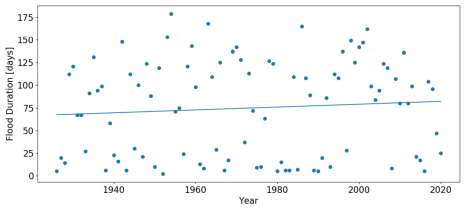

(f) Overall flood duration at Neak Luong.

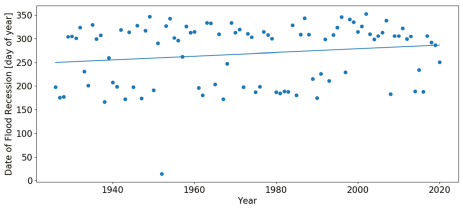

(g) Date of flood recession at Neak Luong.

Figure 3.12: Results of hydrological analysis at Neak Luong, long time series.

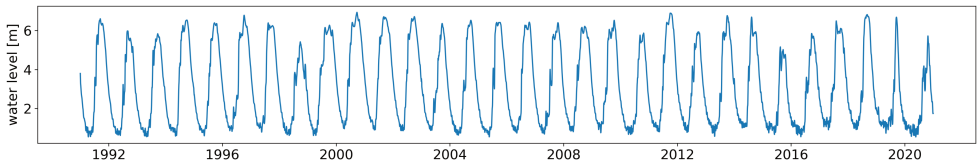

(a) Water levels at Tan Chau 1990-present.

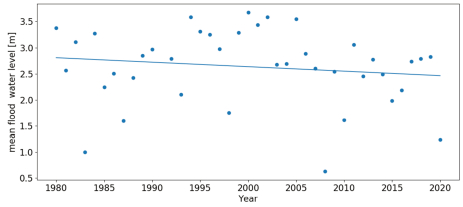

(b) Mean flood water levels at Tan Chau.

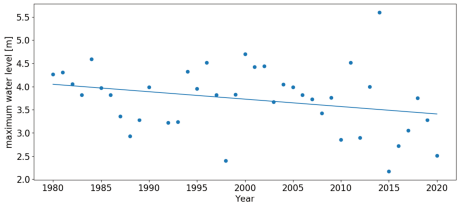

(c) Maximum water level at Tan Chau.

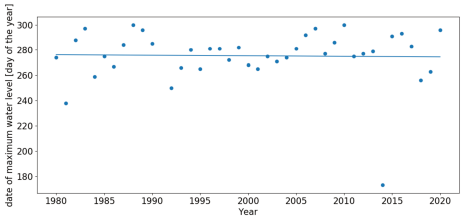

(d) Date of maximum water level at Tan Chau.

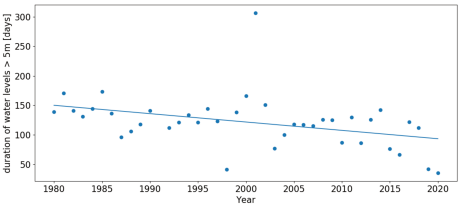

(e) Flood duration over 2 m at Tan Chau.

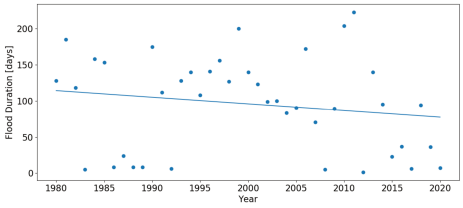

(f) Overall flood duration at Tan Chau.

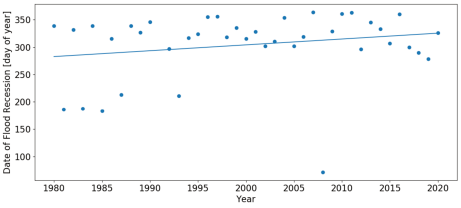

(g) Date of flood recession at Tan Chau.

Figure 3.13: Results of hydrological analysis at Tan Chau.

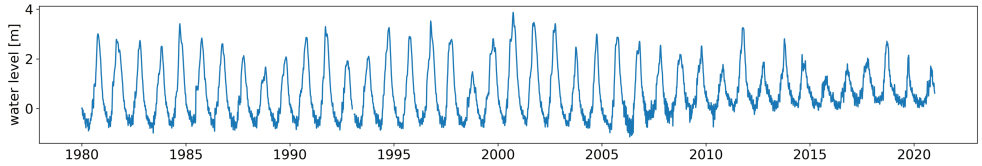

(a) Water levels at Chau Doc 1990-present.

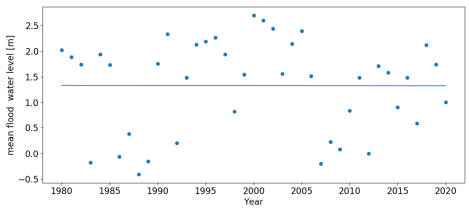

(b) Mean flood water levels at Chau Doc.

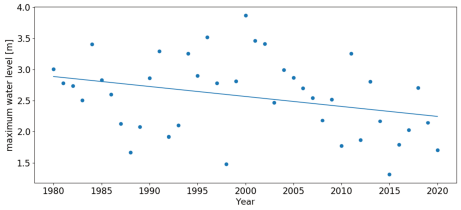

(c) Maximum water level at Chau Doc.

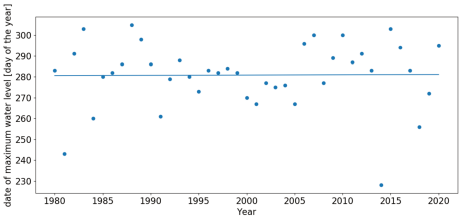

(d) Date of maximum water level at Chau Doc.

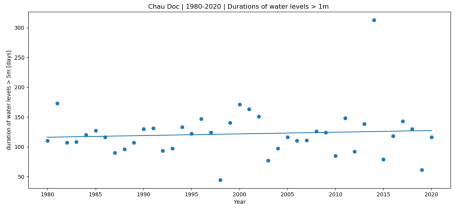

(e) Flood duration over 2 m at Chau Doc.

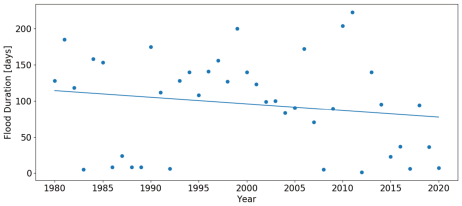

(f) Overall flood duration at Chau Doc.

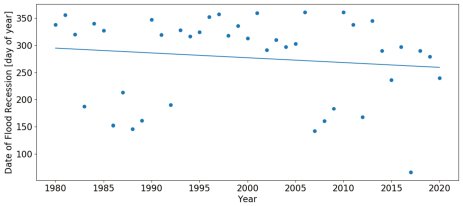

(g) Date of flood recession at Chau Doc.

Figure 3.14: Results of hydrological analysis at Chau Doc.

3.3 Comparing Precipitation Datasets and Identifying Trends

Precipitation is another component of the hydrological cycle that is essential to the understanding of hydrological dynamics in the Cambodian Mekong Delta as a whole and to the case study area explored in Chapters 4.3 and 6 in particular. This section aims to provide a comparison of available data, both locally measured and remotely sensed, as well as an analysis of the long-term trends that emerge from this data.

3.3.1 Data Availability: Local Rainfall Measurements vs. Remotely Sensed Series

Overall, there are eleven precipitation stations either within or in the vicinity of the areas of interest in the Cambodian Mekong Delta. Eight of them were installed by the Mekong River Commission and two by the United Nations Development Programme (UNDP) (see Figure 3.15). One was installed in the course of the project in the framework of which this thesis was conducted.

The MRC stations are Koh Khel, Prey Lvear, Angkorborey[7], and Koh Thom West of the Bassac, Peam Raing (Leuk-Dek) between the Bassac and the Mekong, and Neak Luong and Peam Chor East of the Mekong. These stations form part of the MRC observation network and coincide with the hydrological stations at Koh Kehl and Neak Luong. The UNDP installed two measurement stations West of the Bassac, one at Khao Thum[8] and one at Borey Cholsar. They were installed as part of the project *Strengthening Climate Information and Early Warning Systems in Cambodia to Support Climate Resilient Development and Adaptation to Climate Change*, funded through the GEF-Least Developed Countries Fund. In the course of this project, 24 Automatic Weather Stations (AWS) and 29 Automatic Hydrological Stations (AHS) were installed across Cambodia. In March 2019, they were handed over to the Ministry of Water Resources and Meteorology (MOWRAM), which has maintained them since then (UNDP, 2021). Finally, one station on the western bank of the Bassac river was installed in 2020 in the course of the project of which this thesis forms a part, in cooperation between the IRD and the ITC.

One considerable limitation on the reliability of the data listed above, however, is the duration over which the various stations provide data as well as their sensor type and temporal resolution. In terms of sensors and temporal resolution, two basic types exist - manual instruments providing once- or twice-daily data, and automatic stations providing near-realtime information every 15 minutes. Furthermore, some stations exhibit gaps during those periods for which they do nominally provide data. The manual measurements at Angkorborey, for instance, are listed as lasting from from 2001 to 2007 in the metadata provided by the MRC. However, data

[7] Angkorborey (Angkor Borey in its alternative anglicised spelling.) is given twice in the map because two different stations were maintained at different points in time in similar locations.

[8] Here, it is likely that the name of the station is a variation of "Koh Thom". The UNDP does not provide exact location data - it is thus difficult to pinpoint whether these two stations truly coincide.

is missing for several months in 2005. Another issue is the reliability of measurements in themselves. Especially the stations that require manual readouts are often older and their placements sometimes not ideal, as emerged during field visits. For instance, Figure 3.16 shows the pluviometer used for manual rainfall measurements at Koh Khel meteorological station. As can be seen, the instrument is located near trees and buildings, which can potentially cause rain shadow during precipitation events and lead to an underestimation of the rainfall volume. While these issues are likely resolved in many places by the proper installation of more modern, automated equipment, their effect must still be considered when evaluating longer time series.

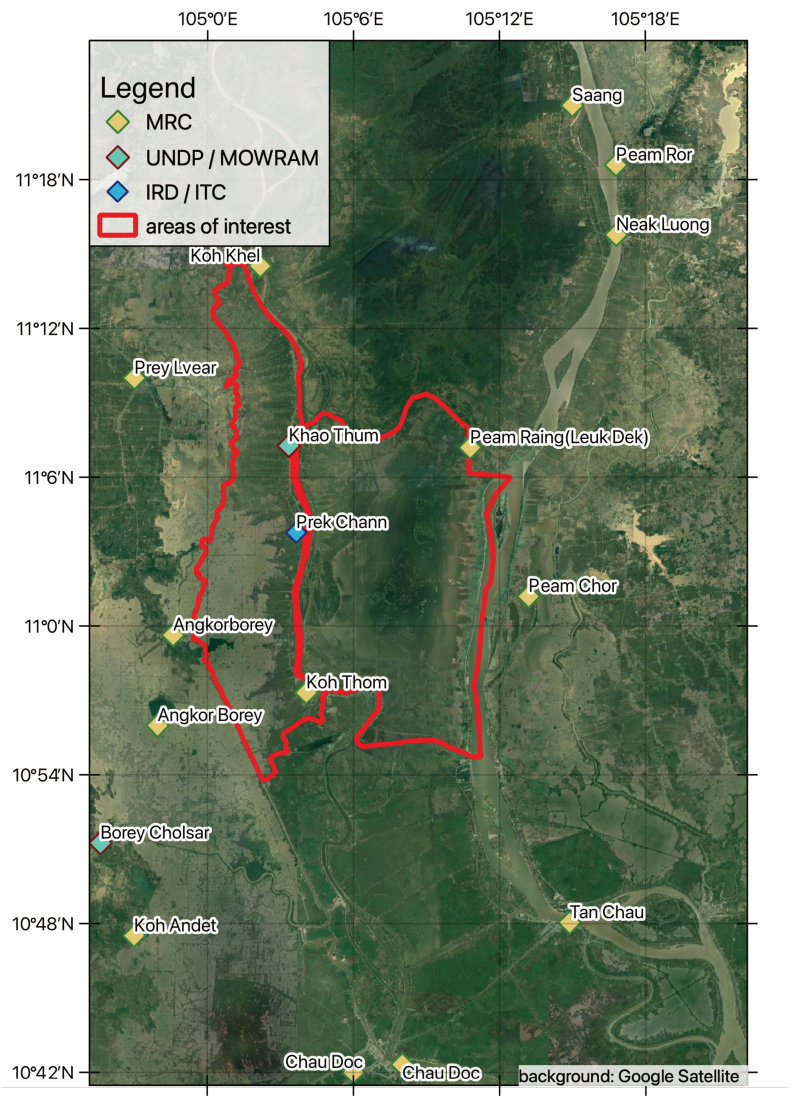

Figure 3.15: Location of rainfall stations in and near the area of interest.

In the analysis below, in-situ rainfall data from the UNDP station at Koh Thom, the MRC

Country	Station	Measurement Type	Interval	Start	End
Cambodia	Angkor Borey	Manual	1-6 times p/day	2001-01-01	2007-12-31
	Angkorborey	Telemetry	15 minutes	2018-06-02	2021-02-20
	Koh Andet	Manual	1-6 times p/day	2001-01-01	2012-12-31
	Koh Khel	Manual	1-6 times p/day	2007-03-19	
		Telemetry	15 minutes	2021-06-16	
	Koh Thom	Manual	1-6 times p/day	2007-01-01	2007-12-31
	Kompong Trabek	Manual	1-6 times p/day	1922-01-01	2012-12-31
	Neak Luong	Manual	1-6 times p/day	2007-03-19	
	Peam Chor	Manual	1-6 times p/day	2007-01-01	2012-12-31
	Peam Raing(Leuk Dek)	Manual	1-6 times p/day	2001-01-01	2003-12-31
	Peam Ror	Manual	1-6 times p/day	2001-01-01	2007-12-31
	Saang	Manual	1-6 times p/day	2001-01-01	2012-12-31
Viet Nam	Chau Doc	Manual	1-6 times p/day	2007-04-18	
		Telemetry	15 minutes	2010-08-14	
		Manual	1-6 times p/day	1920-01-01	2007-12-19
	Tan Chau	Manual	1-6 times p/day	2007-04-10	
		Telemetry	15 minutes	2010-08-14	
		Manual	1-6 times p/day	1997-12-31	2006-12-31

Table 3.3: Overview of all rainfall measurement stations from which data was used in the course of this thesis

station at Koh Khel, and the field station at Prek Chann in the case study area are used. These were chosen because they are located at the intersection of Zone A and B. Since rainfall events can be highly localized, this spatial proximity to both sub-zones is an important factor. Furthermore, these stations continue to provide either consistent time series stretching back several years, or reliable high-resolution NRT data.

The second data type used for precipitation analysis in this thesis is remotely sensed data in the form of CHIRPS. CHIRPS stands for *Climate Hazards group Infrared Precipitation with Stations*. It is a quasi-global dataset spanning latitudes from 50 °S to 50 °N, at the resolution of 0.05 °. Data is provided at daily, pentadal (5-day), and monthly resolution. Originally, CHIRPS was created in order to support the Famine Early Warning Systems Network (FEWS NET) of the United States Agency for International Development. It further developed approaches previously used with success in thermal infrared precipitation products such as the Rainfall Estimate (RFE2) dataset by the US National Oceanic and Atmospheric Administration (NOAA) or the TAMSAT African Rainfall Climatology And Time series (TARCAT) by the University of Reading. At its core, CHIRPS provides global Cold Cloud Duration (CCD) rainfall estimates based on the Tropical Rainfall Measuring Mission Multi-satellite Precipitation Analysis version 7 (TMPA 3B42 V7) and station data incorporated through smart interpolation (Funk et al., 2015). One

considerable advantage of CHIRPS is that it provides consistent daily data going back to 1981, which facilitates trend analyses over longer time periods in data-sparse areas.



Figure 3.16: The pluviometer at Koh Khel meteorological station, photographed in 2020 by Sylvain Massuel.

3.3.2 Methods

To compare precipitation data provided by CHIRPS and measured in-situ, CHIRPS data at daily resolution was first extracted from the cloud computing platform Google Earth Engine (cf. Section 3.4.1.3). It was then compared to the in-situ measurements at Koh Khel, Khao Thum (UNDP), and Angkorborey (NRT, MRC), as well as the meteorological station installed at Prek Chann in the course of this project. Subsequently, daily and monthly precipitation sums were compared between series, as well as the frequency of high-intensity precipitation events. In addition, the root mean square error (RMSE, see Equation 3.1) was calculated to compare the series of rainfall events between stations. Finally, a trend and break point analysis was carried out on the CHIRPS precipitation series to detect changes in the temporal dynamics of precipitation

patterns in the area of interest over the past forty years. As for the trend analysis on water levels, the non-parametric Mann-Kendall test (Hamed and Ramachandra Rao, 1998) was harnessed for this purpose.

$$RMSE = \sqrt{(\frac{1}{n}) \sum_{i=1}^{n} (y_i - x_i)^2} \tag{3.1}$$

Where n is the number of observations, y_i is the measured time series value in CHIRPS and x_i is the time series value of in-situ measurements.

3.3.3 Results and Discussion

The results of the analysis of rainfall data are given in Figures 3.17 to 3.21, as well as Table 3.4. One observation that emerges even from a purely visual comparison is that there is considerable heterogeneity between stations, both on a daily and monthly level. Looking at Figure 3.17, which shows the daily rainfall amounts registered in October 2021 at the three in-situ stations, as well as the values extracted from CHIRPS, it emerges that CHIRPS tends to overestimate rainfall amounts on days on which the in-situ stations register low or no precipitation. In contrast, it fails to capture high-intensity events such as those registered on the 1st, the 5th, and the 17th at Koh Khel. Similar observations can be made when looking at the monthly rainfall sums for 2021, shown in Figure 3.18. During the first three months of the year, CHIRPS registers far higher rainfall amounts than the in-situ stations. During months with higher rainfall values, in contrast, it is in relatively good agreement with at least one in-situ station - with Koh Thom in April, Koh Khel in May, Koh Thom again in June, and so forth. It is noteworthy that the in-situ stations show similarly high deviations amongst themselves as in comparison to CHIRPS. In April 2021, for instance, when both CHIRPS and the UNDP station at Koh Thom registered total rainfall values of almost 200 mm, both the MRC station at Koh Khel and the field station at Prek Chann barely registered half that amount. Similarly, in May, the in-situ station at Koh Khel and CHIRPS both registered just below 150 mm rainfall, while the field station hovered around 100 mm and the UNDP station barely surpassed 50 mm. Both the monthly and daily comparison reveal that the discrepancies between the in-situ stations do not follow a fixed pattern which could be explained through instrument bias, for instance.

The fact that the agreement between individual stations and CHIRPS data is no higher than the agreement between the in-situ stations themselves is also highlighted by Table 3.4, which shows the RMSE for the comparison of monthly precipitation sums since 2020 between all data sources. The smallest overall RMSE was reached in the comparison between MRC data at Koh Khel and CHIRPS data, followed by the comparison between MRC data and measurements collected at the field station at Prek Chann. In contrast, the highest RMSE was evidenced by the comparison between UNDP and MRC data.

Further insights into the dynamics of rainfall are provided by Figure 3.19. Here, all dates of 2021 for which data for all four stations was available (223 days) were sorted into categories depending on how many mm of rainfall were registered at each station. The results show that the patterns are generally similar between the three in-situ stations, especially between the UNDP and MRC station. CHIRPS, on the other hand, evidently slightly overestimates the number and magnitude of low-intensity rainfall events and underestimates high-intensity events.

Overall, these results points towards considerable spatial heterogeneity in terms of rainfall events in the study area. The stations at Prek Chann and Koh Thom lie 6.5 km apart but still register significantly different rainfall sums for individual events, as can be seen in the comparison of daily values in October 2021. Some of that might be due to local conditions at the stations, though no systematic bias can be detected between them. In terms of spatial configuration, the station at Koh Khel is located approximately 13.5 km further North. For individual rainfall events, it exhibits similarly unsystematic variations in comparison to values measured at other in-situ stations. When it comes to the comparison of the magnitude and frequency of rainfall events, though, Figure 3.19 shows that the UDNP and field station exhibit slightly more similar patterns, with the MRC station registering a few more medium-intensity events. This similarity might be due to their spatial proximity.

When it comes to CHIRPS, it is notable that with regard to RMSE values, it is a fairly good predictor for local rainfall values, especially for the MRC an field station, with RMSE results of 42.03 mm and 54.93 mm respectively. These values are similar to those reported by Dandridge et al. (2019), which compared the use of different satellite-based precipitation products in Southeast Asia and found that for elevations between 0 and 100 m, CHIRPS showed an average RMSE of 85.41 mm in comparison to local stations. The same study also noted

an effect observed in this present analysis - namely that CHIRPS shows a better agreement with locally measured data during the wet season season than during the dry season. The authors equally found that CHIRPS often registers low-intensity rainfall events on days that are completely dry according to in-situ stations. Only on 66.8% of all days does CHIRPS correctly make the rainfall / no-rainfall distinction. Part of the reason for this is certainly also that the CHIRPS values are extracted and averaged out for an area across the zone of interest, within which, as we have seen, rainfall is highly heterogeneous according to in-situ stations.

Despite these caveats, the results outlined so far indicate that CHIRPS can be seen as an acceptable predictor of local rainfall characteristics. This is also supported by existing studies, which found that CHIRPS performed well, especially in comparison to other remotely sensed products. Both Dandridge et al. (2019) and Gummadi et al. (2022) report that it outperformed datasets such as the Tropical Rainfall Measuring Mission (TRMM) Multi-Satellite Precipitation Analysis (TMPA), the Global Precipitation Climatology Project, the Climate Prediction Centre (CPC) Merged Analysis of Precipitation, and the Tropical Applications of Meteorology using SATellite and ground-based observations rainfall estimate (TAMSAT).

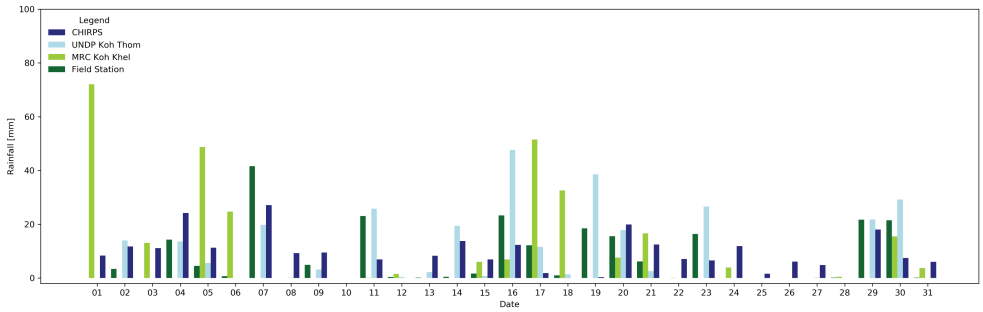

Figure 3.17: Comparison of daily rainfall sums registered by CHIRPS, and by the stations in Koh Thom, Prek Chann, and Koh Khel in October 2021.

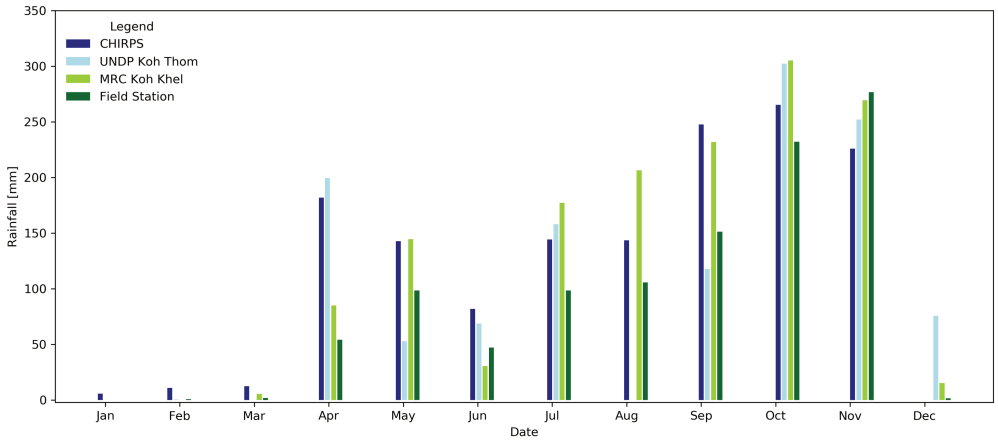

Figure 3.18: Comparison of monthly rainfall sums registered by CHIRPS, and by the stations in Koh Thom, Prek Chann, and Koh Khel in October 2021.

	UNDP	MRC	Field Station
CHIRPS	67.3	42.03	54.93
UNDP	-	83.16	64.84
MRC	-	-	51.42

Table 3.4: RMSE of monthly precipitation sums [mm] compared between stations.

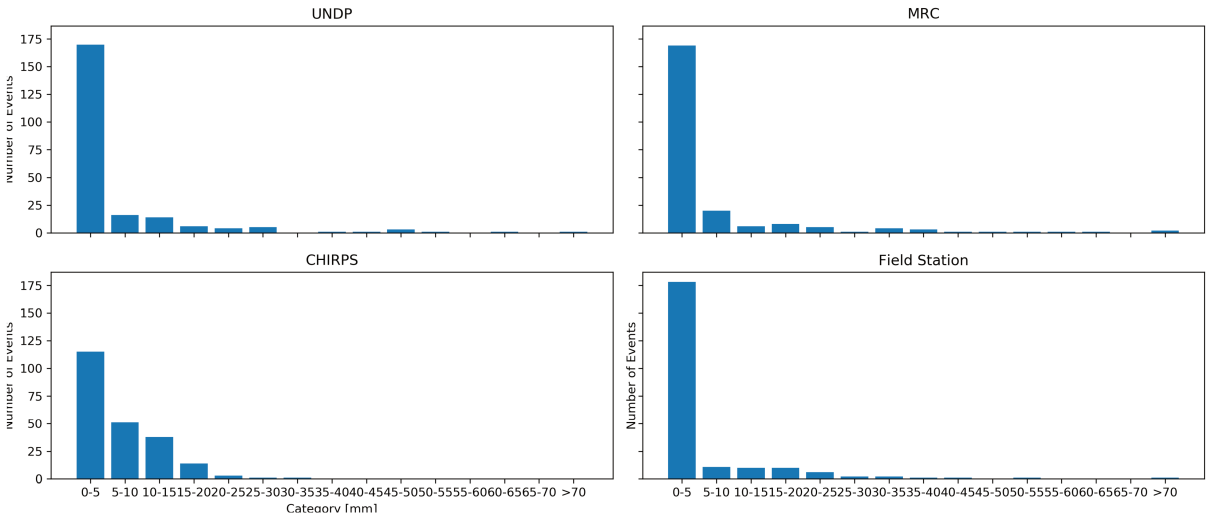

Figure 3.19: Comparison of frequency of rainfall events by intensity registered by CHIRPS, and measured at the meteorological field station at Prek Chann, the MRC station in Koh Khel, and by the UNDP Station at Kho Thom in 2021.

The long-term trend analysis using CHIRPS data since 1981 revealed few significant results.

Solely monthly precipitation in December was found to have increased significantly. This is also visible in Figure 3.20, which shows the rainfall sums for each month since 1981. Figure 3.21, which gives average yearly rainfall distributions for each decade since 1981 also shows that the years since 2011 have seen slightly wetter Septembers and Octobers, though this trend does not meet the requirements for statistical significance (p=0.065 for September and p=0.362 for October). However, the decadal curves illustrate the typical bimodal rainfall distribution across the year in the area of interest.

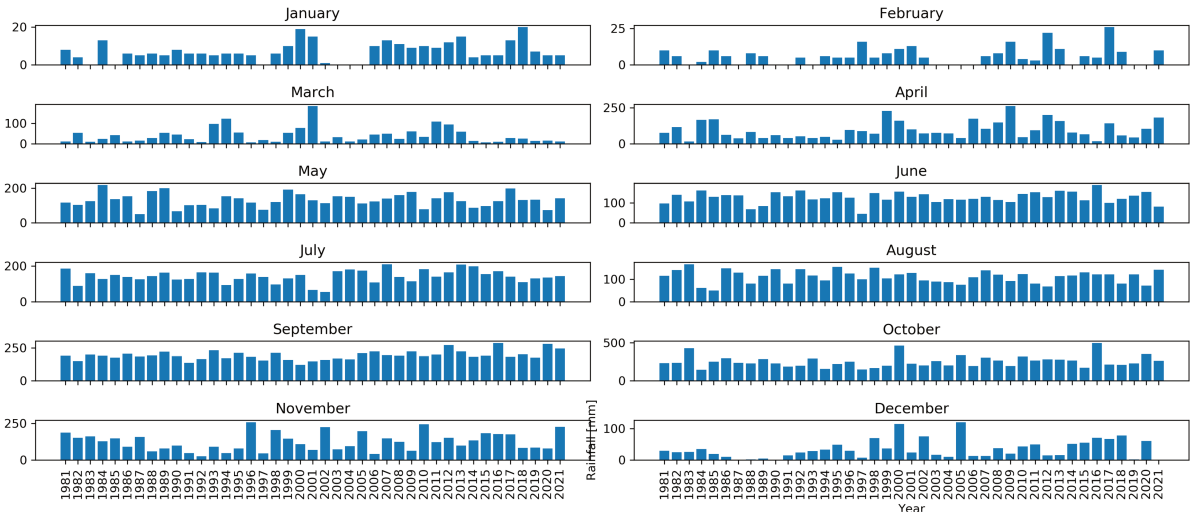

Figure 3.20: Comparison of monthly rainfall sums since 1981 as registered by CHIRPS

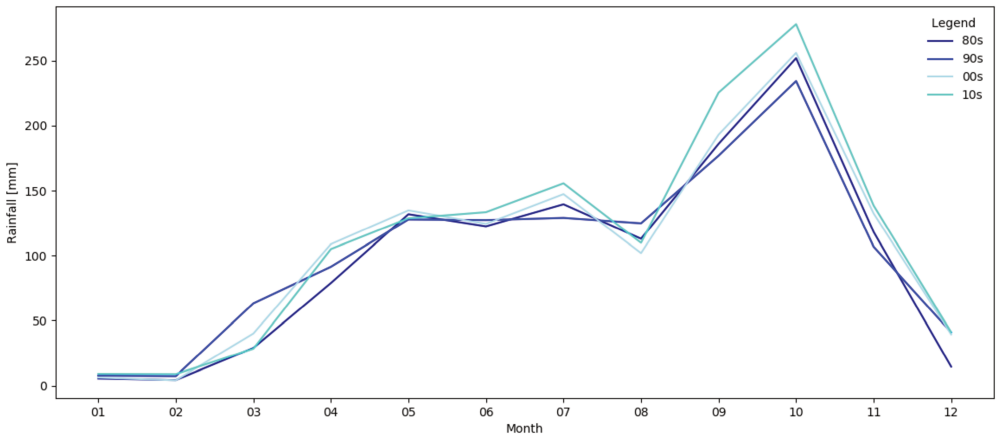

Figure 3.21: Comparison of average rainfall sums per month in every decade since the 1980s as registered by CHIRPS.

3.4 Identifying Inundation Dynamics and Trends Through Satellite Imagery

As outlined in the introductory chapter to this thesis, inundations play an essential role in the hydrological cycle of the Mekong Delta. They furthermore contribute to a wide range of regulating ecosystem services that support the biodiversity and agricultural productivity of the Mekong Delta, from depositing nutrient-rich sediments on the floodplains to recharging shallow aquifers (Kondolf et al., 2018; Boretti, 2020; Kummu and Sarkula, 2008; Dang et al., 2018). It is therefore crucial to understand the temporal and spatial patterns of inundations in the area of interest to this thesis - and how they have changed over the past few decades. However, several obstacles had to be overcome in order to gain insights into these aspects at the local scale.

Previous research existed on the how hydrological changes in the Mekong basin impacted annual inundations in the Mekong Delta, especially their incidence, duration, and spatial pattern of annual inundations. However, these studies were set at larger scales, often focused on Vietnam, and based on different hydrological and hydrodynamic models or on past series of remote sensing imagery (Heng et al., 2021; Try et al., 2020; Li et al., 2019; Shin et al., 2020; Mohammed et al., 2018; Burbano et al., 2020). Each of the proposed modeling approaches comes with its own limitations and simplifying assumptions, as well as with a challenge regarding parametrisation in the relatively data-sparse region of the Mekong Basin. In terms of remote sensing, freely accessible, consistent long-term image time series such as Landsat and MODIS can provide some insights into how the spatial patterns of inundations have shifted (Aires et al., 2020; Dang et al., 2016; Fayne et al., 2017). However, many of these series are limited in terms of the temporal and spatial resolution of images, and, in the case of optical images, exhibit data sparsity during the wet season due to cloud cover. They also have difficulties accounting for water areas dissimulated by natural vegetation. Due to the limitations inherent in each approach, the existing studies are unable to produce both sufficiently extensive time series and adapted spatial and temporal resolutions for analysing long term flood dynamics at local scales.

An alternative path is now available in the form of the Sentinel constellation by the European Space Agency (ESA). Its Sentinel-1 and 2 satellites, launched between 2014 and 2017 (Potin et al., 2019), provide freely available optical and SAR data, at a return period of five to six days

and a spatial resolution of up to 10 m. This makes Sentinel a valuable basis to better understand dynamic hydrological processes, such as inundations, at local scales. Both Sentinel-1 and -2 data have been widely used in hydrological applications, separately and in combination (Twele et al., 2016; DeVries et al., 2020; Tsyganskaya et al., 2018). On the floodplains of the Mekong delta, Quang et al. (2019) and Pham-Duc et al. (2017) both use Sentinel-1 to track annual inundations. However, the disadvantage of the Sentinel series lies in its comparatively short duration, which makes it impossible to observe long-term trends.

To address these challenges, a new method was developed in the course of this thesis to analyse long-term flood dynamics in the Cambodian upper Mekong delta, in order to infer the impact of basin-wide hydrological alterations on local hydro-ecological systems. To circumvent barriers of data sparsity and limitations of any single method, a multi-method approach was employed to reconstruct a time series of daily inundation extents, based on local water level measurements since 1991 and on Sentinel-derived flood maps. It hinges on the construction of a Water Level - Flood Link (WAFL), as is outlined below.

3.4.1 Materials and Methods

An overview of the methodology employed in this analysis is given in Figure 3.22.

The multi-method approach outlined here is based on local knowledge acquired in the course of fieldwork and through exchanges with other researchers working in the area. Besides in-situ measurements, the researchers working on the project of which this thesis forms a part acquired an in-depth qualitative understanding regarding the development projects implemented in the area, local agricultural practices, and local hydrological processes.This understanding provided the context for this approach.

At the core of this methodology is the establishment of a water level - flood link (WAFL). This is achieved by deriving a time series of inundation extents from Sentinel-1 and -2 imagery, and then linking them to locally-measured water levels using a correlation model to take into account propagation delay times. As a subsequent step, a time series of inundation extents is back-calculated on the basis of WAFL.

The accuracy of the WAFL is assessed using Sentinel and Landsat images, as well as the TanDEM-X digital elevation model (12 m resolution). For one thing, WAFL-derived inundation extents are compared to inundation maps directly derived from Landsat and Sentinel-2. For another, they are compared to inundation extents derived from TanDEM-X. In addition, the effect of local land cover variables, especially natural vegetation such as shrubland and trees, on the inundation classification are evaluated using a land use land cover (LULC) classification based on Landsat images.

Finally, the changes in inundation incidences and durations in the Cambodian upper Mekong delta over the past three decades are quantitatively and qualitatively assessed according to break points derived from the hydrological analysis outlined in Section 3.2.

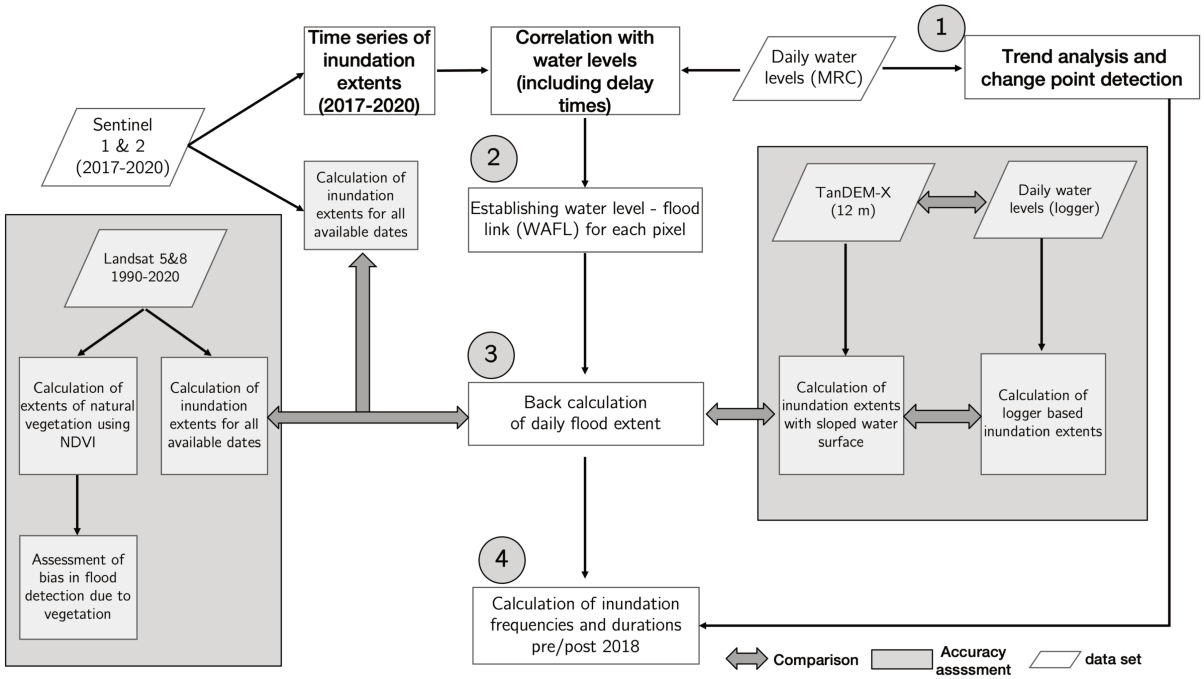

Figure 3.22: Overall analysis workflow for the assessment of inundation trends in the study area.

3.4.1.1 Sentinel-1 and 2

The ESA's Sentinel-1 constellation consists of two satellites, Sentinel-1A and Sentinel-1B, which were launched in 2014 and 2016 respectively. Both satellites have a return period of 12 days, resulting in a combined Sentinel-1 overpass frequency of 6 days. They collect C-band synthetic aperture radar (SAR) imagery in a variety of polarizations, instrument modes, and resolutions.

For this study, interferometric wide swath (IW) images in VV and VH polarization at 10 m resolution are used. The image bands of which a Sentinel-1 tile consists are given in Table 3.5

Like Sentinel-1, the ESA's Sentinel-2 collection consists of a pair of satellites. Sentinel-2A was launched in 2015, followed by Sentinel-2B in 2017. Both satellites have a return period of 10 days, resulting in a combined Sentinel-2 image frequency of 5 days. The constellation provides multi-spectral optical imagery for a total of 12 spectral bands ranging from the blue to the short wave infrared spectrum. All Sentinel-2 bands are given in Table 3.6 below.

Both Sentinel-1 and -2 images were used to generate a series of flood maps for the area of interest for the period 2017-2020. 2017 was chosen as a starting point because the Sentinel satellite constellation was fully in place beginning that year. For this purpose, the series of Sentinel-1 and 2 images available on Google Earth Engine (GEE, Gorelick et al. (2017)) was analysed.

First, images were subjected to multiple pre-treatments. Sentinel-2 images were atmospherically corrected using the sen2cor algorithm (Main-Knorn et al., 2017) and clouds were masked based on the QA band. Sentinel-1 images underwent pre-processing based on the European Space Agency's Sentinel-1 toolbox. Metadata was updated with a restituted orbit file, border noise and thermal noise were removed, and radiometric calibration and orthorectification were applied. In addition, a refined Lee speckle filter (Lee, 1983) was implemented.

Table 3.5: Sentinel-1 bands, their resolutions, and wavelengths.

Name	Resolution	Wavelenght	Description
HH	10 meters	5.405GHz	Single co-polarization, horizontal transmit/horizontal receive
HV	10 meters	5.405GHz	Dual-band cross-polarization, horizontal transmit/vertical receive
VV	10 meters	5.405GHz	Single co-polarization, vertical transmit/vertical receive
VH	10 meters	5.405GHz	Dual-band cross-polarization, vertical transmit/horizontal receive

Table 3.6: Sentinel-2 bands, their resolutions, and wavelengths.

Sentinel-2 SR Band	Description	Native Resolution	Wavelength
B1	Aerosols	60 meters	443.9nm (S2A) / 442.3nm (S2B)
B2	Blue	10 meters	496.6nm (S2A) / 492.1nm (S2B)
B3	Green	10 meters	560nm (S2A) / 559nm (S2B)
B4	Red	10 meters	664.5nm (S2A) / 665nm (S2B)
B5	Red Edge 1 (RE1)	20 meters	703.9nm (S2A) / 703.8nm (S2B)
B6	Red Edge 2 (RE2)	20 meters	740.2nm (S2A) / 739.1nm (S2B)
B7	Red Edge 3 (RE3)	20 meters	782.5nm (S2A) / 779.7nm (S2B)
B8	Near Infrared (NIR)	10 meters	835.1nm (S2A) / 833nm (S2B)
B8A	Red Edge 4 (RE4)	20 meters	864.8nm (S2A) / 864nm (S2B)
B9	Water vapor	60 meters	945nm (S2A) / 943.2nm (S2B)
B11	Short-wave Infrared 1 (SWIR 1)	20 meters	1613.7nm (S2A) / 1610.4nm (S2B)
B12	Short-wave Infrared (SWIR 2)	20 meters	2202.4nm (S2A) / 2185.7nm (S2B)

3.4.1.2 Landsat

As briefly mentioned above, the Landsat satellites maintained by the North American Space Agency (NASA) provide optical imagery. The standout characteristic of this satellite series is its consistency over multiple decades. The first Landsat satellite was launched in 1972 - Landsat 1 - since then, the mission has provided a consistent archive of earth observation imagery. Landsat 1 - 3, carrying a Multi-spectral Scanner (MSS) provided a spatial resolution of 60 m and four spectral bands in the green, red, and near infrared (1 and 2) spectrum for the period between 1972 and 1983. Landsat 4 and 5 also both still carried MSS onboard, but were also equipped with a Thematic Mapper that recorded a larger variety of spectral bands, seven in total. They provide earth observation scenes at a spatial resolution of 30 m between 1982 and 1993, and 1984 and 2012 respectively. They were succeeded by Landsat 7[9], launched in 1999, and Landsat 8, launched in 2013 (Tollefson, 2013). In September 2021, NASA launched Landsat 9. First images from the mission were released at the beginning of November (NASA Earth Observatory, 2021; Masek et al., 2020). The return period of Landsat is 16 days, which allows for the monitoring of processes with moderate temporal dynamics, but places some restrictions on observing highly dynamic processes such as floods. Nonetheless, Landsat has been used for a wide range of

[9]Landsat 6 was lost in a launch failure in October 1993.

Name	Wavelength	Description
B1	0.435-0.451 µ	Ultra blue, coastal aerosol
B2	0.452-0.512 µ	Blue
B3	0.533-0.590 µ	Green
B4	0.636-0.673 µ	Recd
B5	0.851-0.879 µ	Near Infrared
B6	1.566-1.651 µ	Shortwave Infrared 1
B7	2.107-2.294 µ	Shortwave Infrared 2
QA AEROSOL		Aerosol attributes

Table 3.7: Landsat 8 bands.

Name	Wavelength	Description
B1	0.45-0.52 µ	Blue
B2	0.52-0.60 µ	Green
B3	0.63-0.69 µ	Red
B4	0.77-0.90 µ	Near Infrared
B5	1.55-1.75 µ	Shortwave Infrared
B7	2.08-2.35 µ	Shortwave Infrared
ATMOS OPACITY		Atmospheric Opacity
CLOUD QA		Cloud Quality Assessment

Table 3.8: Landsat 5 bands.

large-scale and long-term analyses, from reconstructing a crop history of the US (Johnson, 2019) and creating a global forest cover dataset (Hansen et al., 2013), to monitoring worldwide changes in open water areas (Pekel et al., 2016).

In this thesis, Landsat 5 and 8 were used and an overview of their spectral bands is provided in Tables 3.7 and 3.8 respectively. Landsat 7 was not used due to the fact that images recorded after May 2003 are affected by a failure of the satellite's Scan Line Corrector, which causes stripes in each image for which no data is available. All Landsat images were used via Google Earth Engine (see below), where they are already available in atmospherically corrected form.

3.4.1.3 Google Earth Engine

All remote sensing analyses conducted in the course of this thesis were carried out on the cloud computing platform Google Earth Engine (GEE) (Gorelick et al., 2017). Launched by Google in 2010, it provides a catalogue of remote sensing data, which includes NASA's Landsat and the ESA's Sentinel archives - both in pre-processed form - as well as more specialized datasets, such

as CHIRPS. However, GEE's most considerable advantage is that it outsources computations to Google's servers. Users can launch analyses via the online Javascript API (cf. Figure 3.23) or a locally installed Python API. Then, computations are carried out remotely, which minimizes the computational load on the side of the user. This is a significant advantage for large-scale and long-term analyses, since these often exceed the computational capacity at individual researchers' disposal (Amani et al., 2020).

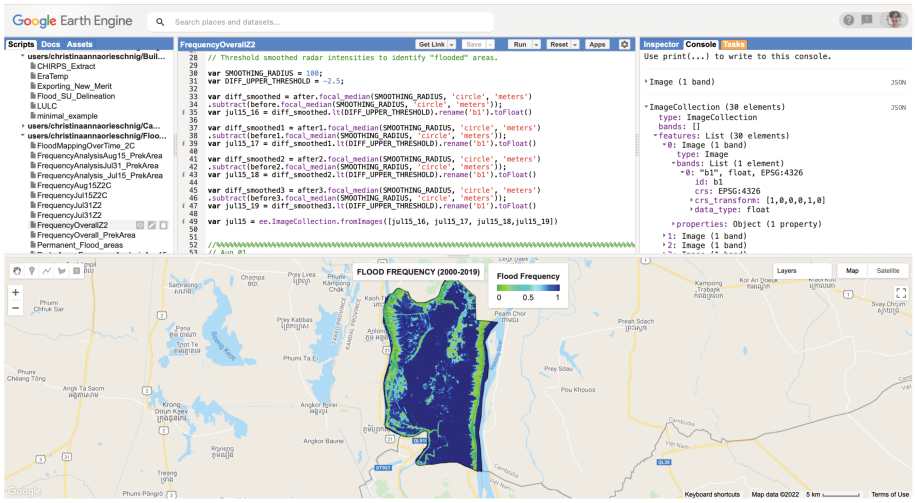

Figure 3.23: The online Javascript interface of Google Earth Engine.

Since its inception, GEE has been widely used in the remote sensing community (Tamiminia et al., 2020). The types of studies conducted on the platform vary wildly, ranging from global-scale land use change analyses to local malaria tracking (Kumar and Mutanga, 2018). Furthermore, GEE has engendered several high-profile studies, such as Hansen et al. (2013), who published a study of global forest loss in Science, and Pekel et al. (2016), whose study on global surface water occurrence and change was published in Nature. Furthermore, GEE has served as the framework for a number of studies in Cambodia and the Mekong Delta (Markert et al., 2018; Venkatappa et al., 2019; Rudiyanto et al., 2019; Binh et al., 2021; Van Tran et al., 2020).

3.4.1.4 Detecting Flood Extents Using Sentinel-1 and 2

To classify each image into flooded and not flooded areas, three spectral indices were first calculated for the optical images: the Normalized Difference Vegetation Index (NDVI, Rouse J.W.

et al. (1974), Equation 3.2), the Normalized Difference Moisture Index (NDMI, Wilson and Sader (2002), Equation 3.3) and the Normalized Difference Water Index (NDWI, McFeeters (1996), Equation 3.4).

$$NDVI = \frac{NIR - Red}{NIR + Red} \tag{3.2}$$

$$NDMI = \frac{NIR - SWIR}{NIR + SWIR} \tag{3.3}$$

$$NDWI = \frac{Green - NIR}{Green + NIR} \tag{3.4}$$

Then, an unsupervised K-means classification approach was chosen (Arthur and Vassilvitskii, 2007; Frank et al., 2016) to identify flooded areas in both Sentinel-1 and -2 images. This classification approach was selected because it can be applied equally to optical and SAR images, and because no local calibration of threshold values is required. As the training period for the classifier, a time window during the 2018 wet season - from September 25 to October 01 - was used due to the large flood extents and sharp contrast between open water and dry areas at this time. Validation of the flood classification was carried out using a total of 2340 points, set manually on the basis of SPOT-6 high-resolution imagery, on four different dates at different stages during the flood cycle: 2017/01/29, 2018/06/24, 2018/08/04, and 2019/01/27. On this basis, a confusion matrix and the kappa coefficient (Congalton, 1991) of the classification were calculated. After validation, the classifier was applied to the entire collection of Sentinel images, and the extents of open water areas were extracted for each image. Finally, the time series of inundation extents was exported, smoothed using a 3-day rolling mean, and scaled down to a daily time step using linear interpolation.

3.4.1.5 Establishing a Water Level - Flood Link (WAFL)

In the dynamics of inundations on large floodplains, a temporal lag is typically observed between the change in river water level and the change in flood extent (Zhang et al., 2017). Time is needed

to fill the water bodies when the river flood occurs, accounting for a temporal lag between the flood dynamics and the river water levels. Similarly, the flood recession on the floodplains is out of phase with the river water level drop, since inundated areas decrease more slowly due to the retention of water by dykes and other floodplains structures. This results in hysteresis effects on the relationship between river water levels and the inundated surfaces (Hughes, 1980; Kummu et al., 2014). Lag times are controlled by the ease with which water can flow between the river and the floodplains, depending on hydraulic controls such as dykes, canals, bank heights, local topography, and water level gradients. Physically-based models require geometric data of the main hydraulic connections and dykes, which are not accessible at this scale. Even high-resolution DEMs are often insufficient in terms of horizontal resolution and vertical accuracy to capture the hydraulic controls by dykes in the area, many of which are below 1 m in height. Due to the low terrain gradient, a water level rise of a few centimetres is enough to act as a tipping point for water to spill over certain dykes and induce several hectares of additional inundated surfaces.

To account for this lag time, the correlative method for flood curves developed by Lamagat et al. (1993) was used. Initially developed to identify correlations between gauging stations, this approach has been used with satellite data series in both the Tana river delta in Kenya by Leauthaud et al. (2013), and at the Niger and Senegal rivers by Bader et al. (2016) (flooded areas) and Belaud and Bercher (2010) (satellite altimetry). It was developed to model the propagation of flood waves, specifically in areas with low slope gradients and observable hysteresis effects in rating curves - such as deltaic floodplains. This approach combines kinematic elements with statistical methods. Its main advantage is that it identifies optimal correlation factors not between the overall time series of flood extents and water levels in the river, but between a set number of sub-sections of the time series. Consequently, it can account for the varying time delays depending on the phase of the flood cycle. Therefore, the time delay is expressed as a function of the river water level, while the flood extent at a given time is a function of the water level observed some days before.

Once the delay times had been made explicit, each inundation map was extracted from the time series of Sentinel-1 and 2 images and assigned a corresponding water level. Then, a flood count and water level link parameter were calculated for each pixel in the areas of interest. The approach used to achieve this is depicted in Figure 3.24. The binary flood maps - flooded pixels

having been assigned a value of 1 - were stacked. Subsequently, the sum of times each pixel was registered as flooded was calculated. As a result, pixels that represent permanent water areas, which are always detected as flooded, have a flood count equal to the number of images in the analysis. Pixels on elevated terrain areas that are never flooded have a flood count of zero. Next, flood counts are linked to water levels measured at Koh Khel. Each pixel was assigned the lowest water level (cm resolution) at which it was detected as being inundated.

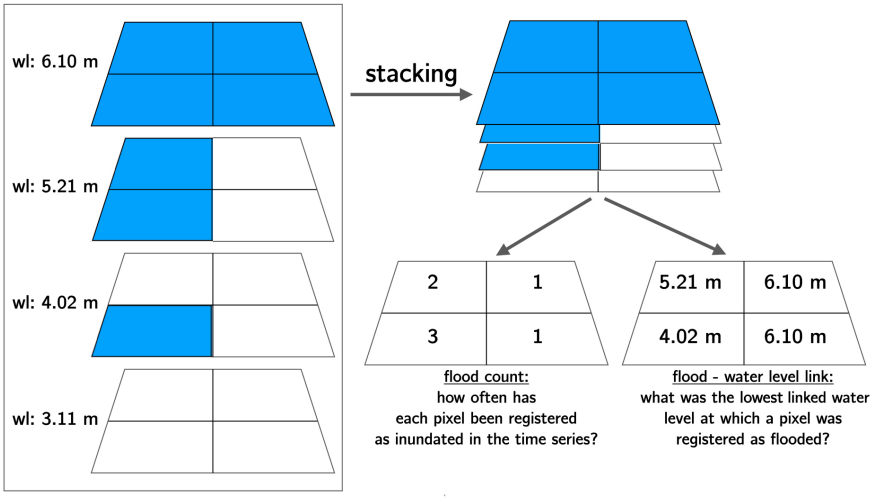

Figure 3.24: Logic workflow for creating the water level - flood link (WAFL). Example of an area with 4 pixels, and 4 images corresponding to 4 different water levels at Koh Khel. Blue areas represent flooded pixels.

3.4.1.6 Comparing the Flood Link With Inundation Extents Derived from Landsat and TanDEM-X

Since the link was established on the basis of relatively recent images from the second half of the 2010s it became necessary to ascertain to which extent it was capable of delivering accurate estimates of inundated areas based on water levels from the 1990s and the 2000s. To this end, two approaches were chosen. The first was a comparison of inundation extents generated on the basis of the WAFL with those directly derived from Landsat images from the period 1991-2020. The second was to use the TanDEM-X (12m) Digital Elevation Model (DEM), which is based on SAR imagery collected in the early 2010s, to generate estimates of flood extents and compare them with those generated on the basis of WAFL.

In order to assess the accuracy of the WAFL, the inundation extents that it found were

compared with two other sources of information on inundations: inundation maps derived from historical Landsat imagery and inundation extents estimated from the TanDEM-X elevation model.

For the comparison with Landsat, a total of 94 optical Landsat-5 and -8 images were used.

To derive inundation maps from Landsat images, the same spectral indices as for Sentinel were calculated, and the images were then partitioned into flooded and dry areas by an unsupervised k-means algorithm. These maps were then compared with the inundation extents generated using the WAFL and the water level observed at the date the image was taken. First, the total inundated area was derived for each of the 94 images and compared to the calculated inundated area. Second, six Landsat images from flood seasons during the period of interest (1991-2020) were chosen to identify discrepancies in spatial inundation patterns. These images, at a time step of about five years, were selected because they provide rare cloud-free wet-season scenes. They date from 1991/11/29, 1995/11/05, 2000/08/31, 2005/08/21, 2013/09/12, 2015/09/11, and 2020/11/28.

The second method of testing the applicability of WAFL was to derive inundation maps from the TanDEM-X (12 m resolution) elevation model, provided by the German aerospace agency (Rizzoli et al., 2017). This DEM was used to assess the extent of inundation patterns as if they were solely linked to differences in detectable terrain elevation in the study area. To establish the comparison, flood extents were generated from the DEM by super-imposing a planar water surface onto the DEM and classifying all areas that were beneath the elevation of that surface as flooded. The planar water surface itself takes into account a North-South slope, based on water level measurements at Koh Khel and in-situ measurements at the western end of a Prek at the center of Zone A. Similar to the Landsat measurements, a comparison of the size of inundated areas was carried out, along with spatially explicit comparisons of the distribution of inundations.

The comparison was also performed locally, directly based on in-situ measurements. The in-situ water level measurements were carried out using a differential pressure logger (Onset Hobo MX2001), with a complete time series available from September 2020 to April 2021 at 15-minute intervals. First, a pseudo water level in the floodplains within a radius of 1km of the logger was generated. This was achieved using inundation extents detected through Sentinel images, and the DEM-derived elevation-area curve of the zone, and based on the assumption that

the water level is horizontal in such a small area (see Figure 3.25c). This pseudo water level was then compared with the levels measured in-situ. In reverse, the in-situ water level measurements were transformed into estimates of the size of the inundated areas within this 1 km radius around the logger, using the same curve. Finally, the inundation curves in this sub-area observed from Sentinel, and generated from WAFL and TanDEM-X were compared.

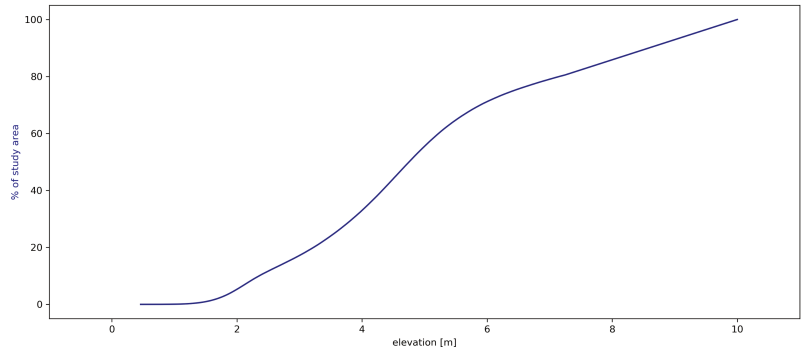

(a) Elevation-area curve Zone A

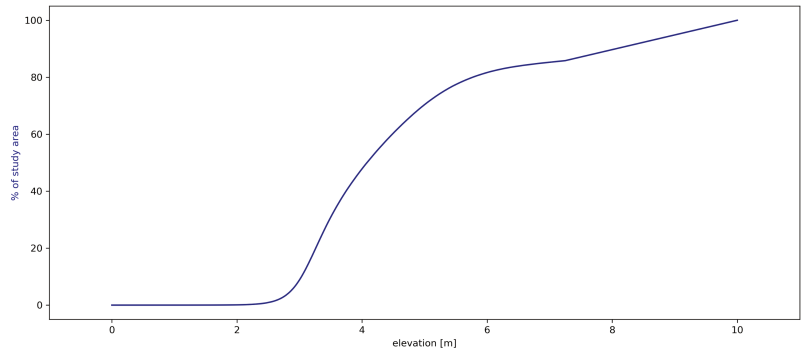

(b) Elevation-area curve Zone B

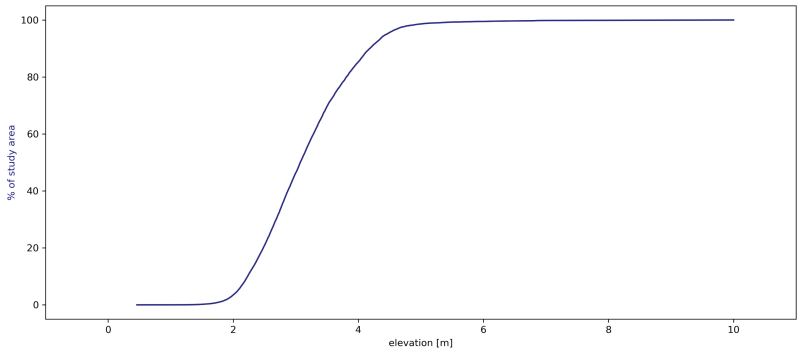

(c) Elevation-area curve in the 1km-radius around the logger in Zone A

Figure 3.25: Elevation-area curves according to TanDEM

3.4.1.7 Land Use Classification: Detecting Natural Vegetation

Finally, vegetation is another element that remains to be tested to assess the applicability of the WAFL. Natural vegetation, such as shrubland and forests, can easily obscure open water surfaces due to canopy cover, especially in optical remote sensing imagery (Tsyganskaya et al., 2018; Pekel et al., 2016; Plank et al., 2017). Therefore, discrepancies between calculated and observed inundated areas might also be due to this obscuring effect, rather than the performance of the classification method. In Cambodia especially, it is known that forest loss has been a notable issue over the past few decades. Driven by economic developments and the Cambodian government's policy of land concessions, forested areas decreased by 12.4% between 2000 and 2012 alone (Davies et al., 2015). Lohani et al. (2020), evaluating forest loss in Cambodia between 1993 and 2017, found that, overall, 19% of primary forest was lost, that the rate of deforestation is accelerating, and that the majority of deforestation is centered in the floodplain, with 31% of forests there having been lost since the 1990s.

To assess the long-term change of land cover in the area of interest and to gauge the extent of these changes on the detection of inundations, an approach relying on a simple thresholding method using the NDVI was chosen. The NDVI was calculated for composite Landsat images for the dry seasons 1990/1991, 2000/2001, 2010/2011, and 2020/2021 for the months between March and May, which are the driest in the region. Then, areas exhibiting an NDVI of over 0.55 (Nath and Acharjee, 2013; Hashim et al., 2019) were classified as likely forest and shrubland. Further on in the analysis, the obscuring effect of canopy cover was taken into consideration by considering low-lying areas classified as natural vegetation, which were otherwise surrounded by open water surfaces, as likely flooded.

3.4.1.8 Flood Dynamics Analysis: Calculating Inundation Durations and Incidences

As a final step in this analysis, flood extent maps were used to generate inundation durations and incidences for each pixel (10 m) in the study area for the comparison periods identified on the basis of the hydrological time series. The term "inundation incidence" refers to the percentage of years in each of the two comparison periods during which any one pixel was flooded. Six different incidences were calculated: the overall annual inundation incidence (the % of years

during the period that a given pixel is flooded, regardless of the date), along with inundation incidences at dates of interest to agricultural practices in the area, identified on the basis of interviews with stakeholders. These are the 15th of July, the 31st of July, the 15th of August (of importance for harvesting early wet season crops), the 31st of August, and the 25th of September (of importance for rainy season cultivation and planting of recession crops).

3.4.2 Results

3.4.2.1 Detection of Inundation Extents

In total, 119 Sentinel-2 and 360 Sentinel-1 images, taken between 2017/01/01 and 2020/12/31 were processed. This means that, on average, one image is available every three days. An example of an inundation map derived from a Sentinel-2 image on the basis of the k-means classification is given in Figure 3.26 below. The average accuracy of the classification of flooded areas lay at 96.5%, with a Kappa value of 0.785. However, it must be mentioned that these values at least partly result from the fact that the validation data used was itself derived from remote sensing imagery. Though it was set on the basis of high-resolution imagery, and with first-hand knowledge of the study area in mind, the validation points were still only set in unambiguous areas. Consequently, areas such as flooded vegetation or inundated rice fields prior to planting that cannot be easily discriminated as either flooded or not in satellite imagery are underrepresented, and their ambiguities missing from the validation results.

Dynamics of inundation extents in Zone A and B, detected on the basis of optical and SAR Sentinel imagery and in relation to water levels at Koh Khel, are shown in Figure 3.27. A good general correspondence between the dynamics of the two curves can be observed. A time delay between the dynamics of the water level curves and the response of the inundated areas can be clearly seen. Large inundated areas correspond to high water levels several days prior, justifying the use of the Lamagat model as explained in the previous section.

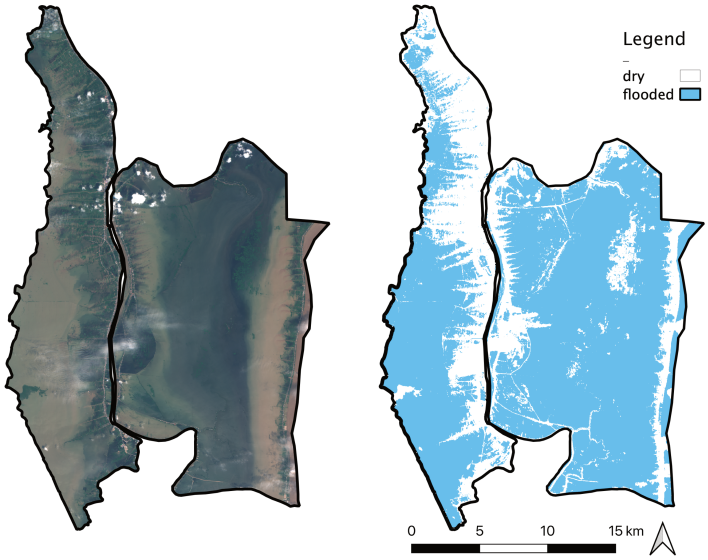

Figure 3.26: Example of classification using k-means and optical Sentinel data on 2018-10-01

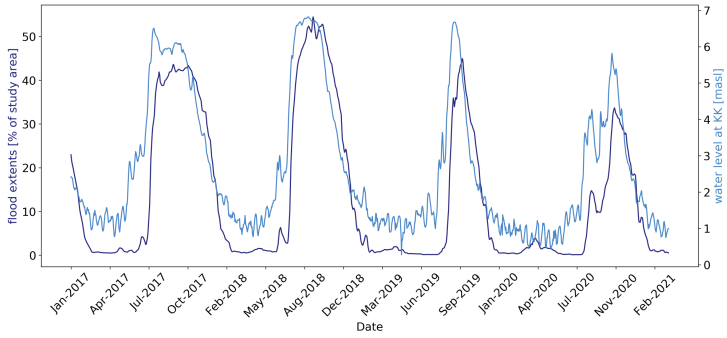

(a) Zone A

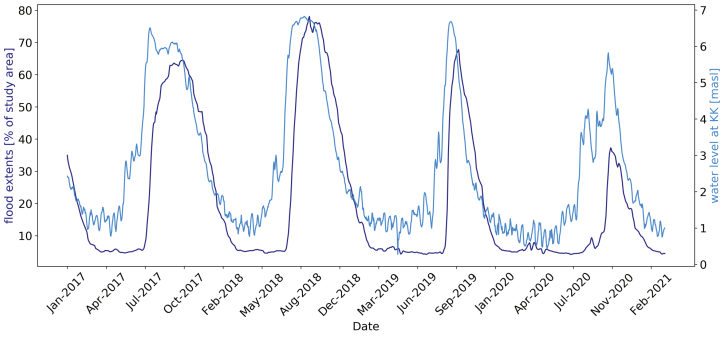

(b) Zone B

Figure 3.27: Dynamics of inundation extents and water levels measured at Koh Khel in the areas of interest 2017-2020.

3.4.2.2 The Water level flood link (WAFL)

The water level flood link (WAFL) was calculated in accordance with the methodology described above. It is given in Figure 3.28, alongside the TanDEM-X elevation model. As can be seen, the WAFL shows similar elevation gradients to those seen in the DEM.

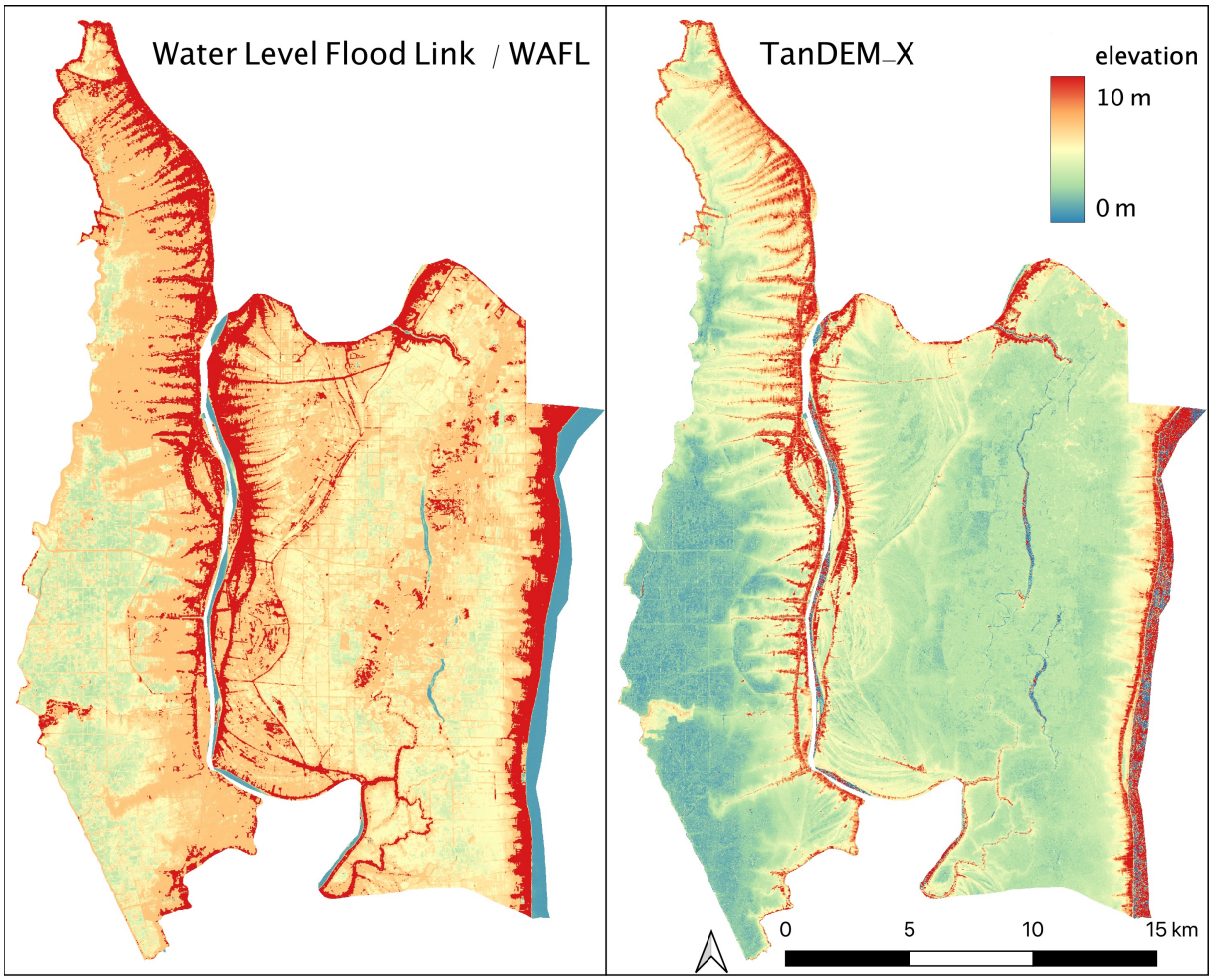

Figure 3.28: Side-by-side comparison of the water level at which each pixel becomes flooded, according to the WAFL, and the TanDEM-X terrain elevation model.

3.4.2.3 Comparison of Calculated Inundation Extents with Flood Maps Derived from Sentinel and Landsat and Influence of Natural Vegetation

In terms of comparing the inundation extents calculated using the WAFL with flood maps derived from Sentinel- and Landsat images, there is widespread agreement, though idiosyncratic variations remain.

Figure 3.29, shows the agreement between WAFL- and Sentinel-2 derived inundation extents at three dates during the flood seasons in 2018, 2019, and 2020. The 2018 image is partially obscured by clouds that are misclassified as dry areas in the Sentinel-derived inundation map. For the 2019 and 2020 images, average classification accuracies lie at 90.60%.

The agreement between the calculated flood extents based on WAFL and those observed in the 94 Landsat images used in this analysis is shown in Figures 3.30 and 3.31. It emerges that in terms of overall inundated areas, there is a strong agreement between the two methods. As Figure 3.30 shows, there are some deviations in years that saw heavy floods, during which calculated inundation extents are lower than those obtained through Landsat classification.

In addition, it can be noted that the spatial distribution of inundations varies between the two methods of detection and that the deviations are more extensive the further back in time the points of comparison lie. For example, Figure 3.31 shows that WAFL-derived inundation maps detect extensive inundated areas in Zone B, while these areas are dry according to the Landsat classification. In contrast, areas of medium elevation in Zone A (transition zones between Boeung and Chamkar) appear as flooded in the 1990s and early 2000s in Landsat images, but are registered as dry by WAFL. The strong agreement between the total water surfaces obtained by the two methods may thus be contingent. This hypothesis will be further investigated in the discussion section.

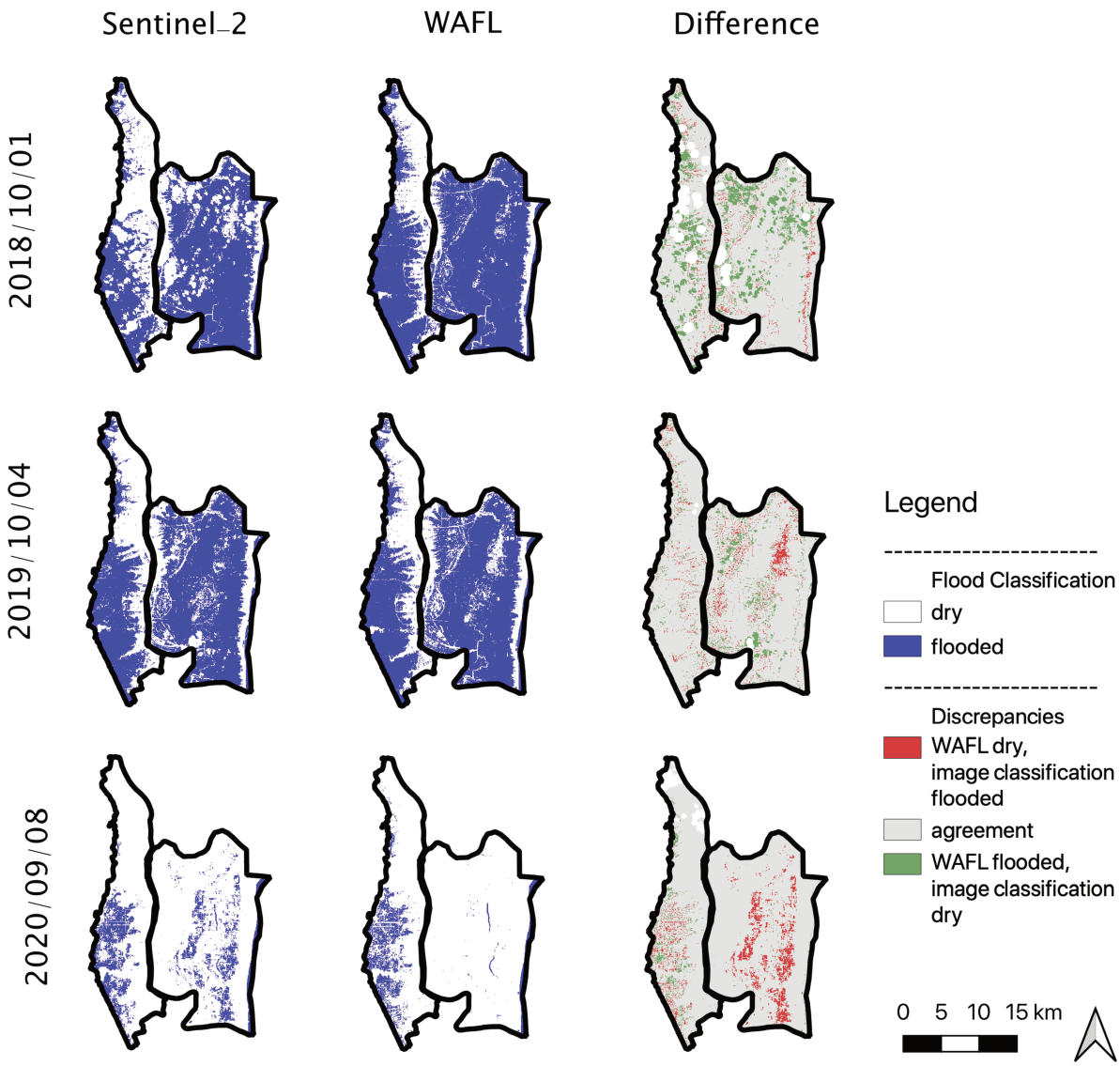

Figure 3.29: Comparison of WAFL-derived inundation extents, and extents directly derived from Sentinel-2 images in 2018, 2019, and 2020.

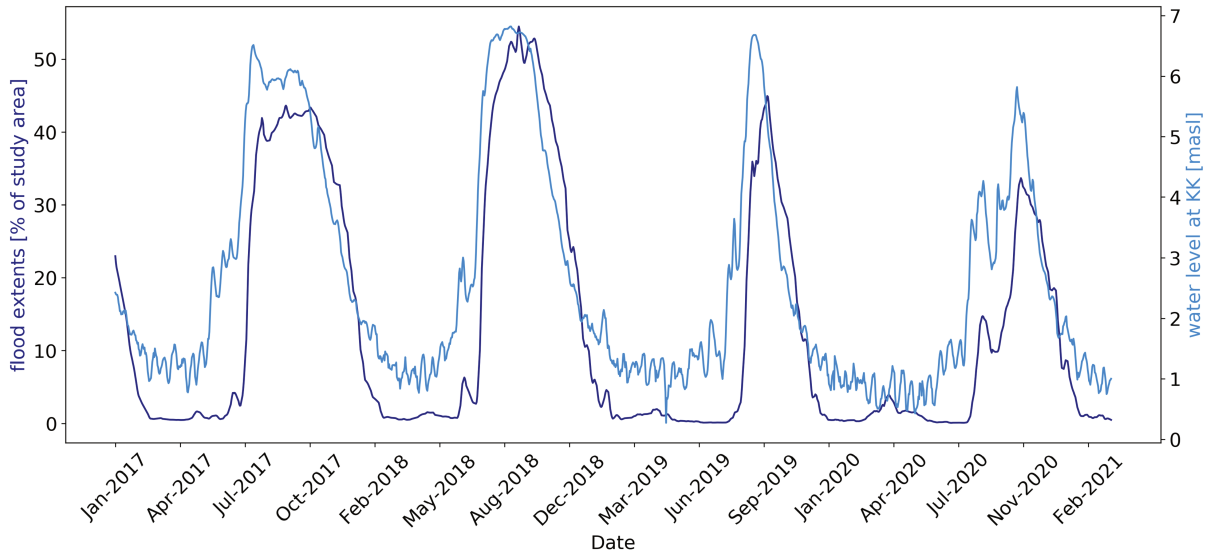

(a) Zone A

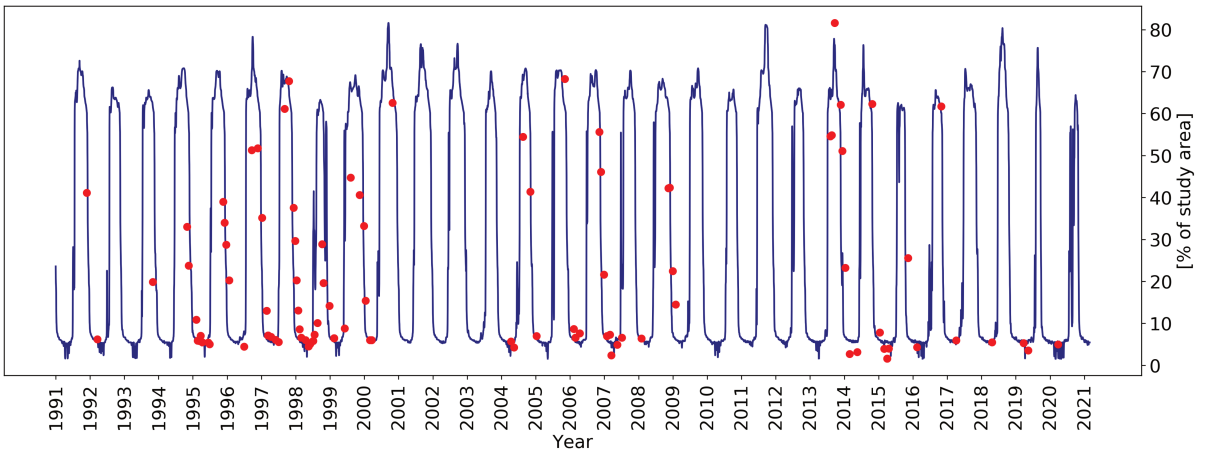

(b) Zone B

Figure 3.30: Comparison of inundated areas - time series derived from the WAFL, and individual Landsat-5 and -8 images

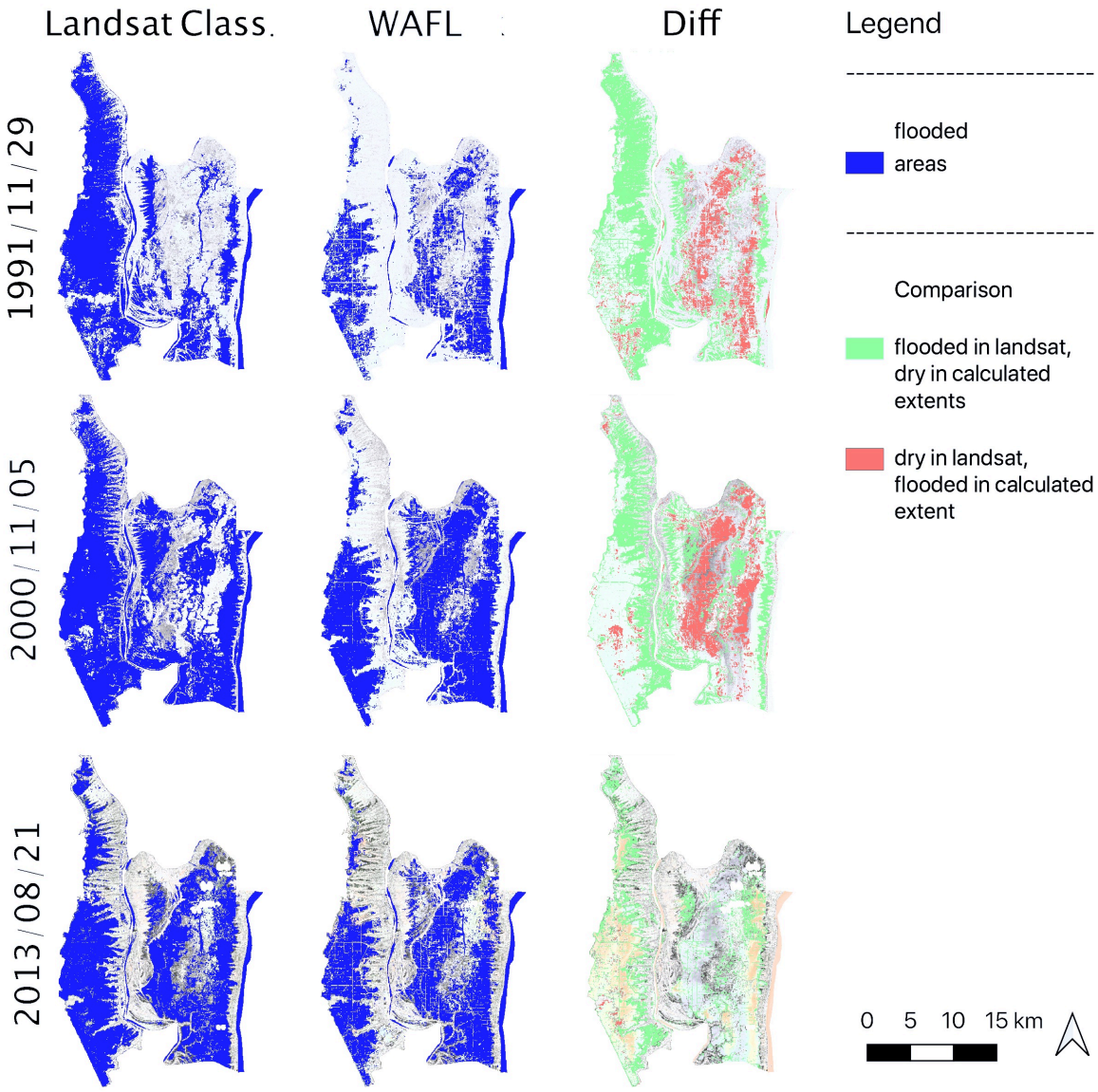

Figure 3.31: Comparison of inundation extents derived from the WAFL and Landsat-5 and -8 images

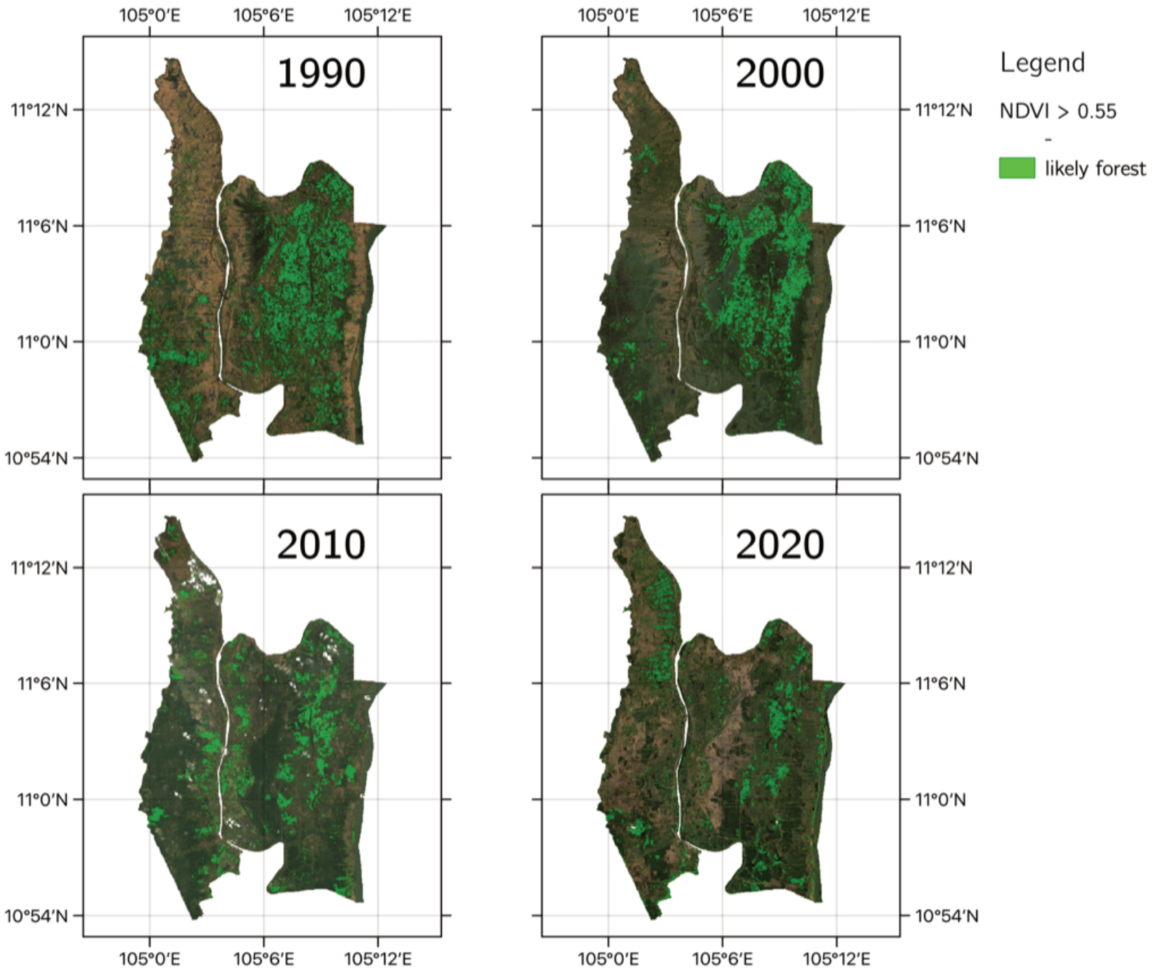

Figure 3.32: Distribution of natural vegetation in the early 1990s, 2000s, 2010s, and present.

The analysis of the extents of natural vegetation indicates that extensive areas of shrubland and regularly flooded forests were present in Zone B in the 1990s, but that they shrunk to a fraction of their former size by 2020 due to large-scale conversions to rice fields. As Figure 3.32 shows, the decrease between 1990 and 2000 is limited, at ca. 2% of the overall area. After that, there is a sharp decline: -42% in comparison to 1990 levels by 2010, and -62% by 2020. Such findings are supported by interview data.

In Zone A, the development is different. Here, natural vegetation detected in the early 1990s is located in the southwestern part of the study area. This patch of vegetation decreased considerably between 1990 and 2000 - by 64% in fact - due also to conversion to rice fields. After that, the overall extents of detected natural vegetation rebounded and even gained 20% in area in comparison to 1990. However, the increased extent of the detected natural vegetation

is more likely to be due to the planting of fruit trees such as mango, whose areas, according to interviews and agricultural statistics, have sharply increased over the last 10 years.

Furthermore, the analysis of the extents of natural vegetation shows that there is an extensive overlap between those areas that are detected as flooded in WAFL-derived maps, but not by those generated directly from Landsat images. The Overlap line of Table 3.9 shows that upwards of 93% of pixels that exhibit these discrepancies coincide with the detected extents of natural vegetation. This indicates that the floods that are actually present may be masked by canopy cover and are thus undetectable by Landsat imagery. If one considers that all forest pixels that overlap with areas being detected as dry by Landsat and wet by the WAFL are indeed flooded, agreement scores between the two methods for detecting flood extents increase from an average of 79.75% to 87.16% for Zone A, and from 68.49% to 87.18% for Zone B.

	Zone	1991	1995	2000	2005	2013	2015	2020
Agreement between LS and WAFL	A	67.64	68.85	74.98	81.85	85.68	85.87	93.37
[% of study area]	B	72.25	49.14	57.49	53.08	78.35	78.00	91.11
LS Wet - WAFL Dry	A	25.83	16.14	20.03	8.71	6.09	8.41	4.37
[% of study area]	B	6.93	14.68	19.76	11.06	8.9	20.13	7.37
LS Dry - WAFL Wet	A	6.53	15.00	4.99	9.44	8.22	5.72	2.25
[% of study area]	B	20.82	36.19	22.75	35.87	12.75	1.86	1.50
Overlap of LS dry area with forest	A	99.93	99.93	99.93	99.93	97.09	99.93	99.89
[% of dry area]	B	99.97	99.97	99.97	99.97	93.42	99.95	99.96
Corrected agreement	A	74.17	83.84	79.97	91.28	93.66	91.59	95.62
[% of study area]	B	93.06	85.32	80.23	88.94	90.26	79.86	92.61

Table 3.9: A comparison of the agreement and discrepancies between the WAFL-derived inundation extents (WAFL) and the Landsat-derived flood maps (LS).

3.4.2.4 Comparison of Calculated Inundation Extents with Flood Maps Derived from TanDEM-X

When it comes to the flood extents derived from TanDEM-X and their comparison with the inundation maps created using the WAFL, several salient points can be observed. The comparison between TanDEM-X derived inundation maps in the 1-km radius around the in-situ sensor in Zone

A and direct inundation observations from Sentinel images reveals a very good correspondence (see Figure 3.33). Some hydraulic elements, like dykes, do not appear in TanDEM-X. This leads to an overestimation of flooded areas with the DEM. We can also expect that these elements slow the filling of the area, introducing some delay between the water level measured at the sensor and the response in terms of inundations. This can be observed in Figures 3.34a and 3.34b which show a lag time of a few days between the two curves. In addition, it emerges that the WAFL underestimates flood extents in this particular part of the study area in comparison to both the Sentinel-derived flood extents and those calculated from the TanDEM-X.

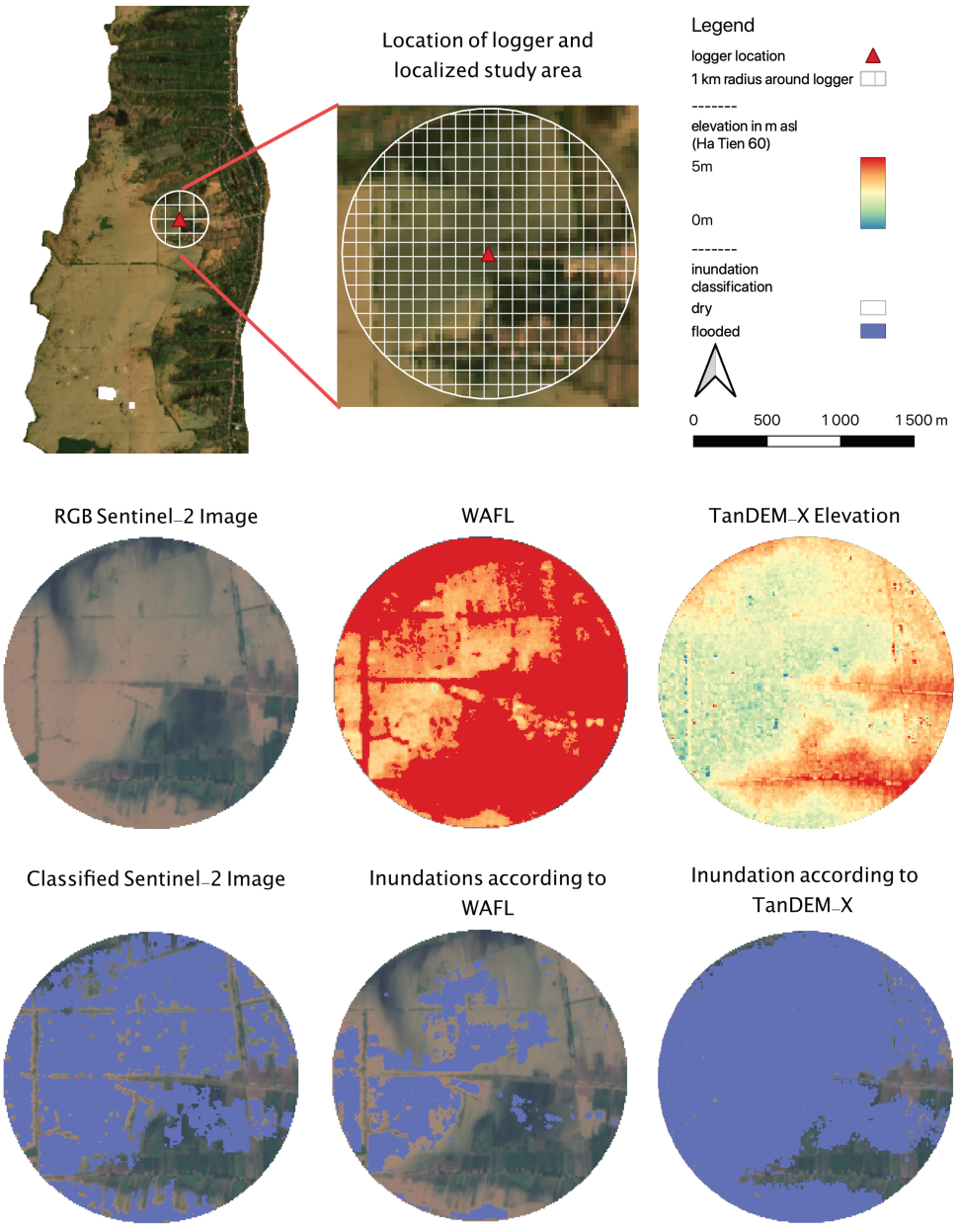

Figure 3.33: Local comparison of TanDEM-X-derived flood extent and WAFL-derived flood extent observed through Sentinel images.

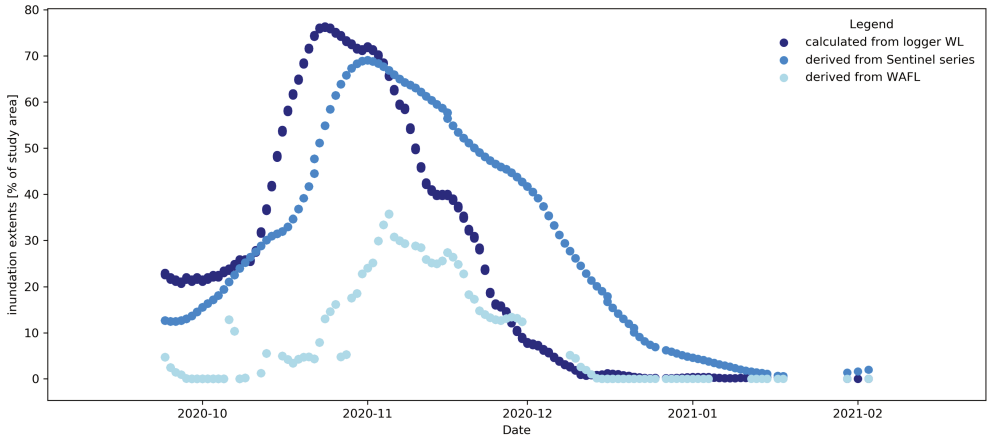

(a) Percentage of flooded area in the 1 km radius around the in-situ logger at Prek Chann West (PCW), derived from Sentinel, and calculated via the elevation-area curve of the TanDEM-X and WAFL.

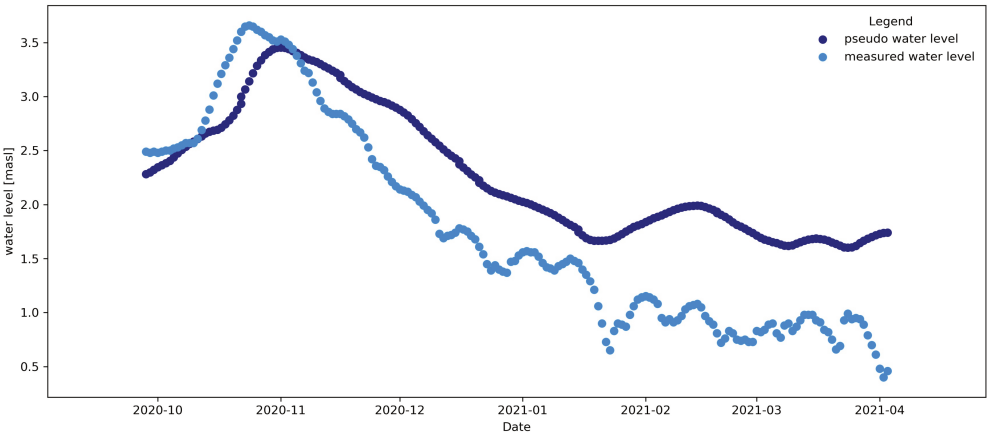

(b) Comparison of the pseudo-water-level calculated from the remote sensing observations and the TanDEM-X elevation-area curve, and the values measured by the in-situ logger

Figure 3.34: Comparison of DEM with local water level data.

At a larger scale, the quality of this correspondence decreases, which illustrates the limitation of the DEM (especially to capture hydraulic connections and barriers) and of the assumption of a planar water surface. We can also expect errors due to propagation times not being evenly distributed throughout the area.

The water level at which pixels become flooded according to the WAFL is generally higher than their elevation in the TanDEM-X model (see Figure 3.28). The exception to this is the center of Zone B. Here, the WAFL shows some areas that become flooded at higher water levels than the surrounding terrain, while the TanDEM-X registers continually low elevations.

As a consequence of this discrepancy between the WAFL and TanDEM-X elevations, TanDEM-X-derived flood extents are generally higher than those calculated using the WAFL (see Figure 3.35), even when taking into account a North-South slope of the water surface area.

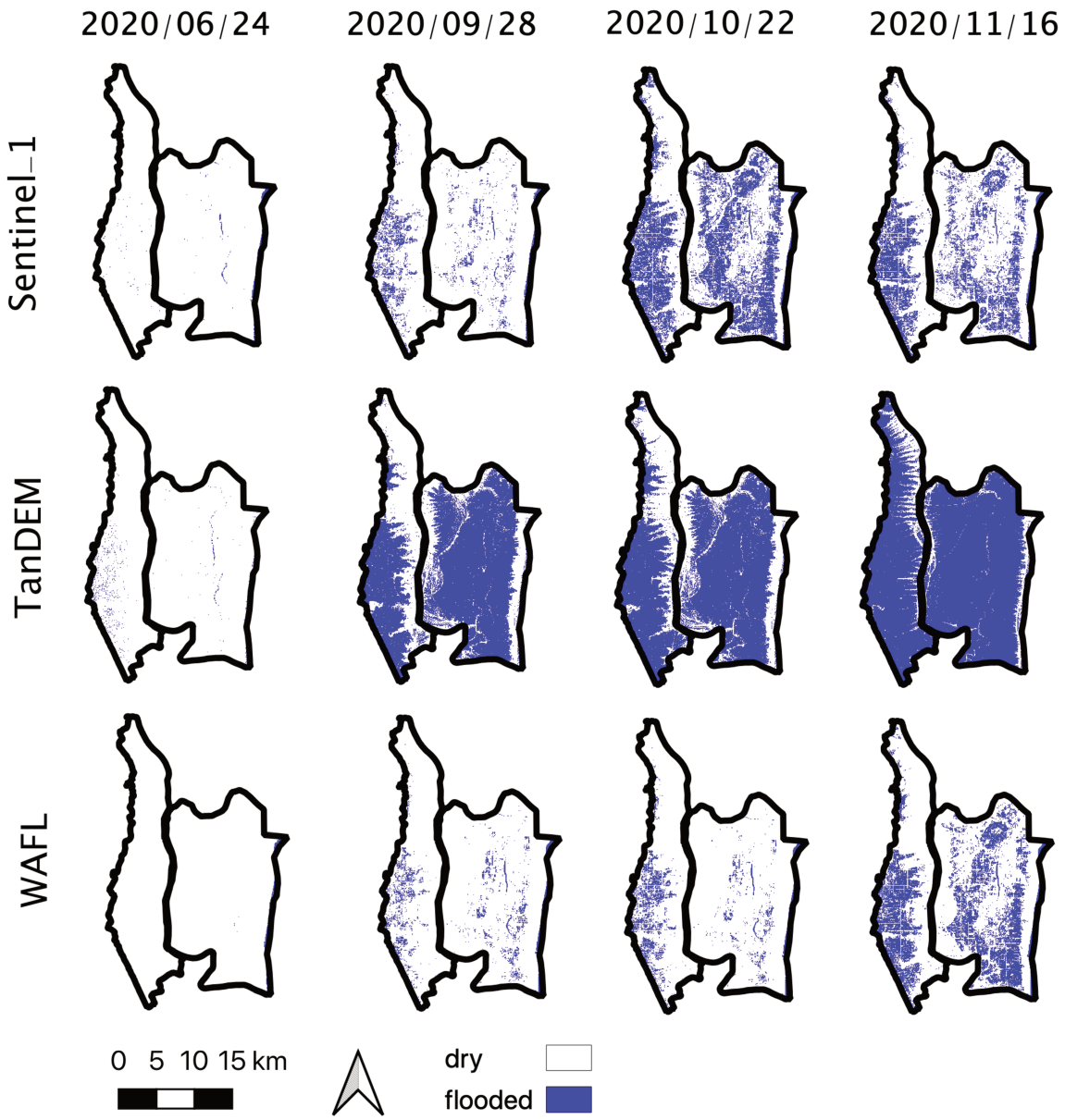

Figure 3.35: Comparison of inundation extents derived from TanDEM-X, and calculated from the WAFL, and as observed from Sentinel-1 for four dates during the 2020 flood season.

3.4.2.5 Changes in Inundation Incidence, Durations, and Patterns Pre- and Post-2008

When the WAFL is applied to the entirety of the water level time series to generate inundation maps, several trends emerge for the comparison periods 1991-2008 and 2009-2020. These trends

are summarized in Table 3.10. It emerges that average annual inundation durations in both zones have decreased. In some areas of both zones, this decrease is as much as 39 days in comparison to the baseline period 1991-2008. In Zone A, the average decrease, at 15 days, was lower than in Zone B, at 23 days.

As for inundation incidence, a similar overall declining trend can be noted. However, the magnitude of this decline is unevenly distributed across the flood season. Overall, there is a sharp decrease in inundation incidence in July and early August in both Zone A and B. In Zone A, the largest mean decrease, at -20% of years per period, can be observed in late July. In Zone B, this is the case for mid-August, at -23%. In contrast, the decrease in mean inundation incidence is limited in late September, a time at which the flood peak would traditionally have occurred already. At this time, the average inundation incidence remains unchanged in Zone B, and only declines by -8% in Zone A. On an annual basis, the decline in inundation incidence is much larger in Zone B, at -6% than in Zone A at -2%.

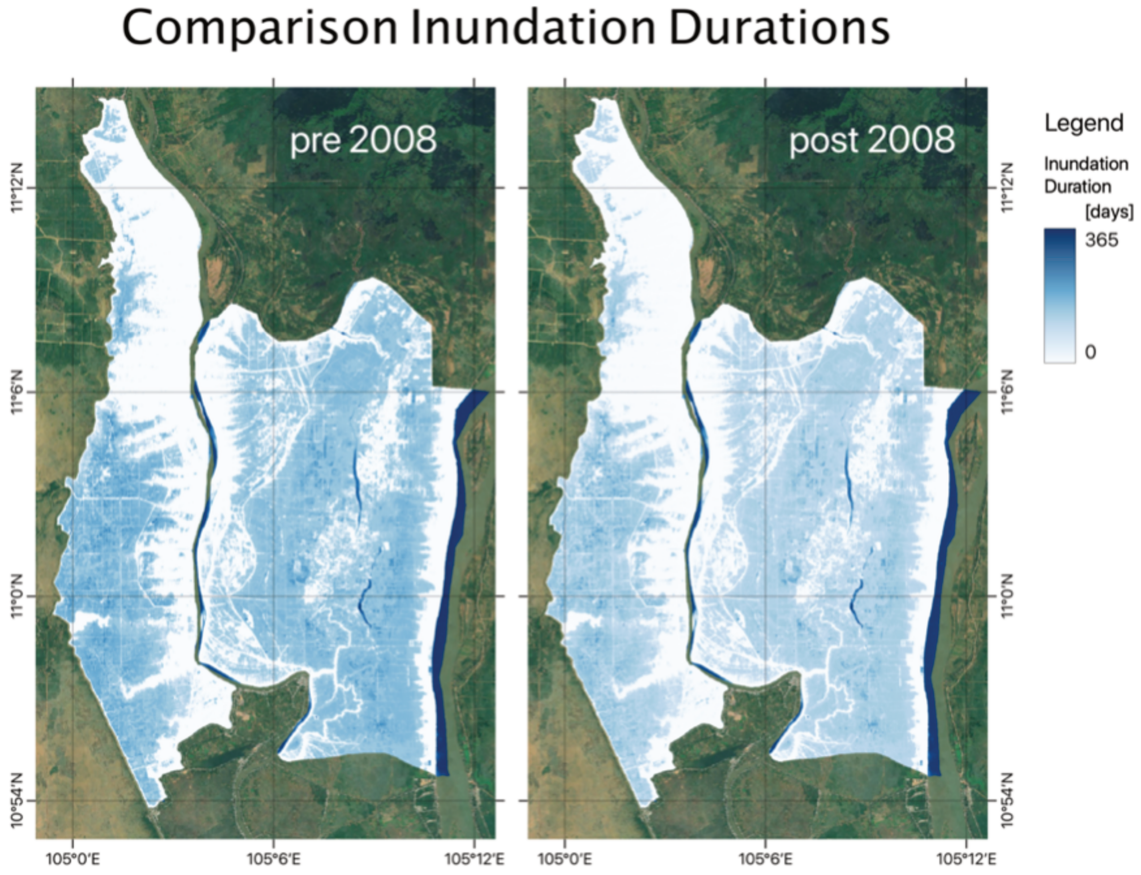

Figure 3.36: Change in inundation durations pre- and post-2008

Parameter		Pixel-based changes in inundation incidence [% of years/period]						Changes in inundation duration [days]
		Jul 15	Jul 31	Aug 15	Aug 31	Sep 25	Overall	
Zone A	Max +	5	5	5	20	15	12	4.81
	Mean	-19	-20	-18	-16	-8	-2	-15.21
	Max -	-53	-41	-64	-33	-38	-25	-39.25
Zone B	Max +	5	5	5	15	15	12	5.17
	Mean	-13	-11	-23	-7	0	-6	-22.97
	Max -	-51	-48	-43	-35	-38	-30	-39.14

Table 3.10: Average changes in inundation incidence and durations in Zone A and B pre- and post-2008 for individual pixels. Given are the largest increase in flood incidence and duration for any individual pixel in the study area (Max +), the largest decrease for the same (Max -), as well as the average change in incidence and duration across all pixels in the study area.

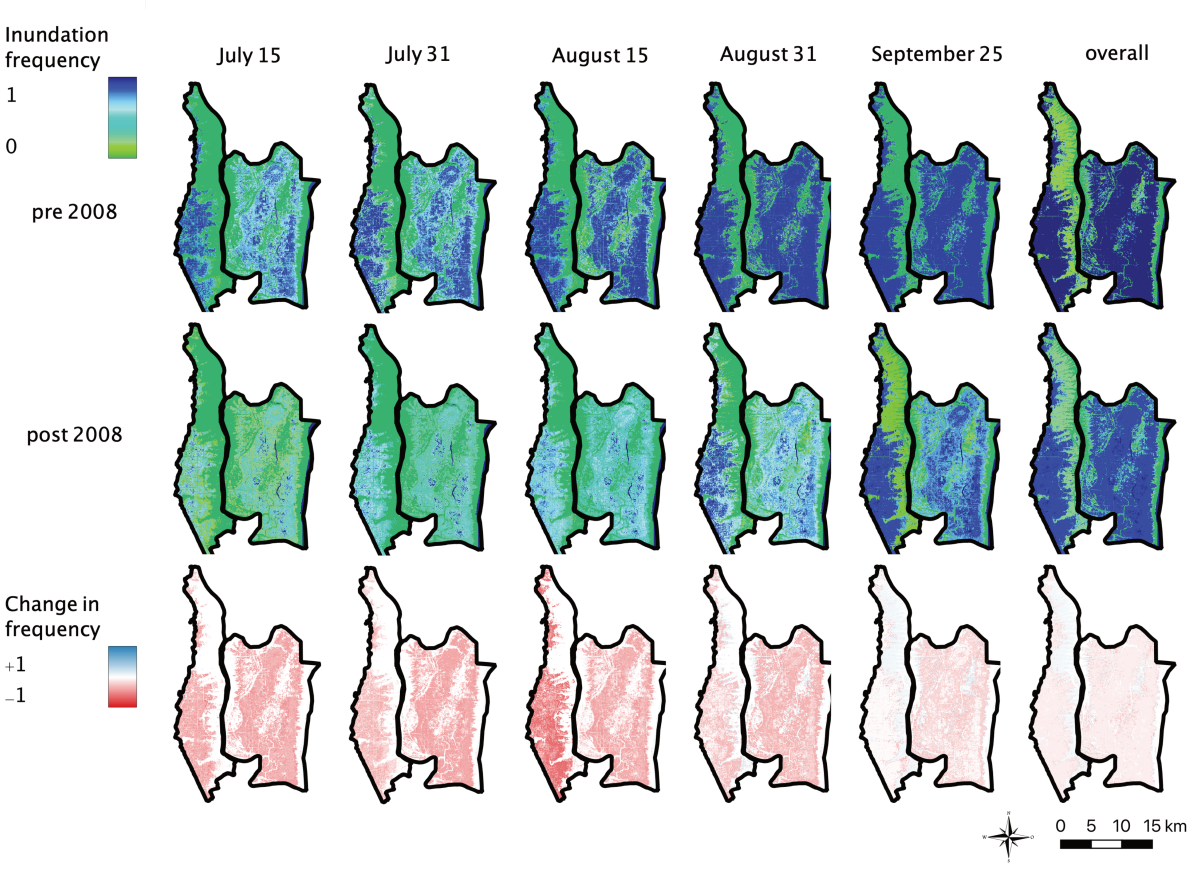

Figure 3.37: Visual comparison of inundation incidences pre- and post-2008

3.4.3 Discussion

3.4.3.1 Local Hydrological Trends and their Reflection of Basin-Wide Changes

Hydrological trends in the Cambodian upper Mekong delta closely mirrored those observed in basin-wide studies, with shorter flood durations and lower wet season water levels. Furthermore, the division of comparison periods into a pre- and post-2008 series mirrors the break point found in basin-wide studies, such as Yun et al. (2020) and Heng et al. (2021).

3.4.3.2 Inundation Mapping Using Sentinel: Between Biases and the Value of Observing Local Dynamics

In terms of inundation dynamics, curves of flood extents closely correspond to those of locally measured river water levels, both for Zone A and B. The most noticeable difference between the two zones is that the delay time between the two curves is larger for Zone B than for Zone A, which may be due to its larger width, as well as the relatively shorter length of the Preks connecting the river to the floodplains. In combination, these terrain characteristics mean that floods take longer to reach the center of Zone B than of Zone A. Another resulting characteristic that can be observed for both Zones is that shorter flood durations result in lower maximum inundation extents. This means that even if the peak water levels of two years match up closely, the peak inundation extents won't be the same if the flood duration is shorter.

3.4.3.3 Validity of the WAFL: Balancing Natural Vegetation, Sedimentation, and Terrain Correspondence

The comparison between WAFL-derived inundation extents and flood maps extracted from Sentinel-2 imagery reveals several advantages and drawbacks of the proposed methodology. First, it clearly illustrates the benefit of using the WAFL-reconstructed inundation extents for the image during the 2018 flood season. The optical Sentinel-2 images at this date show several gaps, left by cloud masking. However, not all clouds were properly detected by the masking algorithm and those that remain are falsely classified as dry areas in the Sentinel-derived flood map, leading

to inconsistencies with the WAFL classification. The drawbacks of the methodology are most clearly revealed in the image from the 2020 flood season. Here, it is visible that the agreement of the two flood classifications is considerably higher in Zone A than in Zone B. Particularly, the WAFL classification in Zone B fails to capture some of the areas detected as inundated in the Sentinel-2 images. This may be due to the fact that water level dynamics in this year deviated considerably from the previously observed norm, with an early peak followed by a lowering of levels, before abruptly rising again towards the season's main peak. It can be conjectured that the correlative relationship established to characterise the delay time between water levels and the response of inundated areas failed to adequately capture this development. Whether this is an isolated response is hard to assess, since similar early peaking patterns cannot be found anywhere else in the data.

In terms of which factors most impact the detection of floods and the applicability of the WAFL, natural vegetation emerges as the central element in the comparison with Landsat images. This is particularly apparent as the binary classification into flooded and not flooded areas that was chosen in this approach limits the possibility of detecting flooded vegetation. Overall, the comparison with Landsat-derived inundation maps highlights the potential of the WAFL for reconstructing past inundation extents. In general, while the WAFL also has some issues mistaking areas with natural vegetation for dry areas, even when they are flooded, this misclassification is much less frequent than with Landsat. There are two main reasons for that. First, Sentinel-1 SAR has the capacity to detect water under vegetation layers (Tsyganskaya et al., 2018). And second, at the time the Sentinel images were recorded (2017-20) there was already much less natural vegetation in the study area than at the time that many of the Landsat images used in this analysis were taken (cf. Figure 3.32).

A second discrepancy in the comparison with Landsat is observed on higher-lying terrain in the study area. Here, Landsat continually registers inundations in the 1990s and early 2000s, which the WAFL fails to capture. That may be due to the fact that at the time that the Landsat images were recorded, these areas actually were flooded regularly, but that by the time the Sentinel-images were taken, this had changed. Some possible explanations for that could be the construction of local infrastructure (such as small dams and dykes), the natural deposition of sediments, or the raising of land through geotechnical projects. (It is not rare to see farmers raising the level of their land to build houses or plant trees.) The regular distribution of this

discrepancy in flood prevalence between Landsat and WAFL-derived maps seems to speak more for the second option. In terms of sediment deposition on the floodplains of the Mekong delta, Hung et al. (2014) found an average annual deposition of 6.86 kg/m^2 in the Vietnamese Mekong delta in Tam Nong district in Dong Thap province. This corresponds to an annual increase of 6 mm in height. These deposition rates are likely to be higher on the Cambodian side of the border due to the absence of dams and dykes. According to Manh et al. (2014), deposition on the Cambodian floodplains is indeed up to six times higher than in Vietnam, ranging from 19 to 23% of the annual sediment load at Kratie, rather than the 1 to 6% deposited in the compartmentalised floodplains in Vietnam.

When it comes to the comparison of the WAFL with TanDEM-X and the inundation extents derived on both bases, using a planar water surface superimposed on the DEM on the basis of in-situ water levels, seems to be a valid approach on a local scale. From a physical perspective, it appears that the water level registered by the logger could be construed to represent the inflow into the Boeung area, while the pseudo water level derived from Sentinel can be seen as the storage response, with local hydrological processes mirroring the dynamics of those of a reservoir (the Boeung) filling and emptying. This is typical for flood storage cells: the inflow-outflow is governed by the difference in levels between the main connection point and the mean level in the area. The delay is directly linked to the volume of water stored in the considered area and the flow rate. When there is no obstacle in the considered area, the delay is very short and water level can be considered as horizontal (propagation effects are not visible at a daily time step). When dykes limit the flow propagation, the filling of the area is made possible by small openings in dykes (usually made by farmers to irrigate their rice fields). Then it takes a longer time to fill the area. During flood recession, the processes are inverted: water level decreases rapidly in the Preks that are well-connected to the Bassac, while water is stored in the floodplains. Water is kept as long as possible in rice fields (by clogging the dykes) and recedes progressively by gravity (surface and subsurface drainage) and evapotranspiration.

However, the accuracy of this approach diminishes considerably when applied at the scale of the entire study area. At this scale, the assumption of a horizontal water surface slope no longer holds. Even when superimposing a sloped water surface over the entire DEM and taking into account correlations between the station at Koh Khel and the logger, the discrepancy remains high due to the complexity of the hydrological processes in the area. Broadly, this leads to an

overestimation of inundated extents derived from TanDEM-X. However, the use of the DEM does have the advantage of absolutely removing the interference of natural vegetation, as evidenced by the discrepancies in the center of Zone B observed in Figure 3.35.

3.4.3.4 Decreasing Flood Incidence and Durations in the Cambodian Mekong Delta: Patterns and Impacts

Despite limitations in the detection of the full flood extents in the 1990s and early 2000s, the analysis clearly shows a pronounced decrease in the incidence and duration of floods, especially in July and the first half of August. Large swaths of the study area, which were regularly flooded during these months in the 1990s, now remain dry until the second half of August. Taken together with the trends of earlier flood recession and the shorter flood durations outlined above, this means that overall, inundations in the Cambodian Mekong delta arrive later, recede earlier, and have lower magnitudes.

To a certain extent, this is in line with previous basin-wide studies such as Yun et al. (2020) and Hecht et al. (2018) that investigated the impacts of climate change and hydropower development. Their main findings were that a lower wet season discharge was to be expected in the future as a result of these developments, along with a higher dry season discharge. In terms of inundations, however, these higher dry season discharges do not balance the lack of inundations during the wet season that are key for the ecological functioning of the floodplains. Similarly, the results are in line with observations by Aires et al. (2020), who found a declining trend in inundation extents in their analysis of the Vietnamese and Cambodian Mekong delta using MODIS data.The same study also found inundations to be delayed by about two weeks in the Cambodian part of the Mekong delta. The present study indicates a longer delay, which may be due to differences in both the time frame and the spatial resolution of the data used. Figure 3.37 indicates that the incidences with which pixels were flooded in late July prior to 2008 are now only attained in late August or early September. Similar parallels exist in the work of Heng et al. (2021). In their modelling study of the Cambodian floodplains - one of the few taking this region as its focus - the authors conclude that total flood extent is projected to decline by 18% by 2040.

These alterations are anathema to the formerly predictable hydrological regime of the re-

gion, and are likely to have wide-reaching consequences for agriculture and fisheries. Greater variability in the dates of the flood arrival and its recession may, for instance, result in shifts in the planting and harvesting times for recession crops and an increased need for irrigation water (Erban and Gorelick, 2016). As far as fisheries are concerned, the later onset of floods and overall decrease in inundation durations limit the period during which fish populations can regenerate in the shallow waters on the floodplains (Hortle, 2009b). Compounded with the decrease in natural vegetation, which provides valuable structural habitat features, this is likely to negatively impact fish population dynamics.Vu et al. (2021) showed a close correlation between the long-term decline in commercial fish catches and declining peak water levels in the Mekong delta. Furthermore, local-level data obtained by the authors from fishermen in the area show fish catch to be much lower in years when the water level at Koh Khel exceeds 4 m for a lower number of days. These changes in inundation extents and durations are likely to impact food security in the region. Burbano et al. (2020), for example, link the shorter flood durations in the Tonle Sap region and the Mekong delta floodplains to shifts in dietary protein from fish to meat, and, consequently, land use changes resulting from the need to accommodate cattle.

Shorter inundation durations and lower incidence also reduce the spatial and temporal extent of the terrestrial-aquatic interface that many regulating ecosystem services depend on. This includes processes such as pest regulation, nutrient deposition, and soil and ground water recharge (Brown and My Phung, 2010; Chen et al., 2011).

Finally the analysis also shows that, even though large changes have occurred in the basin over the past three decades, the link between river water levels and inundation extents has remained relatively static. In contrast to the major changes on the Mekong itself, its hydraulic connections to its floodplains seem to have changed comparatively little, which may be related to the still limited development of water control infrastructure in the Cambodian upper Mekong delta.

3.5 Conclusion : Characterising the Hydrological Dynamics of the Cambodian Mekong Delta

Overall, it can be summarized that the Cambodian Mekong Delta has seen significant shifts in hydrological patterns over the past few decades. While precipitation patterns have remained relatively stable on average, river water levels and, consequently, inundations have seen considerable changes. Trends point toward a later arrival of the flood and a shorter overall duration.

The WAFL has been found to delineate inundation extents with acceptable accuracies. For one thing, it has a smaller propensity for mistaking flooded vegetation for dry areas than inundation maps derived from Landsat images. For another, it is based on actual physical observations and thus avoids overestimating inundation extents, a pitfall to which flood maps derived from superimposing a sloped water surface on the TanDEM-X DEM are prone. In terms of improving the approach, it is possible to envision an additional layer of correction of the Sentinel-derived maps on the basis of TanDEM-X to remove any remnants of vegetation interference, as well as the improvement of the water surface slope on the scale of the floodplains. Furthermore, a spatialisation of delay times could lead to more regionally adapted results. And finally, a correction based on long-term sedimentation rates is conceivable.

Based on the identification of a change point in the local hydrological series in 2008 that conforms to previous basin-wide studies linking this change to acceleration of hydropower development on the Mekong mainstream, inundations durations and incidences between two periods, 1991-2008 and 2009-2020 were compared. This comparison showed a small decrease in overall inundation incidence as well as a sharp decrease in inundation incidence at specific dates in July and the first half of August. The results also indicate a decrease in average inundation durations of up to 39 days per year. Overall, this is likely to have considerable adverse impacts on agricultural cycles, fish reproduction, and regulating ecosystem services such as soil and ground water recharge.

Considering all the limitations outlined above, the WAFL offers a valuable path to reconstructing a consistent time series of inundation extents going back to the 1990s. For the purpose of assessing long-term changes in spatial inundation patterns this is invaluable - especially

considering the alternatives of having only sparse amounts of contemporary optical data, data with insufficient spatial and temporal resolution, or no spatial data at all.

On a more general level, the analyses in this chapter has also allowed a better understanding of some overall characteristics of the hydrology of the region, from the propagation of tidal influence upstream to the likely impact that the impact of connections to floodplains have on the attenuation of flood peaks on the mainstream of the Bassac.

Finally, this chapter has also provided a thorough evaluation of the hydrological data available for the area, both in-situ and derived from earth observation approaches. This serves as a valuable basis for the analyses presented in subsequent chapters, and especially for the modeling approach presented in Chapter 6.

4

Understanding Preks - their Origins, Management, and Significance for Local Agroecosystems

Following the thorough analysis of regional hydrological and land cover dynamics in the Cambodian Mekong delta presented in the previous chapter, this chapter will "zoom in" to a local level. At this level, several research questions outlined for this thesis that relate to more small-scale processes will be addressed. In particular, this chapter will discuss what role local infrastructure in the form of Preks plays in catalyzing regional processes at a local level, what ecosystem services the people in the Prek area benefit from, and how these are linked to hydrological processes.

In order to do address these issues, a multi-method approach combining interviews with local

stakeholders, archival research, and remote sensing was used. This chapter first introduces the small-scale case study area in which field work was carried out and which forms the center of the analyses presented in this part of this thesis. Then, it delves into the defining landscape feature in this area - the Preks. An overview will be given of their general characteristics, origins, and history, with a particular focus on the recent development projects that aimed to improve their functionalities. Next, one of the core elements of this thesis will be presented - the fieldwork and interviews that were carried out with farmers and local officials in the case study area. In particular, insights into ecosystem services, agricultural practices, water management, and local governance of the Prek system will be outlined. Finally, a remote sensing analysis of land cover in the case study area that combines optical and SAR images will be presented. As will be outlined below, many of the benefits that the local population derives from Preks are related to agriculture. Therefore, it is crucial to understand land use practices and patterns in the region. Partly, this is achieved through interviews with farmers, which allow for the characterization of cropping practices. However, to gain a better spatialized understanding of cultivation cycles, remote sensing is used. The overall approach of this analysis, with a particular focus on the comparison of classification methods, is outlined and results are presented.

4.1 Case Study Area: Location and Characteristics

The case study area in which the local-level analyses presented in this chapter, as well as for the modelling approach outlined in the following chapter, were conducted is shown in Figure 4.2. It is located at the center of the larger Zone A, which was described in the previous chapter. In the East, its border is formed by the Bassac, in the West by the Prek Ambel. Overall, this area encompasses ten Preks. From North to South, they are Prek Cham Kroum, Prek Me Srok, Prek Lok, Prek Pok, Prek Hom, Prek Nou, Prek Put, Prek Chann, Prek Touch, and Prek Thom. They connect the Bassac to the floodplains in the interior of the study area, or to the Prek Ambel in the West. These varying Prek configurations are a principal reason why this area was chosen as the case study area for this thesis. Some connect to larger water courses, such as Prek Cham Kroum, which forms the northern border of the delineated study area, and Prek Thom, which forms the southern border. Others, such as Prek Put, end in a dead end in the study area. A third type, finally, connects to a network of smaller-scale canals in the floodplains. Furthermore, some Preks

have been rehabilitated as part of international development projects or local initiatives, while others have not. The general characteristics of all Preks in the study area are given in overview Table 4.1, and a full description of each Prek, photographic documentation, and a preliminary description of their use by the local population is provided in Appendix B. In total, the case study area covers a little over 43 km^2.

Generally, the case study area is characterized by a land use gradient along the length of the Preks. A typical landscape configuration is shown in Figure 4.1. As mentioned briefly in the previous section, the areas that are elevated due to past sedimentation and which are now rarely flooded are called *Chamkars*. These Chamkars are located along the Bassac river as well as along the head ends of Preks and, in the West, the Prek Ambel. Here, villages are located and flood-sensitive crops such as vegetables and fruit trees are cultivated. The Chamkars slope away into two directions - towards the "tail end" of the Preks, the floodplain *Boeung* areas in the East, and towards the lower areas located between Preks, in the North and South. Boeung areas, in the floodplains, are regularly flooded. In terms of crops, rice and maize take over as the principal crops. Where Boeungs and Chamkars meet, there are what is termed Transition Areas in this thesis and "Pseudo-Chamkars" in some of the engineering reports discussed below. These areas are flooded from time to time, but not every year. What crops are grown here depends on farmers' individual assessment of the likelihood with which each of their plots will be flooded.

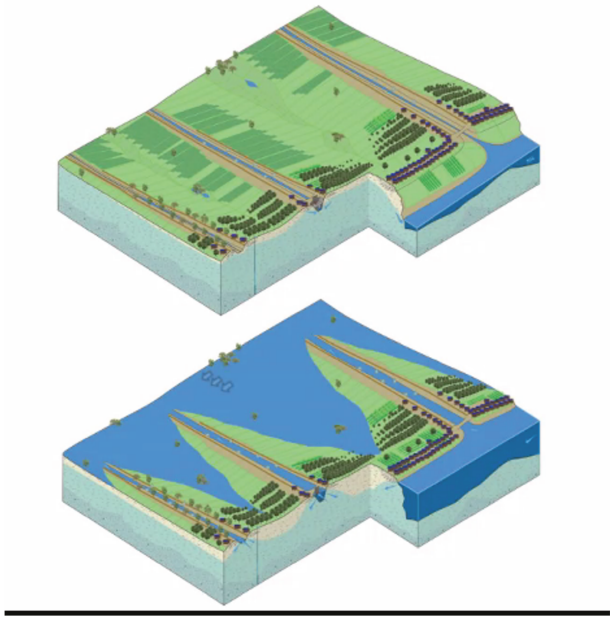

Figure 4.1: Landscape configuration in the Prek Area during the wet and dry season, by Sylvain Massuel.

Administratively, the case study area is located in the Province of Kandal, Kaoh Thum District, and the Commune of Prek Sdei. There are several small villages located along the Bassac, with houses centered around a National Road 21, a road running in parallel to the river, and around the easternmost parts of the Preks. In addition, there is one village in the Northwest of the study area on the bank of the Prek Ambel. This village is inhabited primarily by Cham people. The Cham are a Muslim minority community with a history in the region that reaches back several hundred years. After the defeat of the last Cham principality by the Vietnamese in 1720, many settled along the river north of Chau Doc (Biggs, 2004).

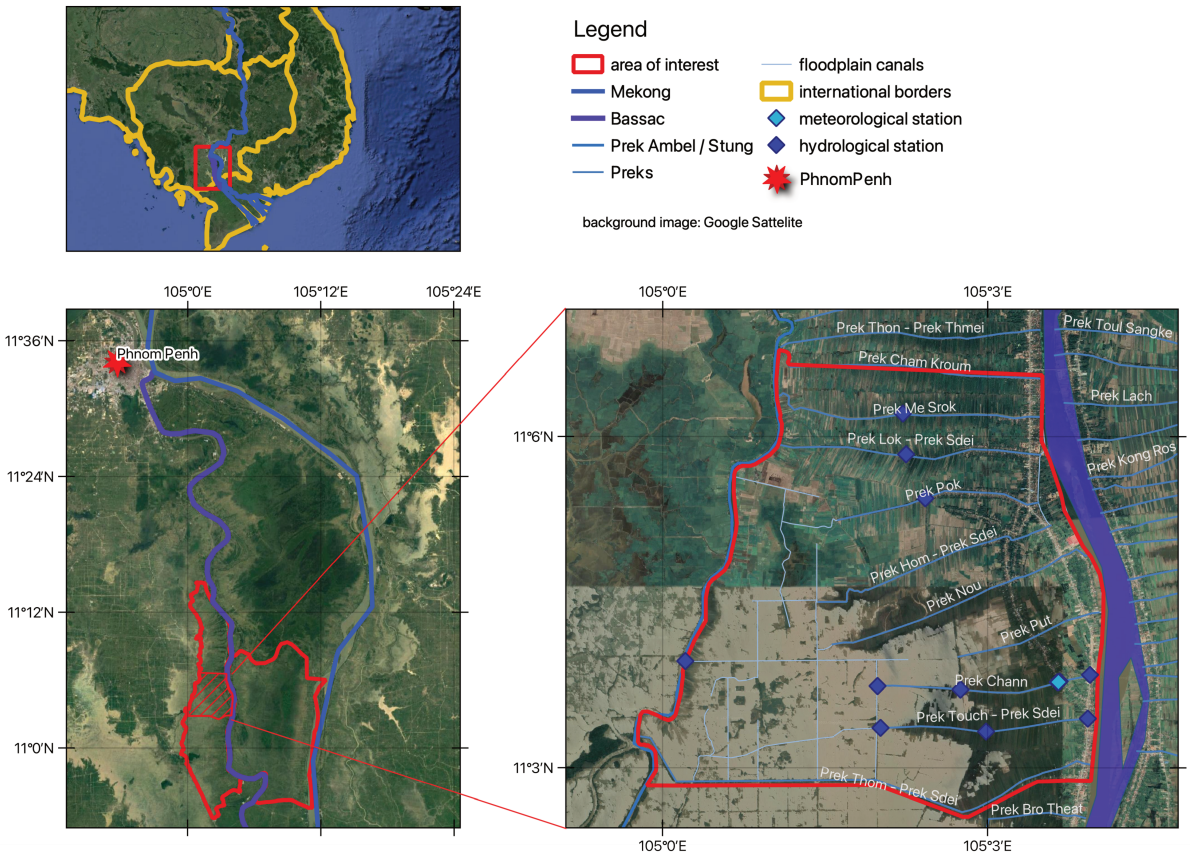

Figure 4.2: Location of the case study area in the Cambodian Mekong delta.

Name	Length [m]	Connection Type	Rehabilitation Status
Prek Cham Kroum	4659.95	Prek Ambel	Not rehabilitated
Prek Me Srok	3592.61	Prek Ambel	Rehabilitated (2017), international project
Prek Lok	4403.52	Prek Ambel	Not rehabilitated
Prek Pok	3535.57	Canal / Floodplain	Not rehabilitated
Prek Hom	4365.34	Canal	Not rehabilitated
Prek Nou	3702.91	Canal	Not rehabilitated
Prek Put	2552.81	Floodplain	Not rehabilitated
Prek Chann	3745.18	Canal	Rehabilitated (2017), international project, with gate
Prek Touch	3621.63	Canal	Not rehabilitated
Prek Thom	2351.14	Canal	Rehabilitated (2020), local excavation initiative

Table 4.1: Overview of information on the ten Preks in the case study area.

4.2 Exploring the History of Preks: From Historical to Modern Engineering Reports

Part of understanding the diverse roles that Preks fulfill today, especially in terms of cultural ecosystem services, is to acquire a sense of their historical importance in the region, their original development, and what they have come to mean for the local population. This section looks at the history of the Preks through the lens of reports written by engineers in various periods, beginning in the early 20th century. To collect these sources, archival research was carried out in the National Archives of Cambodia in Phnom Penh in 2020. It must be noted that, unfortunately, many documents from the period of the French Protectorate and the years after World War II were destroyed during the regime of the Khmer Rouge in the 1970s. For the National Library, the proportion of records that were exterminated during that time lies at 80%. It is reasonable to assume that similar percentages apply to the National Archives. These missing documents are conspicuous when trying to follow cross-references in the files, or when searching through collections of maps and images with missing entries. Most of the documents that were examined stem from the time between 1900 and 1935. In addition to the physical records in the National Archives in Phnom Penh, the digital archives of the French National Library were consulted, as well as the Archives d'Outre Mer in Aix-en-Provence, France, which host many documents related to the country's colonial past.

4.2.1 From Indigenous Discoveries to Colonial Priority

The oldest written sources on the Cambodian Preks stem from the time of the French colonial administration in the early 20th century. The history of French colonial presence in Cambodia begins in 1863, when officers from the French navy stationed in neighbouring Vietnam persuaded King Norodom to relinquish control over Cambodian foreign affairs through a treaty with France. This control was progressively extended through a series of reforms until both the King's resistance and a local guerilla rebellion were overcome in 1897 and the French representation in Phnom Penh assumed authority over the executive. Even though Cambodia was nominally a Protectorate of France, rather than a colony, the King's authority had been reduced to a minimum and the French administration took charge of the affairs of the state. Cambodia effectively remained integrated into French Indochina until after World War II (Tully, 2005).

One of the principal priorities of the French administration was the modernization of the country, especially with regard to infrastructure such as roads, canals, and railways, and agricultural practices. The aim, ultimately, was to make colonies accessible, increase productivity, and gain profit from the land. Civil engineers and agronomists played a major part in this enterprise. In fact, several institutions, societies, and schools were founded particularly for the purpose of educating colonial engineers, such as the École nationale supérieure d'agriculture coloniale (1902) and the Société française des ingénieurs coloniaux (1895) (Vacher, 1999).

On the floodplains of the Mekong in Cambodia, one of the primary challenges that these colonial engineers and agronomists faced was that much of the land in the area was low-lying and marshy, and remained water logged for long periods. The space for growing high-value crops such as cotton was therefore limited. One of the solutions to this problem were the Preks - or *canaux de colmatage* in the French terminology. Colmatage, in general, refers to the process of raising land through improving the conditions for sedimentation.

The first organised studies on the concept of colmatage that appear on the record began in 1906. A first suggestion for such a study was discussed in an exchange of correspondence between Captain Gatard, the head of the Service Hydraulique Agricole, and the head engineer of the Direction Générale des Travaux Publics (File Nr. 5656 in the National Archives of Cambodia).

Gatard feels that a deepening of the Prek channels to increase agricultural potential is essentially inefficient. He believes that it would bring sediments, yes, but that the main issue for agricultural productivity is a lack of water during the dry season. He further states that cultivation is only possible very near the stream (where water is provided through capillarity) or in the lowlands where water from the flood is retained the longest. In fact, he even states his fear that colmatage might ruin the rice fields that are located in those areas. Instead, he proposes building a large number of small reservoirs in the lowlands for the provision of irrigation water during the dry season. He also speaks out in favour of better control over water inflow and outflow in the Preks, for example using stoplogs, and believes that sediment deposits in the Preks themselves have positive effects since they contribute to the retention of flood water for use during the dry season. Overall, he opposes the further study of colmatage systems.

Nonetheless, such a study was implemented at Stung Trang, near Kratie. It appears that the general consensus was that the topographical configuration of the area was well-suited to the purposes of the study. Precise elevation measurements and profiles were created, water samples taken, water levels measured, and temperatures measured. Detailed descriptions of the methods and results, as well as the formulae derived to describe colmatage are available in a report from the 28th of May 1909 by the Service Hydraulique Agricole (M. Jumeau, File Nr. 5654). Overall, the results seem to have been promising, though there was some criticism later on (report by M. Moreau, 15th of June 1909, same file) that the topographical configuration was very particular and that further studies were necessary before a generalisation of results was possible. It is mentioned that a second field study, at Prey Veng, was underway at the time.

Most immediately useful for the purposes of this thesis is a study conducted by Lieutenant Raymond Barthélemy (Administrateur Des Services Civils), first published as a report in 1908, and later re-published in the *Revue Indochinoise* in 1913 (Barthélemy, 1913). His aim was to describe the general principles of the Prek/Chamkar system, using both the field experiment at Stung Trang and observations at already existing Preks. In his report he emphasizes that he heavily involved locals in his study:

> Dans cette étude, nous avons tenu le plus grand compte des observations des habitants, ils ont été pour nous des guides excellents, cette question du percement de canaux de colmatage les intéresse vivement, non seulement ils ont toujours

consenti à nous renseigner lorsque nous avions recours à eux, mais ils sont le plus souvent d'eux-mêmes venus au devant de nous pour nous demander de comprendre dans nos projets des preks qu'ils nous indiquaient pour nous montrer les meilleurs emplacements et la manière la plus économique d'y exécuter les travaux. - *Premières études de colmatage du Mékong, File Nr. 25754, p.7*[1]

Furthermore, through his interactions with the locals, he also gathered a legend of the origins of the Preks, which is given in more detail in the typewritten version of the report (File 8990):

Les Tiams[2] avaient autrefois trouvé un procéde de se procurer cette terre précieuse; voici la légende qui m'a été racontée par de vieux Cambodgiens. Le Che Tiam Ania Khou, aieul du Gouverneur Tiam de Kanchor habitait il y a un siècle *(NB: early 1800s)* le petit village de Dey Dos, sur la rive droite du Mékong; sa maison avait vue sur le fleuve et derrière elle se trouvait un grand beng qui se remplissait tous les ans au moment des crues, mais assez tardivement. Ania Khou avait acheté dans la province de Sambor une superbe pirogue qui était fort lourde, son idée était de faire pénétrer cette pirogue dans le grand beng qui était derrière sa maison et de l'utiliser pour le transport des bois et des paillottes blanches qu'il irait chercher à la montagne en traversant le beng. Mais les flancs de la berge sont presque à pic à Dey Dos, et tous ses efforts pour hisser la pirogue, pour lui faire franchir le bourrelet, furent vains; elle était trop lourde et la berge trop abrupte du côté du fleuve. Ania Khou eut alors l'idée de creuser un canal d'une profondeur de sept ou huit coudées *(NB: ca. 3.5-4 m)* et d'une largeur égale à celle de la lourde pirogue, pensant de profiter du moment de la plus haute crue de l'année pour faire pénétrer sa pirogue par ce canal dans le grand Beng. Le plan d'Ania Khou réussit à merveille et lorsque la crue eut atteint le niveau du fond du canal, les eaux du fleuve se précipitèrent dans le Beng dont le niveau était encore de plusieurs mètres en contre-bas, la pirogue fut violemment poussée vers la nappe d'eau dormante et y flatta, mais il advint que les eaux du fleuve se précipitaient avec tant de force, qu'elles élargirent le canal

[1] See Appendix C for translations.

[2] It seems like Tiam might be a spelling variant of Cham. Kompong Cham, for example is denoted as 'Kompong Tiam' in several old maps in the archive. Furthermore, later on in the text, Barthelemy uses the phrasing "par plusieurs Tiams et Cambodgiens", which suggests a duality between these two groups and makes it likely that it is indeed the Muslim minority group that is referred to here.

> qui, en deux mois, atteignit une largeur de soixante coudées *(NB: ca. 30 m)*. De plus, les eaux limoneuses du fleuve se précipitant dans des eaux plus claires et qui n'étaient pas à la même température, déposaient rapidement leur limon et lorsque la décrue arriva, le vieux Tiam ne fut pas peu surpris de voir que la superficie de terre cultivable avait considérablement augmenté derrière sa maison et qu'un double bourrelet de terre fertile était nettement dessiné au débouché du nouveau prek dans le Beng.

Barthélemy goes on to summarise that in subsequent years, many followed this example and breached the banks of the Mekong to create Preks, until several mésroks and governors placed restrictions on such projects since they interrupted the circulation on the paths along the river. It was only under the Résident Supérieur Luce (Luis-Paul Luce, 1856-1931, Résident Supérieur du Cambodge 1900-01 and 1905-11) that construction of the Preks was assigned a higher priority in the context of furthering agriculture than the continuity of roads. According to Barthélemy, the measures proposed by Luce regarding the construction of the Preks was met by strong approval of the local population.[3]

In his report, Luce furthermore describes the general functioning and morphology of Preks. He mentions the way that Boeungs function as buffers during the wet season, attenuating the flood peak, and even goes as far to liken the great Cambodian lakes to gigantic Boeungs. He also formulates several laws on the functioning of Preks – the first one, for example, stating that there is always a temporal delay between the rise and fall of water levels in the main stream and the Boeungs. Furthermore, several factors that can have positive and negative impacts on the process of colmatage, such as temperature differences, the presence of vegetation etc. are considered. Finally, Barthélemy outlines some general principles that need to be adhered to when constructing Preks – for example that their entry level should be no lower than the mainstream water level on the 15th of July, since the sediment-laden waters needed for colmatage only arrive in the second half of that month.

Barthélemy's conclusions are that the construction of Preks is a valuable measure to increase

[3]The conflict of interests between Preks and roads are also mentioned in other files. For example, one report notes that during the construction of colonial road VII in Kandal, several Preks were closed off. The same report also includes observations about how land quickly became infertile in the region due to a lack of nutrient input from the flood.

agricultural productivity in Cambodia and that it should be implemented on a general basis.

A last feature of Barthélemy's report that deserves to be underlined are the schematic figures he includes, several examples of which are given in Figures 4.3 to 4.5. They compare the typical landscape configuration of European with Cambodian rivers, and show the effect of Prek construction on landscape configuration.

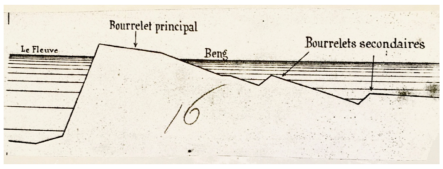

(a) Landscape configuration without a Prek connecting the mainstream with the floodplains.

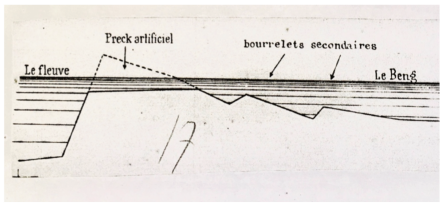

(b) Landscape configuration wit a Prek connecting the mainstream with the floodplains.

Figure 4.3: Figures from Lt. Barthélemy's report, illustrating the difference between flood patterns with and without Preks.

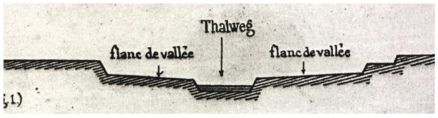

(a) Landscape configuration of a typical stream in Europe, with the terrain rising on either side.

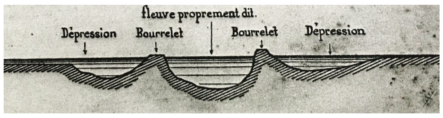

(b) Landscape configuration of a stream in Cambodia, with the terrain sloping away from the river.

Figure 4.4: Figures from Lt. Barthélemy's report, illustrating the difference between flood patterns with and without Preks.

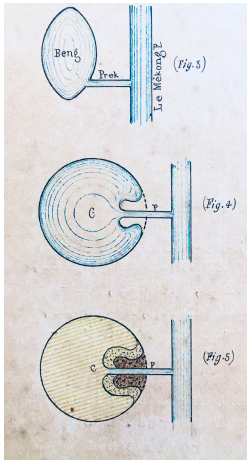

Figure 4.5: Figure from Lt. Barthelemy's report, illustrating sediment deposition in the Boeung following a Prek's construction.

In later exchanges about concrete measures for projects by the Direction Hydraulique Agricole (File 5654), Barthélemy goes into more detail on the projects he envisions, giving estimates of the lengths of Preks required and the ensuing costs. In this file, a great number of details is available – such as the general price of Chamkar land, which is given at 50 piastres for 1 masenkongseng (Cambodian unit of area measurement. This corresponds to ca. 2,000 francs per hectare.) The costs for the Preks that are proposed vary between just over 100, to just over 1000 piastres, with lengths varying between 50 m and 790 m. It is further estimated that a single Prek can create at least six hectares of land per year. Taking into account the price for Chamkar land, Barthélemy concludes that a Prek could pay for its own construction in the very first year.

An important takeaway from these figures is that the Preks that were proposed at the time do not correspond to the channels that are known today, most of which amount to several kilometers in length and evolved over time from the original breaches. The lengths proposed by Barthélemy are much shorter, constituting, in most cases, only a breach in the river bank.

Apart from the information about the concrete development of Preks, some insights could be gained into the development of irrigation initiatives during this period.

Through the letters of Martin Flacourt, the Head of the Services Agricoles et Commerciaux, it is evident how irrigation became a more and more important part in increasing the agricultural capacity of Cambodia during the early 20^{the} century.

File 5654 includes reflections about projects that were being undertaken in 1909-10 to increase irrigation capacities. At the time, some manual irrigation practices were to be found across the country, but most agriculture was rainfed. It appears that an irrigation programme was launched in 1903, with a view towards stabilising agricultural production. As the report states:

> Il ne s'agit donc pas ici de conquérir, pour un peuple qui ne saurait les exploiter, de nouveaux terrains propres à la culture, mais simplement de régulariser, au moyen des irrigations, une récolte qui ne dépend que de la quantité d'eau de pluie annuelle et aussi de sa répartition au cours du développement des diverses phases de la culture.
>
> *- Rapport au sujet d'un programme de travaux d'hydraulique agricole (10th of May 1910, FileNr 5654), Direction Générale des Travaux Publics*

From the same report it can further be gleaned that there were two trial areas for irrigation projects: Prek Chlong and Prek Thnot. Each project was subsidized with ca. 5 Million francs. Some conclusions that were drawn from these projects were, for example, that the maximum yield of 1 ha paddy rice with irrigation is 1.7 t. Furthermore, calculations about how to pay for irrigation infrastructure (for example through additional taxes on the raised rice production) are given.

However, the initiative for irrigation projects did not only come from government agencies. File Nr. 5652 details a 1907 initiative taken by 50 residents of Prek They/Prek Sdey village in Kasthom province, who came together in a sort of association to dig a canal of 5 km in length and 2-3 m in depth to irrigate large areas of Chamkar land. From letters exchanged between provincial representatives and the central government in Phnom Penh, it appears that in this case, an initial breach of the river bank already existed, but that the aim was to lengthen this channel. It is remarked, however, that the project is being implemented without a detailed plans in a "façon rudimentaire". From the documentation it seems like there were quite some administrative troubles in getting the project approved, but that the group was persistent.

From these early documents, several insights into the development of Preks in the early 20th century can be derived. It becomes clear that the functioning of Preks was not, in itself, an invention by French engineers, but that it was well-known among the local population for at least a century, and, if the story recorded by Barthélemy is accurate, discovered by members of a

minority group. Furthermore, it becomes evident that there was considerable enthusiasm on the side of the local population to see Prek and canal projects implemented - and that they took the initiative themselves in multiple cases. The fact that the construction of Preks was assigned a high priority by the colonial government is evidenced by the fact that they were given precedence over the continuity of roads.

However, these early documents also show that the Preks of the period are not equivalent to the Prek channels that exist today, neither in form nor purpose. Especially from the notes and observations on the ideal properties of Preks by Barthélemy, it can be seen that their main purpose was to increase sedimentation in the Boeung areas and create new fertile Chamkar land, though he also mentions the regulating effect on flood attenuation. As is outlined in the next section, Preks are now seen to fulfill a much larger range of ecosystem services, serving as a source of dry-season irrigation water chief among them. Anathema to this is Barthélemy's suggestion to ensure that Prek entrances are no lower than the river water level in mid-July to prevent the inflow of sediment-poor water.

4.2.2 Post-Colonial Period and the Khmer Rouge

French colonial rule in Cambodia ended after World War II, in 1953. In theory, Cambodia had already declared its independence from France eight years earlier in March 1945. At the time, Japan was in control of much of Southeast Asia and urged colonial territories to make a bid for independence. However, when Japan surrendered in August 1945, Allied forces occupied Phnom Penh and French control was reinstated. The French only granted full independence to the country in 1953 after King Sihanouk had mounted a highly public campaign to apply international pressure on the colonial administration. Sihanouk subsequently abdicated in favour of his father in order to participate in politics. After becoming prime minister, however, he declared himself Chief of State and governed Cambodia under a one-party rule until 1970, a time also referred to as the Sangkum period. He was eventually removed through a coup d'état in 1970 and succeeded by Lon Nol, the Prime Minister, who declared the Khmer Republic. While there were many factors leading to the coup, one of the main reasons for was Sihanouk's policy of neutrality and his toleration of North Vietnamese activities on Cambodian soil in the course of the war in neighbouring Vietnam. Lon Nol's government abandoned this stance and took

the side of the United States in the conflict. However, Cambodian communist forces mounted a resistance, claiming Sihanouk as a figurehead for their movement, and were subsequently subjected to extensive American carpet bombing in the East of the country (Tully, 2005; Kiernan, 2002).

No concrete information could be found on the development of Prek channels during this period. Part of the reason for this is that no documents covering these years were available in the National Archives of Cambodia. However, it can be assumed that the existing infrastructure of the Preks was maintained during this period, perhaps even extended. The reason why such conjecture seems reasonable is that agriculture held a high priority in the ideology of Sihanouk and the Sangkum period in general. Public figures were encouraged to perform manual agricultural labour and Sihanouk himself gifted farm equipment to villages and had himself photographed working in fields. In the 1960s, as much as 80% of the population was employed in agriculture (Ayres, 2000b,a). According to Dumas (1990), both farmer- and state-managed irrigation systems were expanded during this period. However, the provinces bordering Vietnam experienced considerable disruptions throughout the 1950s, 60s, and 70s as the Vietnam war continued to be fought. During this period, the United States dropped approximately 500,000 tons of explosive on Cambodia. Even at the beginning of the 21st century, almost 50% of villages report unexploded ordnance. Furthermore, bomb-induced deforestation in the course of the war shifted hydrological conditions in the area (Lacombe and Pierret, 2013). Nevertheless, Preks appear to have been maintained, as the current configuration of the landscape evidences that they continued to fulfill their original purpose. Today, elevated Chamkar areas have formed along the Preks, after a century of deposition processes.

While it is difficult to evaluate any measures that might have been taken to extend the system of Preks and canals in the Cambodian Mekong delta in the years 1953-1975, the years that follow held a dramatic shift that has been extensively documented. In 1975, Lon Nol's government collapsed under the onslaught of the Cambodian communist forces. Subsequently, the country became Democratic Kampuchea, under the rule of the Communist Party of Kampuchea (CPK), alternatively known as the Khmer Rouge and led by Pol Pot (Tully, 2005). The Khmer Rouge aggressively pursued the ideal of creating a self-sufficient agrarian society entirely independent of Western influence. Directly after communist forces entered Phnom Penh in 1975, inhabitants were ordered to leave the nation's cities and move to the countryside. Here, many were forced

to participate in the construction of irrigation infrastructure which, the Khmer Rouge believed, was the key to increasing agricultural gains. However, the design of canals was not based on calculations grounded in civil engineering, or even on local experience values. Instead, a rectangular network of canals and dykes reaching from North to South and East to West was created, often spaced so as to create units of four hectares. Ultimately, the vision of the CPK was to create a nested canal network - arranged in 10 x 10 km grids, encompassing smaller 1 × 1 km grids, which, in turn, feature 100 m × 100 m grids - in order to supply sufficient irrigation water for rice production (Tyner et al., 2018; Tyner and Rice, 2020; Dumas, 1990; Coakley et al., 2019).

In short order, these structures were built, but without the use of heavy machinery. Instead, construction work was completed through forced manual labour under abject conditions, to the point where the rural labour camps in which people were forced to work became known as *Killing Fields*. In total, approximately 2 million Cambodians are estimated to have died in the four years until the Khmer Rouge regime was toppled, representing 25% of the population at the time (Tabeau and Zwierzchowski, 2013). Nonetheless, the construction of irrigation infrastructure was widely completed under these conditions Tyner et al. (2018) estimates that 7,000 kilometers of canals and dikes, as well as over 350 reservoirs were completed during the Khmer Rouge regime. However, many structures had averse rather than positive effects on local hydrological conditions. Due to the lack of control structures, rapid drainage of upland areas occurred in many parts of the country, alongside flooding of lowland areas. Often, improper design of these structures resulted in failure within a few years. Many eroded away in the course of subsequent floods. Most analyses considering the extent and effectiveness of the irrigation schemes implemented by the Khmer Rouge echo the standard total view (STV) defined by Michael Vickery, which characterizes it as a typical manifestation of a poorly managed regime ultimately doomed to failure (Vickery, 1984; Rice and Tyner, 2017; Dumas, 1990)

In the case study area of this thesis, a network of canals stemming from this period exists in the Boeung areas in the West and Southwest, as shown in Figure 4.2. Furthermore, the dyke that delineates the southern border of the study area appears to have originated at this time as well. The remnants of concrete gate structures that exist here are referred to as "Pol Pot" gates by the local population. One of these structures is shown in Figure 4.6. It is not known which, if any, measures the Khmer Rouge took to maintain or extend the Prek channels themselves during this

period, though it can be conjectured, judging by the spatial configuration of the landscape today, that some efforts were made to deepen them to ensure connectivity with the newly constructed canal network to guarantee an influx of river water for irrigation purposes.



Figure 4.6: A "Pol Pot" gate in the dyke that forms the southern border of the case study area.

4.2.3 Development after the Khmer Rouge and Rehabilitation Projects since the 1990s

In early 1979, the Khmer Rouge regime was toppled by Vietnamese forces. In the following years, conditions slowly began to stabilize. During these years the history of Preks is traceable once more only in the larger context of agricultural developments. According to Dumas (1990), farmers began to reverse some of the measures implemented by the Khmer Rouge - for instance by blocking canals to prevent drainage. However, two major obstacles remained that impacted heavily on the maintenance and development of agrarian infrastructure. For one thing, many people were unfamiliar with the conditions in the land that they now found themselves farming. Writing in the late 1980s, Dumas (1990) describes the following situation:

> The main problem is that many farmers have settled into new lands as a result of the dislocations that occurred under the Khmer Rouge regime. They are still

> unfamiliar with the rainfall and flood conditions of the new areas to which they have moved. Even farmers returning to their original lands are faced with changes in the hydrology of their new area. - p. 276

In addition, land remained state-owned until 1989, and farmers had relatively few means to invest in the cultivation of their fields. Dumas (1990) observes that conditions improved slowly and that as resources actually owned by farmers increased, they began to perform water management on an individual basis. Part of these efforts became rehabilitating salvageable parts of irrigation structure from pre-Khmer Rouge times, which had not been maintained in the interim, as well as some Khmer Rouge canals.

Coordinated efforts by the government to improve agricultural practices and infrastructure began in the mid-1980s, under the auspices of the Ministry of Agriculture, particularly the Department of Hydrology. However, a significant obstacle to the development and implementation of projects was the lack of expertise, as a vast number of intellectuals and members of the educated echelons of society either been targeted and killed by the Khmer Rouge, or had fled the country. During this period, international organizations began to implement projects related to irrigation infrastructure in the region. For instance, (Dumas, 1990) mentions a small-scale irrigation programme in Kompong Cham that was set up in cooperation between the Department of Hydrology and the American Friends Service Committee, a Quaker organization. It is in the context of such rehabilitation and development projects that concrete information on the Preks becomes available once more during the 1990s.

After Vietnam withdrew from Cambodia in 1989 following pressure from both the US and the Soviet Union, a peace agreement was reached in 1991 that was endorsed by the UN Security Council. Subsequently, a peacekeeping operation that included both soldiers and civil servants was established in Cambodia under the control of a United Nations Transitional Authority. The 1990s continued to be tumultuous, including free elections followed by a coup led by Second Prime Minister Hun Sen, who still rules Cambodia to this day. It was only in the early 2000s that the situation began to stabilize on a more permanent basis, marked, not least, by Cambodia's entry into ASEAN (Association of Southeast Asian Nations) (Chandler and Overton, 2021).

It is during this period that development projects in the agrarian sector began to multiply

rapidly. The French Development Agency (Agence Française du Développement, AFD), for instance, became involved in the country in 1993 (AFD, 2021), the Japan International Cooperation Agency (JICA) in 1996, and the Australian Department of Foreign Affairs and Trade (DFAT) launched its *Cambodia Agricultural Value Chain Program (CAVAC)* in 2008 (DFAT).

Systematic Prek rehabilitation was first financed by AFD and implemented by MoWRAM between 1999 and 2003. This pilot project was carried out in the framework of a initiative called *PADAP - Programme d'Appui au Développement de l'Agriculture Périurbaine*. The project was centered around two canals in S'ang District and aimed to test rehabilitation measures and the effects on cropping developments. The initial study, led by AGRISUD International, received a positive evaluation in 2004, highlighting value gains, increased agricultural output, and initiatives by the local population. At the same time, JICA was also financing their first Prek rehabilitations. After an initial study on the functioning of the system was undertaken in 1996-1997, JICA financed the rehabilitation of four Preks on the right bank of the Mekong in 2001-2002. Following their initial project, AFD extended its Prek rehabilitation scheme through the *Northwest Irrigation Sector Project (NWISP)*. The overall project aim was to intensify and diversify agricultural systems, as well as to make them more resilient. In this context, a polder was created in 2009-10 between Prek Ta Roat and Ta Ong in S'ang District, Prek Ambel Commune. In 2013, AFD launched the project WASP (*Water and Agriculture Sector Programme*) to rehabilitate almost thirty Preks in Kandal Province over the course of four years. Rehabilitation work on the first thirteen Preks was launched in 2015, in cooperation with the MoWRAM as well as the consulting agencies SOFRECO and SBK Research and Development. Work on these Preks was largely completed in 2017. This was followed by a second rehabilitation phase which targeted a total of twelve Preks and ended in 2020. In 2020, another project that includes rehabilitation efforts related to Preks was launched by MoWRAM and the AFD - *Water Resource Management and Agro-Ecological Transition in Cambodia (WAT4CAM)*. Financed by the AFD and the European Union, its stated aim is to improve irrigation systems management and integrated water resources management in Cambodia. One of its four components is the *Rehabilitation and completion of irrigation and drainage infrastructures*, which includes the rehabilitation and modernization of 20 to 40 Preks (SOFRECO, 2017; Pratx, 2017; MoWRAM, 2021).

At this point it must be briefly outlined what Prek rehabilitation entails. Preks are, by design,

trapezoidal channels that connect the river mainstream to the floodplains at a certain depth. Over time, however, sediments are deposited in the canals, reducing their cross section. Bank collapses and erosion can further impair the vector functionality of Preks. Rehabilitation projects primarily aim to reinstate this functionality by deepening the Prek beds and restoring - or even extending - its profile. In addition, rehabilitation projects typically include the construction or improvement of roads along the Prek. In some cases, control structures such as gates are also constructed to regulate the seasonal inflow of water from the river or outflow from the Boeung. Bank vegetation is removed (Pratx, 2017; SOFRECO, 2017). Figure 4.7 shows a comparison of Prek Chann and Touch in 2020, the former of which is rehabilitated, the latter of which isn't.

One of the main questions in rehabilitation projects is the scale of earthenworks to be implemented. The deeper the bed of the Prek is lowered, the better water availability will be throughout the dry season, but the higher costs for geotechnical works are. For this reason, engineers during the WASP project distinguished between deep and shallow calibration projects. Deep calibration involves lowering the bed level to an elevation that guarantees year-round inflow, typically 0 m asl. Shallow calibration, in contrast, only lowers the bed level to 1.5 m asl. This allows inflow for most of the year. During the height of the dry season, however,pumps are neccessary to supply the Prek with water. A large pump is used to lift water from the Bassac into the Prek so that farmers can use their own smaller pumps to irrigate their fields with water from the Prek, which they also do along Preks that are deeply excavated. At some Preks that have not yet been rehabilitated, this practices already exists, with "water sellers" providing their service - and those of their pumps - in return for a seasonal fee from the farmers who benefit from the practice (SOFRECO, 2017). In the case study area of this thesis, two Preks have been rehabilitated, both in deep calibration - Prek Me Srok and Prek Chann. At Prek Chann, a gate was also constructed to control water flows (cf. Figure 4.9).



(a) Head of a Preks Chann (rehabilitated) and Touch (not rehabilitated).



(b) Tail of a Preks Chann (rehabilitated) and Touch (not rehabilitated).

Figure 4.7: Aerial view of rehabilitated and not rehabilitated Preks.



(a) Head of a Prek at which a pump is being used during the dry season to lift water into the Prek.



(b) Pump used to lift water from the Bassac into the Prek.

Figure 4.8: Pumping at the end of the Prek.



Figure 4.9: Aerial view of the rehabilitated Prek Chann, the gate at its head, and the Bassac in the background.

While rehabilitation projects have reported a considerable number of positive effects, some

problems have also occurred in the course of the projects, often related to a mismatch between the assumptions of engineers and the reality of stakeholder practices and hydrological processes. In several instances, bank collapses happened, which obstructed the flow of water in the Prek once more. This was the case at Prek Chann, for instance. The reasons for these collapses have been conjectured by engineers to be a combination of water pressure from the Chamkar soils and erosion effects (SOFRECO, 2017). Another frequent problem is erosion around control structures such as gates. If these are not opened in time during the wet season the shear forces of the water once they are opened can easily damage the structure, as shown in Figure 4.10b.

Finally, it also needs to be mentioned that the rehabilitation practices described above only appertain to official projects initiated in the framework of collaboration between the Cambodian government and various international actors. However, there are also local initiatives for Prek rehabilitation - or at least excavation. Sediment deposition in the Preks is one of the most commonly reported problems that restricts water inflow. Therefore, regular excavations are organized by some village chiefs to maintain the vector functionality of the Preks. In most cases, these excavations are limited to the heads of the Preks, where the majority of sedimentation happens (see interviews below). However, in the case study area one major locally-organized excavation project was observed during the field work. Here, several kilometers of Prek Thom at the southern end of the case study area were excavated. The results of excavation and the border between excavated and not excavated Prek stretches is shown in Figure 4.11. Sometimes these excavations also have economic motives, as the sediment that is extracted from the Preks can be sold to farmers wishing to raise their land as well as for construction purposes. These initiatives are also sometimes supported by the administration at the communes and district administration, and by the provincial offices of the MoWRAM.



(a) Bank collapse at Prek Chann.

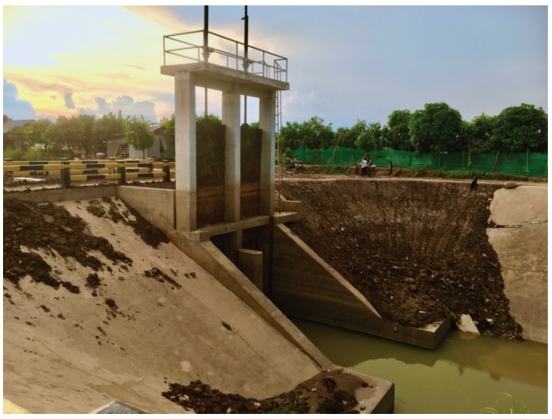

(b) Damage at a gate following inundations.

Figure 4.10: Common issues with rehabilitated Preks.



(a) Aerial view of the excavated part of Prek Thom.



(b) Transition between excavated section and not excavated section.

Figure 4.11: Local excavation initiative at Prek Thom.

4.3 Understanding the Significance of Preks for Agriculture and Communities

Now that the history of Preks has been traced from their origins to the present day, the focus of this thesis must shift to their contemporary role. As mentioned above, Preks' shapes and nominal functions have evolved considerably since their inception as *canaux de colmatage*. This thesis aims to understand, conceptualize, and model the ecosystem services related to the hydrological processes in the area, as catalyzed by Preks. Stock of hydrological processes has been taken, at a larger scale, in the previous chapter already. The focus of this section now lies on outlining what

has been learned about Prek-related ecosystem services, and the associated water management practices. To gain this knowledge, a series of interviews and field surveys was carried out. In the following sub-sections, the methodology of this fieldwork will be outlined, followed by an overview of the main ecosystem services, agricultural practices in the area, and the role of local governance. Several of the results presented below - notably the data gathered on land use, irrigation practices, and average yields - is used in Chapter 6, in the ecohydrological model.

4.3.1 Overview of Field Work and Interview Methodology

Overall, four field trips to Cambodia were organized in the course of this thesis - one in December 2018, one in June 2019, another in November 2019, and a final one in the period between February and May 2020. Unfortunately, two of these trips were cut short, in 2018 due to personal illness, and in March 2020 due to the onset of the COVID-19 pandemic. To compensate for missing data, a colleague from the Royal University of Agriculture (RUA) in Phnom Penh carried out further field visits during autumn 2020 and spring 2021, to conduct interviews in areas that had been underrepresented in the interviews completed up until that point. In order to allow data consolidation, a hosted SQL database was created, alongside a HTML data entry portal (see Figure 4.12).

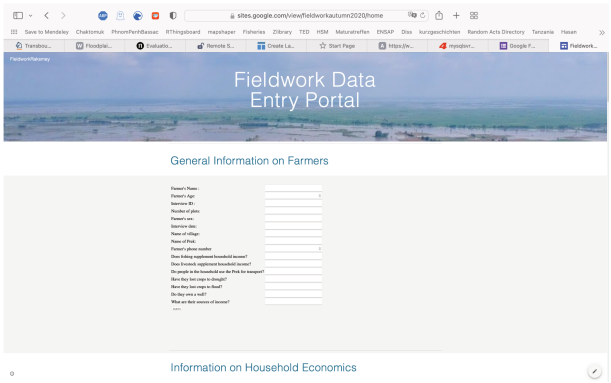

Figure 4.12: HTML-based data entry portal to consolidate fieldwork results.

For the interviews, a semi-structured form was chosen, following Matsukawa et al. (2016), Dumaresq et al. (2020), and Pratx (2017). In this form, most question were pre-defined, but it also gave considerable room for additional information to be collected from interviewees which may not have been envisioned during the original draft of the questionnaire (DiCicco-Bloom and

Crabtree, 2006). This is also the result of the initial pilot phase of the interviews in 2019. At the beginning of the fieldwork, two questionnaires were used – one for a closed survey and one for a semi-structured interview. After the first day, however, the questionnaires were merged into one due to the fact that once a conversation was begun, additional information was gained that could not have been recorded using only a closed-survey questionnaire. The new questionnaire combined elements from both the closed survey and the semi-structured interview. This also allowed for a statistical analysis of the results (though the sample size was limited due to the restrictions in fieldwork that arose in 2020), as well as the collection of important additional information that cannot be captured purely through closed-survey questions.

Broadly speaking, there were two phases of developing the interview structure. The first phase, during the June 2019 field trip, aimed to understand the types of ecosystem services linked to Preks and their hydrological functioning that locals benefit from (see Appendix 4 for a brief description of results from this initial phase). The second phase, starting in November 2019, strove to make these services quantifiable and to develop a more in-depth understanding of agricultural and water management practices. The questionnaires for this approach were piloted in November 2019 and applied in February-March 2020. Three different versions were developed - one for farmers, another for village chiefs, and the third for the heads of Prek User Committees (PUC), who are elected locally to be responsible for Prek water management. Generally, PUCs fall into the broader category of Water User Associations (cf. Ivars and Venot (2018)). [4] Further interviews were planned with representatives of the MoWRAM, the Chief of the Commune, and private water sellers. Unfortunately, these could not take place because fieldwork was cut short due to the pandemic. During the fieldwork in February and March 2020, a very extensive section on agricultural practices such as fertilizer and pesticide application, and tilling was included in the questionnaire. This later served as the basis for an agronomic analysis in an MSc thesis written in the framework of the COSTEA project (see Vandôme (2020)). During the interviews carried out in autumn 2020 and spring 2021, this section was scaled down considerably. Copies of all the questionnaires used can be found in Appendix E.

The interviews (see Figure 4.13) themselves were carried out in a variety of locations. Some were conducted directly in the fields of the farmers, which offered the advantage that they

[4]These committees are established in the course of rehabilitation projects, to ensure proper maintenance of the Prek once construction is finished. The head of the PUC is elected democratically. Their main task is to coordinate maintenance efforts between farmers who benefit from Preks For further details, see Section 4.3.6.

could point to salient features in-situ, demonstrate practices, and showcase equipment. Other interviews took place in the respondents' homes, in the villages along the Preks. These are usually one-storey buildings constructed on pillars, with an open-air living and storage area on the ground floor and closed living quarters on the first floor, accessible via stairs or ladders. The interviews were held in Khmer, with colleagues and students from RUA and ITC acting as translators.



(a) Interview in a village chief's house.



(b) Interview in a mango orchard.



(c) Typical house in the study area.



(d) Interview in a fisherman's house at the Prek Ambel.



(e) Interview in a rice field.

Figure 4.13: Interviews in the case study area.

4.3.2 Geographic and Demographic Information on Respondents

In the first phase of fieldwork, 19 people were interviewed - two at each Prek except Prek Put, where only one respondent was located. In the second phase, eight village chiefs, the chief of one Prek User Committee (PUC at Prek Chann), and 67[5] farmers were interviewed. Among the farmers who were interviewed, two were not strictly speaking farmers. One was a Cham fisherman, who also owns some livestock but no land, and who lives in the Cham village at the end of Prek Cham Kroum. The other was a scavenger – a woman who owns no land herself, and who does not farm, but who collects the remains of crops after harvests from other people's fields. The information gathered from these interviewees covers 149 plots, with 201 responses to which crops were cultivated, as one plot is sometimes used for the cultivation of several crops. This represents ca. 116 ha, which amounts to 2.7% of the study area.

Of the interviewed farmers, 24% were women and 76% were men. The distribution of their ages is shown in Figure 4.14. The age of the interviewees ranged from 28 to 72, with an average of 47 years, with the majority falling into the age groups of 31-40 and 51-60. Generally, it has to be noted that there might be a slight skewing of results due to the fact that Buddhist rules prevent farmers over 50 from either fishing or tending to livestock, according to information from respondents. Among the interviewees, 52% were over this age.

The geographical distribution of interviewed farmers along Preks in the study area is shown in Figure 4.15. As mentioned above, the distribution is uneven. The reason for this is that limited time was available for the interviews due to the pandemic. It must also be noted that most of the interviews at Prek Thom were conducted at its tail end, with farmers whose activities are centered in the Boeung areas.

[5] 37 during in February - March 2020, and the others between November and March 2021 by a colleague from RUA.

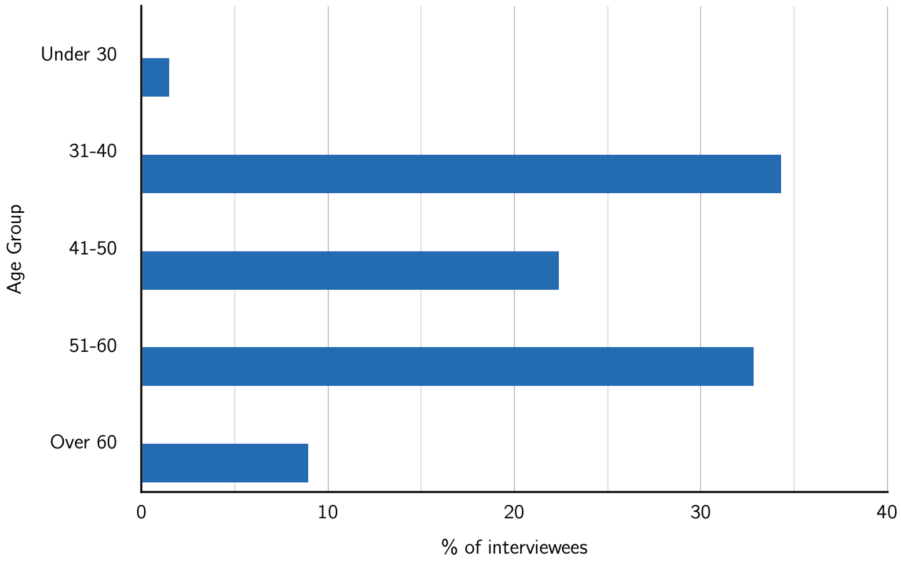

Figure 4.14: Ages of the farmers who were interviewed.

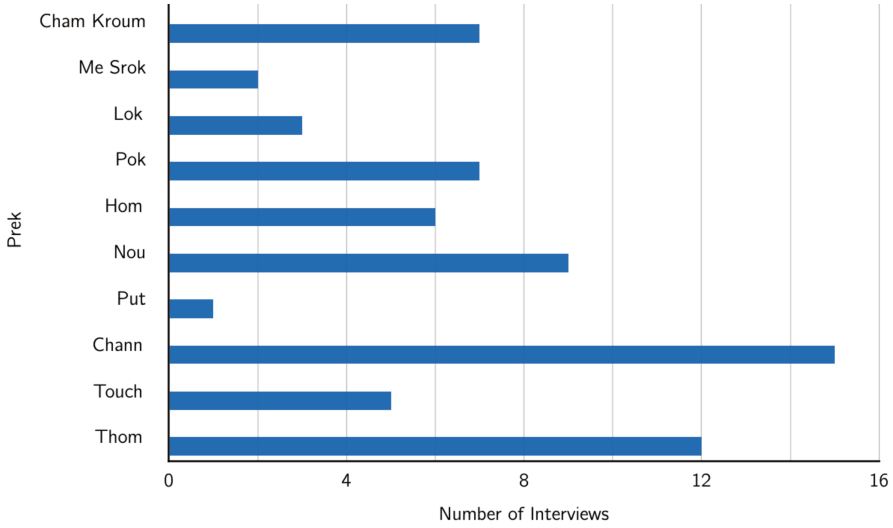

Figure 4.15: Preks at which farmers were interviewed.

The economic circumstances of interviewees varied wildly. The median annual household income from agriculture reported was approximately 3 000 USD, with a minimum of 246 USD and a maximum of 6 700 USD. In addition to cultivating crops and rearing livestock, many people also have secondary incomes from construction work, running a small restaurant or shop, a remittance from family members living in the city, working in garment factories, and selling their own agricultural labour. For a detailed classification of production and income systems in the study area, see Vandôme (2020).

4.3.3 Outlining Ecosystem Services and their Relation to Prek Channels

Some information on the ecosystem services to which the Preks contribute existed already before fieldwork began. Engineering reports such as SOFRECO (2017) listed irrigation, transport by boat, sediment supply, mitigation of flood damage, domestic water supply, fishing, and sedimentation as the principle benefits of Preks in general and rehabilitated Preks in particular.

Generally, it has to be noted that the largest number of ecosystem services is used by those interviewees who are economically less well-off. For instance, in one village the most prosperous interview participant – who also happens to be a village chief – only uses the Prek for irrigation purposes, whereas the least well-off amongst the interviewees derive domestic water, irrigation water, major parts of their diet (in the form of bank vegetation and fish) as well as means of transport and nutrient-laden sediments from the Prek.

4.3.3.1 Provisioning Ecosystem Services

During the interviews, it became apparent that the majority of ecosystem services from which the local inhabitants benefit directly fall under the category of provisioning ecosystem services, though some interviewees explicitly remarked on regulating services as well, which will be examined in the next section.

Irrigation Water Supply Generally, it can be said that the main importance of the Prek for the interviewees lies in its provision of water for crop irrigation. Most of the interviewees grow crops such as mangoes, cucumbers, beans, corn or sugarcane in the Chamkar area of the Preks and rice in the Boeung (see Section 4.3.4 for a more in-depth profile). Most of these crops are irrigated regularly with water from the Preks or the canal system in the Boeung.

Alternative sources of irrigation water exist as well, though they are limited. For instance, some farmers pump from adjacent plots or small-scale ponds located in the inter-Prek areas (see Figure 4.16) just after the flood. In many cases, ponds were excavated to use the soil to raise land elsewhere. A secondary effect is that they can retain flood water after recession, which can be used for irrigation during the early dry season. Groundwater is rarely used for irrigation if it can

be helped, as there are concerns about arsenic contamination (see Tweed et al. (2020)). Some farmers (13% of respondents) have wells on their plots or at their houses, but none were observed to be in use. The exception is a small area near the head of Prek Put. Here, pumps are used regularly for irrigation according to local interview respondents, as the Prek only carries water for one or two months per year during the high flood. However, even here, there are initiatives to draw water from the adjacent Prek Nou rather than use groundwater.

It can therefore be surmised that the supply of irrigation water is indeed one of the principal benefits that the local population derives from Preks, especially during the dry season, with few alternatives available.



Figure 4.16: Pond dug in the inter-Prek area. the extracted soil was used to raise land elsewhere.

Natural Vegetation Besides using the water from the Preks for irrigation to grow their crops, farmers also benefit from the natural vegetation that grows in the Prek system - either directly along the banks of Preks, or in areas of the Boeung and Chamkar that are not actively used to grow crops.

Overall, 54% of interviewees stated that they use the natural vegetation that grows along the banks of the Prek, on the Chamkar land, or in the Boeung. The main uses given were for food and feeding livestock. For the latter, people who rear cattle cut grass on the banks of the Preks as well as in fallow areas in the Boeung (see Figure 4.17). For food, people use mostly morning glory (*Ipomoea aquatica*), and ivy gourd (*Coccinia grandis*), as well as the flowers of water hyacinths (*Eichhornia crassipes*). Many of them also grow some plants themselves on the banks of the Prek for household consumption, like tomatoes and cucumbers. In the case of the rehabilitated Preks, interviewees mentioned that the latter use had been restricted, as the banks

are to be kept clear of vegetation as much as possible.

In addition, interviewees stated that they used the natural vegetation for fuel, fish traps and medicinal plants.

It was difficult for participants to estimate the frequency of usage of natural vegetation for food. Most said that they use the plants they find along the Prek or in the Boeung to supplement their diets a few times per week throughout the year.

Details on using bank vegetation as fuel were given by one farmer who was observed cutting trees along the Prek. He stated that he cuts trees that grow in front of someone else's plot, but that he does not have to pay for it - though the veracity of that statement is questionable. He said that he cuts two trees per year, which result in two cubes of solid wood. Each cube could be sold for ca. 40,000 Riel, but he said he keeps it mostly for home use.

Another use for the bank vegetation is for constructing fish traps. Here, branches from trees that grow in the case study area are cut off and placed on a type of scaffolding in the water, a system locally called "samras". This offers an attractive shelter to fish, and they can be caught there more easily.

In terms of medicinal uses of bank vegetation, only one respondent said that she uses it for this purpose. The medicinal purpose in question was the use of dried herbs to soothe menstrual cramps.

A final point that must be noted on this issue is that there are apparently some concerns related to the use of natural vegetation. One farmer, in particular, noted that his family used to supplement their diets frequently with plants that grow along the Prek and on the Chamkars. However, he stated that they ceased to do so due to concerns over extensive pesticide use. Three more farmers also voiced concerns about using grass that grows along the Preks to feed their cattle out of concerns about pesticide contamination.



(a) A woman collecting natural vegetation for medicinal purposes along Prek Thom before it was excavated.



(b) A farmer cutting grass for his cattle on the banks of Prek Chann.

Figure 4.17: Uses of natural vegetation in the study area.

Transport Some of the interviewees use the Preks as transportation routes for their boats. However, several of the interviewees had recently disposed of their boats - either because they were broken and they couldn't afford to repair them, or because they were now using the better road that had been constructed during Prek rehabilitation and no longer needed transport by water.[6]

During the interviews, a 21% of respondents said that they use the Prek for transport. The majority own their own boat; one borrows it from a family member when they need to use it.

Boats are used to transport farm equipment, pesticides and fertilizers, seeds, and parts of the harvest. Furthermore, people stated that they use boats to go to their Boeung plots periodically to check on the status of their crops. Those who do own boats say they use them along the Preks, in the canals at the end of the Preks, as well as on the Boeung during the wet season. The months of high-frequency boat usage seem to be between November and January, during the period of recession rice cultivation - provided, of course, that there is sufficient water in the Preks. The interviewee in the Cham village at the end of Prek Me Srok also stated that they used their family boat on Prek Ambel, and to transport goods to sell on the market along the Prek and over the Bassac to Koh Thom.

[6]Road construction or repair was frequently named as one of the major benefits of rehabilitation. Also cf. Appendix 4

However, the general use of boats seems to have declined over recent years. One farmer noted that not many families still use boats. According to him, the use of boats on the Prek as a means of transport was much more widespread until about ten years ago. The reason for that is that back then, there was much more livestock in the area – both because prices for livestock were high, and because cows were used to plough fields. Boats were needed to transport agricultural implements, and the grass that was cut in the Boeung and along the Prek, to feed the livestock. Nowadays, livestock prices have fallen, and tractors are widely available, so boats have often become superfluous. In fact, during the fieldwork, it was even observed as one family took apart their boat to re-purpose the wood, see Figure 4.18.



(a) A family taking apart their boat to re-purpose it as construction material.



(b) Transport by boat on a Prek.

Figure 4.18: Boats used for transport in the study area.

Livestock 55% of the interviewed farmers own livestock. The most commonly kept livestock is cattle, followed by chickens and pigs. According to one interviewed village chief, far more farmers used to raise cattle, especially cows. But since the price of cattle has fallen considerably, many have given up on livestock farming. Those who do still have cattle, though, use the water from the Preks to wash and water the animals (see Figure 4.19b). Furthermore, they use the grass that grows along the Prek as fodder, as mentioned above. (One of the interviewees, however, noted that it is not as nutritious as the grass that can be found on the Chamkars.) In addition, they purchase rice straw from farmers. For more details, see Chapter 4.3.4 and Vandôme (2020).



(a) Cattle in front of a house in a village along a Prek.



(b) Cattle being watered and washed in a Prek.

Figure 4.19: Cattle in the case study area.

Domestic Water Supply The majority of interviewees has access to clean water from a communal pipe. The price for one cubic meter of water (1 m^3) of water from this supply lies at 2000 Riel (0.50 USD). The average use seemed to lie at 15 – 25[3] m per month. However, several interviewees stated that they used water from the Prek to supplement their domestic consumption for uses such as washing clothes, cleaning, and personal hygiene. One interviewee stated that since she started using water from the rehabilitated Prek Chann, her water bill had been cut in half, from 30 000 to 15 000 Riels (7.40 to 3.70 USD) per month.

Fishing Of the farmers interviewed, 30% said that at least during one point in the year they fished either in the Prek, in the Boeungs, in the Prek Ambel, or in the canals. The majority of respondents fished only to cover their families' needs, with only three of the interviewees explicitly stating that they sell the fish that they catch. The fish is sold either directly at Koh Thom market, or to middlemen who then bring it to Phnom Penh.

Furthermore, several interviewees noted that they used to fish, but no longer pursue the practice, either because they have too little time, or because the fish catch radically decreased. One of the interviewees attributed this decrease (he estimated it to lie at 80%) to widespread illegal fishing activities using electroshocks. The interviewee living in the Cham village, states that the fish populations also dramatically decreased in the Boeung over the years. He used to fish in the Boeung twice per week during the wet season. In the 2019/20 wet season, however,

he only fished there one time in total, which might be related to the short duration of the flood that year.

The general consensus is that the peak fishing period is between November and January, during flood recession. At this time, fish that have prospered in the flooded Boeung are channelled by the water that is draining to the Bassac. One interviewee stated that during this time, they could catch as much as 30-40 kg of fish in the Prek over the course of five days.One more aspect that was mentioned by multiple fishermen is that the catch in the canals and in the Boeung is also dependent on the phase of the moon. This is likely to be related to the varying water levels mentioned in Section 3.2.3 and the resulting currents.

One particular fishing practice needs to be mentioned. One interviewee stated that their family uses the Boeung plot they own partly for rice cultivation, but partly to rear fish. Part of the plot is lower than the other, and they refer to it as a 'pond'. In this pond, they let fish mature, before using their pump to extract the water. This technique is also known as *bear fishing*.

Finally, the interviewee in the Cham village also noted that commercial fishing activities were prohibited from March onwards by the Fisheries Ministry, to protect fish procreation.[7]

At this point it must be noted that the importance of fishing as an element of livelihoods appears to be much larger in neighbouring areas than in the case study area under scrutiny here. In the area bracketed by the Mekong and the Bassac, villages whose main economic activity is fishing exist, with fish traps set up almost permanently and some people - often of Vietnamese ethnicity - living on house boats nearby. These traps, though illegal, use vegetation arranged as shelters and food incentives to attract fish so that they can be caught. Even though they have theoretically been outlawed by the government, they can still be seen frequently in the region.

[7] In fact, the official "closed fishing season" lasts from the beginning of June to the end of September, according to information from the Ministry (Kunthear and Khmer Times, 2018; Sivutha and The Phnom Penh Post, 2021a)



(a) A farmer fishing in a rehabilitated Prek.



(b) Fish catch in a handwoven basket.



(c) A young man installing nets in a Prek. They will be left for a few days before he comes back to collect the catch.



(d) Fish catch in a river village near the border of Vietnam.

Figure 4.20: Three simple graphs

4.3.3.2 Regulating Ecosystem Services

The second major group of ecosystem services that was inquired after in the interviews were regulating ecosystem services. As was to be expected, these proved more difficult to quantify for individual farmers, but an informative picture of a local perspective nonetheless emerged.

Water Retention and Flood Damage Reduction Water retention and peak flood attenuation is one of the regulating ecosystem services detailed in SOFRECO (2017). Already Barthélemy (1913) likened the rudimentary Prek system he observed at the beginning of the 20th century to the Tonle Sap Lake in terms of its water storage and flood peak attenuation capacity.

However, few farmers in the study area reported any impact of the Prek system or its

rehabilitation on preventing flood damage to crops. Farmers at rehabilitated Preks did not state that they experienced any difference in the impact of floods in comparison to before. The majority of farmers reported that they kept the areas of their plots that are flooded regularly clear of any crops that could be damaged during this time. Some mentioned extreme events that lay several years back and did result in larger damage, but none that they could relate to the Preks.

This indicates that there are few benefits of flood regulation in the Prek system on a local level - but that these are only effectively felt by downstream communities, as indicated in the hydrological analysis in Section 3.2. It also points towards the fact that the rehabilitation of a single Prek changes relatively little in the flood patterns at its tail end, which, in turn, can be seen as an indicator of the fact that the flood also arrives via neighbouring Preks and the canal network.

Sediment and Nutrient Cycling In contrast to regional flood retention, the benefit of sediment deposition is keenly felt by farmers in the study area. Eight of them noted that they used the sediments from the Preks to raise their lands and that they appreciated (partial) inundation of their plots during the flood season because it brought 'good earth' and kept their lands fertile. In addition, some also excavate the sediments from the Prek channels directly to sell at a profit - see the information provided by village chiefs in Section 4.3.6 for further information.

Ground- and Soil Water Recharge Groundwater is used relatively infrequently in the case study area due to concerns about arsenic contamination and the availability of clean drinking water from a communal pipe and Prek water for irrigation. Only in the area of Prek Put, which is dry for most of the year, do farmers still use wells regularly for irrigation, according to the information gathered in the interviews. For this reason, the direct effects of groundwater recharge by Preks and the floods that they catalyze were not a fruitful topic of discussion during the interviews.

However, two farmers did talk in depth about the benefits of soil water recharge. They stated that shorter flood durations over the past few years, but especially during the 2019-20 season, had left soils relatively dry. One farmer said that infiltration depths of the soils in his plots only reached 20-30 cm that year and that, consequently, he needed to irrigate sooner and more

intensively to provide sufficient water for his crops. Apart from the shorter flood duration, he also said that the development of soil crusts that inhibit infiltration contributed to this issue. The reason for the development of these crusts, he believes, is the over-use of fertilizer and pesticides, which destroy soil structure.

Pest Regulation During the interviews, it emerged that for many farmers, crop losses due to pests were a more pressing concern than floods or droughts. Extended flooding can contribute to reducing several aspects of this concern.

Most importantly, several farmers stated that floods are a major contributing factor to the reduction of rat populations, which cause considerable damage to rice, vegetables, and even fruit trees. Especially for rice fields, rats are a concern. One farmer noted that his rice crop was decimated from 160 to 40 bags by rats last year. Other estimates of rice crop losses due to rats lie at 30%. To combat rats, farmers take measures such as electrical traps, rat poison, and setting off fireworks in the fields to scare them away. Also cutting away grass that grows on the borders of plots has been mentioned as a step to take to exterminate rats, since it deprives them of their shelters. The abundance of rats is a well-known problem in the region, and the focus of several initiatives for integrated pest management (Flor et al., 2018; Castilla et al., 2020; Jahn et al., 1999).

The most frequently mentioned natural factor for rat population control was regular flooding. In fact, the majority of farmers who engaged on the issue of pest control mentioned that a considerable negative impact of the short duration of the 2019 flood was the fact that rats were abundant during the following dry season. Overall, eight farmers stated that they believe floods contribute to the decimation of rat populations. When asked to elaborate, three farmers detailed that rat populations are particularly decimated when the flood water reaches up to the level of the road at the middle of the Prek, or over the crest of the Prek. One farmer also stated that a fast rise in water levels also contributes to the death toll among rats, since many of them have their nests in the banks of the Prek and do not have the time to retreat if the flood arrives quickly.

Another aspect of regular inundations' contribution to pest control is that several farmers are of the opinion that large enough floods can also help reduce the damage done to crops by insects. One farmer also noted that he would welcome Prek rehabilitation because it would

reduce stagnant water in the Prek, which is a breeding ground for insects.

4.3.3.3 Cultural Ecosystem Services

Investigating cultural ecosystem services related to the Prek system in the case study area proved to be difficult. Partially, this is due to the fact that they were only peripherally inquired after during the interviews. Partially, however, it is also likely that the historical context outlined above contributes to the fact that there are no readily evident local traditions, stories, spiritual practices, or songs related directly to the Prek channels, or the Prek system as a whole. Due to the major population movements in the aftermath of the Khmer Rouge period, many families have been living in the area only for one generation. In addition, it must be noted that such enquires are generally difficult, even more so when responses are translated.

To a certain extent, Prek channels provide recreational value to the local population. On multiple occasions, for example, children could be seen playing in the Preks when they had sufficient water - swimming and jumping from bridges.

It can also be surmised that the Preks contribute to the formation of a local and regional identity on a deeper level. Even though some farmers have plots at more than one Prek, the majority possesses a Chamkar and a Boeung plot at the same Prek at which their homestead is also located. This means that the majority of their life and labour is organized along the length of Prek channels. Villages and communities, too, are organized along the Preks.

However, to delve into the complexities of identity formation and the underlying social processes, a far more targeted and in-depth approach would be necessary. For this reason, cultural ecosystem services will not be considered further in the framework of this thesis.

4.3.4 Characterising Agricultural Practices

The data collected during the interviews allowed for an in-depth characterization of agricultural practices in the area, to further shed light on the role that Preks play in contributing to provisioning ecosystem services. An extensive account of a typology of farming systems in the study area,

based on data collected in February and March 2020, is available in Vandôme (2020).[8] This section provides an overview of the agricultural practices reflected in the entirety of the interview data collected in the course of this thesis. This will form an important element of the modelling approach presented in the next chapter, as average values are used as baseline inputs for the calculation of future likely yields.

4.3.4.1 Characteristics of Survey Respondents' Holdings

In total, the 67 farmers who were interviewed in the course of this thesis own 149 plots, covering a total of 116 ha. On average, a farmer owns 2.5 plots ($\sigma = 1.23$). Part of the reason for this is historical. According to information by one interviewee in his 60s, each household was allocated a Boeung plot, a Chamkar plot, and a plot of land in the village when the Vietnamese relinquished control over the region in 1989 and individual land management became possible again, followed by private land ownership in 2001 (though many people still hold land use right on state-owned land, rather than actual ownership). Over the past forty years, property structures have shifted relatively little, though some respondents rent additional plots from farmers who no longer cultivate them themselves. In total, 84% of the plots of farmers who were interviewed belonged to them, 12% were rented, and 4% were shared between relatives. Recently, the sale of land has also become more common. Part of the reason for this is that outside investors are moving into the region, prominently from China.[9] Seven was the maximum number of plots owned by a single farmer in the study area.

The average size of a plot in the study area is 0.8 ha ($\sigma = 1.07$ ha), with a maximum size of 8 ha. Generally, Boeung plots tend to be larger, at an average of 1.20 ha ($\sigma = 1.28$ ha) than either plots located in transition areas ($\bar{x} = 1.05$ ha, $\sigma = 1.75$ ha) or on Chamkars ($\bar{x} = 0.46$ ha, $\sigma = 0.44$ha). Typically, multiple crops are cultivated on a single Chamkar plot ($\bar{x} = 1.41$ on average, $\sigma = 0.68$) and plots located in the transition zone ($\bar{x} = 1.28$ha, $\sigma = 0.47$ha). In contrast, Boeung plots are almost exclusively cultivated with rice, though in several cycles. Figure 4.21 shows the distribution of crops among the different zones in the study area.

[8] It must be noted that this data under-represents Boeung areas, as the interview focus was only shifted there in autumn 2020.

[9] Chinese companies and the government have (co-)financed several infrastructure projects in the region, including in the case study area. The bridge across the Mekong at Koh Thom just North of the case study area is an example of this.

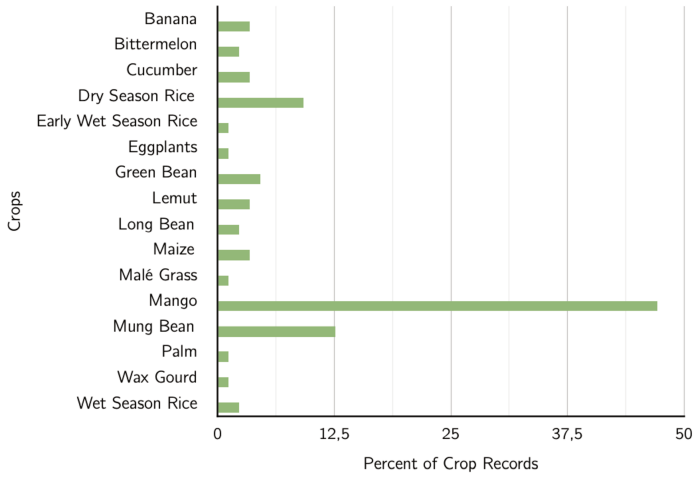

(a) Crop distribution on Chamkars.

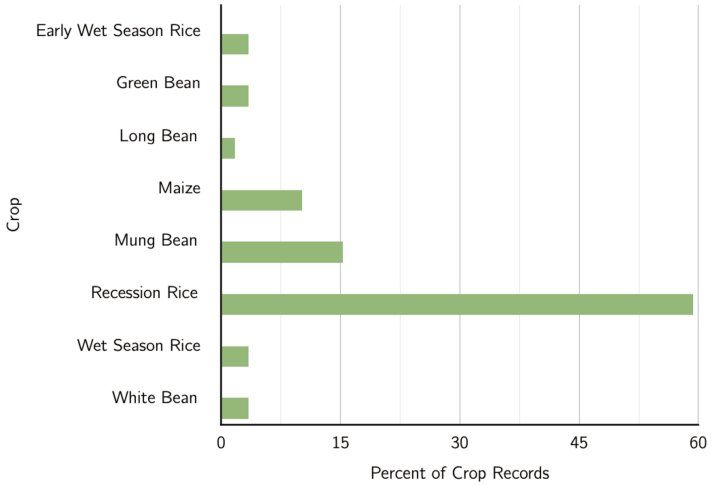

(b) Crop distribution in Transition Areas.

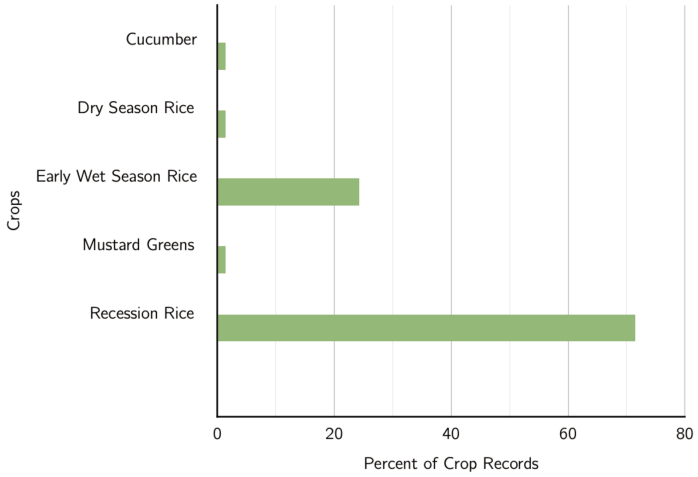

(c) Crop distribution in Boeungs

Figure 4.21: Crop distribution in the case study area.

Crop	Planting Time	Harvest Time	Daily Irrigation [h/ha]	Average Yield	Upper 25% Yield	Average Price Per Unit in USD
Bittermelon	March	May-June	6.52	6.67	6.67	1.67
Early Wet Season Rice	April - May	July - August	2.90	6.10	11	2.75
Mustard greens	June	July	12.50	1.41	1.41	0.35
Wet season rice	September	December	2.82	4.08	5	1.25
Eggplants	October	March	1.85	5.56	5.56	1.39
Mung bean	November or March	February or May	1.87	2.48	4.80	1.20
Recession rice	October - December	January - March	1.88	5.73	9.12	2.28
White bean	October-November	January	0.00	1.35	1.35	0.34
Wax gourd	November	January	1.67			0.00
Green bean	November - December	February - March	0.00	2.71	3.57	0.89
Long bean	December	January	0.95	6.00	6.00	1.50
Dry season rice	December - January	March - April	1.91	5.66	8.57	2.1425
Cucumber	Variable	Variable	7.98	5.22	6.67	1.67
Maize	Variable	Variable	0.45	4.94	6.22	1.56
Fruit trees	year-round	year-round	1	10.8	19.9	4.975
Male Grass	year-round	year-round				

Table 4.2: Average practices for different crops grown in the case study area.

4.3.4.2 Average Cropping Practices

The average planting and harvest dates, irrigation practices, yield, and revenue for them are given in Table 4.4. Vandôme (2020) also produced a visual representation of the farming itineraries for the different crops, reproduced in Figure 4.22. Broadly, the crops grown in the study area can be organized into three groups - rice, fruit trees such as mango and lemut, and vegetables like different varieties of beans, eggplants, and cucumbers.

Vegetables The latter group - vegetables - are grown on Chamkars and on transition zone plots either during the dry season, or in sections of these plots for which flood frequencies are low. For some vegetable crops, the planting dates are mostly uniform, for instance for mung beans. In contrast, crops like cucumbers and eggplants are grown at various times of the year in various plots on Chamkars, in transition zones and in Boeungs. As Table 4.2 shows, vegetables are among the most profitable crops in the study area. However, they are also fairly labour-intensive to grow. Beans, for instance, are picked by hand.

One difficulty with information on vegetables is that many of them are not well-represented in the fieldwork dataset. For instance, only one farmer growing eggplants was interviewed, and only two interviewees provided information on growing bitter melon. This is one of the reasons why vegetables were grouped together as a single crop type in the modeling process - to reduce the uncertainty and noise in the data by averaging them out according to the area each crop occupies in the fieldwork data.

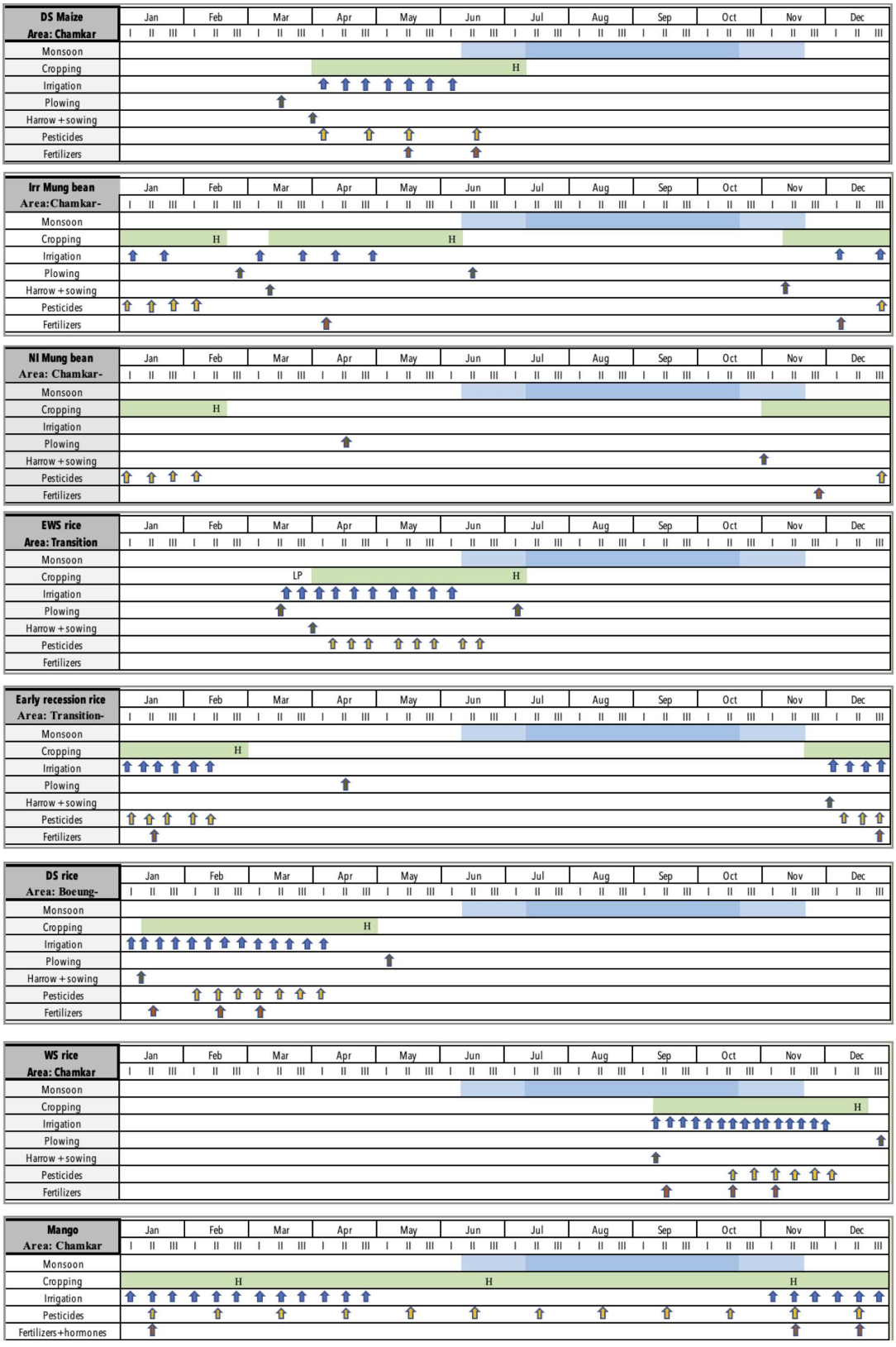

Figure 4.22: Cropping practices for different crops in the study area, as characterized by Vandôme (2020).

Fruit Trees In contrast, extensive information is available on the cultivation of fruit trees, especially mangoes (see Chapter 5). In total, 41 farmers provided information on the practices involved in growing mango trees. They are one of the most widely cultivated crops in the study area. In fact, especially on the Chamkar areas of the two northernmost Preks in the study area – Prek Cham Kroum and Prek Me Srok, it appears that little else is grown.

One of the farmers stated that five to ten years ago, there was a general switch to mangoes due to the high prices for the fruit back then. Some farmers also changed to planting mango trees because of what could be termed situational peer pressure. One of them said he switched from vegetables to mangoes because his plot is narrow, and he was afraid that the new trees of his neighbours would cast shade on his plot and inhibit the growth of his vegetables.

However, the price has since dropped. Furthermore, there are other issues mango growers are facing. Several farmers stated that they lost crops not only due to insects, droughts or floods, but also because hormones for inducing flowering in mango trees sometimes did not work.

As a consequence, some farmers are pursuing strategies to raise the quality of their products to increase the price. Most commonly, it was observed that young mango fruits were covered in paper bags. Farmers said that this was to protect their skin in order to be able to sell them to Thailand for as much as 1500 Riel per kg.

Other farmers are thinking about switching crops again. One interviewee told us that he wants to switch back to rice because mango is no longer very profitable and buying rice for family needs from the market is very expensive. However, he says that he is waiting for his neighbours to make the switch also, because he is afraid that if he is the only one planting rice in the midst of mangoes, rats will converge onto his plot.

Other fruit trees grown in the area include banana and lemut trees. However, only four plots that were (partially) used to grow these trees appeared in the data. Since their management is similar to mangoes in terms of irrigation and pesticide spraying, there were therefore lumped together with mangoes for the land use classification and the model described below.

Rice Finally, there is rice - the most common crop in the study area, especially in the Boeungs. Overall, four different kinds of rice cultivation can be distinguished - recession rice, dry season

rice, early wet season rice, and wet season rice.

Recession rice is the most widespread type of rice cultivation in the study area. As its name suggests, it is planted as the flood recedes from plots, usually when there are a few centimeters of water left, or when the soil is still very muddy from being submerged. This means that the planting and harvesting times for recession rice vary considerably, as is reflected in Table 4.4. In some plots, the flood sometimes recedes as early as the end of October, while it lingers until December in others. Generally, water availability is least problematic for this type of rice, since the soil is saturated at the beginning of cultivation, and water levels in the Preks and canals are still relatively high. In addition, there are still significant amounts of precipitation towards the end of the year. Still, if floods recede quickly, water levels in the Bassac are low, and rainfall insufficient, these crops can experience drought stress (see Section 4.3.4). In some cases, it can also be problematic if the flood recedes too late. In that case, recession rice can only be planted with a delay - and it misses out on natural precipitation during the latter part of the year.

Dry season rice can only be cultivated if sufficient irrigation water is available. It is usually an option on plots where recession rice could be planted and harvested relatively early - in December or January - or on plots that are close to canals and Preks that experience consistent inflow during the dry season. But even then, the expenses for pumping the required amounts of water are often prohibitive. Overall, this is not a common practice in the area - only seven farmers engage in it.

Far more common is the cultivation of early wet season (EWS) rice. Cultivation begins in April or May, when precipitation begins to set in. As the water levels in the river rise at the beginning of the wet season, irrigation becomes possible once more. The most critical issue with EWS rice is that it must be harvested before the arrival of the flood - usually July or early August. If this is not the case, the crop may be lost partially or completely.

Finally, there is wet season rice - which is grown on elevated plots while much of the case study area is flooded. It is partially rainfed and partially sustained through irrigation with water lifted from the full canals and Preks. Like dry season rice, though, this is not a common practice in the case study area, partially because it has the lowest average yields of all the different types of rice cultivation (cf. Table 4.4).

Irrigation During the surveys, farmers were asked how frequently they irrigate their various crops and how long each irrigation session lasts. Most respondents were able to provide detailed information on these issues with a high degree of certainty. In addition, they were asked to explain their reasoning behind choosing to irrigate a plot or not. While some farmers named factors such as soil moisture and monitoring precipitation amounts, most said that it was a matter of routine that they adhered to because their neighbours also did.

To irrigate their crops, farmers use small pumps (see Figure 4.23a) that the majority owns themselves, though three respondents have mentioned renting them or sharing them with family members. These pumps are mobile and can be moved between plots (see Figure 4.23b). On average, farmers own one or two (average: 1.4) pumps. The average pump capacity lies at ca. 7.5 HP (5593 W). Most pumps used to pump water directly from a water source to the destination plots have between 5 and 7 HP. Pumps are placed at various elevations on the banks of Preks. To supply pumps, PVC pipes are used. To distribute water along fields, flexible plastic tubes are used in most cases (see Figure 4.23c and 4.23d). The reason for this is that it allows farmers greater flexibility in where to direct the flow of water (see Figure 4.23e). Furthermore, these tubes can be laid across the path on the banks of the Prek without impeding traffic - carts, tractors, and small motorbikes that farmers use for transport.

In some Preks where natural water inflow from the Bassac ceases during the dry season, water is pumped into the Prek during these times. In some places, this is being organised by village chiefs, in other places by private farmers. Sometimes the pumping is officially sanctioned, sometimes, it appears, the village chief is not even aware of it. Table 4.3 shows a summary of the current state of knowledge about pumping practices within the Prek as well as between the Prek and the Bassac or canals, from North to South. It must be emphasized, however, that this information may not be entirely reliable, as contradictions between what was reported by village chiefs and farmers, and what was observed in the field, were evident.

Prek	Currently pumping into the Prek?	Notes
Cham Kroum	N	According to the village chief, no pumping takes place. However, according to a farmer, 20-30 families get together to pay for renting a pumping machine from the commune for a few days during the dry season.
Me Srok	N	Pumping has not been necessary since rehabilitation. Beforehand, a communal pumping machine could be requested. However, that was not necessary often since farmers along the Prek mainly grow mango and lemut trees, which have limited water needs.
Lok	N	No pumping into the Prek.
Pok	Y	A pump at the head of the Prek is organised by the farmers who need the water, and reported to the village chief. This normally happens in March or April.
Hom	?	Some farmers said yes, some farmers said no. The village chief was not interviewed.
Nou	Y	Water is being pumped into the Prek from the canal at the end of the Prek by a private water seller.
Put	N	Since Prek Put is heavily affected by sedimentation, water inflow only happens one or two months per year. During the dry season, water from Prek Nou is used to supply the fields in the North of the Prek.
Chann	N	Not since rehabilitation. However, a pump was installed within Prek earlier this year to balance out bank collapses. These have been fixed now.
Touch	N	No pumping into the Prek.
Thom	N	A private water seller was pumping into the Prek before the excavation of the Prek in 2020. He has moved his operation to outside the study area since inflow now happens continuously.

Table 4.3: Overview of Preks in the case study area with regard to whether they are supplied with water via pumps during the dry season. State 2020.



(a) A pump lifting water at Prek Thom before excavation.



(b) A woman transporting a small pump to her plot.



(c) Irrigation via plastic tubes at Prek Nou.



(d) Gravity irrigation at Prek Cham Kroum.



(e) A farmer irrigating eggplants.

Figure 4.23: Irrigation practices in the area.

Crop	Planting Time	Harvest Time	Daily Irrigation Hours Per Hectare	Average Yield	Upper 25% Yield	Average Price Per Unit in USD
Bittermelon	March	May-June	6,52	6,67	6,67	1,67
Early Wet Season Rice	April - May	July - August	2,90	6,10	11	2,75
Mustard greens	June	July	12,50	1,41	1,41	0,35
Wet season rice	September	December	2,82	4,08	5	1,25
Eggplants	October	March	1,85	5,56	5,56	1,39
Mung bean	November or March	February or May	1,87	2,48	4,80	1,20
Recession rice	October - December	January - March	1,88	5,73	9,12	2,28
White bean	October-November	January	0,00	1,35	1,35	0,34
Wax gourd	November	January	1,67			0,00
Green bean	November - Decmber	February - March	0,00	2,71	3,57	0,89
Long bean	December	January	0,95	6,00	6,00	1,50
Dry season rice	December - January	March - April	1,91	5,66	8,57	2,1425
Cucumber	Variable	Variable	7,98	5,22	6,67	1,67
Maize	Variable	Variable	0,45	4,94	6,22	1,56
Fruit trees	year-round	year-round	1	10,8	19,9	4,975
Malé Grass	year-round	year-round				

Table 4.4: Average irrigation hours (per day and hectare), and yield for all crops in the study area.

4.3.4.3 Livestock

Among the interviewees, 37 keep livestock. Most of them keep a small number of cows (3-4) to sell for meat, though two farmers also raised pigs. Several interviewees reported having given up on keeping livestock since it had become unprofitable.

Some of the farmers who raise cows also sell the manure they produce. One farmer said that he sold manure three times per year to Takeo. Another farmer detailed that they had to sell the manure to Takeo because farmers in Kandal prefer chemical fertilizers. Apparently, the farmers in Takeo use the manure to fertilize fields for the cultivation of rainy season rice. The farmer said that they have dams in Takeo to protect the area, and can spread the dung over a longer period of time before cultivation, without it being swept away by the flood

Farmers largely use hay from natural vegetation that grows in the Boeung, as well as rice straw to feed the cattle. Some of them also let the cattle graze along the Prek and in the Boeung (see Figure 4.24d). Most of them, however, seem to raise them directly at their houses. During the fieldwork, several farmers were also observed watering and washing their cattle in the Prek.

One concept that also occurred in relation to cattle was the practice of prowa cows. The interviewee in the Cham village at the end of Prek Me Srok raises cows who belong to someone else under prowa. Ultimately, the owner has the benefit of selling mature cows, but the farmer who raises them gets to keep some of the benefits, in this case every second calf born.

Four farmers who were interviewed also raise pigs. Most of the farmers interviewed also raise chickens at their houses. While the majority only raise chickens for family needs, and are

not considered more closely, some of them also raise chickens to sell at the market.



(a) Pigs being raised in a sty at Prek Nou.



(b) Chickens being raised at Prek Put.



(c) Cattle being watered in Prek Nou.



(d) Cattle grazing at Prek Thom.

Figure 4.24: Livestock in the study area.

4.3.4.4 Crop Losses Due to Droughts, Floods, and Pests

Floods Out of the 67 farmers interviewed, 27 (31%) reported having lost crops to floods over the last five years. Most (11) losses were reported for 2018, with an average of 41% of the crop being lost by the farmers affected. Some losses were also reported for 2015, 2017 (with an average of 31% of the crop being lost), 2019 (<10% of the crop lost), and 2020 (70% of the crop lost). Mango trees, rice, and vegetable crops were affected.

The losses to rice occurred in late June and early July for EWS rice, and at the end of September and in October for wet season rice. However, there was also some dry season rice that was lost in February 2018 after a surprising return of the flood in several Boeung plots (the farmer suspects due to a gate being opened). Mango trees were mostly lost in August, which also holds true for vegetables.

There are several interesting aspects that emerged during the interviews related to crop losses due to floods. To begin with, several farmers stated that they lost their mango trees to floods not due to the roots of trees being damaged by excessive moisture, but because the mechanical stress uprooted them. One farmer, who lost 10 out of 200 trees in this way, noted that he usually puts up wooden constructions to support the trees, to prevent such losses.

On average, farmers lost ca. 38% of their yield when their plots were affected by floods. Most reported that the losses were not distributed evenly across their plots, but were centred at the back end of Chamkar plots, or the lower areas of Boeung plots. The estimates for water levels at the time when losses occurred ranged between 40 and 100 cm.

Another notable aspect is that several farmers also mentioned crops being used due to floods caused by heavy rains and the strong winds that accompany them.

Finally, two farmers also pointed out that they believe the main cause of the flood-related crop losses in their plots is bad drainage.

Drought In total, 33% of farmers who were interviewed reported crop losses due to droughts. Unlike for the losses caused by floods, drought losses occurred evenly distributed across the plots. Furthermore, the average percentage of yield lost was estimated by farmers to be slightly higher than for flood losses, at an average of 57%.

The majority of reported losses concerned rice. Either recession rice, which must have been planted late, was lost in February or March due to a lack of rainfall and a dearth of irrigation water. Or EWS rice was lost for the same reasons, mostly in May.

Other crops for which losses were reported are maize, green bean and mung bean. These ranged between 30 and 100% of the corp and occurred mostly at the height of the dry season, between April and May.

An in-depth analysis of the effects of drought in the study are is provided by Vandôme (2020), based on both field data and a modelling approach using the FAO software CROPWAT 8.0.

Pests As mentioned above, for many farmers, pests are actually a bigger concern in terms of crop losses than either floods or droughts, with 83% of farmers who responded to the question reporting losses. To put this in numbers, farmers report that they have lost an average of 30% of (mostly rice) crops to rats, with losses reaching as far as 75%, and an average of 38% (mostly mangoes) to insects. In addition, crop loss risk factors compound each other. In very dry years, rat populations are higher. One farmer who lost their entire rice crop to an unexpected return of the flood in February 2018 also stated that they could not replant the crop because rats during this time of the year would have eradicated the young rice plants.

4.3.5 Assessing Alternative Roles: Perspective of a Landless Scavenger

One of the interviewees, does not own or farm any land herself, but still profits from agriculture by scavenging fields after harvest to look for produce that was left behind. She also fishes for snails in the canals behind the Preks and sells chickens. A particularly interesting aspect of this interview was that she was able to give a (subjective) comparison of agricultural production between Prek areas, since her scavenging activities take her to Prek Pok, Prek Chann, Prek Touch, as well as along the Prek Ambel and outside the study area.

As a scavenger, she collects rice and vegetables that are left behind after the farmers harvest on their plots. In doing so, she can collect considerable quantities of produce. Last year, she collected a total of 53 bags of rice, at a weight of 70-80 kg each. 43 of these bags were collected between January and March, and ten between April and June. To reach this amount of rice collected, she has to work practically every day between 7 am and 5 pm, sometimes aided by her elderly mother. She uses her bicycle for transport along the Preks, and her husband picks up the finished bags of rice on his motorcycle. Out of the 53 bags she collected, she keeps 10 for family needs throughout the year, and sells the rest for 1,000 Riel/kg to middlemen. She says that 2019 was an exceptionally good year for her because it was wet during the harvest period between January and March and the rice harvesting machines left a lot behind as a consequence. As a harvesting implement, she uses a hand sickle.

The interviewee also collects leftovers of white bean, green bean, and other vegetables. She keeps 3 kg of beans for family needs and sells the rest – for 4,500 Riel per kg of green bean and

3,000 Riel per kg of white bean. Last year, she said she spent 4-5 days per month collecting these crops, and managed to collect ca. 10 kg per day.

When asked to compare agricultural production between Preks in the different years, she noted that crop yields at Prek Chann as well as the snail populations in the Prek and the canals behind it have increased since the rehabilitation.

A final note on scavenging activities that the she added is that they are apparently common in the area. She even stated that school students scavenge on the weekends to support school canteens.

In addition to selling the rice and vegetables she scavenges, the interviewee also raises and sells chickens. These live in the shrubland in the vicinity of her house, and in the natural vegetation along the Prek. She says she also feeds them paddy rice. Three times per year she can sell five to ten chickens, for 35,000 – 38,000 Riel per head. However, she also raises particularly expensive cocks (currently seven), which she can sell for 100,000 Riel each.

Apart from selling agricultural products and chickens, the interviewee also fishes in the Preks and the canals network in the Boeung, especially canal 24. She states that she fishes during the whole year, every weekend for ca. 6 hours. Each time, she says she manages to catch ca. 30 kg of snails and 1-2 kg of fish that accidentally get caught in her nets. As a fishing implement, she uses a bicycle wheel the spikes of which have been removed and replaced with a hand-woven string net. According to Ms. Hang, catch is mostly stable across the year, though peak fishing periods are during heat waves, since the animals then come out of their hiding places, and during flood recession. She sells the catch to middlemen from Phnom Penh – for 3,500 Riel per kg of snails and 7,000 Riel per kg of fish.

Finally, two interesting perspectives emerged from this interview related to hydrological issues. For one, the interviewee stated that she joined a meeting of the Cambodian People's Party (CPP)in February 2020 at Prek Put at which it was suggested to fill the Prek up. Currently, there is only water in Prek Put in July and August, but this is not used for irrigation – also because it is of low quality since a pig farmer supposedly drains their wastewater into the Prek. The final decision over the future of the Prek lies with the head of the Pagoda which lies on its north bank. As a second point of interest, she also noted that the fields along Prek Put are often irrigated

through wells, since the Prek cannot be used for water supply.

4.3.6 The Role of Local Governance: Outlining the Roles of Village Chiefs and Prek User Committees

4.3.6.1 Information from Village Chiefs

Overall, eight interviews with village chiefs and one interview with a PUC chief were conducted in the course of the fieldwork in February and March 2020. This section gives a summary of general aspects that emerged from the interviews, as well as a closer discussion of a few salient points. The information gleaned from these interviews illustrates how local communities influence water flows in the area. While these have not yet been accounted for in the model to be described below, they offer interesting insights into feedback loops to be incorporated into calculations later on.

General Observations The level of detail the village chiefs could provide on issues of Prek management, agriculture and general management procedures varied vastly. Some could provide the exact numbers of the villagers and confident estimates about crop production and Prek water usage, while others did not even know whether fields in their village area were flooded during the wet season.

On average, village chiefs are 66 years old and have held their positions for 17 years. All of them were men. They primarily define their tasks as managing village affairs and communicating problems at village level to the commune. Only one village chief stated that his primary task was to represent the CPP on a local level. All village chiefs mentioned that they paid particular attention to matters of infrastructure – in terms of road and Prek maintenance. Two of them also emphasized that they were particularly concerned with security issues, with one detailing that he was struggling to deal with illegal gambling, cockfights, drunken violence, and drugs. In terms of communication, all village chiefs said that they regularly interacted with the commune level to report any larger issues. One of them said that he had one monthly meeting with him, the others did not specify the intervals. Some village chiefs stated that there was a general assembly

of village chiefs and the commune chief once per year and that it had been held at Koh Thom recently.

Rehabilitation At the Preks that have been rehabilitated, the village chiefs say that they are happy that the project was implemented, despite some of the difficulties that have arisen as a consequence, such as bank collapses.

At the Preks that have not yet been rehabilitated, several chiefs stated that they wanted their Preks to be rehabilitated. At Prek Thom and Prek Touch, an excavation is being organised by the village chiefs, though it only includes a deepening of the Prek and no road construction.

Water Use During the interviews, village chiefs made several observations related to water use that had not been included in the questionnaire, which are summarized here.

The village chief at Prek Chann stated that before rehabilitation, many people drilled wells, but used them only as a source of irrigation water, since the water quality was too bad for it to be used for household purposes. At Prek Chann, water from the Prek is also used for non-drinking household purposes like cleaning, washing laundry etc. Similarly, the village chief at Prek Me Srok has stated that since the completion of rehabilitation no pumping ventures have been necessary to supply the Prek with water.

Two village chiefs stated that (temporary) earthen dams are built across the Preks from time to time – at Prek Nou and Prek Put. At Prek Nou, the dams are used to channel water during the dry season, to supply pumps that lift water to distribution channels. At Prek Put, on the other hand, where there is generally little water, the dams are used as bridges by private farmers. It requires the permission of the village chief to build them, and he says he insists they have culverts to let the flood through in July and August.

As mentioned above, at Prek Nou, water, which flows naturally into the Prek, is pumped to distribution channels. These lie in the South of the Prek, and also supply fields that lie in the vicinity of Prek Put, since the latter Prek is dry for the majority of the year. Three pumping machines are used to lift the water from Prek Nou to the distribution channels. These pumps are operated by the village chief, a vice chief and a private person. Two of them have 24 HP,

and one 38 HP. One pump operates on electricity, the other two on gasoline. According to one village chief, ca. 30 ha are supplied using these pumps. The one he operates is run for five to six hours every two weeks between December to March.

At Prek Pok, a pumping machine is used to supply the Prek with water between March and April. The village chief states that it is organised by the people who need water at this time, and that they report to him and he forwards the information to the commune level.

Agriculture The village chiefs interviewed, in addition to the questions asked during the interview, made various observations on the agriculture in the study area. Some of them are relayed here for the sake of completeness.

One village chief noted that there was a dramatic decrease in rice crops this year because of an overabundance of herbicide-resistant grass. He estimated the decrease to lie at 40%.

Several village chiefs commented on recent changes in crops. One of them noted that people were interested in cultivating fruit trees, but that for many investment costs were too high. As a consequence, he noted, people lost motivation and abandoned Chamkar plots. Another village chief noted the decrease in diversity in crops. He said that ca. 15 years ago, tobacco was the main crop on Chamkar areas, and was grown alongside potatoes, chilies, rice, white bean and maize. Now, mango is the main crop along the Prek, and rice is just cultivated in the short term. More fertilizer is needed, along with hormones and pesticides, and the investment costs for farmers to make the transition were considerable. He noted that ca. 10% of them did not make it and either rent out or sold their land. However, he also noted that due to the low water levels in the Prek, mangoes are the only crop that can be grown with a reasonable level of profitability.

Gate Operation at Prek Chann One of the main aims of the interviews with village and PUC chiefs was to discover the reasoning behind gate operation, as well as the patterns of its opening and closing, to incorporate the data into the hydrological model accordingly. Unfortunately, reliable-seeming information could only be gleaned from one village chief interviewed. The information provided by the PUC chief at Prek Chann (see note below) was inconsistent and in itself contradictory.

According to Meas Chrik, 68, village chief of Por Andet village at Prek Chann, the gate operation is as follows:

The gate is closed completely in late June, when the water level in the Bassac begins to rise at the beginning of the rainy season. The reasons given for closing the gate at this time are:

- Avoiding the early floodwater in the Bassac, since this water includes many water plants and residues.
- Avoiding crop losses. Some farmers along the Prek are still cultivating at this point, and delaying the arrival of the flood gives them the opportunity to harvest at the appropriate time.

The gate is then opened ca. one and a half months later in August, but only to ca. 1.5 m above the bottom of the Prek to avoid fast inflow. Generally, the opening of the gate is executed very slowly to avoid erosion. The reasons given for opening the gate are:

- The deteriorating water quality in the Prek. Opening the gate allows for inflow from the now high-quality Bassac water.
- The high difference in water levels. According to Mr. Meas, the water level difference is ca. 3.5 m at this point between the Prek- and Bassac-side of the gate. If the difference is higher still, the danger of bank erosion during gate opening grows sharply.

In December, the gate is opened further still to ca. 3 m above the bottom of the Prek to keep the metal structure out of the water, since the village chief is worried about rusting. It remains in this position until the end of the dry season.

The opening and closing of the gate requires four to five people, chosen by the village chief. The equipment needed consists of a key and a lever that is connected with a wheel to operate the opening and closing mechanism. It is stored locally. The decision to open or close the gate is taken together with the PUC and the commune chief.

Mr Meas also notes that originally, one of the main purposes of the gate in his understanding was flood protection. However, since the completion of the rehabilitation, floods have generally

been small according to his view. He doesn't think that the gate is useful to keep water in the Prek but believes that water availability is now much better than before rehabilitation.

Locally Organized Prek Excavation One topic that was discussed in detail with village chiefs were excavation activities at their Preks. A detailed description of the large-scale excavation that took place at Prek Thom is provided below. However, several other village chiefs also commented on excavations at their Preks.

At Prek Cham Kroum, the village chief stated that a project for a Prek-wide excavation had been proposed by him several times, to deepen the Prek and extend the profile. However, there is some opposition among the village population because several families along the Prek would have to be resettled. No resolution of the conflict has been reached.

At Prek Chann, some excavations were ongoing at the time of the field visit, to remove the material from bank collapses following rehabilitation. Otherwise, excavations at this Prek have ceased since rehabilitation. Equally, there have not been excavations at Prek Me Srok since the completion of rehabilitation, except for the work that is currently being done to fix bank collapses in the village area. However, the village chief says he is thinking about organising smaller excavations to repair bank collapses further along the Prek, which are not being repaired as part of the current project.

At Prek Lok, excavations take place every year in strategic places, like the head of the Prek. According to the village chief, the people report to him and he forwards information to the commune. In turn, the commune representatives come to observe the situation and reach a decision on excavation. The village chief states that funds for the excavation are provided by the government – an annual average of 1 million Riel. Furthermore, the chief says that he raises ca. 5,000 Riel per family per year to cover excavation costs. Costs are furthermore covered by selling the material that is excavated from the Prek. The material is sold in partial compensation by the private companies charged with the excavation of the Prek. Recipients are farmers in the vicinity of the Prek who aim to raise their land. It has furthermore been noted that due to the profitability of such ventures, the initiative for excavation has also come from private companies themselves. Excavation work at Prek Lok takes place between March and April.

Excavation at Prek Thom and Prek Touch One of the most remarkable observations in the study area during this field visit was the excavation that is ongoing at Prek Thom, in the south of the study area. Here, the entire Prek is being excavated in a sharp trapezoidal profile.

In an interview with the village chief it emerged that the project is driven by a private sector company. It is mutually beneficial to the company and the village, because the company gets to keep and sell the soil that is excavated, while the village profits from the improved Prek profile and better water inflow.

According to the village chief, the project was discussed in advance between the village chiefs of the affected villages, the commune chief, and the company. The company also provided a model of the proposed Prek profile as a decision basis. During this meeting, the village chief emphasized that he made sure the excavation would reach to the very end of the Prek. He also says that he consulted with the people in his village before making a final decision.

The people in the village, they said, would have preferred a French project, because rehabilitations by French engineers usually also include roads, which this one doesn't. They would have wanted the same sort of project as was implemented at Prek Chann – but without a gate. The village chief noted that in 2006/07 there were some talks about a rehabilitation project financed by international development agencies, but that ever came to pass.

For now, the villagers are purportedly happy with the excavation because of the prospect of improved water availability. According to the village chief, nobody had to be resettled. He furthermore said that the excavation started at the end of December and that the Prek is usually dry between January and July – so no major inconvenience for agriculture was expected. A private water seller who operated a pump at the Prek moved to another Prek outside the study area. The excavation is expected to be finished in April.

The village chief says that he expects some bank collapses, but none as severe as at Prek Chann. He says he believes the profile implemented at Prek Thom is safer because of the long slopes and the narrow bottom. The bed of the Prek is supposed to be lowered by 3 m along the whole length of the Prek. However, he also noted that there are no exact measurements or plans available.

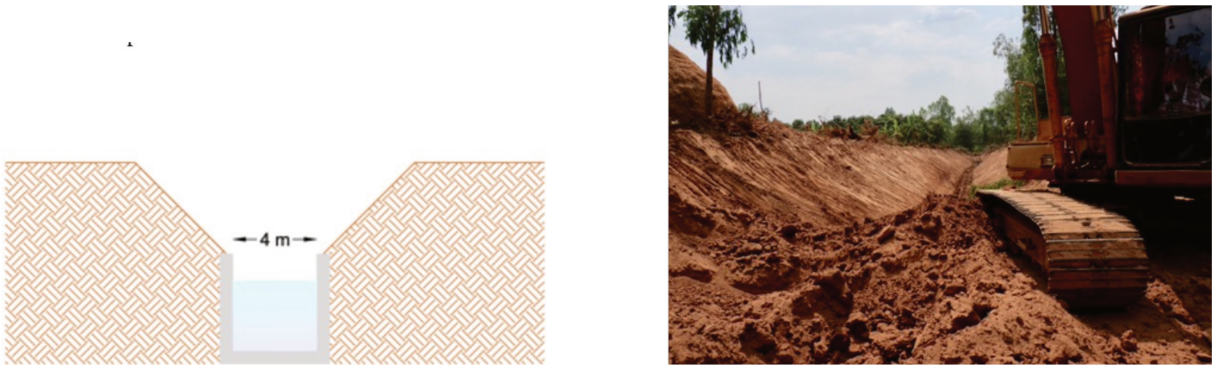

(a) The repair of bank collapses proposed at Prek Me Srok.

(b) Excavator at Prek Thom.

Figure 4.25: Construction projects at the Preks.

Bank Collapse Repair at Prek Me Srok An issue that deserves special attention are the bank collapses which occurred at Prek Me Srok in 2017, after rehabilitation was completed. According to the village chief, the collapses at this Prek threatened three houses, just in front of which the road was destroyed. The village chief, Heng Leang, reported the collapses to the commune chief, who reported them to ministry, who in turn alerted AFD.

Currently, efforts to protect buildings from bank collapses are underway at the Prek. To this end, the lower banks over the first 250 m of the Prek in the village area are being substituted by a concrete channel (width: 4m).

Mr. Heng says he was invited to the water ministry to discuss options of the repair of the Prek banks. Directly after the meeting he relayed the information to the people in the village. He says that he doesn't expect the new system to completely prevent collapses, since the water will rise above the concrete channel during the rainy season.

The current construction work in the village area has no direct negative impacts on agricultural production because of the water inflow from the Prek Ambel end of the Prek. There are further, smaller, bank collapses behind the village, but AFD won't be repairing them and for the moment water is flowing freely so they are of no major concern. The villagers might fix them themselves in the future, but they are no concrete plans at the moment.

4.3.7 Summarizing the Results of Fieldwork

Overall, the interviews conducted in the course of fieldwork have provided a solid understanding of the general agricultural practices in the area, as well as of water management and the organizational difficulties the latter entails. They have outlined that providing irrigation water, especially during the dry season, is the principal priority of Preks in the eyes of the respondents. It has also emerged that many local stakeholders have a very nuanced understanding of the various regulating ecosystem services that the flood in the area contributes to, from pest regulation to sediment deposition.

Furthermore, one of the principal outcomes of the interviews has been to quantify and characterize ecosystem services - or at least to ascertain whether it was possible. For agricultural practices, which largely rely on the provision of irrigation water through the Preks and canals, extensive information has been collected and analyzed statistically to provide a basis for further analyses. In contrast, quantifying services such as the use of natural vegetation and fish catch has been difficult for several reasons. To begin with, practices have shifted considerably over the last years. According to multiple respondents, fish catch has declined dramatically and the use of natural vegetation now entails concerns of pesticide contamination. Another reason is that it was nigh impossible to calculate the average use of either resource due to a paucity of information. For instance, while all respondents could readily answer whether they fish in the Preks or use natural vegetation, estimating a frequency proved difficult for them, as their uses, over the past years, had changed considerably.

In contrast, an aspect on which much clarity could be gained was the attitude towards rehabilitation projects and general water management practices. It emerged that rehabilitation is generally seen in a positive light by local communities, and that water inflow into the Prek is seen as the main benefit, alongside the construction of better roads along the Prek, which allow for transport without having to rely on boats. The construction of inflow management structure such as gates, in contrast, is seen critically - for one thing because it limits transport possibilities, for another because they require management that, if carried out improperly, can lead to erosion and injury.

Another issue that became clearer is that many respondents don't implicitly associate the

rehabilitation state of "their" Prek with the arrival or recession of the flood as a whole. This suggests that flow dynamics in the Boeung play an essential role during the early flood phase.

Overall, the interviews have yielded a clearer understanding of local land cover dynamics, water management practices, and ecosystem services. However, as mentioned at the beginning of this chapter, all of this is presents a snapshot of a fraction of the case study area. In order to better quantify provisioning services in particular, a more spatialized understanding of key aspects of flood and land cover dynamics is necessary. The methodology of WAFL, presented in the last chapter, can provide the former based on water levels in the Bassac river. To provide the latter - an understanding of land cover distribution in the study area as a whole - another approach was utilized. The next section of this chapter aims to outline the path that was taken to assess land cover dynamics in the case study area as a whole through remote sensing.

4.4 Conclusion:Appreciating the Influence of Communities and Individual Actors on Hydrological Processes

The second major part of this thesis has addressed the history of Prek channels, as well as their current role in the provision of ecosystem services and LULC patterns in a case study area located ca. 70 km South of Phnom Penh.

The history of Preks was traced through historical engineering reports, starting in the early 20th century. According to French colonial engineers, Preks were originally constructed by the local population by breaching the elevated river banks to allow sedimentation in low-lying areas. Their aim was to raise land to create more elevated areas for high-value crops. French engineers adopted Prek construction and during the early 20th century the Cambodian Mekong delta saw a systematic extension of Preks along the banks of the Bassac and the Mekong. After the end of the French protectorate following World War II, records on the maintenance of Preks become sparse, though they are likely to have been maintained as agriculture held a high priority in the agenda of the government. During the Khmer Rouge regime in the 1970s, an extensive network of canals was constructed in the lowlands at the tail end of the Preks. Following the fall of the Khmer Rouge and the resettlement of displaced people, the focus of international

development projects in this region of Cambodia fell on Preks and their rehabilitation. Since the 1990s, multiple projects have sought to restore their former functionality to enhance the prosperity and resilience of local agricultural communities.

The effectiveness of this approach as well as the high regard that local communities have for rehabilitation projects also became apparent during the surveys conducted with stakeholders in the case study area. Village chiefs and farmers at every Prek were interviewed and detailed data on cropping practices, irrigation, and the role of Preks for ecosystem services was collected.

This data showed that the primary use of Preks for local communities lies in the provision of irrigation water, especially during the dry season. Farmers use individual, mobile pumps to lift water from the Preks to their plots and distribute it either through gravity irrigation or using plastic pipes. In addition, Prek water is used to water cattle, and to meet non-dietary household needs. Furthermore, local inhabitants also fish in the Preks and in the flooded lowland areas during the wet season, though multiple interviewees noted a steep decline in fish catch over the past years, which they attribute to changes in inundations as well as illegal fishing practices. People also use the natural vegetation that grows along the banks of the Preks for food and fuel. To a certain extent, the interviewees also broached the issue of the role of Preks in catalyzing floods for regulating ecosystem services - such as pest regulation, especially by decimating rat populations, as well as soil- and groundwater recharge and sediment deposition.

Overall, this chapter has outlined the multiple ways in which local communities interact with the local agro-ecosystem in general, and with hydrological processes in general. From the historical initiation of Prek formation via artificial bank breaches, to modern-day rehabilitation projects and pumping practices, humans shape the Prek system as much as the Prek system shapes their livelihoods.

5

Assessing Landcover Dynamics through Supervised Classification Remote Sensing Approaches

As outlined in the previous chapter, the interviews yielded a detailed picture of local cropping practices.[1] However, to assess ecosystem services on the level of the study area as a whole, a more spatialized understanding of land use / land cover (LULC) is necessary. For this reason, a remote sensing approach was chosen using Sentinel-1 and 2 and a supervised classification approach. Supervised classification allows the user to pre-define the classes into which images will be divided. Using a training dataset, a classifier learns to recognize each class and can then

[1]This chapter has been published as a paper: Orieschnig, C.A., Belaud, G., Venot, J.P., Massuel, S. and Ogilvie, A., 2021. Input imagery, classifiers, and cloud computing: Insights from multi-temporal LULC mapping in the Cambodian Mekong Delta. European Journal of Remote Sensing, 54(1), pp.398-416.

delineate it in the images to be processes. For the purposes of this study, six broad land use classes are defined: open water surfaces, bare/fallow land, urban/village areas, fruit trees, rice fields, and vegetable fields. Out of these, urban areas - located along the main road that runs in parallel with the river - and fruit trees are relatively static over the course of a year (neglecting urban spread and the planting or cutting down of trees). The other classes are highly dynamic. During the wet season, large swaths of low-lying land in the west and southwest of the area are inundated. Subsequently, these areas see one or two cycles of rice cultivation, before lying fallow for part of the year. The higher terrain in the east of the study area sees a complex mosaic of fields lying fallow and being cultivated. Figure 5.1 shows an RGB overview of the LULC dynamics in the study area during the dry season.

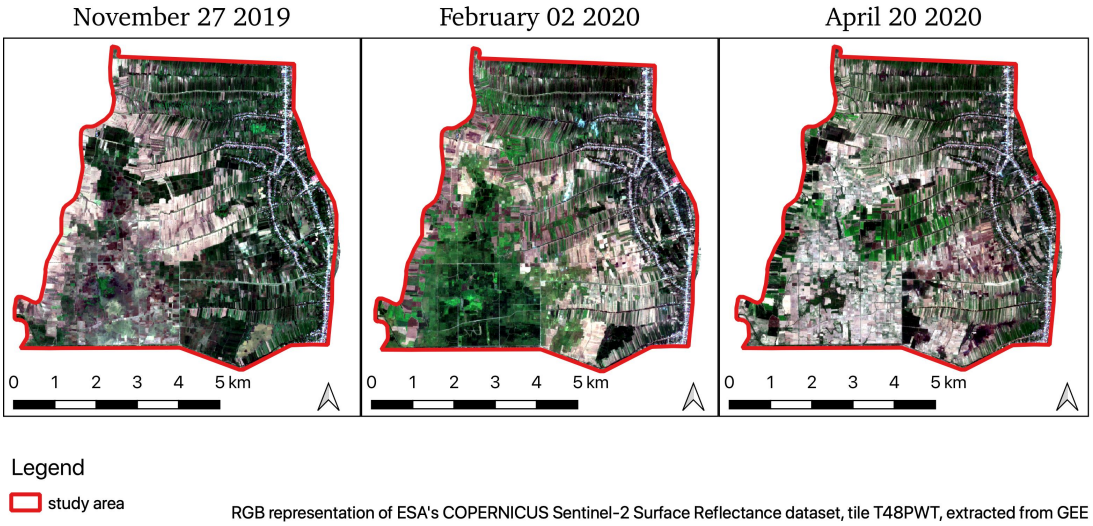

Figure 5.1: Landcover dynamics in the study area during the dry season, RGB Image.

However, before land cover maps for the study area could be derived with any great certainty, it was necessary to test and compare the different methods available on the chosen earth observation platform in this thesis, GEE. This meant comparing different classifiers, combinations of input imagery, and training data sets in order to achieve a classification with maximum accuracy on which further analyses could be based.

Like majority of LULC studies, this analysis uses supervised classification methods. Although some researchers have used unsupervised classification (Mohammady et al., 2015; O'Hara et al., 2003), supervised classification is often preferred due to the possibility of setting a predefined number of labelled output classes. To harness these advantages, a variety of classifiers

is available for supervised classification. Among the most frequently used are machine learning algorithms such as Support Vector Machines (SVM), Random Forest (RF), and K Nearest Neighbour (KNN) (Talukdar et al., 2020). Furthermore, advanced machine learning approaches such as artificial neural networks (ANN), convolutional neural networks (CNN), and deep neural networks (DNN) have seen more widespread use in recent years (Jozdani et al., 2019).

A number of papers compared these classifiers in LULC applications. Talukdar et al. (2020) compare RF and SVM, along with more advanced machine learning methods in a study area along the Ganga river in India. The authors conclude that the RF algorithm overall performs best. In contrast, Nery et al. (2016) find that SVM reaches the highest classification accuracies for LULC analyses after comparing it with KNN, RF, Learning Vector Quantization (LVQ), Recursive Partitioning Regression Trees (RPART), and Stochastic Gradient Boosting Methods (GBM) in a study area in Western Australia. The same conclusion was reached by Thanh Noi and Kappas (2017), who compared RF, KNN, and SVM classifications of Sentinel-2 imagery in the Red River Delta in Vietnam. Shelestov et al. (2017) weighed the merits of some of the classifiers available in GEE against external methods, including an ensemble neural networks, for crop classification using optical Landsat-8 images. They found decision-tree classifiers to perform best in GEE, though neural networks outperformed them.

Most of these comparison papers focus on contrasting the performance of classifiers applied to a single date rather than in a multi-temporal situation. In addition, none yet specifically compare classifiers in the context of cloud computing platforms, many of which only offer a limited number of native implementations. In addition, with a few notable exceptions (Hütt et al., 2016), many papers only approach the classifier comparison on the basis of a single imagery type, with a fixed set of bands, and a single source of training data.

However, no comparison existed so far for the classifiers available for LULC on GEE, nor for a multi-temporal situation in a highly dynamic area, as is necessary in the case of the case study area. To address this lack of knowledge, an assessment of the response of four supervised classifiers available in the online Javascript API of the GEE cloud computing platform, to the use of different combinations of input imagery, training data, and band sets for the purpose of land use and land cover analyses. These classifiers are Naive Bayes (NB), Classification and Regression Trees (CART), Random Forest (RF), and Support Vector Machines (SVM). While it

Table 5.1: Overview of image datasets used.

Dataset Nr	Imagery	Band Set
1	Sentinel-1	Full
2	Sentinel-1	Reduced
3	Sentinel-1	Minimal
4	Sentinel-2	Full
5	Sentinel-2	Reduced
6	Sentinel-2	Minimal
7	Sentinel-1 & 2	Full
8	Sentinel-1 & 2	Reduced
9	Sentinel-1 & 2	Minimal

is possible to implement further supervised classification methods, such as fully convolutional neural networks (FCNN), or deep neural networks (DNN) in GEE, this requires the external training of the models on the TensorFlow platform (Abadi et al., 2016). Since this approach involves several billable components of Google Cloud, it is not included.

The comparisons are made using Sentinel-1 SAR and Sentinel-2 optical imagery, both separately and in combination. In addition, the impact on classifier performance of the type of the training set, as well as the choice of bands, texture features, and spectral indices is tested. For this purpose, two different sets of training points (one based on field data, one derived from high-resolution satellite imagery) and three different sets of training bands (varying in the number of additional indexes and texture features used for classification) are used.

5.1 Data Used

A general outline of the classification workflow is given in Figure 5.3. Figure 5.2 gives an overview of the temporal distribution of images and training data points used in this thesis for the purposes of LULC classification. Following pre-processing, 9 datasets are generated on which the classifiers are tested. These datasets derive from the use of different imagery types alone and in combination, as well as different band sets (see Table 5.1). Parameter tuning, calibration, and validation is performed for each of the 9 datasets separately, using both the limited training points derived from fieldwork, and the extended training points generated on the basis of the SPOT-6 and 7 images, resulting in 18 different configurations of input data for each of the four classifiers. Finally, the best-performing algorithm is chosen and applied to the optical, radar, and combined dataset to generate a LULC classification spanning the entire period between 01/11/2019 and 31/10/2020.

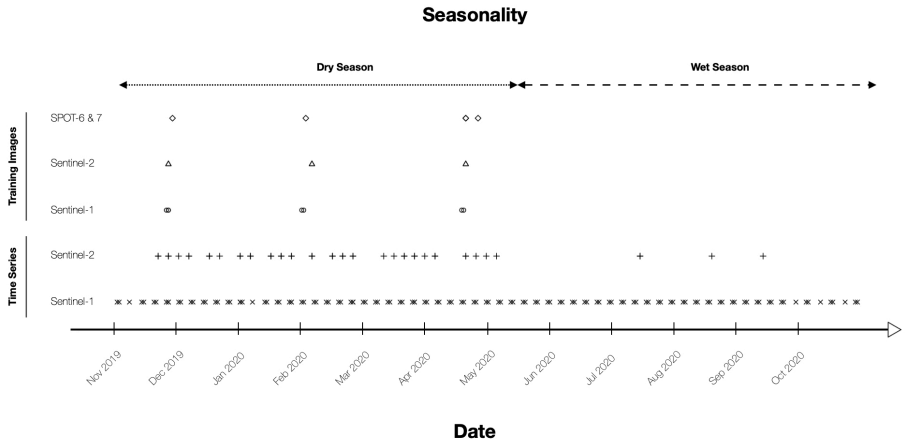

Figure 5.2: Temporal distribution of training images and image time series used in this analysis, throughout the wet and dry season in the study area.

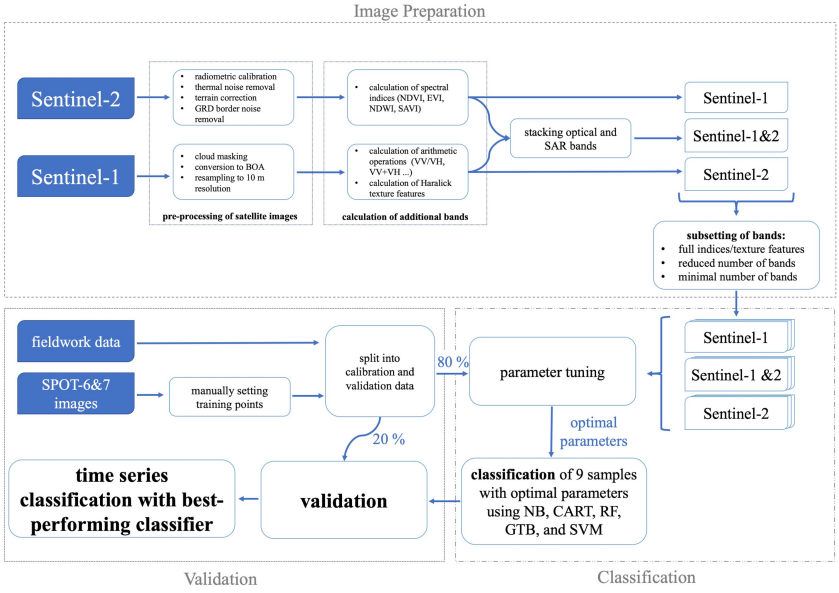

Figure 5.3: Classification workflow

5.2 Image Pre-Processing

To a certain degree, both Sentinel-1 and 2 images are already provided in pre-processed form in GEE.

Sentinel-1 images undergo pre-processing during ingestion in GEE based on the ESA's Sentinel-1 toolbox. In this process, metadata is updated with a restituted orbit file, border noise

and thermal noise is removed, and radiometric calibration and orthorectification are applied. The fact that images are provided in pre-processed form in GEE's Javascript API removes one of the main hurdles many researchers face in using SAR data. In fact, several studies have used GEE as a source of SAR images, even though their analyses were subsequently conducted in different environments (Tamiminia et al., 2020; Amani et al., 2020).

As a basis for classification, additional bands are generated for SAR imagery using the original VV and VH bands (cf. Table 3.5). Three of these are based on arithmetic operations ($\frac{VV}{VH}$, $VV - VH$, $\frac{VV+VH}{2}$) which previous studies found to yield increased accuracies for LULC approaches (Slagter et al., 2020). The others are based on a classic Grey Level Co-occurence Matrix (GLCM), encompassing Haralick texture features (Haralick et al., 1973). These features describe image texture through interpretable descriptors and have been found to add valuable information for LULC analyses. (Clerici et al., 2017; Lin et al., 2020; Mishra et al., 2019). Texture features are calculated separately for both the VV and VH polarization, parameterized with a 5x5 window size. Following previous studies (Nizalapur and Vyas, 2020), angular second moment (ASM), contrast (CONTRAST), correlation (CORR), inverse difference moment (IDM), entropy (ENT), dissimilarity (DISS), and variance (VAR) are used as added bands for classification. Following the calculation of the texture features, a refined Lee speckle filter (Yommy et al., 2015) is applied to smooth the original VV and VH bands in order to reduce speckle, since not all sdatasets use the generated texture bands.

Sentinel-2 images are available in pre-processed form in GEE. The sen2cor algorithm (Main-Knorn et al., 2017) has been applied to transform Top of the Atmosphere (TOA) reflectance to surface reflectance (BOA). For this analysis, all bands are automatically re-sampled to 10 m resolution by the GEE processing algorithm. For the time series calculation, a cloudy pixel threshold of $< 20\%$ is introduced, and the remaining clouds are masked using a simple bit-mask based on the QA band.

Additional spectral indices (cf. Table 5.2) are calculated on the basis of native bands (cf. Table 3.6) o generate ancillary layers of information that serve as input for the classification algorithms, which past studies have found to be valuable in increasing classification accuracies (Godinho et al., 2016). These are based on a range of bands employed in past studies for various LULC analyses using different classification algorithms (Ouattara et al., 2020).

Table 5.2: Spectral indices calculated for optical Sentinel-2 imagery

Index	Calculation	Reference
Enhanced vegetation index	$EVI = 2.5 * \frac{NIR-Red}{NIR+6*Red-7.5*Blue+1}$	Huete et al. (2002)
Two-band enhanced vegetation index	$EVI2 = 2.4 * \frac{NIR-Red}{NIR+Red+1}$	Jiang et al. (2008)
Green normalised difference vegetation index	$GNDVI = \frac{NIR-Green}{NIR+Green}$	Gitelson et al. (1996)
Modified normalised difference water index	$MNDWI = \frac{Green-SWIR2}{Green+SWIR2}$	Xu (2006)
Modified soil adjusted vegetation index	$MSAVI = NIR + 0.5 - (0.5 * \sqrt{(2*NIR+1)^2} - 8*(NIR-(2*Red)))$	Qi et al. (1994)
Normalised difference red edge index	$NDRE = \frac{NIR-RE}{NIR+RE}$	Gitelson and Merzlyak (1996)
Normalised difference moisture index	$NDMI = \frac{NIR-SWIR}{NIR+SWIR}$	Wilson and Sader (2002)
Normalised difference built-up index	$NDBI = \frac{SWIR-NIR}{SWIR+NIR}$	Zha et al. (2003)
Normalised difference vegetation index	$NDVI = \frac{NIR-Red}{NIR+Red}$	Rouse J.W. et al. (1974)
Normalised difference water index	$NDWI = \frac{Green-NIR}{Green+NIR}$	McFeeters (1996)
Normalised difference water index 2	$NDWI2 = \frac{NIR-SWIR2}{NIR+SWIR2}$	Gao (1996)
Normalised ratio vegetation index	$NRVI = \frac{\frac{Red}{NIR}-1}{\frac{Red}{NIR}+1}$	Baret and Guyot (1991)
Ratio vegetation index	$RVI = \frac{Red}{NIR}$	Jordan (1969)
Soil-adjusted vegetation index	$SAVI = \frac{NIR-Red}{NIR+Red+1} + 2$	Huete (1988)
Specific leaf-area vegetation index	$SLAVI = \frac{NIR}{Red+SWIR2}$	Lymburner et al. (2000)
Simple ratio vegetation index	$SRVI = \frac{NIR}{Red}$	Birth and McVey (1968)

5.3 Creation of Image Datasets

In total, parameter tuning, calibration, and validation is performed on nine image datasets (cf. Table 5.1).

First, three main sets of images are created - one containing only SAR imagery, one containing optical imagery, and one in which images are created by stacking all available optical and SAR bands into a single image. Then, each of the three imagery sets is further subdivided into three tiers depending on how many bands are used for classification(see Table 5.3). One tier includes a band set that encompasses all native bands, spectral indices, and texture features. A reduced band set includes the native image bands as well as some indices and texture features. Finally, a minimal set consists only of the VV and VH bands for SAR, and the RGB bands for optical imagery.

Table 5.3: Band sets of spectral indices and texture features. For the combined imagery set, these bands are stacked.

Band Set	**SAR Imagery**	**Optical Imagery**
Full Set	VV, VH, $\frac{VV}{VH}$, $VV-VH$, $\frac{VV+VH}{2}$, ASM, CONTRAST, CORR, DISS, IDM, ENT, VAR	R, G, B, RE2, RE3, NIR, RE4, SWIR1, SWIR2, NDVI, NDBI, NDWI, MNDWI, MSAVI, GNDVI, NDRE, NDWI2, EVI, EVI2, NRVI, RVI, SAVI, SLAVI, SRVI
Reduced Set	VV, VH, $\frac{VV}{VH}$, $VV-VH$, $\frac{VV+VH}{2}$	R, G, B, RE2, RE3, NIR, RE4, SWIR1, SWIR2, NDVI, SAVI
Minimal Set	VV, VH	R,G,B

5.4 Classifiers and Parameter Tuning

Each dataset is calibrated with 80% and validated with 20% of both the fieldwork and the SPOT-based training data, for each of the four classifiers. Preceding calibration, each classifier undergoes parameter tuning. A short description of each classifier as well as the associated tuning parameters is given below.

5.4.1 Naïve Bayes (NB)

This classifier relies on a simple probabilistic approach that is based on the Bayes theorem (John and Langley, 2013). It is referred to as naïve because it relies on the assumption of conditional independence between every pair of features, and a Gaussian probability distribution (Zhang, 2005). In reality, this condition is frequently not met, particularly in more complex situations and datasets. Nonetheless, several studies have found the simplistic approach to yield satisfying results (Johnson and Iizuka, 2016; Diengdoh et al., 2020), particularly in cases where only a limited number of input features is available. This may be due to the fact that, in general, even a small training set is sufficient to minimize the average risk of the classification error and compute the decision surface. Some studies have also argued that dependence distribution among classes could also account for the surprisingly good performance of NB (Kuncheva, 2006). In GEE's implementation of NB, the only parameter that needs to be tuned for performance is the smoothing factor λ.

5.4.2 Classification and Regression Trees (CART)

CART classifiers belong to the family of decision tree classifiers. The basic approach of this type of classifier is to find the attribute or threshold that splits a training dataset most effectively into subsets. This split then becomes a node in the tree, with the two subsets forming branches. Each subset is then split into further subsets until only a non-splitable end node (also known as a 'leaf node') remains. The main criterion in performing every split is the normalized information gain (Shalev-Shwartz and Ben-David, 2014). Once grown using the training dataset, the decision tree can then be applied to new samples. A considerable disadvantage of this approach is its high sensitivity to the training dataset. Even globally negligible modifications in the training data can lead to fundamentally different tree structures (Shelestov et al., 2017). To improve classifier performance, the number of leaf nodes in each tree (maxNodes) is tuned.

5.4.3 Random Forest (RF)

Random Forest (RF) is a recursive partitioning technique that is based on the construction of an ensemble of classification and regression trees (hence the term forest). Each tree is trained using the same method as described above for CART. However, to increase computational efficiency, each tree only utilizes a random subset of features at each node – this step also reduces correlation (and accounts for the second element in the nomenclature of the classifier). Trees are bundled together computationally through bootstrap aggregating ("bagging") (Breiman, 1996). The final classification result for a new sample is then obtained through a majority vote of individual tree results. Overall, this approach is less sensitive to overfitting and noisy data, two of the most considerable pitfalls of CART approaches (Breiman, 2001). For RF tuning, the number of trees (nTree) and the number of variables per split (mTry) have to be optimized. Past studies found that satisfactory, stable results could be produced with a number of trees ranging between 200 and 500 (Belgiu and Dragut, 2016). To find the optimal RF model, this study tested nTree = [50 : 750] with a step size of 50, and mTry = [1:15] with a step size of 1.

5.4.4 Gradient Tree Boosting (GTB)

Like RF, Gradient Tree Boosting (GTB) algorithms utilize an ensemble of decision trees. However, its basic approach differs in that it limits the complexity of trees, confining each individual tree to a weak prediction model. It achieves classification accuracy by iteratively combining an ensemble of these weak learners into strong ones by minimizing a differentiable loss function at every step, following a gradient descent procedure (Friedman, 2002). To reduce correlation between trees, each new tree is constructed on the basis of a stochastically selected subset of training data. Recent studies have shown GTB algorithms, such as XGboost (Chen and Guestrin, 2016) to outperform classifiers such as SVM, RF, and KNN (Godinho et al., 2016), especially on unbalanced datasets. However, GTB are often prone to overfitting, a risk that can be minimized through parameter tuning.

In terms of parameters to be adjusted, the number of trees (nTree) is varied between 50 and 200, with a step size of 10. Furthermore, GTB requires a parameter to be specified to determine how many nodes a decision tree in the ensemble can have. Since GTB is based on weak learners, the maxNodes parameter is typically low, with a range of [2:10] with a step size of 1 being tested in this study. In addition, the sampling rate for stochastic gradient tree boosting, and the shrinkage rate, which controls the learning rate of the algorithm, need to be optimized. In this study, a range of [0.45:75] with a step size of 0.5 was tested for the former, and [0.005, 0.01, 0.05, 0.1, 0.25, 0.5] for the latter. Finally, all three loss functions available in GEE for GTB were compared – least squares, least absolute deviation, and Huber. It must be noted that recommendations for nTree tuning usually include larger numbers of tree. Elith et al. (2008), for example, recommend nTree=1000 for tuning as a rule of thumb. However, the GEE implementation of GTB currently produces an error when more than 200 trees are employed for the data configuration in this study. This may be due to the fact that GTB was only recently implemented in GEE by the developers' team and will be further discussed below.

5.4.5 Support Vector Machines (SVM)

The founding principle of this approach is to find the boundary that maximizes the distance from the nearest data point of all classes (Noble, 2006). These points are used for the construction

of support vectors, which, in turn, form the basis for the computation of the maximum-margin hyperplane that serves as a boundary. The dimensionality of this hyperplane is determined by the number of features to be used for classification. For non-linear data, a kernel is applied to transform low-dimensional data to make it separable via the SVM approach in a higher-dimensional sphere (Cortes and Vapnik, 1995). Frequently used kernels include linear, Gaussian Radial Basis Function (RBF), sigmoid, and polynomial kernels (Amari and Wu, 1999). The main advantage of SVM is its high potential for generalization.

In terms of tuning SVMs, the first choice to make is to pick a kernel. For LULC approaches, RBF and Linear kernels are frequently used (Kavzoglu and Colkesen, 2009; Shi and Yang, 2015). Then the cost parameter C needs to be optimized, as well as the γ value in case the RBF kernel is used. The γ value determines the RBF kernel width and thus affects the smoothing of the hyperplane which divides classes. The C parameter sets the threshold for permitted misclassification of non-separable training data (Thanh Noi and Kappas, 2017). If it is too large, it can lead to over-fitting (Ghosh and Joshi, 2014). This study follows (Li et al., 2014) in using ten C values ($2^{[-2;7]}$) as well as ten γ values ($2^{[-5;4]}$) for parameter tuning.

5.5 Validation and Statistical Analysis

Finally, the classification results of each algorithm using each combination of imagery, band set, and training data is validated. For this, the remaining randomly selected 20% of the field work and SPOT-based datasets are used. Overall accuracy as well as producer and consumer accuracies are calculated (Congalton, 1991). To ascertain whether the choice of input imagery, training data, and band set has statistically significant impacts on classifier performance, the non-parametric Kruskal Wallis test (Kruskal and Wallis, 1952) is used.

5.6 Results

5.6.1 Optimal Tuning Parameters

The tuning parameters that yielded the highest accuracies for each classifier and each of the 9 image subsets, and that are used in the remaining of the analysis, are given in Table 5.4, the full set of tuning parameters and their associated accuracies are given in the supplementary materials. The results show that the parameter values yielding the highest accuracies varied considerably for RF (nTree and mTry) and for SVM (C and γ). For RF, the nTree used for the final analysis varies between 50 and 600, and nTry ranges from 1 to 14. For SVM, optimal classification accuracy is achieved using C values that vary along the full tuning spectrum. Similarly, the optimal γ value for the RBF kernel ranges from 2^{-5} to 2^{4}. There are no discernible trends along the lines of imagery type, band sets, or training datasets.

In contrast to this, the optimal values for the tuning parameter λ for NB and CART's maxNodes vary little. In the case of λ, most combinations of imagery, band sets, and training data show little sensitivity to value tuning. Where differences in accuracies depending on λ are observable, the highest accuracies can be reached with $\lambda = 1 * 10^{-10}$. As for maxNodes, the CART classifier globally reaches its highest accuracies using either 5 or 6 nodes.

As for GTB, parameter tuning revealed low sensitivities for some parameters, and higher discrepancies in accuracies for others. The type of loss function employed, for example, has a virtually untraceable effect on accuracies. The shrinkage function, on the other hand, showed optimal values between 0.01 and 0.25, and the sampling rate between 0.6 and 0.75. For nTree and maxNodes there was a noticeably larger variation for optimal parameter values for the fieldwork training set, than for the extended training set. In the former, values for nTree ranged between 50 and 190 and for maxNodes between 3 and 10. In the latter, the optimal value for nTree lay between 160 and 200, and for maxNodes between 9 and 10.

Band Set	Image Source / Classifier	Parameter	Sentinel-1 All bands	Sentinel-1 Restricted	Sentinel-1 Minimum	Sentinel-2 All bands	Sentinel-2 Restricted	Sentinel-2 Minimum	Sentinel-1 and 2 All bands	Sentinel-1 and 2 Restricted	Sentinel-1 and 2 Minimum
Fieldwork training set	NB	λ	-	-	-	-	-	-	0	-	-
	CART	maxNodes	6	6	5	6	6	5	6	6	5
	RF	nTree	100	600	150	250	200	250	350	400	500
		mTry	14	4	2	14	4	2	3	1	2
	GTB	nTree	180	170	170	190	130	50	80	160	190
		maxNodes	7	3	10	10	10	10	6	8	9
		shrinkage	0.01	0.05	0.1	0.01	0.05	0.1	0.25	0.1	0.05
		samplingRate	0.7	0.7	0.75	0.65	0.7	0.7	0.6	0.7	0.65
		loss function	-	-	-	-	-	-	-	-	-
	SVM	C (linear)	16	1	0.5	0.25	0.25	0.25	16	1	8
		C (RBF)	128	1	16	128	128	128	-	-	2
		γ	0.03	-	0.03	16	16	16	0.03	0.06	0.03
SPOT training set	NB	λ	0	-	-	-	-	-	0	-	-
	CART	maxNodes	6	6	6	6	5	5	6	6	6
	RF	nTree	400	450	400	550	50	500	400	450	400
		mTry	8	4	2	11	1	1	8	4	2
	GTB	nTree	200	190	200	180	190	190	160	190	180
		maxNodes	10	9	10	9	10	9	10	10	9
		shrinkage	0.1	0.25	0.1	0.25	0.05	0.05	0.1	0.25	0.05
		samplingRate	0.7	0.75	0.75	0.75	0.65	0.75	0.75	0.7	0.65
		loss function	-	-	-	-	-	-	-	-	-
	SVM	C (linear)	0.25	0.25	0.25	128	128	64	0.25	0.25	0.25
		C (RBF)	2	2	16	64	64	64	2	2	16
		γ	0.03	-	0.03	16	16	16	0.03	-	0.03

Table 5.4: Optimal tuning parameters.

5.6.2 Overall Accuracy

The maximum overall accuracies achieved by each classifier depending on imagery type, band set, and training data, are given in Table 5.5. Accuracies over 85%, which previous studies have deemed satisfactory for LULC purposes (Denize et al., 2018; Khan et al., 2020; Steinhausen et al., 2018), are highlighted in bold.

The results show that GTB globally reached the highest overall accuracy, at 94%. This value is reached using combined imagery, the extended dataset derived from SPOT imagery, and both the full and the reduced band set. RF also yields similarly high values (93%) using the same combination of imagery, training dataset and bands. For the fieldwork dataset, the highest accuracies are also reached by GTB and RF. GTB yields an overall accuracy of 93% for the full and 92% for the reduced band sets using combined optical and SAR imagery. For the same input configuration, RF yields accuracies of 92% and 91% respectively. Furthermore, GTB and RF also reach accuracies of over 85% using all other combinations of bands and training sets for the combination of Sentinel-1 and 2 imagery, and for the use of the extended training set and the full and reduced band sets for optical-only imagery.

SVM using a linear kernel and combined optical and SAR imagery is third in terms of overall accuracy. Accuracies of up to 92% are achieved using the extended training dataset and the reduced band set. Like RF, SVM also yields high accuracies when trained using the fieldwork dataset and the reduced band set. It furthermore attains accuracies of 88% and 86% respectively

Imagery	Training Set	Band Set	Overall Accuracy [%] NB	CART	RF	GTB	SVM RBF	SVM Linear
Optical	**Fieldwork**	**Full**	35	70	75	72	63	66
		Reduced	46	70	76	75	58	69
		Minimal	49	63	70	67	58	53
	Extended	**Full**	32	71	**85**	**85**	60	75
		Reduced	63	75	**86**	**85**	61	75
		Minimal	53	60	75	72	61	60
SAR	**Fieldwork**	**Full**	42	59	61	53	55	54
		Reduced	23	66	67	55	52	52
		Minimal	21	55	64	66	51	50
	Extended	**Full**	9	55	61	69	57	56
		Reduced	1	54	75	71	56	55
		Minimal	1	54	74	65	55	52
Combined	**Fieldwork**	**Full**	48	**88**	**92**	**93**	21	**88**
		Reduced	72	**88**	**91**	**92**	19	**90**
		Minimal	60	81	**85**	**87**	24	73
	Extended	**Full**	53	81	**93**	**94**	32	**86**
		Reduced	69	82	**93**	**94**	32	**92**
		Minimal	49	66	**85**	**87**	46	79

Table 5.5: Overall accuracies

for the use of the full band set and both training data sets. For the variation of SVM using an RBF kernel, the overall classification accuracy does not surpass 63%.

The CART classifier reaches overall accuracies of up to 88%, when trained using combined imagery, the fieldwork dataset and either the full or reduced band sets. Far below this mark is the Naive Bayes classifier. Its highest overall accuracies, at 72%, is reached using the combined optical and SAR imagery.

5.6.3 SAR- and Optical-Only vs. Combined Imagery

Overall, the results show a marked increase in accuracy for the majority of classifiers when combined imagery is used, as opposed to SAR and optical-only imagery. For RF, optical-only imagery led to an average accuracy of 78% across training and band sets. For SAR-only imagery, this average lay at only 67%. The combination of both imagery types, however, yielded an average accuracy of 90%. Similarly, the CART, SVM, and NB classifiers also yielded their best accuracies using the combined imagery.

As illustrated in Figure 5.4, the combined imagery yielded considerably higher accuracies for NB, CART, RF, and SVM using a linear kernel than optical or SAR images alone. For CART and RF, the improvement in accuracy when using combined imagery in comparison to optical-only imagery is statistically significant ($p \geq 0.95$). In addition, the CART classifier using optical imagery shows considerable variability with respect to accuracies. The improvement in comparison to using SAR-imagery only is statistically significant for NB, CART, RF, and SVM using a linear kernel. However, for SVM using an RBF kernel, the reverse is true - the combined imagery yields considerably lower accuracy values than either optical- or SAR-only imagery.

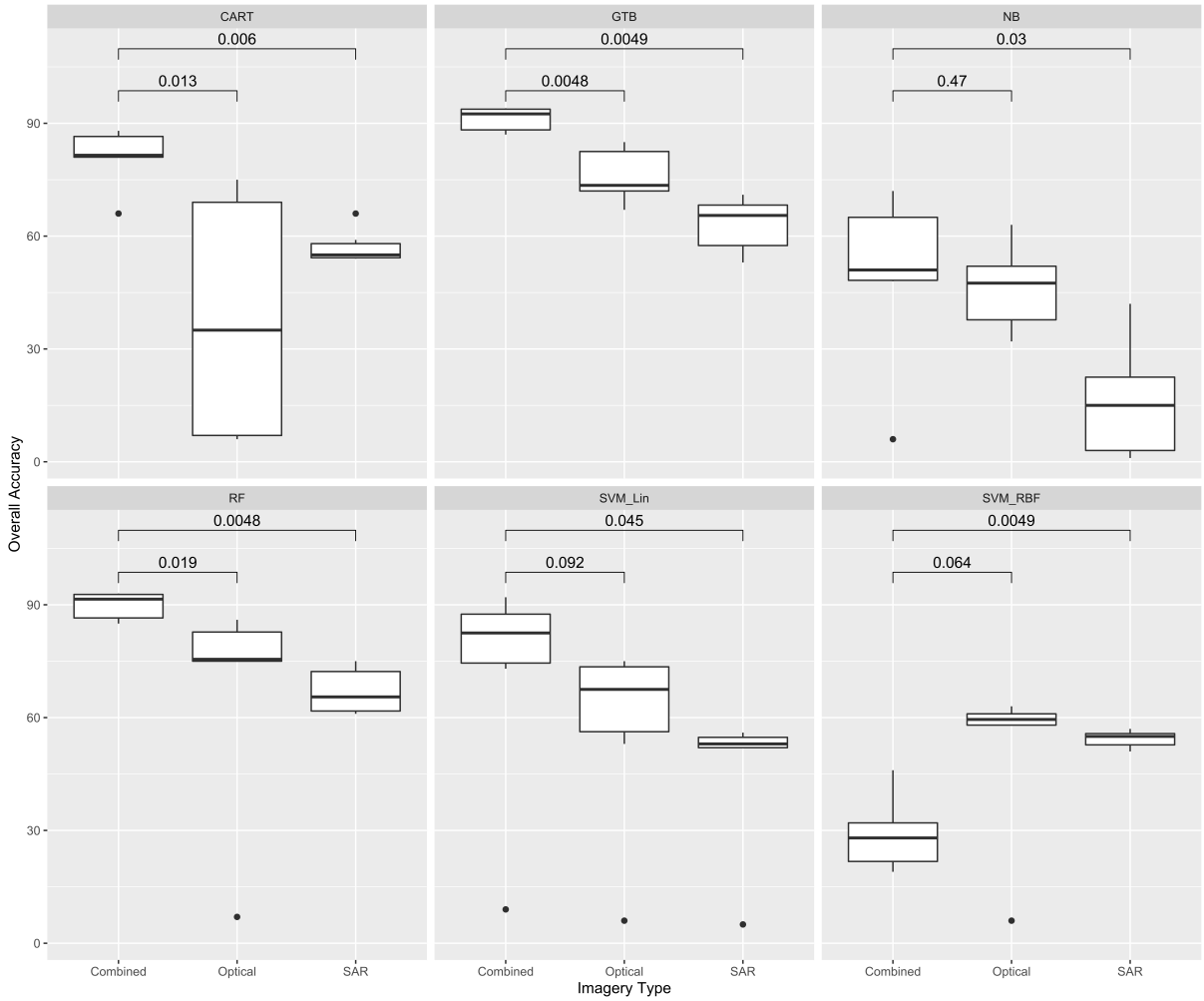

Figure 5.4: Box plot of overall accuracies by imagery used and classifier, and significance of variation of accuracies depending on imagery type used.

5.6.4 Choice of Training Data and Band Sets

In general, the extended training data yielded the highest overall accuracies for GTB, RF and SVM using both a linear and RBF kernel. For CART and NB, however, the training set based on fieldwork data led to higher accuracies. GTB, RF and SVM using a linear kernel also yielded accuracies of over 85% using the fieldwork dataset (cf. Table 5.5 and supplementary materials). It can be noted that the use of the extended data set leads to a higher accuracy improvement in optical and SAR-only imagery than in the combined imagery. For example, for RF applied to optical imagery, the average overall accuracy achieved using the fieldwork dataset lies at 74%, whereas the extended dataset yields an average overall accuracy of 82%. In contrast, for combined imagery the average RF using fieldwork training data lies at 89%. Using the extended dataset only increases this average overall accuracy to 90%.

As for the band set, it emerges that the extended and fieldwork datasets produce comparable accuracies for CART, RF, and GTB. SVM using a linear kernel, however, produces distinctly higher accuracies on the basis of the reduced band set. Furthermore, SVM using the RBF kernel produces its highest overall accuracies when the minimal band set is used.

5.6.5 Accuracy by Class

The accuracy with which each land cover class is classified by each algorithm varies considerably. Consequently, this impacts the overall classification accuracy at different points in the time series of images between 01/11/2019 and 31/10/2020, when the classes have a different predominance.

Water, for example, has a relatively high consumer and producer accuracy (cf. Table 5.6). While NB tends to errors of omission, mis-classifying water as urban areas, the other classifiers succeed in delineating surface water regions with fairly high confidence. RF and GTB in particular delineate water well, with producer accuracies of 98% and 97%, and consumer accuracies of 97% and 98% respectively, followed by SVM (97% and 96% respectively). Consequently, inundated areas, as they can be observed in November, are represented well.

In contrast, the classifiers exhibit greater difficulties in separating bare/fallow land from urban areas, and vegetable fields from rice paddies. While CART, RF, GTB, and SVM succeed

Table 5.6: Producer and Consumer accuracies for NB, CART, RF and SVM using a linear kernel. SVM (RBF) is not included due to low accuracies.

	Producer Accuracy						Consumer Accuracy					
Classifier	Water	Urban	Fallow	Fruit	Rice	Veg.	Water	Urban	Fallow	Fruit	Rice	Veg.
NB	86	75	89	40	83	58	100	79	79	84	64	39
CART	89	91	94	91	87	59	85	91	96	89	88	59
RF	98	96	95	95	85	79	97	96	97	93	91	81
GTB	97	98	97	97	79	82	98	96	98	94	92	80
SVM (Linear)	97	96	93	97	72	66	96	97	99	87	88	79

well in classifying the permanent urban areas in the East of the study area, they also tend to mis-classify fields lying fallow during the dry season as urban areas. The discrepancy between the size of the areas classified as fallow across the year depending on which classifier is used is also shown in Figure 5.6. In terms of consumer accuracy, SVM using a linear kernel can boast the best performance in delineating urban and fallow land. In contrast, RF and GTB exhibit a better performance in separating rice paddies and vegetable plots, both in terms of producer and consumer accuracies.

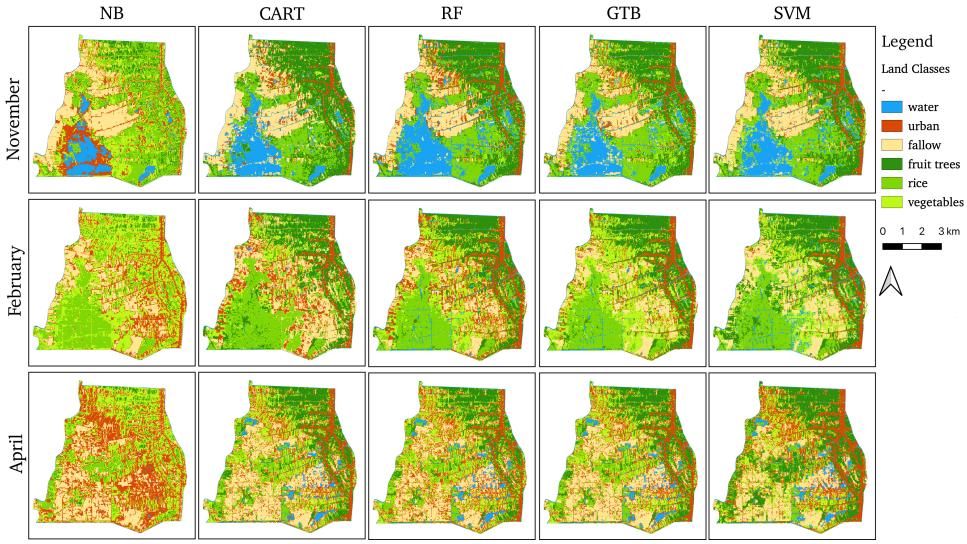

Figure 5.5: Comparison of classification results using the best-performing configuration of NB, CART, RF, and SVM (linear). SVM (RBF) is not included due to low accuracies.

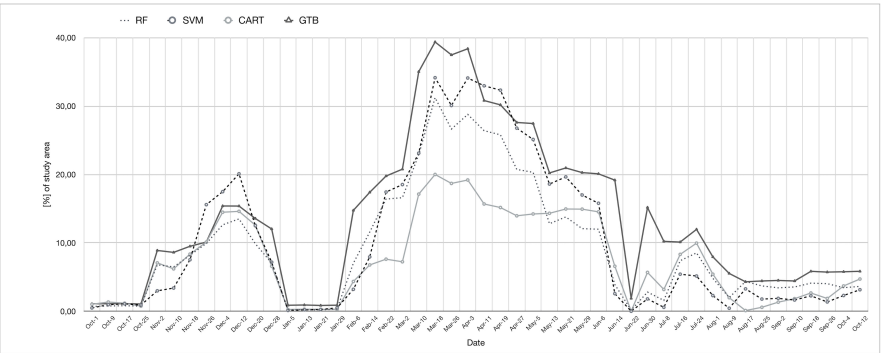

Figure 5.6: Time series of areas classified as bare / fallow using the training point set based on SPOT-images and RF, CART and SVM (linear) between October 2019 and September 2020. NB and SVM (RBF) are not included due to low accuracies.

5.7 Discussion

5.7.1 Benefits of Combining Imagery

Most saliently, this study highlights the multiple benefits of combining Sentinel-1 and 2 imagery for various classifiers. For all classifiers except SVM using an RBF kernel, combined imagery yields the highest classification accuracy. Especially for SVM using a linear kernel, the combination of optical and SAR imagery brings a relative increase in overall classification performance. This is in line with several studies that have found marked benefits in adding information from radar images to optical ones for LULC classification (Denize et al., 2018; Van Tricht et al., 2018). What is notable in this study is the consistent and considerable increase in accuracy that results from the combination of image sources. Tavares et al. (2019), for example, note a rise in accuracy from 89% using Sentinel-2 only to 91% using combined imagery. Similarly small accuracy improvements were reported by (Lu et al., 2018). In contrast, the present study finds increases in accuracy of up to 15 percentage points. In addition, it can be noted that the combination of imagery also leads to a reduction of the impact of the training dataset. It can be conjectured that this is due to the fact that additional layers of information counter-balance the noise in training data and make it more easily separable for classifiers.

5.7.2 Configuring Input Parameters and Data for Optimal Results

Broadly, the results of the analysis illustrated the wide variations in the values of optimal parameters leading to the best classification accuracies for RF and SVM, as well as the considerable impact of the choice of kernel for SVM. Regarding the RF parameter of nTree, for example, previous studies (e.g. (Thanh Noi and Kappas, 2017)) found that accuracies tended to increase with a rising number of classification trees in each random forest, and that further increasing the number of trees led to stability in the accuracy of the results, starting at ca. 250 trees. Others also note that forests with a larger number of trees do not necessarily perform better than those with fewer (Oshiro et al., 2012). The present analysis shows that optimal accuracy values for some data configurations can be reached at nTree = 50 already, and that increasing the number of trees can lead to a noticeable decrease in accuracy. This underscores the importance of performing parameter tuning prior to applying each of these classifiers in a new setting, with varying input data configurations. As the tuning results for GTB show, the importance of parameter tuning is also dependent on the quality of the training dataset. While optimal parameter values for nTree and maxNodes varied little for the extended training set, greater discrepancies in values needed to achieve optimal overall classification accuracies were observed using the fieldwork-based training dataset.

In terms of band sets and training data, this analysis illustrates the nuanced balance between adding additional layers of information through texture features and spectral indices, and introducing noise that can detract from classification accuracies. Most prominently, it emerges that it isn't necessarily the set of bands with the highest number of additional indices and texture features that yields the highest accuracies. Nor is it the minimalist approach taking as a basis of classification only the bare minimum of raw bands. Rather, it is the set of curated raw bands and spectral indices, as well as bands arithmetically calculated from the SAR imagery's VV and VH bands, that leads to the highest classification performance. Most probably, this is due to the fact that any additional information offered by certain spectral indices is drowned out by the noise that other, less meaningful, indices produce. This result underlines findings from previous studies, such as da Silva et al. (2020), which concluded that the NDVI, EVI, and SAVI offer the highest additional values for LULC approaches.

5.7.3 Overall Classifier Performance

When it comes to comparing algorithms in terms of accuracy, this analysis shows that the GTB and RF classifiers exhibit the consistently best performance under a number of different input data configurations, with GTB slightly exceeding RF in terms of accuracy. It must be highlighted that GTB achieved this performance, despite the fact nTree is currently limited to less than 200. Though SVM shows similarly high classification accuracies for combined imagery and the use of a reduced band set, GTB and RF performance is consistently superior with regard to all constellations of input data – imagery type, training dataset, and band set. It is only in certain land cover classes – such as the separation of urban areas and bare land – that SVM outperforms RF and GTB. Several previous studies have debated the compared performance of RF and SVM. Ma et al. (2017) found RF to be generally superior in a review of object-based LULC classification approaches, as did Talukdar et al. (2020) in a comparison of machine learning approaches for LULC classification. Rana and Venkata Suryanarayana (2020) by contrast, found SVM performance to be superior, especially in combination with a principal component approach. In addition, several studies have also factored GTB into the comparison. For example, Georganos et al. (2018) found the XGboost implementation of GTB to systematically outperform RF and SVM, especially on the basis of an extended feature set. Overall, it appears that SVM performs well when studies aim to fine-tune parameters and investigate specific applications, whereas RF offers more solid, generalizable applications for LULC approaches, and a lower sensitivity to various input data. This higher sensitivity of SVM to the types of input imagery and the training data set is in line with findings from earlier studies. Pelletier et al. (2017), for example, compared the effect of training data noise on supervised LULC classification using SVM and RF. The results found RF to be significantly more robust towards both random and systematic noise of training labels.

As for the other classifiers available in GEE that were tested in this study, it emerges that NB is ill-suited for LULC applications, with low overall accuracies. CART, on the other hand, yielded solid results for the combined imagery type. In particular, it can be noted that this classifier performed better when trained using only the fieldwork data. It can be conjectured that this may be due to the more precise nature of the points in this training data set. Even though there are fewer overall than in the extended dataset, and they are unevenly distributed between

classes, their label attribution carries a higher certainty. As mentioned above, a higher label noise is likely to have been introduced in the extended dataset derived from SPOT during its creation (Frenay and Verleysen, 2014). CART appears to be more sensitive to noise of this kind in the input data, which can be related to the fact that, unlike RF, it only relies on a single threshold to define a node to split data into subsets. In RF, where this process is repeated multiple times, noise can be balanced out more easily. The discrepancy in the classification for CART depending on the training point set is illustrated starkly by contrasting Figures 5.5 and 5.6, the former of which was generated with the configuration of input parameters yielding the highest accuracies (meaning the fieldwork training point set for CART), and the latter of which used the extended dataset generated on the basis of SPOT images as input. In the former, the extents of bare land towards the end of the dry season are higher in the CART classification than in RF or SVM. In the latter, the reverse is true.

5.7.4 Final Classification Configuration and LULC Development Throughout the Year

Overall, the analysis so far has illustrated the the considerable benefits of using a combination of optical and SAR imagery in supervised multi-temporal LULC classifications in Google Earth Engine. When using GTB, the accuracies of these classifications can reach up to 94%, despite some current limitations in the classifier configuration. The results so far also reveal that combining Sentinel-1 and Sentinel-2 imagery improves overall classification accuracy by 10 – 15 percentage points in comparison to analyses based on optical-only imagery. Furthermore, the results show that combining different sources of imagery reduces the impact of the size and quality of the training data set. This study also further highlights that out of all the classifiers available in Google Earth Engine, GTB yields the highest overall classification accuracies, performing best in a variety of combinations of input data, training points, and band sets.

In general, the use of the extended training data, with points set manually on the basis of high-resolution SPOT imagery, leads to higher accuracies, despite the higher label noise in comparison to the smaller fieldwork dataset. It can equally be concluded that a carefully selected set of native bands, spectral indices, and texture features used as a basis for classification

results in equal or better classifier performance than either a minimalist set, or a large variety of additional bands, especially when using SVM. This underscores the delicate balance between adding indices and texture features as auxiliary layers of information for classification, and the noise that is introduced through their addition, which may impede classification accuracy.

Therefore, the final configuration of the LULC classifier chosen to characterize large-scale land use in the case study area is a GTB classifier, using a combination of Sentinel-1 and 2 imagery, the reduced band set, and the SPOT-based training set.

Using this classifier, twelve images covering the period between 2020 and 2021 were classified. The input Sentinel-1 and -2 images are mean composites of each month. In order to increase the accuracy of the detection of urban areas - which, as outlined above, is sometimes confused with fallow areas - and fruit trees a post-classification step was added. Permanent areas, defined as those that were mapped as either urban or fruit trees in 11 out of 12 images, were masked and the classification was then re-run over the remainder of each image. Finally, the re-classified images were exported and the relative percentage of each land cover class was calculated.

When possible, images recorded towards the middle of the month were selected in order to have equal temporal intervals between the land cover classification. However, due to cloud cover during the wet season in particular, this was not always possible. For June and October 2020, several images had to be composited in order to create a relatively cloud-free representation of the study area.

This classification provided the basis for the delineation of units for the model described in the next chapter. They were furthermore used to calculate various factors related to land cover, as will be outlined below.

5.8 Conclusion - Understanding Ecosystem Services and Land-cover Dynamics on a Local Scale through Earth Observation

This chapter has presented a thorough comparison of LULC classification methods using Sentinel-1 and 2 optical and SAR imagery to derive a land cover classification for the case study area, with maximum accuracy. The considerable influence of the choice of classifier and its parametrisation, as well as of the selection of input bands, training data, and imagery has been highlighted.

As a final element in characterizing the Prek system in the case study area, a monthly LULC analysis was carried out using combined Sentinel-1 and -2 imagery and a supervised Gradient Tree Boosting (GTB) method. As training data, manually set points were used, which were based on both high-resolution SPOT and information on land use practices and the spatial configuration of crops gathered in the course of the field work presented in the previous chapter.

The monthly LULC maps derived from the land use analysis and the data on average crop distribution, irrigation practices, and yields, serves as input for the model outlined below.

6

Linking Hydrology and Ecosystem Services to Understand Current Challenges and Assess Future Perspectives

So far, this thesis has taken a close look at regional hydrological dynamics and trends in land cover, and has provided an assessment of agricultural practices, ecosystem services, and challenges related to hydrological processes and water management in the case study area. However, to answer the remaining research questions outlined in the beginning, a more abstract approach is necessary. The role of Preks and the related ES have been explored qualitatively, but to go further in a quantitative assessment, especially in the view of improving Prek design in adaptation to global changes, a new model formalizing the interactions between the hydrological system and the related services was constructed.

To this end, an eco-hydrological model was constructed in the course of this thesis. It aims to make explicit the role of Prek channels in particular, as well as the Prek system in general, in providing the ecosystem services outlined in the previous chapter, and to simulate future scenarios. The model was built on the basis of data collected from local stakeholders in the course of fieldwork, and derived from the remote sensing analyses presented in Sections 3.4 and 5. It was then used to simulate four future scenarios relating to hydrological dynamics in the Mekong, temperature and precipitation patterns over the case study area, as well as different scenarios regarding the extent of Prek rehabilitation to assess whether this could help local communities adapt to global changes. The ecosystem services considered in the model were divided into two main categories - flood-related and not flood-related ES.

This chapter first expands on the ecosystem services to be modelled, the divide between flood- and not-flood-related ecosystem services, and their link to hydrological processes. Next, it provides an overview of the conceptual framework of the model, and how the hydrological processes in the area are modelled, including adaptations of methods described in previous chapters. It then outlines the modelling methodology used - the choice of modelling platform, the data, the delineation of modelling units, the calculation of flood- and not-flood related ES, as well as the parametrization of the model. Then, it explains how scenarios were constructed and on which data basis. Subsequently, results are outlined and discussed, and the limitations of the current modelling approach given.

6.1 Objectives: Representing the Links Between Hydrological Processes and Flood-Related and Not-Flood-Related Ecosystem Services

Ultimately, this model aims to represent the links between the hydrological processes at work in the case study area, and the ecosystem services from which the local population benefits. This section outlines these ecosystem services and explains in depth why they were divided into flood-related and not-flood-related ES. Furthermore, their links to hydrological processes are made explicit, and the scales at which they will be considered are outlined.

As becomes evident from the description of the case study area in previous chapters and from the analysis of hydrological processes in the Cambodian Mekong delta, the annual monsoon floods are the defining characteristic of the region in terms of hydrology. Annual inundations form the basis for agricultural practices, by providing the necessary soil moisture and nutrients for lowland rice cultivation, recharge groundwater, regulate pests, and provide an environment for fish populations to regenerate. During the wet season, large swaths of land which are usually divided into smaller units by canals, small-scale dykes, and boundaries between individual fields, become one coherent body of water that is involved in the provision of all these ecosystem services.

In contrast, during the dry season, flow processes in the network of Prek channels and lowland canals are the determining factor for whether key ecosystem services can be provided or not. While some crops are rain-fed, relying solely on natural precipitation, the majority depends on irrigation, using the Preks and canals as a main source of water. For most of the farmers interviewed, the provision of irrigation water by the Prek system is the main benefit that they derive from it, and the primary reason they see rehabilitation projects and excavations in a positive light.



(a) Inundated parts of the study area.



(b) Receding flood water.



(c) The case study area during the dry season.

Figure 6.1: The case study area during different seasons.

For this reason, a fundamental distinction was made in the conceptualisation of the model - between ecosystem services directly related to the floods and those that are independent of them.

As a result of the division into flood-related and non-flood-related ES, the role of the Preks is conceptualised differently during the dry and the wet season. During the wet season, Preks and lowland canals act primarily as conduits of flooding and drainage. Water limitations are generally not a problem during these months, except in the case of the severely degraded Prek

Put. In contrast, during the dry season, the Preks take on more of a storage function, providing the volumes of water necessary for irrigation, and establishing a flow connection between the lowland canal system and the Bassac mainstream.

The flood-related ecosystem services that are included in the model outlined below are soil- and groundwater recharge, the provision of habitats for fish reproduction, flood peak attenuation, pest regulation, and the deposition of sediments - and thus nutrients.

Most of these flood-related ecosystem services fall into the category of regulating ecosystem services. Sediment deposition could be argued to be provisioning to a certain extent, since some farmers and communities excavate sediments from their plots or the Prek channels and sell them so that others may actively raise their land. The provision of habitats for fish reproduction, though, more explicitly contributes to a provisioning service - especially since fish form an important element in the diet of the local population. However, as mentioned above, quantifying the average amounts of fish people derive from the system is difficult, not just due to the varying individual estimations given by interviewees, but also due to the fact that fish catch has declined dramatically in recent years according to many of them. The reasons given for this decline are numerous, such as overfishing and illegal fishing practices such as using electroshocks. Investigating the complex nexus of causality related to the decline in fish populations is beyond the scope of this thesis. Therefore, only one component - the existence of inundation-season habitats for reproduction - will be considered here.

It must also be noted that not all of the flood-related ecosystem services are felt by farmers in the case study area. Flood peak attenuation, for instance, through the storage of water volumes in the Boeung areas, benefits downstream communities, rather than the stakeholders in the area of interest. Similarly, groundwater recharge in the Boeungs is of little interest to the local population, since few of them have wells there and even fewer use them during the dry season. To a certain extent, groundwater recharge from the Preks during the period in which their water levels are high may be more important in this context (see below). However, since groundwater flow in the region is known to follow a North-South gradient (Kazama et al., 2007), and groundwater is an important resource in neighbouring Vietnam, groundwater recharge in the shallow aquifers of the Cambodian Mekong delta is still included in the model.

The calculation of flood-related ecosystem services is partially based on information provided

ES	Type	variable	Reasoning
Flood peak attenuation	Flood-related	Flood volume	The volume of water stored in the case study area corresponds to peak attenuation downstream.
Groundwater recharge	Flood-related	Flood extents and duration	The magnitude of groundwater recharge depends on the infiltration capacity and how long certain areas are under water.
Provision of fish habitats	Flood-related	Flood extents, duration, and average depth	The provision of fish habitats depends on how long areas of the Boeung are flooded, and how deep or shallow the water is.
Sediment deposition	Flood-related	Flood extents and duration	Sediment deposition depends on the sedimentation rate (see below) and how long Boeung areas are flooded.
Pest regulation	Flood-related	Flood extents and duration above threshold	Pest regulation depends on whether water levels inundate rat habitats for a duration of over 14 days .
Agricultural production on SUs	Not flood-related	Water availability in the Preks (water level)	Based on the interviews, the major hydrological constraint for production is the availability of irrigation water.

Table 6.1: The ecosystem services calculated in the model, and the hydrological factors on which they depend.

by the interviewees during field work - such as the flood extents and duration necessary for pest regulation. Partially, however, they are estimated on the basis of literature values. This applies to rates of sedimentation, as well as groundwater recharge. Values from studies in adjacent areas were used and services calculated proportional to the inundated area at each time step, as outlined below. The general factors used to calculate each ES are given in Table 6.1.

The non-flood-related ecosystem services considered in this thesis are entirely of a provisioning nature: provision of water for irrigation, livestock, and household needs, especially during the dry season. As will be outlined in more detail below, this ES is evaluated on the basis of the required volumes of water calculated from data gathered during the interviews, and the volumes of water available in the channel network at any time step.

Some non-flood-related provisioning ES are not considered numerically in the model. For instance, at non-rehabilitated Preks, many locals make use of the bank vegetation. They use branches from trees to construct fish traps and as fuel for their homes. They supplement their diets with ivy gourd and morning glory, and grow vegetables and fruit at banks of the Preks close to their houses. This is no longer possible at rehabilitated Preks, where banks are to be kept clean and free of vegetation - at least in theory. Consequently, these ES are lost in favour of better water provisioning capabilities.

One more significant difference between flood-related and not flood-related ecosystem services that needs to be outlined at this point is the scale at which they are calculated. Flood-related ecosystem services are provided by a continuous area of inundated floodplains. Though water depths vary, this area forms one coherent water body with properties that are assumed to

be homogeneous, as will be outlined below. In contrast, the provision of not flood-related ES is highly variable across the study area, depending on the crops cultivated in each area and the availability of water in every single Prek and channel in the Boeung area.

Consequently, the calculation of flood-related and not-flood related ES was carried out at two different scales. Flood-related ES are calculated across the entire inundated area. For the calculation of not flood-related ES, the case study area was subdivided into separate modelling units - reach segments and surface units. Reach segments are Preks and Boeung channels, which function as conduits and sources of irrigation water. Surface units (SUs) are areas with a homogeneous elevation, land cover progression, and soil properties. As will be outlined in further detail below, SUs were delineated based on the monthly LULC maps derived from Sentinel-1 and 2 images.

6.2 Conceptualisation of the Model Configuration and Description of Calculation of Processes Relevant to ES

Now that the general ES to be modelled have been outlined, it is important to outline the spatial configuration and the general calculation of processes that are relevant to flood-related and not flood-related ES. This section provides an overview of all the elements necessary to the modelling process, and their general calculation, including the adaptation of methods presented in previous chapters.

In terms of flood-related ES, sediment deposition, groundwater recharge, the provision of habitats for fish reproduction, downstream flood peak attenuation, and pest regulation were considered. In terms of not-flood-related ES, the provision of irrigation water and thus crop production in the agro-ecosystem were calculated.

A simplified version of the model and calculation workflow is shown in Figure 6.2. As can be seen, there are two time steps for the calculation. At a daily time step, the case study area is divided into flooded and not flooded areas. At the same daily time step, flood characteristics such as its extent and volume are calculated for the later determination of flood-related ecosystem services. For not flood-related ES, the existence of a water deficit is determined using a

combination of an inflow model and a water balance equation. To this end, the Preks and lowland canals were represented as a network of longitudinal reach segments (RS). Furthermore, for not-flood-related ecosystem services, the surface area were sub-divided into modelling units (referred to as surface units - SUs) based on elevation, slope, and land cover.

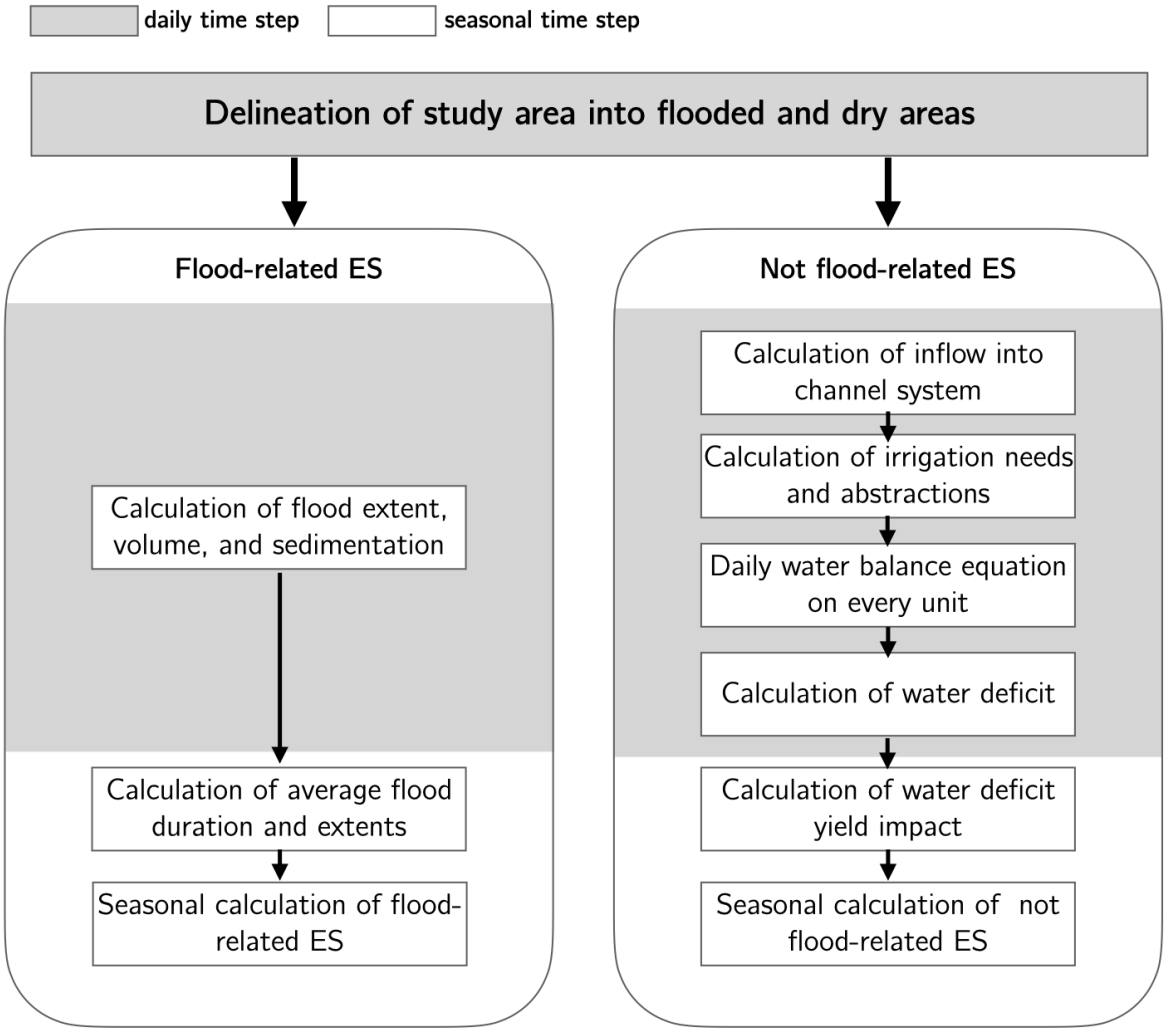

Figure 6.2: Simplified conceptual model.

At a seasonal time step, the ecosystem services are calculated based on the previously calculated daily values. A "season" in the context of the model is defined as one hydrological cycle starting and beginning at the height of the dry season in mid-April. As a baseline period, the year between 2020/04/15 and 2021/04/14 was used, as in-situ data is available during this time for calibration.

The main expected outputs of the model are a measure of the increases and decreases in

ecosystem services for each future development scenario.

The overall spatial configuration of the case study area in terms of modelling units is shown in Figure 6.3. As the Figure shows, the systems consists of the Bassac mainstream to the right, with upstream and downstream boundary conditions, and the daily averaged water levels at the center of the river segment bordering the case study area. From there, individual RS branch out into the case study area, part of which is flooded. Water from these RS is lifted onto individual SUs along the length of the RS. The connections between RS are conceptualised as thresholds and calculated as weirs, as will be outlined in more detail in subsequent sections. This section now offers a description of the principal hydrological processes at work in each element of the conceptualisation.

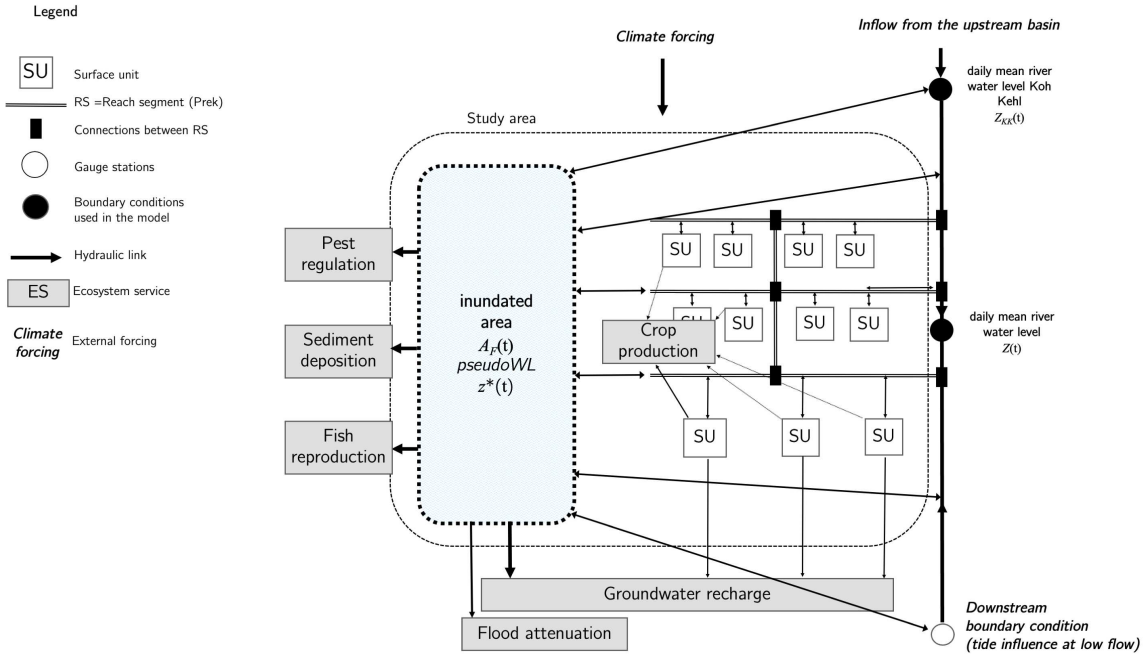

Figure 6.3: Overall conceptualisation and relevant elements of the model.

6.2.1 Flooded Areas

To begin with, there are the annual monsoon inundations, which form one of the most significant hydrological processes in the area. Their recent dynamics can be observed from inundation maps derived from Sentinel-1 and -2 images using an unsupervised classifier in GEE, as outlined in Section 3.4.1.4. The progression of inundation extents in the case study area is shown in Figure

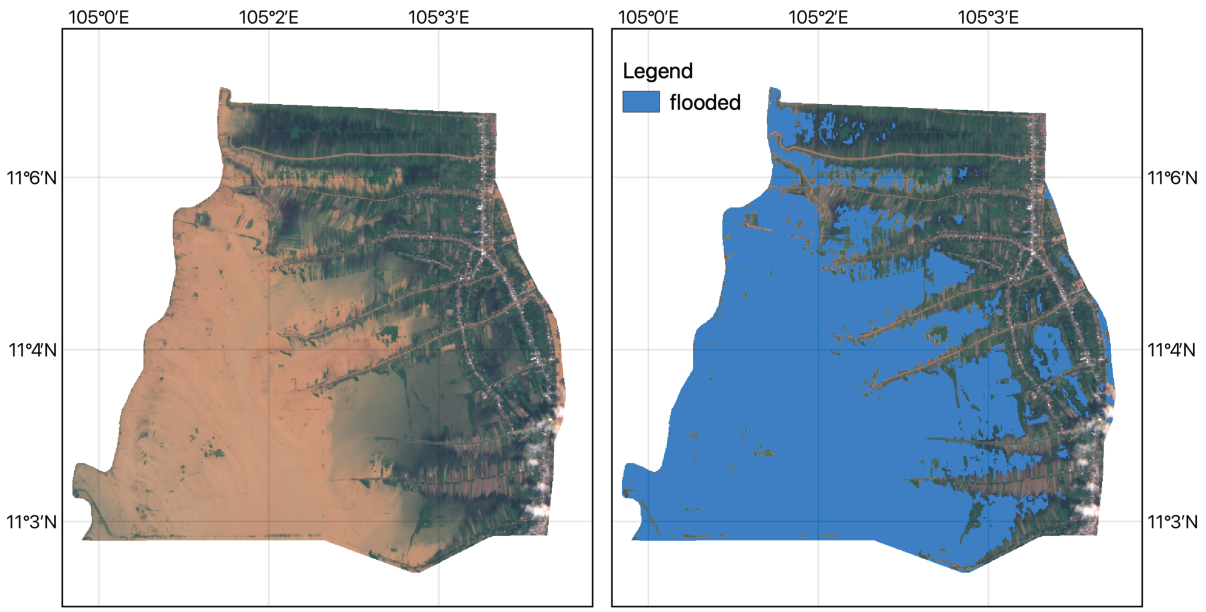

Figure 6.5: RGB Sentinel-2 image taken in the case study area on 2018/09/13 (left) and flood extent detected using the unsupervised classifier (right).

6.4 and an example of the unsupervised classification is given in Figure 6.5.

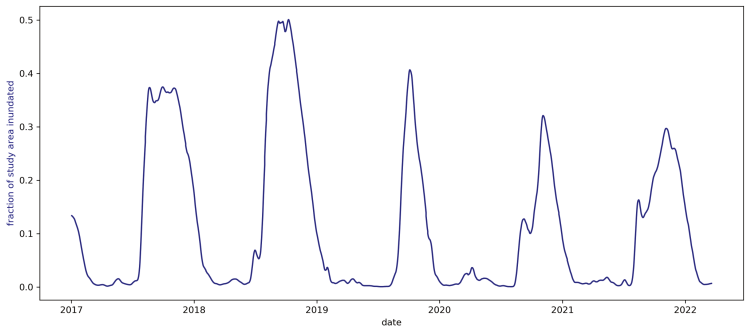

Figure 6.4: Flood extents in the case study area.

During the wet season, inundations are caused by water levels overtopping the banks of the lowland channels and Preks during the wet season. Inundations typically begin in the Boeung areas, then encroach along the lower inter-Prek areas and begin to flood Chamkar plots from their tail ends. It must be noted at this point that inundations can begin at the tail ends of Preks which are still dry themselves. Water can flow from Preks with deeper bed levels into the canal network and then spread throughout the Boeung, initiating inundations.

During flood recession, the processes are reversed. Water drains from the elevated Chamkar areas both towards the inter-Prek areas and towards the tail ends of the Preks. From there, it further drains into the canal network and the Preks and towards the Prek Ambel, the Bassac, or the South of the case study area.

Flooded are modelled using the WAFL (cf. Section 3.4). Making an explicit, correlative link between upstream water levels and flooded areas at a daily time step, the WAFL makes it possible to overcome limitations such as a lack of knowledge about the exact geometric configuration of hydraulic links in the case study area, and exact terrain elevation. For the calculation of flood-related ecosystem services, variables such as the daily extents of inundations, average inundation depths, and overall inundation duration for each pixel are determined.

In addition, the inundation extents derived from Sentinel-1 and -2 images, were adapted and expanded to gain further insights into the hydrological processes in the case study area. First, they were used to determine maximum infiltration rates via pseudowaterlevels. Second, the applicability of the WAFL for predicting inundation extents in the case study area was tested. These calculations are outlined below in Section 6.3.5.

6.2.2 Non-Flood Areas

For the calculation of processes in not flooded areas, three types of elements were employed in the model - surface units, reach segments, and connection between reach segments.

6.2.2.1 Surface Units

The predominant hydrological processes in the not-flooded parts of the case study area are common processes observed in similar environments. The main terms of the hydrological balance are precipitation, evapotranspiration, deep percolation, and irrigation.

Regarding the latter, gravity irrigation[1] can frequently be observed in the area, with water

[1] Gravity irrigation is the predominant irrigation method in the study area. Two instances of sprinkler irrigation and three plots on which drip irrigation were implemented were observed during fieldwork, but mostly in close vicinity to village areas.

flowing from the head of the plot at the bank of the Prek where it is pumped to lower-lying areas at the tail end of the plot, in inter-Prek area. As will be outlined in more detail in subsequent sections, inputs from pumping are estimated based on the fieldwork data and precipitation is taken from field measurements.

6.2.2.2 Reach Segments

In reach segments, the most significant processes are channel flow and pumping onto surface units, the latter of which has already been outlined above.

Channel flow refers to the flow of water between the Bassac, the Prek Ambel and the network of Preks and lowland channels in the Boeungs. Whether or not this flow happens at all is determined by the relative bed elevation of the channels, as well as threshold effects at their junctions. For instance, it is known from interviews with stakeholders that the heads of Preks - such as Prek Nou - preferentially see sediment deposition and thus hinder inflow of water from the Bassac into the Preks. Another regulatory element that exists on some Preks are gates. Installed at rehabilitated Preks, they can prevent inflow into and outflow from the Prek. In the case study area only one such gate exists - at Prek Chann. Its operational schedule, as outlined in the previous chapter, is somewhat uncertain and therefore not taken into consideration in the modelling of flows.

Along each Prek, there is a pronounced water level slope. This is illustrated by the near-realtime water level measurements provided by the loggers installed in Prek Chann and in Prek Touch.

In Prek Chann, a total of four loggers were installed starting in May 2020: two at the gate at its head, one up- and one downstream of it, one at a point where a smaller side channel drains into the Prek, and one at its western end. Furthermore, a logger is installed in the canal adjoining Prek Chann in the West. However, some of them - such as the logger at the western end - were out of order intermittently due to physical damage. The entirety of the data series is shown in Figure 6.6, and a selection of data from June and September 2020 is given in Figures 6.7 and 6.8 respectively. These illustrate a clear water level gradient between the Bassac and the interior floodplains, along the length of the Prek. During the dry season (represented by the June

image), the water level slope is relatively minor, making up a few centimeters between the head of the Prek and its western end. However, it is notable that the considerable daily water level variations in the Bassac, caused by tidal influence, are reflected only to a very limited degree in the water levels within the Prek. During the wet season (September), the water level slope is much more significant, reaching over 0.5 m between the two extremes of the Prek. However, since the calculation of water flow into and out of the Prek takes on particular significance during the dry season due to its role as a source of irrigation water during this period, the water levels stemming from this period are used as a primary source for calibration.

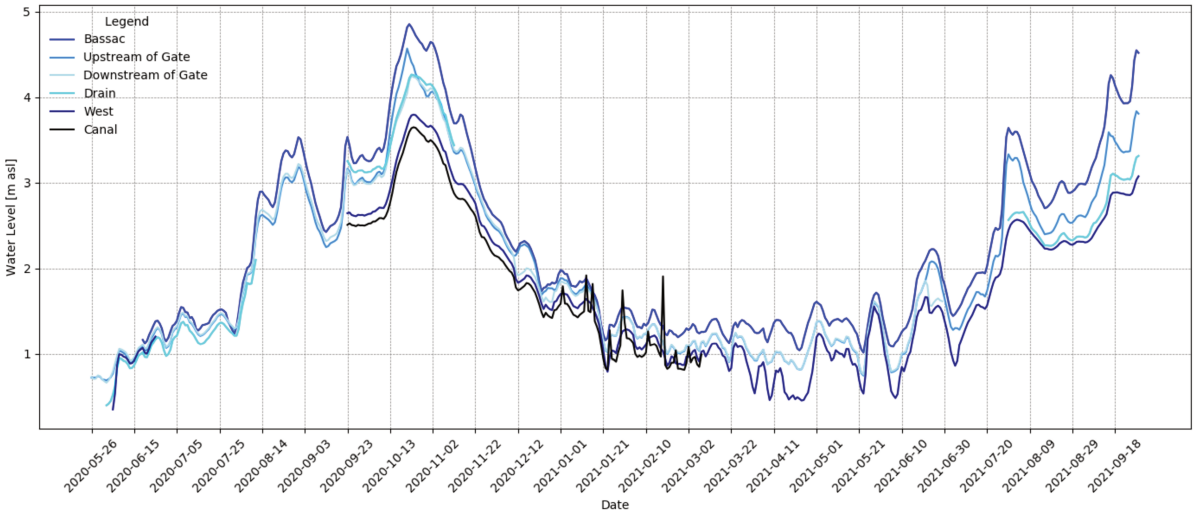

Figure 6.6: Comparison of water levels registered by all loggers in Prek Chann and the Bassac, 2020-2021.

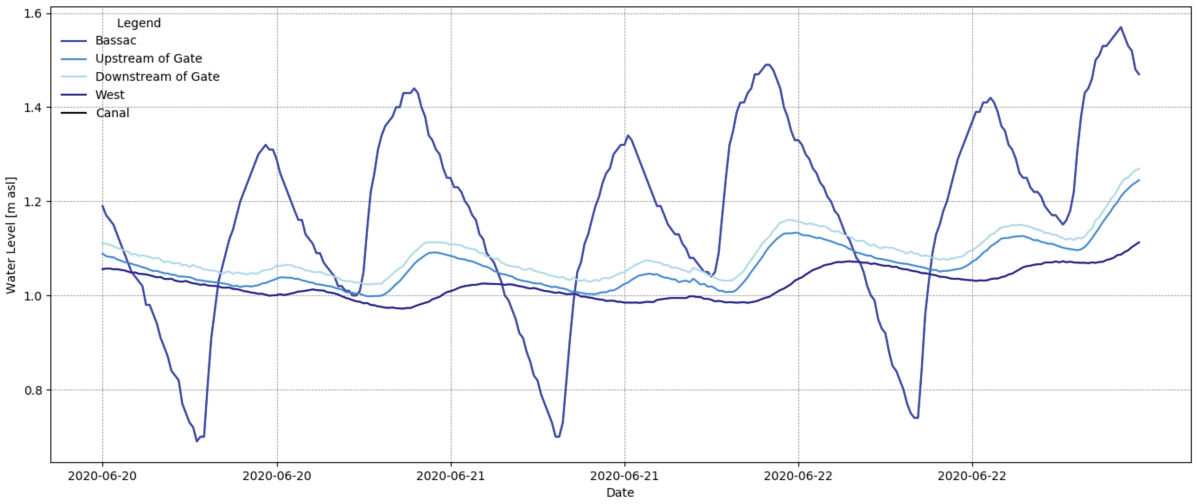

Figure 6.7: Comparison of water levels registered by all loggers in Prek Chann and the Bassac, 20-22 June 2020

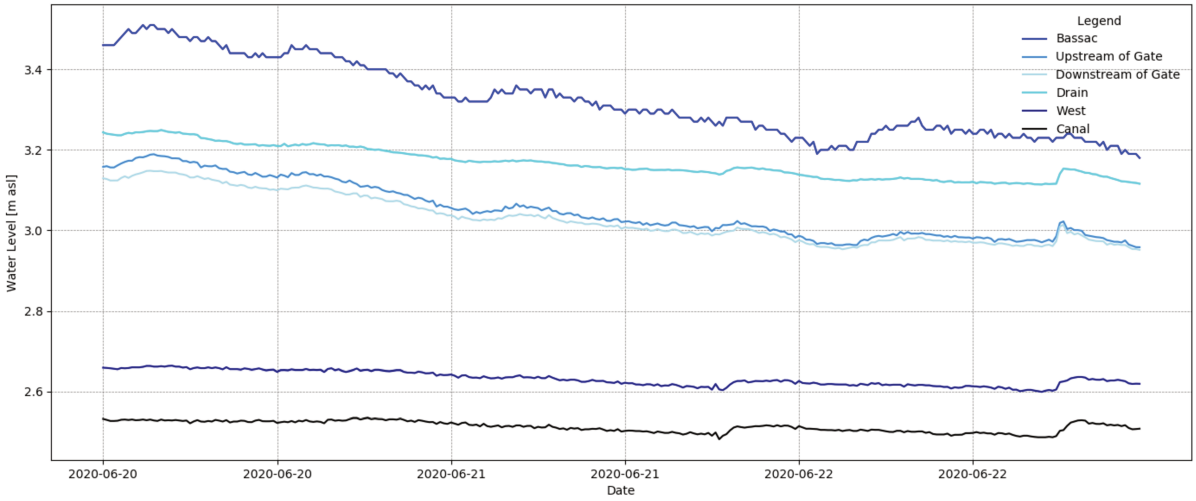

Figure 6.8: Comparison of water levels registered by all loggers in Prek Chann and the Bassac, 24-6 September 2020

In Prek Touch, only one logger has been installed, at the bridge at the head of the Prek (see schema in Figure 6.9 and cf. Figure 3.2). It is located at 3.49 m asl, the level of the Prek's bed. Unfortunately, the logger only provides consistent data for a fairly short period, at the start of the wet season 2021. As Figure 6.10 shows, the Prek is dry until the Bassac water level consistently exceeds its bed level.

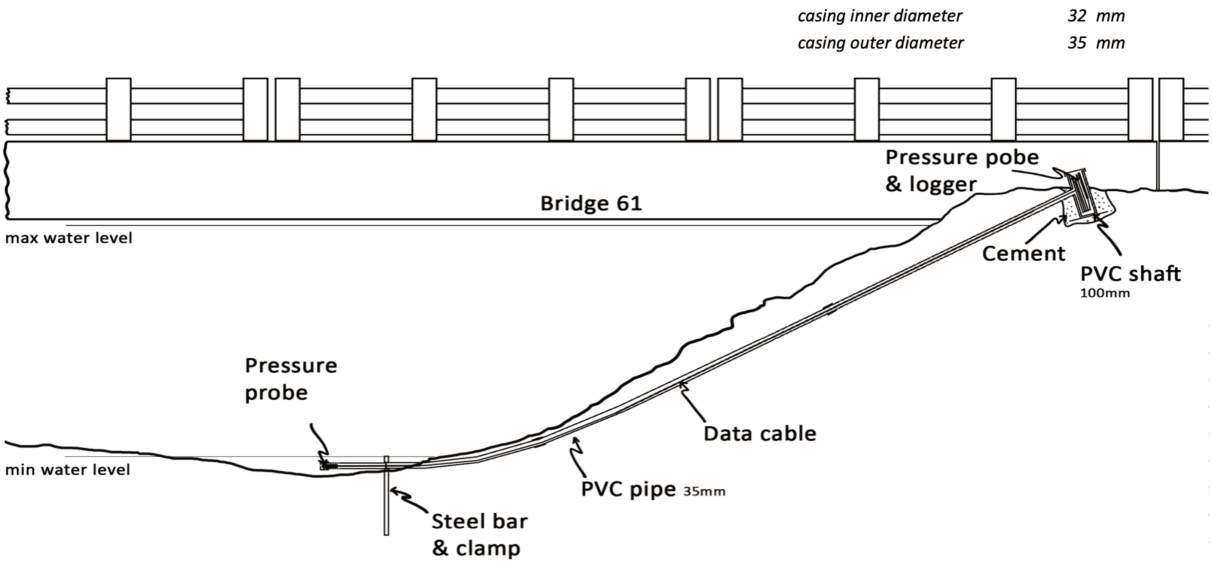

Figure 6.9: Logger set-up at the bridge at Prek Touch. Figure by Sylvain Massuel.

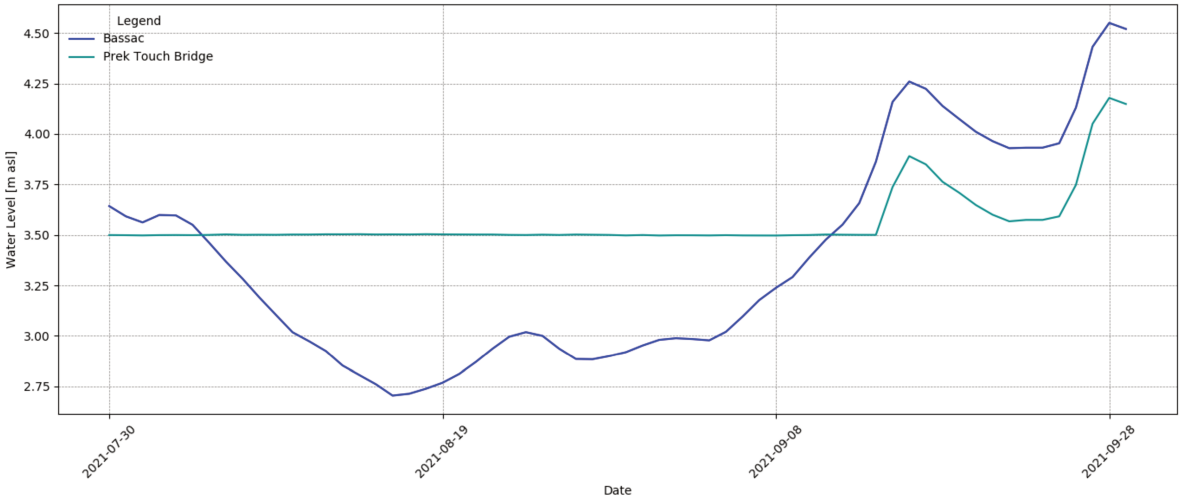

Figure 6.10: Comparison of water levels registered by the logger at Prek Touch bridge and the one in the Bassac, July-September 2021.

From field observations, it is furthermore known that the flow direction within the Preks during times that water levels are low may be influenced by individual irrigation events. A farmer pumping water from the Prek onto their fields at the center of the Prek may cause an observable flow towards this extraction point from both the head and the tail end of the Prek.

6.2.2.3 Connections Between Reach Segments

The connections between reach segments control the flow of water between the Bassac, the Prek Ambel, Preks, and lowland channels. In this model, they are conceptualised as small thresholds, taking the form of rectangular weirs. From the fieldwork, it is known that the intersections between RS are hotspots for sediment deposition, to the point where locally organized excavation projects focus on these areas in particular to allow inflow into the Preks during the dry season.

6.2.3 External Drivers

The external drivers that influence hydrological processes in the case study area are changing climate variables as well as changes in inflow due to modifications in upstream hydrological processes. These modifications are due to climate change, large infrastructure projects, and land use changes (cf. Chapter 2).

The changes in inflow are represented by water levels at Koh Khel and at the logger in the case study area, which are modified in the scenarios. The water level at Koh Khel is used for the calculation of WAFL-derived flooded areas, an the logger in the case study area serves as an input for the calculation of inflow in the system of RS.

6.3 Modelling Methodology

6.3.1 Choice of Modelling Platform

As outlined in the simplified conceptual model at the beginning of this chapter, the first step in the calculation is the division of the case study area into flooded- and not-flooded areas, before ecosystem services are calculated separately for each zone. This means that the modelling platform has to be capable of both representing the complex hydrological processes in the study area (cf. section 3.4) and their connection to ecosystem services.

A wide range of models and modelling platforms for hydrological processes is available, some even specifically designed for applications in deltaic environments. Furthermore, many of them also include some capabilities for the calculation of ecosystem services. In addition, there is also a wide range of models for the calculation of ecosystem services that incorporate the calculation of hydrological processes to a certain extent. Nonetheless, the model for this thesis was built from scratch in Python. The reasons for this lie in the spatial configuration and terrain characteristics of the study area, as well as the complexity of hydrological processes.

Many existing hydrological models adapted for floodplains environments are grid-cell-based, and aim to solve the shallow water equations in 2D environments, such as LISFLOOD-FP, Delft3D, Mike Flood, ISIS-Infoworks, HEC-RAS 2D, and Telemac among others. However, to properly parametrize these models for the case study area, detailed geometric information would be necessary. This is due to the numerous small-scale dykes which delineate field borders and restrict flows. A dyke with a crest height of less than a meter and a width of only a few dozen centimeters can determine whether several hectares of land become flooded - or not. Such small-scale structures are difficult to represent, even in high-resolution DEMs such as TanDEM

with a horizontal resolution of 12 m. Extensive manual adjustments and calibration might make it possible to represent flow processes in the case study area in hydrodynamic models, but that would still leave limitations with regard to the calculation and representation of ecosystem services, since many of these platforms don't have dedicated modules to consider these processes. In contrast, models focused on the calculation of ES, such as InVEST (Integrated Valuation of Ecosystem Services Tradeoffs, Sharp et al. (2020)) and ARIES (ARtificial Intelligence for Ecosystem Services, Villa et al. (2014)), lack the necessary functionalities to represent the complexity of flow processes in the area.

Another option that was considered for the modelling aspects of this thesis is the Soil Water Assessment Tool (SWAT), which offers great flexibility in terms of both hydrological processes and ecosystem services (Arnold, 1994; K. R. Douglas-Mankin et al., 2010; Francesconi et al., 2016). However, like LISFLOOD, it is based on grid cells, which makes it difficult to represent small-scale local terrain variations. While work-arounds exist for some aspects - such as super-imposing a channel system on the grid cells - a major limitation of SWAT is also that it is catchment-based and the model developed here is focused on a much smaller sub-section of a deltaic floodplain.

On larger scales, all of these limitations are of minor importance, and past studies have successfully applied all these tools for analyses in the Mekong Basin and Delta. Xing et al. (2017) used Delft3D to analyse flow and sediment dynamics in the delta's Song Hau channel. Shrestha et al. (2013) used SWAT to estimate the impact of climate change on sediment yield in a sub-basin of the Mekong in Laos, and Truong and Do (2018) used it together with MIKE-11 and MIKE HYDROBasin to estimate the cumulative impacts of hydropower projects on the delta floodplains. Hawker et al. (2017) used LISFLOOD for intermediate-scale inundation modelling in the delta, at a grid size of 540 m. More recently, Quoc Thanh et al. (2019) used Delft3D to calculate the impact of dyke systems on downstream hydrodynamics in the Vietnamese Mekong Delta. In the Cambodian part of the delta, Heng et al. (2021) used a combination of the IWRM-Sub model, which was constructed by the MRC, SWAT, and the ISIS hydrodynamic model, to calculate the impact of future development and climate change on the floodplains at 1 km x 1 km resolution. Also in the Cambodian Mekong Delta and at the same scale, Horton et al. (2022) used a combination of the basin-wide IWRM model, MIKE-11, and IWRM-Sub to project flood extents in the entire delta in 2050. As can be seen from the scale and resolution of these models,

local effects are not taken into consideration.

Another software option that was considered in the context of this thesis was OpenFLUID (Fabre et al., 2010, 2013). Developed by UMR LISAH in Montpellier, this modelling platform allows users to construct highly individualised, spatially explicit models depicting a variety of landscape processes. Its main advantage is that it is not grid-cell-based, but allows for the use of complex geometries of varying sizes. It has furthermore been used successfully in systems with multiple in- and outlets (Rudi, 2019). It distinguishes between surface areas (SU), which share common properties in terms of soil, land cover, slope, and elevation, and reach segments (RS), which are longitudinal elements used to represent channels (see Figure 6.11a). Each process to be modelled is encapsulated in a separate simulator, written in the C++ programming language, with inputs and outputs that allow simulators to be plugged together in various configurations (see Figure 6.11b). Much of the model outlined below took inspiration from the set-up and a simulator for overland flow was even coded on this platform. However, due to temporal constraints and a lack of familiarity with C++, the final model was constructed in Python.

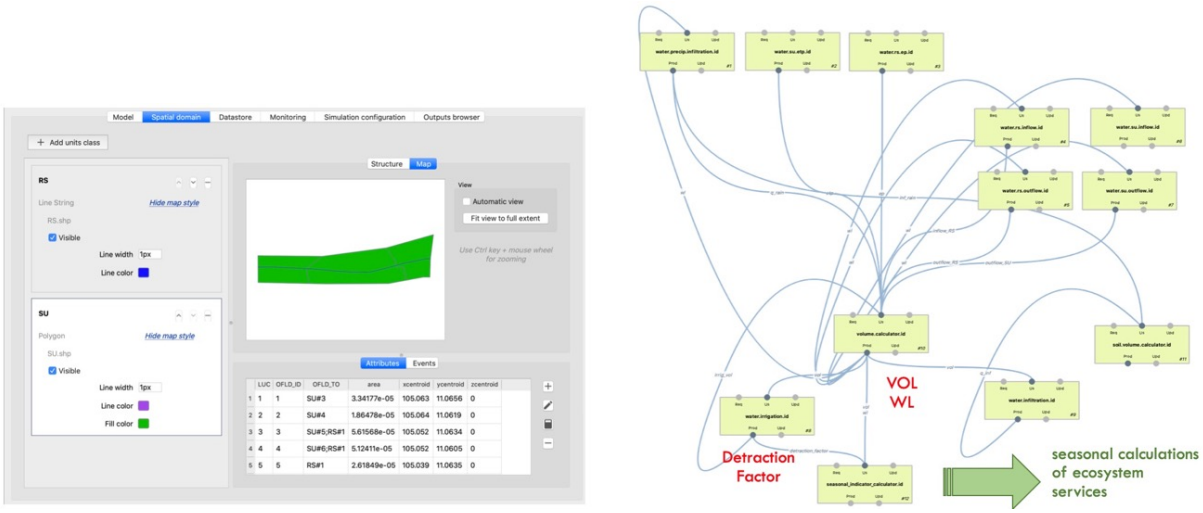

(a) Spatial configuration of sample study area in OpenFLUID, using RS and SU.

(b) Simulator network for hydrological processes on each unit of the case study area in OpenFLUID.

Figure 6.11: OpenFLUID interface.

The model outlined below was coded in Python 2.7.6 (Python Core Team, 2019) using the Anaconda Navigator (Anaconda, 2016) version of Jupyter Notebook. Jupyter Notebook was chosen since it supports literate programming, combining code, text, execution results, and visualisations such as figures and GIFs (see Figure 6.12). All of this contributes to the

self-documenting Jupyter Notebook files, making them easily shareable and reproducible as long as dependencies are made explicit (Pimentel et al., 2019).



Figure 6.12: Code and visualisations of the module for non-flood-related ES in Jupyter Notebook.

6.3.2 Data Used

The data used for this model can be divided into two different categories: data used to delineate the modelling units and define their properties in the baseline scenario, and data that is varied depending on which scenario is modelled and that is used for calibration, validation, and sensitivity testing.

6.3.2.1 Land Cover Data

Into the former category fall the TanDEM-X elevation model, the WAFL-derived flood extents described in Section 3.4, and the LULC classification outlined in Section 5. The LULC classification was further used to determine land-use related coefficients for the calculation of evapotranspiration and the determination of overall yield (cf Sections 6.3.6.4 and 6.3.6.5). In addition, the agricultural characteristics depending on the crops in the SUs - average irrigation hours, average and maximum yield, as well as price per unit - were calculated from the data gathered in interviews. They are shown in Table D.3 in Appendix D.

6.3.2.2 Soil Data

Furthermore, various existing soil classifications in the study area were taken into consideration. This included classifications by Crocker (1962), White et al. (2000), and the FAO (1997). However, these classifications were all conducted at large scales - country-wide in the case of Crocker (1962) and White et al. (2000) and worldwide in the case of the FAO. The delineations of soil types therefore have limited accuracies in the study area. According to the FAO classification, the Chamkar areas in the vicinity of the Bassac are Eutric Fluvisols, which indicate medium clayey soils, and the Chamkar areas further towards the Boeungs, the transition zones, as well as the Boeungs themselves are Eutric Gleysols, which correspond to sandy clay loam to clay. Crocker (1962) draws a similar border, with Bassac-adjacent Chamkar areas classified as Alluvial Lithosols and the remaining case study area simply as Brown Alluvial Soils (loamy or clayey soils). According to White et al. (2000), who proposed a soil classification specifically for rice-growing areas in Cambodia, the study area falls under the category of Prateah Lang soils, which denote sandy soils over clay.[2] Unfortunately, no systematic in-situ survey of soils could be carried out due to fieldwork being cut short. From field observations, also reflected in Vandôme (2020), it appears that Chamkar areas are characterized by more sandy soils, while Boeung areas feature deeper, more clayey soils. In transition zones, soils were observed to vary from silty-clay in the lower-lying areas that are more frequently flooded to silty-sand in more elevated zones that only rarely see floods. In contrast, a borehole created with an auger drill at Prek Chann, near the water level in the center of the Prek (see Figure 3.2 indicated the presence of brown clay up until a depth of 1 m, and grey clay at a depth of 1-3 m. Due to the uncertainty in the soil typology of the area and its delineation, soil properties were assumed to be uniform over the area in the model for simplicity's sake. However, three different soil types were compared in the sensitivity testing stage of the modelling process: silty clay, sandy clay loam, and clay loam. Their average hydraulic values according to Carsel and Parrish (1988) and Saxton and Rawls (2006) are given in Table D.4 in Appendix D. In addition, the infiltration rates determined from the analysis of pseudowaterlevels in Section 6.3.5.2 below were taken into consideration.

[2]Unfortunately, no high-resolution map is available and from the map provided in White et al. (2000), it might also be that the case study area falls under Orung soils, which have a very similar colour as Prateah Lang soils in the legend. Orung soils denote loam or clay over sand. However, since they only make up 1-2% of the entire area under consideration in the map, Prateah Lang soils are the more likely candidate.

6.3.2.3 Water Levels: Hydraulic Boundary Conditions

The case study area is bracketed by two hydrological stations maintained by the MRC - Koh Khel upstream and Chau Doc downstream. In addition, a pressure logger was installed in the Bassac in 2020 in order to have local water measurements, taking account of the superimposed of upstream influences of upstream inflow and backwater effect (cf. Section 3.2.3).

As an external boundary condition, water level data from the station at Koh Khel and the logger at the Bassac in the study area was used. For the calculation of inundated areas, the values at Koh Kehl are used, together with WAFL. The values from the logger are used as input for the calculation of water levels in the network of RS. Values from both sources are modified for scenario simulation to represent upstream shifts due to climate change, hydropower infrastructure, and land use change.

Furthermore, the data from the loggers in the Preks and the channels (see Figure 3.2) was used to validate the water levels calculated in the course of each model run.

6.3.2.4 Climate Data: Temperature and Precipitation

For precipitation and temperature data, in-situ data from the meteorological station installed in the case study area was used. For the determination of long-term averages, CHIRPS and ERA5 Daily Aggregates were extracted from GEE (see Section 3.3 for details). ERA5 is a climate reanalysis product produced by ECMWF - Copernicus Climate Change Service. It provides consistent global data on meteorological parameters such as air temperature, wind speed, air pressure, and dew point temperature since 1979, though at a moderate resolution of 27 830 meters. Sediment concentrations measured by the MRC at Koh Khel and Phnom Penh were used to establish a baseline and then varied in accordance with estimations for future developments according to the literature. Finally, the geometry of the Prek channels and canal network was estimated based on the in-situ measurements taken during the fieldwork, as well as values provided in engineering reports such as SOFRECO (2017) and MoWRAM and AFD (2022). For rehabilitated Preks, a bed level of 0 m asl is assumed. For not rehabilitated Preks, a level of 2.5 m is assumed. The exception to this is Prek Put, which has a considerably higher bed

level, estimated for the purposes of this calculation at 4 m.

6.3.3 Delineating the Prek System into Modelling Units

Before the actual calculation workflow could be defined, the study area needed to be divided into smaller modelling units. As outlined above, the model presented here follows OpenFLUID in delineating a network of reach segments (RS) in the form of Preks and lowland canals, and subdividing the study area into surface units (SU) which share similar properties.

Delineating the RS - which correspond to the Preks and primary lowland canals - could be carried out on the basis of already available geometry files as well as high-resolution SPOT satellite imagery. A choice was made not to delineate smaller drains as little is known about their geometry or location. Overall, 30 such segments were delineated, shown in Figure 6.14a. In contrast, delineating the SUs was a more difficult endeavour. A balance had to be struck between a higher spatial resolution, allowing for the representation of small-scale terrain features, and limiting the number of units for the sake of computational complexity. As a first step, RS were considered as separating lines between SU. Beyond that, the division into Boeungs (flooded annually), transition areas (sometimes flooded), and Chamkars (never flooded) was considered, as well as the average elevation and slope. Finally, a progression of land use was considered by overlaying the results of the LULC classification for each month for the season 2020-2021 (see Figure 6.13). This made it possible to identify areas that share a similar cropping schedule, such as single rice cropping, double rice cropping, or single rice cropping followed by a crop such as maize. On this basis, 129 SUs were delineated manually in QGIS. The results are shown in Figure 6.14b. This latter aspect, the inclusion of cropping practices based on both interviews and remote sensing also arguably adds an socio-hydrological dimension to the model, though merely a basic one that could be extended, as will be outlined later on. While based on physical data and the results of quantitative numerical analyses, the process of delineating units was based on individual judgement and the visual assessment of area similarity.

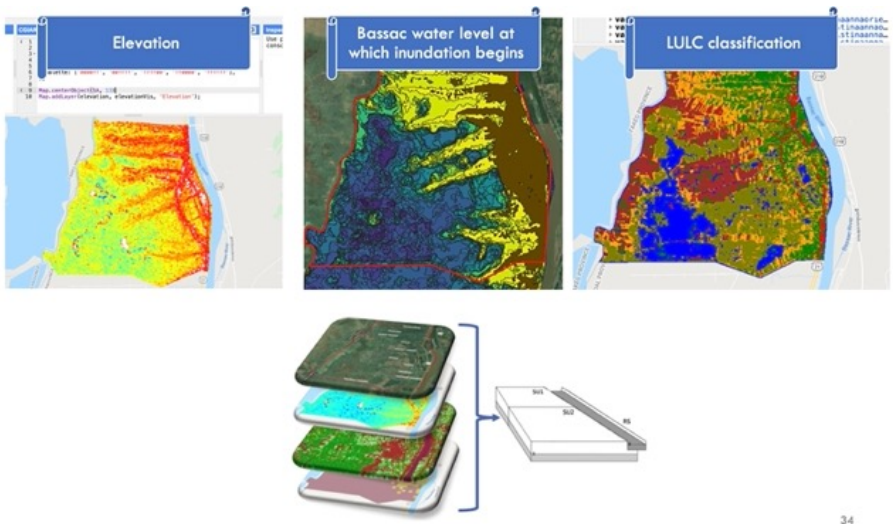

Figure 6.13: Delineation of RS and SUs, carried out manually in QGIS.

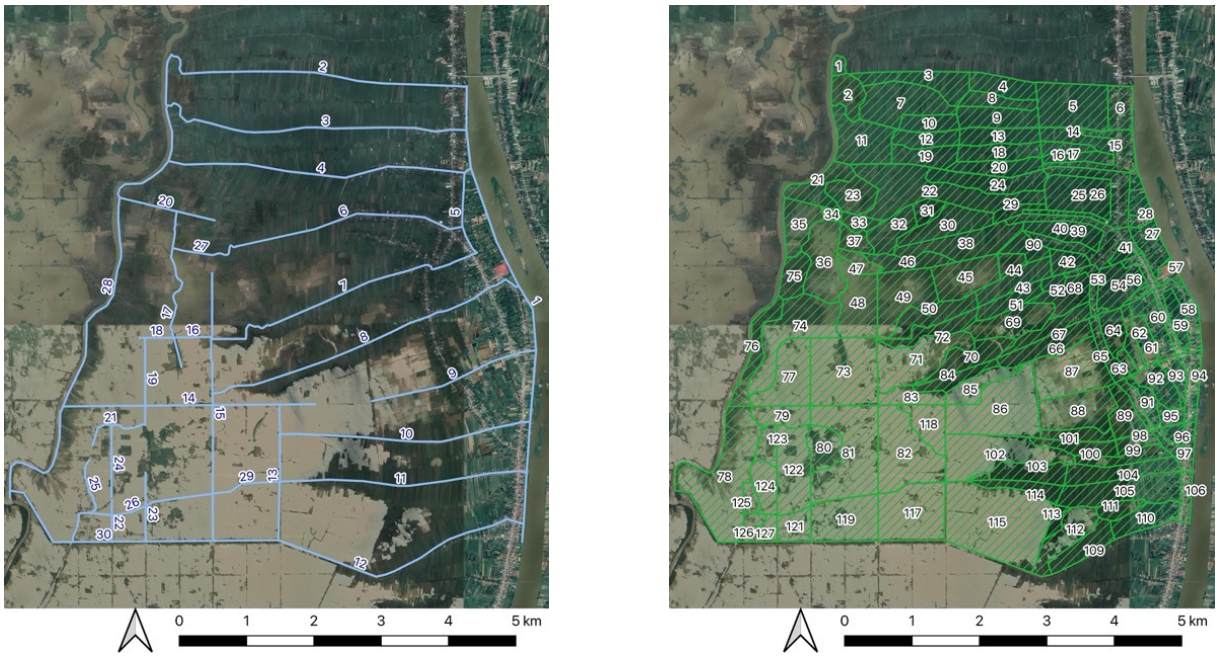

(a) Delineation of reach segments.

(b) Delineation of surface units.

Figure 6.14: Delineation of modelling units. Background image: Google Earth.

Once the delineation of SUs was concluded, the characteristics for each unit were calculated. From the TanDEM-X elevation model, an area-elevation-curve for each unit was extracted. Similarly, in each unit, the area percentages of each land cover class in each month were extracted from the LULC classification. Finally, the average K_C, K_Y and CN values, as well as irrigation requirements and optimal yields for each crop, were calculated for each unit, based on the relative area share of each land cover class in each unit. The result of these calculations were

saved to two separate CSV files to characterize each unit - one containing the area-elevation curve, the other the land-use-related parameters.

A final element related to the spatial delineation of the Prek system is the definition of a network of irrigation sources. Each SU was assigned one RS that serves as its source of irrigation water. This assignment was clear for some units - such as those surface units bordering directly on a Prek. For others, though, it was a more difficult matter and often based on knowledge of the study area or common farming practices. For instance, it emerged from the interviews that for some areas adjoining Prek Put, Prek Nou served as a source of irrigation water. Since Prek Put is practically dry year-round and Prek Nou contains water several months into the dry season, farmers have organized a distribution network containing a double-pumping system. However, it must nonetheless be noted that this assignment of RS to SU as irrigation sources is a simplification and the origin of uncertainties. For instance, in the Boeung areas, several canals might serve as irrigation sources, rather than just one. Similarly, alternative sources such as wells or ponds located at the end of plots are neglected. However, it appears from the interviews that these sources of irrigation water are used only by a small minority of farmers.

6.3.4 Choice of Modelling Period, Time Step, and Baseline Scenario

Each model run spans the duration of one year, to allow the comparison of the impact of the monsoon inundations on the annual provision of ES. For this reason, the modelling period begins and ends at the height of the dry season, when there are no flood-related ES and the provision of not-flood-related ES is at a minimum. The 15th of April was chosen as a starting and end date for each simulation.

As a time step for the simulation, a daily interval was chosen. Partially, this is due to considerations of keeping the computational efforts involved in the calculation limited. The water levels used in the scenarios outlined in Section 6.4 are based on these long-term values.

In terms of baseline scenario, the season 2020-21 was chosen, meaning the period between April 15 2020 and April 14 2021. The reason for this is that the meteorological station and the water level loggers were installed in the case study area in spring 2020. This means that for the season 2020-21, in-situ data in the Preks and canals is available for calibration and validation.

Similarly, sufficient Sentinel-1 and 2 images for a monthly LULC were available during this period. In addition, the majority of survey data used to characterize agricultural practices stems from spring 2020. However, there are a few drawbacks to choosing this period as a reference, especially with regard to flood-related ecosystem services. As outlined briefly in section 3.2.3 and visible in Figure 3.27, the 2020 monsoon inundations were far shorter than typical, and had far lower extents. From this point of view, it would be better to use a hydrologically average year, based on the time series of the past 30 years. Otherwise, future changes in flood-related ES are evaluated in comparison to a situation that is already less than ideal, as can partly be seen in the descriptions of the decrease in fish populations given by interviewees. However, for the moment, the value of available in-situ data outweighs these considerations.

6.3.5 Preliminary Calculations

A final step before the calculation of the model could commence was to complete two preliminary calculations to verify data and methods used in the model. These calculations are, on the one hand, the validation of the estimation of inundation surfaces using the WAFL, and, on the other hand, the estimation of maximum infiltration rates using pseudowaterlevels. The former verifies that the WAFL, a methodology developed at the scale of the Cambodian Mekong delta, yields relevant results at the local level. The latter uses inundation dynamics during the recession phase to identify an average infiltration rate in the area.

6.3.5.1 Validating the WAFL in the case Study Area

As outlined in Chapter 3.4, this method was developed to re-construct past inundation extents on the basis of water levels. In this chapter, however, the WAFL is used to predict inundation extents. Therefore, a further analysis to determine the predictive capabilities of WAFL had to be conducted before it could be used to determine inundation extents for future scenarios.

For this purpose, the water levels measured during the 2021 monsoon inundations, which were not used in the original WAFL development, were used to predict inundation extents. These predicted extents were then compared to those observed from Sentinel-1 and -2 images. The

results are shown in Figures 6.15 and 6.16. Figure 6.15 provides a visual comparison of WAFL- and Sentinel-derived inundation extents at the beginning of June, July, August, September, October, and November. It shows that the overall evolution is reproduced with acceptable levels of accuracy in terms of amplitude and timing of the flood, information which is essential for the purpose of the model. However, the figures also show that at the beginning and end of August, the WAFL tends to underestimate inundation extents in the Boeung slightly. This is mirrored in Figure 6.15, which compares the size of the overall inundated areas derived from both approaches. After an initial peak in mid-August, the WAFL-derived extents decline much faster than the observed ones. As outlined in Section 3.2.3, this pattern of an initial peak followed by a decline in river water levels and then the main flood season peak is typical in the hydrological dynamics in the Bassac. From initial examination it appears that the WAFL registers a much faster flood recession than was actually observed, both after the initial peak and the main one. This is logical, as water retained by local structures, such as dykes around rice fields, is not considered in its calculation. In addition, there is the fact that after the main flood peak, rice cultivation begins in those plots that are no longer flooded. Since the classification of Sentinel images was carried out for only two classes - not flooded and flooded - irrigated rice fields with young plants are often detected as flooded, even though this state is brought about by irrigation, not natural dynamics. In those instances where this latter issue is the reason for the mismatch between calculated and observed inundation extents, the fact that the WAFL does not register it as flooded is actually beneficial to the accuracy of calculations, because the water needed for irrigating rice fields is extracted from the canal network.

A final point that needs to be raised is that calculated inundation extents rarely follow the boundary lines of SUs. Therefore, different SUs might be partially flooded at each time step, according to the WAFL. To decide whether they are considered for the calculation of not-flood-related ES, a simple threshold was implemented. If less than 20% of a SU are flooded it is taken into consideration for the calculation of not-flood-related ES. Part of the reason for this choice are local patterns of cultivation. In many cases, farmers begin to cultivate the elevated areas of their Chamkar plots while those located in the direction of inter-Prek areas are still flooded.

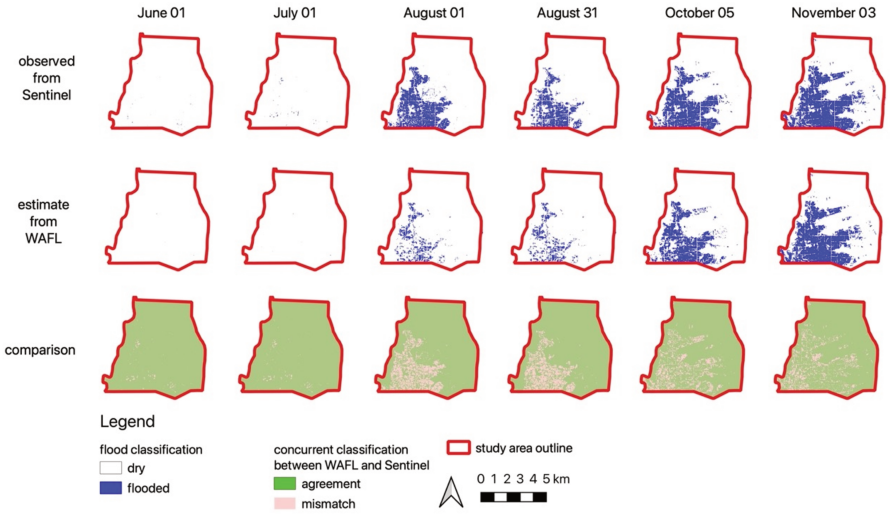

Figure 6.15: Comparison of inundation extents estimated from WAFL and observed in Sentinel-1 imagery for the 2021 flood.

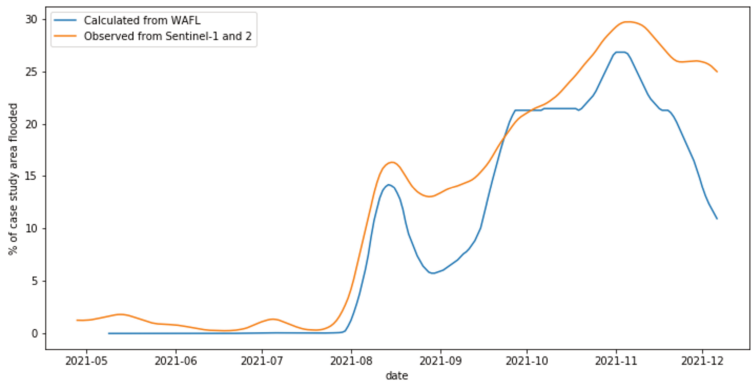

Figure 6.16: Comparison of observed inundation extents and inundation extents calculated on the basis of WAFL for the 2021 wet season.

6.3.5.2 Estimating the Maximum Infiltration From Recession Dynamics

Data on soil characteristics such as infiltration rates is sparse in the case study area. Therefore, maximum infiltration rates were derived from changes in the extent of inundated surfaces derived from Sentinel-1 and -2. As can be observed when looking at the flood extents in the case study area (cf. Figure 6.4), there there is a period each year during flood recession when the decrease in flood extents is almost linear in shape. During this time, a steady rate of recession is reached.

During recession, five factors contribute to the change in inundated surfaces - infiltration,

evaporation, open-channel outflow from the case study area, precipitation, and irrigation. Irrigation can make the flooded areas appear larger than they naturally are. Farmers pump water onto their fields to irrigate their crops, using channels as water sources. These irrigated fields, especially rice fields, can be mistaken as naturally flooded surfaces by the Sentinel-classification, as a simple binary classifier was employed to delineate inundation extents. In addition, it can also be assumed that, as the water level decreases, it reaches the thresholds at which connections are cut. The outflow to neighboring water bodies is then largely reduced and tends to zero as the flood recedes.

To derive infiltration rates from the curve of inundated areas, pseudowaterlevels were used. This concept was already introduced in Section 3.4, for instance in Figure 3.33. It calculates the assumed average water level (in m asl) in the flooded areas of the study area by linking its area-elevation curve with the extent of inundations observed from Sentinel-1 and -2 images. The pseudowaterlevel calculated for the case study area for the period 2017-2022 is shown in Figure 6.17. Marked in red is the quasi-linear phase of flood recession. For the 2016/17 - 2020/21 recession phases, this quasi-linear section is between ca. 2.5 and 0.7 m, for the 2015/16 and 2021/22 phases, it is between approximately 1.7 and 0.5 m. For each year, a linear trendline was calculated to determine the daily rate of flood recession. On average, recession is calculated to occur at a decrease in pseudowaterlevel of 2.57 cm/day, with a standard deviation of 0.41 cm. For the purposes of this model, it is assumed that this recession is accounted for mostly by infiltration.

Not included in these estimates are the effects of precipitation and irrigation, which increase inundated areas, and evaporation and outflow, which decrease them. It is assumed that, to a certain extent, these effects have a lower magnitude and compensate for each other to some extent. Nevertheless, this estimation of infiltration rates provides an idea of an order of magnitude, rather than exact values.

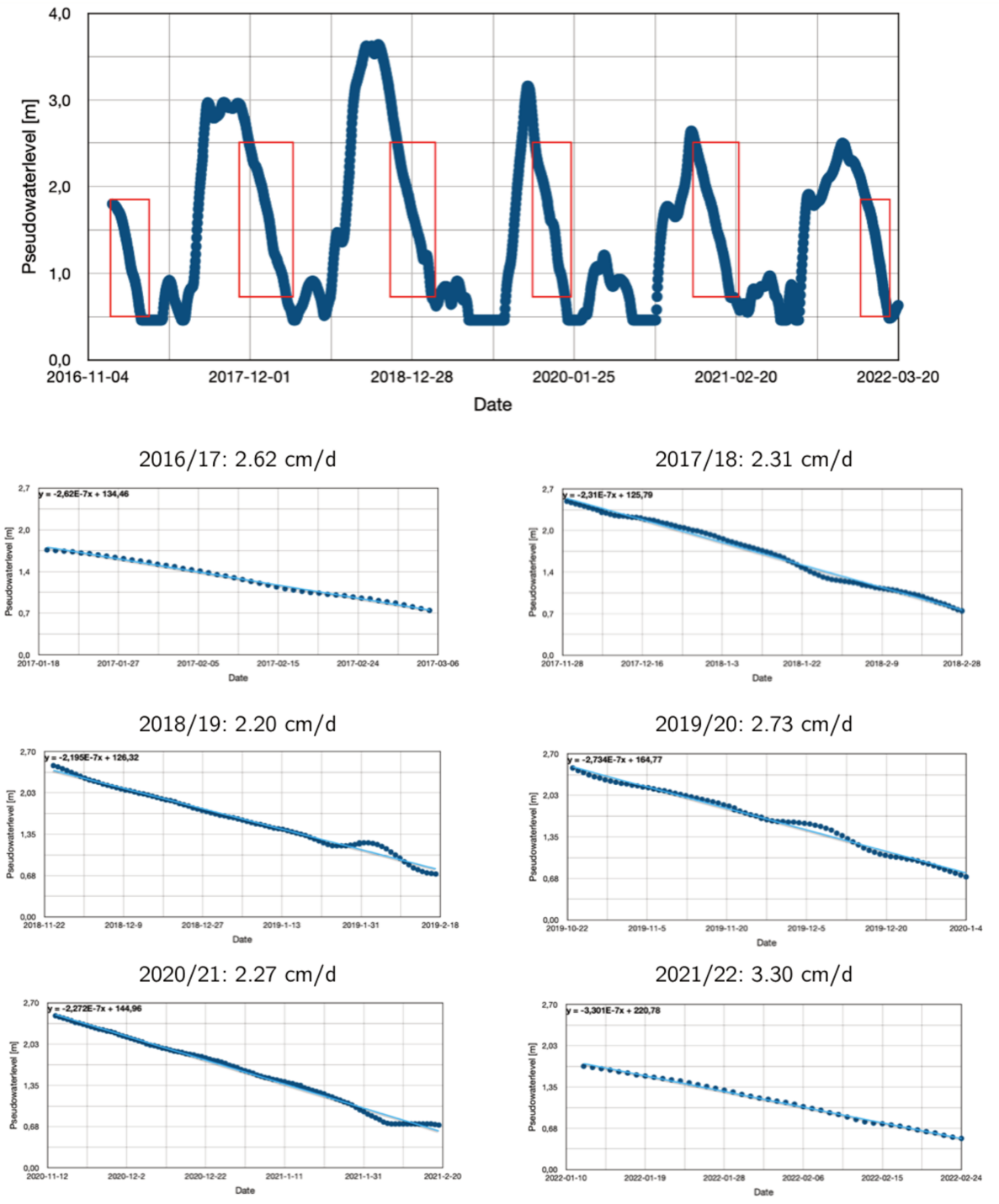

Figure 6.17: Pseudowaterlevel in the case study area 2017-2022 and detail of the quasi-linear phase of recession of each year, as well as the average recession rates during this time.

6.3.6 Calculation Workflow

6.3.6.1 Overview of Calculation Workflow

The detailed calculation workflow is given in Figure 6.18. It consists of two main parts: one is the calculation of flood-related ecosystem services, the other the calculation of not-flood-related ecosystem services. That means that the first principal step in the model is to determine which parts of the case study area are flooded at each time step. At the same time, the total inundated area and, on the basis of the area-elevation curve extracted from TanDEM, the total water volume in the study area are calculated at each time step.

Subsequently, the inundated areas are treated as a single unit, rather than separate SUs and RS, as these distinctions all but disappear during the flood. This flooded area is calculated for each time step and, at the end of the simulation, the overall average inundation duration is determined. On this basis, the seasonal flood-related ecosystem services are then calculated. The variables used and the rationale behind them is outlined in Section 6.3.6.3 and Figure 6.2.

The second major branch of the model is the calculation of not-flood-related ES. This involves more complex calculations at a daily time step, which are spatially explicit for each SU and RS. First, inflow into the RS from the Bassac and the Prek Ambel is calculated. Then, the irrigation volume required for each SU is determined on the basis of the table that characterizes its land use pattern. Then, the water balance for each SU is calculated. Water inputs are precipitation and irrigation volumes. They are added to the surface storage. Infiltration transfers water from the surface to the soil storage. From there, the volume of water plants use for evapotranspiration (ET) is detracted. If soil storage is exceeded, percolation adds water to groundwater storage. At the end of each time step in each SU, it is registered whether sufficient water was available to meet crop water requirements. If this was not the case, the water deficit is noted. Then, to conclude the calculations at each time step, the new water volumes in the reach segments after abstractions for irrigation purposes are calculated.

At this point, several limitations need to be highlighted. For one thing, surface runoff is not considered in the current version of the model. As noted previously, most Chamkar plots slope away into two directions: towards the Boeung in the West and towards the inter-Prek area in the

North or South. Yet overland flow towards these areas is not currently part of the model because of two factors. First, there is the fact that it would involve considerable complexity, even more so due to the small gradients, multiple connections with other units, and small-scale structures such as mini-dykes constructed to delineate plots and prevent runoff. Second, not-flood-related ES are of primary importance mostly during the dry season, when available water volumes are restricted. It was thus assumed that runoff would for that reason be limited in importance.

The second major element of the water balance that is neglected are groundwater dynamics and possible associated flows back to open channels. From measurements in a well at Prek Chann as well as circumstantial evidence such as bank collapses, it is clear that it happens that the groundwater table in the Chamkar areas is elevated above the bed level of the Preks, though its exact elevation varies. It can be conjectured that during the wet season, when water levels in the Preks are typically high, an influent situation dominates, with Prek water infiltrating into the surrounding banks and Chamkar areas. After the flood, this situation reverses into an effluent one, with water that was stored in the banks exfiltrating back into the Prek. During the dry season, excess irrigation water that raises the groundwater table might also contribute to this. By not including this process in the model, a source of Prek water other than the inflow from the Bassac and the Prek Ambel is neglected. The primary reason why this process is not considered so far is the severely limited knowledge of subsurface dynamics and aquifer configurations in the area. Grain size distribution and dimensions of aquifers and aquitards are unknown. At some Preks, especially rehabilitated ones, it is possible that the bed penetrates the aquitard and is thus in permanent connection with the groundwater table. However, no sufficient information on these processes is available. For this reason, it was assumed that the contributions of groundwater to the water level in the Preks remains relatively limited. Whether the calculation is robust in spite of this assumption will be discussed in subsequent sections.

Once the calculations at the daily time step for the non-flood-related ES is finished, the overall effect on provisioning services is determined on the basis of water deficits. As noted previously, these provisioning services relate solely to agricultural production. The use of natural vegetation, for instance for dietary, medicinal, and fuel purposes, is not taken into consideration except on a qualitative basis. For all crops, the likely yield reduction as a response of water stress is calculated, as is outlined in detail in Section 6.3.6.4.

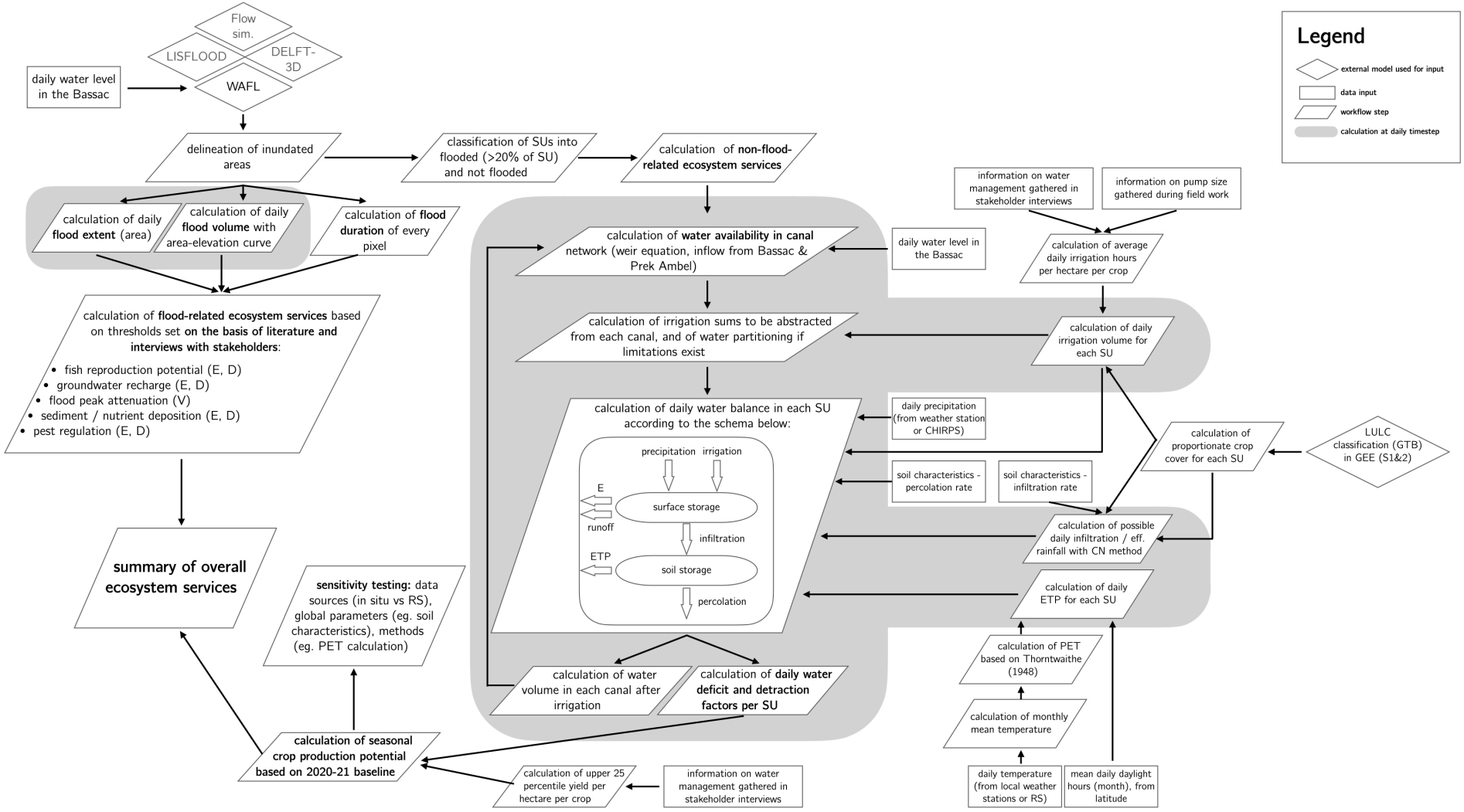

Figure 6.18: Model architecture and calculation workflow.

The final modelling step puts both flood- and not-flood-related ES into perspective by comparing them to the baseline scenario of the 2020-21 cultivation season.

Currently, the model takes between 20 and 30 minutes to run one simulation. So far, the computational efficiency has not been optimized, since the main objective was to make an explicit link between hydrological variables and ES, assessed at the season scale, rather than having an accurate determination of flows at every time step.

6.3.6.2 Calculation of Inundation Extents using WAFL

As noted in the description of the overall workflow of the model, the first crucial step is to delineate flooded areas in the case study area at every time step. In this version of the model, this is achieved using the WAFL, which is described in detail in Section 3.4. The WAFL provides a straightforward, though not very nuanced, estimation of inundation extents. Complex local flow processes and small-scale terrain variations that lead to large-scale variations in inundated areas are already implicitly considered in this approach due to its derivation from observed inundation extents and measured water levels.

6.3.6.3 Calculating Flood-Related Ecosystem Services

Calculating the Inundated Area and Stored Volume Inundated areas, inundation volumes, and inundation durations are calculated for the WAFL. Based on the daily water levels measured at Koh Khel station, it is calculated which pixels are flooded at every time step. Their areas are then added up to calculate the entire flooded area. To calculate the stored volumes, the area-elevation curve of the case study area, derived from TanDEM-X is used.

Provision of Habitats for Fish Reproduction To calculate the impact of hydrological processes on the provision of fish habitats, this thesis evaluates the average duration, extent, and depth of inundations on the floodplain and compares it to to the baseline scenario. These values are calculated by computing the average water level during the flood, then calculating the corresponding inundation extent, duration, and depth. The latter is computed on the basis of the study

area's elevation-area curve.

Pest Regulation According to information from the interviews, rat populations are decimated when sufficient water levels are achieved for sufficient durations. Two interviewees stated that the water levels needed to reach at least the middle of the Preks at which they were being interviewed, for at least two weeks.

To calculate whether a pest regulation effect would be achieved, the areas described by the farmers were delineated in a shape file, and the average WAFL value of the pixels in question was calculated, at 6.43 m. If this value was exceeded for over 14 days, the condition for pest regulation was set to be satisfied in the model.

Soil and Groundwater Recharge As a simplistic approach to groundwater recharge, the maximum infiltration at K_{sat} was assumed over the entire flooded area for the entire duration of the inundation period. Initial variations in the infiltration speed could be calculated, including a more physical determination of the movement of the wetting front according to Heber Green and Ampt (1911). However, since the initial infiltration time until saturated conditions are reached takes up a comparatively small amount of time in the majority of the area, these variations are neglected for now.

A further assumption that is made with regard to groundwater recharge is that there is no limit with regard to the amount that can infiltrate. Some field data collected in the course of the COSTEA project indicates that there might be an aquitard at 5-6 m below ground level, measured at Prek Chann. This would mean that it is a mere 2-4 m below ground level in the Boeung, depending on the location under consideration, if the aquitard were horizontal. What is known, however, is that there is groundwater flow along a North-South axis, towards Vietnam (Kazama et al., 2007). It is therefore assumed that the aquifer is either sufficiently deep to absorb all water that is infiltrated during the flood, or that groundwater flow transports excess water to Vietnam before it can lead to limits on infiltration.

Sediment and Nutrient Deposition Sediment deposition - and thus nutrient input in the study area - are estimated on the basis of inundation extents and durations, as well as average sediment

concentrations during the flood season. Sedimentation rates are assumed to be homogeneous across the study area, and to set in as soon as a pixel becomes flooded. The total sedimentation in the case study area over the course of the wet season is thus calculated by multiplying daily sedimentation rates with the inundation extent at each time step. As can be seen from the overview Table in Appendix A, the MRC maintained multiple stations at which sediment concentration or Total Suspended Solids (TSS) were measured. However, many of these stations ceased their activities in 2017, 2018, or 2019. For this reason, two values are examined more closely to determine at baseline: the TSS concentration measured at Koh Khel between 1993 and 2017 and the suspended sediment concentration (SSC) measured at a station called OSP-MRC, located in Phnom Penh just upstream of the diffluence of the Bassac, between 2011 and 2018. Other, more recent or complete measurements at upstream stations could be considered, for instance at Kratie, but the further away a station is located, the larger the likelihood that sediment concentrations have changed in the interim due to deposition or erosion - especially due to the flow into the Tonle Sap Lake - to a higher degree than the changes over time at Koh Khel.

The TSS series at Koh Khel has the advantage that it offers a long-term view of the development of the concentrations of suspended solids. However, TSS alone cannot serve as a proxy for sediment concentrations due to differences arising from the sampling methods for TSS and SSC. TSS was originally conceived as a water quality parameter. In the MRC data, it is based on a water sample taken in the top 0.3 m of the stream. Since heavier sediments tend to be present at deeper water depths, they are often underrepresented in TSS samples, which leads to an overall underestimation of sediment concentrations. In contrast, SSC samples are based on the depth-integrated method and thus give more accurate results (Kummu and Varis, 2007; Gray et al., 2000). Therefore, TSS is used merely as a way to estimate the temporal development of overall sediment dynamics, whereas the SCC values in Table 6.2 are used to calculate average sediment deposition.

The TSS concentrations at Koh Khel, measured by the MRC between 1993 and 2017 are given in Figure 6.19. As can be seen, concentrations in the 1990s reached much higher peaks during the wet season months than in the 2000s or 2010s. Furthermore, it is known from the analysis of the hydrological series outlined in Section 3.2.3 that the year 2008 can be seen as a break point. Therefore, the values measured between 2010 and 2017 were used to calculate average monthly TSS concentrations in the Bassac at Koh Khel. They are given in Table 6.2.

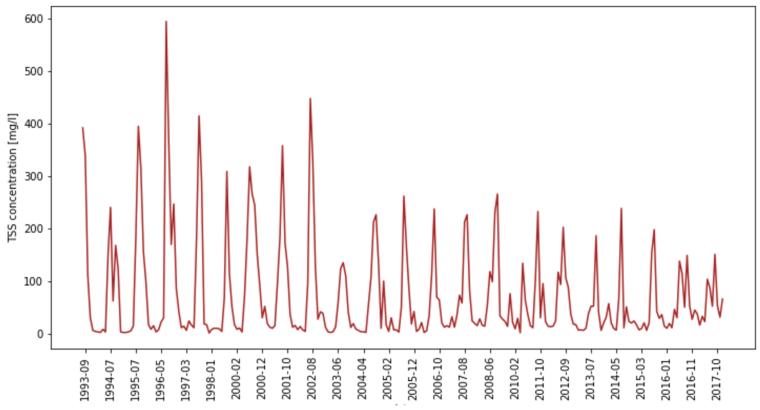

Figure 6.19: TSS concentrations measured at Koh Khel 1993-2017

At OSP-MRC in Phnom Penh, suspended sediment concentrations (SSC) were measured during 2011-2014, as well as during 2018. The average monthly values calculated on the basis of this data are given in Table 6.2 below.

Month	**TSS concentration [mg/l]**	**SSC concentration [mg/l]**
1	19.50	22.65
2	20.66	14.10
3	12.76	16.80
4	21.09	17.10
5	16.53	28.99
6	73.38	78.28
7	123.14	184.13
8	116.32	290.73
9	114.23	238.97
10	47.69	98.28
11	26.18	61.23
12	39.76	33.30

Table 6.2: Average monthly TSS And SSC concentrations at Phnom Penh since 2011.

As the comparison of the two columns in Table 6.2 shows, TSS concentrations are far lower than the actual sediment concentrations. This conforms to trends well-observed in the literature.

The calculation of sedimentation rates is implemented using the formula outlined in Winterwerp (2007):

$$D = c_b * W_s \tag{6.1}$$

where D is the deposition rate, c_b is the suspended sediment concentration and W_s is the settling velocity. The parameter c_b is assumed to be the same as the SSC measured in the main stream of the Bassac. This is a considerable simplification and neglects the spatial distribution of sedimentation, and the fact that differing concentrations have been reported between river mainstreams and laterals (Belaud and Paquier, 2000, 2001). It will be discussed further in subsequent sections.

W_s is calculated following Zhiyao et al. (2008), as:

$$W_s = \frac{\nu}{d} d_*^3 [38.1 + 0.93 d_*^{12/7}]^{-7/8} \tag{6.2}$$

where ν is the kinematic viscosity, d is the particle median diameter, and d_* is a dimensionless particle diameter calculated as:

$$d_* = (\frac{(s-1)*g}{\nu^2})^{1/3} d \tag{6.3}$$

where s is the relative particle density (sediment density / fluid density, ρ_s/ρ), g is the acceleration of gravity (Camenen, 2007).

As a particle diameter, the values measured by Hung et al. (2014) in the Vietnamese Mekong delta were used, which gives the median at 12.5 μm. The same study gave an average value for s of 2.65. Furthermore, the average water temperature for the calculation of the kinematic viscosity ν is also taken from Hung et al. (2014), at approximately 30 degrees C during the wet season. These results were echoed by Gratiot et al. (2017).

Finally, erosion needs to be taken into account. While sediments are being deposited on the floodplains, erosion leads to a certain degree of resuspension, reducing the final overall sediment deposition. The magnitude of resuspension depends on the cohesiveness of the sediments,

as well as on the shear stress exacted by the flow of water across the floodplains. Since the inundation process is, for the moment, estimated from the WAFL and the flow processes within the floodplains are thus not being considered, the erosion rate is estimated as a proportion of the deposition rate based on the average values given for 83 different parameter sets in Hung et al. (2014), at an average resuspension factor of 0.8.

Flood Peak Attenuation Finally, flood peak attenuation as a benefit to downstream communities is calculated on the basis of the water volumes retained in the case study area during the flood rise. Following Chapter 3.2.2, the start of the inundation period is defined as the date with the highest daily water level variation during the season, while the flood peak is defined as the date with the highest water level (after the implementation of a 3-day rolling mean to eliminate spikes due to measurement errors or local variations).

6.3.6.4 Calculating Not-Flood-Related Ecosystem Services

Not-flood-related ecosystem services were calculated for all SUs at any one time step. As a first step, the water levels in all Preks and lowland channels are calculated based on inflow from neighbouring RS as well as the Bassac and the Prek Ambel. Then, it is determined whether the water volumes contained in these channels fulfill the irrigation water demand of SUs that use them as sources. Subsequently, the water balance is calculated in each individual SU, using precipitation and irrigation as inputs, percolation and evapotranspiration as outputs, and updating the surface and soil storage terms, with the transport between them being calculated as infiltration. As a last step, the water volumes post-irrigation are updated in all channels and Preks.

Calculating Prek and Channel Water Volumes The inflow and outflow of water into RS is calculated based on the weir equation (cf. Section 6.2.2.3. The reason for this choice of equation is that it is known from field trips that there is often a threshold, formed by an accumulation of sediments, between the Preks and the Bassac as well as the channels and the Preks. This arises from the fact that increased rates of sedimentation can be observed in these areas. [3]

[3]This was furthermore confirmed during interviews. Several village chiefs, for instance at Prek Nou, explained that local excavations were organized at the Prek heads because inflow was restricted due to sedimentation there.

Furthermore, the weir equation is able to account for the link between water levels and flow between adjoining RS even where parameters like geometry and roughness are uncertain. The higher the denivelation between two water bodies, the larger the flow rate. Two situations are typical: free flow and submerged flow. In the former, the RS having the higher water levels empties into the RS without a downstream influence to consider. In this case, the standard equation used is:

$$Q = \alpha * C_d * \sqrt{2g} * h_1^{\frac{3}{2}} * l \tag{6.4}$$

In the case of submerged flow, the flow is limited due to the small denivellation between water levels in the RS. The corresponding equation is:

$$Q = \alpha * C_{d2} * \sqrt{2g} * h_2 * \sqrt{h_1 - h_2} * l \tag{6.5}$$

$$C_{d2} = 1.5 * \sqrt{3} * C_d \tag{6.6}$$

in which Q is the discharge, h_1 is the higher water level above the weir crest, h_2 is the lower water level above the weir crest, g is the gravitational acceleration, l, is the weir length, C_d is the discharge coefficient for non-submerged weirs, assumed at the standard value of 0.385, C_{d2} is the discharge coefficient for submerged weirs (here taken as unity, allowing continuity of discharge at the limit between free and submerged flows), and α is a correction factor to be optimized through calibration to account for the fact that both C_d and the weir length are estimations. Whether a weir is submerged or not is decided on the basis of the difference between h_1 and h_2: If $h_1 > 1.5 * h_2$, the weir counts as in free flow (Eq. 6.3.6.4), otherwise it is submerged (Eq. 6.3.6.4).

The term α needs to be subject to calibration, validation, and sensitivity testing. This is outlined in Section 6.3.7.2. Actual connections in the study area are often complex and

unmeasured, so geometry (weir length and crest height) as well as discharge coefficients are unknown a priori. Therefore, standard weir lengths were estimated from SPOT high-resolution satellite imagery, and both α and the crest height were subjected to calibration (see below). Since $\alpha * C_d$ values include all unmeasured effects, they can deviate considerably from the theoretical value of 0.385.

The input water level in the Bassac and the Prek Ambel is calculated on the basis of the in-situ data that the logger in the Bassac has been registering since June 2020, and the upstream water level at Koh Khel. Unfortunately, the logger has not yet registered a complete April-to-April seasonal cycle and thus can't serve as direct input. However, the water levels it records were correlated to those at Koh Khel to make an estimate of local water levels possible. As the results of the hydrological analysis have shown (cf. Section 3.2.3), the relationship between upstream and downstream water levels varies considerably between the wet and the dry season. To compensate for this, a method analogous to the Lamagat approach (cf. Section 3.4.1) was used, and the optimal correlation for each month was calculated.

Using the equations above, a flow between RS a new water volume is calculated in each RS at the start of every time step. Based on the assumed geometry, this volume is then converted into a new water level. The corresponding mathematical expression is given below in Equation 6.3.6.4. Here, V_t denotes the volume of water in a RS, with a water level $z_{2,t}$ at time t, supplied by the river or another RS where water level $z_{1,t}$ is known. The flow Q_t given by the weir equation (see Equations 6.3.6.4 and 6.3.6.4) and is equal to

$$Q_t = \frac{dV_t}{dt} = A_t * \frac{dz_2}{dt} \tag{6.7}$$

The area A is a function of z_2, as well as Q in the case of submerged flow, giving a differential equation that is solved with a fourth-order Runge-Kutta scheme (see Appendix F).

In the code, the calculation is carried out through a loop over the different RS, starting from the upstream boundary condition (the water level in the Bassac), and iterating across the different RS according to the flow direction during flood rise and recession. Variations during a time step are bounded so that $z_1 = z_2$ at most. At the end of this loop, the volume is available in each RS.

Following this, the irrigation volumes abstracted from each RS in the ideal scenario are calculated. If these volumes aren't available, the magnitude of the water restrictions is noted and the water input into the SUs drawing water from the RS affected reduced in the next time step.

Water Balance Loop Over SUs The central element of the calculation of not-flood-related ES is the water balance on every SU that is calculated in a loop at every time step. Precipitation and irrigation serve as inputs to the surface storage volume. Water from surface storage is transferred to soil storage through infiltration. From soil storage, plants can abstract water for evapotranspiration (ET)[4]. If soil moisture is above field capacity, percolation occurs as input to groundwater layers.

Precipitation

The precipitation data used as an input for initial calculations of the baseline scenario is taken from meteorological station installed by the UNDP in Koh Thom, since it has made data available over the entirety of the baseline period (2020-04-15 - 2021-04-14). To evaluate future scenarios, precipitation data was modified in accordance with projections in the literature, see Section 6.4. Furthermore, the data used was compared with CHIRPS for the purpose of sensitivity testing.

Irrigation

Irrigation data is based on the information gathered during the interviews on the frequency of irrigation sessions for every crop, as well as the average duration of session. It furthermore uses data collected by Pratx (2017) and in the course of the field trip in February - March 2020 by Vandôme (2020) on the average configuration of the irrigation systems and capacity of pumps, which was found to lie at 60 m^3/h. Building on this information, average irrigation requirements in m^3/d were calculated for each land cover class. Then, the average daily irrigation needs in every month were calculated for each SU based on the percentage of LULC classes that cover it at each time step.

Actual Evapotranspiration

[4]Calculation follows the FAO methodology (Allen et al., 1998), for each of the crops in the SU at the time of simulation.

Potential evapotranspiration (PET) was calculated using the *PyETo* Python package using the Thornthwaite (1948) empirical method. This was used rather than the standard FAO Penman-Monteith method Allen et al. (1998) because it has comparatively minimalistic input data requirements. PET is calculated based on monthly air temperature and monthly mean daily daylight hours, estimated from latitude. Future applications may want to consider a refinement through a transition to the standard Penman-Monteith method.

To calculate actual ET (AET), PET is multiplied with a crop coefficient K_c. This crop coefficient was based on the crop detected in the LULC classification, with values for individual crops taken from the literature (see Table D.1). For the vegetable LULC category calculated through the remote sensing approach, an average for the vegetables found in the interviews was calculated and weighted according to their relative area. K_C values were based on the tables provided by the FAO (Allen et al. (1998), Steduto et al. (2012)).

Infiltration

Infiltration is calculated on the basis of the curve number method, which was developed by the US Department of Agriculture's (USDA) Soil Conservation Service (SCS). It is an empirical method to calculate the amount of infiltration and runoff from rainfall events and irrigation.

$$R = \frac{(P - 0.2S)^2}{P + 0.8 * S} \tag{6.8}$$

$$CN = \frac{25400}{254 + S} \tag{6.9}$$

Where R is the accumulated runoff depth (mm), P is the accumulated input volume (mm), S is the potential maximum retention (mm), and I_a is the initial abstraction. In application, S is calculated from the curve number CN (see Equation 6.3.6.4 above). CN itself is taken from literature values, based on the soil group and land cover (Boughton, 1989; Choi et al., 2019; Hawkins et al., 2008). Furthermore, it is modified depending on antecedent moisture conditions (AMC), meaning that where soils have seen particularly large or particularly sparse irrigation

or rainfall amounts, CN is modified. When the accumulated 5-day antecedent water input is below 36 mm, $CN-I$ is used, when it is above 53 mm $CN-III$ is used. Otherwise, the standard $CN-II$ is used (Bos et al., 2009; Silveira et al., 2000). All CN values used in the calculations for this thesis are given in table D.5. For the purposes of this thesis, hydrological soil group C (moderately fine to fine soil texture) was chosen. The curve numbers corresponding to the different land cover classes are given in Table D.5 in Appendix D. It also includes the variations (CN-I and CN-III) depending on the antecedent soil moisture at the start of the time step.

To calculate infiltration, the theoretical runoff R is subtracted from the existing volume of water stored at the surface (V_{surf}), as well as the inputs in the form of precipitation ($Precip$) and irrigation ($Irrig$):

$$Inf = Precip + Irrig + V_{surf} - R \tag{6.10}$$

Since overland flow is currently not considered in this simulation, as outlined above, the calculated Q is simply added to the surface water volume V_{surf}

Percolation

To calculate percolation, another simplifying assumption was made - namely that it occurs if the soil storage capacity in the root zone is exceeded. The depth of the root zone is estimated at 1 m, based on literature about the average principal rooting depths of paddy rice, mango trees, and various vegetables grown in the area Uga et al. (2013); Feldman (1994); CARR (2014) Evidently, the average rooting depth is highly dependent on the LULC categories. For now, no differentiation between SUs was implemented for the sake of simplicity. However, future applications should spatialise this variable. Potential soil storage (S_{soil}) is calculated simply on the basis of soil storage capacity, derived from Table D.4. Soil storage volumes at every time step (V_{soil} as the total volume of water par unit area, in and below the root depth), as well as percolation ($Perc$), are then calculated on the basis of infiltration, previous soil storage volumes,

and AET.

$$V_{soil} = Inf + V_{soil,t-1} - AET \tag{6.11}$$

$$Perc = max(V_{soil} - S_{soil}; 0) \tag{6.12}$$

Outputs Calculated at Every Time Step

At every time step, several parameters are calculated and stored to memory. These are the V_{surf}, V_{soil}, combined inputs from irrigation and precipitation ($Precip + Irrig$, for the calculation of AMCs), water deficits arising from insufficient water volumes in the channel network, and percolation volumes ($Perc$). These are saved to a data frame and then treated further once the calculation of daily water balances has been concluded.

Calculation of Seasonal Provisioning Services The calculation of seasonal provisioning services follows the approach implemented in the FAO's CROPWAT software (see Allen et al. (1998)), in using a yield response factor K_y to characterize the effect of water scarcity on the yield of various crops:

$$1 - \frac{Y_a}{Y_x} = K_y(1 - \frac{AET}{ET_x}) \tag{6.13}$$

where Y_x is the maximum yield without limiting factors, based on crop variety, ET_x is the evapotranspiration in case crop water requirements are fully met ($ET_x = K_c * PET$), and AET is the actual evapotranspiration possible under given conditions. Y_a, then, is the actual yield. The K_y values used in this thesis (see Table D.1 were taken from the FAO Irrigation and Drainage Paper No. 33 (cf. Allen et al. (1998) and Steduto et al. (2012)). Furthermore, K_Y values for some crops, which were not available in the original FAO publication, were taken from Karanja (2006), Sekendur (2017), Azevedo et al. (2018), Lovelli et al. (2007), and Sezen et al. (2005). For some vegetables, such as long bean, wax gourd, and bittermelon, no data specifically for the

species could be found. In such cases, it was substituted with data from a species in the same family. Bittermelon, for instance (*Momordica charantia*) belongs to the family of *Cucurbitaceae*. Thus, data for squash (genus *Curcurbita*) is used (see Table D.2).

Y_x is estimated on the basis of the data gathered in interviews, taking the average of the upper 25th percentile, after the removal of outliers. Once the calculation of the daily water balance is concluded, and the proportion of actual to maximum evapotranspiration known for each time step, a final yield calculation loop is run over every unit to determine the overall response. For now, this is done on a monthly basis, to account for the different kinds of rice cultivation, for instance. It is furthermore assumed that each month contributes equally to final crop yield. Evidently, this is a simplifying assumption and with a view towards improving the model, different growth stages of the various crops ought to be taken into consideration.

6.3.6.5 Summary of Model Outputs

Overall, at the end of the model run, the following outputs are provided:

- Flood-Related ES
  - Area extent, average duration, and average depth of habitats for fish reproduction. In m^2, d, and m, and as percentage change compared to the baseline scenario.
  - Total volume stored in the case study area during the flood rise, which contributes to flood peak attenuation in m^3, and as percentage change compared to the baseline scenario.
  - Average seasonal sediment deposition in kg/m^2 and as percentage change compared to the baseline scenario.
  - Seasonal groundwater recharge in m^3 and as percentage change compared to the baseline scenario.
  - Pest regulation as a binary parameter - whether it happens or not.
- Non-flood-related ES
  - Average crop yield in all SUs and the case study area as a whole, in % of optimal yield and as percentage change compared to the baseline scenario.

6.3.7 Parametrization and Sensitivity

For calibration and validation, data that the loggers in Prek Chann collected during the 2021 wet season was used. Due to the relative data sparsity in the area, merely the water level in the Preks could be subjected to these steps. Other important output parameters, such as yield, sediment deposition, or groundwater recharge could not be assessed so far.

Sensitivity analysis, to gauge the relative impact of different parameters on model outputs and thus its overall performance, was performed on soil parameters, channel geometry - particularly bed elevation - and the use of different precipitation data. Soil parameters and channel geometry are two parameters that were estimated on the basis of knowledge of the study area gathered during field work, as well as existing literature in the form of studies carried out in the wider region and engineering reports written about Preks. However, they are nonetheless estimations and it was necessary to gauge how small variations in them could affect the overall model output.

It has to be noted that calibration, validation, and sensitivity testing were only carried out to a preliminary degree so far. Due to temporal restrictions and a lack of data, these steps were only implemented manually, rather than automatically using regression, variance-based, or entropy-based methods, as is recommended for hydrological modelling (Song et al., 2015; Devak and Dhanya, 2017).

6.3.7.1 Parametrization and Validating Channel Flow Through In-Situ Water Levels

To calibrate the flow function in the model, water levels measured by the loggers in Prek Chann and Prek Touch were used (cf. Figure 3.2), as well as those of the logger in the Bassac.

To calibrate the flow module in the simulation, the coefficient α in Equation 6.3.6.4 was manually adjusted, alongside the assumed weir height. Since the aim is to find a water level that is representative for the entirety of the Prek, a mean value of all the loggers in Prek Chann was calculated for each date, and the RMSE (cf. Equation 3.1) between this mean and the simulated water level in the Prek was calculated. Since only one water level is measured in Prek Chann this calculation was not necessary, but apart from that the same procedure was observed. The values tested, in each combination, as well as their RMSE are given in Table 6.3. Examples of a

Run	Alpha	Weir Height	RMSE Chann	RMSE Touch
1	1.0	0.3	0.3187	0.2186
2	1.0	0.5	0.3168	0.1999
3	1.0	0.7	0.3144	0.2050
4	1.3	0.3	0.3184	0.2179
5	1.3	0.5	0.3164	0.2037
6	1.3	0.7	0.3123	0.2058
7	1.6	0.3	0.3148	0.2172
8	1.6	0.5	0.3134	0.2080
9	1.6	0.7	0.3125	0.2065
10	1.8	0.3	0.3179	0.2116
11	1.8	0.5	0.3137	0.1943
12	1.8	0.7	0.3119	0.2066
13	2.1	0.3	0.3166	0.2110
14	2.1	0.5	0.3152	0.1952
15	2.1	0.7	0.3140	0.2067

Table 6.3: Weir height and α values for flow calibration at Prek Touch and Prek Chann, with resulting RMSE

simulation run during calibration at Prek Chann and Prek Touch are given in Figures 6.20 and 6.21 respectively.

Prek Touch data is relatively sparse and was thus used only for calibration. Prek Chann data was split in half. 2020 data was used for calibration while 2021 data was used for validation.

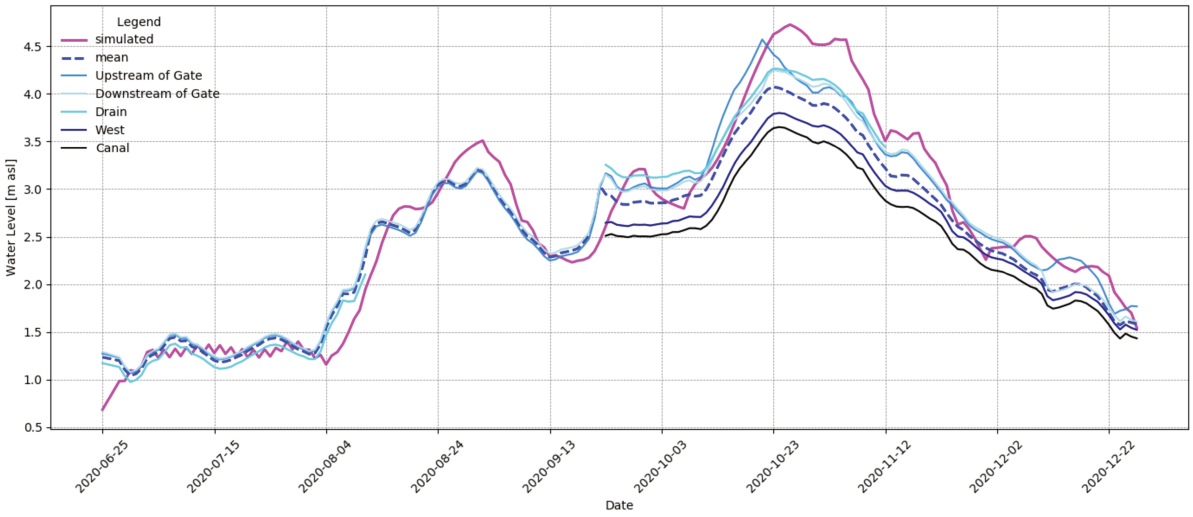

Figure 6.20: Example of simulation run with α=0.016 and z_{weir} = 0.5 at Prek Chann

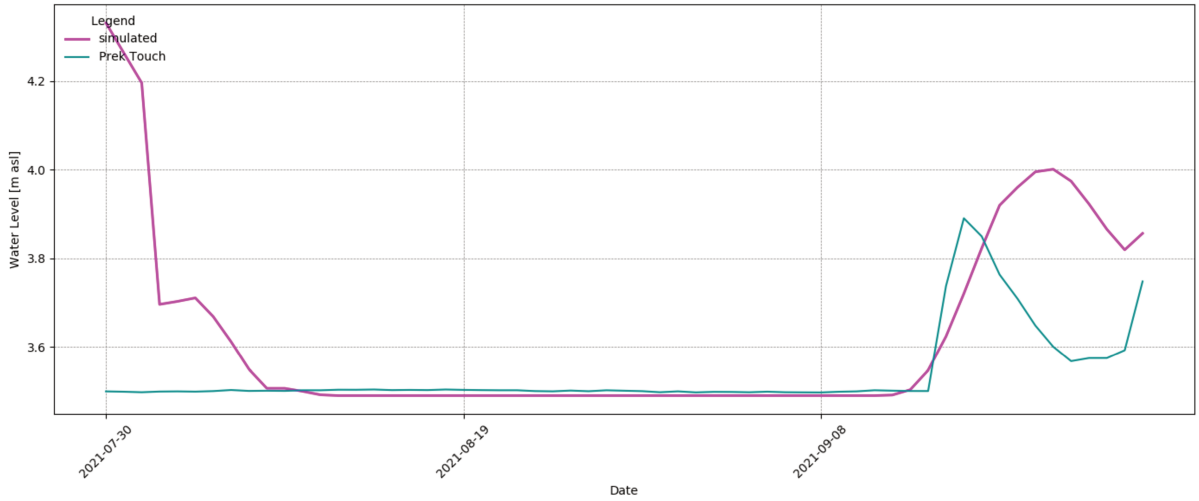

Figure 6.21: Example of simulation run with α=0.018 and z_{weir} = 0.3 at Prek Touch

Based on the results above, an α value of 0.018 and a z_{weir} value of 0.5 were chosen for the overall model. The calibration model run - applying the simulation to the data collected at Prek Chann in 2021 - yielded a RMSE of 0.11 m.

6.3.7.2 Sensitivity Testing

As mentioned above, the sensitivity of various estimated parameters needs to be assessed before the model can be used to simulate future scenarios. The parameters that were evaluated here are soil parameters - specifically K_s, different precipitation data products, and the estimated geometry (bed level) of the Preks. There are different systems for testing the sensitivity of various input parameters. For this simplistic approach the straightforward "one at a time" approach was chosen. It is, however, also possible to test parameters two by two or to employ more evolved methods, such as Morris or GLUE (Gan et al., 2014). The use of these methods can be envisioned for future, more refined versions of the model.

Soil Parameters The soil data used in this analysis is based on a few qualitative field assessments, as well as large-scale maps of soil types in the area. Therefore, the effect of this choice is evaluated by varying the soil input parameters. To this effect, different K_s values (cf. Table D.4 and Section 6.3.5.2) were tested and compared.

The results are given in Table 6.4. As was to be expected, the total seasonal groundwater recharge varies depending on K_s, given the same average inundation extent during the wet season. Values lie between 530 l/m^2 and, assuming high permeability, 33285 l/m^2. This illustrates the high uncertainty arising from assumptions made about soil properties in the area, with variations of several orders of magnitude to be expected depending. For the purposes of the simulation, a K_s value of 0.026 m/d was retained, as estimated from the flood recession analysis.

		Seasonal Groundwater Recharge		
Origin	K_s [m/d]	(m^3)	(m^3/m^2)	(l/m^2)
silty clay (literature)	0.005	3222780	0.53	530
clay loam (literature)	0.062	39962479	6.57	6572
sandy clay loam (literature)	0.314	202390624	33.28	33284
pseudowaterlevel max	0.033	21270352	3.50	3500
pseudowaterlevel mean	0.026	16758459	2.76	2760
pseudowaterlevel min	0.022	14180234	2.33	2330

Table 6.4: Variation in seasonal groundwater recharge in the baseline scenario, depending on K_s (in m/d) and average inundation extents.

Sensitivity to Precipitation Data To gauge the impact of the accuracy of rainfall data sources, two different products were compared: the rainfall amounts extracted from CHIRPS and those measured in-situ by the meteorological stations at Prek Chann, by the one installed by the UNDP, and by the one at Koh Khel (cf. Section 3.3). There are several days - or even weeks - during the baseline period during which one station among the three does not provide data. For this reason, an average of locally measured data was used.

A visual representation of results is shown in Figures 6.22 and 6.23 below. It shows that the use of local precipitation products results in a higher simulated yield, especially in areas along Preks that experience water scarcity during the dry season, such as Prek Touch. Rice production increases by 23.91% in comparison to the baseline scenario that uses CHIRPS. Vegetable and fruit yield increase by 28.47% and 20.3% respectively. This indicates that the precipitation patterns calculated from local stations, with fewer precipitation events of higher intensity, weigh more heavily towards closing the irrigation water gap in the simulation than the more frequent

but lower-intensity events registered by CHIRPS.

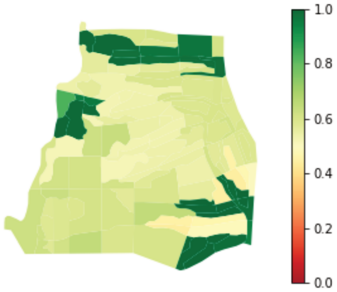

(a) Baseline scenario using CHIRPS precipitation: Calculated yield as fraction of optimal yield.

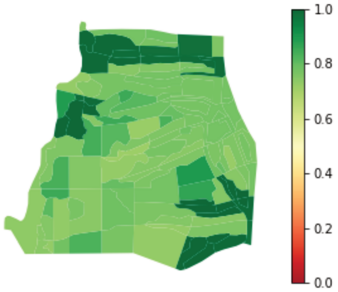

(b) Baseline scenario using local rainfall: Calculated yield as fraction of optimal yield.

Figure 6.22: Variation of calculated yield as fraction of optimal yield, depending on the precipitation product used.

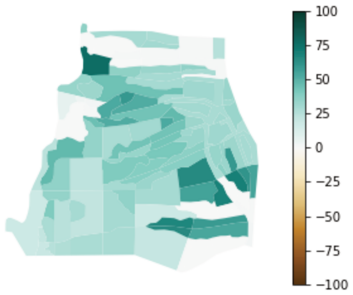

Figure 6.23: Percentage change of yield depending on the use of precipitation product.

Channel Geometry As outlined above, the geometry of channels, especially unrehabilitated ones, is based on estimates grounded in knowledge acquired during fieldwork as well as information from engineering reports. However, the impact of said estimates and how closely they represent reality needs to be assessed. For this reason, four different geometry configurations were tested in which the bed level of Preks was varied. While rehabilitated Preks (Prek Me Srok, Prek Chann, Prek Thom) remained at a bed level at 0 m asl, not rehabilitated ones were varied by -1, -0.5, +0.5 and +1 m. For this simulation, too, the average of local precipitation measurements was used.

The results of this variation are given in Figures 6.24, 6.25, and 6.26, as well as Table 6.5 below. They show that lowering the bed level of the RS by 1 m significantly increases the

yields of rice (+7.38%), vegetables (+8.32%), and fruit (+4.19%). Smaller increases can also be observed if bed levels are lowered by 0.5 m. In contrast, raising bed levels only leads to negligible yield losses. Raising them by 1 meter, for instance, only results in losses of 0.22 to 0.4% of overall yield. This is probably due to the fact that those channels that are already experiencing dry season water scarcity at their current elevation are impacted little by rising bed levels, and rehabilitated Preks would have to be raised by more than 0.5 - 1 m to significantly affect water availability.

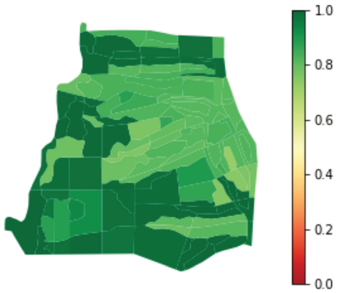

(a) RS lowered by 1 m.

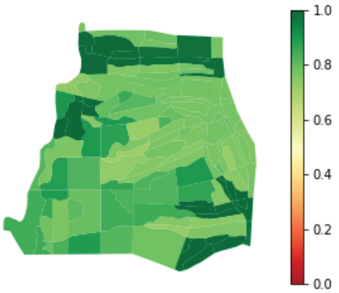

(b) RS lowered by 0.5 m.

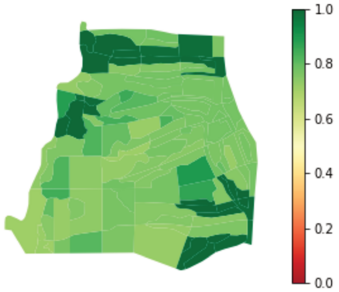

(c) RS raised by 0.5 m

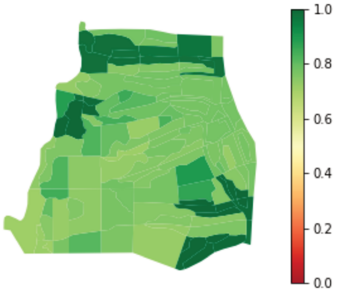

(d) RS raised by 1 m

Figure 6.24: Variation of calculated yield as fraction of optimal yield, depending on the bed level of Preks.

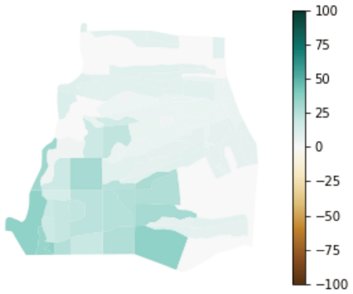

(a) RS lowered by 1 m.

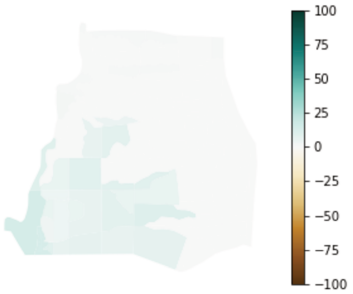

(b) RS lowered by 0.5 m.

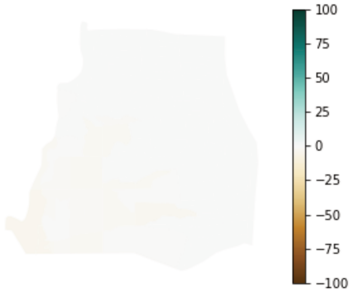

(c) RS raised by 0.5 m

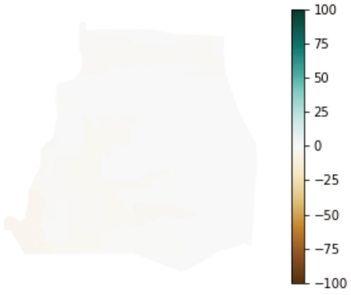

(d) RS raised by 1 m

Figure 6.25: Percentage change in comparison to the baseline using in-situ precipitation products, depending on the bed level of Preks.

	+1 m	**+ 0.5 m**	**- 0.5 m**	**-1m**
Rice	-0.4	-0.21	1.56	7.38
Vegetables	-0.49	-0.3	1.76	8.32
Fruit	-0.22	-0.01	0.42	4.19

Table 6.5: Percentage change of yield in comparison to the baseline scenario using local precipitation measurements of the three main types of crop in the case study area.

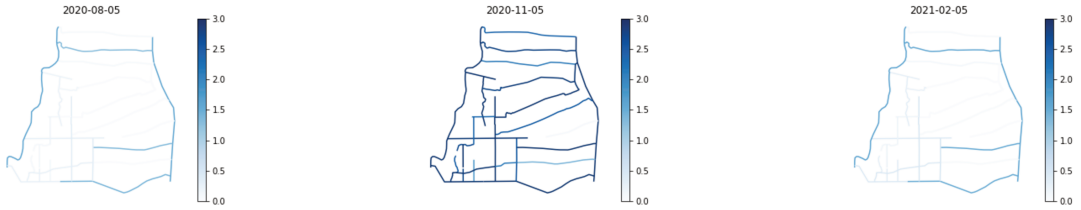

(a) RS lowered by 1 m.

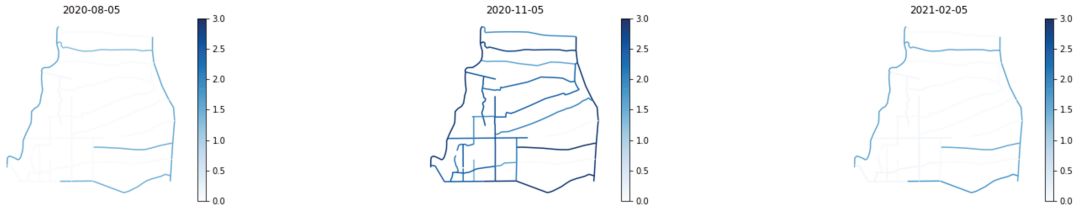

(b) RS lowered by 0.5 m.

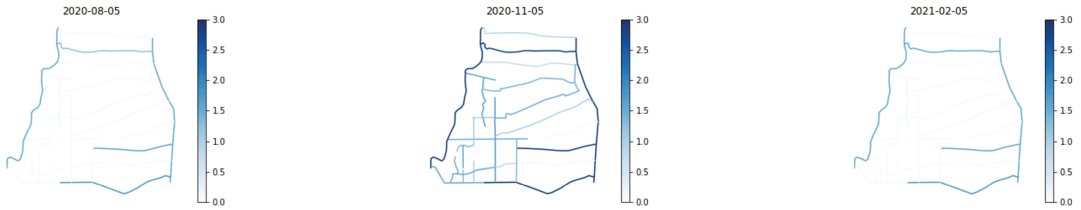

(c) RS raised by 0.5 m.

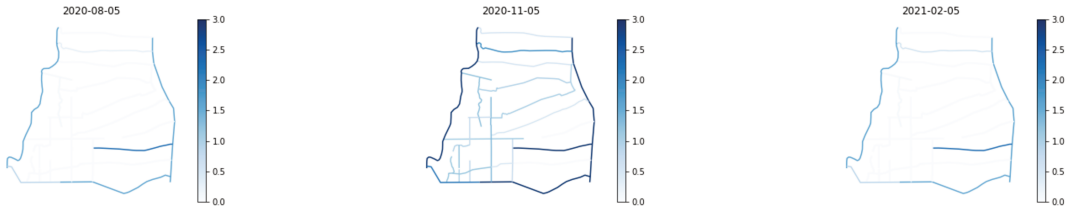

(d) RS raised by 1 m.

Figure 6.26: Variation of water level in Preks [in m above Prek bed level] depending on bed elevation.

6.4 Formalizing Future Perspectives: Defining and Simulating Possible Scenarios

As stated in the introduction to this chapter, the overall aim of this model is to quantitatively characterize the impacts of different possible scenarios for future development. First, though, these scenarios need to be outlined. Future scenarios were constructed with regard to four

parameters - temperature, precipitation, river stages, and Prek configuration. Temperature and precipitation are likely to change in the study area itself due to climate change over the coming years. River stages will evolve based on upstream factors such as the construction of hydropower plants and the variation of precipitation patterns due to climate change. The configuration of Preks, finally, might be modified through rehabilitation projects or locally organized excavations.

The change in temperatures and precipitation is taken from Supharatid et al. (2022). This study uses the 18 Coupled Model Intercomparison Project Phase 6 (CMPI6) to project the local manifestations of climate change in mainland Southeast Asia under two SSP-RCP (shared socioeconomic pathway-representative concentration pathway) scenarios: RCP 4.5 and RCP 8.5. It provides estimates for temperatures and monthly precipitation amounts in Cambodia by 2050.

Similarly, future projections for river water levels are simulated in this thesis based on Hoang et al. (2019). This study modelled the impact of climate change, hydropower, and irrigation schemes on the flow of the Mekong by the 2050s. It assumes maximum hydropower development, with all currently projected dams being in operation, as well as an expansion of irrigated areas. As for climate change, both RCP 4.5 and RCP 8.5 are modelled. The study also provides projections of flow changes at several MRC stations, including Kratie in Cambodia. In order to use these projections, a correlative link was established on a monthly basis between Kratie, Koh Khel, and the logger in the case study area. A visual comparison of the water level elevation at the three stations is provided in Figure 6.27. This follows the same procedure as described above, based on the methodology of the Lamagat method.

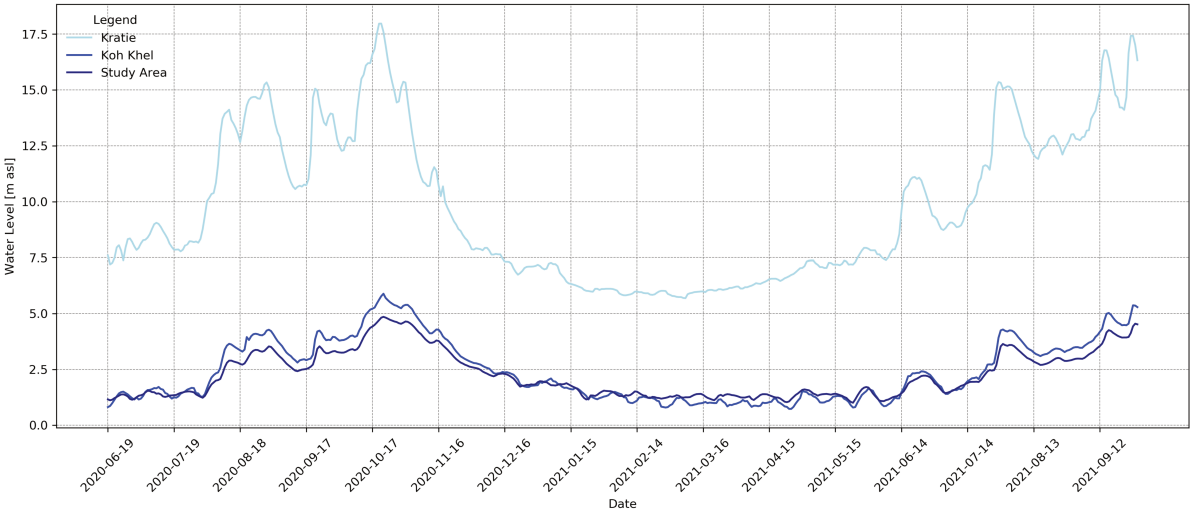

Figure 6.27: Comparison of water levels in m asl at Kratie, Koh Khel, and in the case study area in 2020-21.

One further point that must be noted is that the baseline scenario for Hoang et al. (2019) study was calculated on the basis of the time series 1971-2000. Therefore, the same period was used to calculate the water levels at Kratie to which the percentage changes listed as results in the model for mid-century projections are applied. Furthermore, the projections are for the development of discharge, not water levels at Kratie. Consequently, a rating curve was back-calculated at Kratie based on available water level and discharge measurements, and discharge projections converted to water levels before they were cast for the downstream stations. This rating curve is given in Figure 6.28. It appears that the discharge provided by the MRC is itself based on water level measurements and a rating curve, rather than direct measurements. To convert projected discharge to water levels at Kratie, a polynomial formula was derived from the rating curve:

$$wl = -8.787 * 10^{-9} * Q^2 + 0.0007 * Q + 4.0966 \tag{6.14}$$

where wl is the water level at Kratie and Q is the discharge. The R^2 value of this curve for the baseline period is 0.9951.

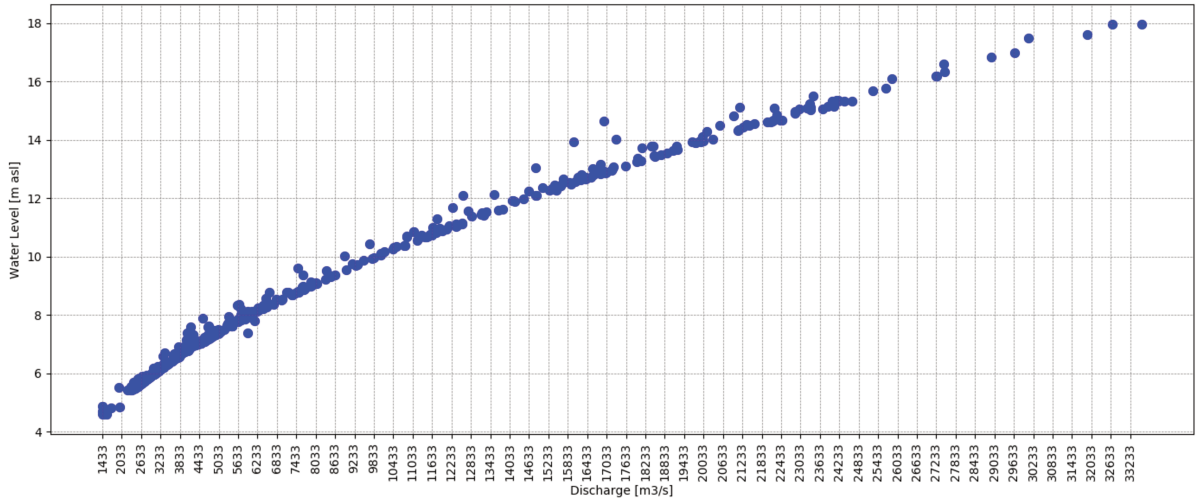

Figure 6.28: Rating curve at Kratie, showing water levels in relation to discharge.

To test the application of the rating curve, the discharge given at Kratie by the MRC for the period 2020-21 was converted to water levels using the rating curve and compared to the water levels provided by the MRC. The result shows good agreement and is given in Figure 6.29 below.

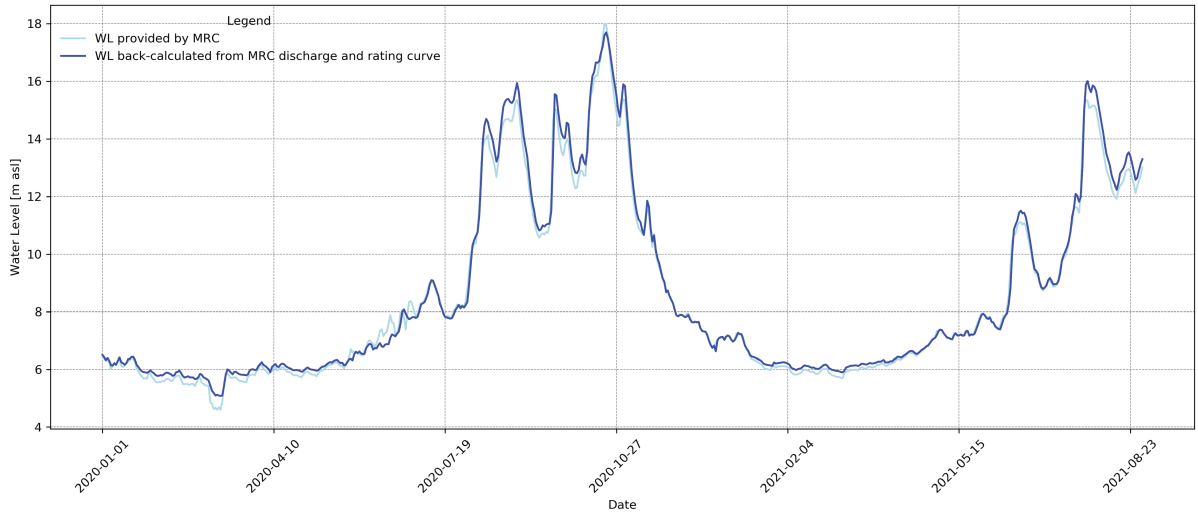

Figure 6.29: Comparison of water levels provided by the MRC and water levels back-calculated from provided discharge values on the basis of the reconstructed rating curve.

The result of this procedure to derive projections for future water levels at Koh Khel and in the case study area via Kratie is given in Figure 6.30. As can be seen, the pronounced triple-peaking pattern that is discussed in Section 3.2.3 and which is also evident in Figure 6.27 is absent in this projection. The reason for this is that the daily baseline water level was calculated on a multi-year basis using the time series between 1971 and 2000. On the one hand, this forms a

considerable limitation in terms of how realistic the simulated water levels are. On the other hand, applying the change factors provided by Hoang et al. (2019) to a more recent series, such as the water levels in 2020-21, disregards the fact that considerable hydrological shifts have taken place in the two decades since the baseline period on the basis of which they were calculated has ended.

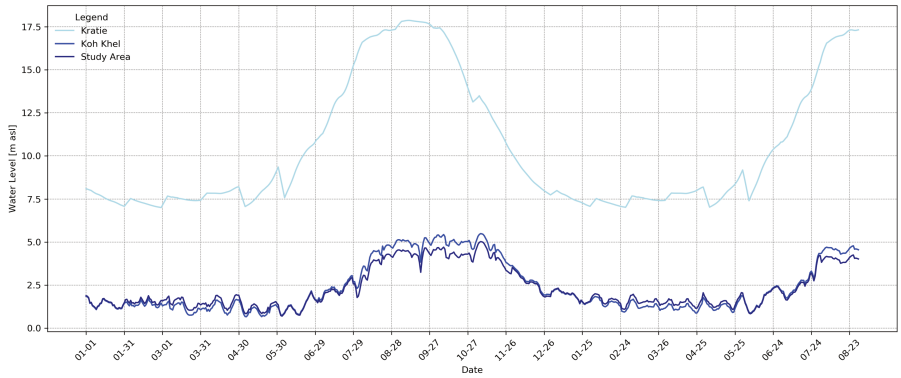

(a) Future water levels at Kratie, Koh Khel, and in the case study area according to scenario RCP 4.5.

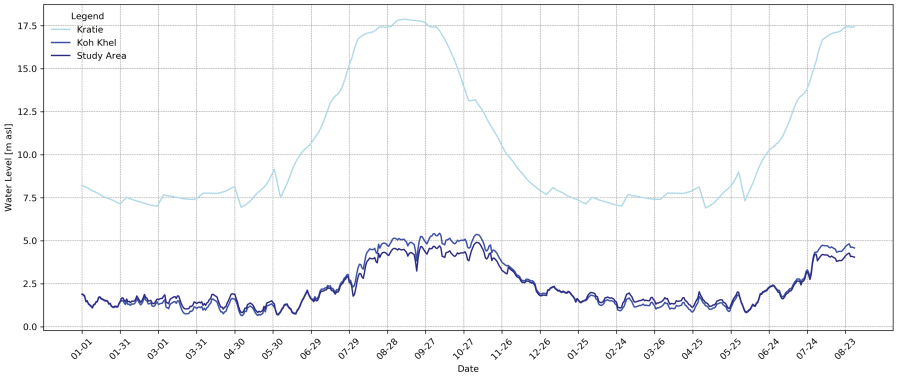

(b) Future water levels at Kratie, Koh Khel, and in the case study area according to scenario RCP 8.5.

Figure 6.30: Future water level projections according to climate change scenarios RCP 4.5 and RCP 8.5.

As Figure 6.30 shows, the two scenarios are very similar with regard to the development of water levels. Nonetheless, their comparison offers an interesting prospect, also with regard to how sensitive the model is to minor upstream water level variations.

Finally, the rehabilitation of Preks is simulated by setting the bed level of all individual Preks to 0, assuming uniform deep calibration.

In total, four scenarios are modelled in the application of the model presented in this thesis.

The precipitation, temperature and water levels projected by Supharatid et al. (2022) and Hoang et al. (2019) for 2050 under RCP 4.5 and 8.5, both with and without Prek rehabilitation. For the rehabilitation scenario, is assumed that all remaining unrehabilitated Preks are rehabilitated, with the exception of Prek Put.

Scenarios:

- **Scenario 1**: RCP 4.5, full dam and irrigation development, no rehabilitation
- **Scenario 2**: RCP 8.5, full dam and irrigation development, no rehabilitation
- **Scenario 4**: RCP 4.5, full dam and irrigation development, full rehabilitation
- **Scenario 5**: RCP 8.5, full dam and irrigation development, full rehabilitation

It has to be noted that this implementation of scenarios still leaves considerable room for refinement. For the moment, only average changes for temperatures and precipitation on a national scale were implemented, and a blanket rehabilitation of Preks - not taking into account the installation of gates or the different types of rehabilitation projects - was assumed. In reality, far more nuanced scenarios ought to be considered, with variations in upstream dam and irrigation development, as well as the number of Preks rehabilitated and the type of rehabilitation. Furthermore, the scenario data used was taken from only two relatively recent studies, rather than compared between different ones at different scales. All of these aspects could be improved still in the further development of the model. The results presented below are therefore initial projections to give an idea of both future development and model capabilities.

6.5 Results and Discussion: Different Scenario Impacts on the Prek System and the Ecosystem Services it Provides

The results of the calculation of not-flood related ecosystem services are shown in Figures 6.31 and 6.32 as well as Table 6.6 below. They show that, without rehabilitation, conditions in 2050 would result in consistent yield reductions, both under Scenario 1 and 2. Both scenarios are similar with regard to the magnitude of yield reductions - between 1% and just over 16%, with

Scenario 2 resulting in slightly higher losses. In terms of the spatial distribution of losses, many of them occur in Boeung areas. This is partly due to canals falling dry and partly due to the fact that areas on which cultivation would have begun already in the 2020 baseline scenario may be flooded still, as the flood peak occurs later in the projected wet season flow. Furthermore, higher temperatures and ET values require additional irrigation amounts to compensate and it is possible that the irrigation schedule constructed on the basis of farmer information in 2020 cannot cover these addition needs.

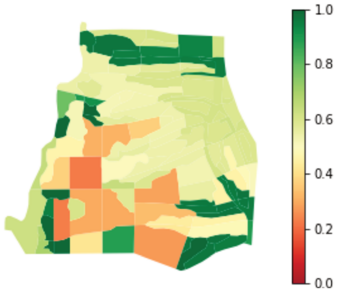

(a) Calculated yield as fraction of optimal yield: Scenario 1

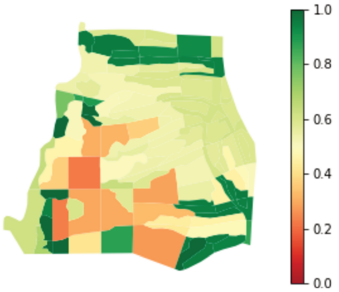

(b) Calculated yield as fraction of optimal yield: Scenario 2

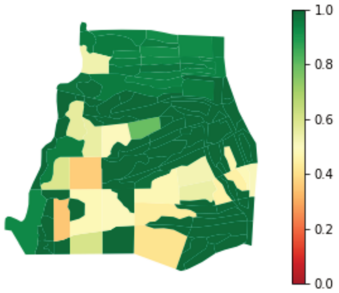

(c) Calculated yield as fraction of optimal yield: Scenario 3

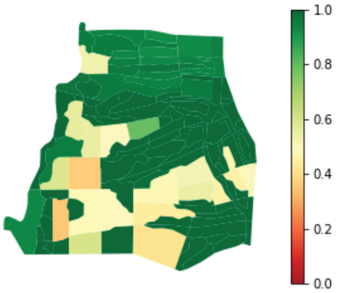

(d) Calculated yield as fraction of optimal yield: Scenario 4

Figure 6.31: Calculated yield as fraction of optimal yield: Scenarios, 1, 2, 3, and 4.

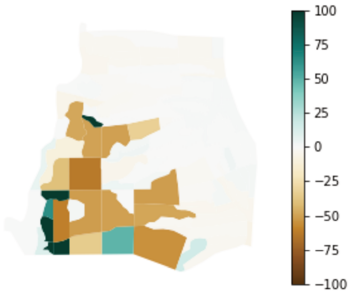

(a) Percentage change in comparison to baseline scenario: Scenario 1

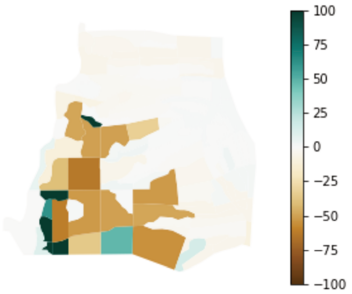

(b) Percentage change in comparison to baseline scenario: Scenario 2

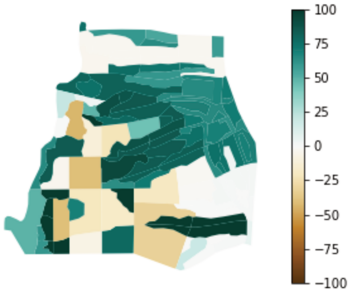

(c) Percentage change in comparison to baseline scenario: Scenario 3

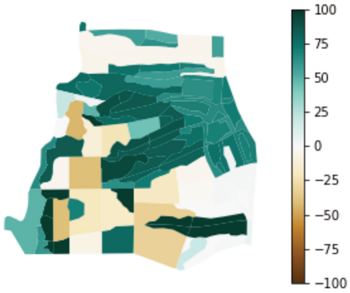

(d) Percentage change in comparison to baseline scenario: Scenario 4

Figure 6.32: Percentage change of yield in comparison to the baseline scenario.

	Scenario 1	**Scenario 2**	**Scenario 3**	**Scenario 4**
Rice	-15.63	-16.27	30.62	30.40
Fruit	-1.27	-2.12	28.71	27.80
Vegetables	-11.48	-12.31	42.53	42.03

Table 6.6: Percentage change of yield in the main crops in the case study area in comparison to the baseline scenario.

In contrast, Scenarios 3 and 4, for which rehabilitation was implemented on all Preks, show that considerable increases in yields are possible under future conditions. In areas such as those bordering on the already rehabilitated Prek Me Srok and Prek Chann, little change is noticeable. However, areas which experienced water scarcity due to a lack of inflow from the Bassac can now fully benefit from dry season water availability, partially also due to the higher dry season water levels in the projected future flows. One aspect that must be noted in particular is that even while Chamkar areas prosper, some Boeung areas still see losses in comparison to the baseline

scenario. This is likely due to the shift in the flood peak, which is discussed below, and the fact that the LULC properties in the model are, as of now, static. This limitation is discussed in detail in the next section.

With regard to flood-related ecosystem services, it emerges that the flood in the scenarios projected on the basis of data collected between 1971 and 2000 is still more extensive than the flood observed in 2020-21. As shown in Table 6.7, the maximum water level would increase from 5.89 to 6.35 m, and it would occur later - in early November. Furthermore, both average and maximum inundation extents would increase - by 7.57% and 17.98% respectively in Scenario 1 and by 8.01% and 16.85% respectively in Scenario 2. As can be seen in Figure 6.33, the maximum flood extents are very similar, with RCP 4.5 having slightly more inundated areas in the Western part of the case study area. Similarly, the maximum volume retained would increase considerably, by 40.80% and 35.15% in either scenario. In contrast, the amount of groundwater recharge increases only slightly (by 7.57% and 8.01% respectively) and neither scenario results in water levels high enough to result in pest regulation. Sediment deposition even decreases slightly, from 16.52 kg/m^2 to 13.23 kg/m^2 and 13.64 kg/m^2 respectively. This is due to the relationship between overall flood duration and the average flooded area.

	Baseline (2020-21	Scenario 1		Scenario 2	
		Absolute	Percentage Change	Absolute	Percentage Change
maximum water level [m asl]	5.89	6.35	7.81	6.26	6.28
date of maximum water level	2020-10-22	2050-11-04	-	2050-11-04	-
groundwater recharge [m^2]	16758459	18026648	7.57	18101643	8.01
pest regulation	No	No	-	No	-
maximum inundation extents [km^2]	11.49	13.56	17.98	13.43	16.85
average inundation extents [km^2]	6.08	6.54	7.57	6.57	8.01
maximum volume retained [m^2	659737918340	928889585910	40.80	891609833703	35.15
average inundation depth [m]	0.67	0.76	13.43	0.74	10.45
sediment deposition [kg/m^2]	16.42	13.23	-19.43	13.64	-16.93

Table 6.7: Results of simulation of flood-related ecosystem services for Scenario 1 and 2.

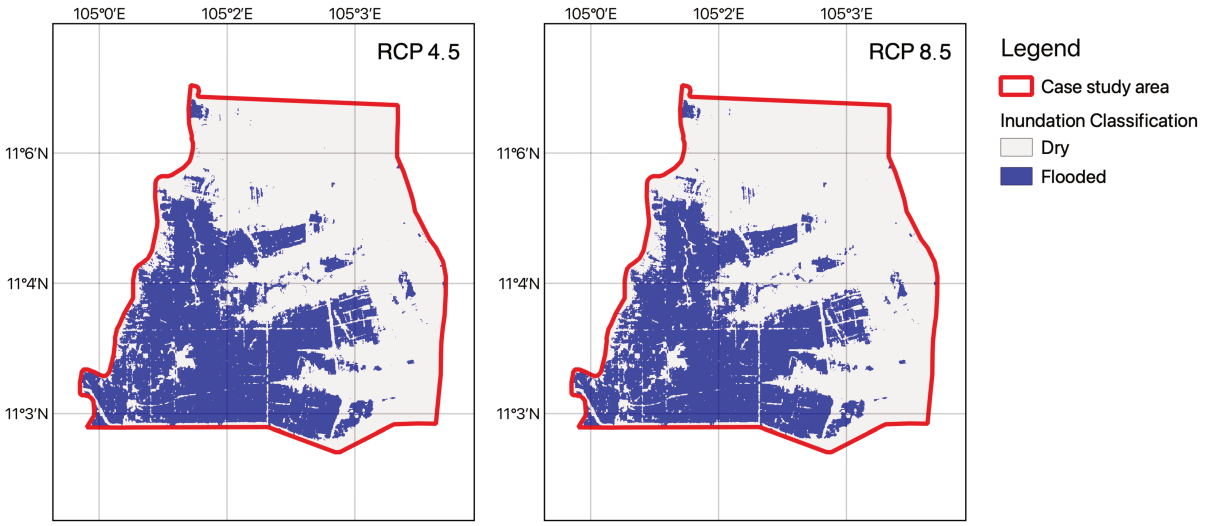

Figure 6.33: Maximum inundation extents for each climate change scenario.

Overall, it can be noted that not flood-related ecosystem services would see a considerable decrease by 2050 in the Scenarios where no rehabilitation is implemented, while blanket rehabilitation would allow an increase in yields of rice, fruit, and vegetables. Flood-related ecosystem services, in contrast, would increase, save for pest regulation and average sediment deposition. The flood peak would be slightly higher but later. However, there are several limitations to the current modelling approach, which are discussed in detail below.

6.6 Limitations and Possibilities for Further Model Development

The model in its current form aims to serve as a prototype, rather than a finished product. There are still multiple areas in which it could substantially benefit from refinement and more detailed input information. Some of them are conceptual in nature, others arise from the fact that processes could not be accounted for in the model due to a lack of knowledge, and some originate from a paucity of reliable data.

To begin with, as sensitivity testing has shown, the de facto bed elevation of the Preks and lowland canals has a significant effect on the calculation of flow and thus the available water

volumes for irrigation. Yet the elevation used in the simulation for not rehabilitated canals is a mere estimation, based on qualitative observations during fieldwork as well as on engineering reports using data from other Preks in the wider region. Topographic surveys along the length of several Preks - for instance during the dry season when they are devoid of water - could greatly improve the accuracy of simulations for not rehabilitated scenarios.

Similarly, the lack of detailed knowledge on soil and subsurface properties, especially infiltration coefficients, porosity values, and the presence and depth of aquitards, poses a substantial limitation with regard to the simulation. Not only does it limit the accuracy of infiltration estimates - and thus the availability of water for evapotranspiration from the soil storage term - it also obscures possible groundwater interactions to the point where it became unfeasible to include them in this prototype model. A distributed soil survey across the case study area as well as soil cores could provide these key pieces of information and clarify at which order of magnitude the subsurface system operates. As mentioned above, there are some indications, for instance, that excess irrigation water filtrates back to the Prek during extensive dry-season irrigation. Yet this is hardly reflected in the groundwater storage term in the current model. Once information on soil and subsurface properties becomes available, adding a simulation module to represent filtration processes in Chamkar areas would become possible.

Another aspect that has been neglected so far and that imposes limitations is surface storage and flow. With the current assumed infiltration properties, the surface storage term has shown that the amounts that fail to infiltrate on a daily basis during the dry season are comparatively small. However, field observation indicate that there is some exchange between individual plots. Since the SUs that serve as the basis for this model comprise multiple plots, this effect is somewhat dampened, as a lot of the water that is transferred between plots through surface runoff may still stay within the same SU. Without doubt, though, some exchange occurs between the areas delineated SUs in reality. Once the soil properties are better-known and the infiltration rates can thus be calculated with a greater degree of certainty, it would be advisable to take surface flow processes into account.

Furthermore, more sensitivity testing ought to be carried out with regard to the spatial configuration of simulation units, both surface units and reach segments. Currently, the model is based on a delineation grounded in knowledge acquired during fieldwork. However, it is

likely that the subdivision of reach segments, for instance, leads to uncertainties, especially when segments are relatively short. The reason for this is that flow is currently calculated at a daily time step. For example, reach segment 16 is a mere 0.5 km in length and, as a lowland canal, fairly shallow. If it is used as an irrigation source, it is possible that the entire volume in the segment is used up in a single calculation time step and a lack of water registered. In reality, however, water would flow into this segment from neighbouring, larger segments, at the same time as farmers' pumps extract it, thus preventing the channel from falling dry. Simultaneously, however, a limitation is also imposed by not dividing longer RS into multiple units. This is clearly illustrated by the validation data at Prek Chann, which shows the water level slope between the head of the Prek and its tail. Furthermore, field observations have shown that even individual pumping activities in one part of the Preks can influence its flow direction during the height of the dry season. During the same period, some villages have erected temporary earthen dams across their Preks to concentrate what little water is available in one of its sections. This is not to mention the gate that currently exists at Prek Chann and which regulates in- and outflow during some months of the year. All of these complexities have been neglected so far. For future simulations, it would be beneficial to further subdivide RS, to take account of inhomogeneities along their lengths as well as of water level slopes. At the same time, the time step of the flow calculation would have to be downscaled to avoid the unrealistic emptying of shorter segments.

Next, a considerable limitation of the current model is that it is solely based on the LULC dynamics of the 2020-2021 season. While grounded in extensively tested remote sensing analyses using field data as input, the classification used to characterize areas is nonetheless static. That means that currently, future farmer decisions with regard to planting different crops at different times of the year depending on hydrological framework conditions varying between scenarios are not taken into consideration. Instead, it is assumed that the monthly crop distribution remains static. It is known from interviews that this is not the case, and that there are already some plans by farmers to switch away from the cultivation of mango, for instance, in the medium term. On a smaller temporal scale, farmers unquestionably adjust cultivation practices - planting and harvesting earlier or later - depending on the hydrological situation in the area. This means the spatial distribution of the crops doesn't stay the same. Such decisions too are currently not represented. For instance, rice planting on low-lying units would commence later if floods retreat later in future scenarios. However, since these areas are registered as flooded in the 2020-21

LULC classification, these delayed crops cannot be represented. This model configuration thus precludes the modelling of LULC responses to future scenarios. To address this issue, it might be feasible to add a LULC decision model. Using information from the surveys and the 2020-21 LULC categorization, it could identify cultivation pathways and decision and timing factors. Furthermore, larger economic considerations could also be taken into account. For the moment it is assumed that water availability is the only constraint farmers in the region face. However, the availability of pesticides and fertilizers, as well as labour force also play crucial roles in the calculation of overall yield.

A further aspect that represents a major limitation of the model in its current form is the simplistic estimation of flooded areas on the basis of WAFL. While it serves as a quick and efficient means of calculation and has been shown to represent reality with an acceptable degree of accuracy, it still comes with considerable caveats. For one thing, it is a black box model with regard to the flow processes in the floodplain, which engenders uncertainty with regard to processes such as sediment deposition.[5] Crucially, however, the WAFL fails to take into account the influence of Prek rehabilitation on inundation processes. By default, this method assumes that the hydraulic link between a river and its floodplains remains relatively static. However, Prek rehabilitation alters that very link. So far, it has been assumed that the rehabilitation of one or two Preks has a negligible impact on this link. To a certain extent, this is supported by the validation procedure WAFL was subjected to (cf. Section 3.4.3). Among others, the comparison with inundation maps based on historical Landsat images showed a fairly good match, even though no Preks were rehabilitated at the time that these images were taken, and two were rehabilitated during the period that WAFL is based on. Nonetheless, it is extremely likely that the blanket rehabilitation of Preks in the case study area would modify this link to the point where WAFL estimates are no longer accurate. Furthermore, in the current model, the impact of outflow from the Boeung areas to the Bassac on Prek water levels is also neglected due to the use of WAFL. It is assumed that since this occurs at the end of the wet season, when river water levels are still fairly, high, sufficient water is still available in Preks to meet irrigation requirements and the exact contribution from outflow is therefore relatively negligible. However, these issues cold be addressed by refining the calculation of inundations by employing a more

[5]When it comes to sediment deposition, it would also be beneficial to install sediment traps at a few points in the floodplain to provide validation data for deposition processes. Hung et al. (2014) carried out such measurements in the Vietnamese delta, but as has been noted, sedimentation is likely to be higher on the Cambodian floodplains due to a lack of regulation infrastructure.

complex, dedicated flow model, such as Delft3D or LISFLOOD. The challenge of using these models, and the principal reason why they have not been implemented so far, are their extensive parametrization requirements. Especially terrain characteristics such as small-scale dykes would necessitate intensive calibration before reliable results could be produced.[6]

Another simplification that poses constraints on the validity of the current model are the assumptions with regard to sedimentation. For one thing, the spatial distribution of sedimentation is being neglected - instead sediment concentrations in the inundated floodplains are assumed to be the same as in the river mainstream. In future versions of the model, a statistical relationship could be established to account for the known discrepancies between these concentrations. Furthermore, if an advanced flow model were to be used, it would also be possible to calculate parameters such as shear stress in the floodplain to calculate resuspension rather than having to estimate it as a fraction of deposition on the basis of previous studies.

Another aspect that must be highlighted with regard to model limitations and uncertainty is the construction of scenarios, specifically future water level projections. As outlined above, the water level scenarios used in this analysis are based on a single study by Hoang et al. (2019), which provides estimates only for an upstream station at Kratie, which are further based on the period 1971-2000. Applying this scenario and transferring it to the water levels in the case study area resulted in a loss of the typical multi-peaking pattern observed in the area, likely because the multi-year average of daily water levels was used, rather than one particular year. In addition, the future water levels projected in the scenarios on the basis of this data were already exceeded by the water levels observed in recent years. They are therefore to be taken with a measure of scepticisim and refined when possible. Furthermore, there were doubts pertaining to the data provided by the MRC, specifically to issues such as gauge elevation and changes in the rating curve. When a rating curve was constructed using the full series of water levels and discharge measurements given at Kratie, for instance, the back-calculation of discharge yielded unrealistic results. For future model applications, a greater number of scenarios ought to be compared, taking into account projections that allow for the conservation of typical local flow patterns. Furthermore, factors such as projected changes in sediment concentration, and different rehabilitation scenarios (deep vs. shallow calibration, number of Preks to be rehabilitated etc.)

[6]Unfortunately, topographic data are required at a vertical resolution and accuracy which are not currently available. Future satellite missions may partially solve this lack of information,but it is likely that small interventions by farmers, such as building small dykes to retain water, would affect the flow distribution.

should be taken into account.

Finally, there are several limitations that must be noted with regard to the conceptual complexity of the model. Several aspects of local water management that are well-known from the results of the field work have been neglected, such as the practice of double-pumping, building temporary dams across Preks, and gate operation at Prek Chann. If a RS network with more sub-segments were to be delineated, these processes could be taken into consideration - provided, of course that sufficient information is available on their temporal dynamics. Alternatively, it could be envisioned to represent these aspects through an agent-based decision model. For instance, a condition could be added that double-pumping at non-rehabilitated Preks becomes feasible once a certain percentage of SUs along the Prek is experiencing acute water stress.

6.7 Conclusion: Deriving a Systematic Understanding and Possible Future Outlooks from Numerical Modelling

This chapter has outlined a numerical modelling approach towards representing flood-related and not-flood-related ecosystem services in the case study area. Based on the insights gained and data collected during field work, as well as on remote sensing analysis and literature values, a workflow was constructed to allow the simulation of future scenarios with regard to shifts in precipitation and temperatures, water level, and the rehabilitation of Preks.

The results have shown that under the future scenarios simulated, not-flood-related ecosystem services would decline by 2050, with yields of rice, fruit, and vegetables decreasing by up to 16% with the current Prek configuration. If blanket rehabilitation were to be implemented, in contrast, they would increase by up to 43%. Under the simulated water levels, flood-related ecosystem services would increase, with higher inundation extents, retention volumes, and and groundwater recharge. Only average sediment deposition would decrease, and pest regulation would remain the same as in the baseline scenario - lacking due to insufficiently high water levels.

However, the process of model construction, validation, and sensitivity testing has also highlighted a number of issues with the current setup that remain to be resolved. First, there are the uncertainties resulting from a lack of data in the study area related to factors such as soil

properties and the elevation of channel beds, as well as the fact that surface flows between units and subsurface flows were neglected. Furthermore, there are the limitations imposed by using the LULC characteristics from the 2020-2021 season as a baseline for yield calculation, as well as the use of WAFL as a blackbox model for flood calculation. Another issue is the data used for the construction of scenarios. The water levels for future scenarios, for instance, don't account for the regionally typical multi-peaking pattern, since they are based on a multi-year average. In addition, the baseline period on which are used to calculate future water levels lies several years in the past, calling into question the accuracy of simulations.

Overall, it can be summarized that the model outlined above presents a promising prototype to be refined further as information becomes available and scenarios are more clearly constructed.

7

Conclusion, Discussion, Perspectives

The Cambodian Mekong delta is a unique area in terms of hydrological processes and agro-ecosystems. Distinct from its Vietnamese counterpart through a lack of hydraulic infrastructure, it is a focal point for cascading effects of upstream developments, yet also one of the most productive areas in Southeast Asia in terms of agriculture and fisheries. Yet it has also offered a gateway towards exploring more universal processes, shared by deltaic areas worldwide, developing transferable methods, and drawing more generic conclusions.

This thesis has sought to explore the link between ecosystem services and hydrological processes, to explore the impact of large-scale changes and their translation to the regional level, as well as to examine how canal networks can be used to respond to these changes at a local level. In particular, it has aimed to elucidate the role of the Prek channels, which are characteristic for the Cambodian Mekong delta. Taking one case study area just North of the border to Vietnam as their focus, the analyses outlined in this thesis have attempted to shed light on the complex

set of ecosystem services from which the local population benefits, as well as their connection to Prek channels and large-scale hydrological processes. Finally, this thesis laid the foundation for estimating the impact of future projected developments on local hydrological processes and ecosystem services. Through these analyses, it has become possible to answer the research questions first outlined in the introduction.

What are the current patterns of regional hydrological dynamics at the scale of the Cambodian upper Mekong delta, and which trends have manifested themselves over the past three decades? In terms of the hydrological dynamics at the scale of the Cambodian upper Mekong delta, three components have been considered - water levels in the Mekong and the Bassac, precipitation over the area, and inundation extents and dynamics. They were analyzed over two large zones of interest - one on the right bank of the Bassac and one bracketed by the Bassac and the Mekong.

A statistical analysis identified the year 2008 as a hydrological break point in the water level series of the past thirty years, provided at four stations maintained by the Mekong River Commission (MRC). Overall, the annual monsoon floods have been found to arrive later and recede sooner, amounting to shorter durations and sharper peaks in water levels. Furthermore, a comparison of both daily and near-realtime measurements taken at stations along the Bassac between Phnom Penh and Chau Doc has highlighted typical bi-daily and bi-monthly water level variations linked to tides and moon phases, as well as a characteristic pattern of multiple flood peaks during the wet season, which might be related to hydraulic thresholds for floodplain connections and upstream processes such as the reverse flow into the Tonle Sap Lake.

A comparison of precipitation data, measured locally at three in-situ stations and estimated through remote sensing products in the form of CHIRPS has revealed that remotely sensed data typically overestimates frequent low-intensity rainfall events and underestimates high-intensity events. However, an inter-station comparison showed that considerable heterogeneity also exists between in-situ stations and that CHIRPS is still valuable due to the consistent long-term data it provides. A trend (and break point) analysis on the CHIRPS data for the region did not yield any significant break points in the precipitation time series. It also did not reveal many significant trends in long-term precipitation. A decadal comparison of monthly rainfall sums has shown

that precipitation amounts in September and October were slightly higher in the 2010s than in previous decades. The only statistically significant trend, however, is the increase in precipitation in December.

A final element of the analysis of hydrological processes at regional scales has been the development of a methodology to construct a novel water level - flood link (termed WAFL), in order to re-construct past inundation extents and assess long-term changes in the spatial pattern and timing of monsoon floods. By linking locally measured water levels to inundation maps derived from Sentinel-1 and 2 images taken between 2017 and 2020, a foundation was established on the basis of which inundation extents can be estimated using historical water levels. The robustness of this approach has been assessed using the TanDEM-X 12 m elevation model and inundation maps as well as LULC classifications derived from historical Landsat-5 and -8 images. Overall, this approach showed that WAFL is capable of estimating inundation extents with overall accuracies of 87% to 93% in comparison to historical inundation maps. It also revealed that the incidence of inundations has decreased sharply in the early traditional wet season in July and the first half of August (at an average of -21%) and that the average duration of inundations has decreased by 19 days in comparison to the pre-2008 period.

How are regional and local hydrological processes being affected by reported basin- and delta-wide changes? A comparison of the results obtained at the scale of the Cambodian Mekong Delta with insights derived from a literature review show that basin-wide trends brought about by the extensive development of hydropower infrastructure, climate change, and land use change are reflected closely in the regional and local water level dynamics.

The hydrological break point identified in the Cambodian Mekong delta in the year 2008, for instance, mirrored the results of large-scale studies. Yun et al. (2020) examined the impact of both climate change and hydropower development on the entirety of the Mekong basin, including its Chinese part and attained the break point of 2008 through a Mann-Kendall test at Yun Jing Hong station in China. Han et al. (2019), focusing on the impacts of climate change and human activities on the flow regime of the Lancang, found the same break point for the same station and noted that this corresponding to the interception of river flow by the Nuozhadu reservoir, the largest to be constructed on the river at that time. Li et al. (2017), investigating flow changes

across the entire Mekong basin detected a slightly later change point in 2009 at Chiang Saen station in Northern Thailand, near the border to Myanmar and Laos, also using the Mann-Kendall test.

Furthermore, the trends towards shorter food durations and sharper flood peaks have also been evidenced in studies conducted at larger scales. In a review of the impact of dams on the Mekong's hydrology, Hecht et al. (2018) noted the reduction of the annual flood pulse as one of the main negative effects, especially in terms of floodplain ecology and fisheries. Similarly, Pokhrel et al. (2018) found that the annual flood pulse in the lower basin would be dampened by 50% and delayed by one month. This is also echoed by Chua et al. (2022), who found the duration of the flood season to have decreased by 26 days at Kampong Cham and by 40 days at Phnom Penh due to a later start and an earlier end.

The attribution of the causes of these changes is tilted towards hydropower infrastructure having larger impacts than other drivers, such as land use change or climate change. Binh et al. (2020), for instance, found that the relative impact of infrastructure outweighs that of climate change in their study of long-term alterations in the Mekong's flow regime adaptation resulting possible strategies for the Vietnamese part of the delta. Similarly, Shin et al. (2020) found that historically, it was climate variability that governed variations in surface water dynamics in the Mekong basin. Since 2009, however, the authors find that the impacts of dams have increased steadily in their influence and have come to dominate.

What are the roles that Preks play in catalyzing these processes at the local level? At the local level of the case study area, the Preks' primary role in catalyzing hydrological processes is to act as a vector of flooding and drainage during the wet season, though the extent to which they can fulfill this functionality depends on their rehabilitation status to a large degree. At the beginning of the flood season, when river water levels rise, Preks begin to flood as soon as water levels in the Bassac exceed the bed elevation at the head of the Preks. Frequently, this head elevation is higher than in other parts of the Prek, as the head is a hotspot for sedimentation. Consequently, threshold effects are observable and focused excavations are sometimes organized by communities, such as at Prek Nou. During the flood rise, Preks serve as conduits for water from the Bassac towards the floodplains in the Boeung areas. This dynamic inverses once the

flood peak has passed. Then, water drains through the Preks back into the river mainstream.

Another component of the system the importance of which must not be underestimated, though, is the network of smaller lowland canals in the Boeung at the tail end of the Preks, which was constructed during the Khmer Rouge regime. It appears that the bed elevation of these canals is often lower than that of Preks, especially non-rehabilitated ones. Consequently, they can serve as a vector for both flooding and drainage even when Preks have fallen dry. For instance, it can be observed that at the tail end of some non-rehabilitated Preks, inundations actually begin before the Prek itself is flooded, as water is transported through rehabilitated Preks, such as Prek Chann, and then flows north and south through the canal network before overspilling the banks of the canals. Similarly, at the end of the wet season, water continues to drain through the canals - especially towards the South - even after not-rehabilitated Preks have fallen dry.

Finally, it must be noted that the role of the Preks during the dry season in terms of hydrology differs considerably from its role during the wet season. In the months between November and June, the Preks' main functionality is no longer as a conduit of water, but rather as a reservoir from which anthropogenic flows originate. Farmers pump Prek water onto their fields to irrigate their crops, thereby creating a steady flow of water from the Prek "reservoir" onto the surrounding surface areas. This, in turn, contributes to surface runoff, infiltration, and evapotranspiration flows.

The role of Preks for sub-surface flows is harder to estimate due to a lack of data. As noted in Chapter 6, it can be conjectured that during the wet season, when water levels in the Preks are typically high, an influent situation dominates, with Prek water infiltrating into the surrounding banks and Chamkar areas. After the flood, this situation reverses into an effluent one, with water that was stored in the banks exfiltrating back into the Prek. To some extent, this is evidenced by bank collapses, which appear to be partially due to high soil water pressure. Furthermore, there is some evidence that water infiltrating from irrigation during the dry season filtrates back to the Prek. At some rehabilitated Preks, it appears that the Prek is even in direct connection with the groundwater table.

What are the ecosystem services from which people in the Prek area benefit? How are these linked to hydrological processes? Broadly, the ecosystem services from which people

benefit in the area can be delineated into flood-related and not-flood related ones. Flood-related ecosystem services are largely of a regulating nature. The annual monsoon inundations, catalyzed by the Preks, deposit valuable nutrient-laden sediments on the plots in the Boeung area. Further, they recharge soil- and groundwater, providing a basis for recession rice cultivation. During the wet season, floods provide valuable shallow-water habitats on the floodplains in which populations of fish, which form an integral part of the local diet, can regenerate. Another regulating service that can be felt immediately by the population in the area is the regulation of pests. Rat populations especially are reduced provided that the flood level is high enough for a sufficient duration. On a larger scale, inundations in the Cambodian Mekong delta also provides flood attenuation, though it is downstream communities who benefit from this regulating service.

In terms of not-flood-related ecosystem services, the Preks serve as valuable sources of water. Primarily, this water is used for irrigation, but several people interviewed in the case study area also use it to water their cattle and for non-dietary household needs. Furthermore, it is a common practice to fish in the Preks - though catches have declined recently - and to collect natural vegetation along their lengths, which is then used for food, fuel, or, in some cases, medicinal purposes. At non-rehabilitated Preks, where no regulations to the contrary exist, people also plant fruit and vegetables on the banks of the Prek and use the branches of the trees that grow along their banks as construction material and for fish traps. While there is water in the Prek, locals further use them as routes for transport, though this practice seems to be in decline, particularly at rehabilitated Preks, where better roads were constructed on the banks.

How will future developments and trends impact hydrology in the Prek area, and in consequence, the ecosystem services to which it is linked? What measures can be taken to mitigate or prevent negative impacts? The regional hydrological analysis and the newly constructed model for not-flood-related and flood-related ecosystem services in the case study area have shown that river water levels are the principal driver of inundations in the area. Flood-related ecosystem services are thus largely dependent on upstream developments, including climate change-induced shifts in precipitation patterns over the Mekong basin, and hydropower development on the Mekong mainstream and its tributaries. Going by the overall consensus in the literature (Hoang et al., 2016; Yun et al., 2020; Binh et al., 2020), which points towards shorter floods, and lower flood peaks, flood-related ecosystem services would thus be set to

decline. In contrast, this was not reflected in the modelled scenarios, as they use projections from a study by Hoang et al. (2019), which are based on the average of the pre-2000 period in Kratie. This further illustrates the importance of reliable upstream projections - and the comparison of different projections - when estimating future flood-related ecosystem services in the Prek area.

In contrast, the availability of water in the Preks during the dry season and thus the provision of the majority of not-flood-related ecosystem services is dependent on two factors: river water levels and the bed elevation of Preks and canals, which governs when natural inflow from the river becomes possible. Most future projections (Hoang et al., 2019; Hecht et al., 2018; Yun et al., 2020) see an increase in dry season flows due to the impact of both climate change and hydropower development. However, the simulations carried out using the eco-hydrological model developed in the course of this thesis show that they would still be too low to provide sufficient inflow of water into the Preks at their current bed level to fulfill water needs, especially in combination with climate change drivers over the case study area. However, the model also shows that rehabilitation is an effective counter-measure to these developments. Lowering the bed level of the Preks ensures inflow and thus water provisioning services. Consequently, agricultural production increases in the modelled scenarios in which Prek levels were lowered, despite other negative drivers.

Possibilities for Further Development While the methods presented in the course of this thesis have largely succeeded in answering the research questions outlined at the beginning of this thesis, there are several possibilities for further improvement.

Most fundamentally, the methods could be refined if more detailed information about the case study area became available. As outlined above, only a limited amount of information available in the case study area. Part of this is due to the fact that fieldwork was cut short, for instance with regard to the number of interviews that could be conducted. In part, it is also because only little information on aspects such as soil properties and subsurface configurations could be collected so far. Similarly, the training dataset for the LULC classification was limited for the same reason. The data that does exist from secondary sources had to be scrutinized carefully. For instance, while the MRC data was invaluable in the course of its thesis, it was also a source of uncertainty since metadata was unavailable and aspects such as gauge elevation and rating curve changes

over the course of the time series remained opaque.

Furthermore, the current setup of the numerical model presented in the last chapter of this thesis is, as emphasized, a prototype with room for improvement in multiple ways - from refining scenarios and inundation calculation to adding modules for subsurface and overland flow. Its use of LULC and cropping data from the 2020-21 season further limits its flexibility with regard to future developments, and especially the responses of the local communities to these developments. Similarly, the WAFL only offers a limited capability for estimating inundation extents for future scenarios and thus flood-related ecosystem services, contingent on the static nature of river-floodplain connections. While developed at a regional scale, it proved to apply well at a finer scale, due, in large part, to the resolution of Sentinel products. However, its application at finer scales could be refined through adapted delay times according to the distance of pixels to the reference gauge.

Other studies conducted in the Cambodian Mekong delta have faced similar limitations and issues, even though many of them were conducted at a larger scale. Horton et al. (2022), for instance, used MIKE-11, a 1D flood propagation model, and IWRM-Sub, a 2D flood duration and extent model to assess the impacts of future development scenarios on the Cambodian Mekong delta. However, this study used the digital elevation model derived from the Shuttle Radar Topography Mission (SRTM), which is of limited use in the case study area due to the fact that its data was recorded prior to 2009, it has a limited accuracy in particularly flat areas, and its 90 m resolution would not be enough to represent the low terrain gradients and small-scale topography features in the case study area. Possible alternatives are the use of TanDEM-X (12m), though this has also been shown to have limitations in the course of this thesis, as well as the error-reduced version of SRTM - Multi-Error-Removed-Improved-Terrain (MERIT) DEM (cf. Hawker et al. (2019)). With more accurate DEM information, the use of models that use the full St. Venant's equations - such as Delft3D, MIKE21, and LISFLOOD - could be envisioned in the case study area. However, even then the sheer number of connections to be represented would make these models difficult to parametrize. To this end, data assimilation from remote sensing and airborne data acquistion could be explored.

Finally, there are aspects of large-scale developments that have not yet been taken into account conceptually, such as the impact of sea level rise and sediment starvation. These current

shortcomings offer avenues towards possible improvements in multiple ways. For instance, agent-based decision modules could be added to take into account adaptation processes in local communities and their land-use practices in response to drivers of change (cf. Richard et al. (2022)). Similarly, further modules based on socio-hydrology and eco-hydrology could be added to refine the representation of processes and future simulations.

Overall, however, the initial performance of the model is promising. It offers an innovative, multi-method approach to modelling the interactions between ecology and water, also taking account of the human dimension by integrating agricultural practices such as integration.

Transferability and Larger Context A final aspect of this thesis that needs to be highlighted is that it carries implications for the larger conceptual context in which it was presented, and that several of its results are transferable to similar areas worldwide. This applies particularly to the results pertaining to LULC classification, the WAFL, and the newly developed eco-hydrological model.

The LULC analysis conducted in the course of this thesis has provided a widely applicable comparison of the performance of supervised classification methods on the cloud computing platform Google Earth Engine. Future studies can benefit from these results with regard to their choice of input imagery, band selection, and training dataset - as well as the process of optimizing their tuning parameters.

The WAFL provides an avenue towards re-constructing historical inundation extents and changes in inundation processes in otherwise data-sparse areas. The ultimate aim of the developed methodology is to provide long-term insights into the spatial dynamics of inundations in tropical deltas. Applying the approach to the Mekong delta showed that this is possible with acceptable average accuracies of 87% in comparison to historical inundation maps derived from Landsat. Such comparisons have also highlighted the limitations of the WAFL with regard to long-term changes in local terrain configuration, and the challenges posed by LULC characteristics such as the presence of natural vegetation. For an application in other study areas, this means that a basic knowledge of changes in local conditions is a prerequisite for the development and application of the WAFL. An awareness of landcover dynamics - which can be assessed through historical LULC analysis - or significant shifts in terrain elevations and the river-floodplain

connections, notably due to the construction of water control infrastructures, is crucial. It must also be noted that the WAFL is primarily applicable in areas where inundations are correlated largely with dynamics in river water levels. This refers to areas in which the influence of local precipitations and groundwater is limited and where there are few obstacles to the flow of water into and out of the floodplain. This can be mostly the case in semi-arid places but also in tropical areas like in the Mekong delta, as demonstrated in this study by the comparison of water level dynamics and Sentinel-derived inundation extents. Where historical records of water levels are available, as a first step in the application of WAFL, such an analysis should be used to elucidate the applicability of the methodology. However, in areas where inundations are significantly correlated with processes such as local precipitation or groundwater logging, adjustments to the correlation model can be made by introducing new input variables, provided time-series are available. Another possible extension of the WAFL is its use to detect the influence of hydraulic infrastructures by illustrating discrepancies between expected and observed inundation extents. A similar application of the Lamagat correlation model was already proposed by Bader et al. (2016).

The eco-hydrological model, finally, demonstrates the importance of small-scale observations and modelling approaches. Despite significant simplifications and limitations, it can represent local processes well, and is well-adapted to a data sparse environment. While it can be improved with regard to further quantification, a better description of various components, and possible further validation with in-situ data, it offers a transferable alternative approach to the down-scaling of coarser modelling data. This could offer interesting opportunities to represent local processes and explore scenarios in similar study areas across the globe, especially in (tropical) delta floodplains characterized by irrigation channels where similar questions of upstream influences and local development scenarios prevail, such as in the Tana river delta in Ethiopia and Kenya (Mwamlavya et al., 2021), the Indus river delta in Pakistan (Irfan et al., 2019; Kravtsova et al., 2009; Atif et al., 2021; Syvitski et al., 2013), and the Inner Niger Delta in Mali (Neal et al., 2012; O'Brien et al., 2020).

With regard to the larger conceptual context, this thesis has harnessed concepts from both ecohydrology and socio-hydrology and illustrated ways in which the two disciplines can be integrated, also with regard to the use of the framework of ecosystem services. The ecohydrological model presented in this thesis integrates a human dimension in multiple ways. First, it uses the

anthropocentric ES framework. Second, it partly bases the delineation of its modelling units on human agricultural practices. The information necessary to do so partially stems from first-hand information given by the actors involved. To spatialize it, this first-hand information was used as the basis of a supervised remote sensing classification. This approach illustrates how actor-based data can be used to inform numerical approaches, and how the conceptual distance between socio- and ecohydrology can be bridged. In addition, potential future developments in the model further explore this interstitial sphere, such as the incorporation of retroactions between land use and sociological dynamics into the ecohydrological model.

Overall Conclusion Overall, this thesis provides an innovative look at the ecohydrological approach to deltaic agro-ecosystems such as those present on the floodplains of the Cambodian Mekong delta. It combines multiple methods and uses them to articulate the processes in the Prek system from diverse angles, as any single method would provide only a limited, partial view. In addition, it can be seen as a contribution to ecohydrology as a whole that the model in this thesis accounts explicitly for the human element of agro-ecosystems by integrating information on cultivation practices gathered in the course of fieldwork, and delineating homogeneous surface units on this basis.

The results presented in this thesis have illustrated that the Cambodian Mekong Delta is tied closely into the developments, both hydrological and ecological, in the larger Mekong region. Basin-wide trends in hydrological dynamics are reflected in both local water levels and the incidence and duration of monsoon inundations on the deltaic floodplains. Large-scale developments such as the decrease in fish populations are keenly felt by local communities, as has emerged from interviews. Most of the local stakeholders who were interviewed demonstrated a deep awareness of the larger nexus of cause and effect into which their communities are tied. Several of them talked about how they saw upstream hydropower development shift the rhythm of the river. Others drew the link between dwindling inundation extents and soil water deficiencies and the abundance of rat populations. However, it has also emerged that they see local measures, in particular the rehabilitation of the Preks, as a way to address the negative impacts that they are facing as a result of these developments.

The Preks themselves tie the floodplains of the Cambodian Mekong Delta much more closely

to the river and its distributaries than its Vietnamese counterpart. Largely devoid of gates and dykes, they act as a vector for flooding and drainage, as a conduit for sedimentation and fish, as a route for transport and a source of irrigation water. Rehabilitating them to make water inflow possible year-round is perceived as uniformly positive by the stakeholders who were interviewed, despite issues such as bank collapses and re-settlements of individual families. The increased availability of irrigation water as well as the accompanying roads on the Prek banks are seen as the biggest benefits, as they increase the production potential of farmers' plots as well as the ease of accessing them.

The challenges that the Cambodian Mekong Delta faces are symptomatic for, if not identical to, the situation of numerous deltas worldwide. Some methods presented in this thesis, such as the WAFL and LULC classification, and - to a certain extent - the numerical model can be transferred to similar deltaic areas to shed light on the shifts in hydrological processes and their impacts. Universally, though, it can be stated that deltaic areas are at the mercy of developments that happen at much larger scales - upstream hydropower development, basin-wide climate change impacts, and global sea level rise to name but a few. There is little deltaic communities can do to influence these developments. They can, however, adapt - and in this local infrastructure such as the Preks play a crucial role, as this thesis has demonstrated. For over a century, Preks have contributed to the enhancement of agriculture in the Cambodian Mekong Delta, raising land for the cultivation of high-value crops, and providing irrigation water when it is needed most. Despite the social and political upheavals of the 20th century, they have remained integral to the community structure and agricultural practices in the region. With sufficient care, maintenance, and the beneficial effects of rehabilitation projects, they will be able to catalyze crucial ecosystem services to support local communities well into an as of yet uncertain future.

Availability of Publications, Code, and Data

Parts of this thesis have been published as papers:

Orieschnig, C., Venot, J.P., Massuel, S., Eang, K.E., Chhuon, K., Lun, S., Siev, S. and Belaud, G., 2022. A Multi-Method Approach to Flood Mapping: Reconstructing Inundation Changes in the Cambodian Upper Mekong Delta. Journal of Hydrology, p.127902.

Orieschnig, C.A., Venot, J.P, Massuel, S., Eang, K.E., Kong, C., Lun, S., and Belaud, G., Datasets for the assessment of changes in the incidence, extents, and spatial patterns of inundations in in the Cambodian Mekong Delta, based on a water level - flood link calculated from in-situ water levels, and Sentinel-derived inundation maps, *Data In Brief*. In Press.

Orieschnig, C. A., Belaud, G., Venot, J. P., Massuel, S., and Ogilvie, A. (2021). Input imagery, classifiers, and cloud computing: Insights from multi-temporal LULC mapping in the Cambodian Mekong Delta. *European Journal of Remote Sensing*, 54(1), 398-416.

Furthermore, the code written on Google Earth Engine is available in the following repositories:

Preliminary flood frequency analysis at the scale of Zone A and B (from which the WAFL was derived): `https://code.earthengine.google.com/?accept_repo=users/christinaannaorieschnig/FloodFrequencyAnalysisJP`

Flood mapping at the scale of the case study area: `https://code.earthengine.google.com/?accept_repo=users/christinaannaorieschnig/GEE_Sentinel_1_2_FloodMapp`

ingMekongCambodia

Comparison of LULC Classifiers:

https://code.earthengine.google.com/?accept_repo=users/christinaannaorieschnig/New_LULC

Extraction of data for model input: https://code.earthengine.google.com/?accept_repo=users/christinaannaorieschnig/PythonModelInput

Modified scripts for flood detection, WAFL extraction etc. to make them more easily transferable to other regions: https://code.earthengine.google.com/?accept_repo=users/christinaannaorieschnig/ThesisResults

The code for the ecohydrological model, as well as the baseline data necessary is available in the following Github repository:

https://github.com/christina-orieschnig

Overall, approximately 25,000 lines of code were written in GEE, and 30,000 lines in Python in the course of the thesis.

Bibliography

M. Abadi, P. Barham, J. Chen, Z. Chen, A. Davis, J. Dean, M. Devin, S. Ghemawat, G. Irving, M. Isard, M. Kudlur, J. Levenberg, R. Monga, S. Moore, D. G. Murray, B. Steiner, P. Tucker, V. Vasudevan, P. Warden, M. Wicke, Y. Yu, and X. Zheng. TensorFlow: A System for Large-Scale Machine Learning. In *12th {USENIX} Symposium on Operating Systems Design and Implementation ({OSDI} 16)*, pages 265–283, Savannah, GA, 11 2016. {USENIX} Association. ISBN 978-1-931971-33-1. Cited on page 236.

AFD. Cambodge | AFD - Agence Française de Développement, 2021. URL `https://www.afd.fr/fr/page-region-pays/cambodge`. Cited on page 188.

M. Ahmed, H. Navy, L. Vuthy, and M. Tiongco. Socioeconomic assessment of freshwater capture fisheries in Cambodia: report on a household survey. Technical report, Mekong River Commission Secretariat., Vientiane, 1998. Cited on page 81.

F. Aires, J.-P. Venot, S. Massuel, N. Gratiot, B. Pham-Duc, and C. Prigent. Surface Water Evolution (2001–2017) at the Cambodia/Vietnam Border in the Upper Mekong Delta Using Satellite MODIS Observations. *Remote Sensing*, 12(5):800, 3 2020. doi: 10.3390/rs12050800. Cited on pages 137 and 167.

H. Alexandersson. A homogeneity test applied to precipitation data. *Journal of Climatology*, 6 (6):661–675, 1 1986. doi: 10.1002/joc.3370060607. Cited on page 116.

R. G. Allen, L. S. Pereira, D. Raes, and M. Smith. *Crop evapotranspiration : guidelines for computing crop water requirements*. Food and Agriculture Organization of the United Nations, 1998. ISBN 9251042195. Cited on pages 296, 297, and 299.

M. Amani, A. Ghorbanian, S. A. Ahmadi, M. Kakooei, A. Moghimi, S. M. Mirmazloumi, S. H. A. Moghaddam, S. Mahdavi, M. Ghahremanloo, S. Parsian, Q. Wu, and B. Brisco. Google Earth Engine Cloud Computing Platform for Remote Sensing Big Data Applications: A Comprehensive Review. *IEEE Journal of Selected Topics in Applied Earth Observations and Remote Sensing*, 13:5326–5350, 2020. doi: 10.1109/JSTARS.2020.3021052. Cited on pages 143 and 238.

S. Amari and S. Wu. Improving support vector machine classifiers by modifying kernel functions. *Neural Networks*, 12(6):783–789, 7 1999. ISSN 0893-6080. doi: 10.1016/S0893-6080(99)00032-5. Cited on page 243.

Anaconda. Anaconda Software Distribution, 2016. URL `https://www.anaconda.com/`. Cited on page 273.

H. Apel, N. N. Hung, T. T. Long, and V. K. Tri. Flood Hydraulics and Suspended Sediment Transport in the Plain of Reeds, Mekong Delta. In F. Renaud and C. Kuenzer, editors, *The Mekong Delta System*, pages 221–232. Springer, Dordrecht, Heidelberg, 2012. doi: 10.1007/978-94-007-3962-8{_}8. Cited on page 95.

J. Arnold. SWAT - Soil and Water Assessment Tool, 1994. URL `https://agris.fao.org/agris-search/search.do?recordID=US2019X00576`. Cited on page 272.

D. Arthur and S. Vassilvitskii. k-means++: The advantages of careful seeding. In *Proceedings of the eighteenth annual ACM-SIAM symposium on Discrete algorithms*, pages 1027–1035. Society for Industrial and Applied Mathematics, 2007. Cited on page 144.

S. Atif, M. Umar, and F. Ullah. Investigating the flood damages in Lower Indus Basin since 2000: Spatiotemporal analyses of the major flood events. *Natural Hazards*, 108(2):2357–2383, 9 2021. doi: 10.1007/s11069-021-04783-w. Cited on page 334.

D. Ávila-García, J. Morató, A. I. Pérez-Maussán, P. Santillán-Carvantes, J. Alvarado, and F. A. Comín. Impacts of alternative land-use policies on water ecosystem services in the Río Grande de Comitán-Lagos de Montebello watershed, Mexico. *Ecosystem Services*, 45:101179, 10 2020. doi: 10.1016/J.ECOSER.2020.101179. Cited on page 71.

D. Ayres. Tradition, Modernity, and the Development of Education in Cambodia. *Comparative Education Review*, 44(4):440–463, 11 2000a. doi: 10.1086/447629. Cited on page 184.

D. M. Ayres. *Anatomy of a Crisis: Education, Development, and the State in Cambodia, 1953-1998*. University of Hawaii Press, 2000b. ISBN 9780824861445. doi: doi:10.1515/9780824861445. URL https://doi.org/10.1515/9780824861445. Cited on page 184.

B. M. d. Azevedo, C. N. V. Fernandes, D. V. Vasconcelos, A. C. Garcia, L. G. M. d. Figueredo Júnior, and T. V. d. A. Viana. Irrigation depths and yield response factor in zucchini cultivation. *Revista Brasileira de Engenharia Agrícola e Ambiental*, 22(6):401–406, 6 2018. doi: 10.1590/1807-1929/agriambi.v22n6p401-406. Cited on page 299.

J.-C. Bader, G. Belaud, J.-P. Lamagat, T. Ferret, and P. Vauchel. Modélisation de propagation d'écoulement entre lits mineur et majeur sur les fleuves Sénégal et Niger. *Hydrological Sciences Journal*, pages 1–20, 10 2016. doi: 10.1080/02626667.2016.1148815. Cited on pages 145 and 334.

I. G. Baird, K. Manorom, A. Phenow, and S. Gaja-Svasti. Opening the Gates of the Pak Mun Dam: Fish Migrations, Domestic Water Supply, Irrigation Projects and Politics. *Water Alternatives*, 13(1):141–159, 2020. Cited on pages 86 and 121.

E. Baran, N. Chum, M. Fukushima, T. Hand, K. G. Hortle, T. Jutagate, and B. Kang. Fish Biodiversity Research in the Mekong Basin. In *The Biodiversity Observation Network in the Asia-Pacific Region*, pages 149–164. Springer, Tokyo, 2012. doi: 10.1007/978-4-431-54032-8{_}11. Cited on page 79.

F. Baret and G. Guyot. Potentials and limits of vegetation indices for LAI and APAR assessment. *Remote Sensing of Environment*, 35(2-3):161–173, 2 1991. ISSN 0034-4257. doi: 10.1016/0034-4257(91)90009-U. Cited on page 239.

R. Barthélemy. Étude sur les colmatages du Mékong. *Revue Indochinoise*, 19(4), 1913. Cited on pages 59, 177, and 205.

G. Belaud and N. Bercher. Calibration of a propagation model in large river using satellite altimetry Water and Energy Saving: A Novel Low-Cost Solution for Water Wells View project Solar Induced Fluorescence View project. In *6th International Symposium on Environmental Hydraulics*, pages 23–25, 2010. doi: 10.1201/b10553-143. Cited on page 145.

G. Belaud and A. Paquier. Estimation of the total sediment discharge in natural stream flows using a depth-integrated sampler. *Aquatic Sciences*, 62(1):39, 2000. doi: 10.1007/s000270050074. Cited on page 292.

G. Belaud and A. Paquier. Sediment Diversion through Irrigation Outlets. *Journal of Irrigation and Drainage Engineering*, 127(1):35–38, 2 2001. doi: 10.1061/(ASCE)0733-9437(2001)127:1(35). Cited on page 292.

M. Belgiu and L. Dragut. Random forest in remote sensing: A review of applications and future directions. *ISPRS Journal of Photogrammetry and Remote Sensing*, 114:24–31, 4 2016. ISSN 0924-2716. doi: 10.1016/J.ISPRSJPRS.2016.01.011. Cited on page 241.

S. Benedikter. Extending the Hydraulic Paradigm: Reunification, State Consolidation, and Water Control in the Vietnamese Mekong Delta after 1975. *Southeast Asian Studies*, 3(3):547–587, 2014. doi: https://doi.org/10.20495/seas.3.3{_}547. Cited on page 102.

L. Bertassello, M. C. Levy, M. F. Müller, S. Archfield, and S. Pande. Sociohydrology, ecohydrology, and the space-time dynamics of human-altered catchments. *Hydrological Sciences Journal*, 66(9):1393–1408, 2021. doi: 10.1080/02626667.2021.1948550. Cited on page 66.

D. Biggs. Fixing the Delta: History and the Politics of Hydraulic Infrastructure Development and Conservation in the Mekong Delta. In *Environmental change and agricultural sustainability in the Mekong Delta*, pages 35–44. Springer, Dordrecht, 2011. doi: 10.1007/978-94-007-0934-8{_}3. Cited on page 102.

D. A. Biggs. *Between the rivers and tides: a hydraulic history of the Mekong Delta, 1820-1975*. PhD thesis, University of Washington, 2004. Cited on pages 102 and 174.

D. A. Biggs. *Quagmire : Nation-building and nature in the Mekong Delta*. University of Washington Press, 2010. ISBN 0295801549. Cited on page 102.

D. V. Binh, S. A. Kantoush, M. Saber, N. P. Mai, S. Maskey, D. T. Phong, and T. Sumi. Long-term alterations of flow regimes of the Mekong River and adaptation strategies for the Vietnamese Mekong Delta. *Journal of Hydrology: Regional Studies*, 32:100742, 12 2020. ISSN 2214-5818. doi: 10.1016/J.EJRH.2020.100742. Cited on pages 58, 328, and 330.

N. A. Binh, H. S. Nhut, N. N. An, T. A. Phuong, N. C. Hanh, G. T. P. Thao, T. T. Pham, P. V. Hong, L. T. T. Ha, D. T. Bui, and P. V. Hoa. Thirty-Year Dynamics of LULC at the Dong Thap Muoi Area, Southern Vietnam, Using Google Earth Engine. *ISPRS International Journal of Geo-Information*, 10(4):226, 4 2021. doi: 10.3390/ijgi10040226. Cited on page 143.

M. I. Bird, W. E. Austin, C. M. Wurster, L. K. Fifield, M. Mojtahid, and C. Sargeant. Punctuated eustatic sea-level rise in the early mid-Holocene. *Geology*, 38(9):803–806, 9 2010. doi: 10.1130/G31066.1. Cited on page 93.

G. S. Birth and G. R. McVey. Measuring the Color of Growing Turf with a Reflectance Spectrophotometer 1. *Agronomy Journal*, 60(6):640–643, 11 1968. ISSN 0002-1962. doi: 10.2134/agronj1968.00021962006000060016x. Cited on page 239.

A. Boretti. Implications on food production of the changing water cycle in the Vietnamese Mekong Delta. *Global Ecology and Conservation*, 22:e00989, 6 2020. doi: 10.1016/J.GECCO.2020.E00989. Cited on pages 78 and 137.

M. G. Bos, R. A. L. Kselik, R. G. Allen, and D. Molden. *Water Requirements for Irrigation and the Environment*. Springer Science & Business Media, 2009. ISBN 978-1-4020-8947-3. Cited on page 298.

W. Boughton. A review of the USDA SCS curve number method. *Soil Research*, 27(3):511, 1989. doi: 10.1071/SR9890511. Cited on page 297.

K. A. Brauman, G. C. Daily, T. K. Duarte, and H. A. Mooney. The Nature and Value of Ecosystem Services: An Overview Highlighting Hydrologic Services. *Annual Review of Environment and Resources*, 32(1):67–98, 11 2007. doi: 10.1146/annurev.energy.32.031306.102758. Cited on page 70.

L. Breiman. Bagging Predictors. *Machine Learning*, 24(2):123–140, 1996. ISSN 08856125. doi: 10.1023/A:1018054314350. Cited on page 241.

L. Breiman. Random Forests. *Machine Learning*, 45:5–32, 2001. Cited on page 241.

P. R. Brown and N. T. My Phung. Pattern and dynamics of rodent damage to lowland irrigated rice crops in An Giang, Vietnam. *International Journal of Pest Management*, 57(1):67–76, 10 2010. doi: 10.1080/09670874.2010.529954. Cited on page 168.

S. T. Buckton and R. J. Safford. The avifauna of the Vietnamese Mekong Delta. *Bird Conservation International*, 14(4):279–322, 12 2004. doi: 10.1017/S0959270904000346. Cited on page 100.

T. Buishand. Some methods for testing the homogeneity of rainfall records. *Journal of Hydrology*, 58(1-2):11–27, 8 1982. doi: 10.1016/0022-1694(82)90066-X. Cited on page 116.

M. Burbano, S. Shin, K. Nguyen, and Y. Pokhrel. Hydrologic changes, dam construction, and the shift in dietary protein in the Lower Mekong River Basin. *Journal of Hydrology*, 581: 124454, 2 2020. doi: 10.1016/J.JHYDROL.2019.124454. Cited on pages 80, 137, and 168.

G. Bussi, S. E. Darby, P. G. Whitehead, L. Jin, S. J. Dadson, H. E. Voepel, G. Vasilopoulos, C. R. Hackney, C. Hutton, T. Berchoux, D. R. Parsons, and A. Nicholas. Impact of dams and climate change on suspended sediment flux to the Mekong delta. *Science of The Total Environment*, 755:142468, 2 2021. doi: 10.1016/J.SCITOTENV.2020.142468. Cited on pages 86 and 97.

B. Camenen. Simple and General Formula for the Settling Velocity of Particles. *Journal of Hydraulic Engineering*, 133(2):229–233, 2 2007. doi: 10.1061/(ASCE)0733-9429(2007)133:2(229). Cited on page 292.

I. Campbell and C. Barlow. Hydropower Development and the Loss of Fisheries in the Mekong River Basin. *Frontiers in Environmental Science*, 8:200, 10 2020. doi: 10.3389/fenvs.2020.566509. Cited on pages 81 and 86.

I. C. Campbell. *The Mekong*. Academic Press, 2009. doi: 10.1016/C2009-0-01620-1. Cited on page 74.

I. C. Campbell. Biodiversity of the Mekong Delta. In *Springer Environmental Science and Engineering*, pages 293–313. Springer Netherlands, 2012. doi: 10.1007/978-94-007-3962-8{_}11. Cited on pages 100 and 101.

T. Campbell, K. Pin, P. Ngor, and Z. Hogan. Conserving Mekong Megafishes: Current Status and Critical Threats in Cambodia. *Water*, 12(6):1820, 6 2020. doi: 10.3390/w12061820. Cited on page 101.

J. Carew-Reid and L. Taylor. Natural systems and climate change resilience in the Lower Mekong

Basin. In *Biodiversity Conservation in Southeast Asia*, pages 175–206. Routledge, 7 2017. doi: 10.4324/9781315313573-10. Cited on page 81.

M. H. Carpenter, C. A. Kennedy, H. Bijl, S. A. Viken, and V. N. Vatsa. Fourth-order runge-kutta schemes for fluid mechanics applications. *Journal of Scientific Computing*, 25(1-2):157–194, 11 2005. doi: 10.1007/BF02728987. Cited on page 468.

M. K. V. CARR. The Water Relations and Irrigation Requirements of Mango (Mangifera indica L.): A Review. *Experimental Agriculture*, 50(1):1–23, 1 2014. doi: 10.1017/S0014479713000288. Cited on page 298.

R. F. Carsel and R. S. Parrish. Developing joint probability distributions of soil water retention characteristics. *Water Resources Research*, 24(5):755–769, 5 1988. doi: 10.1029/WR024i005p00755. Cited on pages 49, 275, and 418.

N. P. Castilla, A. M. Stuart, O. Makara, K. Sathya, S. Somany, V. Kumar, and B. A. Ratna Hadi. Characterization of cropping practices, pest constraints, and yield variation in irrigated lowland rice of Cambodia. *Crop Protection*, 135:104906, 9 2020. doi: 10.1016/J.CROPRO.2019.104906. Cited on page 207.

D. P. Chandler and L. C. Overton. Cambodia, 2021. URL `https://www.britannica.com/place/Cambodia.Accessed13February2022.` Cited on page 187.

C.-F. Chen, N.-T. Son, L.-Y. Chang, and C.-C. Chen. Monitoring of soil moisture variability in relation to rice cropping systems in the Vietnamese Mekong Delta using MODIS data. *Applied Geography*, 31(2):463–475, 4 2011. doi: 10.1016/J.APGEOG.2010.10.002. Cited on page 168.

S. Chen, X. Mao, and M. K. Shukla. Evaluating the effects of layered soils on water flow, solute transport, and crop growth with a coupled agro-eco-hydrological model. *Journal of Soils and Sediments*, 20(9):3442–3458, 9 2020. doi: 10.1007/s11368-020-02647-7. Cited on page 65.

T. Chen and C. Guestrin. XGBoost. In *Proceedings of the 22nd ACM SIGKDD International Conference on Knowledge Discovery and Data Mining*, pages 785–794, New York, NY, USA, 8 2016. ACM. doi: 10.1145/2939672.2939785. Cited on page 242.

D. Choi, H. Park, Y. J. Kim, J.-W. Jung, W.-J. Choi, Y. G. Her, and K.-S. Yoon. Curve Numbers for Rice Paddies with Different Water Management Practices in Korea. *Journal of Irrigation*

and Drainage Engineering, 145(5):06019003, 5 2019. doi: 10.1061/(ASCE)IR.1943-4774.0001382. Cited on page 297.

V. T. Chow. *Open-channel hydraulics*. Blackburn Press, New Jersey, 1959. ISBN 9781932846188. Cited on page 115.

S. D. X. Chua, X. X. Lu, C. Oeurng, T. Sok, and C. Grundy-Warr. Drastic decline of flood pulse in the Cambodian floodplains (Mekong River and Tonle Sap system). *Hydrology and Earth System Sciences*, 26(3):609–625, 2 2022. doi: 10.5194/hess-26-609-2022. Cited on page 328.

J. Claude. The continental fossil record and the history of biodiversity in Southeast Asia. In *Biodiversity Conservation in Southeast Asia*, pages 20–32. Routledge, 7 2017. ISBN 9781315313573. doi: 10.4324/9781315313573-2. Cited on page 79.

N. Clerici, C. A. Valbuena Calderón, and J. M. Posada. Fusion of Sentinel-1A and Sentinel-2A data for land cover mapping: a case study in the lower Magdalena region, Colombia. *Journal of Maps*, 13(2):718–726, 11 2017. doi: 10.1080/17445647.2017.1372316. Cited on page 238.

C. Coakley, M. Munro-Stasiuk, J. Tyner, S. Kimsroy, C. Chhay, and S. Rice. Extracting Khmer Rouge Irrigation Networks from Pre-Landsat 4 Satellite Imagery Using Vegetation Indices. *Remote Sensing*, 11(20):2397, 10 2019. doi: 10.3390/rs11202397. Cited on page 185.

D. Coates, P. Ouch, U. Suntornratana, T. Nguyen, and S. Viravong. Biodiversity and fisheries in the Mekong River Basin. *Mekong Development Series*, 2:1–30, 2003. Cited on page 79.

J. Coleman and D. Prior. Deltaic Environments of Deposition. In *Sandstone Depositional Environments*, volume 58, pages 139–178. AAPG Special Volumes, 1982. Cited on page 94.

J. M. Coleman and H. H. Roberts. Deltaic coastal wetlands. In *Coastal Lowlands*, pages 1–24. Springer, Dordrecht, 1989. doi: 10.1007/978-94-017-1064-0{_}1. Cited on pages 92, 93, and 94.

R. G. Congalton. A Review of Assessing the Accuracy of Classifications of Remotely Sensed Data. *Remote Sensing of Environment*, 37:35–46, 1991. doi: https://doi.org/10.1016/0034-4257(91)90048-B. Cited on pages 144 and 243.

R. Constanze and H. E. Daly. Natural Capital and Sustainable Development. *Conservation Biology*, 6(1):37–46, 3 1992. doi: 10.1046/j.1523-1739.1992.610037.x. Cited on page 68.

C. Cortes and V. Vapnik. Support-vector networks. *Machine Learning*, 20(3):273–297, 9 1995. ISSN 0885-6125. doi: 10.1007/BF00994018. Cited on page 243.

T. L. Cosslett and P. D. Cosslett. *Water Resources and Food Security in the Vietnam Mekong Delta*. Springer International Publishing, Cham, 2014. ISBN 978-3-319-02197-3. doi: 10.1007/978-3-319-02198-0. Cited on page 96.

R. Costanza, R. d'Arge, R. de Groot, S. Farber, M. Grasso, B. Hannon, K. Limburg, S. Naeem, R. V. O'Neill, J. Paruelo, R. G. Raskin, P. Sutton, and M. van den Belt. The value of the world's ecosystem services and natural capital. *Nature*, 387(6630):253–260, 5 1997. doi: 10.1038/387253a0. Cited on page 68.

J. Costenbader, J. Broadhead, Y. Yasmi, and P. B. Durst. Drivers Affecting Forest Change in the Greater Mekong Subregion (GMS): An Overview. Technical report, FAO, Rome, 2015. Cited on page 88.

C. Crocker. The general map of the Kingdom of Cambodia and the exploratory survey of the soils of Cambodia. In *"Agriculture." Atlas of Cambodia: maps on socio-economic development and environment.* Royal Cambodian Government Soil Commission/USAID. Save Cambodia's Wildlife., Phnom Penh, second edition, 1962. Cited on page 275.

R. Cronin, B. Eyler, and C. Weatherby. Letters from the Mekong. Technical report, The Stimson Center, 2016. URL `www.stimson.org`. Cited on page 90.

V. S. da Silva, G. Salami, M. I. O. da Silva, E. A. Silva, J. J. Monteiro Junior, and E. Alba. Methodological evaluation of vegetation indexes in land use and land cover (LULC) classification. *Geology, Ecology, and Landscapes*, 4(2):159–169, 4 2020. doi: 10.1080/24749508.2019.1608409. Cited on page 251.

C. Dandridge, V. Lakshmi, J. Bolten, and R. Srinivasan. Evaluation of Satellite-Based Rainfall Estimates in the Lower Mekong River Basin (Southeast Asia). *Remote Sensing*, 11(22):2709, 11 2019. doi: 10.3390/rs11222709. Cited on pages 133 and 134.

T. A. Dang and T. H. Tran. Application of the Mike21C model to simulate flow in the lower Mekong river basin. *SpringerPlus*, 5(1):1982, 12 2016. doi: 10.1186/s40064-016-3637-8. Cited on page 86.

T. D. Dang, T. A. Cochrane, M. E. Arias, P. D. T. Van, and T. T. de Vries. Hydrological alterations from water infrastructure development in the Mekong floodplains. *Hydrological Processes*, 30(21):3824–3838, 2016. doi: 10.1002/hyp.10894. Cited on page 137.

T. D. Dang, T. A. Cochrane, and M. E. Arias. Quantifying suspended sediment dynamics in mega deltas using remote sensing data: A case study of the Mekong floodplains. *International Journal of Applied Earth Observation and Geoinformation*, 68:105–115, 6 2018. doi: 10.1016/J.JAG.2018.02.008. Cited on page 137.

V. T. Danh and H. V. Khai. Household demand and supply for clean groundwater in the Mekong Delta, Vietnam. *Renewables: Wind, Water, and Solar*, 2(1):4, 12 2015. doi: 10.1186/s40807-014-0004-7. Cited on pages 97 and 98.

G. I. Davies, L. McIver, Y. Kim, M. Hashizume, S. Iddings, and V. Chan. Water-borne diseases and extreme weather events in Cambodia: Review of impacts and implications of climate change. *International Journal of Environmental Research and Public Health*, 2015. doi: 10.3390/ijerph120100191. Cited on page 149.

R. S. de Groot. Environmental functions as a unifying concept for ecology and economics. *The Environmentalist*, 7(2):105–109, 1987. Cited on page 68.

J. M. Delgado, B. Merz, and H. Apel. A climate-flood link for the lower Mekong River. *Hydrology and Earth System Sciences*, 16(5):1533–1541, 5 2012a. doi: 10.5194/hess-16-1533-2012. Cited on page 78.

J. M. Delgado, B. Merz, and H. Apel. Monsoon Variability and the Mekong Flood Regime. In F. Renaud and C. Kuenzer, editors, *The Mekong Delta System*, pages 233–244. Springer, Dordrecht, Heidelberg, 2012b. doi: 10.1007/978-94-007-3962-8{_}9. URL `http://link.springer.com/10.1007/978-94-007-3962-8_9`. Cited on page 95.

J. Denize, L. Hubert-Moy, J. Betbeder, S. Corgne, J. Baudry, and E. Pottier. Evaluation of Using Sentinel-1 and -2 Time-Series to Identify Winter Land Use in Agricultural Landscapes. *Remote Sensing*, 11(1):37, 12 2018. doi: 10.3390/rs11010037. Cited on pages 245 and 250.

M. Devak and C. T. Dhanya. Sensitivity analysis of hydrological models: review and way forward. *Journal of Water and Climate Change*, 8(4):557–575, 12 2017. doi: 10.2166/wcc.2017.149. Cited on page 301.

B. DeVries, C. Huang, J. Armston, W. Huang, J. W. Jones, and M. W. Lang. Rapid and robust monitoring of flood events using Sentinel-1 and Landsat data on the Google Earth Engine. *Remote Sensing of Environment*, 240:111664, 4 2020. ISSN 0034-4257. doi: 10.1016/J.RSE.2020.111664. Cited on page 138.

B. DiCicco-Bloom and B. F. Crabtree. The qualitative research interview. *Medical Education*, 40(4):314–321, 4 2006. doi: 10.1111/j.1365-2929.2006.02418.x. Cited on page 193.

V. L. Diengdoh, S. Ondei, M. Hunt, and B. W. Brook. A validated ensemble method for multinomial land-cover classification. *Ecological Informatics*, 56:101065, 3 2020. doi: 10.1016/J.ECOINF.2020.101065. Cited on page 240.

D. A. Dinh, B. Elmahrad, P. Leinenkugel, and A. Newton. Time series of flood mapping in the Mekong Delta using high resolution satellite images. *IOP Conference Series: Earth and Environmental Science*, 266:12011, 5 2019. doi: 10.1088/1755-1315/266/1/012011. Cited on page 95.

D. Duc Tran, G. Van Halsema, P. J. Hellegers, L. Phi Hoang, T. Quang Tran, M. Kummu, and F. Ludwig. Assessing impacts of dike construction on the flood dynamics of the Mekong Delta. *Hydrology and Earth System Sciences*, 22(3), 2018. doi: 10.5194/hess-22-1875-2018. Cited on pages 57 and 96.

C. Duke. Mangroves of the Kien Giang Biosphere Reserve Vietnam. Technical report, Deutsche Gesellschaft fur Internationale Zusammenarbeit (GIZ), Rach Gia, 2013. Cited on page 100.

D. Dumaresq, K. van Nguyen, J. Pittock, M. Oo, K. Sok, T. van Hieu, and L. Blessington. The paradoxical values of traditional deep water floating rice systems. *Global Food Security*, 26: 100391, 9 2020. doi: 10.1016/J.GFS.2020.100391. Cited on page 193.

L. P. Dumas. Obstacles Facing Farmer-Managed Irrigation Systems in the State of Cambodia. In R. Yoder and J. Thurston, editors, *Design issues in farmer-managed irrigation systems : proceedings of an international workshop of the Farmer-Managed Irrigation Systems Network*, page 319, Ching Mai, Thailand, 1990. International Irrigation Management Institute. ISBN 9290901101. Cited on pages 184, 185, 186, and 187.

N. V. Dung, B. Merz, A. Bárdossy, T. D. Thang, and H. Apel. Multi-objective automatic calibration of hydrodynamic models - development of the concept and an application in

the Mekong Delta. *Hydrology and Earth System Sciences*, 15(4):1339–1354, 1 2011. doi: https://doi.org/10.5194/hess-15-1339-2011. Cited on pages 117 and 121.

N. L. Duy, T. V. K. Nguyen, D. V. Nguyen, A. T. Tran, H. T. Nguyen, I. Heidbüchel, B. Merz, and H. Apel. Groundwater dynamics in the Vietnamese Mekong Delta: Trends, memory effects, and response times. *Journal of Hydrology: Regional Studies*, 33:100746, 2 2021. doi: 10.1016/J.EJRH.2020.100746. Cited on pages 94, 97, and 98.

D. A. Edmonds, R. L. Caldwell, E. S. Brondizio, and S. M. O. Siani. Coastal flooding will disproportionately impact people on river deltas. *Nature Communications*, 11(1):4741, 12 2020. doi: 10.1038/s41467-020-18531-4. Cited on page 57.

P. R. Ehrlich and H. A. Mooney. Extinction, Substitution, and Ecosystem Services. *BioScience*, 33(4):248–254, 4 1983. doi: 10.2307/1309037. Cited on page 68.

J. Elith, J. R. Leathwick, and T. Hastie. A working guide to boosted regression trees. *Journal of Animal Ecology*, 77(4):802–813, 7 2008. doi: 10.1111/j.1365-2656.2008.01390.x. Cited on page 242.

L. E. Erban and S. M. Gorelick. Closing the irrigation deficit in Cambodia: Implications for transboundary impacts on groundwater and Mekong River flow. *Journal of Hydrology*, 535: 85–92, 2016. doi: 10.1016/j.jhydrol.2016.01.072. Cited on page 168.

L. E. Erban, S. M. Gorelick, and H. A. Zebker. Groundwater extraction, land subsidence, and sea-level rise in the Mekong Delta, Vietnam. *Environmental Research Letters*, 9(8):084010, 8 2014. doi: 10.1088/1748-9326/9/8/084010. Cited on page 98.

S. Eslami, P. Hoekstra, N. Nguyen Trung, S. Ahmed Kantoush, D. Van Binh, D. Duc Dung, T. Tran Quang, and M. van der Vegt. Tidal amplification and salt intrusion in the Mekong Delta driven by anthropogenic sediment starvation. *Scientific Reports*, 9(1):18746, 12 2019. doi: 10.1038/s41598-019-55018-9. URL `http://www.nature.com/articles/s41598-019-55018-9`. Cited on page 104.

B. Eyler. *Last days of the mighty Mekong*. Zed Books, London, 2019. ISBN 178360722X. Cited on pages 74, 79, 80, 81, 82, 83, 88, and 90.

J.-C. Fabre, X. Louchart, F. Colin, C. Dagès, R. Moussa, M. Rabotin, D. Raclot, P. Lagacherie, and M. Voltz. OpenFLUID : a software environment for modelling fluxes in landscapes. In *International Conference on Integrative Landscape Modelling*. Editions Quae, 2 2010. ISBN 978-2-7592-0859-3. Cited on page 273.

J.-C. Fabre, M. Rabotin, D. Crevoisier, A. Libres, C. Dagès, R. Moussa, X. Louchart, P. Lagacherie, D. Raclot, and M. Voltz. OpenFLUID : an open-source software environment for modelling fluxes in landscapes. In *EGU General Assembly*, 4 2013. Cited on page 273.

M. Falkenmark. Water and Mankind: A Complex System of Mutual Interaction. *Ambio*, 6(1): 3–9, 1977. ISSN 00447447, 16547209. URL `http://www.jstor.org/stable/4312233`. Cited on page 66.

FAO. FAO/Unesco Soil Map of the World - World Soils Resources Report 60 - Reprinted with updates as Technical Paper 20. Technical report, ISRIC, Wageningen, 1997. Cited on page 275.

J. V. Fayne, J. D. Bolten, C. S. Doyle, S. Fuhrmann, M. T. Rice, P. R. Houser, and V. Lakshmi. Flood mapping in the lower Mekong River Basin using daily MODIS observations. *International Journal of Remote Sensing*, 38(6):1737–1757, 3 2017. doi: 10.1080/01431161.2017.1285503. Cited on page 137.

L. Feldman. The Maize Root. In *The Maize Handbook*, pages 29–37. Springer New York, New York, NY, 1994. doi: 10.1007/978-1-4612-2694-9{_}4. Cited on page 298.

R. Flor, K. Chhay, V. Sorn, H. Maat, and B. Hadi. The Technological Trajectory of Integrated Pest Management for Rice in Cambodia. *Sustainability*, 10(6):1732, 5 2018. doi: 10.3390/su 10061732. Cited on page 207.

W. Francesconi, R. Srinivasan, E. Pérez-Miñana, S. P. Willcock, and M. Quintero. Using the Soil and Water Assessment Tool (SWAT) to model ecosystem services: A systematic review. *Journal of Hydrology*, 535:625–636, 4 2016. doi: 10.1016/J.JHYDROL.2016.01.034. Cited on page 272.

E. Frank, M. A. Hall, and I. H. Witten. The WEKA Workbench, 2016. Cited on page 144.

B. Frenay and M. Verleysen. Classification in the Presence of Label Noise: A Survey. *IEEE*

Transactions on Neural Networks and Learning Systems, 25(5):845–869, 5 2014. doi: 10.1109/TNNLS.2013.2292894. Cited on page 253.

J. H. Friedman. Stochastic gradient boosting. *Computational Statistics & Data Analysis*, 38(4):367–378, 2 2002. doi: 10.1016/S0167-9473(01)00065-2. Cited on page 242.

T. Fuller. Cambodia revives Pol Pot's deadly canals, December 4. *The New York Times*, 2008. URL `https://www.nytimes.com/2008/12/04/world/asia/04iht-canal.4.18410736.html`. Cited on page 103.

C. Funk, P. Peterson, M. Landsfeld, D. Pedreros, J. Verdin, S. Shukla, G. Husak, J. Rowland, L. Harrison, A. Hoell, and J. Michaelsen. The climate hazards infrared precipitation with stations—a new environmental record for monitoring extremes. *Scientific Data*, 2(1):150066, 12 2015. doi: 10.1038/sdata.2015.66. Cited on page 130.

Y. Gan, Q. Duan, W. Gong, C. Tong, Y. Sun, W. Chu, A. Ye, C. Miao, and Z. Di. A comprehensive evaluation of various sensitivity analysis methods: A case study with a hydrological model. *Environmental Modelling & Software*, 51:269–285, 1 2014. doi: 10.1016/J.ENVSOFT.2013.09.031. Cited on page 303.

B. C. Gao. NDWI - A normalized difference water index for remote sensing of vegetation liquid water from space. *Remote Sensing of Environment*, 1996. doi: 10.1016/S0034-4257(96)00067-3. Cited on page 239.

S. Georganos, T. Grippa, S. Vanhuysse, M. Lennert, M. Shimoni, S. Kalogirou, and E. Wolff. Less is more: optimizing classification performance through feature selection in a very-high-resolution remote sensing object-based urban application. *GIScience & Remote Sensing*, 55(2):221–242, 3 2018. doi: 10.1080/15481603.2017.1408892. Cited on page 252.

A. Ghosh and P. Joshi. A comparison of selected classification algorithms for mapping bamboo patches in lower Gangetic plains using very high resolution WorldView 2 imagery. *International Journal of Applied Earth Observation and Geoinformation*, 26:298–311, 2 2014. ISSN 0303-2434. doi: 10.1016/J.JAG.2013.08.011. Cited on page 243.

C. P. Giersch. Across Zomia with merchants, monks, and musk: process geographies, trade networks, and the Inner-East–Southeast Asian borderlands. *Journal of Global History*, 5(2):215–239, 7 2010. doi: 10.1017/S1740022810000069. Cited on page 82.

A. A. Gitelson and M. N. Merzlyak. Signature Analysis of Leaf Reflectance Spectra: Algorithm Development for Remote Sensing of Chlorophyll. *Journal of Plant Physiology*, 148(3-4): 494–500, 1 1996. doi: 10.1016/S0176-1617(96)80284-7. Cited on page 239.

A. A. Gitelson, Y. J. Kaufman, M. N. Merzlyak, A. A. Gitelson, Y. J. Kaufman, and M. N. Merzlyak. Use of a green channel in remote sensing of global vegetation from EOS-MODIS. *Remote Sensing of Environment*, 58(3):289–298, 12 1996. doi: 10.1016/S0034-4257(96)00072-7. Cited on page 239.

S. Godinho, N. Guiomar, and A. Gil. Using a stochastic gradient boosting algorithm to analyse the effectiveness of Landsat 8 data for montado land cover mapping: Application in southern Portugal. *International Journal of Applied Earth Observation and Geoinformation*, 49: 151–162, 7 2016. doi: 10.1016/J.JAG.2016.02.008. Cited on pages 238 and 242.

E. Gómez-Baggethun, R. de Groot, P. L. Lomas, and C. Montes. The history of ecosystem services in economic theory and practice: From early notions to markets and payment schemes. *Ecological Economics*, 69(6):1209–1218, 4 2010. doi: 10.1016/J.ECOLECON.2009.11.007. Cited on page 68.

N. Gorelick, M. Hancher, M. Dixon, S. Ilyushchenko, D. Thau, and R. Moore. Google Earth Engine: Planetary-scale geospatial analysis for everyone. *Remote Sensing of Environment*, 202:18–27, 12 2017. doi: 10.1016/J.RSE.2017.06.031. Cited on pages 140 and 142.

N. Gratiot, A. Bildstein, T. T. Anh, H. Thoss, H. Denis, H. Michallet, and H. Apel. Sediment flocculation in the Mekong River estuary, Vietnam, an important driver of geomorphological changes. *Comptes Rendus Geoscience*, 349(6-7):260–268, 10 2017. doi: 10.1016/J.CRTE.2017.09.012. Cited on page 292.

J. R. Gray, G. D. Glysson, L. M. Turcios, and G. E. Schwarz. *Comparability of Suspended-Sediment Concentration and Total Suspended Solids Data science for a changing world*. No. 4191. US Department of the interior, US Geological Survey, 2000, 2000. Cited on page 290.

B. Grizzetti, D. Lanzanova, C. Liquete, A. Reynaud, and A. Cardoso. Assessing water ecosystem services for water resource management. *Environmental Science & Policy*, 61:194–203, 7 2016. doi: 10.1016/J.ENVSCI.2016.04.008. Cited on page 70.

K. Grunewald and O. Bastian. *Ecosystem services : concept, methods and case studies*. Springer, Heidelberg, 2015. ISBN 9783662441428. Cited on pages 68, 69, and 71.

S. Gummadi, T. Dinku, P. B. Shirsath, and M. D. M. Kadiyala. Evaluation of multiple satellite precipitation products for rainfed maize production systems over Vietnam. *Scientific Reports*, 12(1):485, 12 2022. doi: 10.1038/s41598-021-04380-8. Cited on page 134.

V. C. Hackbart, G. T. de Lima, and R. F. dos Santos. Theory and practice of water ecosystem services valuation: Where are we going? *Ecosystem Services*, 23:218–227, 2 2017. doi: 10.1016/J.ECOSER.2016.12.010. Cited on page 71.

C. R. Hackney, S. E. Darby, D. R. Parsons, J. Leyland, J. L. Best, R. Aalto, A. P. Nicholas, and R. C. Houseago. River bank instability from unsustainable sand mining in the lower Mekong River. *Nature Sustainability*, 3(3):217–225, 3 2020. doi: 10.1038/s41893-019-0455-3. Cited on page 118.

C. R. Hackney, G. Vasilopoulos, S. Heng, V. Darbari, S. Walker, and D. R. Parsons. Sand mining far outpaces natural supply in a large alluvial river. *Earth Surface Dynamics*, 9(5):1323–1334, 9 2021. doi: 10.5194/esurf-9-1323-2021. Cited on page 118.

T. Hallouin, M. Bruen, M. Christie, C. Bullock, and M. Kelly-Quinn. Challenges in Using Hydrology and Water Quality Models for Assessing Freshwater Ecosystem Services: A Review. *Geosciences*, 8(2):45, 1 2018. doi: 10.3390/geosciences8020045. Cited on page 71.

A. S. Halls and K. G. Hortle. Flooding is a key driver of the Tonle Sap dai fishery in Cambodia. *Scientific Reports*, 11(1):3806, 12 2021. doi: 10.1038/s41598-021-81248-x. Cited on page 80.

K. H. Hamed and A. Ramachandra Rao. A modified Mann-Kendall trend test for autocorrelated data. *Journal of Hydrology*, 204(1-4):182–196, 1 1998. doi: 10.1016/S0022-1694(97)00125-X. Cited on pages 116 and 132.

Z. Han, D. Long, Y. Fang, A. Hou, and Y. Hong. Impacts of climate change and human activities on the flow regime of the dammed Lancang River in Southwest China. *Journal of Hydrology*, 570:96–105, 3 2019. doi: 10.1016/J.JHYDROL.2018.12.048. Cited on page 327.

T. J. Hanebuth, U. Proske, Y. Saito, V. L. Nguyen, and T. K. O. Ta. Early growth stage of a large delta — Transformation from estuarine-platform to deltaic-progradational conditions

(the northeastern Mekong River Delta, Vietnam). *Sedimentary Geology*, 261:108–119, 6 2012. doi: 10.1016/j.sedgeo.2012.03.014. Cited on pages 93 and 94.

P. Hanington, Q. T. To, P. D. T. Van, N. A. V. Doan, and A. S. Kiem. A hydrological model for interprovincial water resource planning and management: A case study in the Long Xuyen Quadrangle, Mekong Delta, Vietnam. *Journal of Hydrology*, 2017. doi: 10.1016/j.jhydrol.2017.01.030. Cited on page 58.

M. C. Hansen, P. V. Potapov, R. Moore, M. Hancher, S. A. Turubanova, A. Tyukavina, D. Thau, S. V. Stehman, S. J. Goetz, T. R. Loveland, A. Kommareddy, A. Egorov, L. Chini, C. O. Justice, and J. R. G. Townshend. High-Resolution Global Maps of 21st-Century Forest Cover Change. *Science*, 342(6160):850–853, 11 2013. doi: 10.1126/science.1244693. Cited on pages 142 and 143.

R. M. Haralick, K. Shanmugam, and I. Dinstein. Textural Features for Image Classification. *IEEE Transactions on Systems, Man, and Cybernetics*, SMC-3(6):610–621, 11 1973. doi: 10.1109/TSMC.1973.4309314. Cited on page 238.

D. M. Harper, M. Zalewski, and N. Pacini. *Ecohydrology : processes, models and case studies : an approach to the sustainable management of water resources*. CABI Pub, 2008. ISBN 1845933702. Cited on page 64.

D. Harrison-Atlas, D. M. Theobald, and J. H. Goldstein. A systematic review of approaches to quantify hydrologic ecosystem services to inform decision-making. *International Journal of Biodiversity Science, Ecosystem Services & Management*, 12(3):160–171, 7 2016. doi: 10.1080/21513732.2016.1181105. Cited on page 70.

H. Hashim, Z. A. Latif, N. A. Adnan, and S. Alam. Urban Vegetation Classification with NDVI Threshold Value Method With Very High Resolution (VHR) PLEIADES Imagery. *The International Archives of the Photogrammetry, Remote Sensing and Spatial Information Sciences*, XLII-4/W16:237–240, 2019. doi: 10.5194/isprs-archives-XLII-4-W16-237-2019. Cited on page 149.

L. Hawker, P. Bates, J. Neal, L. Hawker, P. Bates, and J. Neal. Flood Inundation Modelling in Data Sparse Deltas. *EGUGA*, page 5752, 2017. Cited on page 272.

L. Hawker, J. Neal, and P. Bates. Accuracy assessment of the TanDEM-X 90 Digital Elevation Model for selected floodplain sites. *Remote Sensing of Environment*, 232:111319, 10 2019. doi: 10.1016/J.RSE.2019.111319. Cited on page 332.

R. H. Hawkins, T. J. Ward, D. E. Woodward, and J. A. Van Mullem. *Curve Number Hydrology*. American Society of Civil Engineers, Reston, VA, 11 2008. ISBN 978-0-7844-1004-2. doi: 10.1061/9780784410042. Cited on page 297.

W. Heber Green and G. A. Ampt. Studies on Soil Phyics. *The Journal of Agricultural Science*, 4 (1):1–24, 5 1911. doi: 10.1017/S0021859600001441. Cited on page 289.

J. Hecht, G. Lacombe, M. Arias, T. Dang, and T. Piman. Hydropower dams of the Mekong River basin: a review of their hydrological impacts. *Journal of Hydrology*, 568:285–300, 10 2018. doi: 10.1016/j.jhydrol.2018.10.045. Cited on pages 58, 77, 83, 84, 167, 328, and 331.

S. Heng, A. Horton, P. Hok, S. Chung, J. Koponen, and M. Kummu. The Cambodian Mekong floodplain under the future development plans and climate change. *Natural Hazards and Earth System Science*, 65:1–25, 2021. doi: 10.5194/nhess-2021-65. Cited on pages 78, 122, 137, 164, 167, and 272.

P. Hirsch. The Changing Political Dynamics of Dam Building on the Mekong. *Water Alternatives*, 3(2), 2010. Cited on page 87.

P. Hirsch, K. Mørck, J. With, B. Boer, N. Carrard, S. Fitzgerald, and R. Lyster. National Interests and Transboundary Water Governance in the Mekong. Technical report, Australian Mekong Resource Centre, in collaboration with Danish International Development Assistance., 2006. URL `http://www.mekongwaterforum.org/sites/default/files/Hirsch_Jensen_2006_national_interests_and_transboundary_water_governance.pdf`. Cited on page 90.

L. P. Hoang, H. Lauri, M. Kummu, J. Koponen, M. T. H. van Vliet, I. Supit, R. Leemans, P. Kabat, and F. Ludwig. Mekong River flow and hydrological extremes under climate change. *Hydrology and Earth System Sciences*, 20(7):3027–3041, 7 2016. doi: 10.5194/hess-20-3027-2016. Cited on page 330.

L. P. Hoang, R. Biesbroek, V. P. D. Tri, M. Kummu, M. T. H. van Vliet, R. Leemans, P. Kabat, and F. Ludwig. Managing flood risks in the Mekong Delta: How to address emerging challenges

under climate change and socioeconomic developments. *Ambio*, 47(6):635–649, 10 2018. ISSN 0044-7447. doi: 10.1007/s13280-017-1009-4. Cited on pages 78 and 96.

L. P. Hoang, M. T. van Vliet, M. Kummu, H. Lauri, J. Koponen, I. Supit, R. Leemans, P. Kabat, and F. Ludwig. The Mekong's future flows under multiple drivers: How climate change, hydropower developments and irrigation expansions drive hydrological changes. *Science of the Total Environment*, 649:601–609, 2019. ISSN 18791026. doi: 10.1016/j.scitotenv.2018.08.160. Cited on pages 78, 85, 309, 310, 312, 313, 321, and 331.

K. Hortle. Fishes of the Mekong - How Many Species are There? *Catch and Culture*, 15:4–12, 2009a. Cited on page 79.

K. G. Hortle. Fisheries of the Mekong River Basin. *The Mekong*, pages 197–249, 1 2009b. doi: 10.1016/B978-0-12-374026-7.00009-7. Cited on pages 80, 109, and 168.

A. J. Horton, N. V. K. Triet, L. P. Hoang, S. Heng, P. Hok, S. Chung, J. Koponen, and M. Kummu. The Cambodian Mekong floodplain under future development plans and climate change. *Hazards Earth Syst. Sci*, 22:967–983, 2022. doi: 10.5194/nhess-22-967-2022. Cited on pages 272 and 332.

K. Hubacek and J. C. van den Bergh. Changing concepts of 'land' in economic theory: From single to multi-disciplinary approaches. *Ecological Economics*, 56(1):5–27, 1 2006. doi: 10.1016/J.ECOLECON.2005.03.033. Cited on page 68.

A. Huete, K. Didan, T. Miura, E. Rodriguez, X. Gao, and L. Ferreira. Overview of the radiometric and biophysical performance of the MODIS vegetation indices. *Remote Sensing of Environment*, 83(1-2):195–213, 11 2002. doi: 10.1016/S0034-4257(02)00096-2. Cited on page 239.

A. R. Huete. A soil-adjusted vegetation index (SAVI). *Remote Sensing of Environment*, 25(3): 295–309, 1988. ISSN 00344257. doi: 10.1016/0034-4257(88)90106-X. Cited on page 239.

D. A. Hughes. Floodplain inundation: Processes and relationships with channel discharge. *Earth Surface Processes*, 5(3):297–304, 7 1980. doi: 10.1002/esp.3760050308. Cited on page 145.

N. N. Hung, J. M. Delgado, A. Güntner, B. Merz, A. Bárdossy, and H. Apel. Sedimentation in the floodplains of the Mekong Delta, Vietnam Part II: deposition and erosion. *Hydrological*

Processes, 28(7):3145–3160, 3 2014. doi: 10.1002/hyp.9855. Cited on pages 97, 166, 292, 293, and 320.

Hung Van Pham, F. C. Van Geer, V. Bui Tran, W. Dubelaar, and G. H. Oude Essink. Paleo-hydrogeological reconstruction of the fresh-saline groundwater distribution in the Vietnamese Mekong Delta since the late Pleistocene. *Journal of Hydrology: Regional Studies*, 23:100594, 6 2019. doi: 10.1016/J.EJRH.2019.100594. Cited on page 98.

L. Hunt. Mekong River Commission Faces Radical Change, 1 2016. Cited on page 91.

C. Hütt, W. Koppe, Y. Miao, and G. Bareth. Best Accuracy Land Use/Land Cover (LULC) Classification to Derive Crop Types Using Multitemporal, Multisensor, and Multi-Polarization SAR Satellite Images. *Remote Sensing*, 8(8):684, 8 2016. doi: 10.3390/rs8080684. Cited on page 235.

H. Huu Nguyen, P. Dargusch, P. Moss, and D. B. Tran. A review of the drivers of 200 years of wetland degradation in the Mekong Delta of Vietnam. *Regional Environmental Change*, 16(8): 2303–2315, 12 2016. doi: 10.1007/s10113-016-0941-3. Cited on page 102.

IPCC. Climate Change 2013 - The Fifth Assessment Report of the Intergovernmental Panel on Climate Change. Technical report, Intergovernmental Panel on Climate Change, 2013. Cited on page 89.

M. Irfan, A. Qadir, H. Ali, N. Jamil, and S. R. Ahmad. Vulnerability of Environmental Resources in Indus Basin after the Development of Irrigation System. In S. Ricart, A. M. Rico, and J. Olcina, editors, *Irrigation Water Productivity and Operation, Sustainability and Climate Change.* IntechOpen, London, 2019. ISBN 9781789846768. Cited on page 334.

B. Ivars and J.-P. Venot. Entre politiques publiques et matérialité: associations d'usagers et infrastructures d'irrigation au Cambodge. *Natures Sciences Sociétés*, 26(4):383–394, 10 2018. doi: 10.1051/nss/2018053. Cited on page 194.

J. W. Jacobs. The Mekong River Commission: transboundary water resources planning and regional security. *The Geographical Journal*, 168(4):354–364, 12 2002. doi: 10.1111/j.0016-7398.2002.00061.x. Cited on pages 69 and 84.

G. C. Jahn, M. Solieng, P. G. Cox, and C. Nel. Farmer Participatory Research on Rat Management in Cambodia. *Int. Rice Res. Notes*, 24(3):29–31, 1999. Cited on page 207.

Z. Jiang, A. R. Huete, K. Didan, and T. Miura. Development of a two-band enhanced vegetation index without a blue band. *Remote Sensing of Environment*, 112(10):3833–3845, 10 2008. ISSN 0034-4257. doi: 10.1016/J.RSE.2008.06.006. Cited on page 239.

G. H. John and P. Langley. Estimating Continuous Distributions in Bayesian Classifiers. In *Proceedings of the Eleventh conference on Uncertainty in artificial intelligence*, pages 338–345, 8 2013. Cited on page 240.

B. A. Johnson and K. Iizuka. Integrating OpenStreetMap crowdsourced data and Landsat time-series imagery for rapid land use/land cover (LULC) mapping: Case study of the Laguna de Bay area of the Philippines. *Applied Geography*, 67:140–149, 2 2016. doi: 10.1016/J.APGEOG.2015.12.006. Cited on page 240.

D. M. Johnson. Using the Landsat archive to map crop cover history across the United States. *Remote Sensing of Environment*, 232:111286, 10 2019. doi: 10.1016/J.RSE.2019.111286. Cited on page 142.

J. M. Johnston, R. J. Zomer, and M.-c. Wang. Predicting Future Vegetated Landscapes Under Climate Change: Application of the Environmental Stratification Methodology to Protected Areas in the Lower Mekong Basin. In *Ecosystem-Based Management, Ecosystem Services and Aquatic Biodiversity*, pages 561–580. Springer International Publishing, Cham, 2020. doi: 10.1007/978-3-030-45843-0{_}28. Cited on page 89.

C. F. Jordan. Derivation of Leaf-Area Index from Quality of Light on the Forest Floor. *Ecology*, 50(4):663–666, 7 1969. doi: 10.2307/1936256. Cited on page 239.

S. E. Jozdani, B. A. Johnson, and D. Chen. Comparing Deep Neural Networks, Ensemble Classifiers, and Support Vector Machine Algorithms for Object-Based Urban Land Use/Land Cover Classification. *Remote Sensing*, 11(14):1713, 7 2019. doi: 10.3390/rs11141713. Cited on page 235.

W. Junk, P. Bayley, and R. Sparks. The flood-pulse concept in river-floodplain systems. In D. Dodge, editor, *Proceedings of the International Large River Symposium (LARS)*, pages 110–127, Ottawa, 1989. NRC research press. Cited on pages 78 and 79.

K. R. K. R. Douglas-Mankin, R. R. Srinivasan, and J. G. J. G. Arnold. Soil and Water Assessment Tool (SWAT) Model: Current Developments and Applications. *Transactions of the ASABE*, 53(5):1423–1431, 2010. doi: 10.13031/2013.34915. Cited on page 272.

F. Karanja. *Cropwat model analysis of crop water use in six districts in Kenya*. Center for Environmental Economics and Policy in Africa, University of Pretoria, 2006. ISBN 1-920160-35- 3. Cited on page 299.

T. Kavzoglu and I. Colkesen. A kernel functions analysis for support vector machines for land cover classification. *International Journal of Applied Earth Observation and Geoinformation*, 11(5):352–359, 10 2009. doi: 10.1016/J.JAG.2009.06.002. Cited on page 243.

S. Kazama, T. Hagiwara, P. Ranjan, and M. Sawamoto. Evaluation of groundwater resources in wide inundation areas of the Mekong River basin. *Journal of Hydrology*, 340(3-4):233–243, 7 2007. doi: 10.1016/J.JHYDROL.2007.04.017. Cited on pages 98, 103, 260, and 289.

A. Khan, H. Govil, G. Kumar, and R. Dave. Synergistic use of Sentinel-1 and Sentinel-2 for improved LULC mapping with special reference to bad land class: a case study for Yamuna River floodplain, India. *Spatial Information Research*, 28(6):669–681, 12 2020. doi: 10.1007/s41324-020-00325-x. Cited on page 245.

Khmer Times. Japan provides nearly $3 million to MRC, February 27. *Khmer Times*, 2021. URL `https://www.khmertimeskh.com/50818697/japan-provides-nearly-3-million-to-mrc/`. Cited on page 91.

A. Kiem. Analysis of historical trends, variability and changes in hydroclimatic conditions for the Lower Mekong Basin (LMB). Technical report, Mekong River Commission - Climate Change Adaptation Initiative, 2017. URL `https://www.mrcmekong.org/assets/20170502Trends_TechnicalReport_FINAL_forMRC.pdf`. Cited on page 89.

B. Kiernan. Introduction: Conflict in Cambodia, 1945-2002. *Critical Asian Studies*, 2002. doi: 10.1080/1467271022000035893. Cited on page 184.

G. M. Kondolf, Z. K. Rubin, and J. T. Minear. Dams on the Mekong: Cumulative sediment starvation. *Water Resources Research*, 50(6):5158–5169, 6 2014. doi: 10.1002/2013WR014651. Cited on page 86.

G. M. Kondolf, R. J. P. Schmitt, P. Carling, S. Darby, M. Arias, S. Bizzi, A. Castelletti, T. A. Cochrane, S. Gibson, M. Kummu, C. Oeurng, Z. Rubin, and T. Wild. Changing sediment budget of the Mekong: Cumulative threats and management strategies for a large river basin. *Science of The Total Environment*, 625:114–134, 6 2018. doi: 10.1016/j.scitotenv.2017.11.361. Cited on pages 75, 78, and 137.

I. Kossov and The Phnom Penh Post. Mekong River in danger, but MRC is 'weak', May 20. *The Phnom Penh Post*, 2016. URL `https://www.phnompenhpost.com/national/mekong-river-danger-mrc-weak`. Cited on page 91.

I. Kossov, L. Smean, and The Phnom Penh Post. Donors slash funding for MRC, January 14, 2016. URL `https://www.phnompenhpost.com/national/donors-slash-funding-mrc`. Cited on page 91.

V. I. Kravtsova, V. N. Mikhailov, and N. A. Efremova. Variations of the hydrological regime, morphological structure, and landscapes of the Indus River delta (Pakistan) under the effect of large-scale water management measures. *Water Resources*, 36(4):365–379, 7 2009. doi: 10.1134/S0097807809040010. Cited on page 334.

W. H. Kruskal and W. A. Wallis. Use of Ranks in One-Criterion Variance Analysis. *Journal of the American Statistical Association*, 47(260):583–621, 12 1952. doi: 10.1080/01621459.1952.10483441. Cited on page 243.

C. Kuenzer and F. Renaud. Climate Change and Environmental Change in River Deltas Globally. In *The Mekong delta system - Interdisciplinary analyses of a river delta*, pages 7–48. Springer, Dordrecht, 6 2012. ISBN 978-94-007-3961-1. Cited on page 57.

C. Kuenzer, G. Liu, F. Renaud, M. Ottinger, and S. Dech. Asian River Deltas experiencing slow-onset Hazards: Vulnerability, Resilience and Adaptation to Environmental Degradation and Climate Change. In *Proceedings of the International Risk and Disaster Reduction Conference, IRDR.*, Beijing, China, 2011. Cited on page 57.

C. Kuenzer, H. Guo, J. Huth, P. Leinenkugel, X. Li, and S. Dech. Flood mapping and flood dynamics of the Mekong Delta: ENVISAT-ASAR-WSM based time series analyses. *Remote Sensing*, 5:687–715, 2 2013. doi: 10.3390/rs5020687. Cited on pages 57, 95, and 96.

L. Kumar and O. Mutanga. Google Earth Engine Applications Since Inception: Usage, Trends, and Potential. *Remote Sensing*, 10(10):1509, 9 2018. doi: 10.3390/rs10101509. Cited on page 143.

P. Kumar, editor. *The Economics of Ecosystems and Biodiversity: Ecological and Economic Foundations*. Routledge, 12 2012. doi: 10.4324/9781849775489. Cited on page 69.

M. Kummu and J. Sarkula. Impact of the Mekong River Flow Alteration on the Tonle Sap Flood Pulse. *Ambio*, 37(3):185–192, 2008. doi: 10.1579/0044-7447(2008)37[185:IOTMRF]2.0.CO;2. Cited on pages 78 and 137.

M. Kummu and O. Varis. Sediment-related impacts due to upstream reservoir trapping, the Lower Mekong River. *Geomorphology*, 85(3-4):275–293, 3 2007. doi: 10.1016/J.GEOMORPH.2006.03.024. Cited on page 290.

M. Kummu, J. Koponen, and J. Sarkkula. Upstream Impacts on Lower Mekong Floodplains : Tonle Sap Case Study. In *International Conference on Advances in Integrated Mekong River Management*, 2004. Cited on page 76.

M. Kummu, S. Tes, S. Yin, P. Adamson, J. Józsa, J. Koponen, J. Richey, and J. Sarkkula. Water balance analysis for the Tonle Sap Lake-floodplain system. *Hydrological Processes*, 28(4): 1722–1733, 2 2014. doi: 10.1002/hyp.9718. Cited on pages 76 and 145.

L. I. Kuncheva. On the optimality of Naïve Bayes with dependent binary features. *Pattern Recognition Letters*, 27(7):830–837, 5 2006. doi: 10.1016/J.PATREC.2005.12.001. Cited on page 240.

Z. W. Kundzewicz. Ecohydrology-seeking consensus on interpretation of the notion / Ecohydrologie-à la recherche d'un consensus sur l'interprétation de la notion. *Hydrological Sciences Journal*, 47(5):799–804, 2009. doi: 10.1080/02626660209492982. Cited on page 65.

M. Kunthear and Khmer Times. Fishing season ends with ministry warning, May 16. *Khmer Times*, 2018. URL `https://www.khmertimeskh.com/490231/fishing-season-ends-with-ministry-warning/`. Cited on page 204.

G. Lacombe and A. Pierret. Hydrological impact of war-induced deforestation in the Mekong Basin. *Ecohydrology*, 6(5):n/a–n/a, 6 2013. doi: 10.1002/eco.1395. Cited on pages 87 and 184.

J.-P. Lamagat, H. J. Morel-Seytoux, and J. Albergel. Analyse de la propagation des ondes de crues. *Hydrologie Continentale*, 8:113–137, 1993. Cited on page 145.

D. Lanh. Study on integrated water resources utility and environmental flow aims to protect the ecology and the sustainable development of the Mekong Delta (in Vietnamese. Technical report, WRSI Danida project, 2005. Cited on page 121.

C. Leauthaud, G. Belaud, S. Duvail, R. Moussa, O. Grünberger, G. Grünberger, and J. Albergel. Characterizing floods in the poorly gauged wetlands of the Tana River Delta, Kenya, using a water balance model and satellite data. *Hydrol. Earth Syst. Sci*, 17:3059–3075, 2013. doi: 10.5194/hess-17-3059-2013. Cited on pages 59 and 145.

J.-S. Lee. A simple speckle smoothing algorithm for synthetic aperture radar images. *IEEE Transactions on Systems, Man, and Cybernetics*, SMC-13(1):85–89, 1 1983. doi: 10.1109/TS MC.1983.6313036. Cited on page 140.

P. Leinenkugel, M. L. Wolters, N. Oppelt, and C. Kuenzer. Tree cover and forest cover dynamics in the Mekong Basin from 2001 to 2011. *Remote Sensing of Environment*, 158:376–392, 3 2015. doi: 10.1016/J.RSE.2014.10.021. Cited on page 88.

C. Li, J. Wang, L. Wang, L. Hu, and P. Gong. Comparison of Classification Algorithms and Training Sample Sizes in Urban Land Classification with Landsat Thematic Mapper Imagery. *Remote Sensing*, 6(2):964–983, 1 2014. doi: 10.3390/rs6020964. Cited on page 243.

D. Li, D. Long, J. Zhao, H. Lu, and Y. Hong. Observed changes in flow regimes in the Mekong River basin. *Journal of Hydrology*, 551, 2017. doi: 10.1016/j.jhydrol.2017.05.061. Cited on page 327.

D. Li, J. Zhao, and R. S. Govindaraju. Water benefits sharing under transboundary cooperation in the Lancang-Mekong River Basin. *Journal of Hydrology*, 577:123989, 10 2019. doi: 10.1016/J.JHYDROL.2019.123989. Cited on page 137.

X.-l. Li, G. Brierley, D.-j. Shi, Y.-l. Xie, and H.-q. Sun. Ecological Protection and Restoration in Sanjiangyuan National Nature Reserve, Qinghai Province, China. In *Perspectives on Environmental Management and Technology in Asian River Basins*, pages 93–120. Springer Netherlands, Dordrecht, 2012. doi: 10.1007/978-94-007-2330-6{_}6. Cited on page 74.

K.-H. Liao, T. A. Le, and K. V. Nguyen. Urban design principles for flood resilience: Learning from the ecological wisdom of living with floods in the Vietnamese Mekong Delta. *Landscape and Urban Planning*, 155:69–78, 11 2016. doi: 10.1016/J.LANDURBPLAN.2016.01.014. Cited on page 99.

S. Lin and C. Grundy-Warr. Navigating Sino-Thai 'rocky' bilateral ties: The geopolitics of riverine trade in the Greater Mekong Subregion. *Environment and Planning C: Politics and Space*, 38(5):826–833, 8 2020. doi: 10.1177/2399654420911410e. Cited on page 75.

Y. Lin, H. Zhang, H. Lin, P. E. Gamba, and X. Liu. Incorporating synthetic aperture radar and optical images to investigate the annual dynamics of anthropogenic impervious surface at large scale. *Remote Sensing of Environment*, 242:111757, 6 2020. doi: 10.1016/J.RSE.2020.111757. Cited on page 238.

P. Liu, D. DeMaster, T. Nguyen, Y. Saito, V. L. Nguyen, T. K. O. Ta, and X. Li. Stratigraphic Formation of the Mekong River Delta and Its Recent Shoreline Changes. *Oceanography*, 30 (3), 2017. doi: 10.5670/oceanog.2017.316. Cited on pages 76 and 94.

S. Liu, X. Li, D. Chen, Y. Duan, H. Ji, L. Zhang, Q. Chai, and X. Hu. Understanding Land use/Land cover dynamics and impacts of human activities in the Mekong Delta over the last 40 years. *Global Ecology and Conservation*, 22:e00991, 6 2020. doi: 10.1016/J.GECCO.2020.E00991. Cited on page 58.

H. H. Loc, M. Low Lixian, E. Park, T. D. Dung, S. Shrestha, and Y.-J. Yoon. How the saline water intrusion has reshaped the agricultural landscape of the Vietnamese Mekong Delta, a review. *Science of The Total Environment*, 794:148651, 11 2021. doi: 10.1016/J.SCITOTENV.2021.148651. Cited on page 105.

S. Lohani, T. Dilts, P. Weisberg, S. Null, and Z. Hogan. Rapidly Accelerating Deforestation in Cambodia's Mekong River Basin: A Comparative Analysis of Spatial Patterns and Drivers. *Water*, 12(8):2191, 8 2020. doi: 10.3390/w12082191. Cited on pages 87 and 149.

D. P. Loucks. Developed river deltas: are they sustainable? *Environmental Research Letters*, 14 (11):113004, 11 2019. doi: 10.1088/1748-9326/ab4165. Cited on page 92.

S. Lovelli, M. Perniola, A. Ferrara, and T. Di Tommaso. Yield response factor to water (Ky) and water use efficiency of Carthamus tinctorius L. and Solanum melongena L. *Agricultural Water Management*, 92(1-2):73–80, 8 2007. doi: 10.1016/j.agwat.2007.05.005. Cited on page 299.

L. Lu, Y. Tao, and L. Di. Object-Based Plastic-Mulched Landcover Extraction Using Integrated Sentinel-1 and Sentinel-2 Data. *Remote Sensing*, 10(11):1820, 11 2018. doi: 10.3390/rs1011 1820. Cited on page 250.

H. T. Luong. The organisational structure of transnational narcotics trafficking groups in Southeast Asia: a case study of Vietnam's border with Laos. *Trends in Organized Crime*, 23 (4):385–411, 12 2020. doi: 10.1007/s12117-020-09384-w. Cited on page 82.

L. Lymburner, P. Beggs, and C. Jacobson. Estimation of Canopy-Average Surface-Specific Leaf Area Using Landsat TM Data. *Photogrammetric Engineering and Remote Sensing*, 66(2): 183–192, 2000. Cited on page 239.

L. Ma, M. Li, X. Ma, L. Cheng, P. Du, and Y. Liu. A review of supervised object-based land-cover image classification. *ISPRS Journal of Photogrammetry and Remote Sensing*, 130: 277–293, 8 2017. doi: 10.1016/J.ISPRSJPRS.2017.06.001. Cited on page 252.

K. Madani and M. Shafiee-Jood. Socio-Hydrology: A New Understanding to Unite or a New Science to Divide? *Water*, 12(7):1941, 7 2020. doi: 10.3390/w12071941. Cited on page 66.

M. Main-Knorn, B. Pflug, J. Louis, V. Debaecker, U. Müller-Wilm, and F. Gascon. Sen2Cor for Sentinel-2. In L. Bruzzone, F. Bovolo, and J. A. Benediktsson, editors, *Image and Signal Processing for Remote Sensing {XXIII}*. SPIE, 10 2017. doi: 10.1117/12.2278218. Cited on pages 140 and 238.

I. Mallakpour and G. Villarini. A simulation study to examine the sensitivity of the Pettitt test to detect abrupt changes in mean. *Hydrological Sciences Journal*, 61(2):245–254, 1 2016. doi: 10.1080/02626667.2015.1008482. Cited on page 116.

N. V. Manh, N. V. Dung, N. N. Hung, B. Merz, and H. Apel. Large-scale suspended sediment transport and sediment deposition in the Mekong Delta. *Hydrology and Earth System Sciences*, 18(8):3033–3053, 8 2014. doi: 10.5194/hess-18-3033-2014. Cited on pages 97 and 166.

N. V. Manh, N. V. Dung, N. N. Hung, M. Kummu, B. Merz, and H. Apel. Future sediment dynamics in the Mekong Delta floodplains: Impacts of hydropower development, climate change and sea level rise. *Global and Planetary Change*, 127:22–33, 4 2015. doi: 10.1016/J.GLOPLACHA.2015.01.001. Cited on page 97.

K. Markert, C. Schmidt, R. Griffin, A. Flores, A. Poortinga, D. Saah, R. Muench, N. Clinton, F. Chishtie, K. Kityuttachai, P. Someth, E. Anderson, A. Aekakkararungroj, D. Ganz, K. N. Markert, C. M. Schmidt, R. E. Griffin, A. I. Flores, A. Poortinga, D. S. Saah, R. E. Muench, N. E. Clinton, F. Chishtie, K. Kityuttachai, P. Someth, E. R. Anderson, A. Aekakkararungroj, and D. J. Ganz. Historical and Operational Monitoring of Surface Sediments in the Lower Mekong Basin Using Landsat and Google Earth Engine Cloud Computing. *Remote Sensing*, 10(6):909, 6 2018. ISSN 2072-4292. doi: 10.3390/rs10060909. Cited on page 143.

K. Marx. *Captial, Volume One. The Process of Production of Capital.* W.W. Norton & Company, London, 1887. Cited on page 68.

K. Marx. *Critique of the Gotha Program*. First published in: Die Neue Zeit, Bd.1, No. 18, 1891. Cited on page 68.

J. G. Masek, M. A. Wulder, B. Markham, J. McCorkel, C. J. Crawford, J. Storey, and D. T. Jenstrom. Landsat 9: Empowering open science and applications through continuity. *Remote Sensing of Environment*, 248:111968, 10 2020. doi: 10.1016/J.RSE.2020.111968. Cited on page 141.

M. Matsukawa, K. Ito, K. Kawakita, and T. Tanaka. Current status of pesticide use among rice farmers in Cambodia. *Applied Entomology and Zoology*, 51(4):571–579, 11 2016. doi: 10.1007/s13355-016-0432-5. Cited on page 193.

K. McDonough, S. Hutchinson, T. Moore, and J. S. Hutchinson. Analysis of publication trends in ecosystem services research. *Ecosystem Services*, 25:82–88, 6 2017. doi: 10.1016/j.ecoser.2017.03.022. Cited on page 69.

S. K. McFeeters. The use of the Normalized Difference Water Index (NDWI) in the delineation of open water features. *International Journal of Remote Sensing*, 17(7):1425–1432, 5 1996. doi: 10.1080/01431169608948714. Cited on pages 144 and 239.

Mekong River Commission. Annual Report 2012. Technical report, Mekong River Commission, Vientiane, 2014. URL https://www.mrcmekong.org/assets/Publications/governance/MRC-Annual-Report-2012.pdf. Cited on page 91.

Mekong River Commission. Basin-Wide Assessment of Climate Change Impacts on Hydropower Production. Technical report, Mekong River Commission, Vientiane, 2018a. URL https://www.mrcmekong.org/assets/Publications/Basin-wide-Assessment-of-Climate-Change-Impacts-on-Hydropower-Production_report-13May19.pdf. Cited on page 89.

Mekong River Commission. The Council Study - The Study on the Sustainable Management and Development of the Mekong River Basin including Impacts of Mainstream Hydropower Projects - Macro-economic Assessment Report. Technical report, Mekong River Commission, 2018b. URL https://www.mrcmekong.org/assets/Publications/Council-Study/Macro-economic-assessment-report_Council-Study.pdf. Cited on pages 84 and 89.

Mekong River Commission. State of the Basin Report 2018. Technical report, Mekong River Commission, 2019. URL https://www.mrcmekong.org/assets/Publications/SOBR-v8_Final-for-web.pdf. Cited on pages 77 and 81.

Mekong River Commission. Climate Change, 2021. URL https://www.mrcmekong.org/our-work/topics/climate-change/. Cited on page 89.

Mekong River Commission MRC. Agreement on the Cooperation for the Sustainable Development of the Mekong River Basin. Technical report, Mekong River Commission, Chiang Rai, 1995. Cited on page 90.

Mekong River Commission MRC. Overview of the Hydrology of the Mekong Basin. Technical report, Mekong River Commission, Vientiane, 2005. Cited on pages 76, 78, and 92.

L. Mercado and Asia Times. Mekong Commission failure: dam the river and damn the region, December 2. *Asia Times*, 2021. URL https://asiatimes.com/2021/12/mekong-commission-failure-dam-the-river-and-damn-the-region/. Cited on pages 88 and 91.

E. Meselhe, D. Roelvink, C. Wackerman, F. Xing, and V. Q. Thanh. Modeling the Process Response of Coastal and Deltaic Systems to Human and Global Changes: Focus on the

Mekong System. *Oceanography*, 30(3), 2017. doi: 10.5670/oceanog.2017.317. Cited on page 58.

P. S. J. Minderhoud, G. Erkens, V. H. Pham, V. T. Bui, L. Erban, H. Kooi, and E. Stouthamer. Impacts of 25 years of groundwater extraction on subsidence in the Mekong delta, Vietnam. *Environmental Research Letters*, 12(6):064006, 6 2017. doi: 10.1088/1748-9326/aa7146. Cited on pages 58, 81, 97, 98, and 104.

P. S. J. Minderhoud, L. Coumou, G. Erkens, H. Middelkoop, and E. Stouthamer. Mekong delta much lower than previously assumed in sea-level rise impact assessments. *Nature Communications*, 10(1):3847, 12 2019. doi: 10.1038/s41467-019-11602-1. Cited on pages 86 and 104.

V. N. Mishra, R. Prasad, P. K. Rai, A. K. Vishwakarma, and A. Arora. Performance evaluation of textural features in improving land use/land cover classification accuracy of heterogeneous landscape using multi-sensor remote sensing data. *Earth Science Informatics*, 12(1):71–86, 3 2019. doi: 10.1007/s12145-018-0369-z. Cited on page 238.

M. Mohammady, H. R. Moradi, H. Zeinivand, and A. J. A. M. Temme. A comparison of supervised, unsupervised and synthetic land use classification methods in the north of Iran. *International Journal of Environmental Science and Technology*, 12(5):1515–1526, 5 2015. doi: 10.1007/s13762-014-0728-3. Cited on page 234.

I. N. Mohammed, J. D. Bolten, R. Srinivasan, and V. Lakshmi. Satellite observations and modeling to understand the Lower Mekong River Basin streamflow variability. *Journal of Hydrology*, 564:559–573, 9 2018. ISSN 00221694. doi: 10.1016/j.jhydrol.2018.07.030. Cited on page 137.

F. Molle, T. Foran, and M. Kakonen. *Contested waterscapes in the Mekong Region : hydropower, livelihoods and governance*. Earthscan, 2009. ISBN 1844077071. Cited on page 75.

S. Morand and C. Lajaunie. The history and diversity of Southeast Asia. In *Biodiversity Conservation in Southeast Asia*, pages 3–19. Routledge, 7 2017. doi: 10.4324/9781315313573-1. Cited on page 79.

MoWRAM. WAT4CAM, 2021. URL `https://wat4cam-mowram.com/en`. Cited on page 188.

MoWRAM and AFD. Wat4Cam Component 3.1 Mekong Bassac Hydrological and Hydraulic Study. Technical report, Ministry of Water Resources and Management, Phnom Penh, 2022. Cited on page 276.

H. M. Mwamlavya, C. N. Munga, B. M. Fulanda, J. O. Omukoto, P. Z. Thoya, F. Mackay, F. H. Manyenze, and J. C. Groeneveld. Natural resource-use in the Lower Tana River Delta based on household surveys and remote sensing of land cover and land use patterns. *Western Indian Ocean Journal of Marine Science*, 1:115–129, 12 2021. doi: 10.4314/wiojms.vi1/2021. Cited on page 334.

NASA Earth Observatory. NASA and USGS Launch Landsat 9, 9 2021. URL `https://earthobservatory.nasa.gov/images/148888/nasa-and-usgs-launch-landsat-9`. Cited on page 141.

B. Nath and S. Acharjee. Forest Cover Change Detection using Normalized Difference Vegetation Index (NDVI) : A Study of Reingkhyongkine Lake's Adjoining Areas, Rangamati, Bangladesh. *Indian Cartographer*, 33:348–353, 9 2013. Cited on page 149.

National Institute of Statistics. General Population Census of the Kingdom of Cambodia 2019. Technical report, Kingdom of Cambodia, Ministry of Planning, Phnom Penh, 2020. URL `https://www.nis.gov.kh/nis/Census2019/FinalGeneralPopulationCensus2019-English.pdf`. Cited on page 99.

J. Neal, G. Schumann, and P. Bates. A subgrid channel model for simulating river hydraulics and floodplain inundation over large and data sparse areas. *Water Resources Research*, 48(11), 11 2012. ISSN 00431397. doi: 10.1029/2012WR012514. Cited on page 334.

T. Nery, R. Sadler, M. Solis-Aulestia, B. White, M. Polyakov, and M. Chalak. Comparing supervised algorithms in Land Use and Land Cover classification of a Landsat time-series. In *2016 IEEE International Geoscience and Remote Sensing Symposium (IGARSS)*, pages 5165–5168. IEEE, 7 2016. doi: 10.1109/IGARSS.2016.7730346. Cited on page 235.

M. S. Netzer, G. Sidman, T. R. Pearson, S. M. Walker, and R. Srinivasan. Combining Global Remote Sensing Products with Hydrological Modeling to Measure the Impact of Tropical Forest Loss on Water-Based Ecosystem Services. *Forests*, 10(5):413, 5 2019. doi: 10.3390/f10050413. Cited on page 88.

M. Nga. Mekong Delta saltwater intrusion not to be as severe as 2020, 1 2021. Cited on page 117.

P. M. Nguyen, K. Van Le, Y.-D. Botula, and W. M. Cornelis. Evaluation of soil water retention pedotransfer functions for Vietnamese Mekong Delta soils. *Agricultural Water Management*, 158:126–138, 8 2015. doi: 10.1016/J.AGWAT.2015.04.011. Cited on page 94.

N. H. Nhan and N. B. Cao. Damming the Mekong: Impacts in Vietnam and Solutions. *Coasts and Estuaries*, pages 321–340, 1 2019. doi: 10.1016/B978-0-12-814003-1.00019-8. Cited on pages 60, 74, and 77.

V. Nizalapur and A. Vyas. Texture Analysis for Land Use Land Cover (lulc) Classification in Parts of Ahmedabad, Gujarat. *ISPRS - International Archives of the Photogrammetry, Remote Sensing and Spatial Information Sciences*, XLIII-B3-2:275–279, 8 2020. doi: 10.5194/isprs-archives-XLIII-B3-2020-275-2020. Cited on page 238.

W. S. Noble. What is a support vector machine? *Nature Biotechnology*, 24(12):1565–1567, 12 2006. doi: 10.1038/nbt1206-1565. Cited on page 242.

G. C. O'Brien, C. Dickens, C. Baker, R. Stassen, and F. van Weert. Sustainable Floodplains: Linking E-Flows to Floodplain Management, Ecosystems, and Livelihoods in the Sahel of North Africa. *Sustainability*, 12(24):10578, 12 2020. doi: 10.3390/su122410578. Cited on page 334.

C. O'Hara, J. King, J. Cartwright, and R. King. Multitemporal land use and land cover classification of urbanized areas within sensitive coastal environments. *IEEE Transactions on Geoscience and Remote Sensing*, 41(9):2005–2014, 9 2003. doi: 10.1109/TGRS.2003.816573. Cited on page 234.

K. R. Olson and L. W. Morton. Polders, dikes, canals, rice, and aquaculture in the Mekong Delta. *Journal of Soil and Water Conservation*, 73(4):83A–89A, 7 2018. doi: 10.2489/jswc.73.4.83A. Cited on page 99.

T. M. Oshiro, P. S. Perez, and J. A. Baranauskas. How Many Trees in a Random Forest? In *International workshop on machine learning and data mining in pattern recognition*, pages 154–168. Springer, Berlin, Heidelberg, 2012. doi: 10.1007/978-3-642-31537-4{_}13. Cited on page 251.

B. Ouattara, G. Forkuor, B. J. B. Zoungrana, K. Dimobe, J. Danumah, B. Saley, and J. E. Tondoh. Crops monitoring and yield estimation using sentinel products in semi-arid smallholder irrigation schemes. *International Journal of Remote Sensing*, 41(17):6527–6549, 9 2020. doi: 10.1080/01431161.2020.1739355. Cited on page 238.

S. Paik, D. T. P. Le, L. T. Nhu, and B. F. Mills. Salt-tolerant rice variety adoption in the Mekong River Delta: Farmer adaptation to sea-level rise. *PLOS ONE*, 15(3):e0229464, 3 2020. doi: 10.1371/journal.pone.0229464. Cited on page 105.

P. Paris. Anciens canaux reconnus sur photographies aériennes dans les provinces de Ta Kèv et de Châu-doc. *Bulletin de l'Ecole française d'Extrême-Orient*, 31(1):221–224, 1931. doi: 10.3406/befeo.1931.4423. Cited on page 102.

E. Park, H. L. Ho, D. D. Tran, X. Yang, E. Alcantara, E. Merino, and V. H. Son. Dramatic decrease of flood frequency in the Mekong Delta due to river-bed mining and dyke construction. *Science of The Total Environment*, 723:138066, 6 2020. doi: 10.1016/J.SCITOTENV.2020.138066. Cited on page 58.

J.-F. Pekel, A. Cottam, N. Gorelick, and A. S. Belward. High-resolution mapping of global surface water and its long-term changes. *Nature*, 540(7633):418–422, 12 2016. doi: 10.1038/nature20584. Cited on pages 142, 143, and 149.

C. Pelletier, S. Valero, J. Inglada, N. Champion, C. Marais Sicre, and G. Dedieu. Effect of Training Class Label Noise on Classification Performances for Land Cover Mapping with Satellite Image Time Series. *Remote Sensing*, 9(2):173, 2 2017. doi: 10.3390/rs9020173. Cited on page 252.

C. Perrings, C. Folke, and K. Mäler. The ecology and economics of biodiversity loss: the research agenda. *Ambio*, 21:201–211, 1992. Cited on page 68.

A. N. Pettitt. A Non-Parametric Approach to the Change-Point Problem. *Applied Statistics*, 28 (2):126–135, 6 1979. doi: 10.2307/2346729. Cited on page 116.

B. Pham-Duc, C. Prigent, and F. Aires. Surface water monitoring within cambodia and the Vietnamese Mekong Delta over a year, with Sentinel-1 SAR observations. *Water*, 9(6):366, 5 2017. doi: 10.3390/w9060366. Cited on page 138.

H. M. Phan, Q. Ye, A. J. Reniers, and M. J. Stive. Tidal wave propagation along The Mekong deltaic coast. *Estuarine, Coastal and Shelf Science*, 220:73–98, 5 2019. doi: 10.1016/J.ECSS .2019.01.026. Cited on page 117.

T. Piman and M. Shrestha. Project Report 2017-03 Case study on sediment in the Mekong River Basin: Current state and future trends. Technical report, Stockholm Environment Institute, 2017. URL `http://mediamanager.sei.org/documents/Publications/Bangkok/SEI_2017_Report_Mekong_sediment_LoRes.pdf`. Cited on pages 75, 78, and 86.

T. Piman, T. A. Cochrane, M. E. Arias, A. Green, and N. D. Dat. Assessment of Flow Changes from Hydropower Development and Operations in Sekong, Sesan, and Srepok Rivers of the Mekong Basin. *Journal of Water Resources Planning and Management*, 139(6):723–732, 11 2013a. doi: 10.1061/(ASCE)WR.1943-5452.0000286. Cited on pages 75, 79, and 90.

T. Piman, T. Lennaerts, and P. Southalack. Assessment of hydrological changes in the lower mekong basin from basin-wide development scenarios. *Hydrological Processes*, 2013b. doi: 10.1002/hyp.9764. Cited on page 77.

T. Piman, T. A. Cochrane, and M. E. Arias. Effect of Proposed Large Dams on Water Flows and Hydropower Production in the Sekong, Sesan and Srepok Rivers of the Mekong Basin. *River Research and Applications*, 2016. doi: 10.1002/rra.3045. Cited on page 86.

J. F. Pimentel, L. Murta, V. Braganholo, and J. Freire. A Large-Scale Study About Quality and Reproducibility of Jupyter Notebooks. In *2019 IEEE/ACM 16th International Conference on Mining Software Repositories (MSR)*, pages 507–517. IEEE, 5 2019. doi: 10.1109/MSR.2019 .00077. Cited on page 274.

S. Plank, M. Jüssi, S. Martinis, and A. Twele. Mapping of flooded vegetation by means of polarimetric Sentinel-1 and ALOS-2/PALSAR-2 imagery. *International Journal of Remote Sensing*, 38(13):3831–3850, 7 2017. doi: 10.1080/01431161.2017.1306143. Cited on page 149.

Y. Pokhrel, M. Burbano, J. Roush, H. Kang, V. Sridhar, and D. W. Hyndman. A review of the integrated effects of changing climate, land use, and dams on Mekong river hydrology. *Water*, 10(3):266, 2018. doi: 10.3390/w10030266. Cited on pages 58 and 328.

P. Potapov, A. Tyukavina, S. Turubanova, Y. Talero, A. Hernandez-Serna, M. C. Hansen, D. Saah, K. Tenneson, A. Poortinga, A. Aekakkararungroj, F. Chishtie, P. Towashiraporn, B. Bhandari,

K. S. Aung, and Q. H. Nguyen. Annual continuous fields of woody vegetation structure in the Lower Mekong region from 2000-2017 Landsat time-series. *Remote Sensing of Environment*, 232:111278, 10 2019. doi: 10.1016/J.RSE.2019.111278. Cited on page 88.

P. Potin, B. Rosich, N. Miranda, P. Grimont, I. Shurmer, A. O'Connell, M. Krassenburg, and J.-B. Gratadour. Copernicus Sentinel-1 Constellation Mission Operations Status. In *IGARSS 2019 - 2019 IEEE International Geoscience and Remote Sensing Symposium*, pages 5385–5388. IEEE, 7 2019. doi: 10.1109/IGARSS.2019.8898949. Cited on page 137.

A. Poulsen, K. Hortle, J. Valbo-Jorgensen, S. Chan, S. Viravong, K. Bouakhamvongsa, U. Suntornratana, N. Yoorong, T. Nguyen, and B. Tran. Distribution and Ecology of Some Important Riverine Fish Species of the Mekong River Basin. Technical report, Mekong River Commission, Phnom Penh, 2004. Cited on page 121.

O. Pratx. Mémoire Etude du fonctionnement hydro-agricole de canaux d'irrigation : Cas des « preks » sur les rives du Bassac au Cambodge. Technical report, École Nationale du Génie de l'Eau et de l'Environnement de Strasbourg, 2017. Cited on pages 188, 189, 193, and 296.

Python Core Team. Python: A dynamic, open source programming language, 2019. Cited on page 273.

J. Qi, A. Chehbouni, A. Huete, Y. Kerr, and S. Sorooshian. A modified soil adjusted vegetation index. *Remote Sensing of Environment*, 48(2):119–126, 5 1994. doi: 10.1016/0034-4257(94)90134-1. Cited on page 239.

W. Qu, N. Hu, J. Fu, J. Lu, H. Lu, T. Lei, Z. Pang, X. Li, and L. Li. Analysis of the Tonle Sap flood pulse based on remote sensing: How much does the Tonle Sap Lake affect the Mekong River flood? *ISPRS - International Archives of the Photogrammetry, Remote Sensing and Spatial Information Sciences*, XLII-3:1461–1465, 4 2018. doi: 10.5194/isprs-archives-XLII-3-1461-2018. Cited on page 76.

N. H. Quang, V. A. Tuan, N. T. P. Hao, L. T. T. Hang, N. M. Hung, V. L. Anh, L. T. M. Phuong, and R. Carrie. Synthetic aperture radar and optical remote sensing image fusion for flood monitoring in the Vietnam lower Mekong basin: a prototype application for the Vietnam Open Data Cube. *European Journal of Remote Sensing*, 52(1):599–612, 1 2019. doi: 10.1080/22797254.2019.1698319. Cited on page 138.

V. Quoc Thanh, D. Roelvink, M. van der Wegen, J. Reyns, H. Kernkamp, G. Van Vinh, and V. Thi Phuong Linh. Flooding in the Mekong Delta: Impact of dyke systems on downstream hydrodynamics. *Hydrology and Earth System Sciences*, 24(1):189–212, 2019. doi: 10.5194/hess-2019-64. Cited on pages 60, 76, 96, and 272.

N. H. Quyen, T. H. Duong, B. T. Yen, and L. S. Sebastian. Impact of climate change on future rice production in the Mekong River Delta. In *Impact of climate change on future rice production in the Mekong River Delta. Poster paper presented in the 5th International Rice Congress*, Singapore, 10 2018. CGIAR Research Program on Climate Change, Agriculture and Food Security (CCAFS). URL `https://hdl.handle.net/10568/99563`. Cited on page 99.

V. K. Rana and T. M. Venkata Suryanarayana. Performance evaluation of MLE, RF and SVM classification algorithms for watershed scale land use/land cover mapping using sentinel 2 bands. *Remote Sensing Applications: Society and Environment*, 19:100351, 8 2020. doi: 10.1016/J.RSASE.2020.100351. Cited on page 252.

T. A. Räsänen, P. Someth, H. Lauri, J. Koponen, J. Sarkkula, and M. Kummu. Observed river discharge changes due to hydropower operations in the Upper Mekong Basin. *Journal of Hydrology*, 545:28–41, 2 2017. doi: 10.1016/J.JHYDROL.2016.12.023. Cited on page 86.

F. G. Renaud and C. Kuenzer. *The Mekong Delta system : interdisciplinary analyses of a river delta*. Springer, 2012. ISBN 9789400739628. Cited on pages 76 and 98.

F. G. Renaud, J. P. Syvitski, Z. Sebesvari, S. E. Werners, H. Kremer, C. Kuenzer, R. Ramesh, A. Jeuken, and J. Friedrich. Tipping from the Holocene to the Anthropocene: How threatened are major world deltas? *Current Opinion in Environmental Sustainability*, 5(6):644–654, 12 2013. doi: 10.1016/J.COSUST.2013.11.007. Cited on pages 57 and 92.

S. Rice and J. Tyner. The rice cities of the Khmer Rouge: an urban political ecology of rural mass violence. *Transactions of the Institute of British Geographers*, 42(4):559–571, 12 2017. doi: 10.1111/tran.12187. Cited on page 185.

B. Richard, B. Bonté, O. Barreteau, and I. Braud. A situated agent-based model to reveal irrigators' options behind their actions under institutional arrangements in Southern France. *Socio-Environmental Systems Modelling*, 3:17893–17893, 2 2022. doi: 10.18174/SESMO.17893. Cited on page 333.

C. Rigolot. Transdisciplinarity as a discipline and a way of being: complementarities and creative tensions. *Humanities and Social Sciences Communications*, 7(1):100, 12 2020. doi: 10.1057/s41599-020-00598-5. Cited on page 72.

P. Rizzoli, M. Martone, C. Gonzalez, C. Wecklich, D. Borla Tridon, B. Bräutigam, M. Bachmann, D. Schulze, T. Fritz, M. Huber, B. Wessel, G. Krieger, M. Zink, and A. Moreira. Generation and performance assessment of the global TanDEM-X digital elevation model. *ISPRS Journal of Photogrammetry and Remote Sensing*, 132:119–139, 10 2017. doi: 10.1016/J.ISPRSJPRS.2017.08.008. Cited on page 147.

J. Rouse J.W., R. Haas, J. Schell, and D. Deering. Monitoring Vegetation Systems in the Great Plains with ERTS. In S. C. Freden, E. P. Mercanti, and M. A. Becker, editors, *Third Earth Resources Technology Satellite-1 Symposium- Volume I: Technical Presentations NASA SP-351*, volume 30103017, pages 301–217. NASA, 1974. Cited on pages 143 and 239.

G. Rudi. *Modélisation et analyse de services éco-hydrauliques des réseaux de canaux et fossés des agrosystèmes méditerranéens*. PhD thesis, Montpellier SupAgro, 2019. Cited on page 273.

Rudiyanto, B. Minasny, R. M. Shah, N. C. Soh, C. Arif, and B. I. Setiawan. Automated Near-Real-Time Mapping and Monitoring of Rice Extent, Cropping Patterns, and Growth Stages in Southeast Asia Using Sentinel-1 Time Series on a Google Earth Engine Platform. *Remote Sensing*, 11(14):1666, 7 2019. doi: 10.3390/rs11141666. Cited on page 143.

K. E. Saxton and W. J. Rawls. Soil Water Characteristic Estimates by Texture and Organic Matter for Hydrologic Solutions. *Soil Science Society of America Journal*, 70(5):1569–1578, 9 2006. doi: 10.2136/sssaj2005.0117. Cited on page 275.

R. J. P. Schmitt, S. Bizzi, A. Castelletti, J. J. Opperman, and G. M. Kondolf. Planning dam portfolios for low sediment trapping shows limits for sustainable hydropower in the Mekong. *Science Advances*, 5(10), 10 2019. doi: 10.1126/sciadv.aaw2175. Cited on page 84.

J. C. Scott. *The art of not being governed : an anarchist history of upland Southeast Asia*. Yale University Press, 2009. ISBN 9780300169171. Cited on page 82.

F. Sekendur. Effect of water stress at different growth stages of seed pumpkin (cucurbita pepo l.) on seed yield and quality, 2017. Cited on page 299.

S. M. Sezen, A. Yazar, M. Canbolat, S. Eker, and G. Çelikel. Effect of drip irrigation management on yield and quality of field grown green beans. *Agricultural Water Management*, 71(3): 243–255, 2 2005. doi: 10.1016/j.agwat.2004.09.004. Cited on page 299.

S. Shalev-Shwartz and S. Ben-David. Decision Trees. In *Understanding machine learning: From theory to algorithms*, chapter 18. Cambridge University Press, 2014. Cited on page 241.

R. Sharp, J. Douglass, S. Wolny, K. Arkema, J. Bernhardt, W. Bierbower, N. Chaumont, D. Denu, J. Douglass, D. Fisher, K. Glowinski, R. Griffin, G. Guannel, A. Guerry, J. Johnson, P. Hamel, C. Kennedy, C.-K. Kim, M. Lacayo, E. Lonsdorf, L. Mandle, L. Rogers, R. Sharp, J. Toft, G. Verutes, A. L. Vogl, S. Wolny, and S. Wood. InVEST User's Guide Integrated Valuation of Ecosystem Services and Tradeoffs. Technical report, The Natural Capital Project, Stanford University, University of Minnesota, The Nature Conservancy, and World Wildlife Fund, 2020. URL `https://invest-userguide.readthedocs.io/_/downloads/en/3.8.5/pdf/`. Cited on page 272.

A. Shelestov, M. Lavreniuk, N. Kussul, A. Novikov, and S. Skakun. Exploring Google Earth Engine Platform for Big Data Processing: Classification of Multi-Temporal Satellite Imagery for Crop Mapping. *Frontiers in Earth Science*, 5:17, 2 2017. doi: 10.3389/feart.2017.00017. Cited on pages 235 and 241.

D. Shi and X. Yang. Support Vector Machines for Land Cover Mapping from Remote Sensor Imagery. In *Monitoring and Modeling of Global Changes: A Geomatics Perspective.*, pages 265–279. Springer, Dordrecht, 2015. doi: 10.1007/978-94-017-9813-6{_}13. Cited on page 243.

S. Shin, Y. Pokhrel, D. Yamazaki, X. Huang, N. Torbick, J. Qi, S. Pattanakiat, T. Ngo-Duc, and T. D. Nguyen. High Resolution Modeling of River-Floodplain-Reservoir Inundation Dynamics in the Mekong River Basin. *Water Resources Research*, 56(5):e2019WR026449, 5 2020. doi: 10.1029/2019WR026449. Cited on pages 137 and 328.

B. Shrestha, M. S. Babel, S. Maskey, A. van Griensven, S. Uhlenbrook, A. Green, and I. Akkharath. Impact of climate change on sediment yield in the Mekong River basin: a case study of the Nam Ou basin, Lao PDR. *Hydrology and Earth System Sciences*, 17(1): 1–20, 1 2013. doi: 10.5194/hess-17-1-2013. Cited on page 272.

B. Shrestha, T. A. Cochrane, B. S. Caruso, M. E. Arias, and T. Piman. Uncertainty in flow and sediment projections due to future climate scenarios for the 3S Rivers in the Mekong Basin. *Journal of Hydrology*, 540:1088–1104, 9 2016. doi: 10.1016/j.jhydrol.2016.07.019. Cited on page 75.

B. Shrestha, T. A. Cochrane, B. S. Caruso, and M. E. Arias. Land use change uncertainty impacts on streamflow and sediment projections in areas undergoing rapid development: A case study in the Mekong Basin. *Land Degradation & Development*, 29(3):835–848, 11 2017. doi: 10.1002/ldr.2831. Cited on page 88.

B. Shrestha, T. A. Cochrane, B. S. Caruso, and M. E. Arias. Land use change uncertainty impacts on streamflow and sediment projections in areas undergoing rapid development: A case study in the Mekong Basin. *Land Degradation & Development*, 29(3):835–848, 3 2018. doi: 10.1002/ldr.2831. Cited on page 58.

L. Silveira, F. Charbonnier, and J. L. Genta. The antecedent soil moisture condition of the curve number procedure. *Hydrological sciences journal*, 45(1):3–12, 2000. Cited on page 298.

M. Singha, J. Dong, S. Sarmah, N. You, Y. Zhou, G. Zhang, R. Doughty, and X. Xiao. Identifying floods and flood-affected paddy rice fields in Bangladesh based on Sentinel-1 imagery and Google Earth Engine. *ISPRS Journal of Photogrammetry and Remote Sensing*, 166:278–293, 8 2020. doi: 10.1016/J.ISPRSJPRS.2020.06.011. Cited on page 60.

B. Sivakumar. Socio-hydrology: not a new science, but a recycled and re-worded hydrosociology. *Hydrological Processes*, 26(24):3788–3790, 11 2012. doi: 10.1002/hyp.9511. Cited on page 66.

M. Sivapalan, H. H. G. Savenije, and G. Blöschl. Socio-hydrology: A new science of people and water. *Hydrological Processes*, 26(8):1270–1276, 4 2012. doi: 10.1002/hyp.8426. Cited on page 65.

N. Sivutha and The Phnom Penh Post. Fishing season closed down through September 30, June 14. *The Phnom Penh Post*, 2021a. URL `https://www.phnompenhpost.com/national/fishing-season-closed-down-through-september-30`. Cited on page 204.

N. Sivutha and The Phnom Penh Post. MRC gets $13 million for management of Mekong River, June 25. *The Phnom Penh Post*, 2021b. URL `https://www.phnompenhpost.com/national/mrc-gets-13m-management-mekong-river`. Cited on page 91.

B. Slagter, N.-E. Tsendbazar, A. Vollrath, and J. Reiche. Mapping wetland characteristics using temporally dense Sentinel-1 and Sentinel-2 data: A case study in the St. Lucia wetlands, South Africa. *International Journal of Applied Earth Observation and Geoinformation*, 86:102009, 4 2020. doi: 10.1016/J.JAG.2019.102009. Cited on page 238.

R. Sochan and The Phnom Penh Post. US splashes $770K for Mekong management, data sharing, December 11. *The Phnom Penh Post*, 2021. URL `https://www.phnompenhpost.com/national/us-splashes-770k-mekong-management-data-sharing`. Cited on page 91.

SOFRECO. Project Review Report - Technical Assistance for the implementation of Preks of Kandal Component (TA-Preks). Technical report, French Development Agency, 2017. Cited on pages 59, 188, 189, 191, 198, 205, and 276.

X. Song, J. Zhang, C. Zhan, Y. Xuan, M. Ye, and C. Xu. Global sensitivity analysis in hydrological modeling: Review of concepts, methods, theoretical framework, and applications. *Journal of Hydrology*, 523:739–757, 2015. doi: 10.1016/j.jhydrol.2015.02.013. Cited on page 301.

A. Soukhaphon, I. G. Baird, and Z. S. Hogan. The Impacts of Hydropower Dams in the Mekong River Basin: A Review. *Water*, 13(3):265, 1 2021. doi: 10.3390/w13030265. Cited on pages 81, 84, and 87.

D. J. Stanley and A. G. Warne. Worldwide initiation of holocene marine deltas by deceleration of sea-level rise. *Science*, 265(5169):228–31, 7 1994. doi: 10.1126/science.265.5169.228. Cited on page 93.

D. J. Stanley and A. G. Warne. Holocene Sea-Level Change and Early Human Utilisation of Deltas. *GSA Today*, 7(12), 1997. Cited on page 57.

P. Steduto, T. C. Hsiao, E. Fereres, D. Raes, and A. Müller. Crop yield response to water. Technical report, Food and Agriculture Organization of the United Nations, 2012. Cited on pages 297 and 299.

M. J. Steinhausen, P. D. Wagner, B. Narasimhan, and B. Waske. Combining Sentinel-1 and Sentinel-2 data for improved land use and land cover mapping of monsoon regions. *International Journal of Applied Earth Observation and Earth Observation*, 73:595–604, 12 2018. doi: 10.1016/j.jag.2018.08.011. Cited on page 245.

M. A. Stewart and P. A. Coclanis. *Environmental change and agricultural sustainability in the Mekong Delta*. Springer, 2011. ISBN 9400709331. Cited on pages 58 and 92.

Stimson Center. Mekong Dam Monitor, 2022. URL `https://www.stimson.org/project/mekong-dam-monitor/`. Cited on pages 77 and 84.

R. Stone. Hydropower. Mayhem on the Mekong. *Science*, 2011. doi: 10.1126/science.333.6044.814. Cited on page 77.

E. Stopelli, V. T. Duyen, T. T. Mai, P. T. Trang, P. H. Viet, A. Lightfoot, R. Kipfer, M. Schneider, E. Eiche, A. Kontny, T. Neumann, M. Glodowska, M. Patzner, A. Kappler, S. Kleindienst, B. Rathi, O. Cirpka, B. Bostick, H. Prommer, L. H. Winkel, and M. Berg. Spatial and temporal evolution of groundwater arsenic contamination in the Red River delta, Vietnam: Interplay of mobilisation and retardation processes. *Science of The Total Environment*, 717:137143, 5 2020. doi: 10.1016/J.SCITOTENV.2020.137143. Cited on page 94.

D. Suhardiman, M. Giordano, and F. Molle. Scalar Disconnect: The Logic of Transboundary Water Governance in the Mekong. *Society & Natural Resources*, 25(6):572–586, 6 2012. doi: 10.1080/08941920.2011.604398. Cited on page 90.

S. Supharatid, J. Nafung, and T. Aribarg. Projected changes in temperature and precipitation over mainland Southeast Asia by CMIP6 models. *Journal of Water and Climate Change*, 13 (1):337–356, 1 2022. doi: 10.2166/wcc.2021.015. Cited on pages 309 and 313.

J. P. Syvitski, A. J. Kettner, I. Overeem, L. Giosan, G. R. Brakenridge, M. Hannon, and R. Bilham. Anthropocene metamorphosis of the Indus Delta and lower floodplain. *Anthropocene*, 3:24–35, 11 2013. doi: 10.1016/J.ANCENE.2014.02.003. Cited on page 334.

S. Szabo, E. Brondizio, F. G. Renaud, S. Hetrick, R. J. Nicholls, Z. Matthews, Z. Tessler, A. Tejedor, Z. Sebesvari, E. Foufoula-Georgiou, S. da Costa, and J. A. Dearing. Population dynamics, delta vulnerability and environmental change: comparison of the Mekong, Ganges–Brahmaputra and Amazon delta regions. *Sustainability Science*, 11(4):539–554, 2016. doi: 10.1007/s11625-016-0372-6. Cited on pages 57, 58, 60, and 92.

E. Tabeau and J. Zwierzchowski. A Review of Estimation Methods for Victims of the Bosnian War and the Khmer Rouge Regime. In T. Seybolt, J. Aronson, and B. Fischhoff, editors,

Counting Civilian Casualties - An Introduction to Recording and Estimating Nonmilitary Deaths in Conflict, pages 213–246. Oxford University Press, Oxford, 2013. doi: 10.1093/acprof:oso/9780199977307.001.0001. Cited on page 185.

S. Talukdar, P. Singha, S. Mahato, Shahfahad, S. Pal, Y.-A. Liou, and A. Rahman. Land-Use Land-Cover Classification by Machine Learning Classifiers for Satellite Observations—A Review. *Remote Sensing*, 12(7):1135, 4 2020. doi: 10.3390/rs12071135. Cited on pages 235 and 252.

H. Tamiminia, B. Salehi, M. Mahdianpari, L. Quackenbush, S. Adeli, and B. Brisco. Google Earth Engine for geo-big data applications: A meta-analysis and systematic review. *ISPRS Journal of Photogrammetry and Remote Sensing*, 164:152–170, 6 2020. doi: 10.1016/J.ISPRSJPRS.2020.04.001. Cited on pages 143 and 238.

T. Tamura, Y. Saito, M. D. Bateman, V. L. Nguyen, T. O. Ta, and D. Matsumoto. Luminescence dating of beach ridges for characterizing multi-decadal to centennial deltaic shoreline changes during Late Holocene, Mekong River delta. *Marine Geology*, 326-328(326-328):140–153, 10 2012a. doi: 10.1016/j.margeo.2012.08.004. Cited on page 93.

T. Tamura, Y. Saito, V. L. Nguyen, T. O. Ta, M. D. Bateman, D. Matsumoto, and S. Yamashita. Origin and evolution of interdistributary delta plains; insights from Mekong River delta. *Geology*, 40(4):303–306, 4 2012b. doi: 10.1130/G32717.1. Cited on page 93.

P. Tavares, N. Beltrão, U. Guimarães, and A. Teodoro. Integration of Sentinel-1 and Sentinel-2 for Classification and LULC Mapping in the Urban Area of Belém, Eastern Brazilian Amazon. *Sensors*, 19(5):1140, 3 2019. ISSN 1424-8220. doi: 10.3390/s19051140. Cited on page 250.

P. Thanh Noi and M. Kappas. Comparison of Random Forest, k-Nearest Neighbor, and Support Vector Machine Classifiers for Land Cover Classification Using Sentinel-2 Imagery. *Sensors (Basel, Switzerland)*, 18(1), 12 2017. doi: 10.3390/s18010018. Cited on pages 235, 243, and 251.

C. W. Thornthwaite. An Approach toward a Rational Classification of Climate. *Geographical Review*, 38(1):55, 1 1948. doi: 10.2307/210739. Cited on page 297.

T. Q. Toan. Climate Change and Sea Level Rise in the Mekong Delta: Flood, Tidal Inundation, Salinity Intrusion, and Irrigation Adaptation Methods. *Coastal Disasters and Climate Change*

in Vietnam, pages 199–218, 1 2014. doi: 10.1016/B978-0-12-800007-6.00009-5. Cited on pages 95 and 104.

J. Tollefson. Landsat 8 to the rescue. *Nature*, 494(7435):13–14, 2 2013. doi: 10.1038/494013a. Cited on page 141.

M. Torell and A. M. Salamanca. Wetlands Management in Vietnam's Mekong Delta: An Overview of the Pressures and Responses. Technical report, WorldFish Center, 2003. Cited on page 94.

T. Tran. Transboundary Mekong River Delta (Cambodia and Vietnam). In *The Wetland Book*, pages 1–12. Springer Netherlands, Dordrecht, 2016. doi: 10.1007/978-94-007-6173-5{_}40-1. Cited on page 100.

V. K. Tri. Hydrology and Hydraulic Infrastructure Systems in the Mekong Delta, Vietnam. In *The Mekong Delta System*, pages 49–81. Springer, Dordrecht, 2012. doi: 10.1007/978-94-007-3962-8{_}3. URL `http://link.springer.com/10.1007/978-94-007-3962-8_3`. Cited on pages 60 and 95.

N. V. K. Triet, N. V. Dung, H. Fujii, M. Kummu, B. Merz, and H. Apel. Has dyke development in the Vietnamese Mekong Delta shifted flood hazard downstream? *Hydrology and Earth System Sciences*, 21(8):3991–4010, 8 2017. doi: 10.5194/hess-21-3991-2017. Cited on pages 96, 101, and 102.

Y. Trisurat, A. Aekakkararungroj, H.-o. Ma, and J. M. Johnston. Basin-wide impacts of climate change on ecosystem services in the Lower Mekong Basin. *Ecological Research*, 33(1):73–86, 1 2018. doi: 10.1007/s11284-017-1510-z. Cited on page 89.

L. D. Trung, N. A. Duc, L. T. Nguyen, T. H. Thai, A. Khan, K. Rautenstrauch, and C. Schmidt. Assessing cumulative impacts of the proposed Lower Mekong Basin hydropower cascade on the Mekong River floodplains and Delta – Overview of integrated modeling methods and results. *Journal of Hydrology*, 581:122511, 2 2020. doi: 10.1016/J.JHYDROL.2018.01.029. Cited on page 104.

T. D. Truong and L. H. Do. Mangrove forests and aquaculture in the Mekong river delta. *Land Use Policy*, 73:20–28, 4 2018. doi: 10.1016/J.LANDUSEPOL.2018.01.029. Cited on pages 100 and 272.

S. Try, S. Tanaka, K. Tanaka, T. Sayama, G. Lee, and C. Oeurng. Assessing the effects of climate change on flood inundation in the lower Mekong Basin using high-resolution AGCM outputs. *Progress in Earth and Planetary Science*, 7(1):34, 12 2020. doi: 10.1186/s40645-020-00353-z. Cited on pages 89 and 137.

V. Tsyganskaya, S. Martinis, P. Marzahn, and R. Ludwig. SAR-based detection of flooded vegetation – a review of characteristics and approaches. *International Journal of Remote Sensing*, 39(8):2255–2293, 4 2018. doi: 10.1080/01431161.2017.1420938. Cited on pages 138, 149, and 165.

J. Tully. *A Short History of Cambodia: From Empire to Survival*. Allen & Unwin, Crows Nest NSW, 2005. Cited on pages 176 and 184.

S. Tweed, S. Massuel, J. Seidel, K. Chhuon, S. Lun, K. Eang, J. Venot, G. Belaud, M. Babic, and M. Leblanc. Seasonal influences on groundwater arsenic concentrations in the irrigated region of the Cambodian Mekong Delta. *Science of The Total Environment*, 728:138598, 8 2020. ISSN 0048-9697. doi: 10.1016/J.SCITOTENV.2020.138598. Cited on pages 72 and 199.

A. Twele, W. Cao, S. Plank, and S. Martinis. Sentinel-1-based flood mapping: a fully automated processing chain. *International Journal of Remote Sensing*, 37(13):2990–3004, 7 2016. doi: 10.1080/01431161.2016.1192304. Cited on page 138.

J. A. Tyner and S. Rice. Agrarian ruins of the Khmer Rouge. In *Geographies of Post-Industrial Place, Memory, and Heritage*, pages 141–157. Routledge, Milton Park, Abingdon, Oxon ; New York, NY : Routledge, 2021., 10 2020. ISBN 9781003007494. doi: 10.4324/9781003007494-12. Cited on page 185.

J. A. Tyner, M. Munro-Stasiuk, C. Coakley, S. Kimsroy, and S. Rice. Khmer Rouge Irrigation Schemes During the Cambodian Genocide. *Genocide Studies International*, 12(1):103–119, 6 2018. doi: 10.3138/gsi.12.1.07. Cited on page 185.

Y. Uga, K. Sugimoto, S. Ogawa, J. Rane, M. Ishitani, N. Hara, Y. Kitomi, Y. Inukai, K. Ono, N. Kanno, H. Inoue, H. Takehisa, R. Motoyama, Y. Nagamura, J. Wu, T. Matsumoto, T. Takai, K. Okuno, and M. Yano. Control of root system architecture by DEEPER ROOTING 1 increases rice yield under drought conditions. *Nature Genetics*, 45(9):1097–1102, 9 2013. doi: 10.1038/ng.2725. Cited on page 298.

UNDP. Cambodian Climate Hero Profile: Mr Seng Sopha | UNDP Climate Change Adaptation, 2021. URL https://www.adaptation-undp.org/resources/communications-products/cambodian-climate-hero-profile-mr-seng-sopha. Cited on page 128.

H. Vacher. Les figures de l'ingenieur colonial a la fin du XIXe siecle: la formation de la Societe francaise des ingenieurs coloniaux et de l'Ecole speciale des travaux publics. *Le Mouvement social*, 189:47–65, 10 1999. doi: 10.2307/3780204. Cited on page 176.

T. Van Tran, H. Pham Dung Phat, and T. Phi Hoanh Ho Chi. Analysing Drought Intensity in the Mekong River Delta using Time Series Analysis and Google Earth Engine Assessing the impact of climate change on drought and salinisation View project Analysing Drought Intensity in the Mekong River Delta using Time Serie. *International Journal of Geoinformatics*, 16(1), 2020. Cited on page 143.

K. Van Tricht, A. Gobin, S. Gilliams, and I. Piccard. Synergistic Use of Radar Sentinel-1 and Optical Sentinel-2 Imagery for Crop Mapping: A Case Study for Belgium. *Remote Sensing*, 10(10):1642, 10 2018. doi: 10.3390/rs10101642. Cited on page 250.

N. van Zalinge, P. Degen, C. Pongsri, S. Nuov, J. Jensen, V. Nguyen, and X. Choulamany. The Mekong River System. *RAP Publication*, pages 335–357, 2004. Cited on page 79.

P. Vandôme. Agricultural vulnerability to hydrologic hazards in the prek area of the upper Mekong Delta, Cambodia. Technical report, Montpellier SupAgro, Montpellier, 2020. Cited on pages 99, 194, 197, 202, 209, 211, 219, 275, and 296.

M. Venkatappa, N. Sasaki, R. P. Shrestha, N. K. Tripathi, and H.-O. Ma. Determination of Vegetation Thresholds for Assessing Land Use and Land Use Changes in Cambodia using the Google Earth Engine Cloud-Computing Platform. *Remote Sensing*, 11(13):1514, 6 2019. doi: 10.3390/rs11131514. Cited on page 143.

J.-P. Venot and C. B. Jensen. A multiplicity of prek(s) : Enacting a socionatural mosaic in the Cambodian upper Mekong delta. *Environment and Planning E: Nature and Space*, page 251484862110268, 6 2021. doi: 10.1177/25148486211026835. Cited on pages 58 and 72.

J.-P. Venot, J. Vos, F. Molle, M. Zwarteveen, G. J. Veldwisch, M. Kuper, A. Mdee, M. Ertsen, R. Boelens, F. Cleaver, B. Lankford, L. Swatuk, J. Linton, L. M. Harris, J. Kemerink-Seyoum,

M. Kooy, and K. Schwartz. A bridge over troubled waters. *Nature Sustainability*, pages 1–1, 12 2021. doi: 10.1038/s41893-021-00835-y. Cited on page 72.

J.-P. Venot, C. B. Jensen, E. Delay, and W. Daré. Mosaic glimpses: Serious games, generous constraints, and sustainable futures in Kandal, Cambodia. *World Development*, 151:105779, 3 2022. doi: 10.1016/J.WORLDDEV.2021.105779. Cited on page 72.

M. Vickery. *Cambodia: 1975-1982*. South End Press, Boston, 1984. Cited on page 185.

C. Vidthayanon. Field Guide to fishes of the Mekong Delta. Technical report, Mekong River Commission, Vientiane, 2008. Cited on page 100.

F. Villa, K. J. Bagstad, B. Voigt, G. W. Johnson, R. Portela, M. Honzák, and D. Batker. A Methodology for Adaptable and Robust Ecosystem Services Assessment. *PLoS ONE*, 9(3): e91001, 3 2014. doi: 10.1371/journal.pone.0091001. Cited on page 272.

A. V. Vu, K. G. Hortle, and D. N. Nguyen. Factors Driving Long Term Declines in Inland Fishery Yields in the Mekong Delta. *Water*, 13(8):1005, 4 2021. doi: 10.3390/w13081005. Cited on pages 58 and 168.

F. Wagner, V. B. Tran, and F. G. Renaud. Groundwater Resources in the Mekong Delta: Availability, Utilization and Risks. In *The Mekong Delta System*, pages 201–220. Springer, Dordrecht, 2012. doi: 10.1007/978-94-007-3962-8{_}7. Cited on page 98.

Y. Wang, C. Cheng, Y. Xie, B. Liu, S. Yin, Y. Liu, and Y. Hao. Increasing trends in rainfall-runoff erosivity in the Source Region of the Three Rivers, 1961–2012. *Science of The Total Environment*, 592:639–648, 8 2017. doi: 10.1016/J.SCITOTENV.2017.02.235. Cited on page 74.

R. Wassmann, N. D. Phong, T. Q. Tho, C. T. Hoanh, N. H. Khoi, N. X. Hien, T. B. T. Vo, and T. P. Tuong. High-resolution mapping of flood and salinity risks for rice production in the Vietnamese Mekong Delta. *Field Crops Research*, 236:111–120, 4 2019. doi: 10.1016/J.FCR.2019.03.007. Cited on page 58.

W. Westman. How much are nature's services worth? *Science*, 197:960–964, 1977. Cited on page 68.

P. White, T. Oberthur, A. Dobermann, and C. Ros. Classifying soils for agronomists in Cambodia I. The Cambodian agronomic soil classification system (CASC). *Soil Use Manage.*, 16:12–20, 2000. Cited on page 275.

E. H. Wilson and S. A. Sader. Detection of forest harvest type using multiple dates of Landsat TM imagery. *Remote Sensing of Environment*, 80(3):385–396, 6 2002. doi: 10.1016/S0034-4257(01)00318-2. Cited on pages 144 and 239.

K. O. Winemiller, P. B. McIntyre, L. Castello, E. Fluet-Chouinard, T. Giarrizzo, S. Nam, I. G. Baird, W. Darwall, N. K. Lujan, I. Harrison, M. L. J. Stiassny, R. A. M. Silvano, D. B. Fitzgerald, F. M. Pelicice, A. A. Agostinho, L. C. Gomes, J. S. Albert, E. Baran, M. Petrere, C. Zarfl, M. Mulligan, J. P. Sullivan, C. C. Arantes, L. M. Sousa, A. A. Koning, D. J. Hoeinghaus, M. Sabaj, J. G. Lundberg, J. Armbruster, M. L. Thieme, P. Petry, J. Zuanon, G. T. Vilara, J. Snoeks, C. Ou, W. Rainboth, C. S. Pavanelli, A. Akama, A. v. Soesbergen, and L. Saenz. Balancing hydropower and biodiversity in the Amazon, Congo, and Mekong. *Science*, 351(6269):128–129, 2016. doi: 10.1126/science.aac7082. Cited on pages 78 and 79.

J. Winterwerp. On the sedimentation rate of cohesive sediment. In J.-Y. Maa, L. Sanford, and D. Schoellhammer, editors, *Estuarine and Coastal Fine Sediment Dynamics*, pages 209–226. Elsevier, Amsterdam, 2007. Cited on page 292.

P. J. Wood, D. M. Hannah, and J. P. Sadler. *Hydroecology and ecohydrology : past, present and future*. Wiley, 2007. ISBN 0470010185. Cited on page 65.

World Bank. Overview: Development news, research, data | World Bank, 2021. URL `https://www.worldbank.org/en/country/cambodia/`. Cited on pages 99 and 100.

F. Xing, E. A. Meselhe, M. A. Allison, and H. D. Weathers. Analysis and numerical modeling of the flow and sand dynamics in the lower Song Hau channel, Mekong Delta. *Continental Shelf Research*, 147, 2017. doi: 10.1016/j.csr.2017.08.003. Cited on pages 58 and 272.

H. Xu. Modification of normalised difference water index (NDWI) to enhance open water features in remotely sensed imagery. *International Journal of Remote Sensing*, 27(14):3025–3033, 7 2006. doi: 10.1080/01431160600589179. Cited on page 239.

J. Yang, Y. E. Yang, J. Chang, J. Zhang, and J. Yao. Impact of dam development and climate change on hydroecological conditions and natural hazard risk in the Mekong River Basin.

Journal of Hydrology, 579:124177, 12 2019. doi: 10.1016/J.JHYDROL.2019.124177. Cited on page 58.

A. S. Yommy, R. Liu, and S. Wu. SAR Image Despeckling Using Refined Lee Filter. In *2015 7th International Conference on Intelligent Human-Machine Systems and Cybernetics*, pages 260–265. IEEE, 8 2015. doi: 10.1109/IHMSC.2015.236. Cited on page 238.

Y. Yoshida, H. S. Lee, B. H. Trung, H.-D. Tran, M. K. Lall, K. Kakar, and T. D. Xuan. Impacts of Mainstream Hydropower Dams on Fisheries and Agriculture in Lower Mekong Basin. *Sustainability*, 12(6):2408, 3 2020. doi: 10.3390/su12062408. Cited on pages 86, 87, 99, and 105.

X. Yun, Q. Tang, J. Wang, X. Liu, Y. Zhang, H. Lu, Y. Wang, L. Zhang, and D. Chen. Impacts of climate change and reservoir operation on streamflow and flood characteristics in the Lancang-Mekong River Basin. *Journal of Hydrology*, 590:125472, 11 2020. doi: 10.1016/J.JHYDROL.2020.125472. Cited on pages 89, 116, 122, 164, 167, 327, 330, and 331.

M. Zalewski, D. Harper, B. Demars, G. Jolánkai, G. Crosa, G. Janauer, and N. Pacini. Linking biological and physical processes at the river basin scale: the origins, scientific background and scope of ecohydrology. In D. Harper, M. Zalewski, and N. Pacini, editors, *Ecohydrology–Processes, Models and Case Studies*, pages 1–17. CABI, Oxfordshire, 2008. Cited on page 64.

M. Zalewski, E. Kiedrzyńska, I. Wagner, K. Izydorczyk, J. M. Boczek, T. Jurczak, K. Krauze, P. Frankiewicz, M. Godlewska, A. Wojtal-Frankiewicz, M. Łapińska, M. Urbaniak, A. Bednarek, Z. Kaczkowski, I. Gągała, L. Serwecińska, S. Szklarek, R. Włodarczyk-Marciniak, A. Font-Nájera, E. Mierzejewska, M. Połatyńska-Rudnicka, K. Belka, and P. Jarosiewicz. Ecohydrology and adaptation to global change. *Ecohydrology & Hydrobiology*, 8 2021. doi: 10.1016/J.ECOHYD.2021.08.001. Cited on page 65.

Y. Zha, J. Gao, and S. Ni. Use of normalized difference built-up index in automatically mapping urban areas from TM imagery. *International Journal of Remote Sensing*, 24(3):583–594, 1 2003. doi: 10.1080/01431160304987. Cited on page 239.

H. Zhang. Exploring Conditions for the Optimality of Naive Bayes. *International Journal of Pattern Recognition and Artificial Intelligence*, 19(02):183–198, 3 2005. doi: 10.1142/S0218001405003983. Cited on page 240.

W. Zhang, W. Sun, and T. Li. Uncertainties in the national inventory of methane emissions from rice cultivation: field measurements and modeling approaches. *Biogeosciences*, 14(1): 163–176, 1 2017. doi: 10.5194/bg-14-163-2017. Cited on page 144.

S. Zhiyao, W. Tingting, X. Fumin, and L. Ruijie. A simple formula for predicting settling velocity of sediment particles. *Water Science and Engineering*, 1(1):37–43, 2008. Cited on page 292.

C. Zhou, R. van Nooijen, A. Kolechkina, and M. Hrachowitz. Comparative analysis of nonparametric change-point detectors commonly used in hydrology. *Hydrological Sciences Journal*, 64(14):1690–1710, 10 2019. doi: 10.1080/02626667.2019.1669792. Cited on page 116.

C. Zoccarato, P. S. J. Minderhoud, and P. Teatini. The role of sedimentation and natural compaction in a prograding delta: insights from the mega Mekong delta, Vietnam. *Scientific Reports*, 8(1):11437, 12 2018. doi: 10.1038/s41598-018-29734-7. Cited on pages 60 and 94.

A

Overview of Mekong River Commission Observation Network

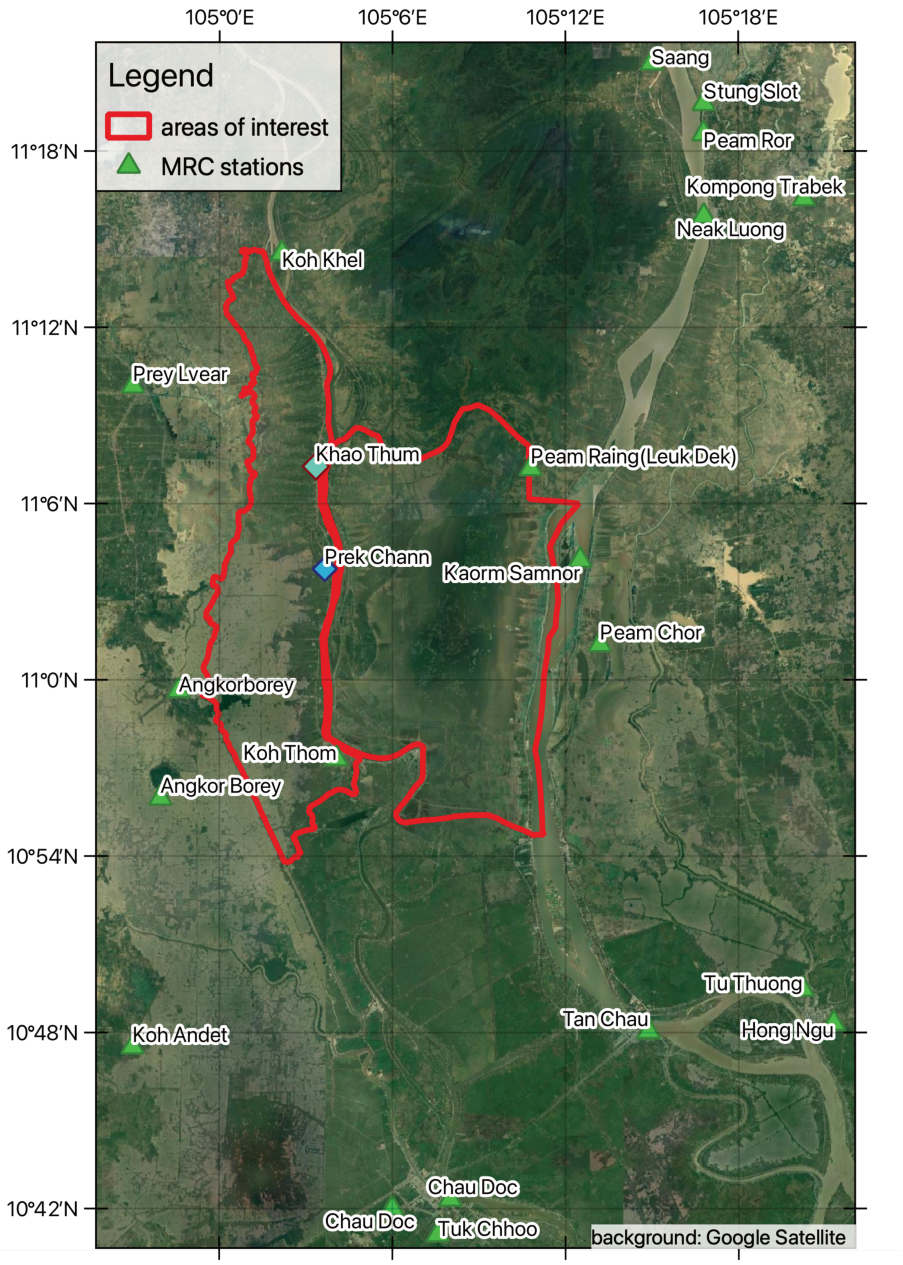

Figure A.1: All MRC measurement stations in the vicinity of the areas of interest in the Cambodian Mekong Delta.

Station	Latitude	Longitude	Parameter	Measurement Type	Unit	Interval	Start	End	River
Angkor Borey	10,933	104,966	Rainfall	Manual	mm	1-6 times p/day	20010101	20071231	Delta
Angkorborey	10,994	104,977	Water Level	Telemetry	m	15 minutes	20180602	20210220	Stung Angkor Borey
			Rainfall	Telemetry	mm	15 minutes	20180602	20210220	Stung Angkor Borey
	11,068	105,209	Water Temperature	Measured	degC	4 times p/month	20041014	20171215	Mekong
			pH	Measured	pH Units	4 times p/month	20041014	20171215	Mekong
			Total Suspended Solids	Measured	mg/l	4 times p/month	20041014	20171215	Mekong
			Nitrite-Nitrate	Measured	mg/l	4 times p/month	20041014	20171215	Mekong
			Total Nitrogen	Measured	mg/l	4 times p/month	20080114	20171215	Mekong
Kaorm Samnor			Total phosphorous	Measured	mg/l	4 times p/month	20041014	20171215	Mekong
			Dissolved Oxygen	Measured	mg/l	4 times p/month	20041014	20171215	Mekong
			Chemical Oxygen Demand	Measured	mg/l	4 times p/month	20041014	20171215	Mekong
			Sulphate calculated by EC	Measured	mS/m	4 times p/month	20041014	20111214	Mekong
			Conductivity	Measured	mS/m	4 times p/month	20041014	20171215	Mekong
			Ammonium	Measured	mg/l	4 times p/month	20041014	20171215	Mekong
Koh Andet	10,792	104,950	Rainfall	Manual	mm	1-6 times p/day	20010101	20121231	Delta
	4,527	111,703	Bentho AAbundance	Average per station	Species Count	2-Yearly	20131230	20171230	Bassac
			Bentho ARichness	Average per station	Species Count	2-Yearly	20131230	20171230	Bassac
			Bentho ATSPT	Average per station	Species Count	2-Yearly	20131230	20171230	Bassac
			Diatoms AAbundance	Average per station	Species Count	2-Yearly	20131230	20171230	Bassac
			Diatoms ARichness	Average per station	Species Count	2-Yearly	20131230	20171230	Bassac
			Diatoms ATSPT	Average per station	Species Count	2-Yearly	20131230	20171230	Bassac
			Littoral AAbundance	Average per station	Species Count	2-Yearly	20131230	20171230	Bassac
			Littoral ARichness	Average per station	Species Count	2-Yearly	20131230	20171230	Bassac
			Littoral ATSPT	Average per station	Species Count	2-Yearly	20131230	20171230	Bassac
			Zooplanktons AAbundance	Average per station	Species Count	2-Yearly	20131230	20171230	Bassac
			Zooplanktons ARichness	Average per station	Species Count	2-Yearly	20131230	20171230	Bassac
			Zooplanktons ATSPT	Average per station	Species Count	2-Yearly	20131230	20171230	Bassac
			Rainfall	Manual	mm	1-6 times p/day	20070319	20210830	Bassac
			Discharge	Daily Calculated	m^3/s	Daily	19910101	20001231	Bassac
Koh Khel			Nitrite-Nitrate	Measured	mg/l	4 times p/month	19930914	20171215	Bassac
			Ammonium	Measured	mg/l	4 times p/month	19930814	20171215	Bassac
			pH	Measured	pH Units	4 times p/month	19930814	20171215	Bassac
			Total Suspended Solids	Measured	mg/l	4 times p/month	19930814	20171215	Bassac
			Conductivity	Measured	mS/m	4 times p/month	19930814	20171215	Bassac
			Total Nitrogen	Measured	mg/l	4 times p/month	20080114	20171215	Bassac
			Sulphate calculated by EC	Measured	mS/m	4 times p/month	19930814	20111214	Bassac
			Dissolved Oxygen	Measured	mg/l	4 times p/month	19930814	20171215	Bassac
			Chemical Oxygen Demand	Measured	mg/l	4 times p/month	19930814	20171215	Bassac
			Water Temperature	Measured	degC	4 times p/month	19930814	20171215	Bassac
			Total phosphorous	Measured	mg/l	4 times p/month	19930814	20171215	Bassac
			Water Level	Manual	m	1-6 times p/day	19900905	20210830	Bassac
			Water Level	Telemetry	m	15 minutes	20210616	20210831	Bassac
			Rainfall	Telemetry	mm	15 minutes	20210616	20210831	Bassac
	10,955	105,068	Rainfall	Manual	mm	1-6 times p/day	20070101	20071231	Bassac
			Nitrite-Nitrate	Measured	mg/l	4 times p/month	20041014	20171215	Bassac
			Conductivity	Measured	mS/m	4 times p/month	20041014	20171215	Bassac
			pH	Measured	pH Units	4 times p/month	20041014	20171215	Bassac
			Total Suspended Solids	Measured	mg/l	4 times p/month	20041014	20171215	Bassac
			Total phosphorous	Measured	mg/l	4 times p/month	20041014	20171215	Bassac
Koh Thom			Total Nitrogen	Measured	mg/l	4 times p/month	20080114	20171215	Bassac
			Chemical Oxygen Demand	Measured	mg/l	4 times p/month	20041014	20171215	Bassac
			Water Temperature	Measured	degC	4 times p/month	20041014	20171215	Bassac
			Ammonium	Measured	mg/l	4 times p/month	20041014	20171215	Bassac
			Dissolved Oxygen	Measured	mg/l	4 times p/month	20041014	20171215	Bassac
			Sulphate calculated by EC	Measured	mS/m	4 times p/month	20041014	20111214	Bassac
Kompong Trabek	11,273	105,338	Water Level	Manual	m	1-6 times p/day	20010101	20061226	
Kompong Trabek			Rainfall	Manual	mm	1-6 times p/day	19220101	20121231	
	11,263	105,280	Rainfall	Manual	mm	1-6 times p/day	20070319	20210830	Mekong
			Discharge	Daily Calculated	m^3/s	Daily	19650101	20021231	Mekong
			Water Level	Manual	m	1-6 times p/day	19260101	20210830	Mekong
			pH	Measured	pH Units	4 times p/month	19930814	20171215	Mekong
			Total Suspended Solids	Measured	mg/l	4 times p/month	19930814	20171215	Mekong
			Chemical Oxygen Demand	Measured	mg/l	4 times p/month	19930814	20171215	Mekong
			Total Nitrogen	Measured	mg/l	4 times p/month	20080114	20171215	Mekong
Neak Luong			Total phosphorous	Measured	mg/l	4 times p/month	19930814	20171215	Mekong
			Dissolved Oxygen	Measured	mg/l	4 times p/month	19930814	20171215	Mekong
			Water Temperature	Measured	degC	4 times p/month	19930814	20171215	Mekong
			Sulphate calculated by EC	Measured	mS/m	4 times p/month	19930814	20111214	Mekong
			Conductivity	Measured	mS/m	4 times p/month	19930814	20171215	Mekong
			Ammonium	Measured	mg/l	4 times p/month	19930814	20171215	Mekong
			Nitrite-Nitrate	Measured	mg/l	4 times p/month	19930914	20171215	Mekong
Peam Chor	11,020	105,220	Rainfall	Manual	mm	1-6 times p/day	20070101	20121231	
Peam Raing(Leuk Dek)	11,120	105,180	Rainfall	Manual	mm	1-6 times p/day	20010101	20031231	Delta
Peam Ror	11,310	105,280	Rainfall	Manual	mm	1-6 times p/day	20010101	20071231	Mekong
Saang	11,350	105,250	Rainfall	Manual	mm	1-6 times p/day	20010101	20121231	Mekong
Stung Slot	11,327	105,280	Water Level	Manual	m	1-6 times p/day	19870510	20061231	
Tuk Chhoo	10,685	105,126	Water Level	Manual	m	1-6 times p/day	20010101	20051231	Kamchay

Table A.1: Overview of MRC measurement stations in the vicinity of the areas of interest in the Cambodian Mekong Delta.

Station	Latitude	Longitude	Parameter	Measurement Type	Unit	Interval	Start	End	River
	10,705	105,134	Rainfall	Manual	mm	1-6 times p/day	20070418	20210830	Bassac
			Discharge	Daily Calculated	m^3/s	Daily	20010101	20071231	Bassac
			Water Level	Daily Minimum	m	Daily	19620101	20061231	Bassac
			Water Level	Daily Maximum	m	Daily	19620101	20061231	Bassac
			Rainfall	Telemetry	mm	15 minutes	20100814	20210831	Bassac
			Discharge	Measured DSMP	m^3/s	Unknown	20090630	20141230	Bassac
			Sediment Concentration	Measured DSMP	mg/l	Unknown	20090630	20141230	Bassac
			Sediment Flux	Calculated DSMP	tonnes/day	Unknown	20090630	20141230	Bassac
			Nitrite-Nitrate	Measured	mg/l	4 times p/month	19850714	20171214	Bassac
			Ammonium	Measured	mg/l	4 times p/month	19850514	20171214	Bassac
			Water Temperature	Measured	degC	4 times p/month	20030114	20171214	Bassac
			Total Suspended Solids	Measured	mg/l	4 times p/month	19870514	20171214	Bassac
			Conductivity	Measured	mS/m	4 times p/month	19850514	20171214	Bassac
Chau Doc			Total phosphorous	Measured	mg/l	4 times p/month	19850614	20171214	Bassac
			Chemical Oxygen Demand	Measured	mg/l	4 times p/month	19850714	20171214	Bassac
			Sulphate calculated by EC	Measured	mS/m	4 times p/month	19850514	20111214	Bassac
			pH	Measured	pH Units	4 times p/month	19850514	20171214	Bassac
			Total Nitrogen	Measured	mg/l	4 times p/month	19880114	20171214	Bassac
			Dissolved Oxygen	Measured	mg/l	4 times p/month	19850514	20171214	Bassac
			Water Level	Manual	m	1-6 times p/day	19600629	20210830	Bassac
			Water Level	Telemetry	m	15 minutes	20100815	20210831	Bassac
	10,700	105,100	Rainfall	Manual	mm	1-6 times p/day	19200101	20071219	
			Evaporation Rate	Daily	mm/d	Daily	19800101	20121231	
			Air Temperature	Daily Maximum	degC	Daily	19781201	20121231	
			Relative Humidity	Daily	%	Daily	19781201	20121231	
			Air Temperature	Daily Minimum	degC	Daily	19781201	20121231	
			Sunshine Duration	Daily	hr	Daily	19790101	20071231	
			Wind Speed	Daily	m/s	Daily	19781201	20071231	
	10,805	105,355	Water Temperature	Measured	degC	4 times p/month	20030614	20031214	
			pH	Measured	pH Units	4 times p/month	19860314	20031214	
			Conductivity	Measured	mS/m	4 times p/month	19860314	20031214	
			Sulphate calculated by EC	Measured	mS/m	4 times p/month	19860314	20031214	
			Nitrite-Nitrate	Measured	mg/l	4 times p/month	19860314	20031214	
Hong Ngu			Ammonium	Measured	mg/l	4 times p/month	19860314	20031214	
			Total Nitrogen	Measured	mg/l	4 times p/month	19890514	20031214	
			Total phosphorous	Measured	mg/l	4 times p/month	19860314	20031214	
			Dissolved Oxygen	Measured	mg/l	4 times p/month	19860314	20031214	
			Total Suspended Solids	Measured	mg/l	4 times p/month	19870914	20031214	
			Chemical Oxygen Demand	Measured	mg/l	4 times p/month	19860314	20031214	
	10,801	105,248	Water Level	Manual	m	1-6 times p/day	19790401	20210830	Mekong
			Water Level	Telemetry	m	15 minutes	20100816	20210831	Mekong
			Water Level	Daily Minimum	m	Daily	19690406	20061231	Mekong
			Water Level	Daily Maximum	m	Daily	19690407	20061231	Mekong
			Water Temperature	Measured	degC	4 times p/month	20030114	20171214	Mekong
			Discharge	Daily Calculated	m^3/s	Daily	20030101	20061231	Mekong
			Discharge	Measured DSMP	m^3/s	Unknown	20090630	20181230	Mekong
			Sediment Concentration	Measured DSMP	mg/l	Unknown	20090630	20181230	Mekong
			Rainfall	Manual	mm	1-6 times p/day	20070410	20210830	Mekong
			Sediment Flux	Calculated DSMP	tonnes/day	Unknown	20090630	20181230	Mekong
Tan Chau			Total Suspended Solids	Measured	mg/l	4 times p/month	19870514	20171214	Mekong
			Conductivity	Measured	mS/m	4 times p/month	19850514	20171214	Mekong
			Ammonium	Measured	mg/l	4 times p/month	19850514	20171214	Mekong
			Total Nitrogen	Measured	mg/l	4 times p/month	19880214	20171214	Mekong
			Dissolved Oxygen	Measured	mg/l	4 times p/month	19850514	20171214	Mekong
			Chemical Oxygen Demand	Measured	mg/l	4 times p/month	19850714	20171214	Mekong
			Sulphate calculated by EC	Measured	mS/m	4 times p/month	19850514	20111214	Mekong
			Nitrite-Nitrate	Measured	mg/l	4 times p/month	19850714	20171214	Mekong
			Total phosphorous	Measured	mg/l	4 times p/month	19850614	20171214	Mekong
			pH	Measured	pH Units	4 times p/month	19850514	20171214	Mekong
			Rainfall	Telemetry	mm	15 minutes	20100814	20210831	Mekong
			Rainfall	Manual	mm	1-6 times p/day	19971231	20061231	
	10,824	105,337	Total Nitrogen	Measured	mg/l	4 times p/month	20040714	20171214	
			Water Temperature	Measured	degC	4 times p/month	20040714	20171214	
			pH	Measured	pH Units	4 times p/month	20040714	20171214	
			Total Suspended Solids	Measured	mg/l	4 times p/month	20040714	20171214	
			Conductivity	Measured	mS/m	4 times p/month	20040714	20171214	
Tu Thuong			Ammonium	Measured	mg/l	4 times p/month	20040714	20171214	
			Total phosphorous	Measured	mg/l	4 times p/month	20040714	20171214	
			Dissolved Oxygen	Measured	mg/l	4 times p/month	20050114	20171214	
			Chemical Oxygen Demand	Measured	mg/l	4 times p/month	20040714	20171214	
			Sulphate calculated by EC	Measured	mS/m	4 times p/month	20040714	20111214	
			Nitrite-Nitrate	Measured	mg/l	4 times p/month	20040714	20171214	

Table A.2: Overview of MRC measurement stations in Vietnam.

B

Description and Documentation of Each Prek in the Case Study Area

This chapter provides a brief description of each Prek as well as photographic documentation. It is primarily based on fieldwork conducted in June 2019, but has been updated with information from later field trips where necessary.

B.1 Prek Cham Kroum

The head of Prek Cham Kroum, the northernmost Prek in the study area, is located close to the 7th Cambodia-China Friendship bridge across the Tonle Bassac. Water can flow freely from the Bassac into the Prek. Directly along the head of the Prek, there is a tight agglomeration of

houses. The Prek itself, though filled with water along its whole length, is overgrown with water hyacinths (*Eichhornia crassipes*). The profile of the Prek is well-defined, though erosion effects are visible in some places. Vegetation is lush along its whole length, with Mango trees being the dominant crop over large stretches.

A particularity of this Prek are a number of cylindrical containers, probably used for the storage of liquids, that can be found in several places along the Prek (though whether those liquids are water, growth enhancers for mango trees, or pesticides could not yet be determined).

It was visible in several places that vegetation along the Prek is being removed. In some spots, cut-down branches of banana and bamboo trees could be seen. In others, there were charred spots on the ground where dried vegetation had been burned.

For the majority of its length, the course of Prek Cham Kroum is very straight. However, at its tail end, it takes a sharp turn to the North and then curves towards its junction with the Prek Ambel in a wide bend. Here the area is covered by grassland and a small settlement is located along the Prek Ambel. According to the information of local inhabitants, the community in this settlement is predominately composed of Cham people.

The junction of the Prek with the Prek Ambel is not easily accessible since several houses are located directly on its banks and no open path leads to the waterfront. In itself, the junction is wide and open, but at the time of observation (June 2019), it was entirely overgrown with water hyacinths to the point where no open water surface was visible anymore. According to interviewees, there is an annual water shortage in the Prek in April and May. Water from the Prek is used for irrigation during both the dry and the rainy season when it is available. Furthermore, people fish in the Prek during the rainy season and use the vegetation found on the banks for their diet – predominantly morning glory (*Ipomoea aquatica*) and ivy gourd (*Coccina grandis*). In addition, some also plant vegetables and fruit on the banks of the Prek – bananas and papayas among others. In the past, the Prek was also commonly used as a source of domestic water, water for livestock and transport by boat during the rainy season. However, these uses ceased because clean water is now available from a communal supply pipe and a new road was constructed, rendering the waterway superfluous as a transport route. On an additional note, one farmer stated that fishing used to be possible in the Prek during both the dry and the rainy season, but that fish populations have declined in the past 10 years.

Furthermore, a Farmer's Water User Community (FWUC) appears to exist at Prek Cham Kroum, and an interviewed farmer is the deputy head of this association. According to him, its chief aims are to prevent the littering of the Prek, to prevent the unauthorized removal of sediments (which can lead to bank collapses) and to coordinate the clearing of vegetation on the bank of the Prek. According to the interviewee the association was created by his excellency Choa Tol, who works in the Ministry of the Interior, and its Khmer name is Pro Chea Kapea. Every farmer who has plots along the Prek belongs to the association. The interviewee's duties as deputy head of the association include patrolling the Prek every 3-5 days to spot any illicit activities. The head of the FWUC is not elected, but chosen by the chief of the village.

The Prek has not been rehabilitated, though it appears that it would be welcomed by the local residents in order to supply sufficient water for irrigation. In 2018, the FWUC coordinated an effort to supply water during the dry season because there was less than usual in the Prek. They asked the commune to assist them in renting a big pumping station to pump water into the Prek as well as to acquire sandbags so that the spread of the irrigation water on the fields could be channeled to crops that have the largest water requirements. According to the interviewee, the effort succeeded and together with the funding the FWUC received from the commune, the individual farmers only had to contribute 2000 Riel each to cover the costs of the operation.



(a) Head of the Prek and China Friendship Bridge.



(b) Mango trees and liquid storage containers.



(c) Grassland and Cham settlement at tail end.



(d) Junction of the Prek and Prek Ambel.



(e) Dense water hyacinth vegetation.



(f) Charred spots from burned vegetation.

Figure B.1: Visual documentation of Prek Cham Kroum.

B.2 Prek Me Srok

At the head of Prek Me Srok, water can flow freely into the Prek. A wooden bridge spans the head of the Prek, a small concrete-paved path leading along the bank of the Bassac. Several boats could be seen navigating the Prek in June 2019 and the water surface was relatively free of water hyacinths. Water is present throughout the Prek and at the time of the visit (ca. 11:30 a.m.), a slight current towards the Prek Ambel was visible.

The profile of the Prek is well-defined throughout and the roads along the Prek are passable.

In some places, charred patches were bank vegetation was removed through burning can be observed. Locally, erosion effects and bank collapses are visible.

Similar to the Prek Cham Kroum, the course of the Prek Me Srok is straight for the majority of its length, but takes a sharp turn to the North at its end, to join with the Prek Ambel after a double curve. At this point, erosion effects are clearly visible on a larger scale and some presence of water hyacinths could be noted.

For comparison purposes, the pumping stations along the Prek Me Srok were georeferenced. Unfortunately, the majority of the pumps had already been removed by farmers in preparation for the inundations during the monsoon season. What remained were blue PVC pipes leading from the Prek to the top of the bank and under the road to the fields. It has to be noted that not all those pumping stations are equipped with individual pumps during the dry season – rather one pump is shifted between several pumping stations. However, while the numbers of pumps and pumping stations might not correspond entirely, the large number of pumping stations still bears testimony to extensive irrigation activities during certain times of the year. Overall, a total of 69 pumping stations could be counted on the Prek's length of 4.700 m. This equals ca. 1.5 pumping stations per 100 m.

Water from the Prek is used for irrigation during the dry season, to water and wash livestock and, for domestic water supply (though not for drinking water). Several interviewees also stated that they use the bank vegetation – specifically, morning glory. One of the interviewees also fishes regularly in the Prek, though he noted that this activity was limited due to declining fish populations.

The Prek has recently been rehabilitated – and several interviewees expressed satisfaction in this regard, appreciating the year-round availability of water in the Prek. The Prek was deepened and the excavated material was used to raise the road on the bank. Before the Prek was rehabilitated, there was a shortage of water during several months of the year for seven years.



(a) Head of the Prek, with bridge.



(b) Boat used to transport goods along the Prek.



(c) Bank collapses along the Prek.



(d) Road and profile along the Prek.



(e) Junction of the Prek with Prek Ambel, erosion effects along the banks.

Figure B.2: Visual documentation of Prek Me Srok.

B.3 Prek Lok

The head of Prek Lok shows extensive sediment deposits separating the current level of the Bassac from the mouth of the Prek, constricting the inflow into the Prek. This area is actually being used as a recreational area by the local population and several people could be observed sunbathing on the sandbanks and swimming in the Bassac. Furthermore, extensive macrophyte floating vegetation covers the water surfaces at the head of the Prek.

Nevertheless, water is present in many parts of the Prek, though water hyacinths cover large areas of the water surface. At one point, there is a ford where a road crosses the Prek

Like Prek Cham Kroum and Prek Me Srok, Prek Lok's tail connects with the Prek Ambel, though without the curve that characterizes this area of the other two Preks. Beside the junction of the Prek Ambel and the Prek Lok, there is a small agglomeration of houses.

Along the Prek, but especially at its tail end, extensive erosion effects are visible.

Two people were interviewed in June 2019 at this Prek – one of them a fisherman who lives at the junction of Prek Ambel and Prek Lok, the other one a farmer who has four plots along the Prek. According to their information, the Prek has never been rehabilitated, but they would welcome such a rehabilitation. The farmer noted that if water were in the Prek year-round, not only would it allow him to grow a second crop of rice, but also to use his boat on the Prek. The farmer, who lives in the village at the head end of the Prek, uses the municipal pipe for the supply of domestic water, but the fisherman uses water from the Prek and Prek Ambel, though he boils it first. The water from the Prek is furthermore used for the watering of livestock. Both interviewees also use the vegetation found along the banks of the canal, especially morning glory, though the fisherman also noted that his family sometimes eats the flowers of the water hyacinths.

At this Prek too the number of visible pumping stations was counted to compare it to Prek Me Srok. Only a total of 8 pumping station over the whole length of the Prek could be observed in June 2019. While this is probably also due to the fact that many pumping stations were removed entirely for the duration of the wet season, it also shows that irrigation activity at this Prek is lower than at Prek Me Srok.



(a) Head of the Prek, with sediment deposits preventing inflow.



(b) Bridge across the Prek in the village area.



(c) Erosion at the tail end of Prek Lok.



(d) Junction of Prek Lok and the Prek Ambel.



(e) Ford across Prek Lok at its tail end.

Figure B.3: Visual documentation of Prek Lok.

B.4 Prek Pok

The head of Prek Pok allows for free inflow into the Prek, although there are some sediment deposits. It has to be noted that the head of Prek Pok and Prek Hom do not lie directly at the Bassac, but rather at another man-made channel. An island with a Pagoda on it separates the heads of these Preks from the Bassac. The channel connecting the heads of Prek Pok and Prek

Hom to the Bassac is called Wat Koh channel and begins just beside the head of Prek Lok. As with Prek Lok, there are sediment deposits and macrophyte floating plant vegetation constricting the free inflow of water into the channel and thus into the Preks it supplies.

Water is present in some parts of the Prek, but there are two fords cutting through it, creating barriers for the water. In the farmer interviews it was stated that this was intentional so that the little water that there is in the Prek would be concentrated in the areas closer to the village to enable the farmers there to irrigate their crops. Consequently, the plots along the tail-half of the Prek are lying fallow during the dry season, as no water for irrigation is available. The ford closer to the village, which dams up the majority of the water present in the Prek, was apparently built in the early months of 2019, and, according to statements made by interviewees, is removed before the rainy season to enable a free flow of water during the annual monsoon inundation.

This Prek, unlike the others described so far, does not end in the Prek Ambel, but rather in a dead end. There is a ford at the end of the Prek, another road crossing through, but no further channels to which it is connected.

The two farmers interviewed at this Prek in June 2019 grow beans, corn and dry season rice on their plots and use the Prek as source for irrigation water and for livestock. One of them also uses it for transport by boat, to fish in occasionally and, in the month of June, to harvest morning glory and ivy gourd on its banks. The Prek has not been rehabilitated and both farmers report a lack of water in the Prek from November to June. Both also agree that they would welcome a rehabilitation project and the increased availability of water throughout the year, especially since some of their plots are currently lying fallow. As noted above, a ford including a small dam was built to concentrate the little water that is available during the dry season in one half of the Prek. Furthermore, there is a coordination among farmers to pump water from the Bassac into the Prek when it is needed. Two or three farmers possess bigger pumps and take on the task of pumping water on demand, charging 10.000-20.000 Riel per hour (open to negotiation) to cover labour and operational costs as well as to make a small profit. The chief of the village is responsible for Prek maintenance and asks the farmers to take care of the Prek vegetation in front of their houses and plots. Apparently, the village chief also coordinated the removal of sediments with a private company. From what the interviewees could say, the company dredged parts of the canal where road accessibility was possible, and used some of the sediments to repair minor bank collapses.

It appears that the company accepted part of the sediments as payment for their services, because they can sell the excavated material to farmers who wish to raise their land. If the company is asked to also dredge parts of the Prek that are more difficult to access, the village chief would have to collect money from the farmers to pay the charges, and that is apparently rather difficult.



(a) Beginning of Wat Koh channel, with sediment deposits.



(b) Wat Koh channel with Prek Pok debranching.



(c) Ford across the Prek, with dammed up water on the right and dry channel on the left.



(d) Bridge across the Prek in the village area.



(e) Fields lying fallow at the tail end of the Prek due to lack of irrigation water.



(f) Ford across the tail-end of the Prek.

Figure B.4: Visual documentation of Prek Pok

B.5 Prek Hom

Prek Hom, like Prek Pok is connected to the Bassac through the Wat Koh channel. However, while Prek Pok debranches from the Wat Koh channel, Prek Hom is its continuation. Effectively, the Wat Koh channel takes a sharp turn to the West and becomes Prek Hom. In this transitional area, a large pool of water exists.

Prek Hom's profile is well-defined throughout. The Prek is broad and apparently of considerable depth, for there is water in the channel throughout. In some places, water hyacinth vegetation is dense. Furthermore, several bank collapses and other, more minor, erosion sites were observed. In several places, people appear to have taken steps to prevent erosion by fortifying the bank with cut-off tree branches .

While its course is mostly straight, Prek Hom takes several turns at its tail end, before ending in a perpendicular irrigation/drainage channel. On the other side of this channel, a smaller water course continues in the direction of Prek Ambel.

At Prek Hom, two farmers were interviewed in June 2019. They grow mangoes, rice, corn, beans and sugarcane along the Prek. The Prek has not been rehabilitated and in this case the two farmers disagree on whether it would be a good idea to do so. The current system is that farmers coordinate among themselves to hire machines to remove sedimentary deposits at the head of the Prek when it is necessary to do so. The costs are split amongst themselves. One of the interviewed farmers is satisfied with this system while the other finds that it is rather expensive and would welcome a rehabilitation of the Prek that would ensure free inflow all year-round. Furthermore, he also stated that an even greater advantage of rehabilitation for him would be the construction of a better road along the Prek. He currently finds it very difficult to transport his equipment and crop from his house at the head of the Prek to his plots at its tail.

Both interviewees use the Prek for irrigation and domestic water supply. One of them also uses it for transport by boat, to water his livestock, for fishing and as a source of food in the form of bank vegetation such as morning glory.

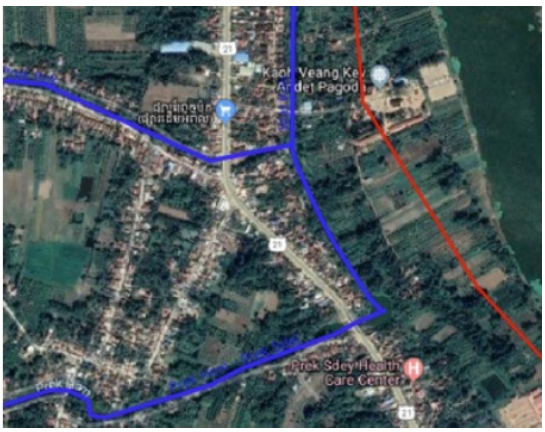

(a) Wat Koh channel, with Prek Pok debranching to the North, then transition from Wat Koh Channel to Prek Hom in the southern bend. Image credit: Google Maps.

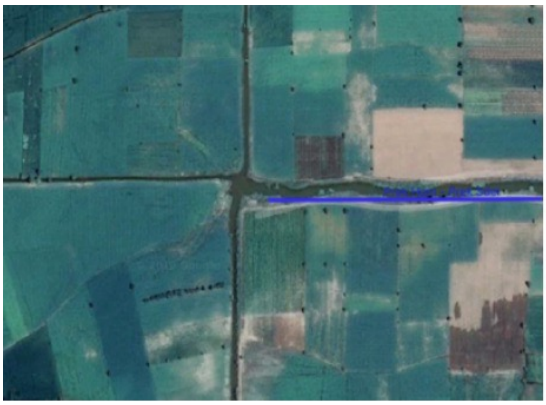

(b) End of Prek Hom, with small channel continuing towards Prek Ambel and perpendicular irrigation channel. Image credit: Google Maps.



(c) Transition zone between Wat Koh channel and Prek Hom.



(d) Erosion zones along the Prek.



(e) Prek profile, filled with water in its tail section.



(f) End of the Prek.

Figure B.5: Visual documentation of Prek Hom

B.6 Prek Nou

Unlike Prek Hom and Prek Pok, the head of Prek Nou lies directly on the Bassac, though it does not debranch in a straight line, but rather in a backwards curve. Nonetheless, a free inflow of water is possible and the Prek is supplied with water throughout. Water hyacinths are abundant in certain places. The Prek's profile is well-defined but erosion is very pronounced in some places. It ends in the same perpendicular channel as Prek Hom.

Two farmers were interviewed on this Prek in June 2019. Both of them use the water from the Prek for irrigation. One of them also uses it for his domestic water supply, to water his livestock and sometimes as a source of food in the form of vegetation that grows on its banks. The other farmer also uses the Prek for transport by boat and fishes in it, though only for domestic use. Beans, mangoes, corn and rice are grown on the plots. Two years ago, the Prek was rehabilitated and consequently, there is enough water in the Prek year-round. Both farmers feel that the rehabilitation was a success and appreciate the continuous availability of water in the Prek. The farmers agree that there used to be a FWUC, more than ten years ago. However, it was dissolved due to conflicting interests. The FWUC put up a blockade so that the Chamkar would not be flooded during the rainy season, but there were other farmers who needed the water. Nowadays, it is the chief of the village who is in charge of Prek maintenance, though according to the information by the interviewees, no strict rules are observed. The farmers are responsible for clearing the vegetation on the banks of the Prek in front of their houses and their plots.



(a) Head of the Prek.



(b) Water hyacinth vegetation.

Figure B.6: Visual documentation of Prek Nou

B.7 Prek Put

Out of all the Preks in the study area, Prek Put is in the worst state of disrepair. Its head is entirely disconnected from the Bassac by sediment deposits. The concrete foundations of an old pumping station that was used to lift water from the Bassac to the Prek are still visible, but the endeavour was abandoned several years ago and the pump has been removed. A dirt road crosses in front of the abandoned pumping station, further separating the head of the Prek from the Bassac.

In itself, the Prek is filled with waste and vegetation and in several places, earthen dams have been erected across what remains of the channel in order to let streets and paths cross over. In some cases, these incorporate pipes in order to let water pass, should it enter the Prek. But even these pipes are often clogged with vegetation or missing entirely. In one case the brick foundation of a garden wall cuts through the Prek completely without any possibility of water passage.

From what remains of it, it can be deduced that Prek Put's original profile was already considerably smaller than that of the other Preks in the study area. Furthermore, it is also the shortest Prek. From what was observed during the field trip, the Prek hardly qualifies as such anymore. Its sedimentation has reached levels to leave it hardly more than a longitudinal depression in the landscape.

According to the information gained in the interview with a local, hardly any water is present in the Prek even in the high period of flooding during the wet season. It does not serve for irrigation purposes – the interviewee stated that it is easier to use water from nearby Prek Nou if it is possible to do so and to abandon the plots if it is not. The only use that can be derived from the Prek is the use of vegetation such as morning glory and bitter melon. Furthermore, the interviewee stated that a rehabilitation of the Prek would entail major conflicts of interest, since several local residents have built their houses directly on the banks of the Prek or very close to it and would have to be resettled.



(a) Head of Prek Put at the Bassac.



(b) Remains of the old pumping station.



(c) Earthen dam across Prek Put.



(d) Prek Put, entirely overgrown.

Figure B.7: Visual documentation of Prek Put

B.8 Prek Chann

Prek Chann diverges perpendicularly from the Bassac and has a straight course all the way to its end. It was rehabilitated in 2017 and the Prek was broadened, deepened and a new road and gate were constructed. The gate is located ca. 700 m inland from the head of the Prek. However, a few hundred meters West of the gate, major bank collapses have occurred since the rehabilitation, posing a constriction on the amount of water that can flow through the Prek. Prek Chann ends in a perpendicular irrigation channel.

Two farmers were interviewed at this Prek in July 2019, one of them being the head of the local FWUC. Both interviewees use the Prek as a source for irrigation water all year round and as a source of water for their livestock. Furthermore, one of them fishes in the Prek all year round. Both of them also state that they use the vegetation that grows on the banks, and one of them plants certain vegetables such as lemongrass, garlic, bitter lemon and Chinese cabbage on the banks himself. They were furthermore in agreement that the rehabilitation of the Prek, which was carried out in 2017, has been a positive change for them, enabling them to use their plots more effectively. One of the interviewees had to move her entire house back by 3 m during the rehabilitation, but still stated that it had been worth it.

Regarding the operation of the gate, the interviewees did not mention any particular conflicts. The head of the FWUC, who was interviewed, is in charge of the operation of the gate. He states that he leaves the gate open between November and June, when there is a shortage of water in the Prek but closes it between June and October in order to prevent soil erosion. While he did not discuss this operation schedule with all the members of the FWUC, he did consult with one other farmer before deciding on it. He also noted that the gate is opened very slowly, since there was an accident in 2018 when the gate was opened abruptly. A farmer who had been fishing in the Prek at the time was swept away by the suddenly rising water and almost drowned.

One major issue at the Prek Chann are the bank collapses that occurred after rehabilitation. As mentioned above, they constrict the flow of water. The head of the FWUC states that he has already contacted the pertinent authorities, but has not yet heard back from them. Apart from deciding on the schedule for gate operation and managing the repair of the bank collapses, the head of the FWUC also coordinates the clearing of the vegetation on the banks of the Prek. The system is that every farmer is responsible for clearing the vegetation that borders on their plots, which seems to work so far. The head of the FWUC said that if someone did not meet their duties, he would consider making them pay for the water from the Prek. All the farmers who have plots along the Prek are in the FWUC. The head is elected democratically.



(a) Head of Prek, as seen from the main street bridge.



(b) Gate constructed during rehabilitation.



(c) Concrete fortification of banks behind the gate.



(d) View towards tail end of the Prek.



(e) Area of massive bank collapse.



(f) Vegetation growing in the Prek.



(g) Tail end of Prek, with irrigation channel.

Figure B.8: Visual documentation of Prek Chann

B.9 Prek Touch

Prek Touch is an unrehabilitated, heavily overgrown Prek with hardly any water present. What water there was seems to have been pumped not from the head of the Prek but from its tail-end, where another irrigation channel, this one filled with water, is located, separated from the Prek by an earthen mound. There is a pump and a plastic pipe to transport water from one channel to the other. This channel at the end of the Prek branches off from a perpendicular drainage/irrigation channel. Furthermore there is a half-sunken, but still operational bridge located at the junction of these two channels that allow for a relatively dry crossing.

The lack of water was evident in the agricultural practices and general vegetation that could be observed along the Prek. A great number of fields lay fallow, though some farmers could be seen attempting to cultivate fruit and vegetables such as cucumbers.

Two farmers were interviewed at this Prek in June 2019. They have crops consisting of mango trees, mung beans and dry season rice in plots along the Prek. The Prek has never been rehabilitated and both interviewees state that there is not sufficient water for them to irrigate crops during the dry season months. (Though one of the farmers stated that there was no water in the Prek between November and July, while the other reported such a lack only between December and April.) Both farmers use the Prek for irrigation and transport by boat during the rainy season. One of them further uses it for domestic water supply and watering his livestock, while the other fishes in the Prek whenever possible. Both of them also report using the vegetation found on the banks, especially morning glory. Furthermore, they stated that there is a private water seller, who supplies the Prek with water when there is no natural inflow during the dry season at the price of 100 $ per ha per crop cycle.

According to the interviewees, there used to be a FWUC until 9 years ago, which was founded and coordinated by the village chief. However, when the village chief died, the association fell apart. Now, it is the current village chief who is nominally in charge of Prek maintenance, but it appears that no measures are being taken. Both farmers seem very enthusiastic about the possibility of Prek rehabilitation and would welcome the extended presence of water in the Prek to grow another cycle of crops.

After the interviews with the farmers, a third interview was conducted at this Prek – namely with the private water seller who uses a big pump to supply the Prek during the dry season when no natural inflow is possible. He is a farmer himself, but has been taking the additional responsibility of pumping water from the Bassac into the Prek for five years. According to him, he started this activity to supply his own family's plots but was approached by other farmers soon after. He bases his pricing policy on the plot size and the crop type and charges between 150 000 and 300 000 Riel per ha per season. Payment is collected at the end of the season, generally without many problems, even though there are currently several people who owe him money. When the pumps are running, he leaves them on for 24 h/day. When water is required in the Prek, he pumps for one week and then takes a break of 2-3 days before beginning again. At the moment, he supplies the plots of ca. 20 farmers with water during the dry season. Asked about the possibility of Prek rehabilitation, the private water seller stated that he would still welcome it. According to him, it would be a big advantage for his own plots if water were available without the necessity of additional pumping activities, which are not a big source of additional income for him.



(a) Pump that is used to lift water into the Prek.



(b) Fields lying fallow at the tail end of the Prek due to lack of water.



(c) Head of the Prek, with pumping station to lift water from the Bassac into the Prek.



(d) Junction of the two irrigation channels, with the half submerged bridge that can be used for crossing.

Figure B.9: Visual documentation of Prek Touch

B.10 Prek Thom

Prek Thom forms the southern border of the study area. It diverges directly from the Bassac and its tail end connects to the Prek Ambel. During this field trip in June 2019 only ca. half the length of the Prek could be visited, as road conditions on the second half were too difficult to continue. At the furthest point of the Prek that was visited, an old concrete construction

is located. It appears that it used to be a gate to regulate the flow through the perpendicular irrigation channel that crosses the Prek at this point, but parts of the construction have been dismantled. The construction that remains seems to serve as a bridge across the perpendicular channel to continue the path along the Prek.

Along the tail-half of the Prek, a second Prek (Prek Khsae 500), which originates at Prek Ambel, runs in parallel to Prek Thom. In the area that was visited during this field trip, only a road on a dam separates those two channels. In some places, pipes have been installed through which water can be transferred from one Prek to the other.

According to the information gathered in the interviews in June 2019, at this Prek, the last rehabilitation took place in 1993. However, since then, sedimentation has clogged up the canal again. The interviewed farmers expressed a very positive attitude towards possible future rehabilitation, since year-round water availability would be a boon to their farming activities. In 2019, the farmers state that they lack water between January and August. There was a private water supplier who pumps water from the Bassac into the Prek for farmers along the Prek to use for their plots. He charges them at varying rates depending on the crop they want to irrigate and the diameter of the pipe that they are using to irrigate. The interviewees use the water from the Prek for irrigation and the vegetation found on the banks for their regular diets both during the dry and the rainy season.

The head of Prek Thom shows considerable sediment deposits and a regular inflow of water currently was not possible possible in 2019 during the first field survey. There is a ferry station at the head of this Prek, which offers the possibility to cross the Bassac.

However, significant changes occurred at Prek Thom during the duration of this thesis. In 2020, the Prek was excavated through a local initiative. The bed was deepened significantly, and the banks straightened, as is outlined in Chapter 4.3.



(a) Ferry station at the head of the Prek.



(b) Head area of the Prek, with sediment deposits and vegetation.



(c) Road leading along the Prek, with rice fields on the other side.



(d) Concrete remnants of a gate, now serving as a bridge.



(e) View from the old gate.

Figure B.10: Visual documentation of Prek Thom

C

Translations of Quotations from Archival Research in Cambodia

In this study, we have taken the greatest account of the observations of the inhabitants, they have been excellent guides for us, this question of the drilling of sealing canals is of great interest to them, not only have they always agreed to inform us when we have had recourse to them, but more often than not they have come to us themselves to ask us to include in our projects the Preks which they have indicated to us to show us the best locations and the most economic way of carrying out the work. - *First Mekong sealing studies, File Nr. 25754, p.7*[1]

The Tiams had once found a way to obtain this precious land; this is the legend

[1] See Appendix C for translations.

that was told to me by old Cambodians. Che Tiam Ania Khou, aunt of Governor Tiam of Kanchor, lived a century ago in the small village of Dey Dos, on the right bank of the Mekong; his house overlooked the river and behind it was a large beng which filled up every year at the time of the floods, but rather late. Ania Khou had bought a beautiful, heavy dugout canoe in Sambor province, and his idea was to take it into the large beng behind his house and use it to transport the wood and white huts that he would fetch from the mountain across the beng. But the sides of the bank are almost sheer at Dey Dos, and all his efforts to hoist the dugout canoe, to get it over the hump, were in vain; it was too heavy and the bank too steep on the river side. Ania Khou then had the idea of digging a channel seven or eight cubits deep and of a width equal to that of the heavy dugout, thinking of taking advantage of the moment of the highest flood of the year to make his dugout penetrate by this channel into the great Beng. Ania Khou's plan succeeded marvellously and when the flood had reached the level of the bottom of the canal, the waters of the river rushed into the Beng whose level was still several meters below, the priogue was violently pushed towards the still water table and flatted there, but it happened that the waters of the river rushed with so much force that they widened the canal which, in two months, reached a width of sixty coudée *(NB: ca. 30 m)*. Moreover, the silty waters of the river, rushing into clearer waters which were not at the same temperature, quickly deposited their silt and when the floods came, old Tiam was not a little surprised to see that the area of cultivable land had considerably increased behind his house and that a double bulge of fertile land was clearly marked out at the outlet of the new prek into the Beng.

It is therefore not a question here of conquering, for a people who cannot exploit them, new lands suitable for cultivation, but simply of regulating, by means of irrigation, a harvest which depends only on the quantity of annual rainwater and also on its distribution during the development of the various phases of the crop.

- Rapport au sujet d'un programme de travaux d'hydraulique agricole (10th of May 1910, FileNr 5654), Direction Générale des Travaux Publics

D

Tables of Values Used in Eco-Hydrological Model

Crop	Kc_{init}	Kc_{mid}	Kc_{end}	Ky_{init}	Ky_{mid}	$Ky_{end}d$
Rice	1,05	1,20	0,75	0,6	1,25	0,4
Vegetables	0,67	1,02	0,73	1,06	1,06	1,06
Fruit trees	0,65	0,824	0,854	0,8	0,8	0,8
Fallow	0,05	0,05	0,05	0	0	0
Water	0	0	0	0	0	0
Urban	0,05	0,05	0,05	0	0	0

Table D.1: K_C and K_Y values for all land cover classes.

Crop	Proportion of Vegetable Area [%]	Crop from FAO Table	Kc_{init}	Kc_{mid}	Kc_{end}	K_y
Bittermelon	2	Squash, zucchini	0,95	0,95	0,75	1,34
Cucumber	4	Fresh market	0,60	1,00	0,75	0,85
Eggplants	1	Squash, zucchini	0,95	0,95	0,75	1,37
Green bean	31	Beans, green	0,50	1,05	0,90	1,07
Long bean	3	Beans, green	0,50	1,05	0,90	1,07
Maize	26	Maize, field	1,20	1,20	0,48	1,25
Mung bean	29	Beans, green	0,50	1,05	0,90	1,07
Mustard greens	1	Lettuce	1,00	1,00	0,95	1,97
Wax gourd	1	Squash, zucchini	0,95	0,95	0,75	0,90
White bean	2	Beans, green	0,50	1,05	0,90	1,07

Table D.2: K_C and K_Y values for all vegetable crops.

Crop	**Planting Time**	**Harvest Time**	**Daily Irrigation [h/ha]**	**Upper 25% Yield [t/ha]**	**Average Price Per [USD/kg]**	
Bittermelon	March	May-June	6,52	6,67	6,67	1,67
Early Wet Season Rice	April - May	July - August	2,90	6,10	11	2,75
Mustard greens	June	July	12,50	1,41	1,41	0,35
Wet season rice	September	December	2,82	4,08	5	1,25
Eggplants	October	March	1,85	5,56	5,56	1,39
Mung bean	November or March	February or May	1,87	2,48	4,80	1,20
Recession rice	October - December	January - March	1,88	5,73	9,12	2,28
White bean	October-November	January	0,00	1,35	1,35	0,34
Wax gourd	November	January	1,67	-	-	-
Green bean	November - Decmber	February - March	0,00	2,71	3,57	0,89
Long bean	December	January	0,95	6,00	6,00	1,50
Dry season rice	December - January	March - April	1,91	5,66	8,57	2,14
Cucumber	Variable	Variable	7,98	5,22	6,67	1,67
Maize	Variable	Variable	0,45	4,94	6,22	1,56
Fruit trees	year-round	year-round	1	10,8	19,9	4,98
Malé Grass	year-round	year-round	-	-	-	-

Table D.3: Agricultural characteristics of the crops recorded in the interviews. For vegetable crops, average values depending on their relative areas were calculated.

Texture **Field capacity [vol/vol]**	θ_r **Wilting point [vol/vol]**	θ_s	α **[cm^{-1}]**	n	K_s **[m/d]**
silty clay	0.07	0.36	0.005	1.09	0.005
0.32	0.05				
sandy clay loam	0.1	0.39	0.959	1.48	0.314
0.32	0.07				
clay loam	0.095	0.41	0.019	1.31	0.062
0.32	0.15				

Table D.4: Hydraulic soil properties according to Carsel and Parrish (1988), with θ_r = residual water content, $\theta_s at$ = saturated water content, α and n = fitting parameters related to particle-size distribution, and K_s = saturated hydraulic conductivity.

Crop	CN-I	CN-II	CN-III
Rice	67	82	91
Vegetables	55	75	88
Fruit trees	40	60	78
Fallow	72	86	94
Water	1	1	1
Urban	81	92	97

Table D.5: Different curve number values according to land use, hydrological soil group, and antecedent soil moisture.

E

Questionnaires used in the field surveys

E.1 Farmers - Initial Survey on Ecosystem Services June 2019

Basic information					
Name					
Telephone					
Prek					
Age bracket					
Gender					
How long have you been living here?					
Occupation					
Agriculture					
Uses of the canal	**Present**		**Past**		
	Dry season	*Wet season*	*Dry season*	*Wet season*	
When is the Prek dry?					
Crops	**Type**	**Planting time**	**Harvest time**	**Where is it grown**	**Irrigation**
Do you have enough water to grow your crops?					
When are you lacking water?					
How many plots do you have?					
How frequent is it that you lose some of your crops to the flood?					
Rehabilitation					
Has the canal been rehabilitated?					
What work has been done on the canal?					
What has changed since the rehabilitation?					
Do you have the feeling that it was a good or a bad thing?					
What are the main positive and negative effects?					
Have there been bank collapses?					
Have there been problems with the Gates?					
Would you want it to be rehabilitated?					

Why?					
What do you expect from rehabilitation?					
Do you think there would be conflicts involved in the rehabilitation?					
Management of the Canal					
Are you using pumps to get water from the canal to your field?					
Do you own your pumps yourself?					
How many pumps do you have?					
What other irrigation infratructure is there?					
Who decides on the operation of the gate?					
On which basis is it decided to close or open gates?					
Are there discussions with the farmers or a fixed schedule?					
Who is responsible for the maintenance of the canal?					
Is there a FWUC?					
Do you pay anything for pumping?					
When was this rate decided and by whom?					

E.2 Farmers - Field Work February-March 2020

Questionnaire Farmers | Interview Nr: _____ Date: _____ Prek: _____

Primary aims: finding out details about crop rotation, irrigation schedule (pumping), well pumping, rationale of decision making, fishing and other livelihoods activities and strategies

Name: _____ Gender: _____

Age :_____ Village/Commune: _____

Telephone number: _____

Please tick relevant sources of income:

- ☐ Agricultural income
- ☐ Livestock rearing
- ☐ Fishing
- ☐ Palm juice/sugar production
- ☐ Small Business
- ☐ Non agricultural incomes
- ☐ Agricultural wage labor
- ☐ Remittance from family member

Part A: Agriculture & Economics

Fill out crop table (A3)

How many **pumps** do you own?

- How big are they (HP)
- Do you move them between plots? If yes, how often do you move them?

If they have a **well** that is not (only) used for irrigation:

- What do you use the water of the well for?
- How often/for how long do you pump water from the well?
- How much fuel do you use per hour of pumping?

Do you own **farm equipment** ?

- If so, what do you own ?

☐ Moto-tiller
☐ Pump
☐ Other :
☐ Sprayer
☐ Plough

- If not, do you rent it ? From whom and for how much ?

Fishing

Do you fish ?

Is the fishing **for your own use or to sell the catch**?

Fishing	Notes/Details	N	D	J	F	M	A	M	J	J	A	S	O
		I II III	I II III	I II III	I II III	I II III	I II III	I II III	I II III	I II III	I II III	I II III	I II III
Boeung													
Canal													
Prek													
Fishing implements													
Average catch (kg per fishing time)													
Fishing times per week?													

When are the **peak fishing periods**?

- Are these periods linked to any weather/climate conditions?
- Is fish catch affected by the tide?
- Is fish catch affected by the moon phases?

Livestock

- Do you have **livestock** ? If so, how many heads ? For what production (milk, meat) ?

- How do you feed your cattle (rice straw/natural vegetation/fodder) ?

- If fodder is purchased, what is the cost of a bag ? How many bags do you buy in a year/season ?

- Do you use the manure ? What for (fertilizing, selling) ?

Do you breed/fatten **pigs**?

- How many?
- How do you feed them?

Do you keep **ducks**? Or do you let duck-farmers graze their animals on your plots?

- How many ducks graze on your plots?
- What is the benefit for you?

Economics

- Do you contract a **loan** in the course of your **farming** activity? If so, what for, and under what conditions (bank, usurer, interest rate) ?

- Do you have **any other long term or short term loan** ? If so, what for, and under what conditions (interest rate) ?

- Could you give precise income for each activity (USD or ₹).

Activities	Livestock	Fishing	Small business	Salary from workplace	Pension fund	Agricultural wage labor
Incomes						
Activities	Motor taxi	Construction worker	Garment worker	Remittance from relatives	Other (specify)	
Incomes						

- What is the share of your farm income in your total income ? (check if it seems logical)

Decision Making

Can you explain, what do you generally take into account to take the **decision to irrigate**? (neighbours, regular schedule, soil moisture, precipitation, water level in Bassac / Prek?)

Can you explain, what do you take into account to take the **decision to plant your crops**? (neighbours, regular schedule, soil moisture, precipitation, water level in Bassac / Prek?)

Crop	Decision to plant	Decision to irrigate

Part B - Agricultural risk and adaptation capacity

Agricultural risk

- Over the last three years, have you **lost crops due to floods** ? Where and when ? Can you quantify the loss (% area, %yield, revenue loss) ?

Year	Crop	Where in your plots?	Loss (Y/N)	Area %	Yield %	Revenue (%)	Date of arrival of the flood	Water level (cm) in field

- Over the last three years, have you **lost crops due to droughts** ? Where and when ? Can you quantify the loss (% area, %yield, revenue loss) ?

Year	Crop	Where in your plots?	Loss (Y/N)	Area %	Yield %	Revenue (%)	Date of loss

Agricultural risk

- Have you lost crops due to **pests**?

If yes, can you estimate how much **[%] you have lost** because of pests?

Which pests affect your plots?

How can they be **controlled**?

Does the **flood also help to control pests** (rats) ?

How long does the flood have to last to get rid of rats? How high does the water have to be?

Does the **speed of the water level increase** has an impact (e.g. rats are killed more efficiently if the water rises fast).

Adaptation Capacity

Do you have **strategies to avoid crop losses due to flooding** (land and water management, sowing dates, crop location, resistant varieties…) ?

Do you have **strategies to avoid crop losses due to drought** (irrigation system, sowing dates, crop location, resistant varieties…) ?

Do you think the **Prek rehabilitation provides an opportunity to decrease the risk of floods** ? How does it protect ?

Do you think the **Prek rehabilitation provides an opportunity to decrease the risk of droughts** ? How does it protect ?

Have you **changed varieties or crops during the past 5 years**? Why (market, water availability, reduce D/F risks, ease of cultivation, rehabilitation) ?

Do you plan **changes in varieties or crops in the coming years** ? Why (market, water availability, reduce D/F risks, ease of cultivation, rehabilitation) ?

Do you plan **new agricultural investments** (pump, tiller, land, fruit trees…) ? If not, why ?

Have you been **impacted by the short duration of the flood last season?** How ? What have you done to deal with the situation ?

Have you been **impacted by the delay of the flood last season**? How ? What have you done to deal with the situation ?

Part C: General Operation and Uses of the Prek

Has the Prek next to your plots been **rehabilitated**?

Is there a **gate** at this Prek?

- What is the purpose of the gate?
    - Is it useful to slow down/avoid floods or to keep water in the Prek?
    - If not: why not?
- Are you involved in deciding when the gate is being opened/closed?

Is there a **Prek User Community** at this Prek?

- What are the main tasks of the PUC?
- Are you involved in the PUC?
- Does the PUC coordinate who gets to pump water at which times?

Before rehabilitation, was someone **operating a pump to supply the Prek** with water?

- Who was it?
- What happened to his pumping business?

Is there (still) any **time** of the year **when water needs to be pumped into the Prek**?

- If yes: From where is it pumped: the Bassac or the canals in the floodplain?
- Who is responsible for it?
    - Name
    - Phone number

Who builds **earthen dams** across the Prek?

- What are they for?
- Does someone coordinate the building?
- What happens to the farmers who don't get water because it is kept in one part of the Prek by the dams?

Do you use the Preks for **transport**?

Do you have a **boat**?

What do you use it **for**?

- Do you use it for your own purpose?
- Do you use it to transport and sell goods for other farmers?

During which months do you use it?

Where do you use it? (Prek/Boeung?)

Do you use the **natural vegetation** that grows along the Prek?

If yes, **what** do you use it **for**?

- ☐ Fuel
- ☐ Construction material
- ☐ Food
- ☐ Fish traps
- ☐ Animal feeding
- ☐ Other :

Where do you find the vegetation that you use in that way?

E.3 Village Chiefs - Field Work February-March 2020

Questionnaire Village Chiefs

Principal aims: finding out if they are involved in irrigation management or the operation of the gate.

Name: _____

Age: _____

Village/Commune: _____

Telephone number: _____

Profession(s): _____

General situation:

How long have you been the chief of the village?

What are your **main tasks**?

Who was **chief before you**? (contact details?)

Do you **communicate** regularly with the PUC chiefs/commune chief or representatives from the water ministry?

- Are these representatives from Koh Thom? Or from Takhmao?
- What do you discuss with them?

Is there a ***PUC*** in the village?

Are **you involved** in the PUC?

What do you think are the **main responsibilities of the PUC** (e.g. road maintenance, operation of the gate, collecting money from farmers who pump)

Does the **PUC influence who gets to pump water** from the Prek, or is every one free to pump when they want?

- If yes, what are the rules?
- How have these rules been designed (by you, the PUC committee, the ministry, the commune)?
- Are some people not respecting the rules?

Are some farmers or the PUC building **earth dams** across the Prek?

- What are they for?
- Who put them up?
- Is this allowed?
- From when to when are these dams installed?

Roles and purpose of the gate

Is there a **gate** at this Prek?

What is the **use/purpose** of the gate?

- Is it useful to slow down/avoid floods?
- Is it useful to o keep water in the Prek? If not: why not?

Do you think the **water availability in the Prek** is better now than it was before rehabilitation?

- Why yes/no?

Who decides when to **open** the gate?

Who decides when to **close** the gate?

Are **you consulted** before these decisions are taken?

On what is the **decision to open** the gate based?

- On the basis of the water level observed? (If yes, on which? In the Bassac, On Prek Ambel, in the Boeung?)
- Is the difference in water levels between one side of the Prek and the other taken into consideration?
- Does the decision depend on the status of farming in the area?

On what is the **decision to close** the gate based?

- On the basis of the water level observed? (If yes, on which? In the Bassac, On Prek Ambel, in the Boeung?)
- Is the difference in water levels between one side of the Prek and the other taken into consideration?
- Does the decision depend on the status of farming in the area?

Technical operation of the gate

Once the decision to operate the gate is taken, **who actually operates the gate?**

Where is the **equipment** to operate the gate kept?

Is the **gate opened / closed in full**?

- If not: To what height is it opened/closed? (1/3, 1/2)?
- Why?

When was the gate opened / closed in:

	2017	2018	2019	2020
Open				
Close				

Do you open only and close **only one time or several times** during the year?

- If several times: when and for what purpose?

Does the **tide** influence the way the gate is open/closed?

Pumping of water into the Prek

Is there a **pumping station** at the Prek in your village?

Before rehabilitation, was someone **operating a pump to supply the Prek** with water?

- Who was it?
- What happened to his pumping business?

Is there (still) any **time** of the year **when water needs to be pumped into the Prek**?

- If yes: From where is it pumped: the Bassac or the canals in the floodplain?

Who is responsible for it? (name, phone number)?

Sediment Management:

Is the Prek **excavated** regularly? (Every year? Every two years? Less often?)

Why is the Prek excavated? To improve the water flow?

When does this happen (which months)?

Who is excavates it?

What happens to the excavated soil?

- Is it sold outside the village?
- If yes, to whom?
- For how much?

How much soil is excavated each time?

- How many truck loads?
- How many cubic meter per load?

What is the **price of a cubic meter of soil**?

Is there anything else that you think is important that you would like to mention?

E.4 Heads of Prek Water User Committees - Field Work February and March 2020

Questionnaire: Heads of Prek User Communities

Principal Aims: Finding out decisions about irrigation / whether there is coordination among farmers / if the PUC is involved in the operation of the gate

Name: _____

Age :_____

Village/Commune: _____

Telephone number: _____

Profession(s): _____

Characterizing the PUC

When was the Prek **rehabilitated**?

When was the PUC **created**?

How many **members** does the PUC have?

Are there regular meetings of the **whole PUC**?

- How many people attend?
- What do you discuss?

Is there a **PUC Committee**?

- How many members?
- Can you list the position and responsibilities of other PUC committee members?
- Does the committee meet regularly?
    - How often?
    - What do you discuss?

How long have you been the **president of the PUC**?

- Was someone else in charge before? Who (ccontact details)?
- Do you hold any other position in the village (soldier, village guard, village chief…)?
- Before being the PUC president, were you the Me Prek?
    - What are the differences between a Me Prek and a PUC president?
- As president or member of the PUC committee have you ever met other PUC presidents/ committee members?
    - When?
    - To do what?
- What are your main tasks as president of the PUC?

What are the main **challenges** of coordinating / managing the PUC?

Do you communicate with the **village chief/commune chief**?

- Do you meet them or communicate by phone?
- What do you discuss with them?

Do you communicate with **representatives from the water ministry**?

- Do you meet them or communicate by phone?
- The people you communicate with, are they from the district (Koh Thom) or the provincial (Takmao) office of the ministry
- What do you discuss with them?

What is the role of the PUC?

- What do you think are the **main responsibilities of the PUC** (e.g. road maintenance, operation of the gate, collecting money from farmers who pump)

- Does the **PUC influence who gets to pump water** from the Prek or is every one free to pump when they want?
    - If yes, what are the rules?
    - How have these rules been designed (by you, the PUC committee, the ministry, the commune)?
    - Are some people not respecting the rules?

- Are some farmers or the PUC building **earthen dams** across the Prek? What are they for? Who put them up? Is this allowed? Who initiated the building? Is the water ministry involved? From when to when are they installed?

Roles and purpose of the gate

Is there a **gate** at this Prek?

What is the **use/purpose** of the gate?

- Is it useful to slow down/avoid floods?
- Is it useful to o keep water in the Prek? If not: why not?

Do you think the **water availability in the Prek** is better now than it was before rehabilitation?

- Why yes/no?

Who decides when to **open** the gate?

Who decides when to **close** the gate?

Are **you consulted** before these decisions are taken?

On what is the **decision to open** the gate based?

- On the basis of the water level observed? (If yes, on which? In the Bassac, On Prek Ambel, in the Boeung?)
- Is the difference in water levels between one side of the gate and the other taken into consideration?
- Does the decision depend on the status of farming in the area?

On what is the **decision to close** the gate based?

- On the basis of the water level observed? (If yes, on which? In the Bassac, On Prek Ambel, in the Boeung?)
- Is the difference in water levels between one side of the gate and the other taken into consideration?
- Does the decision depend on the status of farming in the area?

Technical operation of the gate

Once the decision to operate the gate is taken, **who actually operates the gate?**

Where is the **equipment** to operate the gate kept?

Is the **gate opened / closed in full**?

- If not: To what height is it opened/closed? (1/3, 1/2)?
- Why?

When was the gate opened / closed in:

	2017	2018	2019	2020
Open				
Close				

Do you open only and close **only one time or several times** during the year?

- If several times: when and for what purpose?

Does the **tide** influence the way the gate is open/closed?

Pumping of water into the Prek

Before rehabilitation, was someone **operating a pump to supply the Prek** with water?

- Who was it?
- What happened to his pumping business?

Is there (still) any **time** of the year **when water needs to be pumped into the Prek**?

- If yes: From where is it pumped: the Bassac or the canals in the floodplain?

Who is responsible for it? (name, phone number)

*Does the PUC manage a **fishing system** along the Prek?*

If yes, **how does the system work**?

When was it installed?

Who is involved in it?

Does the PUC monitor **fish catch**? If yes, what is the average catch per season?

Does the PUC use the **fishing rights** themselves or auction them off?

Sediment Management:

Is the Prek **excavated** regularly? (Every year? Every two years? Less often?)

Why is the Prek excavated? To improve the water flow?

When does this happen (which months)?

Who is excavates it?

What happens to the excavated soil?

- Is it sold outside the village?
- If yes, to whom?
- For how much?

How much soil is excavated each time?

- How many truck loads?
- How many cubic meter per load?

What is the **price of a cubic meter of soil**?

Is there anything else that you think is important that you would like to mention?

E.5 Shortened Farmer Questionnaire - Field Work November 2020 and Spring 2021

Questionnaire Farmers | Interview Nr: _____ Date: _____ Prek: _____

Primary aims: finding out details about crop rotation, irrigation schedule (pumping), well pumping, rationale of decision making, fishing and other livelihoods activities and strategies

Name: _____ Gender: _____

Age :_____ Village/Commune: _____

Telephone number: _____

Please tick relevant sources of household income			
	Agricultural income		Small Business
	Livestock rearing		Non agricultural incomes
	Fishing		Agricultural wage labor
	Palm juice/sugar production		Remittance from family member

How many **working persons** are there in your household?

Nr: _____

What are their **non-agricultural** incomes? How high are they?

Person #1		Person #2		Person #3	
Activity	Income	Activity	Income	Activity	Income

Part A: Agriculture & Economics

How many plots do you own?

Plot Nr.	Area (ha)	Location	Number of Crops

Plot Nr.	Crop	Cultivation Period	Irrig. freq. (d)	Irrig. dur (h)	Yield (t)	Revenue	Cost seeds	Cost fertilizer	Cost Pesticide	Cost land prep.	Cost pumping	Cost hired help

Plot Nr.	Crop	Cultivation Period	Irrig. freq. (d)	Irrig. dur (h)	Yield (t)	Revenue	Cost seeds	Cost fertilizer	Cost Pesticide	Cost land prep.	Cost pumping	Cost hired help

How many **pumps** do you own?

- How big are they (HP)
- Do you move them between plots? If yes, how often do you move them?

If they have a **well** that is not (only) used for irrigation:

- What do you use the water of the well for?
- How often/for how long do you pump water from the well?
- How much fuel do you use per hour of pumping?

Fishing

Do you fish ?

If yes:

- Where do you fish? (Boeung / canal / Bassac?)
- How often do you fish (every day / once a week …)?
- How big is your average catch? (kg)

Is the fishing **for your own use or to sell the catch**?

When are the **peak fishing periods**?

- Are these periods linked to any weather/climate conditions?
- Is fish catch affected by the tide?
- Is fish catch affected by the moon phases?

Livestock

- Do you have **livestock** ? If so, how many heads ? For what production (milk, meat) ?

- How do you feed your cattle (rice straw/natural vegetation/fodder) ?

- If fodder is purchased, what is the cost of a bag ? How many bags do you buy in a year/season ?

- Do you use the manure ? What for (fertilizing, selling) ?

Do you breed/fatten **pigs**?

- How many?
- How do you feed them?

Do you keep **ducks**? Or do you let duck-farmers graze their animals on your plots?

- How many ducks graze on your plots?
- What is the benefit for you?

Part B - Agricultural risk and adaptation capacity

Agricultural risk

- Over the last three years, have you **lost crops due to floods** ? Where and when ? Can you quantify the loss (% area, %yield, revenue loss) ?

Year	Crop	Where in your plots?	Loss (Y/N)	Area %	Yield %	Revenue (%)	Date of arrival of the flood	Water level (cm) in field

- Over the last three years, have you **lost crops due to droughts** ? Where and when ? Can you quantify the loss (% area, %yield, revenue loss) ?Agricultural r

Year	Crop	Where in your plots?	Loss (Y/N)	Area %	Yield %	Revenue (%)	Date of loss

Have you lost crops due to **pests**? If yes, which ones?

If yes, can you estimate how much **[%] you have lost** because of pests?

How can they be **controlled**?

Does the **flood also help to control pests** (rats) ?

How long does the fl ood have to last to get rid of rats? How high does the water have to be?

Does the **speed of the water level increase** has an impact (e.g. rats are killed more efficiently if the water rises fast).

Adaptation Capacity

Do you have **strategies to avoid crop losses due to flooding** (land and water management, sowing dates, crop location, resistant varieties…) ?

Do you have **strategies to avoid crop losses due to drought** (irrigation system, sowing dates, crop location, resistant varieties…) ?

Do you think the **Prek rehabilitation provides an opportunity to decrease the risk of floods** ? How does it protect ?

Do you think the **Prek rehabilitation provides an opportunity to decrease the risk of droughts** ? How does it protect ?

Have you **changed varieties or crops during the past 5 years**? Why (market, water availability, reduce D/F risks, ease of cultivation, rehabilitation) ?

Do you plan **changes in varieties or crops in the coming years** ? Why (market, water availability, reduce D/F risks, ease of cultivation, rehabilitation) ?

Have you been **impacted by the low water levels in the Bassac this year?** How ? What have you done to deal with the situation ? What do you think the effects for your plots will be?

Part C: General Operation and Uses of the Prek

Has the Prek next to your plots been **rehabilitated or excavated**? If yes, when?

Is there a **Prek User Community** at this Prek?

- What are the main tasks of the PUC?
- Are you involved in the PUC?
- Does the PUC coordinate who gets to pump water at which times?

Before rehabilitation, was someone **operating a pump to supply the Prek** with water?

- Who was it?
- What happened to his pumping business?

Is there (still) any **time** of the year **when water needs to be pumped into the Prek**?

- If yes: From where is it pumped: the Bassac or the canals in the floodplain?
- Who is responsible for it? (name and phone nr if possible)

Do you use the Preks for **transport**?
Do you have a **boat**?

What do you use it **for**? (private / commercial purposes)

During which months do you use it? How often per week? (every day? once a week?)

Where do you use it? (Prek/Boeung?)

Do you use the **natural vegetation** that grows along the Prek?

If yes, **what** do you use it **for**? (food, fuel, feeding animals?)

Where do you find the vegetation that you use in that way?

F

Runge Kutta Solution

The fourth-order Runge-Kutta solution is calculated as follows.

$$For: \frac{dy(t)}{dt} = y'(t) = f(y(t),t),\ with\ y(t_0) = y_0 \tag{F.1}$$

$$k_1 = f(y^*(t_0),t_0) \tag{F.2}$$

$$k_2 = f(y^*(t_0) + k_1\frac{h}{2}, t_0 + \frac{h}{2}) \tag{F.3}$$

$$k_3 = f(y^*(t_0) + k_2\frac{h}{2}, t_0 + \frac{h}{2}) \tag{F.4}$$

$$k_4 = f(y^*(t_0) + k_3 h, t_0 + h) \tag{F.5}$$

$$y^*(t_0 + h) = y^*(t_0) + \frac{k_1 + 2k_2 + 3k_3 + k_4}{6} h \tag{F.6}$$

This method uses an initial condition $y(t_0) = y_0$ as well as intermediary slope estimates k_1, k_2, k_3, and k_4 as well as their eventual weighted sum to estimate the slope at time step $t_0 + h$. Here, k_1 is the slope at the beginning of the time step, k_2 and k_3 are estimates of the slope at mid-point, used to cover the first and second half of the time step respectively, and k_4 is the estimate of the slope at the endpoint (Carpenter et al., 2005).

G

Revision of Paper Published in the European Journal of Remote Sensing

Input imagery, classifiers, and cloud computing: Insights from multi-temporal LULC mapping in the Cambodian Mekong delta

Christina Orieschnig

Gilles Belaud

Jean-Philippe Venot

Sylvain Massuel

Andrew Ogilvie

G-Eau, IRD, AgroParisTech, Institut Agro, Cirad, INRAE, Univ. Montpellier, 361 rue J.F. Breton, BP 5095, 34196, Montpellier Cedex 5, France.

Corresponding author: Christina Orieschnig, christina.orieschnig@ird.fr / christina.orieschnig@agroparistech.fr, +33 7 51 35 75 08, https://orcid.org/0000-0001-5182-7110

Body word count: 7522

Input imagery, classifiers, and cloud computing: Insights from multi-temporal LULC mapping in the Cambodian Mekong delta

Abstract

The increased availability of open-access Synthetic Aperture Radar and optical earth observation data has engendered numerous land use and land cover (LULC) analyses combining these types of imagery. In parallel, the computational capabilities of cloud platforms have enabled a wider community to perform LULC classifications over long periods and large areas. However, an explicit assessment of how the performance of classifiers available on these cloud platforms responds to and can be optimized for the use of multi-imagery data, has been lacking for multi-temporal LULC approaches. This study carries out such an assessment for the supervised classifiers natively available in the open-access cloud computing platform Google Earth Engine: Naïve Bayes (NB), Classification and Regression Trees (CART), Random Forest (RF), Gradient Tree Boosting (GTB), and Support Vector Machines (SVM). A multi-temporal LULC analysis using Sentinel-1 and 2 is implemented for a study area in the Cambodian Mekong delta. Classifier performance is compared for different combinations of input imagery, band sets, and training datasets. The results show that GTB and RF yield the highest overall accuracy, at 94% and 93% respectively. Combining optical and SAR imagery boosts classification accuracy for CART, RF, GTB, and SVM by 10-15 percentage points. Furthermore, it also reduces the impact of limited training dataset quality for RF, GTB, and SVM.

Keywords: CART, Google Earth Engine; Gradient Tree Boosting, LULC; Random Forest; Sentinel-1 and -2; SVM

Introduction

Over the past years, there has been continuous progress in the availability of satellite products environmental studies. Analyses of long time-series have become possible through the now fully available Landsat archives, which span back to 1972 (Saunier et al., 2017). Simultaneously, high-frequency, high-resolution imagery, provided by the Sentinel constellation enable a wider community of researchers to gain

insights into complex, long-term, large-scale states and processes. Consequently, these products find applications in various disciplines, from archaeology (Schreier, 2020) to marine biology (Foo & Asner, 2019). Particularly analyses in the domain of land use and land cover (LULC) have benefited from the increased availability of imagery. These analyses provide crucial insights into interactions between human populations and their environment, from tracing a crop cover history across the United States (Johnson, 2019) and assessing the impacts of dam construction on land use (Li et al., 2017), to mapping rice cropping in the Vietnamese Mekong Delta (Kontgis, Schneider, & Ozdogan, 2015), and evaluating changes in habitat quality and composition in conservationally significant areas (López, López-Sandoval, Gerique, & Salazar, 2020; Yohannes, Soromessa, Argaw, & Dewan, 2021) and ecosystem service provision (Kusi, Khattabi, Mhammdi, & Lahssini, 2020). Especially the Sentinel constellation by the European Space Agency (ESA), with its spatial resolution of up to 10 m, return frequency of upwards of 6 days, and provision of both optical and Synthetic Aperture Radar (SAR) data provides attractive insights into LULC dynamics. Since its launch in 2014 (Potin et al., 2019), Sentinel has been used for LULC analyses relating to smallholder maize in Africa (Jin et al., 2019), monsoon inundations (Dinh, Elmahrad, Leinenkugel, & Newton, 2019) and rice paddy extents (Minh, Avtar, Mohan, Misra, & Kurasaki, 2019) in the Mekong Delta, and wetland mapping in Canada (Mahdianpari et al., 2018).

However, a considerable hindrance to many analyses has been the computational power required to perform them. LULC studies covering long periods of time, large areas, or high resolutions and image frequencies often exceed the computational resources at individual researchers' disposal. In response, cloud-based services and computing platforms have been developed (Carretero & Blas, 2014). Open-access cloud

computing platforms such as Google Earth Engine (GEE) (Gorelick et al., 2017), OpenEO (Gomes, Queiroz, & Ferreira, 2020), or Open Data Cube (Killough, 2018) now enable any user to cope with the massive amounts of available data. Among the different platforms, GEE is the most widely-used to conduct analyses at large scales and for long time series (Kumar & Mutanga, 2018). Early high-profile applications include Hansen et al. (2013) mapping global forest cover change, and Pekel et al., (2016) creating a dataset of global surface water occurrence, change, and seasonality since the 1980s. More recently, studies have used GEE to map irrigation on the US High Plains over three decades (Deines et al., 2019), to track global annual impervious areas since 1985 (Gong et al., 2020), and to follow wildfire progression in British Columbia (Crowley, Cardille, White, & Wulder, 2019).

However, while the progress with regard to the availability of images and sufficient computational capacity for analyses has yielded fascinating insights, the choice of algorithm for land use classification purposes carries an often-neglected weight. As Thanh Noi & Kappas (2017) point out, the overall accuracy of a LULC analysis depends 'not just on the quantity and quality of the images, but also on the right choice of classification method.'

The majority of LULC analyses use supervised classification methods. Although some researchers have used unsupervised classification (Mohammady, Moradi, Zeinivand, & Temme, 2015; O'Hara, King, Cartwright, & King, 2003), supervised classification is often preferred due to the possibility of setting a predefined number of labelled output classes. To harness these advantages, a variety of classifiers is available for supervised classification. Among the most frequently used are machine learning algorithms such as Support Vector Machines (SVM), Random Forest (RF), Gradient

Tree Boosting (GTB), Maximum Likelihood Classifiers (Orimoloye, Mazinyo, Nel, & Kalumba, 2018; Orimoloye & Ololade, 2020), and K Nearest Neighbour (KNN) (Talukdar et al., 2020). Furthermore, advanced machine learning approaches such as artificial neural networks (ANN), convolutional neural networks (CNN), and deep neural networks (DNN) have seen more widespread use in recent years (Jozdani, Johnson, & Chen, 2019).

A number of papers compared these classifiers in LULC applications. Talukdar et al. (2020) compare RF and SVM, along with more advanced machine learning methods in a study area along the Ganga river in India. The authors conclude that the RF algorithm overall performs best. In contrast, Nery et al. (2016) find that SVM reaches the highest classification accuracies for LULC analyses after comparing it with KNN, RF, Learning Vector Quantization (LVQ), Recursive Partitioning Regression Trees (RPART), and Stochastic Gradient Boosting Methods (GBM) in a study area in Western Australia. The same conclusion was reached by Thanh Noi & Kappas (2017), who compared RF, KNN, and SVM classifications of Sentinel-2 imagery in the Red River Delta in Vietnam. Shelestov et al. (2017) weighed the merits of some of the classifiers available in GEE against external methods, including an ensemble neural networks, for crop classification using optical Landsat-8 images. They found decision-tree classifiers to perform best in GEE, though neural networks outperformed them.

Most of these comparison papers focus on contrasting the performance of classifiers applied to a single date rather than in a multi-temporal situation. In addition, hardly any compare classifiers in the context of cloud computing platforms, many of which only offer a limited number of native implementations. In addition, with a few notable exceptions (Hütt, Koppe, Miao, & Bareth, 2016), many papers only approach

the classifier comparison on the basis of a single imagery type, with a fixed set of bands, and a single source of training data.

In view of the proliferation of studies addressing research questions through multi-temporal analyses using cloud computing platforms, this paper aims to systematically address these knowledge gaps. It presents an assessment of the response of four supervised classifiers available in the online Javascript API of the GEE cloud computing platform, to the use of different combinations of input imagery, training data, and band sets for the purpose of land use and land cover analyses. These classifiers are Naive Bayes (NB), Classification and Regression Trees (CART), Random Forest (RF), Gradient Tree Boosting (GTB), and Support Vector Machines (SVM). While it is possible to implement further supervised classification methods, such as fully convolutional neural networks (FCNN), or deep neural networks (DNN) in GEE, this requires the external training of the models on the TensorFlow platform (Abadi et al., 2016). Since this approach involves several billable components of Google Cloud, it is not included in this paper, which focuses on entirely open-access solutions.

The comparisons are made using Sentinel-1 SAR and Sentinel-2 optical imagery, both separately and in combination. In addition, the impact on classifier performance of the type of the training set, as well as the choice of bands, texture features, and spectral indices is tested. For this purpose, two different sets of training points (one based on field data, one derived from high-resolution satellite imagery) and three different sets of training bands (varying in the number of additional indexes and texture features used for classification) are used.

Study Area

For the purposes of this study, a study area on the floodplains of the Mekong delta in Cambodia was chosen. The region is well known for intra- and inter-annual land use changes (Liu et al., 2020; Ngo, Lechner, & Vu, 2020), making it adapted to test the multi-temporal capacity of classifiers. The area is subject to annual monsoon inundations, which typically last from July until November. For the rest of the year, the floodplain is intensively cultivated, in one to three cropping cycles.

Specifically, an area of 44 km^2 on the right bank of the Bassac river, one of the Mekong's deltaic distributaries, was chosen (see Figure 1). Located about 70 km south of the Cambodian capital Phnom Penh, this area exhibits rapid changes in land use following flood rise and recession, and strong annual variability in cropping calendars and cultivated areas. In the north, it is dominated by fruit trees, especially mango trees, while the south is a patchwork of fields where rice and vegetables like tomatoes, cucumbers, and aubergines are grown. During the dry season, these crops are either irrigated with water pumped from canals, or rely on sparse amounts of rainfall. The rainfall distribution in the area is bimodal, with peaks in the early and late wet season.

Overall, six broad land use classes are defined: open water surfaces, bare/fallow land, urban/village areas, fruit trees, rice fields, and vegetable fields. Out of these, urban areas – located along the main road that runs in parallel with the river – and fruit trees are relatively static over the course of a year (neglecting urban spread and the planting or cutting down of trees). The other classes are highly dynamic. During the wet season, large swaths of low-lying land in the west and southwest of the area are inundated. Subsequently, these areas see one or two cycles of rice cultivation, before lying fallow for part of the year. The higher terrain in the east of the study area sees a complex

mosaic of fields lying fallow and being cultivated. Figure 2 shows an RGB overview of the LULC dynamics in the study area during the dry season.

[Figure 1 about here: Location of the study area on the floodplains of the Cambodian Mekong delta.]

[Figure 2 about here: Landcover dynamics in the study area during the dry season, RGB image.]

Data Used

The data used in this study stems from three sources: the Sentinel satellite constellation maintained by the European Space Agency (ESA), high-resolution SPOT-6 and 7 imagery, and fieldwork in Cambodia. For classifier training, images from three time points in November 2019, February 2020, and April 2020 were used. At all time points, both Sentinel-1 and 2 data are available on either the same or adjacent dates. These dates fall at the beginning, middle, and end of the dry season and account for the main changes in cultivation practices and LULC dynamics (cf. Figure 2). The SPOT-6 and 7 images and the fieldwork data are used for parameter tuning, calibration, and validation. Details on the satellite images used are given in Table 1.

[Table 1 about here: Overview of images used for training the classifiers. (* resampled to 10 m across all bands during pre-processing.)]

[Figure 3 about here: Temporal distribution of training images and image time series used in this analysis, throughout the wet and dry season in the study area.]

Sentinel-1

The ESA's Sentinel-1 constellation consists of two satellites, Sentinel-1A and Sentinel-1B, which were launched in 2014 and 2016 respectively. Both satellites have a

return period of 12 days, resulting in a combined Sentinel-1 overpass frequency of 6 days. They collect C-band synthetic aperture radar imagery in a variety of polarizations, instrument modes, and resolutions. For this study, interferometric wide swath (IW) images in the form of co-polarized VV and cross-polarized VH bands at 10 m resolution are used, as the most widely-spread type of imagery for LULC approaches using SAR (Khan, Govil, Kumar, & Dave, 2020; Ranjan & Parida, 2019; Tavares, Beltrão, Guimarães, & Teodoro, 2019).

In total, six Sentinel-1A and B images taken in descending orbits are used to train and validate the classifiers for three different dates. The study area is located at an intersection area of two Sentinel-1 tiles. To reduce random speckle noise, mean composites of Sentinel-1 images taken on subsequent days were created for each training time point (cf. Table 1). To test the trained classifier and create a LULC time series, 117 SAR images between 01/11/2019 and 31/10/2020 are used. As can be seen in Figure 3, these images are distributed regularly throughout the year.

Sentinel-2

Like Sentinel-1, the ESA's Sentinel-2 collection consists of a pair of satellites. Sentinel-2A was launched in 2015, followed by Sentinel-2B in 2017. Both satellites have a return period of 10 days, resulting in a combined Sentinel-2 image frequency of 5 days. The constellation provides multi-spectral optical imagery for a total of 12 spectral bands ranging from the blue to the short wave infrared spectrum.

Like for Sentinel-1, overlapping Sentinel-2 tiles are available in the study area. To train the classifiers, three composites of six cloud-free optical images are used (cf. Table 1). For the land use time series classification, 47 images between 01/11/2019 and

31/10/2020 are used. However, it must be noted that these images are not distributed regularly across the year. As shown in Figure 3, multiple images are available for every month during the dry season. During the wet season, when cloud cover is high, this is not the case.

3.3. *Data for Calibration and Validation*

This study uses SPOT-6 and 7 images to generate training points for the classification algorithms. SPOT (Satellite Pour l'Observation de la Terre) is a high-resolution satellite operated commercially by Spot Image. It provides panchromatic and multi-spectral images at 1.5-6 m resolution. Complemented by knowledge of the general LULC distribution patterns in the study area, points are set manually where land use classes are discernible with reasonable certainty on the high-resolution images. Overall, 9,000 training points are set – 1500 per training class (cf. Table 2). While this procedure yields an extensive set of training data, it also introduces some class noise. This describes training points that carry erroneous labels, which can impact the quality of the classification. However, it is still salient to harness a dataset generated in this way for comparative purposes, as noise is a common problem in supervised remote sensing approaches (Frenay & Verleysen, 2014; Pelletier et al., 2017).

A final component of the data setup of this paper is ground-truth training data collected at the study site in autumn 2019 and spring 2020. In total, 1,712 training points were collected. The majority were set on site using a manual GPS device (horizontal accuracy: 10 m). In addition, some were set manually using geo-referenced in-situ images from an unmanned aerial vehicle (UAV). However, unlike for the training

data derived from SPOT-6 and 7 images, the training points from the field surveys are not distributed equally between classes. For example, while the November fieldwork training set includes 630 points, its April equivalent only contains 491 (cf. Table 2). While this training sample is smaller and its points are unevenly distributed between classes and dates, the confidence of its label attribution is considerably higher.

[Table 2 about here: Distribution of training data points across the multi-temporal images.]

Methodology

A general outline of the classification workflow is given in Figure 4. Following pre-processing, 9 datasets are generated on which the classifiers are tested. These datasets derive from the use of different imagery types alone and in combination, as well as different band sets (see Table 3). Parameter tuning, calibration, and validation is performed for each of the 9 datasets separately, using both the limited training points derived from fieldwork, and the extended training points generated on the basis of the SPOT-6 and 7 images, resulting in 18 different configurations of input data for each of the four classifiers. Finally, the best-performing algorithm is chosen and applied to the optical, radar, and combined dataset to generate a LULC classification spanning the entire period between 01/11/2019 and 31/10/2020.

[Table 3 about here: Overview of image datasets used.]

[Figure 4 about here: Classification workflow.] (updated)

Image Pre-Processing

To a certain degree, both Sentinel-1 and 2 images are already provided in pre-processed

form in GEE.

Sentinel-1 images undergo pre-processing during ingestion in GEE based on the ESA's Sentinel-1 toolbox. In this process, metadata is updated with a restituted orbit file, border noise and thermal noise is removed, and radiometric calibration and orthorectification are applied. The fact that images are provided in pre-processed form in GEE's Javascript API removes one of the main hurdles many researchers face in using SAR data. In fact, several studies have used GEE as a source of SAR images, even though their analyses were subsequently conducted in different environments (Amani et al., 2020; Tamiminia et al., 2020).

As a basis for classification, additional bands are generated for SAR imagery using the original VV and VH bands (cf. Table B2). Three of these are based on arithmetic operations (VV/VH, VV-VH, (VV+VH)/2) which previous studies found to yield increased accuracies for LULC approaches (Slagter, Tsendbazar, Vollrath, & Reiche, 2020). The others are based on a classic Grey Level Co-occurence Matrix (GLCM), encompassing Haralick texture features (Haralick, Shanmugam, & Dinstein, 1973). These features describe image texture through interpretable descriptors and have been found to add valuable information for LULC analyses.(Clerici, Valbuena Calderón, & Posada, 2017; Lin, Zhang, Lin, Gamba, & Liu, 2020; Mishra, Prasad, Rai, Vishwakarma, & Arora, 2019). Texture features are calculated separately for both the VV and VH polarization, parameterized with a 5x5 window size. Following previous studies (Nizalapur & Vyas, 2020), angular second moment (ASM), contrast (CONTRAST), correlation (CORR), inverse difference moment (IDM), entropy (ENT), dissimilarity (DISS), and variance (VAR) are used as added bands for classification. Following the calculation of the texture features, a refined Lee speckle filter (Yommy,

Liu, & Wu, 2015) is applied to smooth the original VV and VH bands in order to reduce speckle, since not all data datasets use the generated texture bands.

Sentinel-2 images are available in pre-processed form in GEE. The sen2cor algorithm (Main-Knorn et al., 2017) has been applied to transform Top of the Atmosphere (TOA) reflectance to surface reflectance (BOA). For this analysis, all bands are automatically resampled to 10 m resolution by the GEE processing algorithm. For the time series calculation, a cloudy pixel threshold of < 20% is introduced, and the remaining clouds are masked using a simple bit-mask based on the QA band.

Additional spectral indices (cf. Table 4) are calculated on the basis of native bands (cf. Table B1) to generate ancillary layers of information that serve as input for the classification algorithms, which past studies have found to be valuable in increasing classification accuracies (Godinho, Guiomar, & Gil, 2016). These are based on a range of bands employed in past studies for various LULC analyses using different classification algorithms (Ouattara et al., 2020).

[Table 4 about here: Spectral indices calculated for optical Sentinel-2 imagery]

Creation of Image Datasets

In total, parameter tuning, calibration, and validation is performed on nine image datasets (cf. Table 3).

First, three main sets of images are created – one containing only SAR imagery, one containing optical imagery, and one in which images are created by stacking all available optical and SAR bands into a single image. Then, each of the three imagery sets is further subdivided into three tiers depending on how many bands are used for classification(see Table 5). One tier includes a band set that encompasses all native

bands, spectral indices, and texture features. A reduced band set includes the native image bands as well as some indices and texture features. Finally, a minimal set consists only of the VV and VH bands for SAR, and the RGB bands for optical imagery.

[Table 5 about here: Band sets of spectral indices and texture features. For the combined imagery set, these bands are stacked.]

Parameter Tuning and Classification

Each dataset is calibrated with 80% and validated with 20% of both the fieldwork and the SPOT-based training data, for each of the four classifiers. Preceding calibration, each classifier undergoes parameter tuning. A short description of each classifier as well as the associated tuning parameters is given below.

Naïve Bayes (NB)

This classifier relies on a simple probabilistic approach that is based on the Bayes theorem (John & Langley, 1995). It is referred to as naïve because it relies on the assumption of conditional independence between every pair of features, and a Gaussian probability distribution (Zhang, 2005). In reality, this condition is frequently not met, particularly in more complex situations and datasets. Nonetheless, several studies have found the simplistic approach to yield satisfying results (Diengdoh et al., 2020; Johnson & Iizuka, 2016) particularly in cases where only a limited number of input features is available. This may be due to the fact that, in general, even a small training set is sufficient to minimize the average risk of the classification error and compute the decision surface. Some studies have also argued that dependence distribution among classes could also account for the surprisingly good performance of NB (Kuncheva,

2006). In GEE's implementation of NB, the only parameter that needs to be tuned for performance is the smoothing factor λ .

Classification and Regression Trees (CART)

CART classifiers belong to the family of decision tree (DT) classifiers. The basic approach of this type of classifier is to find the attribute or threshold that splits a training dataset most effectively into subsets. This split then becomes a node in the tree, with the two subsets forming branches. Each subset is then split into further subsets until only a non-splitable end node (also known as a 'leaf node') remains. The main criterion in performing every split is the normalized information gain (Shalev-Shwartz & Ben-David, 2014). Once grown using the training dataset, the decision tree can then be applied to new samples. A considerable disadvantage of this approach is its high sensitivity to the training dataset. Even globally negligible modifications in the training data can lead to fundamentally different tree structures (Shelestov et al., 2017). To improve classifier performance, the number of leaf nodes in each tree (maxNodes) is tuned.

Random Forest (RF)

Random Forest (RF) is a recursive partitioning technique that is based on the construction of an ensemble of classification and regression trees (hence the term forest). Each tree is trained using the same method as described above for CART. However, to increase computational efficiency, each tree only utilizes a random subset of features at each node – this step also reduces correlation (and accounts for the second element in the nomenclature of the classifier). Trees are bundled together

computationally through bootstrap aggregating ("bagging") (Breiman, 1996). The final classification result for a new sample is then obtained through a majority vote of individual tree results. Overall, this approach is less sensitive to overfitting and noisy data, two of the most considerable pitfalls of CART approaches (Breiman, 2001). For RF tuning, the number of trees (nTree) and the number of variables per split (mTry) have to be optimized. Past studies found that satisfactory, stable results could be produced with a number of trees ranging between 200 and 500 (Belgiu & Dragut, 2016). To find the optimal RF model, this study tested nTree = [50 : 750] with a step size of 50, and mTry = [1:15] with a step size of 1.

Gradient Tree Boosting (GTB)

Like RF, Gradient Tree Boosting (GTB) algorithms utilizes an ensemble of decision trees. However, its basic approach differs in that it limits the complexity of trees, confining each individual tree to a weak prediction model. It achieves classification accuracy by iteratively combining an ensemble of these weak learners into strong ones by minimizing a differentiable loss function at every step, following a gradient descent procedure (Friedman, 2002). To reduce correlation between trees, each new tree is constructed on the basis of a stochastically selected subset of training data. Recent studies have shown GTB algorithms, such as XGboost (Chen & Guestrin, 2016) to outperform classifiers such as SVM, RF, and KNN (Godinho et al., 2016), especially on unbalanced datasets. However, GTB are often prone to overfitting, a risk that can be minimized through parameter tuning. In terms of parameters to be adjusted, the number of trees (nTree) is varied between 50 and 200, with a step size of 10. GTB further requires a parameter to be specified to determine how many nodes a decision tree in the

ensemble can have. Since GTB is based on weak learners, the maxNodes parameter is typically low, with a range of [2:10] with a step size of 1 being tested in this study. In addition, the sampling rate for stochastic gradient tree boosting, and the shrinkage rate, which controls the learning rate of the algorithm, need to be optimized. In this study, a range of [0.45:75] with a step size of 0.5 was tested for the former, and [0.005, 0.01, 0.05, 0.1, 0.25, 0.5] for the latter. Finally, all three loss functions available in GEE for GTB were compared – least squares, least absolute deviation, and Huber.

Support Vector Machines (SVM)

The founding principle of this approach is to find the boundary that maximizes the distance from the nearest data point of all classes (Noble, 2006). These points are used for the construction of support vectors, which, in turn, form the basis for the computation of the maximum-margin hyperplane that serves as a boundary. The dimensionality of this hyperplane is determined by the number of features to be used for classification. For non-linear data, a kernel is applied to transform low-dimensional data to make it separable via the SVM approach in a higher-dimensional sphere (Cortes & Vapnik, 1995). Frequently used kernels include linear, Gaussian Radial Basis Function (RBF), sigmoid, and polynomial kernels (Amari & Wu, 1999). The main advantage of SVM is its high potential for generalization.

In terms of tuning SVMs, the first choice to make is to pick a kernel. For LULC approaches, RBF and Linear kernels are frequently used (Kavzoglu & Colkesen, 2009; Shi & Yang, 2015). Then the cost parameter C needs to be optimized, as well as the γ value in case the RBF kernel is used. The γ value determines the RBF kernel width and thus affects the smoothing of the hyperplane which divides classes. The C parameter

sets the threshold for permitted misclassification of non-separable training data (Thanh Noi & Kappas, 2017). If it is too large, it can lead to over-fitting (Ghosh & Joshi, 2014). This study follows (Li et al., 2014) in using ten C values ($2^{[-2;7]}$) as well as ten γ values ($2^{[-5;4]}$) for parameter tuning.

Validation and Statistical Analysis

Finally, the classification results of each algorithm using each combination of imagery, band set, and training data is validated. For this, the remaining randomly selected 20% of the field work and SPOT-based datasets are used. Overall accuracy as well as producer and consumer accuracies are calculated (Congalton, 1991). To ascertain whether the choice of input imagery, training data, and band set has statistically significant impacts on classifier performance, the non-parametric Kruskal Wallis test (Kruskal & Wallis, 1952) is used.

Results

Optimal Tuning Parameters

The tuning parameters that yielded the highest accuracies for each classifier and each of the nine image subsets, and that are used in the remaining of the analysis, are given in Table 6. The full set of tuning parameters and their associated accuracies are given in the supplementary materials. The results show that the parameter values yielding the highest accuracies varied considerably for RF (nTree and mTry) and for SVM (C and γ). For RF, the nTree used for the final analysis varies between 50 and 600, and nTry ranges from 1 to 14. For SVM, optimal classification accuracy is achieved using C values that vary along the full tuning spectrum. Similarly, the optimal γ value for the

RBF kernel ranges from 2^{-5} to 2^{4} . There are no discernible trends along the lines of imagery type, band sets, or training datasets.

In contrast to this, the optimal values for the tuning parameter λ for NB and CART's maxNodes vary little. In the case of λ, most combinations of imagery, band sets, and training data show little sensitivity to value tuning. Where differences in accuracies depending on λ are observable, the highest accuracies can be reached with λ = $1*10^{-10}$. As for maxNodes, the CART classifier globally reaches its highest accuracies using either 5 or 6 nodes.

As for GTB, parameter tuning revealed low sensitivities for some parameters, and higher discrepancies in accuracies for others. The type of loss function employed, for example, has a virtually untraceable effect on accuracies. The shrinkage function, on the other hand, showed optimal values between 0.01 and 0.25, and the sampling rate between 0.6 and 0.75. For nTree and maxNodes there was a noticeably larger variation for optimal parameter values for the fieldwork training set, than for the extended training set. In the former, values for nTree ranged between 50 and 190 and for maxNodes between 3 and 10. In the latter, the optimal value for nTree lay between 160 and 200, and for maxNodes between 9 and 10.

[Table 6 about here: Tuning parameters for optimal accuracies for each classifier and band set.] (updated)

Overall Accuracy

The maximum overall accuracies achieved by each classifier depending on imagery type, band set, and training data, are given in Table 7. Accuracies over 85%, which previous studies have deemed satisfactory for LULC purposes (Denize et al., 2018;

Khan et al., 2020; Steinhausen, Wagner, Narasimhan, & Waske, 2018) are highlighted in bold.

The results show that GTB globally reached the highest overall accuracy, at 94%. This value is reached using combined imagery, the extended dataset derived from SPOT imagery, and both the full and the reduced band set. RF also yields similarly high values (93%) using the same combination of imagery, training dataset and bands. For the fieldwork dataset, the highest accuracies are also reached by GTB and RF. GTB yields and overall accuracy of 93% for the full and 92% for the reduced band set using combined optical and SAR imagery. For the same input configuration, RF yields accuracies of 92% and 91% respectively. Furthermore, GTB and RF also reach accuracies of over 85% using all other combinations of bands and training sets for the combination of Sentinel-1 and 2 imagery, and for the use of the extended training set and the full and reduced band sets for optical-only imagery.

Third in terms of overall accuracy is SVM, using a linear kernel and combined optical and SAR imagery. Accuracies of up to 92% are achieved using the extended training dataset and the reduced band set. Like RF, SVM also yields high accuracies when trained using the fieldwork dataset and the reduced band set. It furthermore attains accuracies of 88% and 86% respectively for the use of the full band set and both training data sets. For the variation of SVM using an RBF kernel, the overall classification accuracy does not surpass 63%.

The CART classifier reaches overall accuracies of up to 88%, when trained using combined imagery, the fieldwork dataset and either the full or reduced band sets. Far below this mark is the Naive Bayes classifier. Its highest overall accuracies, at 72%, is reached using the combined optical and SAR imagery.

[Table 7 about here: Comparison of overall accuracies (OA) by classifier, imagery type, training set, and band set. OA values of over 85 are marked in bold.] (updated)

SAR- and Optical-Only vs. Combined Imagery

Overall, the results show a marked increase in accuracy for the majority of classifiers when combined imagery is used, as opposed to SAR and optical-only imagery. For RF, optical-only imagery led to an average accuracy of 78% across training and band sets, for GTB to 76%. For SAR-only imagery, this average lay at only 67% and 63% respectively. The combination of both imagery types, however, yielded an average accuracy of 90% for RF, and of 91 for GTB. Similarly, the CART, SVM, and NB classifiers also yielded their best accuracies using the combined imagery.

As illustrated in Figure 5, the combined imagery yielded considerably higher accuracies for NB, CART, RF, GTB, and SVM using a linear kernel than optical or SAR images alone. For CART, RF, and GTB the improvement in accuracy when using combined imagery in comparison to optical-only imagery is statistically significant ($p < 0.05$). In addition, the CART classifier using optical imagery shows considerable variability with respect to accuracies. The improvement in comparison to using SAR-imagery only is statistically significant for NB, CART, RF, and SVM using a linear kernel. However, for SVM using an RBF kernel, the reverse is true – the combined imagery yields considerably lower accuracy values than either optical- or SAR-only imagery.

[Figure 5 about here: Box plot of overall accuracies by imagery used and classifier, and significance of variation of accuracies depending on imagery type used.]

Choice of Training Data and Band Sets

In general, the extended training data yielded the highest overall accuracies for GTB, RF and SVM using both a linear and RBF kernel. For CART and NB, however, the training set based on fieldwork data led to higher accuracies. GTB, RF and SVM using a linear kernel also yielded accuracies of over 85% using the fieldwork dataset (cf. Table 7 and supplementary materials). It can be noted that the use of the extended data set leads to a higher accuracy improvement in optical and SAR-only imagery than in the combined imagery. For example, for RF applied to optical imagery, the average overall accuracy achieved using the fieldwork dataset lies at 74%, whereas the extended dataset yields an average overall accuracy of 82%. In contrast, for combined imagery the average RF using fieldwork training data lies at 89%. Using the extended dataset only increases this average overall accuracy to 90%.

As for the band set, it emerges that the extended and fieldwork dataset produce comparable accuracies for CART, RF, and GTB. SVM using a linear kernel, however, produces distinctly higher accuracies on the basis of the reduced band set. Furthermore, SVM using the RBF kernel produces its highest overall accuracies when the minimal band set is used.

Accuracy by Class

The accuracy with which each land cover class is classified by each algorithm varies considerably. Consequently, this impacts the overall classification accuracy at different points in the time series of images between 01/11/2019 and 31/10/2020, when the classes have a different predominance.

Water, for example, has a relatively high consumer and producer accuracy (cf. Table 8). While NB tends to errors of omission, mis-classifying water as urban areas, the other classifiers succeed in delineating surface water regions with fairly high confidence. RF and GTB in particular delineate water well, with producer accuracies of 98% and 97%, and consumer accuracies of 97% and 98% respectively, followed by SVM (97% and 96% respectively). Consequently, inundated areas, as they can be observed in November, are represented well.

In contrast, the classifiers exhibit greater difficulties in separating bare/fallow land from urban areas, and vegetable fields from rice paddies. While CART, RF, GTB, and SVM succeed well in classifying the permanent urban areas in the East of the study area, they also tend to misclassify fields lying fallow during the dry season as urban areas. The discrepancy between the size of the areas classified as fallow across the year depending on which classifier is used is also shown in Figure 7. In terms of consumer accuracy, SVM using a linear kernel can boast the best performance in delineating urban and fallow land. In contrast, RF and GTB exhibit a better performance in separating rice paddies and vegetable plots, both in terms of producer and consumer accuracies.

[Table 8 about here: Producer and Consumer accuracies for NB, CART, RF, GTB and SVM using a linear kernel. SVM (RBF) is not included due to low accuracies.] (updated)

[Figure 6 about here: Comparison of classification results using the best-performing configuration of NB, CART, RF, GTB, and SVM (linear).] (updated)

[Figure 7 about here.: Time series of areas classified as bare / fallow using the training point set based on SPOT-images and CART, RF, GTB, and SVM (linear) between

October 2019 and September 2020. NB and SVM (RBF) are not included due to low accuracies.] (updated)

Discussion

Benefits of Combining Imagery

Most saliently, this study highlights the multiple benefits of combining Sentinel-1 and 2 imagery for various classifiers. For all classifiers except SVM using an RBF kernel, combined imagery yields the highest classification accuracy. Especially for SVM using a linear kernel, the combination of optical and SAR imagery brings a relative increase in overall classification performance. This is in line with several studies that have found marked benefits in adding information from radar images to optical ones for LULC classification (Denize et al., 2018; Van Tricht, Gobin, Gilliams, & Piccard, 2018). What is notable in this study is the consistent and considerable increase in accuracy that results from the combination of image sources. (Tavares et al., 2019), for example, note a rise in accuracy from 89% using Sentinel-2 only to 91% using combined imagery. Similarly small accuracy improvements were reported by (Lu, Tao, & Di, 2018). In contrast, the present study finds increases in accuracy of up to 15 percentage points. In addition, it can be noted that the combination of imagery also leads to a reduction of the impact of the training dataset. It can be conjectured that this is due to the fact that additional layers of information counter-balance the noise in training data and make it more easily separable for classifiers.

Configuring Input Parameters and Data for Optimal Results

Broadly, the results of the analysis illustrated the wide variations in the values of

optimal parameters leading to the best classification accuracies for RF, GTB, and SVM, as well as the considerable impact of the choice of kernel for SVM. Regarding the RF parameter of nTree, for example, previous studies (e.g. Thanh Noi and Kappas, 2017) found that accuracies tended to increase with a rising number of classification trees in each random forest, and that further increasing the number of trees led to stability in the accuracy of the results, starting at ca. 250 trees. Others also note that forests with a larger number of trees do not necessarily perform better than those with fewer (Oshiro, Perez, & Baranauskas, 2012). The present analysis shows that optimal accuracy values for some data configurations can be reached at nTree = 50 already, and that increasing the number of trees can lead to a noticeable decrease in accuracy. This underscores the importance of performing parameter tuning prior to applying each of these classifiers in a new setting, with varying input data configurations. As the parameter tuning results for GTB show, the importance of parameter tuning is also dependent on the quality of the training dataset. While optimal parameter values for nTree and maxNodes varied little for the extended training set, greater discrepancies in values needed to achieve optimal overall classification accuracies were observed using the fieldwork-based training dataset.

Broadly, in terms of band sets and training data, this analysis illustrates the nuanced balance between adding additional layers of information through texture features and spectral indices, and introducing noise that can detract from classification accuracies. Most prominently, it emerges that it isn't necessarily the set of bands with the highest number of additional indices and texture features that yields the highest accuracies. Nor is it the minimalist approach taking as a basis of classification only the bare minimum of raw bands. Rather, it is the set of curated raw bands and spectral

indices, as well as bands arithmetically calculated from the SAR imagery's VV and VH bands, that leads to the highest classification performance. Most probably, this is due to the fact that any additional information offered by certain spectral indices is drowned out by the noise that other, less meaningful, indices produce. This result underlines findings from previous studies, such as (da Silva et al., 2020), which concluded that the NDVI, EVI, and SAVI offer the highest additional values for LULC approaches.

Overall Classifier Performance

When it comes to comparing algorithms in terms of accuracy, this analysis shows that the GTB and RF classifiers exhibit the consistently best performance under a number of different input data configurations, with GTB slightly exceeding RF in terms of accuracy. Though SVM shows similarly high classification accuracies for combined imagery and the use of a reduced band set, GTB and RF performance is consistently superior with regard to all constellations of input data – imagery type, training dataset, and band set. It is only in certain land cover classes – such as the separation of urban areas and bare land – that SVM outperforms RF and GTB. Several previous studies have debated the compared performance of RF and SVM. Ma et al. (2018) found RF to be generally superior in a review of object-based LULC classification approaches, as did Talukdar et al. (2020) in a comparison of machine learning approaches for LULC classification. Rana & Venkata Suryanarayana (2020) by contrast, found SVM performance to be superior, especially in combination with a principal component approach. In addition, several studies have also factored GTB into the comparison, though their number is lower due to the fact that this algorithm has only more recently seen widespread use in LULC. For example, Georganos et al. (2018) found the

XGboost implementation of GTB to systematically outperform RF and SVM, especially on the basis of an extended feature set. Overall, it appears that SVM performs well when studies aim to fine-tune parameters and investigate specific applications, whereas RF offers more solid, generalizable applications for LULC approaches, and a lower sensitivity to various input data. This higher sensitivity of SVM to the types of input imagery and the training data set is in line with findings from earlier studies. Pelletier et al. (2017), for example, compared the effect of training data noise on supervised LULC classification using SVM and RF. The results found RF to be significantly more robust towards both random and systematic noise of training labels.

As for the other classifiers available in GEE that were tested in this study, it emerges that NB is ill-suited for LULC applications, with low overall accuracies. CART, on the other hand, yielded solid results for the combined imagery type. In particular, it can be noted that this classifier performed better when trained using only the fieldwork data. It can be conjectured that this may be due to the more precise nature of the points in this training data set. Even though there are fewer overall than in the extended dataset, and they are unevenly distributed between classes, their label attribution carries a higher certainty. As mentioned above, a higher label noise is likely to have been introduced in the extended dataset derived from SPOT during its creation (Frenay and Verleysen, 2014). CART appears to be more sensitive to noise of this kind in the input data, which can be related to the fact that, unlike RF, it only relies on a single threshold to define a node to split data into subsets. In RF, where this process is repeated multiple times, noise can be balanced out more easily. The discrepancy in the classification for CART depending on the training point set is illustrated starkly by contrasting Figures 6 and 7, the former of which was generated with the configuration

of input parameters yielding the highest accuracies (meaning the fieldwork training point set for CART), and the latter of which used the extended dataset generated on the basis of SPOT images as input. In the former, the extents of bare land towards the end of the dry season are higher in the CART classification than in RF or SVM. In the latter, the reverse is true.

Conclusion

Overall, this study illustrates the considerable benefits of using a combination of optical and SAR imagery in supervised multi-temporal LULC classifications in Google Earth Engine. When using GTB, the accuracies of these classifications can reach up to 94%. It reveals that combining Sentinel-1 and Sentinel-2 imagery improves overall classification accuracy by 10 – 15 percentage points in comparison to analyses based on optical-only imagery. Furthermore, the results of the analysis show that combining different sources of imagery reduces the impact of the size and quality of the training data set. This study also further highlights that out of all the classifiers available in Google Earth Engine, GTB yields the highest overall classification accuracies, performing best in a variety of combinations of input data, training points, and band sets.

In general, the use of the extended training data, with points set manually on the basis of high-resolution SPOT imagery, leads to higher accuracies, despite the higher label noise in comparison to the smaller fieldwork dataset. It can equally be concluded that a carefully selected set of native bands, spectral indices, and texture features used as a basis for classification results in equal or better classifier performance than either a minimalist set, or a large variety of additional bands, especially when using SVM. This

underscores the delicate balance between adding indices and texture features as auxiliary layers of information for classification, and the noise that is introduced through their addition, which may impede classification accuracy. Finally, this study also highlights the importance of tuning various input parameters prior to classification, and of comparing basic classifier settings such as the choice of SVM kernel.

Overall, this study showcases the considerable differences in the outputs of LULC analyses on the GEE cloud computing platform that can result from the choice of imagery, input bands, classifiers, and parametrization – which can lead to vast disparities when applied to larger areas. These results can provide preliminary guidance to researchers to improve the accuracy of LULC analyses, which provide essential inputs into studies ranging from agriculture to hydrology.

Acknowledgements

The authors thank the Equipex Geosud project and the Theia network for making the SPOT-6 & 7 images used in this study available free of charge for research purposes, the French Development Agency (AFD) for its support through the COSTEA project, and our colleagues at the Institute of Technology of Cambodia as well as the Royal University of Agriculture for their invaluable partnership and support of field work.

Data and code availability

All the code used to produce the analyses in this study is available in the GEE Javascript environment: code.earthengine.google.com/?accept_repo=users/christinaannaorieschnig/LandCover Supplementary materials are available in the Mendeley data repository here: 10.17632/wjdzrz7r5m.1

Citations from Table 4 (for bibliography): (Baret & Guyot, 1991; Birth & McVey, 1968; Gao, 1996; Gitelson et al., 1996; Gitelson & Merzlyak, 1996; A. Huete et al., 2002; A. R. Huete, 1988; Jiang, Huete, Didan, & Miura, 2008; Jordan, 1969; Lymburner, Beggs, & Jacobson, 2000; McFeeters, 1996; Qi, Chehbouni, Huete, Kerr, & Sorooshian, 1994; Rouse J.W., Haas, Schell, & Deering, 1974; Wilson & Sader, 2002; Xu, 2006; Zha, Gao, & Ni, 2003)

References

Abadi, M., Barham, P., Chen, J., Chen, Z., Davis, A., Dean, J., … Zheng, X. (2016). TensorFlow: A System for Large-Scale Machine Learning. In *12th {USENIX} Symposium on Operating Systems Design and Implementation ({OSDI} 16)* (pp. 265–283). Savannah, GA: {USENIX} Association.

Amani, M., Ghorbanian, A., Ahmadi, S. A., Kakooei, M., Moghimi, A., Mirmazloumi, S. M., … Brisco, B. (2020). Google Earth Engine Cloud Computing Platform for Remote Sensing Big Data Applications: A Comprehensive Review. *IEEE Journal of Selected Topics in Applied Earth Observations and Remote Sensing*, *13*, 5326–5350. https://doi.org/10.1109/JSTARS.2020.3021052

Amari, S., & Wu, S. (1999). Improving support vector machine classifiers by modifying kernel functions. *Neural Networks*, *12*(6), 783–789. https://doi.org/10.1016/S0893-6080(99)00032-5

Baret, F., & Guyot, G. (1991). Potentials and limits of vegetation indices for LAI and APAR assessment. *Remote Sensing of Environment*, *35*(2–3), 161–173. https://doi.org/10.1016/0034-4257(91)90009-U

Belgiu, M., & Dragut, L. (2016). Random forest in remote sensing: A review of applications and future directions. *ISPRS Journal of Photogrammetry and Remote Sensing*, *114*, 24–31. https://doi.org/10.1016/J.ISPRSJPRS.2016.01.011

Birth, G. S., & McVey, G. R. (1968). Measuring the Color of Growing Turf with a Reflectance Spectrophotometer 1. *Agronomy Journal*, *60*(6), 640–643. https://doi.org/10.2134/agronj1968.00021962006000060016x

Breiman, L. (1996). Bagging Predictors. *Machine Learning*, *24*(2), 123–140. https://doi.org/10.1023/A:1018054314350

Breiman, L. (2001). Random Forests. *Machine Learning* , *45*, 5–32.

Carretero, J., & Blas, J. G. (2014). Introduction to cloud computing: platforms and solutions. *Cluster Computing*, *17*(4), 1225–1229. https://doi.org/10.1007/s10586-014-0352-5

Chen, T., & Guestrin, C. (2016). XGBoost. In *Proceedings of the 22nd ACM SIGKDD*

International Conference on Knowledge Discovery and Data Mining (pp. 785–794). New York, NY, USA: ACM. https://doi.org/10.1145/2939672.2939785

Clerici, N., Valbuena Calderón, C. A., & Posada, J. M. (2017). Fusion of Sentinel-1A and Sentinel-2A data for land cover mapping: a case study in the lower Magdalena region, Colombia. *Journal of Maps*, *13*(2), 718–726. https://doi.org/10.1080/17445647.2017.1372316

Congalton, R. G. (1991). *A Review of Assessing the Accuracy of Classifications of Remotely Sensed Data* (Vol. 37). Retrieved from ftp://ftp.inpa.gov.br/pub/incoming/SIGLAB/Edwin/Curso_SIG_SR/SEPARATAS_RS-Amazonia/Remote Sensing Environment/congalton_1991.pdf

Cortes, C., & Vapnik, V. (1995). Support-vector networks. *Machine Learning*, *20*(3), 273–297. https://doi.org/10.1007/BF00994018

Crowley, M. A., Cardille, J. A., White, J. C., & Wulder, M. A. (2019). Multi-sensor, multi-scale, Bayesian data synthesis for mapping within-year wildfire progression. *Remote Sensing Letters*, *10*(3), 302–311. https://doi.org/10.1080/2150704X.2018.1536300

da Silva, V. S., Salami, G., da Silva, M. I. O., Silva, E. A., Monteiro Junior, J. J., & Alba, E. (2020). Methodological evaluation of vegetation indexes in land use and land cover (LULC) classification. *Geology, Ecology, and Landscapes*, *4*(2), 159–169. https://doi.org/10.1080/24749508.2019.1608409

Deines, J. M., Kendall, A. D., Crowley, M. A., Rapp, J., Cardille, J. A., & Hyndman, D. W. (2019). Mapping three decades of annual irrigation across the US High Plains Aquifer using Landsat and Google Earth Engine. *Remote Sensing of Environment*, *233*, 111400. https://doi.org/10.1016/J.RSE.2019.111400

Denize, J., Hubert-Moy, L., Betbeder, J., Corgne, S., Baudry, J., & Pottier, E. (2018). Evaluation of Using Sentinel-1 and -2 Time-Series to Identify Winter Land Use in Agricultural Landscapes. *Remote Sensing*, *11*(1), 37. https://doi.org/10.3390/rs11010037

Diengdoh, V. L., Ondei, S., Hunt, M., & Brook, B. W. (2020). A validated ensemble

method for multinomial land-cover classification. *Ecological Informatics*, *56*, 101065. https://doi.org/10.1016/J.ECOINF.2020.101065

Dinh, D. A., Elmahrad, B., Leinenkugel, P., & Newton, A. (2019). Time series of flood mapping in the Mekong Delta using high resolution satellite images. *IOP Conference Series: Earth and Environmental Science*, *266*, 12011. https://doi.org/10.1088/1755-1315/266/1/012011

Foo, S. A., & Asner, G. P. (2019). Scaling Up Coral Reef Restoration Using Remote Sensing Technology. *Frontiers in Marine Science*, *6*, 79. https://doi.org/10.3389/fmars.2019.00079

Frenay, B., & Verleysen, M. (2014). Classification in the Presence of Label Noise: A Survey. *IEEE Transactions on Neural Networks and Learning Systems*, *25*(5), 845–869. https://doi.org/10.1109/TNNLS.2013.2292894

Friedman, J. H. (2002). Stochastic gradient boosting. *Computational Statistics & Data Analysis*, *38*(4), 367–378. https://doi.org/10.1016/S0167-9473(01)00065-2

Gao, B. (1996). NDWI—A normalized difference water index for remote sensing of vegetation liquid water from space. *Remote Sensing of Environment*, *58*(3), 257–266. https://doi.org/10.1016/S0034-4257(96)00067-3

Georganos, S., Grippa, T., Vanhuysse, S., Lennert, M., Shimoni, M., & Wolff, E. (2018). Very High Resolution Object-Based Land Use–Land Cover Urban Classification Using Extreme Gradient Boosting. *IEEE Geoscience and Remote Sensing Letters*, *15*(4), 607–611. https://doi.org/10.1109/LGRS.2018.2803259

Ghosh, A., & Joshi, P. K. (2014). A comparison of selected classification algorithms for mapping bamboo patches in lower Gangetic plains using very high resolution WorldView 2 imagery. *International Journal of Applied Earth Observation and Geoinformation*, *26*, 298–311. https://doi.org/10.1016/J.JAG.2013.08.011

Gitelson, A. A., Kaufman, Y. J., Merzlyak, M. N., Gitelson, A. A., Kaufman, Y. J., & Merzlyak, M. N. (1996). Use of a green channel in remote sensing of global vegetation from EOS-MODIS. *Remote Sensing of Environment*, *58*(3), 289–298. https://doi.org/10.1016/S0034-4257(96)00072-7

Gitelson, A. A., & Merzlyak, M. N. (1996). Signature Analysis of Leaf Reflectance Spectra: Algorithm Development for Remote Sensing of Chlorophyll. *Journal of Plant Physiology*, *148*(3–4), 494–500. https://doi.org/10.1016/S0176-1617(96)80284-7

Godinho, S., Guiomar, N., & Gil, A. (2016). Using a stochastic gradient boosting algorithm to analyse the effectiveness of Landsat 8 data for montado land cover mapping: Application in southern Portugal. *International Journal of Applied Earth Observation and Geoinformation*, *49*, 151–162. https://doi.org/10.1016/J.JAG.2016.02.008

Gomes, V., Queiroz, G., & Ferreira, K. (2020). An Overview of Platforms for Big Earth Observation Data Management and Analysis. *Remote Sensing*, *12*(8), 1253. https://doi.org/10.3390/rs12081253

Gong, P., Li, X., Wang, J., Bai, Y., Chen, B., Hu, T., … Zhou, Y. (2020). Annual maps of global artificial impervious area (GAIA) between 1985 and 2018. *Remote Sensing of Environment*, *236*, 111510. https://doi.org/10.1016/J.RSE.2019.111510

Gorelick, N., Hancher, M., Dixon, M., Ilyushchenko, S., Thau, D., & Moore, R. (2017). Google Earth Engine: Planetary-scale geospatial analysis for everyone. *Remote Sensing of Environment*, *202*, 18–27. https://doi.org/10.1016/J.RSE.2017.06.031

Hansen, M. C., Potapov, P. V., Moore, R., Hancher, M., Turubanova, S. A., Tyukavina, A., … Townshend, J. R. G. (2013). High-Resolution Global Maps of 21st-Century Forest Cover Change. *Science*, *342*(6160), 850–853. https://doi.org/10.1126/science.1244693

Haralick, R. M., Shanmugam, K., & Dinstein, I. (1973). Textural Features for Image Classification. *IEEE Transactions on Systems, Man, and Cybernetics*, *SMC-3*(6), 610–621. https://doi.org/10.1109/TSMC.1973.4309314

Huete, A., Didan, K., Miura, T., Rodriguez, E. ., Gao, X., & Ferreira, L. . (2002). Overview of the radiometric and biophysical performance of the MODIS vegetation indices. *Remote Sensing of Environment*, *83*(1–2), 195–213. https://doi.org/10.1016/S0034-4257(02)00096-2

Huete, A. R. (1988). A soil-adjusted vegetation index (SAVI). *Remote Sensing of Environment*, *25*(3), 295–309. https://doi.org/10.1016/0034-4257(88)90106-X

Hütt, C., Koppe, W., Miao, Y., & Bareth, G. (2016). Best Accuracy Land Use/Land Cover (LULC) Classification to Derive Crop Types Using Multitemporal, Multisensor, and Multi-Polarization SAR Satellite Images. *Remote Sensing*, *8*(8), 684. https://doi.org/10.3390/rs8080684

Jiang, Z., Huete, A. R., Didan, K., & Miura, T. (2008). Development of a two-band enhanced vegetation index without a blue band. *Remote Sensing of Environment*, *112*(10), 3833–3845. https://doi.org/10.1016/J.RSE.2008.06.006

Jin, Z., Azzari, G., You, C., Di Tommaso, S., Aston, S., Burke, M., & Lobell, D. B. (2019). Smallholder maize area and yield mapping at national scales with Google Earth Engine. *Remote Sensing of Environment*, *228*, 115–128. https://doi.org/10.1016/j.rse.2019.04.016

John, G. H., & Langley, P. (1995). *Estimating Continuous Distributions in Bayesian Classiiers*. Morgan Kaufmann Publishers.

Johnson, B. A., & Iizuka, K. (2016). Integrating OpenStreetMap crowdsourced data and Landsat time-series imagery for rapid land use/land cover (LULC) mapping: Case study of the Laguna de Bay area of the Philippines. *Applied Geography*, *67*, 140–149. https://doi.org/10.1016/J.APGEOG.2015.12.006

Johnson, D. M. (2019). Using the Landsat archive to map crop cover history across the United States. *Remote Sensing of Environment*, *232*, 111286. https://doi.org/10.1016/J.RSE.2019.111286

Jordan, C. F. (1969). Derivation of Leaf-Area Index from Quality of Light on the Forest Floor. *Ecology*, *50*(4), 663–666. https://doi.org/10.2307/1936256

Jozdani, S. E., Johnson, B. A., & Chen, D. (2019). Comparing Deep Neural Networks, Ensemble Classifiers, and Support Vector Machine Algorithms for Object-Based Urban Land Use/Land Cover Classification. *Remote Sensing*, *11*(14), 1713. https://doi.org/10.3390/rs11141713

Kavzoglu, T., & Colkesen, I. (2009). A kernel functions analysis for support vector

machines for land cover classification. *International Journal of Applied Earth Observation and Geoinformation*, *11*(5), 352–359. https://doi.org/10.1016/J.JAG.2009.06.002

Khan, A., Govil, H., Kumar, G., & Dave, R. (2020). Synergistic use of Sentinel-1 and Sentinel-2 for improved LULC mapping with special reference to bad land class: a case study for Yamuna River floodplain, India. *Spatial Information Research*, 1–13. https://doi.org/10.1007/s41324-020-00325-x

Killough, B. (2018). Overview of the Open Data Cube Initiative. In *IGARSS 2018 - 2018 IEEE International Geoscience and Remote Sensing Symposium* (pp. 8629–8632). IEEE. https://doi.org/10.1109/IGARSS.2018.8517694

Kontgis, C., Schneider, A., & Ozdogan, M. (2015). Mapping rice paddy extent and intensification in the Vietnamese Mekong River Delta with dense time stacks of Landsat data. *Remote Sensing of Environment*, *169*, 255–269. https://doi.org/10.1016/j.rse.2015.08.004

Kruskal, W. H., & Wallis, W. A. (1952). Use of Ranks in One-Criterion Variance Analysis. *Journal of the American Statistical Association*, *47*(260), 583–621. https://doi.org/10.1080/01621459.1952.10483441

Kumar, L., & Mutanga, O. (2018). Google Earth Engine Applications Since Inception: Usage, Trends, and Potential. *Remote Sensing*, *10*(10), 1509. https://doi.org/10.3390/rs10101509

Kuncheva, L. I. (2006). On the optimality of Naïve Bayes with dependent binary features. *Pattern Recognition Letters*, *27*(7), 830–837. https://doi.org/10.1016/J.PATREC.2005.12.001

Kusi, K. K., Khattabi, A., Mhammdi, N., & Lahssini, S. (2020). Prospective evaluation of the impact of land use change on ecosystem services in the Ourika watershed, Morocco. *Land Use Policy*, *97*, 104796. https://doi.org/10.1016/J.LANDUSEPOL.2020.104796

Li, C., Wang, J., Wang, L., Hu, L., & Gong, P. (2014). Comparison of Classification Algorithms and Training Sample Sizes in Urban Land Classification with Landsat

Thematic Mapper Imagery. *Remote Sensing*, *6*(2), 964–983. https://doi.org/10.3390/rs6020964

Li, D., Long, D., Zhao, J., Lu, H., & Hong, Y. (2017). Observed changes in flow regimes in the Mekong River basin. *Journal of Hydrology*, *551*, 217–232. https://doi.org/10.1016/J.JHYDROL.2017.05.061

Lin, Y., Zhang, H., Lin, H., Gamba, P. E., & Liu, X. (2020). Incorporating synthetic aperture radar and optical images to investigate the annual dynamics of anthropogenic impervious surface at large scale. *Remote Sensing of Environment*, *242*, 111757. https://doi.org/10.1016/J.RSE.2020.111757

Liu, S., Li, X., Chen, D., Duan, Y., Ji, H., Zhang, L., … Hu, X. (2020). Understanding Land use/Land cover dynamics and impacts of human activities in the Mekong Delta over the last 40 years. *Global Ecology and Conservation*, *22*, e00991. https://doi.org/10.1016/J.GECCO.2020.E00991

López, S., López-Sandoval, M. F., Gerique, A., & Salazar, J. (2020). Landscape change in Southern Ecuador: An indicator-based and multi-temporal evaluation of land use and land cover in a mixed-use protected area. *Ecological Indicators*, *115*, 106357. https://doi.org/10.1016/J.ECOLIND.2020.106357

Lu, L., Tao, Y., & Di, L. (2018). Object-Based Plastic-Mulched Landcover Extraction Using Integrated Sentinel-1 and Sentinel-2 Data. *Remote Sensing*, *10*(11), 1820. https://doi.org/10.3390/rs10111820

Lymburner, L., Beggs, P., & Jacobson, C. (2000). Estimation of Canopy-Average Surface-Specific Leaf Area Using Landsat TM Data. *Undefined*.

Ma, H.-E., Lin, C., & Hai, P. N. (2018). Applying an Object-Based SVM Classifier to Explore Canopy Closure of Mangrove Forest in the Mekong Delta Using Sentinel-2 Multispectral Images (pp. 5402–5405). IEEE. https://doi.org/10.1109/IGARSS.2018.8519127

Mahdianpari, M., Salehi, B., Mohammadimanesh, F., Homayouni, S., Gill, E., Mahdianpari, M., … Gill, E. (2018). The First Wetland Inventory Map of Newfoundland at a Spatial Resolution of 10 m Using Sentinel-1 and Sentinel-2

Data on the Google Earth Engine Cloud Computing Platform. *Remote Sensing*, *11*(1), 43. https://doi.org/10.3390/rs11010043

Main-Knorn, M., Pflug, B., Louis, J., Debaecker, V., Müller-Wilm, U., & Gascon, F. (2017). Sen2Cor for Sentinel-2. In L. Bruzzone, F. Bovolo, & J. A. Benediktsson (Eds.), *Image and Signal Processing for Remote Sensing XXIII* (Vol. 10427, p. 3). SPIE. https://doi.org/10.1117/12.2278218

McFeeters, S. K. (1996). The use of the Normalized Difference Water Index (NDWI) in the delineation of open water features. *International Journal of Remote Sensing*, *17*(7), 1425–1432. https://doi.org/10.1080/01431169608948714

Minh, H. V. T., Avtar, R., Mohan, G., Misra, P., & Kurasaki, M. (2019). Monitoring and Mapping of Rice Cropping Pattern in Flooding Area in the Vietnamese Mekong Delta Using Sentinel-1A Data: A Case of An Giang Province. *ISPRS International Journal of Geo-Information*, *8*(5), 211. https://doi.org/10.3390/ijgi8050211

Mishra, V. N., Prasad, R., Rai, P. K., Vishwakarma, A. K., & Arora, A. (2019). Performance evaluation of textural features in improving land use/land cover classification accuracy of heterogeneous landscape using multi-sensor remote sensing data. *Earth Science Informatics*, *12*(1), 71–86. https://doi.org/10.1007/s12145-018-0369-z

Mohammady, M., Moradi, H. R., Zeinivand, H., & Temme, A. J. A. M. (2015). A comparison of supervised, unsupervised and synthetic land use classification methods in the north of Iran. *International Journal of Environmental Science and Technology*, *12*(5), 1515–1526. https://doi.org/10.1007/s13762-014-0728-3

Nery, T., Sadler, R., Solis-Aulestia, M., White, B., Polyakov, M., & Chalak, M. (2016). Comparing supervised algorithms in Land Use and Land Cover classification of a Landsat time-series. In *2016 IEEE International Geoscience and Remote Sensing Symposium (IGARSS)* (pp. 5165–5168). IEEE. https://doi.org/10.1109/IGARSS.2016.7730346

Ngo, K. D., Lechner, A. M., & Vu, T. T. (2020). Land cover mapping of the Mekong Delta to support natural resource management with multi-temporal Sentinel-1A

synthetic aperture radar imagery. *Remote Sensing Applications: Society and Environment*, *17*, 100272. https://doi.org/10.1016/J.RSASE.2019.100272

Nizalapur, V., & Vyas, A. (2020). Texture Analysis for Land Use Land Cover (lulc) Classification in Parts of Ahmedabad, Gujarat. *ISPRS - International Archives of the Photogrammetry, Remote Sensing and Spatial Information Sciences*, *XLIII-B3-2*, 275–279. https://doi.org/10.5194/isprs-archives-XLIII-B3-2020-275-2020

Noble, W. S. (2006). What is a support vector machine? *Nature Biotechnology*, *24*(12), 1565–1567. https://doi.org/10.1038/nbt1206-1565

O'Hara, C. G., King, J. S., Cartwright, J. H., & King, R. L. (2003). Multitemporal land use and land cover classification of urbanized areas within sensitive coastal environments. *IEEE Transactions on Geoscience and Remote Sensing*, *41*(9), 2005–2014. https://doi.org/10.1109/TGRS.2003.816573

Orimoloye, I. R., Mazinyo, S. P., Nel, W., & Kalumba, A. M. (2018). Spatiotemporal monitoring of land surface temperature and estimated radiation using remote sensing: human health implications for East London, South Africa. *Environmental Earth Sciences*, *77*(3), 77. https://doi.org/10.1007/s12665-018-7252-6

Orimoloye, I. R., & Ololade, O. O. (2020). Spatial evaluation of land-use dynamics in gold mining area using remote sensing and GIS technology. *International Journal of Environmental Science and Technology*, *17*(11), 4465–4480. https://doi.org/10.1007/s13762-020-02789-8

Oshiro, T. M., Perez, P. S., & Baranauskas, J. A. (2012). How Many Trees in a Random Forest? (pp. 154–168). Springer, Berlin, Heidelberg. https://doi.org/10.1007/978-3-642-31537-4_13

Ouattara, B., Forkuor, G., Zoungrana, B. J. B., Dimobe, K., Danumah, J., Saley, B., & Tondoh, J. E. (2020). Crops monitoring and yield estimation using sentinel products in semi-arid smallholder irrigation schemes. *International Journal of Remote Sensing*, *41*(17), 6527–6549. https://doi.org/10.1080/01431161.2020.1739355

Pekel, J.-F., Cottam, A., Gorelick, N., & Belward, A. S. (2016). High-resolution

mapping of global surface water and its long-term changes. *Nature*, *540*(7633), 418–422. https://doi.org/10.1038/nature20584

Pelletier, C., Valero, S., Inglada, J., Champion, N., Marais Sicre, C., & Dedieu, G. (2017). Effect of Training Class Label Noise on Classification Performances for Land Cover Mapping with Satellite Image Time Series. *Remote Sensing*, *9*(2), 173. https://doi.org/10.3390/rs9020173

Potin, P., Rosich, B., Miranda, N., Grimont, P., Shurmer, I., O'Connell, A., … Gratadour, J.-B. (2019). Copernicus Sentinel-1 Constellation Mission Operations Status. In *IGARSS 2019 - 2019 IEEE International Geoscience and Remote Sensing Symposium* (pp. 5385–5388). IEEE. https://doi.org/10.1109/IGARSS.2019.8898949

Qi, J., Chehbouni, A., Huete, A. R., Kerr, Y. H., & Sorooshian, S. (1994). A modified soil adjusted vegetation index. *Remote Sensing of Environment*, *48*(2), 119–126. https://doi.org/10.1016/0034-4257(94)90134-1

Rana, V. K., & Venkata Suryanarayana, T. M. (2020). Performance evaluation of MLE, RF and SVM classification algorithms for watershed scale land use/land cover mapping using sentinel 2 bands. *Remote Sensing Applications: Society and Environment*, *19*, 100351. https://doi.org/10.1016/J.RSASE.2020.100351

Ranjan, A. K., & Parida, B. R. (2019). Paddy acreage mapping and yield prediction using sentinel-based optical and SAR data in Sahibganj district, Jharkhand (India). *SPATIAL INFORMATION RESEARCH*, *27*(4), 399–410. https://doi.org/10.1007/s41324-019-00246-4

Rouse J.W., J., Haas, R. H., Schell, J. A., & Deering, D. W. (1974). Monitoring Vegetation Systems in the Great Plains with Erts. In *Third Earth Resources Technology Satellite-1 Symposium- Volume I: Technical Presentations. NASA SP-351, compiled and edited by Stanley C. Freden, Enrico P. Mercanti, and Margaret A. Becker, 1994 pages, published by NASA, Washington, D.C., 1974, p.309* (Vol. 351, p. 309).

Saunier, S., Northrop, A., Lavender, S., Galli, L., Ferrara, R., Mica, S., … Altena, B.

(2017). European Space agency (ESA) Landsat MSS/TM/ETM+/OLI archive: 42 years of our history. In *2017 9th International Workshop on the Analysis of Multitemporal Remote Sensing Images (MultiTemp)* (pp. 1–9). IEEE. https://doi.org/10.1109/Multi-Temp.2017.8035252

Schreier, G. (2020). Opportunities by the Copernicus Program for Archaeological Research and World Heritage Site Conservation (pp. 3–18). Springer, Cham. https://doi.org/10.1007/978-3-030-10979-0_1

Shalev-Shwartz, S., & Ben-David, S. (2014). Decision Trees. In *Understanding machine learning: From theory to algorithms*. Cambridge University Press.

Shelestov, A., Lavreniuk, M., Kussul, N., Novikov, A., & Skakun, S. (2017). Exploring Google Earth Engine Platform for Big Data Processing: Classification of Multi-Temporal Satellite Imagery for Crop Mapping. *Frontiers in Earth Science*, *5*, 17. https://doi.org/10.3389/feart.2017.00017

Shi, D., & Yang, X. (2015). Support Vector Machines for Land Cover Mapping from Remote Sensor Imagery (pp. 265–279). Springer, Dordrecht. https://doi.org/10.1007/978-94-017-9813-6_13

Slagter, B., Tsendbazar, N.-E., Vollrath, A., & Reiche, J. (2020). Mapping wetland characteristics using temporally dense Sentinel-1 and Sentinel-2 data: A case study in the St. Lucia wetlands, South Africa. *International Journal of Applied Earth Observation and Geoinformation*, *86*, 102009. https://doi.org/10.1016/J.JAG.2019.102009

Steinhausen, M. J., Wagner, P. D., Narasimhan, B., & Waske, B. (2018). Combining Sentinel-1 and Sentinel-2 data for improved land use and land cover mapping of monsoon regions. *International Journal of Applied Earth Observation and Earth Observation*, *73*, 595–604. https://doi.org/10.1016/j.jag.2018.08.011

Talukdar, S., Singha, P., Mahato, S., Shahfahad, Pal, S., Liou, Y.-A., & Rahman, A. (2020). Land-Use Land-Cover Classification by Machine Learning Classifiers for Satellite Observations—A Review. *Remote Sensing*, *12*(7), 1135. https://doi.org/10.3390/rs12071135

Tamiminia, H., Salehi, B., Mahdianpari, M., Quackenbush, L., Adeli, S., & Brisco, B. (2020). Google Earth Engine for geo-big data applications: A meta-analysis and systematic review. *ISPRS Journal of Photogrammetry and Remote Sensing*, *164*, 152–170. https://doi.org/10.1016/J.ISPRSJPRS.2020.04.001

Tavares, P., Beltrão, N., Guimarães, U., & Teodoro, A. (2019). Integration of Sentinel-1 and Sentinel-2 for Classification and LULC Mapping in the Urban Area of Belém, Eastern Brazilian Amazon. *Sensors*, *19*(5), 1140. https://doi.org/10.3390/s19051140

Thanh Noi, P., & Kappas, M. (2017). Comparison of Random Forest, k-Nearest Neighbor, and Support Vector Machine Classifiers for Land Cover Classification Using Sentinel-2 Imagery. *Sensors (Basel, Switzerland)*, *18*(1). https://doi.org/10.3390/s18010018

Van Tricht, K., Gobin, A., Gilliams, S., & Piccard, I. (2018). Synergistic Use of Radar Sentinel-1 and Optical Sentinel-2 Imagery for Crop Mapping: A Case Study for Belgium. *Remote Sensing*, *10*(10), 1642. https://doi.org/10.3390/rs10101642

Wilson, E. H., & Sader, S. A. (2002). Detection of forest harvest type using multiple dates of Landsat TM imagery. *Remote Sensing of Environment*, *80*(3), 385–396. https://doi.org/10.1016/S0034-4257(01)00318-2

Xu, H. (2006). Modification of normalised difference water index (NDWI) to enhance open water features in remotely sensed imagery. *International Journal of Remote Sensing*, *27*(14), 3025–3033. https://doi.org/10.1080/01431160600589179

Yohannes, H., Soromessa, T., Argaw, M., & Dewan, A. (2021). Spatio-temporal changes in habitat quality and linkage with landscape characteristics in the Beressa watershed, Blue Nile basin of Ethiopian highlands. *Journal of Environmental Management*, *281*, 111885. https://doi.org/10.1016/J.JENVMAN.2020.111885

Yommy, A. S., Liu, R., & Wu, A. S. (2015). SAR Image Despeckling Using Refined Lee Filter. In *2015 7th International Conference on Intelligent Human-Machine Systems and Cybernetics* (pp. 260–265). IEEE. https://doi.org/10.1109/IHMSC.2015.236

Zha, Y., Gao, J., & Ni, S. (2003). Use of normalized difference built-up index in automatically mapping urban areas from TM imagery. *International Journal of Remote Sensing*, *24*(3), 583–594. https://doi.org/10.1080/01431160304987

Zhang, H. (2005). Exploring Conditions for the Optimality of Naive Bayes. *International Journal of Pattern Recognition and Artificial Intelligence*, *19*(02), 183–198. https://doi.org/10.1142/S0218001405003983

Appendix A. Table of Abbreviations

[Table A1 about here: Abbreviations used in the text.]

Appendix B. Overview of Native Sentinel-1 and 2 Bands

[Table B1 about here: Sentinel-2 bands, their resolutions, and wavelengths.]

[Table B2 about here: Sentinel-1 bands, their resolutions, and wavelengths]

H

Revision of Paper Published in the Journal of Hydrology

A Multi-Method Approach to Flood Mapping: Reconstructing Inundation Changes in the Cambodian Upper Mekong Delta

Christina Orieschnig[a], Jean-Philippe Venot[b], Sylvain Massuel[b], Khy Eam Eang[c], Kong Chhuon[c], Sambo Lun[c], Sokly Siev[d], Gilles Belaud[b]

[a] *UMR Hydrosciences, AgroParisTech, University of Montpellier, IRD, 300 Av. du Professeur Emile Jeanbrau, 34090 Montpellier, France*
[b] *G-Eau, IRD, AgroParisTech, Institut Agro, Cirad, INRAE, University of Montpellier, 361 rue J.F. Breton, BP 5095, 34196, Montpellier Cedex 5, France*
[c] *Faculty of Hydrology and Water Resources Engineering, Institute of Technology of Cambodia, Russian Blvd., P.O. Box 86, Phnom Penh, Cambodia*
[d] *General Department of Science, Technology and Innovation, Ministry of Industry, Science, Technology and Innovation, 45 Preah Norodom Boulevard, Sangkat Phsar Thmey III, Khan Daun Penh, Phnom Penh 120203, Cambodia*

Abstract

As in many tropical deltas globally, annual floods shape the livelihoods of the largely rural population in the Cambodian Mekong delta. Agricultural cycles are keyed to the flood arrival, peak, and recession, and fish populations depend on inundated floodplains for their regeneration. However, as factors like climate change and hydropower infrastructure development are altering the Mekong's hydrology, the inundation dynamics of its deltaic floodplains are shifting as well. Several studies have assessed the general changes of river discharge and flood extent on a basin- or delta-wide scale. Yet the sustainable development of this region is relying on dynamics at more local and specific scales, which have not been addressed so far.

This paper presents a methodology to track the evolution of hydrological regimes and associated inundations in tropical deltas such as the upper Mekong delta in Cambodia, where it is applied over the past 30 years. Data scarcity and heterogeneity of the environment in this region necessitated the use of combined approaches. We established a link between water levels measured in-situ and

Email address: christina.orieschnig@ird.fr (Christina Orieschnig)

flood maps derived from optical and radar satellite images (Sentinel-1 and -2).The robustness of the link was assessed using Sentinel, Landsat imagery and the TanDEM-X (12m) elevation model. This water level-flood link (WAFL) was then used to reconstruct a daily time series of inundation extents reaching back to the beginning of hydrological measurements in 1991 (30 years). On this basis, changes in the incidence, duration, and spatial distribution of floods were analysed.

The results indicated that WAFL can be used to reconstruct inundation maps with an overall robustness of 87% in comparison to historical inundation maps derived from remote sensing imagery. Comparisons of WAFL-derived flood extents with Landsat images further underscored the significant role of local infrastructure, sedimentation dynamics, and land cover to explain changes in inundation dynamics. WAFL-based analyses revealed that inundation durations have decreased by an average of 19 days when comparing the periods before and after 2008, which was identified as a break point in the hydrological time series. Furthermore, a drastic decrease in inundation the annual frequency with which individual pixels are flooded can be detected during the first half of the traditional flood season, with an average of -21% in early August, negatively impacting water-based livelihoods, from agriculture to fisheries.

Keywords: Mekong delta, Cambodia, inundations, Sentinel-1 and -2, water levels

---

1. Introduction

Tropical deltas worldwide are fundamentally influenced by regional and local hydrological regimes (Kuenzer and Renaud, 2012; Loucks, 2019). Given low terrain gradients, inundation processes are central to their populations' water-based livelihoods. Yet it is often not well-understood what impact large-scale, basin-wide changes have on more local systems, often due to a lack of data. This is illustrated perfectly by the Cambodian Mekong Delta.

As the largest trans-boundary river in Southeast Asia, the Mekong plays a crucial role in the socioeconomic development of the region, with agriculture and fisheries highly dependent on its flow regime (Kondolf et al., 2018; Boretti, 2020; Kummu and Sarkula, 2008). However, recent years have seen considerable shifts in the Mekong's hydrology (Yun et al., 2020; Trung et al., 2020). Its seasonal hydrological regime, defined by a flood pulse - a strong unimodal flow pattern induced by the annual Monsoon precipitation - has altered in terms of timing and magnitude. On a basin-wide scale, numerous studies have traced the reasons for this to a variety of factors, especially hydropower development and climate change (Hecht et al., 2018; Lacombe et al., 2014; Yang et al., 2019; Yun et al., 2020; Li et al., 2017; Pokhrel et al., 2018). For example, Hoang et al. (2019) project that dry season flows in the basin will more than double as a result of hydropower development, while wet season flows will decrease by 16% by 2050. Similarly, Hoang et al. (2016) conclude that climate change will result in a decrease of wet season flows by 7%, and an increase in dry season flows by 33% by 2065.

These basin-wide changes have a particularly adverse impact on downstream hydro-ecological systems in the Cambodian and Vietnamese Mekong Delta (Intralawan et al., 2018; Yoshida et al., 2020). In these areas, the annual inundations[1] fundamentally shape the livelihoods of the local population. They deposit nutrient-rich sediments on the floodplains, benefiting flood-recession agriculture,

[1]This paper uses the terms "flood" and "inundations" synonymously.

contribute to the recharge of soil moisture and groundwater after the dry season months (Dang et al., 2018; Kondolf et al., 2018) and are crucial for the reproductive cycles of fish species, supporting one of the world's most productive systems of inland fisheries (Poulsen et al., 2004; Hortle, 2009; Winemiller et al., 2016). The floodplains of the Mekong are significantly impacted by shifts in the incidence, duration, and spatial patterns of annual inundations as a consequence of basin-wide hydrological changes. This mirrors the situation in other major deltas worldwide, such as the Ganges–Brahmaputra and Amazon deltas (Szabo et al., 2016; Singha et al., 2020).

These factors have mostly been studied at large scales, based on different hydrological and hydrodynamic models or on past series of remote sensing imagery (Heng et al., 2021; Try et al., 2020; Li et al., 2019; Shin et al., 2020; Mohammed et al., 2018; Burbano et al., 2020). However, each of the proposed modeling approaches comes with its own limitations and simplifying assumptions, as well as with a challenge regarding parametrisation in these often relatively data-sparse regions of interest. In terms of remote sensing, freely accessible, consistent long-term image time series such as Landsat and MODIS can provide some insights into how the spatial patterns of inundations have shifted (Aires et al., 2020; Dang et al., 2016; Fayne et al., 2017). However, many of these series are limited in terms of the temporal and spatial resolution of images, and, in the case of optical images, exhibit data sparsity during the wet season due to cloud cover. They also have difficulties accounting for water areas dissimulated by natural vegetation. Due to the limitations inherent in each approach, the existing studies are unable to produce both sufficiently extensive time series and adapted spatial and temporal resolutions for analysing long-term flood dynamics at local scales. An alternative path is now available in the form of the Sentinel constellation by the European Space Agency (ESA). Its Sentinel-1 and 2 satellites, launched between 2014 and 2017 (Potin et al., 2019), provide freely available optical and SAR data, at a return period of five to six days and a spatial resolution of up to 10 m. This makes Sentinel a valuable basis to better understand dynamic hydrological processes, such as inundations, at local scales. Both Sentinel-1 and

-2 data have been widely used in hydrological applications, separately and in combination (Twele et al., 2016; DeVries et al., 2020; Tsyganskaya et al., 2018), including on delta floodplains (Quang et al., 2019; Singha et al., 2020; Pham-Duc et al., 2017). However, the disadvantage of the Sentinel series lies in its comparatively short duration, which makes it impossible to observe long-term trends.

The aim of the present paper is to present a new methodology to analyse long-term flood dynamics in data-sparse tropical deltas, in order to infer the impact of basin-wide hydrological alterations on local hydro-ecological systems. To circumvent barriers of data scarcity and limitations of any single method, we are proposing a novel multi-method approach to reconstruct a time series of daily inundation extents. The application of this approach is illustrated in the Cambodian upper Mekong delta, based on local water level measurements since 1991 and on Sentinel-derived flood maps.

Building on an in-depth qualitative understanding of international development relations and agricultural practices grounded in social sciences and acquired through interviews with farmers and key informants over the last five years (Venot and Jensen, 2021), the proposed solution is to link in-situ water levels with high-resolution inundation maps derived from Sentinel imagery to establish a water level - flood link (WAFL). On the basis of this link, daily inundation maps are reconstructed going back to 1991, and then used to assess changes in inundation incidences, durations, and spatial patterns. This approach helps overcome the paucity and heterogeneity of data available in the area. We further assess the robustness of the WAFL using comparisons with inundation extents and land cover parameters derived from Landsat imagery and the TanDEM-X (12 m) digital elevation model (Rizzoli et al., 2017; Hawker et al., 2019).

2. Study Area

Agriculture, fisheries and livelihoods of the Cambodian upper Mekong delta are deeply influenced by annual monsoon inundations, yet few studies so far have focused on understanding the hydrological dynamics of this area. With a few notable exceptions (Sothea et al., 2006; Heng et al., 2021; Orieschnig et al., 2021), studies have instead focused on the Vietnamese Mekong delta. However, the Cambodian side of the delta exhibits several striking differences to its Vietnamese counterpart - most importantly in terms of water control infrastructure. On the Vietnamese side of the border, an extensive dyke and sluice gate system allows considerable anthropogenic control over inundations (Park et al., 2020; Triet et al., 2017; Quoc Thanh et al., 2019). Such infrastructure is largely absent in the Cambodian part of the delta. Consequently, it can be conjectured that the effects of upstream alterations are more immediately evident in the inundation patterns of this region (Aires et al., 2020).

The study area is located 60 km south of the Cambodian capital Phnom Penh, on the banks of the Mekong and its distributary, the Bassac river. The Koh Khel and Neak Luong hydrological stations are located just north of the study area, on the Bassac and Mekong respectively. Furthermore, the Chau Doc and Tan Chau stations can be found a few kilometres south of the case study area, in Vietnam (see Figure 1).

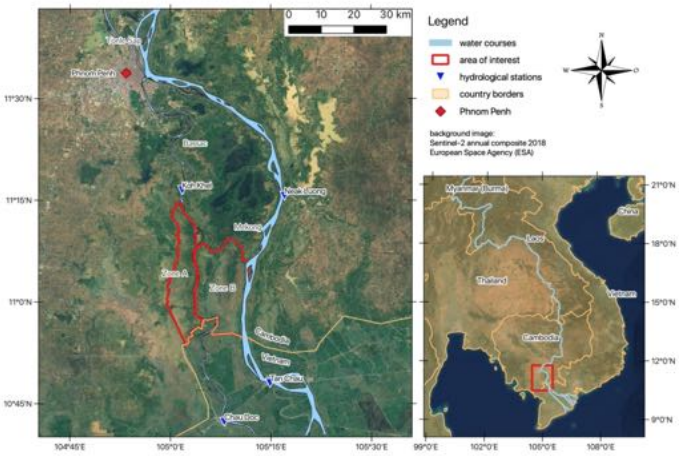

Figure 1: Geographic location of the study area in the Cambodian Mekong delta.

Given low levels of infrastructure development, especially when compared to Vietnam (Biggs, 2010), agriculture and fisheries in the case study area are inextricably keyed to inundation and precipitation dynamics. Typically, wet season precipitation begins in May, with river water levels rising in July to the point of inundating the floodplains. Floods extents usually peak in September and recede in late October and November. After the first rains and before the advent of the floods, farmers engage in what is locally called early wet season cultivation. Then, in the wake of the flood, they practice recession agriculture, harnessing the nutrient-rich sediments deposited during the flood and making use of residual soil moisture. Finally, some farmers engage in dry-season cultivation between March and May, using water stored in low-lying areas and the many drainage channels that crisscross the region (Khem, 2009; Vandôme, 2020; Venot and Jensen, 2021).

Floods are also crucial for small-scale capture fisheries, which provide an

essential component of the daily diet of the local population, and represent a significant share of the revenues of the poorest households in the region (Vilain et al., 2016). During the flood, fish populations regenerate on the floodplains (Hortle, 2009). Fish spawn either directly in the remaining expanses of inundated natural vegetation, or migrate from upstream in their juvenile stages to safely mature in the nutrient-rich shallow waters on the deltaic plains. When flood recession sets in, species migrate back to the main stream of the river, its distributaries, or smaller bodies of inland water, where they are later caught by local fishermen (Vu et al., 2021; Poulsen et al., 2004).

The study area is further divided into two sub-zones with different agricultural landscapes. The first region of interest (Zone A) is located on the right bank of the Bassac (see Figure 1). It encompasses a total area of 206.75 km^2. Its western and northern border are defined by a small distributary of the Bassac, its southern one by the Vietnamese border. Its landscape is characterised by Prek channels. These are human-made, trapezoidal channels, 10 to 50 meters wide and a few kilometers long, which diverge perpendicularly from the Bassac's main stream and connect it to low-lying floodplains by breaching the elevated river banks. In terms of agriculture, a gradient of cultivation can be observed along the length of each Prek. In areas that have been sufficiently raised by sediment deposition and are now rarely flooded (called *Chamkar*), high-value crops such as fruit trees and various vegetables are grown (Pinn et al., 2020).The further the terrain slopes away towards low-lying, regularly flooded areas (*Boeungs*), the more these crops give way to rice and maize.

The second area of interest (Zone B) is located on the opposite bank of the Bassac, and is bracketed between the Bassac in the West and the Mekong in the East (see Figure 1). In the North, it is limited by a canal and a dyke, in the South by the border to Vietnam. It covers an area of 312.65 km^2. This zone is characterized by a large interior floodplain, part of which feature man-made depressions, remnants of shallow reservoirs that were excavated during the Khmer Rouge period in the 1970s. Connecting these depressions to natural streams, a network of canals - also dug during the Khmer Rouge period and

re-excavated since then - spans across the area. Together, these structures support extensive areas of rice cultivation, with cropping calendars attuned to topography and flood timing. Recession rice, planted just after the flood, benefits from residual soil moisture and precipitation in December and January, which reduces the need for irrigation. A second rice crop, dry season rice, is sometimes planted between February and April, though the extent of this crop is usually limited by a lack of irrigation water, which needs to be pumped from canals and shallow reservoirs. Subsequently, early wet season rice is planted in late April or May. It is partially irrigated if water is available, but depends largely on the increased rainfall amounts in late April, May, and June. Typically, it is harvested just before the start of the flood in July.

When the timing, spatial patterns, and magnitude of inundations vary, specific problems result for agriculture, fisheries, and ecosystems in general (Nguyen et al., 2019). For instance, if floods arrive too soon, early wet season crops can be damaged or lost. In contrast, if inundations are shorter than expected, soil moisture and groundwater recharge can be insufficient, and reproduction times for fish populations are cut short. Similarly, a late flood recession can be problematic since it results in recession crops being planted with a delay, meaning flowering and harvesting may be negatively affected by dryer weather. Consequently, the need for irrigation is increased, which can cause issues given the lower water availability and higher overall production costs resulting from pump operation (Koponen et al., 2017). For these reasons, it is crucial to understand the spatial and temporal patterns of inundations in the area and their changes over the past decades.

3. Methodology

An overview of the methodology employed in this analysis is given in Figure 2.

The multi-method approach proposed in this paper is grounded in over five years of interdisciplinary research conducted by the authors. Through months

of collective field work, frequent interviews with multiple stakeholders, and in-situ water level measurements, the team acquired qualitative understanding regarding the development projects implemented in the area, local agricultural practices, and local hydrological processes. This understanding provided the context for the proposed approach, coupling remote sensing methods and hydrological analysis to study inundation trends in the Cambodian Upper Mekong delta.

First, an analysis of local hydrological trends and break points is carried out, to see if changes observed in the upper Mekong delta line up with basin-wide trends. Second, a water level - flood link (WAFL) is established. This is achieved by deriving a time series of inundation extents from Sentinel-1 and -2 imagery, and then linking them to locally measured water levels using a correlation model to take into account propagation delay times. As a third step, a time series of inundation extents is back-calculated on the basis of WAFL.

The robustness of the WAFL is assessed using Sentinel and Landsat images, as well as the TanDEM-X digital elevation model (12 m resolution). For one thing, WAFL-derived inundation extents are compared to inundation maps directly derived from Landsat and Sentinel-2. For another, they are compared to inundation extents derived from TanDEM-X. In addition, the effect of local land cover variables, especially natural vegetation such as shrubland and trees, on the inundation classification are evaluated using a land use land cover (LULC) classification based on Landsat images.

Finally, the changes in inundation incidences and durations in the Cambodian upper Mekong delta over the past three decades are quantitatively and qualitatively assessed according to break points derived from the hydrological analysis.

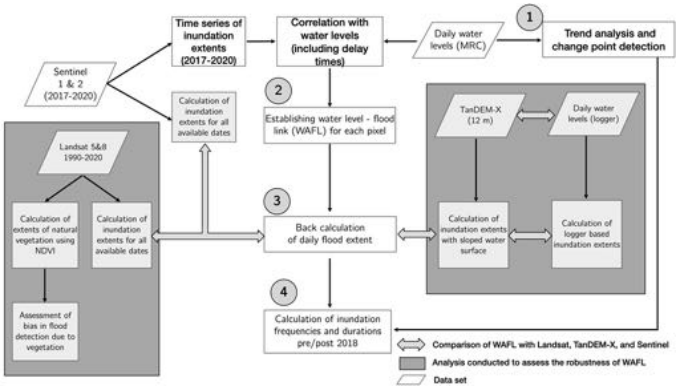

Figure 2: Overall analysis workflow

3.1. Hydrological Analysis: Identifying Trends and Change points

The hydrological analysis was carried out on the time series of water levels measured at four hydrological stations maintained by the Mekong River Commission (MRC). First a trend analysis was implemented using the non-parametric Mann-Kendall test (Hamed and Ramachandra Rao, 1998). Then, a change point detection was carried out using the Pettitt test (Pettitt, 1979), Buishand's range test (Buishand, 1982), and the standard normal homogeneity test (SNH, Alexandersson (1986)). This approach follows the analyses by Mallakpour and Villarini (2016), Yun et al. (2020), and Zhou et al. (2019). The parameters tested were the dates of the flood rise and recession, the overall flood duration, the duration of water levels above local thresholds, the average water level during the flood, and the maximum water level, along with the date at which it was reached each year (see Appendix A in supplementary materials for further explanations). All elevations are given in the local Ha Tien 1960 elevation datum.

The hydrological stations used in this analysis are Koh Khel and Chau Doc on the Bassac, and Neak Luong and Tan Chau on the Mekong (see Figure 1.

At Koh Khel, a continuous time series of daily water level measurements since autumn 1991 is available. At Neak Luong, a series is available since 1926, which is remarkably complete save for two larger gaps in 1946 and 1952-3. For this series, the tests were carried out twice: once on the entirety of the series, and once on a shortened series corresponding to the same duration as that available at Koh Khel. At both Chau Doc and Tan Chau series are available since 1980 and the analysis was conducted on the entirety of the series.

3.2. Detecting Flood Extents Using Sentinel-1 and 2

A series of flood maps was generated from SAR Sentinel-1 and optical Sentinel-2 images for the period 2017-2020. 2017 was chosen as a starting point because the satellite constellation was fully in place beginning that year. For this purpose, the series of Sentinel-1 and 2 images available on the cloud computing platform Google Earth Engine (Gorelick et al., 2017) was analysed. Past studies have illustrated the synergy effects for flood detection in combining both optical and SAR images, for Sentinel in particular (DeVries et al., 2020; Bioresita et al., 2019; Huang et al., 2002). Images were subjected to various pretreatments. Sentinel-2 images were atmospherically corrected using the sen2cor algorithm (Main-Knorn et al., 2017) and clouds were masked based on the QA band. Sentinel-1 images underwent pre-processing based on the European Space Agency's Sentinel-1 toolbox. Metadata was updated with a restituted orbit file, border noise and thermal noise were removed, and radiometric calibration and orthorectification were applied. In addition, a refined Lee speckle filter (Lee, 1983) was implemented.

To classify each image into flooded and not flooded areas, three spectral indices were first calculated for the optical images: the Normalized Difference Vegetation Index (NDVI, Rouse J.W. et al. (1974)), the Normalized Difference Moisture Index (NDMI, Wilson and Sader (2002)) and the Normalized Difference Water Index (NDWI, McFeeters (1996)). For the optical images, these three indices were used as input bands for classification. For Sentinel-1, the VH and VV band were selected. On this basis, an unsupervised K-means classifi-

cation approach was chosen (Arthur and Vassilvitskii, 2007; Frank et al., 2016) to identify flooded areas in both Sentinel-1 and -2 images. This classification approach was selected because it can be applied equally to optical and SAR images, and because no local calibration of threshold values is required. As the training period for the classifier, a time window during the 2018 wet season - from September 25 to October 01 - was used due to the large flood extents and sharp contrast between open water and dry areas at this time. Validation of the flood classification was carried out using a total of 2340 points, set manually on the basis of SPOT-6 high-resolution imagery, on four different dates at different stages during the flood cycle: 2017/01/29, 2018/06/24, 2018/08/04, and 2019/01/27. On this basis, a confusion matrix and the kappa coefficient (Congalton, 1991) of the classification were calculated. This data was also used to determine the optimal number of clusters, which was determined to be two. After validation, the classifier was applied to the entire collection of Sentinel images, and the extents of open water areas were extracted for each image. Finally, the time series of inundation extents was exported, smoothed using a 3-day rolling mean, and scaled down to a daily time step using linear interpolation.

3.3. Establishing a Water Level - Flood Link (WAFL)

In the dynamics of inundations on large floodplains, a temporal lag is typically observed between the change in river water level and the change in flood extent (Zhang et al., 2017). Time is needed to fill the water bodies when the river flood occurs, accounting for a temporal lag between the flood dynamics and the river water levels. Similarly, the flood recession on the floodplains is out of phase with the river water level drop, since inundated areas decrease more slowly due to the retention of water by dykes and other floodplains structures. This results in hysteresis effects on the relationship between river water levels and the inundated surfaces (Hughes, 1980; Kummu et al., 2014). Lag times are controlled by the ease with which water can flow between the river and the floodplains, depending on hydraulic controls such as dykes, canals, bank heights, local topography, and water level gradients. Physically-based models

require geometric data of the main hydraulic connections and dykes, which are not accessible at this scale. Even high-resolution DEMs are often insufficient in terms of horizontal resolution and vertical accuracy to capture the hydraulic controls by dykes in the area, many of which are below 1 m in height. Due to the low terrain gradient, a water level rise of a few centimetres is enough to act as a tipping point for water to spill over certain dykes and induce several hectares of additional inundated surfaces. To account for this lag time, the correlative method for flood curves developed by Lamagat et al. (1993) was used (see Appendix B for more details).

Once the delay times had been made explicit, each inundation map was extracted from the time series of Sentinel-1 and 2 images and assigned a corresponding water level. Then, a flood count and water level link parameter were calculated for each pixel in the areas of interest. The approach used to achieve this is depicted in Figure 9 in Appendix C. The binary flood maps - flooded pixels having been assigned a value of 1 - were stacked. Subsequently, the sum of times each pixel was registered as flooded was calculated. As a result, pixels that represent permanent water areas, which are always detected as flooded, have a flood count equal to the number of images in the analysis. Pixels on elevated terrain areas that are never flooded have a flood count of zero. Next, flood counts are linked to water levels measured at Koh Khel. Each pixel was assigned the lowest water level (cm resolution) at which it was detected as being inundated.

3.4. Comparing the Flood Link With Inundation Extents Derived from Landsat and TanDEM-X

Since the link was established on the basis of relatively recent images from the second half of the 2010s, it became necessary to ascertain to which extent it was capable of delivering accurate estimates of inundated areas based on water levels from the 1990s and the 2000s. To this end, two approaches were chosen. The first was a comparison of inundation extents generated on the basis of the WAFL with those directly derived from Landsat images from the period 1991-

2020. The second was to use the TanDEM-X (12m) Digital Elevation Model (DEM), which is based on SAR imagery collected in the early 2010s, to generate estimates of flood extents and compare them with those generated on the basis of WAFL.

3.4.1. Comparison With Landsat

For the comparison with Landsat, a total of 94 optical Landsat-5 and -8 images were used.

To derive inundation maps from Landsat images, the same spectral indices as for Sentinel were calculated, and the images were then partitioned into flooded and dry areas by an unsupervised k-means algorithm. These maps were then compared with the inundation extents generated using the WAFL and the water level observed at the date the image was taken. First, the total inundated area was derived for each of the 94 images and compared to the calculated inundated area. Second, six Landsat images from flood seasons during the period of interest (1991-2020) were chosen to identify discrepancies in spatial inundation patterns. These images, at a time step of about five years, were selected because they provide rare cloud-free wet-season scenes. They date from 1991/11/29, 1995/11/05, 2000/08/31, 2005/08/21, 2013/09/12, 2015/09/11, and 2020/11/28.

3.4.2. Comparison Using TanDEM-X

A second method of testing the applicability of WAFL was to derive inundation maps from the TanDEM-X (12 m resolution) elevation model, provided by the German aerospace agency (Rizzoli et al., 2017). This DEM was used to assess the extent of inundation patterns as if they were solely linked to differences in detectable terrain elevation in the study area. To establish the comparison, flood extents were generated from the DEM by super-imposing a planar water surface onto the DEM and classifying all areas that were beneath the elevation of that surface as flooded. The planar water surface itself takes into account a North-South slope, based on water level measurements at Koh Khel and in-situ measurements at the western end of a Prek at the center of Zone A. Similar

to the Landsat measurements, a comparison of the size of inundated areas was carried out, along with spatially explicit comparisons of the distribution of inundations.

The comparison was also performed locally, directly based on in-situ measurements. The in-situ water level measurements were carried out using a differential pressure logger (Onset Hobo MX2001), with a complete time series available from September 2020 to April 2021 at 15-minute intervals. First, a pseudo water level in the floodplains within a radius of 1km of the logger was generated. This was achieved using inundation extents detected through Sentinel images, and the DEM-derived elevation-area curve of the zone, and based on the assumption that the water level is horizontal in such a small area (see Figure 20c in Appendix D). This pseudo water level was then compared with the levels measured in-situ. In reverse, the in-situ water level measurements were transformed into estimates of the size of the inundated areas within this 1 km radius around the logger, using the same curve. Finally, the inundation curves in this sub-area observed from Sentinel, and generated from WAFL and TanDEM-X were compared.

3.4.3. Land Use Classification: Detecting Natural Vegetation

A final element of the applicability of the WAFL related to the detection of natural vegetation in the area. Natural vegetation, such as shrubland and forests, can easily obscure open water surfaces due to canopy cover, especially in optical remote sensing imagery (Tsyganskaya et al., 2018; Pekel et al., 2016; Plank et al., 2017). To gauge the extent of this effect on the detection of inundations, an approach relying on a simple thresholding method using the NDVI was chosen. The NDVI was calculated for composite Landsat images for the dry seasons 1990/1991, 2000/2001, 2010/2011, and 2020/2021 for the months between March and May, which are the driest in the region. Then, areas exhibiting an NDVI of over 0.55 (Nath and Acharjee, 2013; Hashim et al., 2019) were classified as likely forest and shrubland. Further on in the analysis, the obscuring effect of canopy cover was taken into consideration by considering low-

lying areas classified as natural vegetation, which were otherwise surrounded by open water surfaces, as likely flooded.

3.5. Flood Dynamics Analysis: Calculating Inundation Durations and Incidences

As a next step, flood extent maps were used to generate inundation durations and incidences for each pixel (10 m) in the study area for the comparison periods identified on the basis of the hydrological time series. The term "inundation incidence" refers to the percentage of years in each of the two comparison periods during which any one pixel was flooded. Six different incidences were calculated: the overall annual inundation incidence (the % of years during the period that a given pixel is flooded, regardless of the date), along with inundation incidences at dates of interest to agricultural practices in the area, identified on the basis of interviews with stakeholders. These are the 15th of July, the 31st of July, the 15th of August (of importance for harvesting early wet season crops), the 31st of August, and the 25th of September (of importance for rainy season cultivation and planting of recession crops).

4. Results

4.1. Trends and Change Points in the Water Level Time Series

Detailed results of the analysis of hydrological trends and change points are given in Appendix D. The statistically significant trends that could be identified are highlighted in this section.

Generally, the water level time series at Koh Khel shows trends towards a later flood rise and an earlier flood recession (the latter is significant at $p < 0.1$). Most significant is the decrease of the duration of water levels at over 4 m^2 ($p=0.022$). A break point is detected by all three homogeneity tests for the hydrological year 2007/08.

[2] A local threshold of 4 m rather than 5 as at Neak Luong was used here because there were several years in the time series when water levels did not exceed 5 m at all.

The water level series at Neak Luong since 1926 exhibits significant trends towards a later flood arrival ($p=0.03$), decreasing maximum water levels ($p<0.001$), and decreasing flood durations at over 5 m ($p<0.001$). The short time series (1990-2020) shows a trend towards an earlier flood recession ($p=0.06$), a shorter flood duration ($p=0.09$), and especially a decreasing average water level during the flood ($p=0.03$), as well as a decrease in the incidence of water levels above 5 m ($p=0.03$). Significant break points were detected 17 years into the time series, which corresponds to the break 2009/10.

At both Tan Chau and Chau Doc, break points were detected for the hydrological year 2007/08. In addition, there is a significant decreasing trend in terms of maximum water levels and flood durations of over 2 m at Tan Chau ($p<0.001$).

Overall, it emerged from the analyses that the hydrological year 2007/2008 significantly separates two statistically homogeneous periods characterised by different flood durations, dates of flood rise and recession, and flood peaks. Consequently, we used the years pre- and post-2008 as comparison periods for the analysis of inundation extents reconstructed using the WAFL.

4.2. Detection of Inundation Extents

In total, 119 Sentinel-2 and 360 Sentinel-1 images, taken between 2017/01/01 and 2020/12/31 were processed. This means that, on average, one image is available every three days. An example of an inundation map derived from a Sentinel-2 image on the basis of the k-means classification is given in Figure 15 in Appendix E. The average accuracy of the classification of flooded areas lay at 96.5%, with a Kappa value of 0.785. Details are given in Table 3 in Appendix E. However, it must be mentioned that these values at least partly result from the fact that the validation data used was itself derived from remote sensing imagery. Though it was set on the basis of high-resolution imagery, and with first-hand knowledge of the study area in mind, the validation points were still only set in unambiguous areas. Consequently, areas such as flooded vegetation or inundated rice fields prior to planting that cannot be easily discriminated

as either flooded or not in satellite imagery are underrepresented, and their ambiguities missing from the validation results.

Dynamics of inundation extents in Zone A and B, detected on the basis of optical and SAR Sentinel imagery and in relation to water levels at Koh Khel, are shown in Figure 3. A good general correspondence between the dynamics of the two curves can be observed. A time delay between the dynamics of the water level curves and the response of the inundated areas can be clearly seen. Large inundated areas correspond to high water levels several days prior, justifying the use of the Lamagat model as explained in the previous section - its results are given in Appendix E in Figures 16 and 17 as well as Tables 4 and 5.

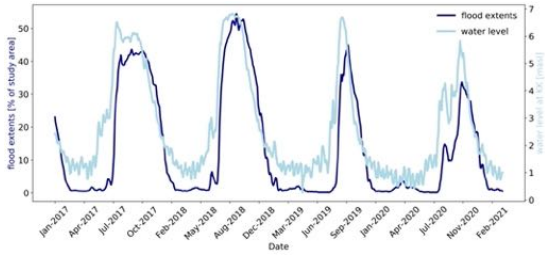

(a) Zone A

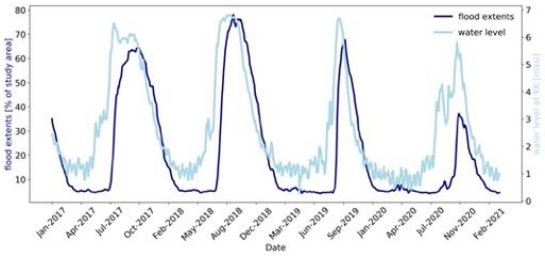

(b) Zone B

Figure 3: Dynamics of inundation extents and water levels measured at Koh Khel in the areas of interest 2017-2020.

4.3. The Water Level Flood Link (WAFL)

The water level flood link (WAFL) was calculated in accordance with the methodology described above. It is given in Figure 4, alongside the TanDEM-X elevation model. As can be seen, the WAFL shows similar elevation gradients to those seen in the DEM.

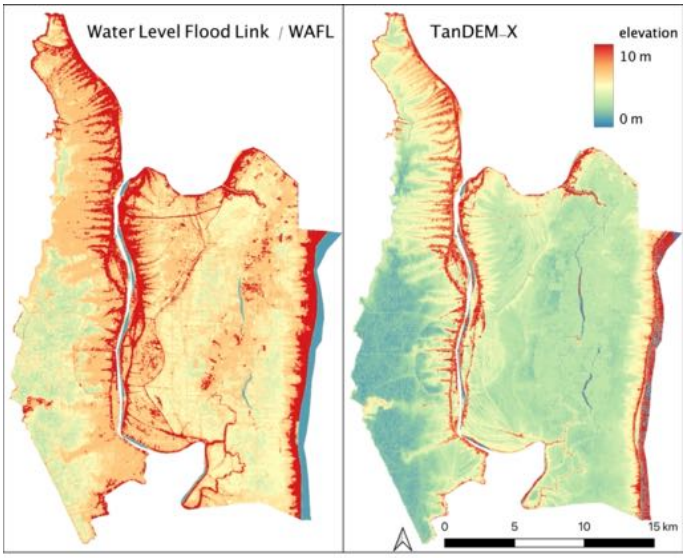

Figure 4: Side-by-side comparison of the water level at which each pixel becomes flooded, according to the WAFL, and the TanDEM-X terrain elevation model.

4.4. Comparison of Calculated Inundation Extents with Flood Maps Derived from Sentinel and Landsat and Influence of Natural Vegetation

In terms of comparing the inundation extents calculated using the WAFL with flood maps derived from Sentinel- and Landsat images, there is widespread agreement, though idiosyncratic variations remain.

The comparison of WAFL-calculated extents with Sentinel images showed an average classification agreement of 90.60% in images that were not obscured by clouds (see Figure 18 in Appendix F). The agreement between the calculated flood extents based on WAFL and those observed in the 94 Landsat images used in this analysis is shown in Figures 5 and 6, which shows the comparison for three specific dates. It emerges that in terms of overall inundated areas, there is a strong agreement between the two methods. As Figure 5 shows, there are some deviations in years that saw heavy floods, during which calculated inundation extents are lower than those obtained through Landsat classification.

In addition, it can be noted that the spatial distribution of inundations varies between the two methods of detection and that the deviations are more extensive the further back in time the points of comparison lie. For example, Figure 6 shows that WAFL-derived inundation maps detect extensive inundated areas in Zone B in the 2010s, while these areas are dry according to the Landsat classification. In contrast, areas of medium elevation in Zone A (transition zones between Boeung and Chamkar) appear as flooded in the 1990s and early 2000s in Landsat images, but are registered as dry by WAFL. The strong agreement between the total water surfaces obtained by the two methods may thus be contingent. This hypothesis will be further investigated in the discussion section.

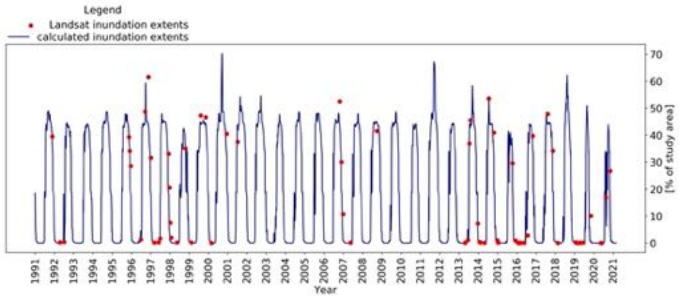

(a) Zone A

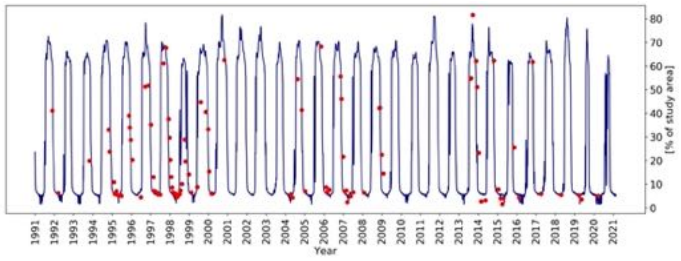

(b) Zone B

Figure 5: Comparison of inundated areas - time series derived from the WAFL, and individual Landsat-5 and -8 images

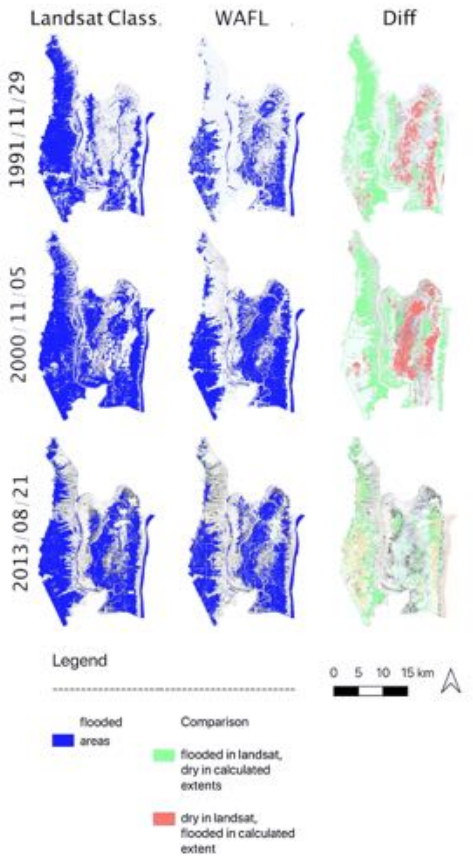

Figure 6: Comparison of inundation extents derived from the WAFL and Landsat-5 and -8 images

The analysis of the extents of natural vegetation indicates that extensive areas of shrubland and regularly flooded forests were present in Zone B in the

1990s, but that they shrunk to a fraction of their former size by 2020 due to large-scale conversion to rice fields. The decrease between 1990 and 2000 is limited, at ca. 2% of the overall area (see Figure 19 in Appendix F). After that, there is a sharp decline: -42% and -62% by 2010 and 2020 when compared to 1990. Such findings are supported by interview data.

In Zone A, the development is different. Here, natural vegetation detected in the early 1990s is located in the southwestern part of the study area. This patch of vegetation decreased considerably between 1990 and 2000 - by 64% in fact - due also to conversion to rice fields. After that, the overall extents of detected natural vegetation rebounded and even gained 20% in area in comparison to 1990. However, the increased extent of the detected natural vegetation is more likely to be due to the planting of fruit trees such as mango, whose areas, according to interviews and agricultural statistics, have sharply increased over the last 10 years.

Furthermore, the analysis of the extents of natural vegetation shows that there is an extensive overlap between those areas that are detected as flooded in WAFL-derived maps, but not by those generated directly from Landsat images. The Overlap line of Table 1 shows that upwards of 93% of pixels that exhibit these discrepancies coincide with the detected extents of natural vegetation. This indicates that these areas may be flooded but their water surface masked by canopy cover and hence not detected by Landsat imagery. If one considers that all forest pixels that overlap with areas being detected as dry by Landsat and wet by the WAFL are indeed flooded, agreement scores between the two methods for detecting flood extents increase from an average of 79.75% to 87.16% for Zone A, and from 68.49% to 87.18% for Zone B.

	Zone	1991	1995	2000	2005	2013	2015	2020
Agreement between LS and WAFL	A	67.64	68.85	74.98	81.85	85.68	85.87	93.37
[% of study area]	B	72.25	49.14	57.49	53.08	78.35	78.00	91.11
LS Wet - WAFL Dry	A	25.83	16.14	20.03	8.71	6.09	8.41	4.37
[% of study area]	B	6.93	14.68	19.76	11.06	8.9	20.13	7.37
LS Dry - WAFL Wet	A	6.53	15.00	4.99	9.44	8.22	5.72	2.25
[% of study area]	B	20.82	36.19	22.75	35.87	12.75	1.86	1.50
Overlap of LS dry area with forest	A	99.93	99.93	99.93	99.93	97.09	99.93	99.89
[% of dry area]	B	99.97	99.97	99.97	99.97	93.42	99.95	99.96
Corrected agreement	A	74.17	83.84	79.97	91.28	93.66	91.59	95.62
[% of study area]	B	93.06	85.32	80.23	88.94	90.26	79.86	92.61

Table 1: A comparison of the agreement and discrepancies between the WAFL-derived inundation extents (WAFL) and the Landsat-derived flood maps (LS).

4.5. Comparison of Calculated Inundation Extents with Flood Maps Derived from TanDEM-X

When it comes to the flood extents derived from TanDEM-X and their comparison with the inundation maps created using the WAFL, several salient points can be observed.[3] The comparison between TanDEM-X derived inundation maps in the 1-km radius around the in-situ sensor in Zone A and direct inundation observations from Sentinel images reveals a very good correspondence (see Figure 21 in Appendix F). Some hydraulic elements, like dykes, do not appear in TanDEM-X. This leads to an overestimation of flooded areas with the DEM compared to WAFL. We can also expect that these elements slow the filling of the area, introducing some delay between the water level measured at the sensor and the response in terms of inundations.[4] In addition, it emerges that the WAFL underestimates flood extents in this particular part of the study area in comparison to both the Sentinel-derived flood extents and those calculated from the TanDEM-X.

At a larger scale, the quality of this correspondence decreases, which illustrates the limitation of the DEM (especially to capture hydraulic connections and barriers) and of the assumption of a planar water surface. We can also

[3] See Figure 20 in Appendix F for the elevation-area curves extracted from TanDEM.

[4] This can be observed in Figures 22a and 22b in Appendix F, which show a lag time of a few days between the two curves.

expect errors due to propagation times not being evenly distributed throughout the area.

The water level at which pixels become flooded according to the WAFL is generally higher than their elevation in the TanDEM-X model (see Figure 4). The exception to this is the center of Zone B. Here, the WAFL shows some areas that become flooded at higher water levels than the surrounding terrain, while the TanDEM-X registers continually low elevations.

As a consequence of this discrepancy between the WAFL and TanDEM-X elevations, TanDEM-X-derived flood extents are generally higher than those calculated using the WAFL (see Figure 7), even when taking into account a North-South slope of the water surface area.

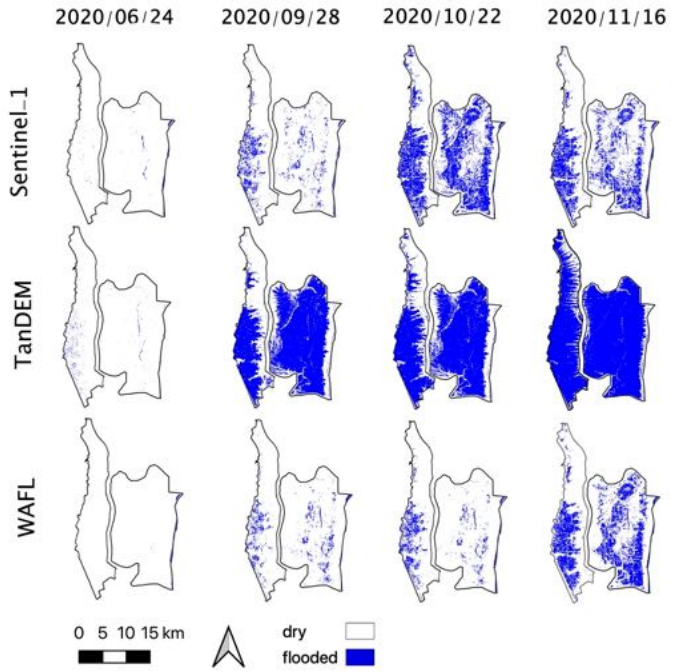

Figure 7: Comparison of inundation extents derived from TanDEM-X, and calculated from the WAFL, and as observed from Sentinel-1 for four dates during the 2020 flood season.

4.6. Changes in Inundation Incidence, Durations, and Patterns Pre- and Post-2008

When the WAFL is applied to the entirety of the water level time series to generate inundation maps, several trends emerge for the comparison periods 1991-2008 and 2009-2020. These trends are summarized in Table 2. It emerges that average annual inundation durations in both zones have decreased. In some areas of both zones, this decrease is as much as 39 days when the two periods are compared. In Zone A, the average decrease, at 15 days, was lower than in

Zone B, at 23 days.

As for inundation incidence, a similar overall declining trend can be noted. However, the magnitude of this decline is unevenly distributed across the flood season. Overall, there is a sharp decrease in inundation incidence in July and early August in both Zone A and B. In Zone A, the largest mean decrease, at -20% of years per period, can be observed in late July. In Zone B, this is the case for mid-August, at -23%. In contrast, the decrease in mean inundation incidence is limited in late September, a time at which the flood peak would traditionally have occurred already. At this time, the average inundation incidence remains unchanged in Zone B, and only declines by -8% in Zone A. On an annual basis, the decline in inundation incidence is much larger in Zone B, at -6% than in Zone A at -2%.

Parameter		Pixel-based changes in inundation incidence [% of years/period]						Changes in inundation
		Jul 15	Jul 31	Aug 15	Aug 31	Sep 25	Overall	duration [days]
	Max +	5	5	5	20	15	12	4.81
Zone A	Mean	-19	-20	-18	-16	-8	-2	-15.21
	Max -	-53	-41	-64	-33	-38	-25	-39.25
	Max +	5	5	5	15	15	12	5.17
Zone B	Mean	-13	-11	-23	-7	0	-6	-22.97
	Max -	-51	-48	-43	-35	-38	-30	-39.14

Table 2: Average changes in inundation incidence and durations in Zone A and B pre- and post-2008 for individual pixels. Given are the largest increase in flood incidence and duration for any individual pixel in the study area (Max +), the largest decrease for the same (Max -), as well as the average change in incidence and duration across all pixels in the study area.

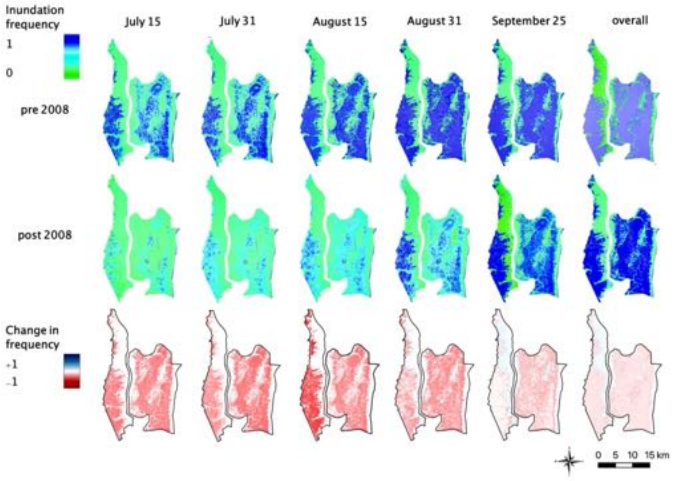

Figure 8: Visual comparison of inundation incidences pre- and post-2008

5. Discussion

5.1. Local Hydrological Trends and their Reflection of Basin-Wide Changes

Hydrological trends in the Cambodian upper Mekong delta closely mirrored those observed in basin-wide studies, with shorter flood durations and lower wet season water levels. Furthermore, the division of comparison periods into a pre- and post-2008 series mirrors the break point found in basin-wide studies, such as Yun et al. (2020) and Heng et al. (2021).

5.2. Inundation Mapping Using Sentinel: Between Biases and the Value of Observing Local Dynamics

In terms of inundation dynamics, curves of flood extents closely correspond to those of locally measured river water levels, both for Zone A and B. The most noticeable difference between the two zones is that the delay time between the two curves is longer for Zone B than for Zone A, which may be due to its

larger width, as well as the relatively shorter length of the Preks connecting the river to the floodplains. In combination, these terrain characteristics mean that floods take longer to reach the center of Zone B than of Zone A.

5.3. Validity of the WAFL: Balancing Natural Vegetation, Sedimentation, and Terrain Correspondence

The comparison between WAFL-derived inundation extents and flood maps extracted from Sentinel-2 imagery reveals several advantages and drawbacks of the proposed methodology. The benefit of using the WAFL-reconstructed inundation extents are best exemplified in the case of the image taken during the 2018 flood season, shown in Figure 18 in Appendix F. The optical Sentinel-2 images at this date show several gaps, left by cloud masking. However, not all clouds were properly detected by the masking algorithm and those that remain are falsely classified as dry areas in the Sentinel-derived flood map, leading to inconsistencies with the WAFL classification. The drawbacks of the methodology are most clearly revealed in the image from the 2020 flood season. Here, it is visible that the agreement of the two flood classifications is considerably higher in Zone A than in Zone B. Particularly, the WAFL classification in Zone B fails to capture some of the areas detected as inundated in the Sentinel-2 images. This may be due to the fact that water level dynamics in this year deviated considerably from the previously observed norm, with an early peak followed by a lowering of levels, before abruptly rising again towards the season's main peak. It can be conjectured that the correlative relationship established to characterise the delay time between water levels and the response of inundated areas failed to adequately capture this development. Whether this is an isolated response is hard to assess, since similar early peaking patterns cannot be found anywhere else in the data.

In terms of which factors most impact the detection of floods and the applicability of the WAFL, natural vegetation emerges as the central element in the comparison with Landsat images. This is particularly apparent as the binary classification into flooded and not flooded areas that was chosen in this approach

limits the possibility of detecting flooded vegetation. Overall, the comparison with Landsat-derived inundation maps highlights the potential of the WAFL for re-constructing past inundation extents. In general, while the WAFL also has some issues mistaking areas with natural vegetation for dry areas, even when they are flooded, this misclassification is much less frequent than with Landsat. There are two main reasons for that. First, Sentinel-1 SAR (on the basis of which the WAFL was derived) has the capacity to detect water under vegetation layers (Tsyganskaya et al., 2018). And second, at the time the Sentinel images were recorded (2017-20) there was already much less natural vegetation in the study area than at the time that many of the Landsat images used in this study were taken (cf. Figure 19 in Appendix F).

A second discrepancy in the comparison with Landsat is observed on higher-lying terrain in the study area. Here, Landsat continually registers inundations in the 1990s and early 2000s, which the WAFL fails to capture. That may be due to the fact that at the time that the Landsat images were recorded, these areas actually were flooded regularly, but that by the time the Sentinel images were taken, this had changed. Some possible explanations for that could be the construction of local infrastructure (such as small dams and dykes), the natural deposition of sediments, or the raising of land through geotechnical projects (it is not rare to see farmers raising the level of their land to build houses or plant trees). The regular distribution of this discrepancy in flood prevalence between Landsat and WAFL-derived maps seems to speak more for the second option. In terms of sediment deposition on the floodplains of the Mekong delta, Hung et al. (2014) found an average annual deposition of 6.86 kg/m^2 in the Vietnamese Mekong delta in Tam Nong district in Dong Thap province. This corresponds to an annual increase of 6 mm in height. These deposition rates are likely to be higher on the Cambodian side of the border due to the absence of dams and dykes. According to Manh et al. (2014), deposition on the Cambodian floodplains is indeed up to six times higher than in Vietnam, ranging from 19 to 23% of the annual sediment load at Kratie, rather than the 1 to 6% deposited in the compartmentalised floodplains in Vietnam. However, this also highlights

one of the principal limitations of WAFL - that it uses recent data to re-construct past inundation extents. As the conjectured effect of sedimentation shows, this may lead to errors where terrain configuration has changed significantly over the past decades. As the likelihood of such significant changes invariably increases over time, this necessarily means that the likely robustness of WAFL-derived maps diminishes the further back in time it is applied.

When it comes to the comparison of the WAFL with TanDEM-X and the inundation extents derived on both bases, using a planar water surface superimposed on the DEM on the basis of in-situ water levels, seems to be a valid approach on a local scale. From a physical perspective, it appears that the water level registered by the logger could be construed to represent the inflow into the Boeung area, while the pseudo water level derived from Sentinel can be seen as the storage response, with local hydrological processes mirroring the dynamics of those of a reservoir (the Boeung) filling and emptying. This is typical for flood storage cells: the inflow-outflow is governed by the difference in levels between the main connection point and the mean level in the area. The delay is directly linked to the volume of water stored in the considered area and the flow rate. When there is no obstacle in the considered area, the delay is very short and water level can be considered as horizontal (propagation effects are not visible at a daily time step). When dykes limit the flow propagation, the filling of the area is made possible by small openings in dykes (usually made by farmers to irrigate their rice fields). Then it takes a longer time to fill the area. During flood recession, the processes are inverted: water level decreases rapidly in the Preks that are well-connected to the Bassac, while water is stored in the floodplains. Water is kept as long as possible in rice fields (by clogging the dykes) and recedes progressively by gravity (surface and subsurface drainage) and evapotranspiration.

However, the robustness of this approach diminishes considerably when applied at the scale of the entire study area. At this scale, the assumption of a horizontal water surface slope no longer holds. Even when superimposing a sloped water surface over the entire DEM and taking into account correla-

tions between the station at Koh Khel and the logger, the discrepancy remains high due to the complexity of the hydrological processes in the area. Broadly, this leads to an overestimation of inundated extents derived from TanDEM-X. However, the use of the DEM does have the advantage of absolutely removing the interference of natural vegetation, as evidenced by the discrepancies in the center of Zone B observed in Figure 7.

5.4. Decreasing Flood Incidence and Durations in the Cambodian Mekong Delta: Patterns and Impacts

Despite limitations in the detection of the full flood extents in the 1990s and early 2000s, the analysis clearly shows a pronounced decrease in the incidence and duration of floods, especially in July and the first half of August. Large swaths of the study area, which were regularly flooded during these months in the 1990s, now remain dry until the second half of August. Taken together with the trends of earlier flood recession and the shorter flood durations outlined above, this means that overall, inundations in the Cambodian Mekong delta arrive later and recede earlier.

To a certain extent, this is in line with previous basin-wide studies such as Yun et al. (2020) and Hecht et al. (2018) that investigated the impacts of climate change and hydropower development. Their main findings were that a lower wet season discharge was to be expected in the future as a result of these developments, along with a higher dry season discharge. In terms of inundations, however, these higher dry season discharges do not balance the lack of inundations during the wet season that are key for the ecological functioning of the floodplains. Similarly, the results are in line with observations by Aires et al. (2020), who found a declining trend in inundation extents in their analysis of the Vietnamese and Cambodian Mekong delta using MODIS data.The same study also found inundations to be delayed by about two weeks in the Cambodian part of the Mekong delta. The present study indicates a longer delay, which may be due to differences in both the time frame and the spatial resolution of the data used. Figure 8 indicates that the incidences with which pixels were

flooded in late July prior to 2008 are now only attained in late August or early September. Similar parallels exist in the work of Heng et al. (2021). In their modelling study of the Cambodian floodplains - one of the few taking this region as its focus - the authors conclude that total flood extent is projected to decline by 18% by 2040.

Overall, the alterations outlined above are anathema to the formerly predictable hydrological regime of the region, and are likely to have wide-reaching consequences for agriculture and fisheries. Greater variability in the dates of the flood arrival and its recession may, for instance, result in shifts in the planting and harvesting times for recession crops and an increased need for irrigation water (Erban and Gorelick, 2016). As far as fisheries are concerned, the later onset of floods and overall decrease in inundation durations limit the period during which fish populations can regenerate in the shallow waters on the floodplains (Hortle, 2009). Compounded with the decrease in natural vegetation, which provides valuable structural habitat features, this is likely to negatively impact fish population dynamics. Vu et al. (2021) showed a close correlation between the long-term decline in commercial fish catches and declining peak water levels in the Mekong delta. Furthermore, local-level data obtained by the authors from fishermen in the area show fish catch to be much lower in years when the water level at Koh Khel exceeds 4 m for a lower number of days. These changes in inundation extents and durations are likely to impact food security in the region. Burbano et al. (2020), for example, link the shorter flood durations in the Tonle Sap region and the Mekong delta floodplains to shifts in dietary protein from fish to meat, and, consequently, land use changes resulting from the need to accommodate cattle.

Shorter inundation durations and lower incidence also reduce the spatial and temporal extent of the terrestrial-aquatic interface that many regulating ecosystem services depend on. This includes processes such as pest regulation, nutrient deposition, and soil and ground water recharge (Brown and My Phung, 2010; Chen et al., 2011).

Furthermore the analysis also shows that, even though large changes have

occurred in the basin over the past three decades, the link between river water levels and inundation extents has remained relatively static. In contrast to the major changes in the hydrology of the Mekong river, its hydraulic connections to its Cambodian floodplains seem to have changed comparatively little, which may be related to the still limited development of water control infrastructure in the region. At this point, it is important to note the fact that the results presented in this study partially mirror those from analyses of basin-wide trends in discharge and water levels because the WAFL has been constructed on the basis of these water levels. The merit of the study, though, lies in illustrating the magnitude of these parallelisms, which depends on the unique terrain configuration of the floodplain and the hydraulic controls that determine the dynamics of inundation processes.

5.5. Generalizability and Transferability to other Case Study Areas

As stated above, the ultimate aim of the developed methodology is to provide long-term insights into the spatial dynamics of inundations in tropical deltas. Applying the approach to the Mekong delta showed that this is possible with acceptable average accuracies of 87% in comparison to historical inundation maps derived from Landsat. Such comparisons have also highlighted the limitations of the WAFL with regard to long-term changes in local terrain configuration, and the challenges posed by LULC characteristics such as the presence of natural vegetation.

For an application in other study areas, this means that a basic knowledge of changes in local conditions is a prerequisite for the development and application of the WAFL. An awareness of landcover dynamics - which can be assessed through historical LULC analysis - or significant shifts in terrain elevations and the river-floodplain connections, notably due to the construction of water control infrastructures, is crucial. It must also be noted that the WAFL is primarily applicable in areas where inundations are correlated largely with dynamics in river water levels. This refers to areas in which the influence of local precipitations and groundwater is limited and where there are few obstacles to the flow

of water into and out of the floodplain. This can be mostly the case in semi-arid places but also in tropical areas like in the Mekong delta, as demonstrated in this study by the comparison of water level dynamics and Sentinel-derived inundation extents. Where historical records of water levels are available, as a first step in the application of WAFL, such an analysis should be used to elucidate the applicability of the methodology. However, in areas where inundations are significantly correlated with processes such as local precipitation or groundwater logging, adjustments to the correlation model can be made by introducing new input variables, provided time-series are available.

6. Conclusion

This paper offers an innovative approach, combining multiple methods and types of data, to elaborate a water level-flood link (WAFL) on the basis of which past daily inundation extents can be reconstructed, as illustrated for the Cambodian upper Mekong delta with a time series starting in 1991. Combining remote sensing and statistical methods with an in-depth knowledge of hydrological processes and agricultural dynamics of the Cambodian upper Mekong delta acquired over several years of research makes it possible to surmount barriers posed by the paucity and heterogeneity of data in this region, and attain a better understanding of changes in inundation dynamics.

The water level - flood link (WAFL) is established on the basis of Sentinel-1 and 2 data collected between 2017 and 2020 and in-situ hydrological measurements. Its robustness is further tested through a comparison with Landsat-derived inundation maps and inundation extents calculated on the basis of TanDEM-X. The results show that the WAFL is capable of acceptably representing past flood extents. For one thing, it has a smaller propensity for mistaking flooded vegetation for dry areas than inundation maps derived from Landsat images. For another, it is based on actual physical observations and thus avoids overestimating inundation extents, a pitfall to which flood maps derived from superimposing a sloped water surface on TanDEM-X are prone.

Nonetheless, it must be noted that due to long-term changes in terrain configuration due to sedimentation, and the construction of local infrastructure, the robustness of the method diminishes the farther back in time it is applied. In terms of improving the approach, it is possible to envision an additional layer of correction of the Sentinel-derived maps on the basis of TanDEM-X to remove any remnants of vegetation interference, as well as the improvement of the water surface slope on the scale of the floodplains. Furthermore, a spatialisation of delay times could lead to more regionally adapted results. And finally, a correction based on long-term sedimentation rates is conceivable.

In the case study area in the Cambodian Mekong delta, the results show a small decrease in overall inundation incidence as well as a sharp decrease in inundation incidence at specific dates in July and the first half of August. The results furthermore indicate that inundations duration are on average 19 days shorter in the period 2008-2020 than in the period 1991-2008. Overall, this is likely to have considerable adverse impacts on agricultural cycles, fish reproduction, and regulating ecosystem services such as soil and ground water recharge.

Considering all the limitations outlined above, the WAFL offers a valuable path to reconstructing a consistent time series of inundation extents going back to the 1990s. For the purpose of assessing long-term changes in spatial inundation patterns this is invaluable - especially considering the alternatives of having only sparse amounts of contemporary optical data, data with insufficient spatial and temporal resolution, or no spatial data at all. The WAFL methodology is applicable to other similar areas in large floodplains, where inundated areas are directly correlated to the water level at a gauging station through hydraulic processes and where historical water level data is available. In some areas, however, long-term shifts and precipitation contributions may require some further developments to improve the methodology.

Declaration of Competing Interest

The authors declare that they have no known competing financial interests or personal relationships that could have appeared to influence the work reported in this paper.

Acknowledgements

The authors thank the French Development Agency (AFD) for its support through the COSTEA project, the Wat-Health project (FSPI-2021), and our esteemed colleagues at the Institute of Technology of Cambodia as well as the Royal University of Agriculture for their invaluable partnership and support during field work.

CRediT Author Statement

Christina Orieschnig: Conceptualisation, Methodology, Software, Validation, Formal Analysis, Writing - Original Draft, Writing- Review and Editing, Visualisation **Jean-Philippe Venot**: Conceptualisation, Methodology, Writing - Review and Editing, Supervision, Project Administration, Funding Acquisition **Sylvain Massuel**: Conceptualisation, Investigation, Resources, Writing - Review and Editing, Project Administration, Funding Acquisition **Khy Eam Eang**: Investigation, Resources **Kong Chhuon**: Investigation, Resources **Sambo Lun**:Investigation, Resources **Sokly Siev**:Investigation, Resources **Gilles Belaud**:Conceptualisation, Methodology, Writing - Review and Editing, Supervision

References

Aires, F., Venot, J.P., Massuel, S., Gratiot, N., Pham-Duc, B., Prigent, C., 2020. Surface Water Evolution (2001–2017) at the Cambodia/Vietnam Border in the Upper Mekong Delta Using Satellite MODIS Observations. Remote Sensing 12, 800. doi:10.3390/rs12050800.

Alexandersson, H., 1986. A homogeneity test applied to precipitation data. Journal of Climatology 6, 661–675. doi:10.1002/joc.3370060607.

Arthur, D., Vassilvitskii, S., 2007. k-means++: The advantages of careful seeding, in: Proceedings of the eighteenth annual ACM-SIAM symposium on Discrete algorithms, Society for Industrial and Applied Mathematics. pp. 1027–1035.

Bader, J.C., Belaud, G., Lamagat, J.P., Ferret, T., Vauchel, P., 2016. Modélisation de propagation d'écoulement entre lits mineur et majeur sur les fleuves Sénégal et Niger. Hydrological Sciences Journal , 1–20doi:10.1080/02626667.2016.1148815.

Belaud, G., Bercher, N., 2010. Calibration of a propagation model in large river using satellite altimetry Water and Energy Saving: A Novel Low-Cost Solution for Water Wells View project Solar Induced Fluorescence View project, in: 6th International Symposium on Environmental Hydraulics, pp. 23–25. doi:10.1201/b10553-143.

Biggs, D.A., 2010. Quagmire : Nation-building and nature in the Mekong Delta. University of Washington Press.

Bioresita, F., Puissant, A., Stumpf, A., Malet, J.P., 2019. Fusion of Sentinel-1 and Sentinel-2 image time series for permanent and temporary surface water mapping. International Journal of Remote Sensing 40, 1–24. doi:10.1080/01431161.2019.1624869.

Boretti, A., 2020. Implications on food production of the changing water cycle in the Vietnamese Mekong Delta. Global Ecology and Conservation 22, e00989. doi:10.1016/J.GECCO.2020.E00989.

Brown, P.R., My Phung, N.T., 2010. Pattern and dynamics of rodent damage to lowland irrigated rice crops in An Giang, Vietnam. International Journal of Pest Management 57, 67–76. doi:10.1080/09670874.2010.529954.

Buishand, T., 1982. Some methods for testing the homogeneity of rainfall records. Journal of Hydrology 58, 11–27. doi:10.1016/0022-1694(82)90066-X.

Burbano, M., Shin, S., Nguyen, K., Pokhrel, Y., 2020. Hydrologic changes, dam construction, and the shift in dietary protein in the Lower Mekong River Basin. Journal of Hydrology 581, 124454. doi:10.1016/J.JHYDROL.2019.124454.

Chen, C.F., Son, N.T., Chang, L.Y., Chen, C.C., 2011. Monitoring of soil moisture variability in relation to rice cropping systems in the Vietnamese Mekong Delta using MODIS data. Applied Geography 31, 463–475. doi:10.1016/J.APGEOG.2010.10.002.

Congalton, R.G., 1991. A Review of Assessing the Accuracy of Classifications of Remotely Sensed Data. Remote Sensing of Environment 37, 35–46. doi:https://doi.org/10.1016/0034-4257(91)90048-B.

Dang, T., Cochrane, T., Arias, M., 2018. Quantifying suspended sediment dynamics in mega deltas using remote sensing data: A case study of the Mekong floodplains. volume 68. doi:10.1016/j.jag.2018.02.008.

Dang, T.D., Cochrane, T.A., Arias, M.E., Van, P.D.T., de Vries, T.T., 2016. Hydrological alterations from water infrastructure development in the Mekong floodplains. Hydrological Processes 30, 3824–3838. doi:10.1002/hyp.10894.

DeVries, B., Huang, C., Armston, J., Huang, W., Jones, J.W., Lang, M.W., 2020. Rapid and robust monitoring of flood events using Sentinel-1 and Landsat data on the Google Earth Engine. Remote Sensing of Environment 240, 111664. doi:10.1016/J.RSE.2020.111664.

Erban, L.E., Gorelick, S.M., 2016. Closing the irrigation deficit in Cambodia: Implications for transboundary impacts on groundwater and Mekong River flow. Journal of Hydrology 535, 85–92. doi:10.1016/j.jhydrol.2016.01.072.

878 Fayne, J.V., Bolten, J.D., Doyle, C.S., Fuhrmann, S., Rice, M.T., Houser, P.R.,
879 Lakshmi, V., 2017. Flood mapping in the lower Mekong River Basin using
880 daily MODIS observations. International Journal of Remote Sensing 38, 1737–
881 1757. doi:10.1080/01431161.2017.1285503.

882 Frank, E., Hall, M.A., Witten, I.H., 2016. The WEKA Workbench.

883 Gorelick, N., Hancher, M., Dixon, M., Ilyushchenko, S., Thau, D., Moore, R.,
884 2017. Google Earth Engine: Planetary-scale geospatial analysis for everyone.
885 Remote Sensing of Environment 202, 18–27. doi:10.1016/J.RSE.2017.06.
886 031.

887 Hamed, K.H., Ramachandra Rao, A., 1998. A modified Mann-Kendall trend
888 test for autocorrelated data. Journal of Hydrology 204, 182–196. doi:10.
889 1016/S0022-1694(97)00125-X.

890 Hashim, H., Latif, Z.A., Adnan, N.A., Alam, S., 2019. Urban Vegetation Clas-
891 sification with NDVI Threshold Value Method With Very High Resolution
892 (VHR) PLEIADES Imagery. The International Archives of the Photogram-
893 metry, Remote Sensing and Spatial Information Sciences XLII-4/W16, 237–
894 240. doi:10.5194/isprs-archives-XLII-4-W16-237-2019.

895 Hawker, L., Neal, J., Bates, P., 2019. Accuracy assessment of the TanDEM-X
896 90 Digital Elevation Model for selected floodplain sites. Remote Sensing of
897 Environment 232, 111319. doi:10.1016/J.RSE.2019.111319.

898 Hecht, J., Lacombe, G., Arias, M., Dang, T., Piman, T., 2018. Hydropower
899 dams of the Mekong River basin: a review of their hydrological impacts.
900 Journal of Hydrology 568, 285–300. doi:10.1016/j.jhydrol.2018.10.045.

901 Heng, S., Horton, A., Hok, P., Chung, S., Koponen, J., Kummu, M., 2021.
902 The Cambodian Mekong floodplain under the future development plans and
903 climate change. Natural Hazards and Earth System Science 65, 1–25. doi:10.
904 5194/nhess-2021-65.

Hoang, L.P., Lauri, H., Kummu, M., Koponen, J., van Vliet, M.T.H., Supit, I., Leemans, R., Kabat, P., Ludwig, F., 2016. Mekong River flow and hydrological extremes under climate change. Hydrology and Earth System Sciences 20, 3027–3041. doi:10.5194/hess-20-3027-2016.

Hoang, L.P., van Vliet, M.T., Kummu, M., Lauri, H., Koponen, J., Supit, I., Leemans, R., Kabat, P., Ludwig, F., 2019. The Mekong's future flows under multiple drivers: How climate change, hydropower developments and irrigation expansions drive hydrological changes. Science of the Total Environment 649, 601–609. doi:10.1016/j.scitotenv.2018.08.160.

Hortle, K.G., 2009. Fisheries of the Mekong River Basin. The Mekong , 197–249doi:10.1016/B978-0-12-374026-7.00009-7.

Huang, C., Davis, L.S., Townshend, J.R.G., 2002. An assessment of support vector machines for land cover classification. International Journal of Remote Sensing 23, 725–749. doi:10.1080/01431160110040323.

Hughes, D.A., 1980. Floodplain inundation: Processes and relationships with channel discharge. Earth Surface Processes 5, 297–304. doi:10.1002/esp.3760050308.

Hung, N.N., Delgado, J.M., Güntner, A., Merz, B., Bárdossy, A., Apel, H., 2014. Sedimentation in the floodplains of the Mekong Delta, Vietnam Part II: deposition and erosion. Hydrological Processes 28, 3145–3160. doi:10.1002/hyp.9855.

Intralawan, A., Wood, D., Frankel, R., Costanza, R., Kubiszewski, I., 2018. Tradeoff analysis between electricity generation and ecosystem services in the Lower Mekong Basin. Ecosystem Services 30, 27–35. doi:10.1016/j.ecoser.2018.01.007.

Khem, S., 2009. Assessment of Double Rice Cropping in the Cambodian Mekong Delta using a Flood Inundation Model. doi:10.13140/RG.2.1.1899.8886.

Kondolf, G.M., Schmitt, R.J.P., Carling, P., Darby, S., Arias, M., Bizzi, S., Castelletti, A., Cochrane, T.A., Gibson, S., Kummu, M., Oeurng, C., Rubin, Z., Wild, T., 2018. Changing sediment budget of the Mekong: Cumulative threats and management strategies for a large river basin. Science of The Total Environment 625, 114–134. doi:10.1016/j.scitotenv.2017.11.361.

Koponen, J., Paiboonvorachat, C., Munoz, A., 2017. The Council Study: Study on the sustainable management and development of the Mekong River, including impacts of mainstream hydropower projects. Report on the Positive and Negative Impacts of Irrigation on the Social, Environment, and Economic Conditions of the Lower Mekong River Basin and Policy Recommendations. Technical Report. Mekong River Commission. Vientiane, Laos PDR. URL: https://www.mrcmekong.org/assets/Publications/Council-Study/Irrigation-report_Council-Study.pdf.

Kuenzer, C., Renaud, F., 2012. Climate Change and Environmental Change in River Deltas Globally, in: The Mekong delta system - Interdisciplinary analyses of a river delta. Springer, Dordrecht, pp. 7–48.

Kummu, M., Sarkula, J., 2008. Impact of the Mekong River Flow Alteration on the Tonle Sap Flood Pulse. Ambio 37, 185–192. doi:10.1579/0044-7447(2008)37[185:IOTMRF]2.0.CO;2.

Kummu, M., Tes, S., Yin, S., Adamson, P., Józsa, J., Koponen, J., Richey, J., Sarkkula, J., 2014. Water balance analysis for the Tonle Sap Lake-floodplain system. Hydrological Processes 28, 1722–1733. doi:10.1002/hyp.9718.

Lacombe, G., Douangsavanh, S., Baker, J., Hoanh, C.T., Bartlett, R., Jeuland, M., Phongpachith, C., 2014. Are hydropower and irrigation development complements or substitutes? The example of the Nam Ngum River in the Mekong Basin. Water International 39, 649–670. doi:10.1080/02508060.2014.956205.

Lamagat, J.P., Morel-Seytoux, H.J., Albergel, J., 1993. Analyse de la propagation des ondes de crues. Hydrologie Continentale 8, 113–137.

961 Leauthaud, C., Belaud, G., Duvail, S., Moussa, R., Grünberger, O., Albergel, J.,
962 2013. Characterizing floods in the poorly gauged wetlands of the Tana River
963 Delta, Kenya, using a water balance model and satellite data. Hydrology and
964 Earth System Sciences 17, 3059–3075. doi:10.5194/hess-17-3059-2013.

965 Lee, J.S., 1983. A simple speckle smoothing algorithm for synthetic aperture
966 radar images. IEEE Transactions on Systems, Man, and Cybernetics SMC-13,
967 85–89. doi:10.1109/TSMC.1983.6313036.

968 Li, D., Long, D., Zhao, J., Lu, H., Hong, Y., 2017. Observed changes in flow
969 regimes in the Mekong River basin. Journal of Hydrology 551, 217–232.
970 doi:10.1016/J.JHYDROL.2017.05.061.

971 Li, D., Zhao, J., Govindaraju, R.S., 2019. Water benefits sharing under trans-
972 boundary cooperation in the Lancang-Mekong River Basin. Journal of Hy-
973 drology 577, 123989. doi:10.1016/J.JHYDROL.2019.123989.

974 Loucks, D.P., 2019. Developed river deltas: are they sustainable? Environmen-
975 tal Research Letters 14, 113004. doi:10.1088/1748-9326/ab4165.

976 Main-Knorn, M., Pflug, B., Louis, J., Debaecker, V., Müller-Wilm, U., Gascon,
977 F., 2017. Sen2Cor for Sentinel-2, in: Bruzzone, L., Bovolo, F., Benediktsson,
978 J.A. (Eds.), Image and Signal Processing for Remote Sensing XXIII, Interna-
979 tional Society for Optics and Photonics. p. 3. doi:10.1117/12.2278218.

980 Mallakpour, I., Villarini, G., 2016. A simulation study to examine the sensitivity
981 of the Pettitt test to detect abrupt changes in mean. Hydrological Sciences
982 Journal 61, 245–254. doi:10.1080/02626667.2015.1008482.

983 Manh, N.V., Dung, N.V., Hung, N.N., Merz, B., Apel, H., 2014. Large-
984 scale suspended sediment transport and sediment deposition in the Mekong
985 Delta. Hydrology and Earth System Sciences 18, 3033–3053. doi:10.5194/
986 hess-18-3033-2014.

McFeeters, S.K., 1996. The use of the Normalized Difference Water Index (NDWI) in the delineation of open water features. International Journal of Remote Sensing 17, 1425–1432. doi:10.1080/01431169608948714.

Mohammed, I.N., Bolten, J.D., Srinivasan, R., Lakshmi, V., 2018. Satellite observations and modeling to understand the Lower Mekong River Basin streamflow variability. Journal of Hydrology 564, 559–573. doi:10.1016/j.jhydrol.2018.07.030.

Nath, B., Acharjee, S., 2013. Forest Cover Change Detection using Normalized Difference Vegetation Index (NDVI) : A Study of Reingkhyongkine Lake's Adjoining Areas, Rangamati, Bangladesh. Indian Cartographer 33, 348–353.

Nguyen, V.K., Pittock, J., Connell, D., 2019. Dikes, rice, and fish: how rapid changes in land use and hydrology have transformed agriculture and subsistence living in the Mekong Delta. Regional Environmental Change 19, 2069–2077. doi:10.1007/s10113-019-01548-x.

Orieschnig, C.A., Belaud, G., Venot, J.P., Massuel, S., Ogilvie, A., 2021. Input imagery, classifiers, and cloud computing: Insights from multi-temporal LULC mapping in the Cambodian Mekong Delta. European Journal of Remote Sensing 54, 398–416. doi:10.1080/22797254.2021.1948356.

Park, E., Ho, H.L., Tran, D.D., Yang, X., Alcantara, E., Merino, E., Son, V.H., 2020. Dramatic decrease of flood frequency in the Mekong Delta due to riverbed mining and dyke construction. Science of The Total Environment 723, 138066. doi:10.1016/J.SCITOTENV.2020.138066.

Pekel, J.F., Cottam, A., Gorelick, N., Belward, A.S., 2016. High-resolution mapping of global surface water and its long-term changes. Nature 540, 418–422. doi:10.1038/nature20584.

Pettitt, A.N., 1979. A Non-Parametric Approach to the Change-Point Problem. Applied Statistics 28, 126–135. doi:10.2307/2346729.

Pham-Duc, B., Prigent, C., Aires, F., 2017. Surface water monitoring within cambodia and the Vietnamese Mekong Delta over a year, with Sentinel-1 SAR observations. Water 9, 366. doi:10.3390/w9060366.

Pinn, T., Reach, S., Buntong, B., Acedo, A., 2020. Vegetable Farming Practices in Cambodia: Case study of Small-scale Vegetable Farmers in Kandal, Kampong Chhnang and Battambang Provinces. Journal of Environmental and Rural Development 11, 57–62.

Plank, S., Jüssi, M., Martinis, S., Twele, A., 2017. Mapping of flooded vegetation by means of polarimetric Sentinel-1 and ALOS-2/PALSAR-2 imagery. International Journal of Remote Sensing 38, 3831–3850. doi:10.1080/01431161.2017.1306143.

Pokhrel, Y., Burbano, M., Roush, J., Kang, H., Sridhar, V., Hyndman, D.W., 2018. A review of the integrated effects of changing climate, land use, and dams on Mekong river hydrology. Water 10, 266. doi:10.3390/w10030266.

Potin, P., Rosich, B., Miranda, N., Grimont, P., Shurmer, I., O'Connell, A., Krassenburg, M., Gratadour, J.B., 2019. Copernicus Sentinel-1 Constellation Mission Operations Status, in: IGARSS 2019 - 2019 IEEE International Geoscience and Remote Sensing Symposium, IEEE. pp. 5385–5388. doi:10.1109/IGARSS.2019.8898949.

Poulsen, A., Hortle, K., Valbo-Jorgensen, J., Chan, S., Viravong, S., Bouakhamvongsa, K., Suntornratana, U., Yoorong, N., Nguyen, T., Tran, B., 2004. Distribution and Ecology of Some Important Riverine Fish Species of the Mekong River Basin. Technical Report. Mekong River Commission. Phnom Penh.

Quang, N.H., Tuan, V.A., Hao, N.T.P., Hang, L.T.T., Hung, N.M., Anh, V.L., Phuong, L.T.M., Carrie, R., 2019. Synthetic aperture radar and optical remote sensing image fusion for flood monitoring in the Vietnam lower Mekong

basin: a prototype application for the Vietnam Open Data Cube. European Journal of Remote Sensing 52, 599–612. doi:10.1080/22797254.2019.1698319.

Quoc Thanh, V., Roelvink, D., van der Wegen, M., Reyns, J., Kernkamp, H., Van Vinh, G., Thi Phuong Linh, V., 2019. Flooding in the Mekong Delta: Impact of dyke systems on downstream hydrodynamics. Hydrology and Earth System Sciences 24, 189–212. doi:10.5194/hess-2019-64.

Rizzoli, P., Martone, M., Gonzalez, C., Wecklich, C., Borla Tridon, D., Bräutigam, B., Bachmann, M., Schulze, D., Fritz, T., Huber, M., Wessel, B., Krieger, G., Zink, M., Moreira, A., 2017. Generation and performance assessment of the global TanDEM-X digital elevation model. ISPRS Journal of Photogrammetry and Remote Sensing 132, 119–139. doi:10.1016/J.ISPRSJPRS.2017.08.008.

Rouse J.W., J., Haas, R., Schell, J., Deering, D., 1974. Monitoring Vegetation Systems in the Great Plains with ERTS, in: Freden, S.C., Mercanti, E.P., Becker, M.A. (Eds.), Third Earth Resources Technology Satellite-1 Symposium- Volume I: Technical Presentations NASA SP-351. NASA. volume 30103017, pp. 301–217.

Shin, S., Pokhrel, Y., Yamazaki, D., Huang, X., Torbick, N., Qi, J., Pattanakiat, S., Ngo-Duc, T., Nguyen, T.D., 2020. High Resolution Modeling of River-Floodplain-Reservoir Inundation Dynamics in the Mekong River Basin. Water Resources Research 56, e2019WR026449. doi:10.1029/2019WR026449.

Singha, M., Dong, J., Sarmah, S., You, N., Zhou, Y., Zhang, G., Doughty, R., Xiao, X., 2020. Identifying floods and flood-affected paddy rice fields in Bangladesh based on Sentinel-1 imagery and Google Earth Engine. ISPRS Journal of Photogrammetry and Remote Sensing 166, 278–293. doi:10.1016/J.ISPRSJPRS.2020.06.011.

Sothea, K., Goto, A., Mizutani, M., 2006. A Hydrologic Analysis on Inundation in the Flooding Area of the Mekong Delta, Cambodia: The Combined

Deterministic and Stochastic Models for Flood Forecasting, in: World Environmental and Water Resource Congress 2006, pp. 1–10. doi:10.1061/40856(200)213.

Szabo, S., Brondizio, E., Renaud, F.G., Hetrick, S., Nicholls, R.J., Matthews, Z., Tessler, Z., Tejedor, A., Sebesvari, Z., Foufoula-Georgiou, E., da Costa, S., Dearing, J.A., 2016. Population dynamics, delta vulnerability and environmental change: comparison of the Mekong, Ganges–Brahmaputra and Amazon delta regions. Sustainability Science 11, 539–554. doi:10.1007/s11625-016-0372-6.

Triet, N.V.K., Dung, N.V., Fujii, H., Kummu, M., Merz, B., Apel, H., 2017. Has dyke development in the Vietnamese Mekong Delta shifted flood hazard downstream? Hydrology and Earth System Sciences 21, 3991–4010. doi:10.5194/hess-21-3991-2017.

Trung, L.D., Duc, N.A., Nguyen, L.T., Thai, T.H., Khan, A., Rautenstrauch, K., Schmidt, C., 2020. Assessing cumulative impacts of the proposed Lower Mekong Basin hydropower cascade on the Mekong River floodplains and Delta – Overview of integrated modeling methods and results. Journal of Hydrology 581, 122511. doi:10.1016/J.JHYDROL.2018.01.029.

Try, S., Tanaka, S., Tanaka, K., Sayama, T., Lee, G., Oeurng, C., 2020. Assessing the effects of climate change on flood inundation in the lower Mekong Basin using high-resolution AGCM outputs. Progress in Earth and Planetary Science 7, 34. doi:10.1186/s40645-020-00353-z.

Tsyganskaya, V., Martinis, S., Marzahn, P., Ludwig, R., 2018. SAR-based detection of flooded vegetation – a review of characteristics and approaches. International Journal of Remote Sensing 39, 2255–2293. doi:10.1080/01431161.2017.1420938.

Twele, A., Cao, W., Plank, S., Martinis, S., 2016. Sentinel-1-based flood mapping: a fully automated processing chain. International Journal of Remote Sensing 37, 2990–3004. doi:10.1080/01431161.2016.1192304.

Vandôme, P., 2020. Agricultural vulnerability to hydrologic hazards in the prek area of the upper Mekong Delta, Cambodia. Technical Report. Montpellier SupAgro. Montpellier.

Venot, J.P., Jensen, C.B., 2021. A multiplicity of prek(s) : Enacting a socionatural mosaic in the Cambodian upper Mekong delta. Environment and Planning E: Nature and Space , 251484862110268doi:10.1177/25148486211026835.

Vilain, C., Baran, E., Gallego, G., Samadee, S., 2016. Fish and the Nutrition of Rural Cambodians. Asian Journal of Agriculture and Food Sciences 4, 2321–1571.

Vu, A.V., Hortle, K.G., Nguyen, D.N., 2021. Factors Driving Long Term Declines in Inland Fishery Yields in the Mekong Delta. Water 13, 1005. doi:10.3390/w13081005.

Wilson, E.H., Sader, S.A., 2002. Detection of forest harvest type using multiple dates of Landsat TM imagery. Remote Sensing of Environment 80, 385–396. doi:10.1016/S0034-4257(01)00318-2.

Winemiller, K.O., McIntyre, P.B., Castello, L., Fluet-Chouinard, E., Giarrizzo, T., Nam, S., Baird, I.G., Darwall, W., Lujan, N.K., Harrison, I., Stiassny, M.L.J., Silvano, R.A.M., Fitzgerald, D.B., Pelicice, F.M., Agostinho, A.A., Gomes, L.C., Albert, J.S., Baran, E., Petrere, M., Zarfl, C., Mulligan, M., Sullivan, J.P., Arantes, C.C., Sousa, L.M., Koning, A.A., Hoeinghaus, D.J., Sabaj, M., Lundberg, J.G., Armbruster, J., Thieme, M.L., Petry, P., Zuanon, J., Vilara, G.T., Snoeks, J., Ou, C., Rainboth, W., Pavanelli, C.S., Akama, A., Soesbergen, A.v., Saenz, L., 2016. Balancing hydropower and biodiversity in the Amazon, Congo, and Mekong. Science 351, 128–129. doi:10.1126/science.aac7082.

Yang, J., Yang, Y.E., Chang, J., Zhang, J., Yao, J., 2019. Impact of dam development and climate change on hydroecological conditions and natural hazard risk in the Mekong River Basin. Journal of Hydrology 579, 124177. doi:10.1016/J.JHYDROL.2019.124177.

Yoshida, Y., Lee, H.S., Trung, B.H., Tran, H.D., Lall, M.K., Kakar, K., Xuan, T.D., 2020. Impacts of Mainstream Hydropower Dams on Fisheries and Agriculture in Lower Mekong Basin. Sustainability 12, 2408. doi:10.3390/su12062408.

Yun, X., Tang, Q., Wang, J., Liu, X., Zhang, Y., Lu, H., Wang, Y., Zhang, L., Chen, D., 2020. Impacts of climate change and reservoir operation on streamflow and flood characteristics in the Lancang-Mekong River Basin. Journal of Hydrology 590, 125472. doi:10.1016/J.JHYDROL.2020.125472.

Zhang, W., Sun, W., Li, T., 2017. Uncertainties in the national inventory of methane emissions from rice cultivation: field measurements and modeling approaches. Biogeosciences 14, 163–176. URL: https://bg.copernicus.org/articles/14/163/2017/, doi:10.5194/bg-14-163-2017.

Zhou, C., van Nooijen, R., Kolechkina, A., Hrachowitz, M., 2019. Comparative analysis of nonparametric change-point detectors commonly used in hydrology. Hydrological Sciences Journal 64, 1690–1710. doi:10.1080/02626667.2019.1669792.

Appendix A: Explanation of the Choice of Hydrological Parameters Chosen for Analysis

These parameters reflect the immediate considerations of farmers with regard to their cultivation practices. The date of the flood arrival, for example, determines whether early wet season crops can be harvested in time, or whether they will suffer damage from the oncoming inundations. Similarly, the date of the flood recession dictates when crops can be planted on the formerly inundated fields and the extent to which they will depend on irrigation at the end of their growing cycle. The dates of the flood rise and recession - and thus the overall flood duration - were defined on the basis of the rate at which water levels rise and fall (Δwl). The date of the largest positive Δwl was taken as the start of the flood, the date of the largest negative Δwl as the date of recession. The number of days between these two dates was taken as the flood duration. Local water level thresholds were chosen on a qualitative basis, based on conversations with stakeholders. They reflect water depths that are conducive to fish reproduction and that farmers feel allow cultivation without constituting potential threats to harvesting.

Appendix B: The Lamagat Correlation Model

Initially developed to identify correlations between gauging stations, the Lamagat approach has been used with satellite data series in both the Tana river delta in Kenya by Leauthaud et al. (2013), and at the Niger and Senegal rivers by Bader et al. (2016) (flooded areas) and Belaud and Bercher (2010) (satellite altimetry). It was developed to model the propagation of flood waves, specifically in areas with low slope gradients and observable hysteresis effects in rating curves - such as deltaic floodplains. This approach combines kinematic elements with statistical methods. Its main advantage is that it identifies optimal correlation factors not between the overall time series of flood extents and water levels in the river, but between a set number of sub-sections of the time series. Consequently, it can account for the varying time delays depending on

the phase of the flood cycle. Therefore, the time delay is expressed as a function of the river water level, while the flood extent at a given time is a function of the water level observed some days before.

Appendix C: Visual Representation of WAFL Calculation

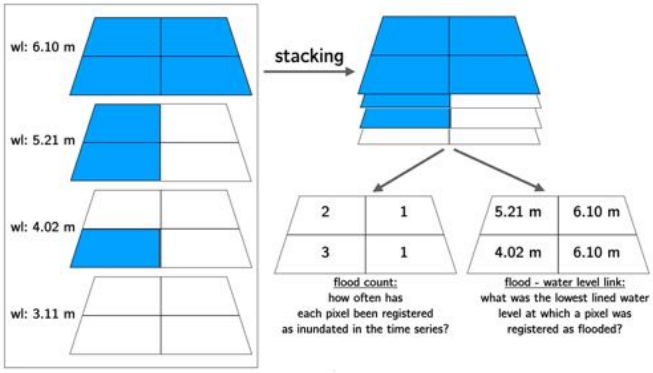

Figure 9: Logic workflow for creating the water level - flood link (WAFL). Example of an area with 4 pixels, and 4 images corresponding to 4 different water levels at Koh Khel. Blue areas represent flooded pixels.

Appendix D: Results of the Hydrological Analysis

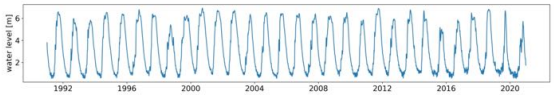

(a) Water levels at Koh Kehl 1990-present.

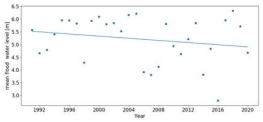

(b) Mean flood water levels at Koh Khel.

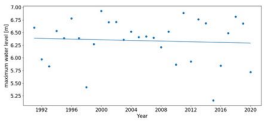

(c) Maximum water level at Koh Kehl.

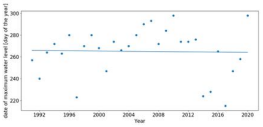

(d) Date of maximum water level at Koh Khel.

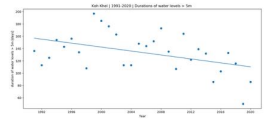

(e) Flood duration over 4 m at Koh Khel.

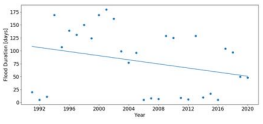

(f) Overall flood duration at Koh Kehl.

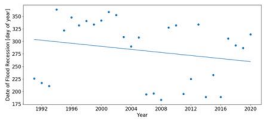

(g) Date of flood recession at Koh Khel.

Figure 10: Results of hydrological analysis at Koh Khel.

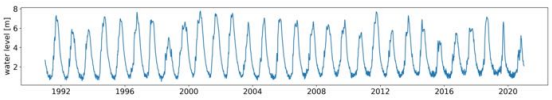

(a) Water levels at Neak Luong 1990-present.

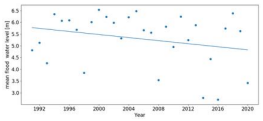

(b) Mean flood water levels at Neak Luong.

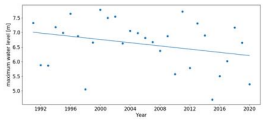

(c) Maximum water level at Neak Luong.

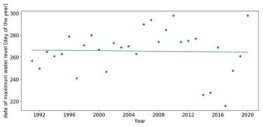

(d) Date of maximum water level at Neak Luong.

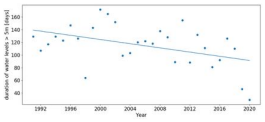

(e) Flood duration over 5 m at Neak Luong.

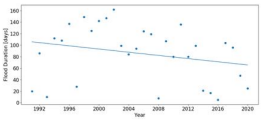

(f) Overall flood duration at Neak Luong.

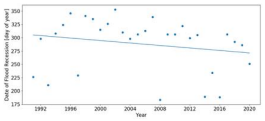

(g) Date of flood recession at Neak Luong.

Figure 11: Results of hydrological analysis at Neak Luong, short time series.

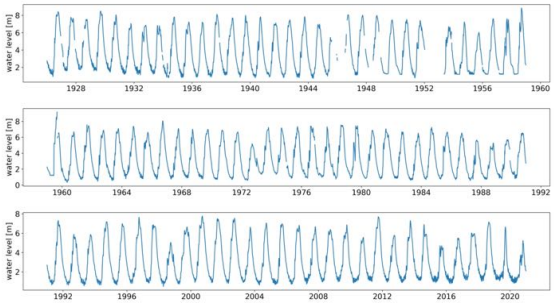

(a) Water levels at Neak Luong 1926-present.

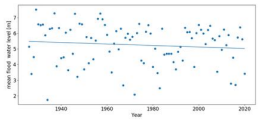

(b) Mean flood water levels at Neak Luong.

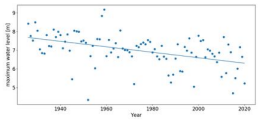

(c) Maximum water level at Neak Luong.

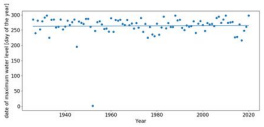

(d) Date of maximum water level at Neak Luong.

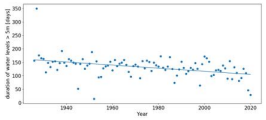

(e) Flood duration over 5 m at Neak Luong.

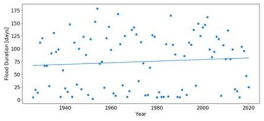

(f) Overall flood duration at Neak Luong.

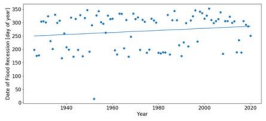

(g) Date of flood recession at Neak Luong.

Figure 12: Results of hydrological analysis at Neak Luong, long time series.

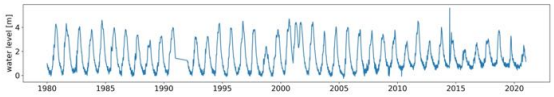

(a) Water levels at Tan Chau 1980-present.

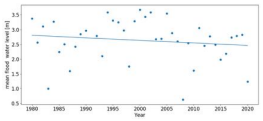

(b) Mean flood water levels at Tan Chau.

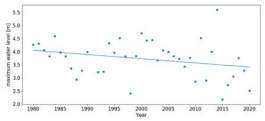

(c) Maximum water level at Tan Chau.

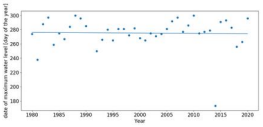

(d) Date of maximum water level at Tan Chau.

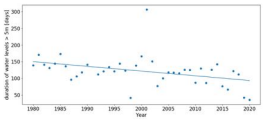

(e) Flood duration over 2 m at Tan Chau.

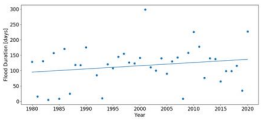

(f) Overall flood duration at Tan Chau.

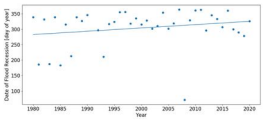

(g) Date of flood recession at Tan Chau.

Figure 13: Results of hydrological analysis at Tan Chau.

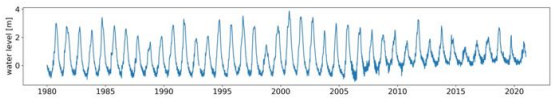

(a) Water levels at Chau Doc 1980-present.

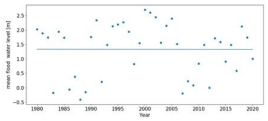

(b) Mean flood water levels at Chau Doc.

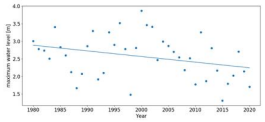

(c) Maximum water level at Chau Doc.

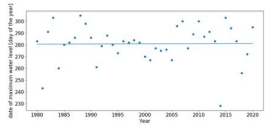

(d) Date of maximum water level at Chau Doc.

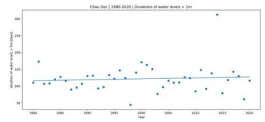

(e) Flood duration over 2 m at Chau Doc.

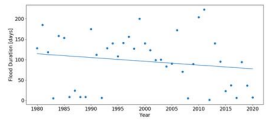

(f) Overall flood duration at Chau Doc.

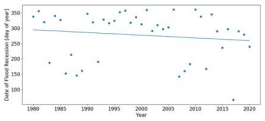

(g) Date of flood recession at Chau Doc.

Figure 14: Results of hydrological analysis at Chau Doc.

Appendix E: Results of the Detection of Inundation Extents Using Sentinel 1 and 2 and the Lamagat Correlation

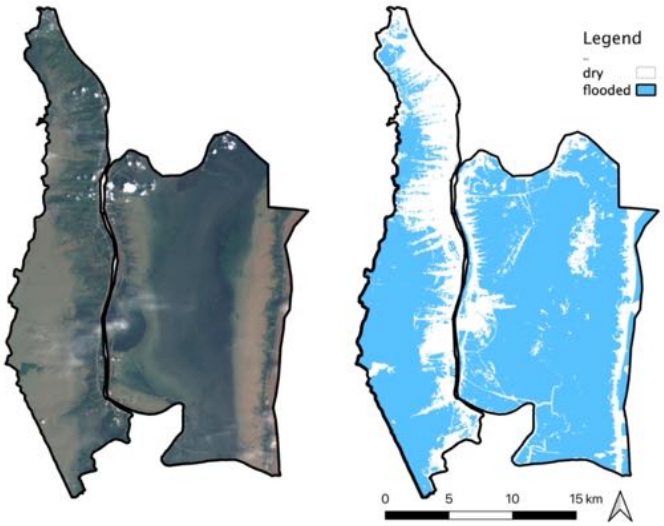

Figure 15: Example of classification using k-means and optical Sentinel data on 2018-10-01

Validation Date	Overall Accuracy Optical	Overall Accuracy Radar	Kappa Optical	Kappa Radar
2017-01-29	0.994	0.984	0.948	0.83
2018-06-24	0.938	0.979	0.757	0.908
2019-09-27	0.993	0.997	0.945	0.993
2019-08-14	0.917	0.917	0.526	0.371
Average	0.961	0.97	0.794	0.776
	0.965		0.785	

Table 3: Accuracy assessment of the inundation classification using Sentinel-1 and 2

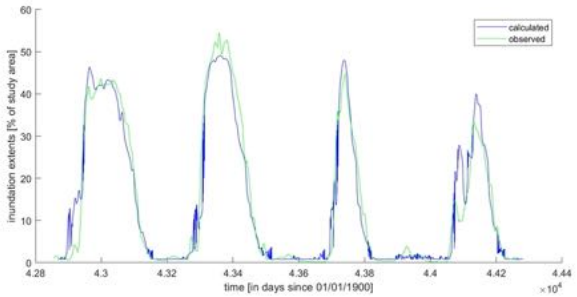

Figure 16: Observed inundation extents and extents calculated from upstream water levels using the Lamagat model, Zone A.

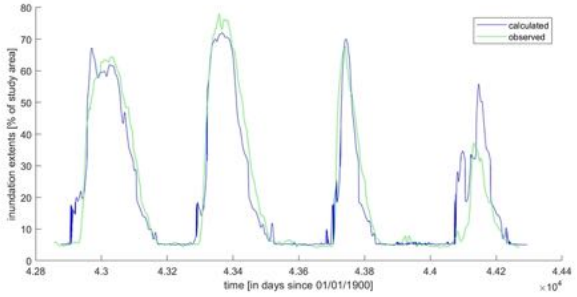

Figure 17: Observed inundation extents and extents calculated from upstream water levels using the Lamagat model, Zone B.

Water Level [m]	Optimal Delay Time
0.67	1
0.87	13.75
0.98	8.75
1.07	8.75
1.15	12.75
1.22	14.75
1.31	11.75
1.41	12.75
1.58	7.75
1.81	18.75
2.05	27.75
2.44	14.75
2.81	17.75
3.17	17.75
3.74	19.75
4.30	11.75
5.14	13.75
5.82	12.75
6.44	15.75

Table 4: Optimal correlation times by water level, Zone A

Water Level [m]	Optimal Delay Time
0.67	2.75
0.87	24.75
0.98	23.75
1.07	23.75
1.15	12.75
1.22	22.75
1.31	28.75
1.41	29.75
1.58	29.75
1.81	29.75
2.05	29.75
2.44	24.75
2.81	19.75
3.17	22.75
3.74	27.75
4.30	23.75
5.14	20.75
5.82	20.75
6.44	21.75

Table 5: Optimal correlation times by water level, Zone B

Appendix F: Comparison With Sentinel, Landsat, and TanDEM-X

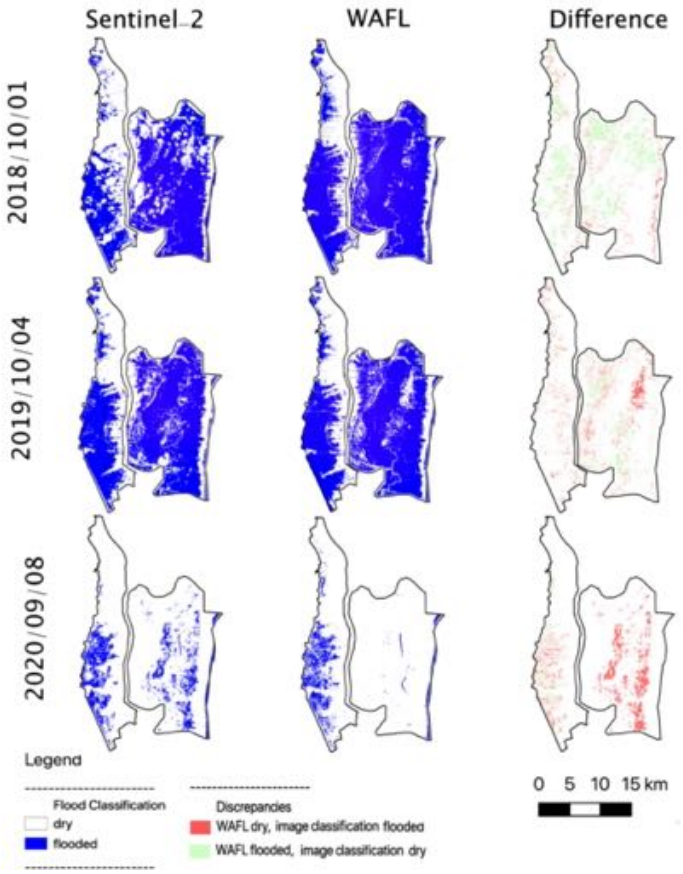

Figure 18: Comparison of WAFL-derived inundation extents, and extents directly derived from Sentinel-2 images in 2018, 2019, and 2020.

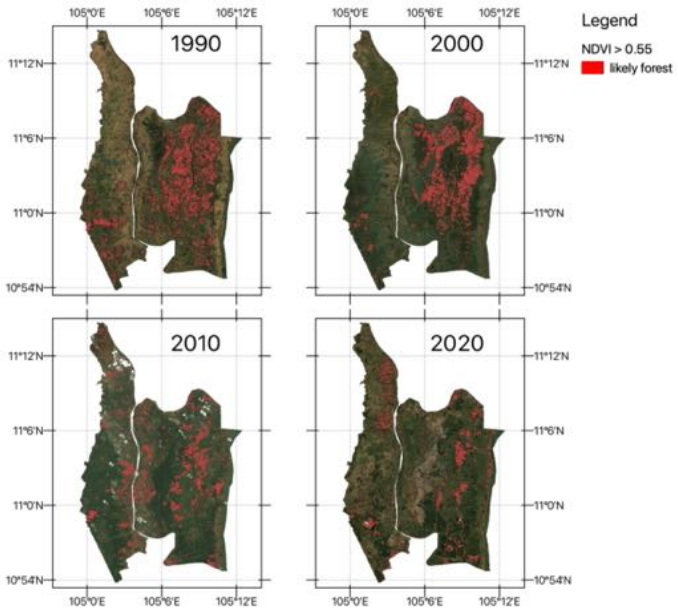

Figure 19: Distribution of natural vegetation in the early 1990s, 2000s, 2010s, and present.

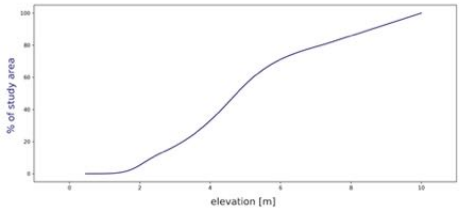

(a) Elevation-area curve Zone A

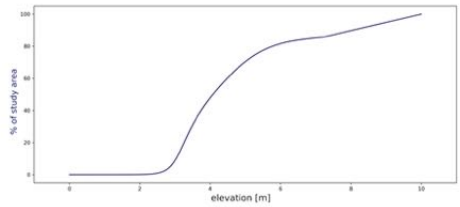

(b) Elevation-area curve Zone B

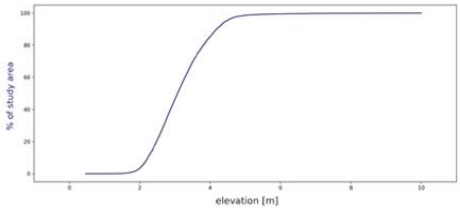

(c) Elevation-area curve in the 1km-radius around the logger in Zone A

Figure 20: Elevation-area curves according to TanDEM

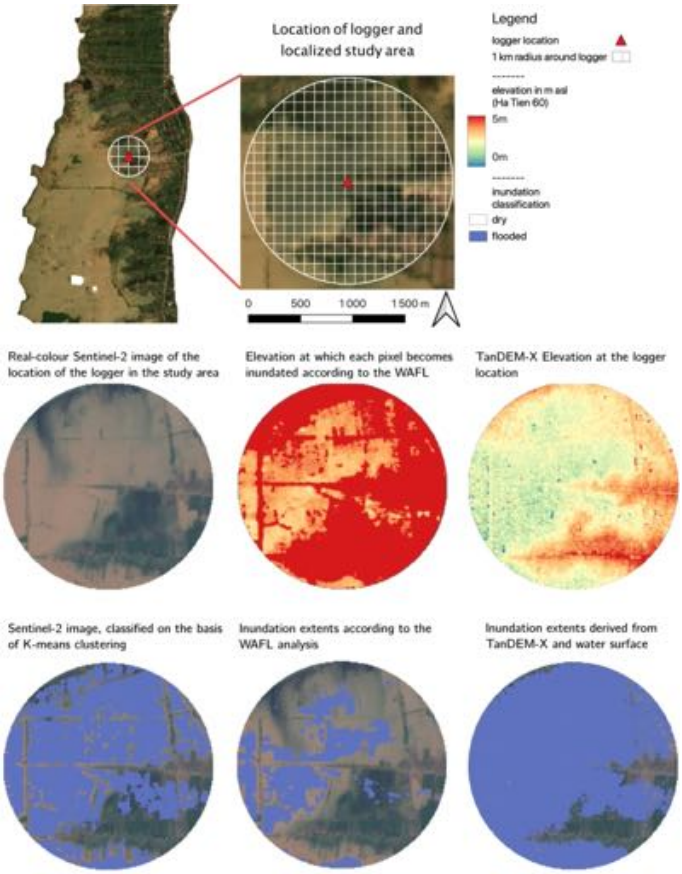

Figure 21: Local comparison of TanDEM-X-derived flood extent and WAFL-derived flood extent observed through Sentinel images.

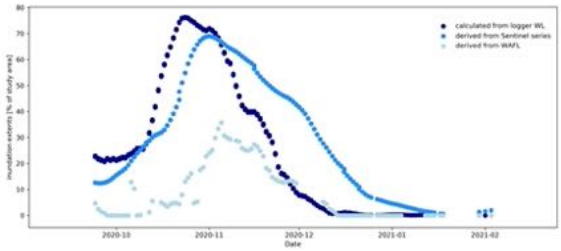

(a) Percentage of flooded area in the 1 km radius around the in-situ logger at Prek Chann West (PCW), derived from Sentinel, and calculated via the elevation-area curve of the TanDEM-X and WAFL.

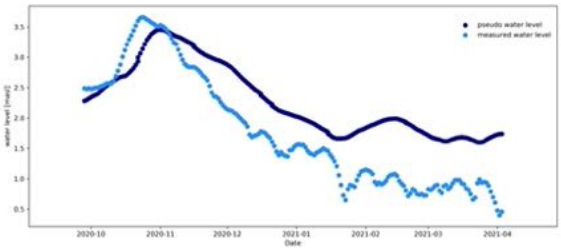

(b) Comparison of the pseudo-water-level calculated from the remote sensing observations and the TanDEM-X elevation-area curve, and the values measured by the in-situ logger

Figure 22: Comparison of DEM with local water level data.

Appendix G: Results of Analysis of Changes in Inundation Patterns in the Cambodian Mekong Delta

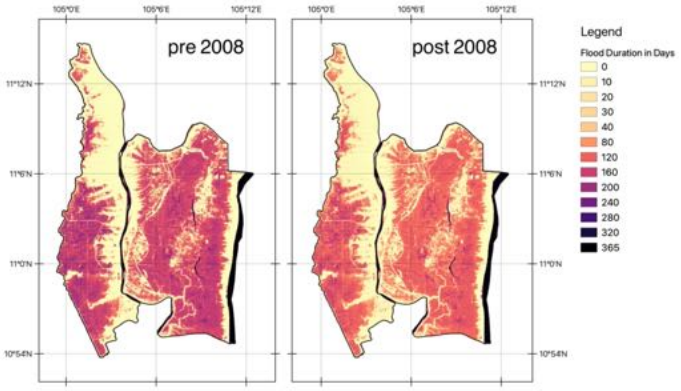

Figure 23: Change in inundation durations pre- and post-2008